Thermodynamic Analysis, Modelling and Control of a Novel Hybrid Propulsion System

by

Anita Raghunath Chaudhari

Doctoral Thesis Submitted in partial fulfilment of the
Requirements for the award of
Doctor of Philosophy of Loughborough University

August 2011

Abstract

Stringent emission regulations imposed by governments and depleting fossil fuel reserves have promoted the development of the automotive industry towards novel technologies. Various types of hybrid power plants for transport and stationary applications have emerged. The methodology of design and development of such power plants varies according to power producing components used in the systems. The practical feasibility of such power plants is a pre-requisite to any further development. This work presents thermodynamic analysis and modelling of such a novel power plant, assesses its feasibility and further discusses the development of a suitable control system.

The proposed system consists of a hybrid configuration of a solid oxide fuel cell and IC engine as the main power producing components. A reformer supplies fuel gas to the fuel cell while the IC engine is supplied with a liquid fuel. The excess fuel from the fuel cell anode and the oxygen-depleted air from cathode of the fuel cell are also supplied to the engine. This gas mixture is aspirated into the engine with the balance of energy provided by the liquid fuel. The fuel cell exhaust streams are used to condition the fuel in the engine to ensure minimum pollutants and improved engine performance. Both, fuel cell and engine share the load on the system. The fuel cell operates on a base load while the engine handles majority of the transient load. This system is particularly suitable for a delivery truck or a bus cycle.

Models of the system components – reformer, solid oxide fuel cell, IC engine and turbocharger were developed to understand their steady state and dynamic behaviour. These models were validated against sources of literature and used to predict the effect of different operating conditions for each component. The main control parameters for each component were derived from these models. A first law analysis of the system at steady state was conducted to identify optimum operating region, verify feasibility and efficiency

improvement of the system. The results suggested reduced engine fuel consumption and a 10 % improvement in system efficiency over the conventional diesel engines.

Further, a second law analysis was conducted to determine the key areas of exergy losses and the rational efficiency of the system at full load operating conditions. The results indicate a rational efficiency of 25.4 % for the system. Sensitivity to changes in internal exergy losses on the system work potential was also determined. The exergy analysis indicates a potential for process optimisation as well as design improvements. This analysis provides a basis for the development of a novel control strategy based on exergy analysis and finite-time thermodynamics.

A dynamic simulation of the control oriented system model identified the transient response and control parameters for the system. Based on these results, control systems were developed based on feedback control and model predictive control theories. These controllers mainly focus on air and fuel path management within the system and show an improved transient response for the system. In a hierarchical control structure for the system, the feedback controllers or the model predictive controller can perform local optimisation for the system, while a supervisory controller can perform global optimisation. The objective of the supervisory controller is to determining the load distribution between the fuel cell and the engine. A development strategy for such a top-level supervisory controller for the system is proposed.

The hybrid power plant proposed in this thesis shows potential for application for transport and stationary power production with reduced emissions and fuel consumption. The first and second law of thermodynamics can both contribute to the development of a comprehensive control system. This work integrates research areas of powertrain design, thermodynamic analysis and control design. The development and design strategy followed for such a novel hybrid power plant can be useful to assess the potential of other hybrid systems as well.

Acknowledgements

I am very grateful to my supervisor Professor Richard K Stobart for his able guidance, encouragement, patience, and for providing a rigid foundation for my career. Without his invaluable support, this work would not have been possible.

I would also like to thank members of the Virtual Research Centre, Professor Nicos Ladommatos, Professor Mike Monaghan, Professor Morgan Heikal, Professor Alex Taylor, Dr Yannis Hardalupas, Professor Hua Zhao, Dr Tom Ma, Dr Thanos Megaritis, Dr Xi Jiang, Dr Zhijun Peng whose contributions during discussions regarding the hybrid system have been invaluable.

I would like to thank University of Sussex and Loughborough University for providing funding for my PhD studies. A special thanks to the staff members of University of Sussex, especially late Professor Richard Grimsdale and Linda Church for their tremendous support received for my work as a teaching assistant. I would also like to thank Dr David Kay for his support with partial differential equations.

Personal thanks to colleagues, especially, Dr. Alexandros Plianos for his assistance with modelling work and my dear friend, Dr. Ireri Ibarra.

Words cannot express the support provided by my parents Raghunath and Aruna Chaudhari, my sister Sheetal Narkhede and my brother-in-law Nikhil Narkhede. Last but not the least; I thank my husband Ioannis, for always standing by me.

I would like to dedicate this work to my father, Professor Raghunath V. Chaudhari, who has always been my inspiration.

Table of Contents

List of Acronyms & Abbreviations

AFR	Air-to-fuel-ratio
APS	Acceleration Pedal Sensor
APU	Auxiliary Power Unit
ATR	Autothermal Reformer
BPS	Brake Pedal Sensor
CHP	Combined Heat and Power
CNG	Compressed Natural Gas
CUTE	Clean Urban Transport for Europe
DMFC	Direct Methanol Fuel cell
ECMS	Equivalent Consumption Minimization Strategy
EGR	Exhaust Gas Recirculation
FTT	Finite time thermodynamics
GT	Gas Turbine
HC	Hydrocarbon
HCCI	Homogenous Charge Compression Ignition
HDS	Hydro-desulphuriser
HEV	Hybrid Electric Vehicle
ICE	Internal Combustion Engine
IRSOFC	Internal Reforming SOFC
LSM	Lanthanum Strontium Manganite
MCFC	Molten Carbonate Fuel cell
MIMO	Multiple-input-multiple-output
MPC	Model Predictive Control
MVEM	Mean value engine model
NMP	Non Minimum Phase

NOx	mono-nitrogen oxides (NO and NO2)
OFR	Oxygen-to-fuel-ratio
PAFC	Phosphoric Acid Fuel cell
PEFC	Polymer Electrolyte Fuel cell
PEM	Polymer Electrolyte Membrane
PEMFC	Polymer Electrolyte Membrane fuel cell
PEN	Positive-Electrolyte-Negative
PI	Proportional Integral
PID	Proportional Integral Derivative
PM	Particulate Matter
PNGV	Partnership for New Generation of Vehicles
POX	Partial Oxidation
PRBS	Pseudo-Random Binary Sequence
PSS	Power System Simulation
RFC	Reversible Fuel Cell
RHE	Reversible Heat Engine
SISO	Single-input-single-output
SOFC	Solid Oxide Fuel cell
SPFC	Solid Polymer Fuel cell
SR	Steam Reformer
TPB	Triple-phase Boundary
TPO	Temperature Programmed Oxidation
VGT	Variable Geometry Turbocharger
VVLT	Variable Valve Lift and Timing
WGS	Water Gas Shift Reactor
YSZ	Yttrium-Stabilized Zirconia

Nomenclature

Symbol	Unit	Description
F	Coulombs	Faraday constant
F_{O2}	-	Fraction of oxygen
J	kg m^2	Moment of inertia of turbocharger
T	K	Temperature
p	Pa	Partial Pressure
V	V	Fuel cell stack soltage
W	kg/s	Mass flow rate
P	Pa	Supply manifold and cathode pressure
V_{sm}	m^3	Volume of supply manifold
R_a	-	Gas constant of air
x	-	Mass Fraction
y	-	Molar Fraction
M	kg/mol	Molecular weight of oxygen, nitrogen, hydrogen, water vapour
m	kg	Mass
Greek		
γ_{cp}	-	Heat capacity ratio of air
η	-	Efficiency
γ	-	Ratio of specific heat capacities of air.
λ	-	Excess oxygen ratio
Subscripts		
$_1$	inlet manifold	
$_2$	output manifold	

A	anode
ae	exhaust from anode to engine
anode	anode
B	burner
Bg	burner gas
Bs	burner solid
C	cathode
cat	catalyst
cathode	cathode
cathode,out	cathode exhaust
ce	exhaust from cathode to engine
cm	compressor motor
conv	Convection
cp1	fuel cell compressor
cp1,out	exhaust from fuel cell compressor
cp2	engine compressor
crit	critical
cv	control volume
di	diesel
e	Engine
f	Fuel
fc	fuel cell
fce	fuel cell exhaust
h2_out	hydrogen at outlet
H2O	Water Vapour
H2	Hydrogen
ic	IC engine
in	inlet
ins	Insulator
isentropic	isentropic
mass,diff	Mass diffusion
mass,in	Mass flow in
mass,out	Mass flow out

$N2$	Nitrogen
$O2$	Oxygen
out	outlet
PEN	fuel cell PEN
R	reformer
rad	Radiation
$react$	reaction
ref_in	reformer inlet
rm	return manifold
rm,out	return manifold exhaust
sm	supply manifold for fuel cell
sm_out	exhaust from fuel cell supply manifold
W	wall
Ω	Ohmic

SOFC

Symbol	Unit	Description
ΔG^0	J/kg	Gibbs Free Energy
ΔH	J/kg	Low heating value of hydrogen
A	m2	cross sectional area
A_c	m2	circumferential area
c_p	J/kg. K	Specific heat (constant pressure)
c_v	J/kg. K	Specific heat (constant volume)
e	J/kg	specific internal energy
E_{Nernst}	V	Nernst Potential
E_x	kJ/mol	Activation energies of x
F	Coulombs	Faraday constant
H	J/mol	enthalpy
h	$W/m^2.K$	Convective heat transfer coefficient
I	A	current
k	W/m.K	Thermal conductivity
K	kg/Pa.s	flow coefficient

k_A, k_C	A/m^2	Anode and Cathode pre-exponential factor
K_{shift}	-	equilibrium constant for shift reaction
L	m	Fuel Cell Length
L	m	length of fuel cell
M	g/mol	Molecular weight
p	Pa	partial pressure
r	m	radius
R_A,R_C	ohm	equivalent resistances of anode and cathode
r_x		reaction rate for species x
V	m3	volume
Greek		
ε	$m^3/s.kg$	Thermal emissivity
ρ	kg/ m^3	density
σ	$W/m^2.K^4$	Stefan-Boltzmann constant
Subscripts		
g	gas	
k	species k	
s	solid	

Reformer

Symbol	**Unit**	**Description**
ϵ_R	-	Reformer void fraction
ϵ_B	-	Burner void fraction
ψ_R	m/s.K	$(v_{R,0}/T_{R,0})/(\overline{MM}_{R,0}/\overline{MM}_R)$
ψ_B	m/s.K	$(v_{B,0}/T_{B,0})/(\overline{MM}_{B,0}/\overline{MM}_B)$
ρ_{cat}	kg/ m^3	Catalyst pellet density
ρ	kg/ m^3	Density
π_e	$J/m^3.s.K$	
ξ	m^2/m^3	Catalyst specific surface area
ΔH_4	J/mol	Reaction enthalpy
ΔH_2	J/mol	Reaction enthalpy

ΔH_1	J/mol	Reaction enthalpy
a	m	reactor width
A_1	m^3/s.kg	Kinetic parameters
A_2	mol/s.kg	Kinetic parameters
B_1	m^3/s.kg	Kinetic parameters
$C_{Bg,j}$	kmol/m^3	Concentration in burner gas phase for species j
$C_{Bs,j}$	kmol/m^3	Concentration in burner solid phase for species j
C_{catB}	J/m^3K	Catalyst thermal capacity
C_{catR}	J/m^3K	Catalyst thermal capacity
C_{gas}	J/m^3K	$\sum_j \left(C_{B,g,j} - C_{B,s,j}\right) MM_j c_{p_j}$
c_p	J/kgK	specific heat
$C_{R,j}$	kmol/m^3	Concentration in reformer for species j
C_W	J/m^3K	Wall thermal capacity
D_1	-	Kinetic parameters
D_2	-	Kinetic parameters
E_1	J/mol	Kinetic parameters
E_2	J/mol	Kinetic parameters
f		Wall shape factor
G	-	Stoichiometric coefficient
H	m/s	burner mass-transfer coefficient
j		j=1,2...7, representing species in reformer and burner
k	s^{-1}	reaction rate constant
K_{cat}	J/m.s.K	Catalyst thermal conductivity
K_W	J/m.s.K	Wall conductivity
MM	kg/kmol	Molar Mass
P	kPa	Pressure
P_{atm}	kPa	Ambient Pressure
P_B	kPa	Burner Pressure
P_R	kPa	Reformer Pressure
R	J/mol K	Ideal gas constant
r	kmol/m^3.s	reaction rate

s_B	m	burner thickness
s_{Bs}	m	burner catalyst thickness
s_R	m	reformer thickness
s_W	m	wall thickness
t	s	Time
T_{Bg}	K	Temperature burner gas phase
T_{Bs}	K	Temperature burner solid phase
T_e	K	Temperature ambient
T_R	K	Temperature Reformer
T_W	K	Temperature wall
U_1	$J/m^2.s.K$	heat exchange coefficient
U_2	$J/m^2.s.K$	heat exchange coefficient
U_3	$J/m^2.s.K$	heat exchange coefficient
U_e	$J/m^2.s.K$	heat exchange coefficient
v	m/s	reformer and burner gas speed
x	m	axial coordinate

Engine

Symbol	**Unit**	**Description**
A_m	m2	internal surface area of engine
C	-	compression ratio
h	J/mol	enthalpy
M	g/mol	Molecular weight
n	-	number of species
Nu	-	Nusselt number
P	Pa	pressure
$P_{motored}$	Pa	motored cylinder pressure
Pr	-	Prandtl number
R	-	Ratio of connecting rod length to crank arm radius

Re	-	Reynolds number
$\dot{s}$	mol/s.m^2	molar surface production rate of species per unit area
$\overline{S_p}$	m/s	mean piston speed
U_t	J/mol.K	total internal energy
V	m^3	Volume
V_c	m^3	clearance volume
V_d	m^3	displacement volume
v_{swirl}	m/s	swirl velocity
w	m/s	average cylinder gas velocity
Y		mass fraction of species k
Greek		
θ	degrees	angle of crank arm
ρ	kg/m^3	density
Ω	s^{-1}	rotation rate of crank arm
Subscripts		
i	initial	
k	kth species	

Turbocharger

Symbol	**Unit**	**Description**
A_{vgt}	m^2	effective flow area for the turbine
D	m	turbine blade diameter
d_c	m	compressor blade diameter
J	kg.m^2	inertia
M	-	Mach number
N_{tc}	RPM	turbocharger speed
P	Pa	pressure
P_2	Pa	turbine outlet pressure
P_c	W	Compressor Power
P_t	W	tubine power

T	K	temperature
U/C	-	blade-speed ratio
U_c	-	compressor blade tip speed
W	kg/s	mass flow rate
W_{2t}	kg/s	turbine exhaust flow rate
Greek		
γ	-	ratio of specific heats
η	-	efficiency
φ	kg/s	normalised compressor flow rate
χ_{vgt}	-	VGT pane position
ψ	-	dimensionless head parameter
ω_{tc}	rad/s	angular speed
$\dot{\omega}_{tc}$	rad/s^2	angular acceleartion of turbocharger
Subscripts		
01	stagnation condition at inlet	
02	stagnation condition at outlet	
c	compressor	
crit	critical	
in	inlet	
is	isentropic	
out	outlet	
t	turbine	

Exergy Analysis

Symbol	**Unit**	**Description**
$ex_{f\,out}$	J/mol	exergy transfer
$ex_{f\,in}$	J/mol	Exergy flow through the system
ex_{ch}	J/mol	Chemical exergy
ex_{ph}	J/mol	Physical exergy
ex_{k}	J/mol	Kinetic exergy

ex_p	J/mol	Potential exergy
h_{in}	J/mol	enthalpy in
h_{out}	J/mol	enthalpy out
$\dot{I}_{cv}$	W	Irreversibility
$\dot{n}$	mol/sec	molar flow rate
$\dot{W}_{cv}$	kW	Work
$\dot{Q}_{cv}$	kW	Heat transfer within the control volume
T_o	K	reference temperature
T_j	K	system temperature
$\dot{Q}_{react}$	W	Heat transfer due to reaction
$\dot{Q}_{surr}$	W	Heat transfer to surroundings
η_R		rational efficiency
$\sum \dot{E}x_{OUT}$	W	sum of exergies flowing out
$\sum \dot{E}x_{IN}$	W	sum of exergies flowing in

List of Figures

List of Tables

Chapter 1. Introduction

1.1. *Fuel cell discovery and development*

The fuel cell was invented by Sir William Grove in 1834 [1]. The actual development of a 5 kW fuel cell was successfully demonstrated by Francis Bacon of Essex, England only in 1959 [2]. Since then, fuel cell research encouraged by space exploration and interest in the hydrogen economy has progressed rapidly.

A fuel cell is an electrochemical device in which chemical energy from the fuel supplied to it is converted directly to electrical energy. A single fuel cell consists of an electrolyte between two electrodes. The electrodes assist in removing and supplying electrons from the fuel and air feeds [1]. The electrolyte conducts the electrons or ions. The transfer of the ions or electrons from one electrode to the other, results in generation of electricity. When multiple cells are interconnected to form a fuel cell stack, the voltages of individual cells are added to create a practical power source. A specified current is achieved by increasing the cross sectional area of the cell.

With depleting natural resources and rising pollution levels, the fuel cell has gained significant importance since the establishment of government initiatives such as the US Partnership for a New Generation of Vehicles (PNGV) [3] and the Fuel Cell and Hydrogen Joint Technology Initiative by the European Commission [4]. Fuel cell systems for both stationary and mobile power production have emerged as commercial products. Fuel cell performance and the application of new structures and materials have correspondingly advanced to support significant performance goals.

The first commercial implementation of fuel cells was by UTC fuel cell who supplied fuel cell power plants for the US space programs [5]. The fuel cells, which have attained

importance in the industry for mass production, are the Polymer Electrolyte Membrane Fuel Cell (PEMFC) and Solid Oxide Fuel Cell (SOFC). The PEMFC is a low temperature fuel cell operating around 100^{o}C and is advantageous for its compact structure and ease of starting. A major hindrance in implementing them in practical applications is the need for pure hydrogen as a fuel.

SOFCs are high temperature fuel cells operating in the range 600- 1000^{o}C. They can operate on various fuels, and have lower costs compared to the PEMFC systems [6]. The SOFCs have already been implemented in MW-class stationary power production systems. While research in fuel cell technology is proceeding rapidly, a cost effective penetration of the power and vehicle propulsion market has not yet been achieved.

1.2. *IC Engine development*

The IC engine is a fascinating and very successful device, with references in history dating as far as 1509: a compression-less IC engine proposed by Leonardo Da Vinci [7].

Progressive developments led to the landmark invention of Carl Otto and Rudolf Diesel. In the meantime, reciprocating engine technology and the rudiments of control were encouraged by the widespread adoption of the steam engine. Fuels tested in the IC engine changed from gun powder, coal gas, hydrogen, hydrogen sulphide, liquid fuels such as benzene, and eventually to petroleum refinery products [8]. In 1857, when commercial oil refining began in California, kerosene was dominantly used for fuelling IC Engines, which, in 1911 was superseded by gasoline[8]. Rudolf Diesel invented the diesel engine based on theories proposed by Léonard Sadi Carnot [7]. In 1897, the first successful diesel engine was developed which well exceeded the efficiencies of existing steam and gasoline engines [7].

The IC engine technology has received a substantial impetus from the adoption of exhaust emissions regulations from the mid 60s onwards. The use of novel injection techniques, variable valve timing, exhaust gas recirculation, variable geometry turbocharger have added to the capability of the engine while at the same time making it more complex to operate and expensive to manufacture. The IC Engine technology is deeply rooted in the transport sector all over the world making it extremely difficult to conceive of any progression to new forms of propulsion power except progressive ones.

1.3. *Trends in power generation in transport and energy sector*

Governments globally are issuing strict emission regulations, forcing manufacturers to explore alternative fuels and technologies for their production and use. In efforts to reduce the emissions and dependency on foreign sources of fuel, extensive research has expanded into renewable sources of energy, alternative and bio-fuels, hybrid technology. As projected in a European Commission report [9], on the basis of frozen-technology reference assumptions, the energy demand of transport sector was expected be at least one-third of the total energy demand by 2010. The emissions from the transport sector alone account for 30% of EU's carbon dioxide emissions [9].

The transport sector is mainly dependent on fuels such as gasoline and diesel. In order to supplant these conventional fuels, infrastructure for fuelling vehicles with alternative fuels will involve heavy costs and a delay for construction of new distribution equipment. Based on extrapolation of data in the reports produced for the European Commission in 2001, the cost effective implementation of alternative fuels in transport sector is expected to happen after 2010 [10]. Further, the methods to reduce greenhouse gas emissions in transport sector include:

- Weight reduction of the vehicle
- Engine performance improvement – Use of technology such as Variable Valve Lift and Timing (VVLT), novel injection techniques, EGR, lean combustion
- Friction and drag reduction
- Major engine changes – This involves the use of hybrid and/or electric powertrains, fuel cell vehicles, conversion of petrol-fuelled engine to diesel, etc.
- Alternative fuels

For stationary power generation systems, the options to reduce emissions considered include:

- Retirement of coal fired plants and use Natural Gas fired combined cycle plants
- Expansion of Renewable energy power plants
- Use of Combined Heat and Power (CHP) plants
- CO_2 removal and storage (sequestration)

The expansion of renewable energy power plants involves significant costs for their construction and commissioning. From 2001 onwards the European Commission has aimed to double the penetration of CHP systems by 2010 [11]. The present technology for

extracting carbon dioxide from various sources is expensive and requires further research into different techniques.

European Commission reports [9-11], clearly indicate significant reduction of emissions by the use of hybrid powertrains, fuel cell vehicles, alternative fuels and use of CHP systems though these techniques are not cost effective. The speculation that these technologies will dominate future energy demands has resulted in extensive research and development throughout the industrial and the academic sectors.

1.4. *Research Motivation*

The natural resources in the world are continually depleting. Technology dependence on supply of conventional fuel is at a risk of becoming obsolete in the coming decades. Combustion is a major means of energy conversion in power production applications. Combustion has low efficiencies of around 30-40 % and can be a significant source of emissions. The energy produced by combustion is thermal and mechanical energy, which is then converted to electrical energy; resulting in losses during conversion from one form of energy to another.

On the other hand, fuel cells, operating on the principles of electrochemistry directly convert energy from the fuel to electrical energy, and thereby promise higher efficiencies. Fuel cell power production can ensure very low levels of pollutant. However, fuel cell power is at a developing stage. Forming an analogy with batteries, fuel cell stacks can work alongside IC engines to offer high efficiency clean power at low load conditions, and to combine with the IC engine for higher load conditions.

A combination of combustion-produced power with electrochemical power production makes good use of the inherent characteristics of both types of power sources. With the current state of technology and infrastructure, it is a more viable option for power production in the near future.

While fuel cell technology is still developing, hybrid systems supplementing engine power production and/or helping reduced emissions have emerged. Such hybrid vehicles usually with two power producing components can potentially lower emissions and fuel consumption, and improve the overall efficiency of the system.

The system proposed in this thesis is a step towards developing an alternative technology system, which can be implemented in the near future, within the current state of technology and infrastructure. The system bridges the time gap between current power production systems based in IC engine and the dawn of cost effective production of fuel cell vehicles/alternative fuel systems.

1.5. *Thesis Structure*

The structure of the thesis is as follows. The hybrid system and its attributes are described in Chapter 2. A literature review focussing on the key components of the system, various analyses for hybrid systems and control development are discussed in Chapter 3. The component modelling in Chapter 4 has four parts, namely the modelling of the SOFC, reformer, engine and the turbine and compressors. The evaluation of the steady state behaviour of the hybrid system and investigation of optimum range of operation for the fuel cell and the diesel engine are discussed in Chapter 5. An exergy analysis for the system is discussed in detail in Chapter 6. The integration of control-oriented models of the system components and examination of the dynamics of the system are described in Chapter 7. The control development is discussed in Chapter 8, Chapter 9, and Chapter 11. Chapter 8 discusses the development of a feedback control system while Chapter 9 discusses the development of a model predictive controller. Chapter 10 summarises the findings in the thesis and draws conclusions from this work. Further control development is discussed as a part of future work in Chapter 11.

1.6. *Scope of work*

The first part of the work in this thesis, presents the modelling of the system components to provide a better understanding of the component behaviour. The models developed are from experimentally verified sources of literature. The component modelling allows determination of the individual control issues and constraints of operation for efficient operation of each component.

A steady state analysis based on the first law of thermodynamics for the system reveals the need for system operation in an optimum range. An exergy analysis on the system examines the hybrid system from a hypothetical reversible system to a practical system. The improvement of rational efficiency of the system by waste heat recovery is discussed. This analysis is also used to support the development of a novel control strategy.

Further, the development of control-oriented model of the system is studied, which identifies the control issues and constraints for the whole system. The necessary changes in operating points, for each component, due to the system configuration are discussed and a possible control strategy is discussed. Controllers based on feedback control and model predictive control theories are designed with the aim of supplying the load on the system within operating constraints. The controller designs are linear and hence valid for a small range of values around a selected operating point. The need for a supervisory controller for power management along with a development strategy is discussed as a part of future work.

A steady state exergy analysis is performed on the system at certain conditions to identify the use of total available energy in the system. This analysis provides an insight into thermal management of the system to improve exergetic efficiency. Further, a strategy to develop a control system based on exergy analysis is discussed. The strategy is based on the principles of finite-time thermodynamics.

1.7. *Research proposition*

The main research objectives of this thesis are:

- The investigation of a novel concept of a hybrid SOFC - diesel engine power plant.
- To develop an understanding of each system component and the hybrid system interactions by means of modelling.
- To investigate the feasibility and performance of the novel hybrid SOFC-diesel engine system for automotive applications by means of system modelling.
- To examine system behaviour and extent of energy usage within the system by conducting analyses based on first and second law of thermodynamics.
- To study and develop control oriented models, and select control parameters for system components and integrated system.
- To develop potential for a high efficiency system through optimum usage of system components by means of an appropriate control strategy.
- To develop controls to stabilise the system
- To investigate use of hierarchical and advanced control methodologies to manage the transient operation of the system

This thesis presents research contributions on the following:

- The understanding of the modelling requirements of a hybrid energy system,
- Issues in modelling and developing controls for complex multi-component systems, in which single-component system solutions are ineffective.
- A strategy for investigating a novel power plant by means of modelling, thermodynamic analyses, which together contribute towards control development.
- The use of an exergy analysis to deduce the system configuration and the investigation of systems from complete reversibility to practical systems.
- A step towards developing an exergy based control approach, contributing to the knowledge in the field of control development for hybrid systems.
- A contribution to the development of greener vehicles.

Chapter 2. The System and its Attributes

2.1. *Background*

The Solid Oxide Fuel Cell being a high temperature fuel cell has the ability to internally reform various fuels and produce electricity. The fuel cell is normally operated up to 95% utilisation factor [6] to avoid fuel starvation. When the fuel utilisation is lower, a considerable amount of fuel is exhausted from the anode. Fuel cell hybrid systems use this excess fuel in a combustor or employ techniques to re-circulate any excess fuel back to the fuel cell.

This fuel can, for example be used to supplement the main fuel of an internal combustion engine. The exhausts from cathode of the fuel cell contain oxygen-depleted air, which can be as a diluent to promote a lower temperature combustion.

Use of hydrogen in fuel cells or combustion devices can produce higher amounts of power with the reaction product being pure water. Burning pure hydrogen in an internal combustion engine poses significant problems due its low octane rating and consequently its tendency to promote knock. Besides, hydrogen is not naturally available and needs to be produced from higher hydrocarbons or hydrides. For use in mobile systems, hydrogen is stored in tanks in compressed or liquid form. The cost of production and transportation of hydrogen in liquid or pressurised gaseous form is significant. Hydrogen, when combined with air can form an extremely explosive mixture, hence involves safety issues for mobile systems. On-board storage of hydrogen involves packaging issues within the vehicle. Hydrogen refuelling facilities throughout the world are limited, but they are gradually developing. This necessitates on-board production of hydrogen by reforming of hydrocarbons.

A study conducted by Mathur, Das and Patro [12-14] shows that substituting part of the diesel in a diesel powered engine by hydrogen resulted in reduction of pollutants and

improved thermal efficiency. To reduce the tendency to knock, diluents such as helium and nitrogen were added to the combustion mixture. Water injection along with nitrogen dilution lowered combustion temperatures resulting in NO_x reductions. Nitrogen as a diluent gave the best engine performance.

With the fuel cell as a source for auxiliary fuel and diluent for the engine, a fuel cell and diesel engine hybrid system is proposed in Figure 2.1. The engine acts as the major power-producing component, while the fuel cell supplies a small portion of the load on the system. This system is suitable for transport as well as stationary power production applications. Owing to the physical size and weight of the fuel cell, in the transport sector, this system is particularly suitable for a bus or a delivery truck cycle rather than small passenger cars. The system can also be used for stationary combined heat and power production plant.

The Solid Oxide Fuel Cell (SOFC) is best suited for this system as compared to the more widely used Polymer Electrolyte Membrane Fuel Cells (PEMFC). PEMFCs are very sensitive to carbon monoxide in the fuel stream and hence, the fuel processing requirements are strict. PEMFCs are also very temperature sensitive, operating below 100 ^{o}C. The system would require special thermal management measures in order to make use of PEMFC technology. The membrane requires that its moisture content is maintained at all times [6], resulting in a requirement for water management. SOFCs on the other hand can reform carbon monoxide as well as various other fuels such as methane, iso-octane, alcohols such as methanol and methanoic (formic) acid [15]. Hence, the SOFC is fuel flexible, allowing the use of various fuels for the system.

2.2. *System operation*

The system, shown schematically in Figure 2.1, consists of an internal combustion engine and a solid oxide fuel cell stack producing power together to supply the load on the system. A methanol steam reformer feeds processed fuel consisting mainly of hydrogen, carbon dioxide, water vapour, carbon monoxide and methanol [16] to the fuel cell. Methanol steam reforming is more convenient to model than diesel reforming due to large availability of data in literature. The engine is supplied with diesel as the main fuel, while the excess fuel from the fuel cell anode is supplementary fuel. The exhausts from the fuel

cell serve to condition the air-fuel mixture in the engine cylinder, and are expected to improve combustion and lower emissions.

The exhaust from the fuel cell anode will contain mainly hydrogen, carbon monoxide, carbon dioxide and water vapour. Addition of trace amounts of hydrogen in a diesel engine has proven to be beneficial to improve engine thermal efficiency and performance [12]. Part-substitution of diesel by hydrogen in the engine also reduces specific fuel consumption of diesel fuel [17].

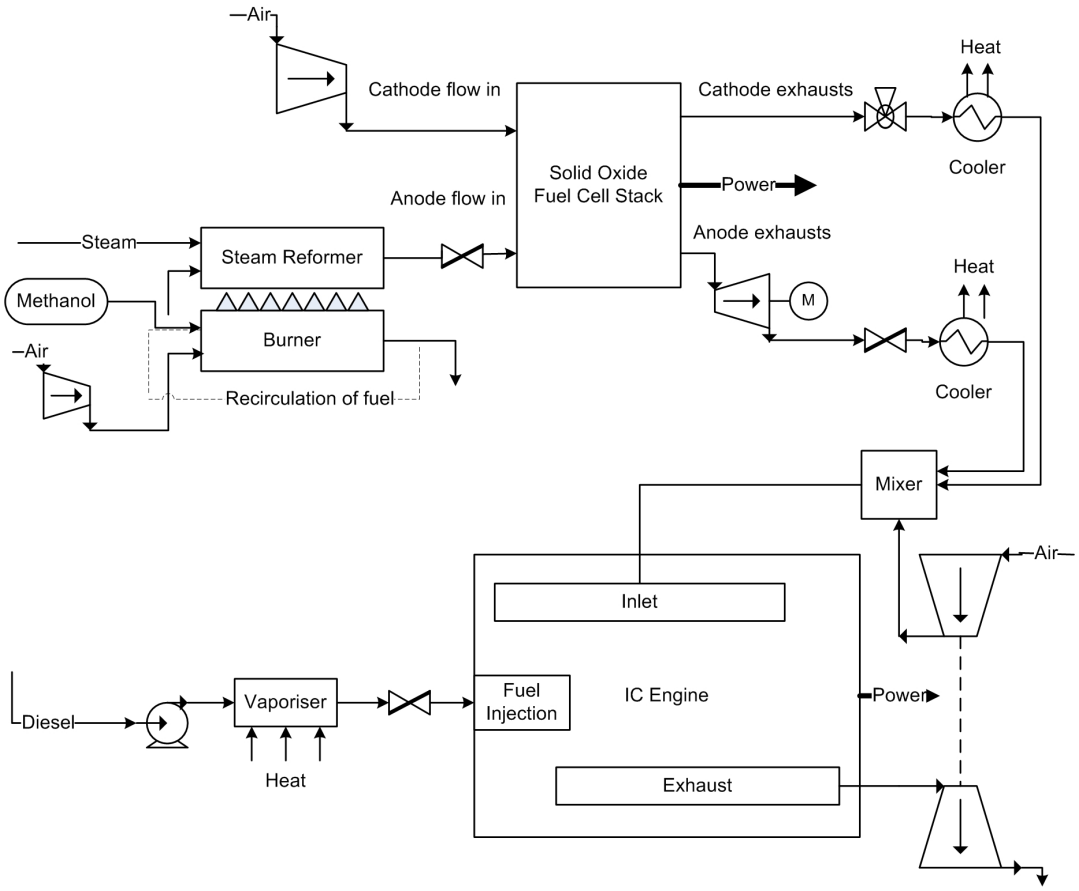

Figure 2.1: System Schematic

In conventional diesel engines, a fraction of the burnt gas is cooled and fed back into the engine to reduce NOx emissions. This system is called exhaust gas recirculation (EGR). This re-circulated gas consists of an inert mixture. The oxygen-depleted air from the cathode consisting of higher percentage of nitrogen, along with carbon dioxide and water vapour from the anode exhausts forms a mixture similar to the composition of EGR used in

IC engines. These warm effluents from the fuel cell can function as a source of an inert mixture hence serving as a form of external EGR.

The load sharing by the fuel cell and the engine is handled such that the engine handles the majority of the transient loads while the fuel cell supplies power at a base load. The use of a high temperature fuel cell in this system facilitates the use of this system as a combined heat and power plant. The heat rejection from the fuel cell and engine exhausts is significant and can be used for providing thermal energy to auxiliary system components requiring thermal energy transfers.

The feasibility and control development for an internal combustion engine system, where a fuel cell assists in supplying part load on the system and conditions the engine fuel is examined in this thesis.

2.3. *System Interconnection and its effects*

The components of the system in Figure 2.1 interact with each other through three main paths,

1. input and exhaust flows of the components,
2. power requirement and delivery of each component,
3. heat flows through the components.

The complex interaction between the components identifies the need for an appropriate control system.

2.3.1. Flow management

The successful operation of the system is mainly dependent on the proper control of flows in the system. Flow control is required for

- Fuel feeds for the reformer and burner
- Steam flow into the reformer
- Air flow into the burner
- Air flow into the fuel cell cathode
- Primary fuel flow into the IC engine
- Air flow into the IC Engine
- Fuel cell cathode exhausts into the IC Engine

The fuel flow required by the reformer is defined by the fuel requirement of the fuel cell. The composition of the reformate will also determine the extent of power production by the fuel cell and the unused fuel exiting from the fuel cell. The fuel flow into the diesel engine is regulated depending on the flow of excess fuel from the fuel cell and the power demand from the engine.

2.3.2. Power management and load distribution

The response of the system and that of the fuel cell and diesel engine at various load conditions must be examined to ensure that the ability to accept load conforms to the industry needs. An important focus of the investigation is the dependence of engine performance improvement on the fuel utilisation of the fuel cell, which potentially creates a conflict. With low fuel utilisation in the fuel cell, the engine receives a correspondingly higher amount of supplementary fuel, which improves its performance. At the same time, the lower fuel utilisation of the fuel cell causes its efficiency to drop. In order to ensure that the overall performance of the system is logical, optimal operating conditions must be determined for the fuel cell and engine. This is an important focus of the research. All hybrid systems have optimum operating conditions and an associated set of methods for finding the optimum. This proposed hybrid system is no exception and the research objectives of this work include an intention to generalise the results to all SOFC-diesel engine hybrid power systems.

The load sharing and power management in the system will depend on the type of application. For example, in a stationary power generation application, the fuel cell stack will supply a base load, which can be determined by the load duration curve of the system. For transport applications such as a bus or a delivery truck cycle, the base load can be determined from the likely duty cycle of the system.

2.3.3. Thermal management

Thermal management is necessary in system components to ensure proper operation and efficient utilisation of rejected heat. The temperature management of the system involves maintaining proper operating temperature for the reformer and the fuel cell. The reaction kinetics are greatly affected by variations in temperature. Excessive temperatures can affect the materials used in the fuel cell and the reformer catalyst. The system requires

heating and cooling at various stages to maintain temperatures for proper operation of components. A thermal analysis will show how heat fluxes can be arranged in a way that reinforces the favourable thermal efficiency of the whole system.

Chapter 3. Literature Review

3.1. *Fuel Cell Systems*

Fuel cell systems for automotive applications have received continued interest due to their ability to operate at near-zero emissions. Hydrogen fuelled fuel cell systems are of particular interest in view of the forthcoming regulations on carbon dioxide emission restrictions.

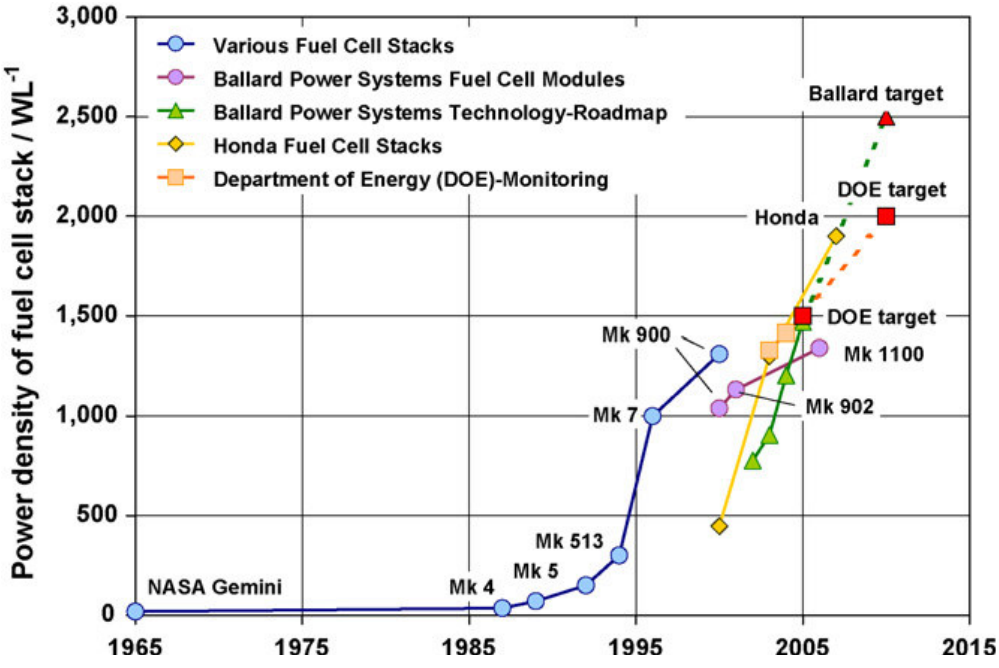

Figure 3.1 – Historic development of volumetric power density of PEM fuel cell stacks including various targets set for the future [18]

The first application of the PEM fuel cell stacks was for the NASA Gemini programme where the volumetric power density was $20Wl^{-1}$ [18]. As shown in Figure 3.1, Ballard Power Systems have achieved a volumetric power density of 1340 Wl^{-1} and further targeted a volumetric power density of $2500Wl^{-1}$. The significant improvement in fuel cell

power densities by various manufacturers as depicted in Figure 3.1 shows the results of increasing research and development efforts on fuel cell systems.
With the initial projects of fuel cell systems already implemented commercially (CUTE), the need to address issues such as lower production costs, improved materials and durability and performance of fuel cell systems has been recognised. The initial applications of fuel cell systems in the transport sector were focussed mainly on buses (CUTE) and now various automotive manufacturers such as Honda, Toyota and Volkswagen are launching the fuel cell vehicles.

The use of solid oxide fuel cell (SOFC) stacks for automotive applications has received less coverage in research and development when compared to the PEM fuel cells [19]. A search for 'SOFC' on the Society of Automotive Engineers' website resulted in 83 hits while that for 'PEM' resulted in 523 hits. Examination of SOFC hybrids for automotive applications and issues are discussed in a study conducted together by Rolls-Royce and Delphi Corporation [19]. The paper reports that issues that need to be resolved before implementing SOFC hybrids in the automobile industry were more tractable than those required for the PEM fuel cell when considering mass production. Delphi Automotive Systems and BMW GmbH have jointly developed an SOFC Auxiliary Power Unit (APU) to supply electric energy to the air conditioning system in an automobile [20]. This APU system is independent of the automobile engine and uses the same fuel as the vehicle's propulsion engine. The use of an SOFC APU can prove to be very beneficial for heavy-duty trucks during the idle conditions. In order to provide power to the sleeper cabin of the truck during the driver's rest period, the main truck engine is run at idle conditions. The use of the engine truck to supply a comparatively small power requirement is highly inefficient and highly polluting [21]. The fuel saving and pollutant reduction by use of SOFC APU has been studied extensively in the USA [21, 22]. The overall fuel consumption for trucks idling for more than 10 hours a day, by the use of an SOFC APU, was reduced by about 5-12 %.

Toyota Motor Corporation has developed a fuel cell hybrid bus. The system consists of a PEM fuel cell stack, secondary batteries and a traction motor [23]. The system simulation results showed that the vehicle efficiency of this bus is 66% better than that of the IC Engine bus.

A paper by Thijssen et al [24] discussed the advantages of ICE/FC hybrids as compared to the conventional ICE –battery hybrids. Simulations were done for an IC Engine – fuel cell APU, where the two modes of operation were modelled. In one mode, the fuel cell provides all power with the engine stopped while in the second mode the IC-engine provides all the power with the fuel cell turned off. The high power levels, decided by a 10 kW switching threshold power, were handled by the IC Engine. Over the total drive cycle the fuel cell was engaged for 76% of the city cycle time. The results clearly indicated a potential to improve fuel consumption and reduce emissions for Fuel-Cell IC engine. The authors have also highlighted a series of technical problems such as rapid system start up and low emission over a drive cycle that require to be overcome before such systems are practical.

Daimler Chrysler AG has proposed a system with a reformer and a shift reactor supplying hydrogen as a supplementary fuel to an IC engine during its cold start phase [25]. When the shift reactors warm up, the hydrogen is fed to a PEM fuel cell. The exhaust gas from the anode of the fuel cell along with the primary fuel is fed to the IC engine to reduce regulated emissions during start up. The fuel cell also provides power to the electrical system of the vehicle. A patent [26] by Audi AG described an IC engine and fuel cell wherein the fuel cell supplies exhaust gas to the engine to reduce NOx emissions. The fuel cell in this patent can be either the PEMFC or the SOFC, which in addition to supplying exhaust gas to the engine, also functions as an APU.

There is extensive ongoing research in combined SOFC – Gas Turbine systems for stationary power generation. The exhaust gas from the fuel cell is used to drive an expander, which is coupled to an electrical generator. Analysis of the system performance at part-load along with design performance is investigated by Costamagna, Magistri and Massardo [27]. Their results show that over 60% efficiency can be achieved at design point, while at part-load the efficiency is always above 50%.

Another study [28] showed the environmental benefit of using fuel cells for transport and stationary power generation. Buses fuelled with diesel and CNG, SPFC and PAFC fuelled by local reformers at bus depots and battery buses were compared for total system emissions. The results indicated lowest emissions by FC buses. The fuel consumption for FC buses reduced by 20-26 % as compared to diesel buses. In stationary CHP generation,

typically the SOFC and the phosphoric acid fuel cells (PAFC) are considered. These fuel cell systems, SOFC CHP, PAFC CHP and SOFC-GT for stationary power generation are mainly compared with the diesel fuelled and natural gas fuelled engines [28]. The advantages of the fuel cell systems are visible in better efficiencies and lower emissions.

Most literature sources discussed the obvious advantages of fuel cells over conventionally used power generation schemes in transport as well as stationary power applications. Fuel cell systems are still developing and require expensive fuelling infrastructure for large-scale implementation. There are many issues with fuel cell systems, which need to be addressed, such as weight/size of the fuel cells, manufacturing costs and sources of fuel. Hybridisation allows the use of pre-existing technology with fuel cells, which are comparatively smaller and more feasible than those used in pure fuel cell systems. The use of fuel cell hybrid systems requires development of novel control techniques.

In the transport industry, efforts have been made to reduce the emissions and fuel consumption with the use of hybrid fuel cell systems. These more commonly include PEM fuel cell-battery hybrids. The possibility of using SOFC-IC engine hybrids in which the fuel cell functions beyond an APU, supporting the main load on the system along with the engine has been discussed in limited sources of literature [19]. As far as the patent literature goes, such SOFC-IC engine hybrids are discussed, but further analysis and development is not reflected in journal publications or other literature reports.

For stationary power generation, the SOFC has already been identified as a potential benefactor. The SOFC-GT systems developed by Siemens Power Generation and Rolls Royce and its partners are receiving a lot of attention. SOFC CHP systems are also being considered for power generation.

The development challenges of weight and cost reduction are yet to be met satisfactorily and hence the successful applications are only expected in future. Existing technology cannot be easily replaced because of its cost effectiveness thus demanding development of systems, which will enable the transition from current technology to future advanced power plants.

3.2. *SOFC*

The solid oxide fuel cell (SOFC) is a high temperature fuel cell, which has been studied in detail with respect to dynamic modelling, prevention of carbon formation, materials, internal reforming and fuel flexibility.

The fuel flexibility of SOFC is discussed in several reports [15, 29, 30]. The effect of various alcohols, hydrocarbon fuels, alkanes and organic acids were tested as fuel sources in some studies [15, 29]. Fukunaga et al [31] investigated the relationship between overpotential and triple-phase boundary of the SOFC. The triple-phase boundary (TPB) in composites is the active site for electrochemical reactions where electrolyte, gas and electrically connected catalyst regions are in contact. The results indicate that the overpotential decreases with increase in length of TPB but an excessive length does not become effective for reduction of overpotential. Overpotential is the difference between the ideal voltage and actual voltage obtained from a fuel cell. This paper discusses the relationship between material limitations and the voltage output of the SOFC. A paper by Deng and Petric [32] discussed the relationship between the length of the TPB versus the grain size, pore size and porosity on the basis of a geometric model.

Petruzzi et al [33] have developed a detailed model for a SOFC APU for transport applications to account for all operating conditions. The model allows evaluation of detailed thermodynamic and electrochemical effects of the stack. The modelling of single cell SOFC is studied by Ota et al and Xue et al [34, 35]. Xue et al [35] have demonstrated a dynamic single tube SOFC model based on the control volume approach with thermodynamic and electrochemical effects. The model is used to investigate the effect of non-uniform distribution of the Nernst potential along the length of the cell. Ota et al[34] studied the micro-tubular SOFC using an object based approach. In the object-based approach, each component model is treated as an object with an explicit interface. The model investigated the current, gas and temperature distribution in the fuel cell and compared the electrical and temperature transient response of a standard cell and a micro-tube cell. An SOFC that includes dynamic effects is developed by Padulles et al [36]. This model [36] has been used for a power system simulation (PSS) and a commercial software package has been further used to develop a control oriented model for SOFC [37, 38].

A polarisation model proposed by Chan et al [39] for the SOFC includes a Butler-Volmer equation for activation polarisation and ordinary and Knudsen diffusion considerations for the concentration polarisation as compared to the commonly used simplified versions of these equations. The voltage drop of the fuel cell is expressed in terms of irreversibility by activation, ohmic and concentration polarisation. This model allows examination of the sensitivity of the cell voltage to anode, electrolyte and cathode thickness. The results show that the sensitivity of cell voltage to anode thickness is lowest and hence the anode-supported cell is preferred over the cathode or electrolyte supported structures. The internal reforming capability of SOFC is investigated by various authors [40-43]. Nagata et al [42] proposed a tubular internal reformer which is inserted into the tubular SOFC stack. This configuration allows achievement of a homogenous temperature distribution. The exhausts from the SOFC are burned in a post-combustor, which provides heat for the pre-reformer and supply air. The simulation results from the model revealed that the exhaust temperature of the SOFC was greatly affected by parameters such as the catalyst density, reforming rate, inlet gas and air temperature, and oxidant re-circulation, while the efficiency of the fuel cell remained unaffected. The effects of internal reforming of methane and of anode gas recirculation in SOFC was studied experimentally by Peters et al [40]. Aguiar et al [41] have developed a steady state model of an indirect internal reformer and the SOFC. The model demonstrates an undesirable cooling effect for the SOFC close to the entrance of the reformer. The effects of catalyst activity, fuel inlet temperature, current density, pressure, co-current and counter-current flow are discussed.

The above papers provided an insight into the modelling, performances and issues associated with SOFCs with internal reforming. The hybrid system discussed in Chapter 2 includes an external reformer, which can process higher hydrocarbons such as diesel. The reformate containing hydrogen and lower hydrocarbons can then be further used in the SOFC.

The dynamic models described in literature allow in-depth understanding of the fuel and temperature distribution and the effects on overpotentials in the SOFC. The development of a control system requires simplified models that capture the transient responses, which will be further demonstrated in Chapter 7 (System Integration).

3.3. *Fuel Pre-processing*

Fuel processing, as defined by Kolb [44], is the conversion of hydrocarbons, alcohol fuels and other alternative energy carriers into hydrogen containing gas mixtures. This hydrogen containing gas mixture is called as the 'reformate'. Reforming, which is commonly used in large scale industrial applications, is the conversion process involved in fuel processing [44]. For fuel cell applications, the reforming process is scaled-down to provide a hydrogen containing mixture. Depending on the type of fuel cell, the 'reformate' is further processed to remove the impurities such as sulphur, carbon monoxide etc.

A review paper on fuel processing for fuel cells [45] discusses the types of fuel cell and the associated fuel processing for low temperature and high temperature fuel cells. The paper highlights the challenges and opportunities for fuel processing which include the need for improving energy efficiency, size reduction and tolerance to carbon monoxide and sulphur in the reformate [45]. The three types of commonly used reformers include the steam reformer, partial oxidation reformer and autothermal reformer. An autothermal reformer combines the endothermic steam reforming with exothermic catalytic partial oxidation processes.

A significant issue with fuel processors is the slow dynamic performance, which can hamper performance in the automotive systems. Studies on reformers for automotive applications include studies by Goebel et al [46], Varesano et al [16] and Peters et al [47]. The fuel processing system studied by Goebel et al [46] consists of an autothermal reformer (ATR), a water gas shift reactor and a preferential oxidation reactor. Water is injected directly into the burner exhaust, which highlights the importance of steam for the reforming process. This also improved the start-up performance with 30% of the power obtained in 20 seconds. Peters et al [47] have studied a methanol steam reformer for a fuel cell powered passenger car with a focus on the dynamics and long term stability of the system. This experimental study, conducted with fixed bed tube reactors with different catalyst loadings, determined that methanol conversion was a function of the catalyst bed length. The results showed that catalyst utilisation was high at the beginning of the catalyst bed and reduced towards the end of the bed. The study also showed that CO formation is proportional to methanol conversion. The study recommended the amount of catalyst required for using the reformer for mobile PEMFC applications.

The experimental work by Goebel et al [46] and Peters et al [47] discussed how steam and catalyst degradation, respectively, affect the performance of a reformer. These factors highlight the need for a controller to prevent catalyst deactivation and to regulate steam proportion in the reformer. Such factors will also determine the limits on the reformer operation to ensure long term functioning of the reformer.

The detailed modelling for a methanol steam reformer for automotive applications is studied by Varesano et al [16]. The chemical kinetic models of the reactions involved in the reformer and the burner are presented which are useful in optimisation of the reactor design to maximise methanol conversion and maintain the operating temperature. The reformer is modelled as a pseudo-homogeneous reactor and the burner as a heterogeneous reactor with solid and gas phases. The results allow the development of an operability map with the optimized design to give up to 97% methanol conversion and maximum temperature below the specified limits. The reformer model discussed in this thesis is primarily based on the study by Varesano et al [16]. The focus for fuel processor modelling in the thesis is mainly to study the dynamics of the reformer and to determine operating constraints for control design.

A thorough analysis of the control requirement for an ethanol fuel processor is done by Biset et al [48]. The control objectives were supplying the necessary hydrogen to the fuel cell during load changes, preventing the ethanol steam reformer from overheating and maintaining high overall system efficiency. Two control structures were proposed and subjected to sensitivity evaluation for the most critical perturbations in the system. This paper suggests a methodology that can be used to examine alternate control strategies.

Görgün et al [49] and Pukrushpan et al [50] have discussed a lumped model of a partial oxidation reformer. Görgün et al [49] has described a design of observers for the fuel processing reactors system with temperature and pressure measurements.

The lumped models discussed [49, 50] do not account for the temperature variation along the length of the reactor, which determines catalyst degradation, extent of fuel conversion and the long term stability of the catalyst.

Lin et al [51] have described a dynamic model of an autothermal reformer (ATR). The rate equations and kinetic parameters were developed from the regression of data obtained experimentally. The control objective being a response to the hydrogen demand, two control structures, i.e. on-supply and on-demand control were suggested. The on demand structure provided a faster response to changes in the hydrogen demand.

Hu et al [52] described a feedback plus feed-forward controller for regulating the temperature of an ATR. The feedback controller did not perform well during large load changes, while the feed-forward controller was sensitive to the disturbances. An advanced controller such as the model predictive controller has been suggested for improved performance.

The reformer modelling presented in this thesis is a detailed distributed model, in which operational issues are evaluated and control requirement is defined.

3.4. *IC Engine*

The hybrid system discussed in this thesis, as discussed in Chapter 2 (The System and its Attributes) involves a diesel engine supplied with hydrogen, as auxiliary fuel and oxygen depleted air from the fuel cell as external EGR. The study of reformer gas composition on HCCI engine combustion for n-heptane, iso-octane and natural gas was conducted by Hossieini et al [53]. The effect of reformer gas in different compositions of hydrogen and carbon monoxide were examined experimentally and by means of a combustion model. Reformer gas was found to be effective in controlling the combustion timing of HCCI combustion, in particular for fuels such as n-heptane which undergo a multiple-stage combustion [53]. Studies by Mathur et al [12-14] have discussed part substitution of diesel in the engine with hydrogen and its impact on the engine thermal efficiency and emissions. The effects of diluents such as water and nitrogen have also been discussed by these authors. Ladommatos et al [54-58] have studied the dilution, thermal and chemical effects of EGR on diesel engine emissions. The effects of carbon dioxide, water vapour, reduction of inlet oxygen and carbon dioxide and water vapour together, are individually studied these paper [54-58]. The results from these papers [12-14, 54-58] are discussed in detail in section 4.3 (Component Modelling-IC Engine) in context with the hybrid system and results from combustion model for the engine. A number of studies have investigated the effects of EGR, EGR composition, dual fuel combustion with hydrogen or reformer gas,

which are all relevant to the method proposed for operating the IC engine described in the hybrid system in this thesis. The main barrier in practically implementing dual fuel combustion is the source of the second fuel. However, the hybrid system proposed in the thesis can potentially operate on a single fuel, allowing a variation of hydrogen fraction and external EGR composition regulation by controlling the loads on the reformer and fuel cell.

3.5. *Control of Fuel Cell Systems*

Fuel cell systems involve a number of operating parameters for efficient performance. The typical operating requirements include prevention of air and fuel starvation, prevention of carbon deposition, maintaining voltage output, maintaining operating temperature and avoiding thermal stresses. A number of studies have been conducted for air and fuel starvation of fuel cell system [38, 59-65]. These studies emphasise that regulation of air and fuel for the fuel cell system are the most important factors in a fuel cell system for achieving good performance.

Mueller et al [59] described a novel controller for rapid load following of solid oxide fuel cells. Decentralised feedback controllers are developed to regulate fuel depletion and for the fuel cell thermal management. To prevent hydrogen depletion in the fuel cell, a current-based fuel controller along with a power demand-based feedforward fuel controller is employed as a controller. This strategy is novel since most sources of literature use only current-based controller for prevention of hydrogen depletion. The results show the load following capabilities of SOFCs.

The paper by Pukrushpan et al [60] described the dynamic modelling and analysis of a fuel cell system. The analysis in [60] provides the basis for the control development described in another study by Pukrushpan et al [61]. The book presents detailed modelling of a PEM fuel cell system including the fuel processor and peripheral components. A feedback controller designed for the fuel cell prevents oxygen starvation while that designed for the fuel processor prevents hydrogen starvation in the fuel cell, protects the partial oxidation reformer from overheating and ensures high system efficiency. This work presents a methodology of control-oriented modelling and control design for fuel cell systems.

On similar lines, Bao et al [64, 65] described a control oriented model for a PEM fuel cell system and compared different controllers for the system. Bao et al [64] have elaborated on three different control configurations namely, a decentralised PI control, a multivariable state feedback control and a nonlinear adaptive control for air and fuel path regulation. The results showed that the multivariable controller provides improved transient response as well as disturbance rejection capability as compared to the decentralized PI controller [64]. Vahidi et al [62] have proposed a hybrid fuel cell system in which a small auxiliary power source allows improved control over oxygen starvation during rapid current transitions. A model predictive controller manages the current distribution between the fuel cell and the auxiliary power source. Further study by Vahidi et al [63] describes a model predictive controller for current management for a hybrid system in which an ultracapacitor bank supplements the fuel cell operation during transients. The objectives of the controller are to regulate the excess oxygen ratio of the fuel cell and the state of charge of the ultracapacitor [63]. Wang et al [38] presents a data drive predictive control for the solid oxide fuel cell. The subspace identification method is used to obtain the necessary input and output data for the fuel cell. The study is restricted to linear predictive control theory.

The above studies for control of fuel cell systems show a similar trend of initially designing simple decentralized controllers and then further designing advanced multivariable controllers, which give improved responses. It was noted that the model predictive control theory is widely used for fuel cell system due to the number of operating constraints in the system and improved transient responses as compared to the feedback control systems. This thesis also discusses the development and issues of decentralized PID controllers for the system and then further describes a model predictive controller. In case of hybrid fuel cell systems, the management of power between components is critical for optimum fuel consumption. Supervisory controllers for power management, based on the Equivalent Consumption Minimization Strategy (ECMS), are described in [66-69]. The ECMS is a discretized method in which the power distribution is optimised at each time step such that the overall fuel consumption is minimised. The ECMS computes the power split between the two power producing components based on quasi-static maps, hence is suitable for a hierarchical control structure. The ECMS strategy requires knowledge of the energy required at the wheels, while T-ECMS is another strategy, which involves online optimisation based on information provided by an on-board telemetry system. The ECMS strategy is proposed as future work in this thesis for the hybrid fuel cell and engine system.

3.6. *Exergy Analysis*

Exergy analysis has been studied extensively in the literature for chemical processes. In transport and stationary power applications, the evaluation of heat recovery and work from the exhaust gas streams can be done with the help of exergy analysis. Exergy is the maximum work, which can be obtained from a given form of energy using the environmental parameters as the reference state [70]. Exergy analysis for a complete system, rather than an individual component, allows evaluation of the exergy losses at each stage in the system. This analysis assesses the quality of fuel usage in the system and can help in determining process or component design flaws.

Exergy analysis for fuel cell systems have been studied by various authors [71-80]. These studies form a pre-requisite to optimising system components and operating conditions as well as thermo-economics of the system. A study of exergy analysis for an internal reforming SOFC – GT system indicated the highest irreversibilities in the internal reforming SOFC (IRSOFC) [79]. Based on these results, the electrical efficiency of the system at appropriate design and operating conditions is 60% with an improvement to 70% by heat recovery [79]. A similar study done for a PEM fuel cell system for transport applications also indicated highest destruction of exergy in the fuel cell stack [81]. This was because the fuel cell was the site of electrochemical reaction. A comparative exergy analysis of methane fuelled SOFC system with 600% theoretical air and stoichiometric air revealed improved first and second law efficiencies and reduced fuel cell irreversibilities for the latter case [80]. A fuel cell micro-power plant was modelled and analysed for the first and second law efficiencies at operating conditions and geometric parameters [78]. The exergetic efficiency of the whole system was 19.4 %. Comparison of results of exergy analysis of hydrogen polymer electrolyte fuel cell (PEFC) micro power plant and DMFC micro-power plant showed that the PEFC system had a higher exergetic efficiency [82]. In the above analyses, the authors have used exergy analysis to determine operating conditions and physical parameters of the system in order to improve system efficiency.

The transient availability analysis of a turbocharged diesel engine was studied by Rakopoulos et al [83]. The availability analysis, performed on an experimentally validated engine model identifies the potential for work recovery during the transient event. Besides the high combustion irreversibilities, those in the exhaust manifold were significantly

higher due to turbocharging. An interesting availability study on an energy recovery system by Stobart [84] follows an approach considering a system with 100% rational efficiency to the actual efficiency by imposing constraints step by step.

The work discussed for fuel cell systems by Barclay in [75, 85] highlights the importance of exergetic efficiency and that the methods used for calculating efficiency for CHP systems are irrationally based on the Carnot limits. Further, the maximum work potential and exergy calculation for hydrogen and methane are discussed using the concepts of chemical equilibrium, equilibrium constants and ideal reversible systems. Similarly the idealised fuel cell with perm-selective membranes, circulators (Van Hoff's box) is discussed by Haywood [86] and Kotas [70]. Perm-selective membranes are idealised components, which allow only a specified species to enter a system, without mixing with the surrounding environment. Circulators are idealised compressors or expanders with extremely large pressure ratios. The work discussed in Chapter 6, is based on this concept. The optimisation and exergy analysis of a simplified gas-turbine power plant by chemical recovery was studied by Alves and Nebra [87].

Literature sources show that exergy analysis studies have been conducted mainly to compare with first law efficiency values, identify maximum irreversibilities in a system or potential for work recovery, component design optimisation, system operating condition optimisation and thermo-economics. Exergy analysis studies with hybrid power plants have been limited in number. With the growing importance of CHP systems and other heat recovery applications in various systems, the exergy analysis provides a reliable means to explore the complete work potential of the system.

3.7. *Availability and Finite-time Thermodynamics*

The concept of using exergy analysis for developing control systems is novel. Such work combining concepts of thermodynamic with control theory is reported by Robinett and Wilson [88-90]. The novel control design combines exergy and entropy, Hamiltonian system, Lyapunov's direct method and Lyapunov's optimal analysis, electric AC power concepts and power flow analysis. The methodology was applied to nonlinear systems and control performance was examined using exergy dissipation and generation terms. The methodology also gave necessary and sufficient conditions for stability of these systems.

Alonso et al [91] have studied the design of a robust control methodology based on the concepts of passivity and irreversible thermodynamic. Ydstie [92] has studied passivity based control via the second law of thermodynamics for distributed chemical processes. A new storage function connecting passivity based control and second law is proposed and the concept of minimum entropy production is discussed [92].

The principles of finite-time thermodynamics are also discussed by Salamon et al [93]. The principles have three categories namely, principles of problem simplification, those related to minimum entropy production and to maximum power. Based on the above principles, a control strategy for minimization of irreversibilities or exergy destruction is proposed in this thesis as future work.

Chapter 4. Component Modelling

4.1. *Solid Oxide Fuel Cell – Fundamentals and modelling principles*

4.1.1. Introduction to SOFC

Solid oxide fuel cells (SOFC) are high temperature fuel cells with abilities to internally reform fuels. These fuel cells can use carbon monoxide as a fuel, hence identified suitable for a number applications where the use of PEM fuel cell may prove to be expensive or inconvenient. The system studied in this thesis, involves the SOFC as an important power-producing component of the system, which supports the fuel combustion in the IC engine. The SOFC is highly suited for this application as compared to other fuel cells due to its properties of internal fuel reforming and ability to provide effluents to condition the engine fuel. This chapter describes the fundamental principles of operation, modelling and control requirement for the SOFC with reference to this system.

The fuel cell is an electrochemical device, which converts chemical energy from fuel to electricity. The cathode of the SOFC reduces the oxygen to oxygen ions. The oxygen ions travel from the electrolyte to the anode, where they react with hydrogen to form water vapour. The hydrogen oxidation reaction and the oxygen reduction reactions occur in the triple-phase boundary of the SOFC material. The triple-phase boundary has two solid phases, i.e. of the solid electro-catalyst and the electrolyte, and one gaseous phase, i.e. of the reacting gas. The length of the triple phase boundary influences the overpotential of the fuel cell [31]. The solid oxide fuel cell consists of porous electrodes and an electrolyte, which are ionic and electronic conductors. The electrodes are made of cermets/ ceramics, anode mixture of ceramic and metal [6]. The requirements of an electrolyte include high ionic and low electronic conductivity at operating temperatures, along with stability in oxidising and reduction conditions [94]. The electrolyte is conventionally made from

zirconia doped with yttria, i.e. yttria-stabilized zirconia (YSZ) [6]. The cathode is conventionally made from Lanthanum Strontium Manganite (LSM) while the anode of the SOFC is a mixture of ceramic and metal. The metal conventionally used is nickel with Yttrium-Stabilized Zirconia (YSZ) [6].

4.1.2. Stack structures and applications of SOFCs

The SOFC has two common architectures, tubular and planar. A single tubular SOFC structure is described in Figure 4.1 and Figure 4.2, while the planar structure is shown in Figure 4.3 and Figure 4.4. The tubular technology was initiated by US Westinghouse Corporation (now Siemens Westinghouse Power Corporation) [94]. The tubular solid oxide fuel cells are manufactured by TOTO while the micro-tubular types by others such as Acumentrics and Adelan. The tubular structure has high fabrication costs but eliminates the need for high-temperature gas tight seals [6].

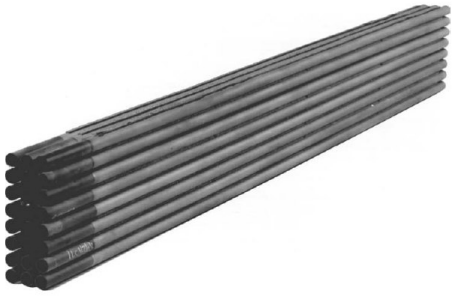

Figure 4.1 - Tubular SOFC stack [6]

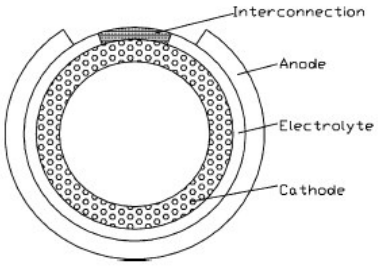

Figure 4.2 - Cross section of tubular SOFC [95]

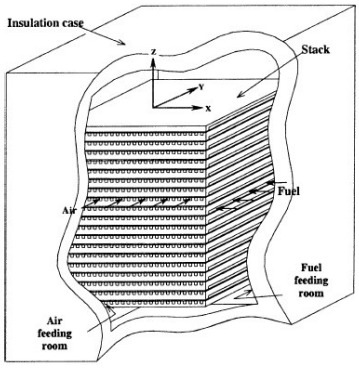

Figure 4.3 - Planar SOFC Stack [33]

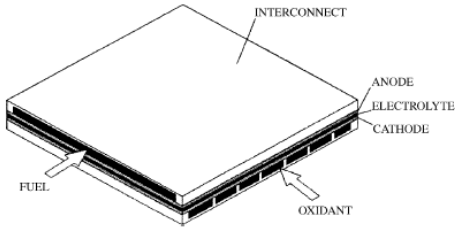

Figure 4.4 - Single cell – Planar Structure [33, 95]

The planar type has better manufacturability [35] and has been adapted by various SOFC manufacturers such as Rolls Royce, Ceres Power, Delphi, Hexis and Ceramic Fuel Cells Ltd. The integrated planar SOFC is developed by Rolls Royce [6]. This structure combines the advantages of the planar and tubular structures [6]. Hexis Ltd (previously Sulzer Hexis Ltd) has developed planar structures in the form of discs with a round aperture at the centre [76].

The structural component of SOFC can be electrolyte supported, anode supported, cathode supported, interconnect supported and substrate supported [94]. The selected structural component provides mechanical strength to the fuel cell. For example, an anode-supported SOFC will have the anode thicker providing mechanical strength to the cell structure. The model discussed in this chapter is for an anode-supported SOFC tubular cell, indicating that the anode provides mechanical strength to the fuel cell.
SOFCs have found applications in the transport and energy sector. In the transport sector, SOFCs are being considered as auxiliary power units (APU), while in the energy sector, large megawatt class power stations are being studied on the SOFC-GT technology.

4.1.3. Modelling principles

As described by Singhal et al [94], the SOFC can be modelled at different levels such as molecular, cell, stack and system level. The molecular level models focus on kinetics of reaction at the electrolyte-electrode interface and conduction in electrolyte and electrode [94]. The cell and stack level models typically consist of integrated flow, thermal and electrochemical models. These models can determine the voltage, current, temperature, pressure and species concentration of the fuel cell. A system level model includes the models for auxiliary components required for the fuel cell operation such as compressors, fuel reformers, heat exchangers and other components required for the system. The system level model is useful for determination of the interaction between the components of the system and are typically used to study the SOFC-GT hybrid systems. The type of model used will depend on the application of the modelling results. A number of distributed control volume models have been discussed in literature [33, 35, 96-98], however for the purpose of understanding the control requirement of the fuel cell and how it would interact with the rest of the components in the hybrid system, a lumped model is discussed in this section. The results of this lumped model are compared with those obtained by the

distributed model developed by Xue et al [35]. The model by Xue et al [35] is divided into control volumes, while the lumped model discussed in the following sections assumes a single control volume.

The modelling approach described below focuses on electrochemical, mass transfer and thermodynamic effects of the SOFC. The thermodynamic effects in the fuel cell depend directly on the mass flow and electrochemical reactions. The model evaluates the heat generation and transfer between the electrodes, electrolyte and the insulator. An overview for a distributed SOFC model is shown in Figure 4.5. The flow, thermal and electrochemical models together can predict the temperature, flow and pressure distribution within the cell, current density, voltage and species concentration.

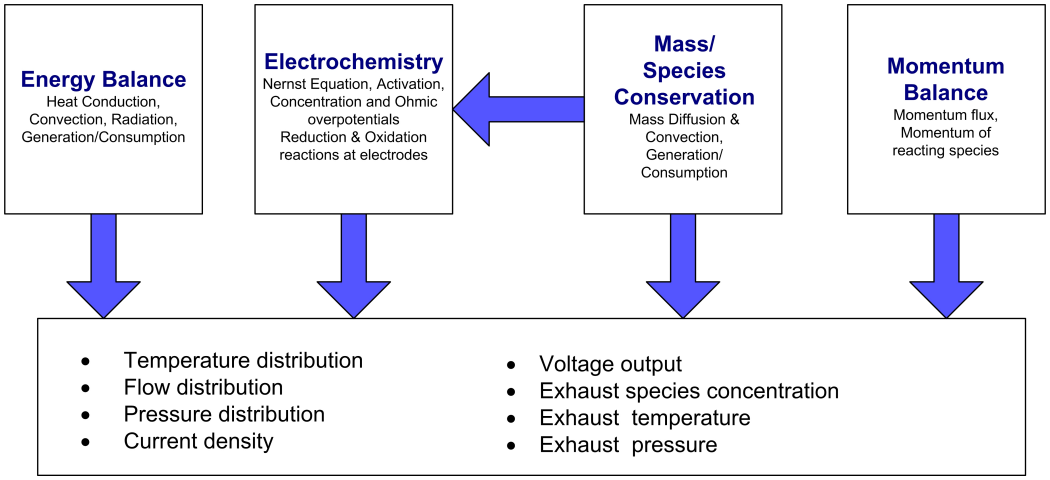

Figure 4.5 - SOFC Model overview

4.1.3.1. Electrochemistry in SOFC

The overpotentials or polarisation effects or voltage losses occurring in the fuel cell are of four types, i.e. activation losses, losses due to fuel cross over and internal current, ohmic losses and concentration losses [6]. These overpotentials are discussed below.

1. The activation losses are caused due to the energy consumed for initiation of the reaction. The activation losses are related to the Butler-Volmer equation, which describes the exchange ion current density. The activation energy, which describes the exchange ion current density, is specific to the reactant and the electrode material. These losses are dependent on the microstructure of the fuel cell, which

includes the triple-phase boundary, grain size and porosity of the anode and cathode channels.

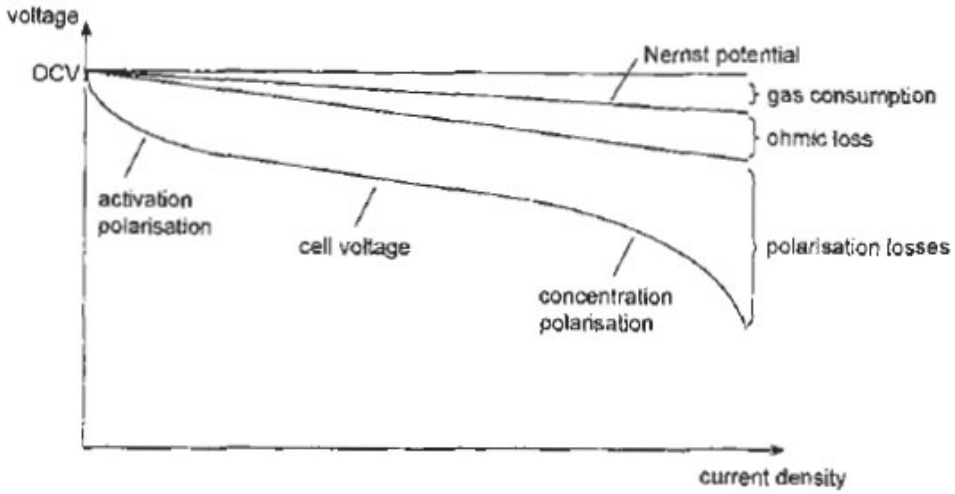

Figure 4.6 - Overpotential for a single cell [94].

2. Fuel cross over and internal currents: This effect is generally negligible in most fuel cells except the direct methanol fuel cell [6]. These losses are not considered in the model described in this section.
3. Ohmic losses: These losses occur due to the electrical resistance offered by the electrodes and the electrolyte.
4. Concentration or mass transport losses: These are caused due to the depletion of reactant at electrode surface [6] due to transport of the reactant and product species. Oxygen reduction and hydrogen depletion causes the partial pressures to drop. These losses depend on how quickly the supply for the fuel and oxidant is replenished. Increasing pressure helps reduce these losses. The concentration overpotential at the cathode and the anode is a function of species partial pressures, current density, diffusivity and microstructures [94].

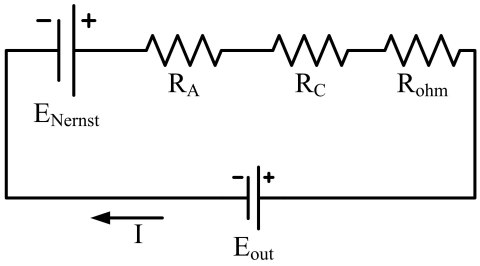

Figure 4.7 - Equivalent circuit diagram

The equivalent circuit diagram for the single SOFC cell is shown in Figure 4.7. The Nernst potential for the SOFC fed with pure hydrogen is given by Eqn. 4.1.

$$E_{Nernst} = -\frac{\Delta G^o}{2F} + \frac{RT}{2F}\ln\left(\frac{p_{H_2} p_{O_2}{}^{1/2}}{p_{H_2O}}\right)$$

Eqn. 4.1

Where ΔG^o is the Gibbs free energy, p_{H_2}, p_{O_2} p_{H_2O} are partial pressures of hydrogen, oxygen and water vapour, R is the universal gas constant, F is the Faraday constant, T is the fuel cell temperature. The equivalent resistances of the cathode R_C and anode R_A are based on experimental characterization [99]. The terms involving E_A and E_C (activation energies) account for the activation losses for the anode and cathode respectively. The pressure ratio term accounts for the concentration losses in the anode and the cathode. The equivalent resistances of the cathode and anode as described by Achenbach [99] are given in Eqn. 4.2 and Eqn. 4.3.

$$R_A = \left[\frac{2F}{RT} k_A A_a^c \left(\frac{p_{H_2}}{P_{anode}}\right)^{0.25} \exp\left(-\frac{E_A}{RT}\right)\right]^{-1}$$

Eqn. 4.2

$$R_C = \left[\frac{4F}{RT} k_C A_c^c \left(\frac{p_{O_2}}{P_{cathode}}\right)^{0.25} \exp\left(-\frac{E_C}{RT}\right)\right]^{-1}$$

Eqn. 4.3

The fuel cell voltage using Kirchoff's laws for the equivalent circuit shown in Figure 4.7 is given below.

$$V_{fc} = E_{Nernst} - (R_A + R_C + R_\Omega)I$$

Eqn. 4.4

4.1.3.2. Flow Model

The mass balance or species conservation equation for the fuel cell is given by the following equation.

$$\frac{dm_i}{dt} = \dot{m}_{in} - \dot{m}_{out} - \dot{m}_{react}$$

Eqn. 4.5

Where '*i*' represents the fuel cell channel, $\dot{m}$ is the mass flow rate, and $\dot{m}_{react}$ is the rate of consumption of the reacting species or rate of formation of the generated species. The term $\dot{m}_{react}$ will be positive for water vapour generation in the anode. For the anode channel, the species are hydrogen and water vapour and for the cathode channel, it is oxygen. $\dot{m}_{react}$ for each channel is given below.

ANODE:

$$\dot{m}_{H_2\,used} = M_{H_2} \times \frac{I}{2F}$$

Eqn. 4.6

$$\dot{m}_{H_2O\,gen} = M_{H_2O} \times \frac{I}{2F}$$

Eqn. 4.7

CATHODE:

$$\dot{m}_{O_2\,used} = M_{O_2} \times \frac{I}{4F}$$

Eqn. 4.8

4.1.3.3. Energy balance of SOFC

Figure 4.8 shows the energy balances within a control volume '*i*' for an SOFC as developed by Xue et al [35]. The data from Xue et al has been used to develop the mass and energy balances for the lumped model based on Figure 4.8.

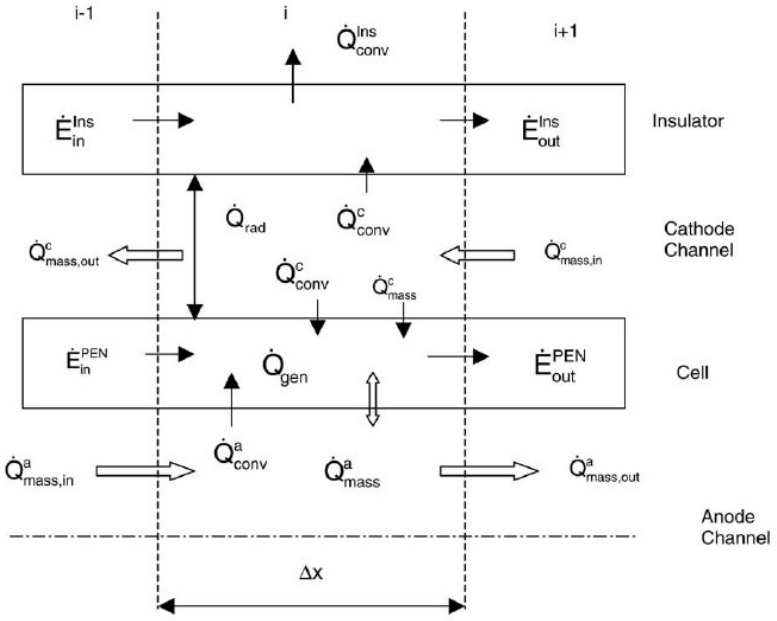

Figure 4.8 - Mass and Energy Balance for a control volume [35].

The energy balance for anode channel of the single tubular cell is given in Eqn. 4.9.

$$\frac{d\left(\sum_k e_k m_k\right)}{dt} = \dot{Q}_{mass,in} - \dot{Q}_{mass,out} - \dot{Q}_{conv} - \dot{Q}_{mass,diff}$$

Eqn. 4.9

where '*e*' is the specific internal energy and '*k*' represents the species in each channel. The energy balance consists of heat flows through the system, convection effect between solid

and gaseous channels, mass diffusion of species from electrode to electrolyte, conduction and radiation from the PEN to the insulator and vice-versa and electrochemical action. These are described below in Eqn. 4.10 - Eqn. 4.13.

$$\dot{Q}_{mass,in} = \left(\sum_k \dot{m}_k H_k \right)_{in}$$

Eqn. 4.10

$$\dot{Q}_{mass,out} = \left(\sum_k \dot{m}_k H_k \right)_{out}$$

Eqn. 4.11

$\dot{Q}_{conv}$ is the heat generated in the fuel cell due to convection between the gas and the solid phase. For the anode channel, the heat transfer due to convection is between the anode and the PEN, while that for the cathode channel is between the cathode and PEN and cathode and the insulator.

$$\dot{Q}_{conv} = hA^c \left(T_g - T_s \right)$$

Eqn. 4.12

$\dot{Q}_{mass,diff}$ is the heat generated in the fuel cell due to diffusion of components.

$$\dot{Q}_{mass,diff} = \sum_k M_k \frac{I}{n_k F} \left(c_p \right)_k \left(T_g - T_s \right)$$

Eqn. 4.13

Energy balance for the PEN and insulator of the fuel cell is given by Eqn. 4.14. However, the last term for heat generated due to the reaction is applicable only to the PEN.

$$\rho V c_p \frac{dT}{dt} = \dot{E}_{in} - \dot{E}_{out} + \sum \dot{Q}_{conv} + \sum \dot{Q}_{mass} + \dot{Q}_{rad} + \dot{Q}_{gen}$$

Eqn. 4.14

The heat transfer due to conduction along the length of the cell is given in Eqn. 4.15.

$$\dot{E}_{in} - \dot{E}_{out} = kA \frac{T_{in} - T_{out}}{L}$$

Eqn. 4.15

The heat transfer due to radiation between the PEN and the insulator is given below.

$$\dot{Q}_{rad} = \frac{\sigma A^c \left(T_{Ins}^4 - T_{PEN}^4 \right)}{1/\varepsilon_{PEN} + \left(r_{PEN} / r_{Ins} \right) \left(\left(1/\varepsilon_{Ins} \right) - 1 \right)}$$

Eqn. 4.16

Eqn. 4.17 gives the heat generated due to the chemical reaction within the PEN.

$$\dot{Q}_{gen} = M_{H_2} \frac{I}{2F} \Delta H_{H_2} + I^2 \left(R_A + R_\Omega + R_C \right)$$

Eqn. 4.17

The term $\dot{Q}_{gen}$ occurs only in the PEN, where heat is generated due to the electrochemical reaction. Excessive temperatures in the SOFC can cause local hot spots and material failure while lower temperatures can affect reaction rates within the fuel cell and result in limited utilisation of the fuel.

4.1.4. Fuel flexibility, Internal reforming and Chemical kinetics

The high temperature operation of the SOFC allows internal reforming to take place and can utilise various fuels. Fuel flexibility studies done by Saunders et al [15, 29] show the effect of various fuels on SOFC voltage and carbon deposition. The ratio of the steam to carbon must be controlled in order to avoid carbon deposition in the fuel cell. Carbon deposition can reduce the active area of the fuel cell by obstructing the triple-phase boundary of the fuel cell and reduce performance.

The mass flow dynamics, thermodynamics and electrochemical effects are coupled; hence, the change in species in the anode affects each of them. The heat generated in the SOFC as described by Eqn. 4.17 has two major terms, one due to the reaction chemistry of hydrogen in the anode and the other due to current flowing through the cell resistances. Similarly, when the SOFC anode consists of a mixture of fuels, the heat generated depends on the reaction chemistry of these fuels. The steam present in the anode can lead to the water gas shift reaction and reforming of fuels such as methane.

The presence of various fuels in the anode also affects the Nernst equation as the free energy of each fuel reaction is considered. It is observed commonly that hydrogen oxidation is a dominating reaction in the anode [94] hence, also produces greater voltage than any other fuel. The voltage produced by the cell depends on the polarisations. Activation polarisation is a function of the activation energy, while concentration polarisation is a function of the transport of reacting species to product species. [94]
The mixture of fuels such as hydrogen, methane and carbon monoxide in the presence of steam in the SOFC anode can undergo various reactions. The reactions do not necessarily follow a certain path and most often do not achieve equilibrium [94]. Due to the interaction

between various species in the anode, a reaction mechanism for the species can effectively determine the extent of the reaction, species produced and heat generated. The extent of the reactions can be determined with the rates of each reaction occurring in the anode. The rate of reactions of each species are a function of the activation energy, order of the reaction specific to the fuel cell material and operating conditions of the fuel cell. For example, if the following reactions are considered for internal reforming of methane in the anode, the species involved include CH_4, H_2O, CO_2, CO and H_2.

$$CH_4 + H_2O \xrightarrow{k_{CH_4}} 3H_2 + CO$$

Steam reforming reaction Eqn. 4.18

$$H_2 + O^{2-} \xrightarrow{k_{H_2}} H_2O + 2e^-$$

Hydrogen oxidation reaction Eqn. 4.19

$$CO + O^{2-} \xrightarrow{k_{CO}} CO_2 + 2e^-$$

Carbon monoxide oxidation reaction Eqn. 4.20

$$CO + H_2O \xrightarrow{k_1} CO_2 + H_2$$

Shift reaction Eqn. 4.21

The rate of reaction for methane reforming is given by [94]

$$r_{CH_4} = k_{CH_4} p_{CH_4}^{m1} p_{H_2O}^{m2} \exp\left(\frac{-E_{CH_4}}{RT}\right)$$

Eqn. 4.22

The rate of reaction for hydrogen oxidation reaction is given by [94]

$$r_{H_2\,oxidation} = k_{H_2} p_{H_2}^{m3} \exp\left(\frac{-E_{H_2}}{RT}\right)$$

Eqn. 4.23

The rate of reaction for carbon monoxide oxidation reaction is given by [94]

$$r_{CO\,oxidation} = k_{CO} p_{CO}^{m4} \exp\left(\frac{-E_{CO}}{RT}\right)$$

Eqn. 4.24

The rate of reaction of the forward and backward shift reaction is given by

$$r_f = k_1 p_{CO} p_{H_2O}$$

Eqn. 4.25

$$r_b = k_1 K_{shift} p_{CO_2} p_{H_2}$$

Eqn. 4.26

Where k denotes the reaction rate constant, p the respective partial pressure of the species, m the order of reaction and E the activation energy of the respective reaction. K_{shift} is the equilibrium constant of the shift reaction given by:

$$K_{shift} = \exp\left(\frac{-\Delta G^{o}_{shift}}{RT}\right)$$

Eqn. 4.27

Where ΔG^{o}_{shift} is the standard Gibbs free energy change of the shift reaction. The rates of change of concentration for carbon monoxide, steam and hydrogen depend on all four reactions and are given by

$$\frac{dr_{CO}}{dt} = \frac{dr_{CH_4}}{dt} + \frac{dr_b}{dt} - \frac{dr_f}{dt} - \frac{dr_{CO\,oxidation}}{dt}$$

Eqn. 4.28

$$dr_{H_2O} = \frac{dr_{H_2\,oxidation}}{dt} + \frac{dr_b}{dt} - \frac{dr_f}{dt} - \frac{dr_{CH_4}}{dt}$$

Eqn. 4.29

$$\frac{dr_{H_2}}{dt} = 3\frac{dr_{CH_4}}{dt} + \frac{dr_f}{dt} - \frac{dr_b}{dt} - \frac{dr_{H_2\,oxidation}}{dt}$$

Eqn. 4.30

The following undesirable reactions may occur if steam proportion is low and lead to carbon formation. Carbon deposits block the reaction sites and reduce the active area of the fuel cell.

Boudouard reaction

$$CH_4 \rightarrow 2H_2 + C$$

Eqn. 4.31

CO hydrogenation

$$CO + H_2 \rightarrow H_2O + C$$

Eqn. 4.32

CH4 decomposition reaction

$$2CO \rightarrow CO_2 + C$$

Eqn. 4.33

The important factors, which require monitoring of internal reforming of fuels other than hydrogen, are the operating fuel cell temperature and fuel to steam ratio in the anode channel.

The model described by Xue et al [35] is simplified to a lumped model which combines the thermodynamic and electrochemical effects in a single tubular fuel cell. This lumped model is compared with the one-dimensional control volume model described by Xue et al. The SOFC is modelled in this chapter for pure hydrogen only. The steps followed in modelling are given in Figure 4.9.

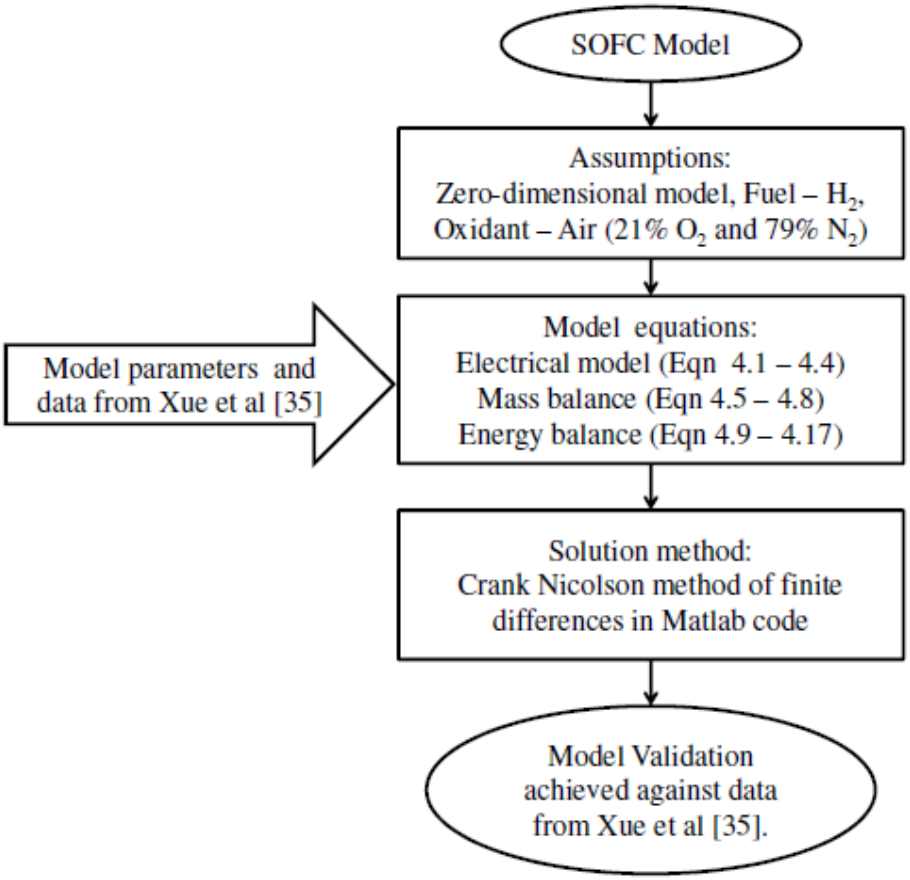

Figure 4.9 – SOFC Model flowchart

4.1.5. Results of tubular SOFC model

Validation

The results of the lumped model described in section 4.1.3 are discussed below with the help of Figure 4.10 to Figure 4.15.

In order to verify the model, operating conditions similar to those used for modelling and experiments by Xue et al [35] were used. The fuel cell model was treated as isothermal with operating temperature of 1123 K, fuel pressure at 3 bar and the cathode as ambient.

The load voltage was specified and the model computed the current generated. The lumped model predicts the fuel cell behaviour closely to the results by Xue et al. However, the results of the lumped model are a better match with the experimental results of Xue et al than their distributed modelling results. This is observed in the polarisation curve shown in Figure 4.10 and the power density curve in Figure 4.11.

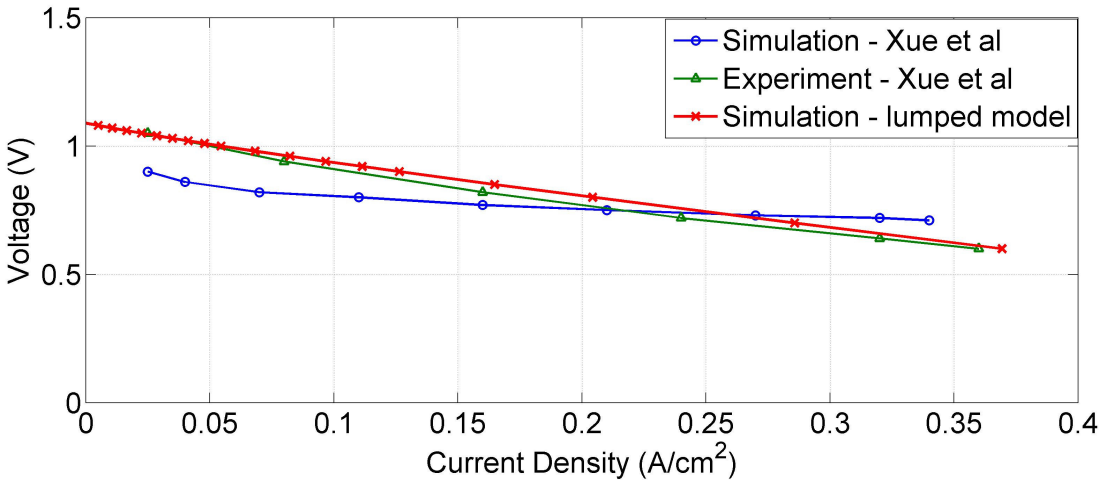

Figure 4.10 – Polarisation curve for the SOFC

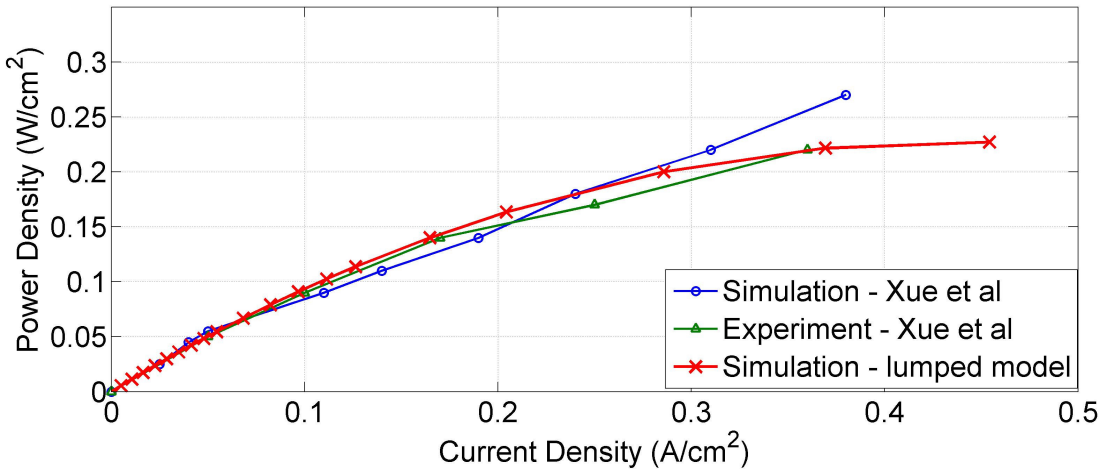

Figure 4.11 –Power density versus current density for the SOFC

Effect of load changes on fuel cell performance

The load voltage for the lumped model was changed from 0.7 V to 0.5 V at 50 seconds and 0.5 V to 0.6 V at 150 seconds to investigate the response of the model at various load conditions. The feed temperature was 1073 K and the inlet pressures of the fuel and air

were 3 bar. The resulting Nernst potential at these load voltages, as shown in Figure 4.12, shows very small variations.

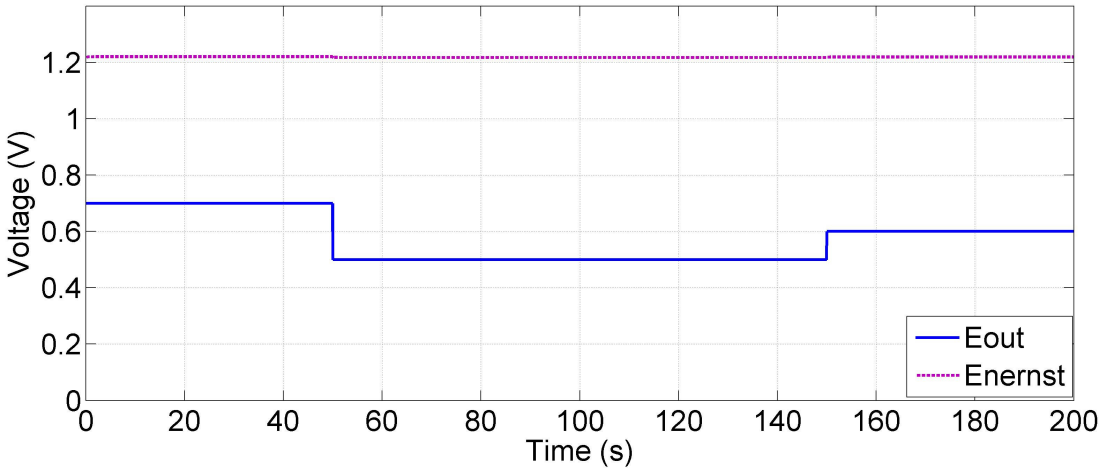

Figure 4.12 – Load voltage and Nernst potential

The Nernst potential depends on the species partial pressures and the temperature of the cell. The variation in pressures, as shown in Figure 4.13, of the anode and cathode channel is small. The pressure is function of the fuel cell temperature and the current, which affects the consumption or generation of species. One of the main effects of change in the load demand is the fuel consumption. The fuel consumption and oxygen usage depends directly

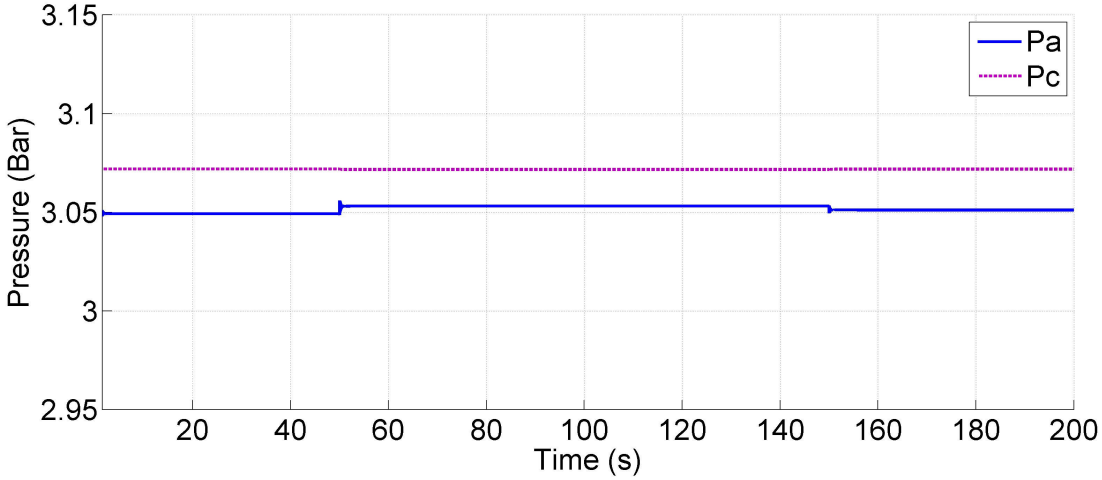

Figure 4.13 – Pressure profiles with varying load conditions

on the load current and affects the partial pressures of the species. In case the fuel or oxidant is completed consumed, the partial pressure drops to zero causing a sharp drop in fuel cell performance. Hence, it is important to supply the fuel cell with sufficient fuel and oxidant to prevent fuel and oxidant starvation. The effect of operating pressure on the fuel cell performance is further discussed in the following section.

The current produced by the fuel cell when the load voltage changes is shown in Figure 4.14. The current produced is a function of the equivalent anode and cathode resistances. These resistances are dependent on the channel pressures and temperatures and can considerably affect the performance of the fuel cell. The power produced in the single cell is with varying load voltage is 4.6 W and shows very small variations. This is shown in Figure 4.15. To develop a fuel cell stack, a number of cells can be arranged in a series-parallel configuration to achieve a stack operating at a desired voltage and power. The fuel cell power and the current shows a fast response for feed temperatures at 1073 K, which is desirable for automotive applications.

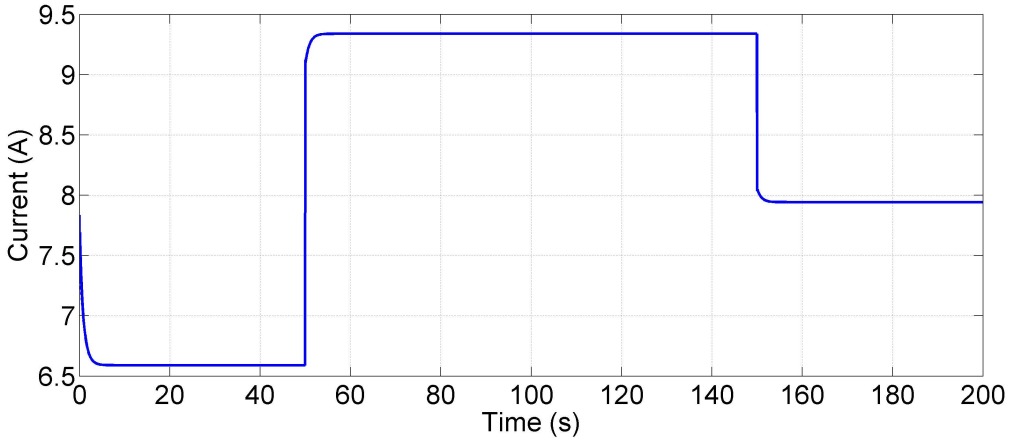

Figure 4.14 – Current generated in fuel cell

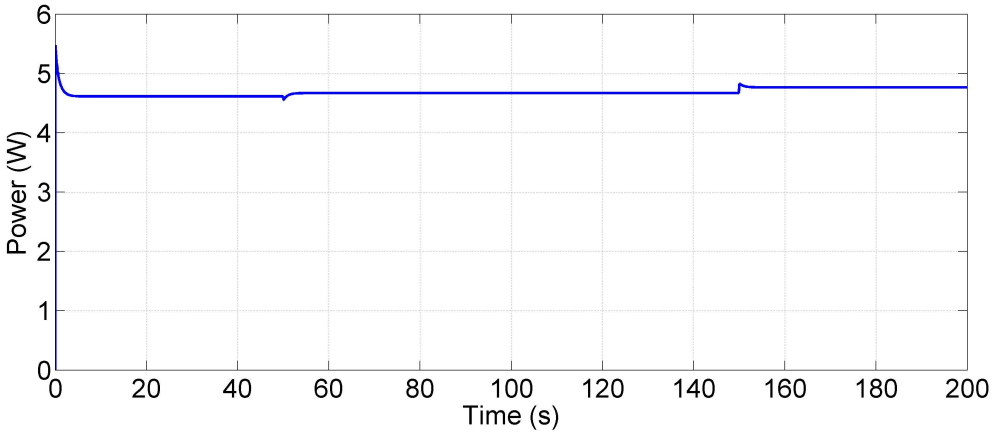

Figure 4.15 – Fuel cell power

The inlet temperature of the fuel cell is 1073 K, which drops and settles to a lower value as shown in Figure 4.16. For constant mass flow rates, the temperature shows an increase when the load voltage decreases. The main source of heat generation in the PEN is the electrochemical reaction, which depends on the current produced in the fuel cell. As a result, the temperature is highest when the current is 9.4 A (between 50-150 seconds). The

temperature of the anode and cathode shows a difference of about 8 K. This difference may be attributed to the structure of the tubular fuel cell, in which the cathode loses heat via convection to the PEN and the insulator, while the anode has thermal energy exchanges only with the PEN.

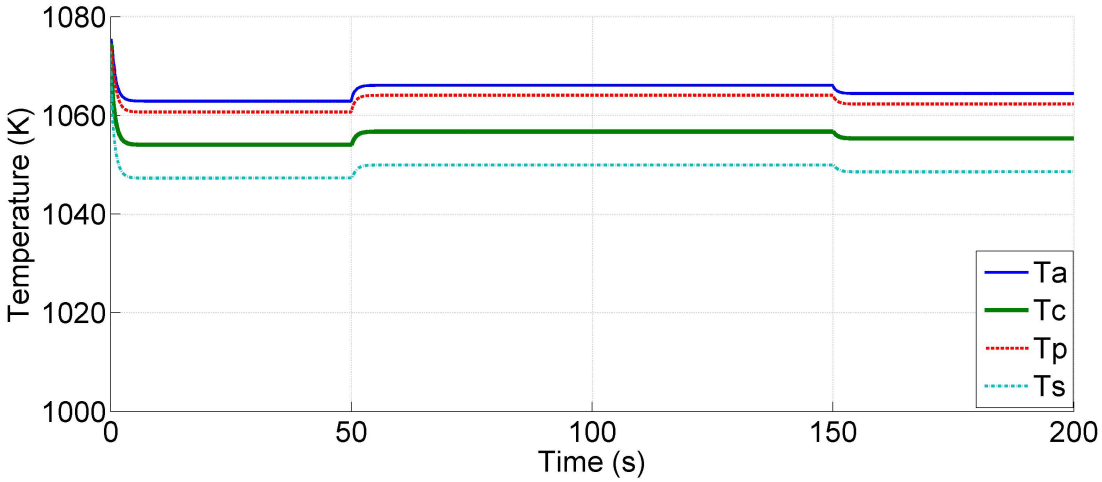

Figure 4.16 – Temperature profile for varying load conditions

Comparison of results with distributed model developed by Xue et al [35]

Comparison of the results of the two models highlights a main difference in temperature trends. The temperature increase with drop in voltage is higher in the lumped model than that in the distributed model developed by Xue et al [35]. For a change in load voltage from 0.5 V to 0.6 V, in the distributed model the temperature changes are of approximately 0.1 K in the PEN while those in the lumped model are 2 K. This difference is due to the different electrochemical models. The distributed model by Xue et al [35] has divided the electrochemical model into parallel sub-cells, each of which produces a current. The current and the Nernst potential in each control volume is different. Hence, the total cell current is the sum of the currents produced in the sub-cells. As a result, the temperature change (for step change in voltage) in the PEN, in each control volume in Xue et al's model, is small. In comparison, the lumped model, assumes a single circuit (as shown in Figure 4.7), which computes the total current in the fuel cell. This fuel cell current value in the lumped model is larger than the current generated in a single control volume in the distributed model and causes the temperature rise to be higher. The lumped model overestimates the effect of load changes on the temperature of the PEN. This indicates that the type of electrochemical model can influence the resulting temperature from the model.

Experimental verification can confirm the most suited electrochemical model for a particular cell.

Effect of operating temperature on the fuel cell performance

The results discussed above in Figure 4.12-Figure 4.16 are for fuel cell feed temperatures of 1073 K. To study the effect of feed temperature, this value was changed to 973 K while all other feed conditions were maintained the same as before. The results are shown in Figure 4.17.

The current and power at the lower feed temperature are clearly lower indicating a reduced performance of the fuel cell. As shown in the figure, the temperatures in the SOFC affect the anode and cathode equivalent resistances, which in turn affect the current production. Operating the fuel cell at a low temperature causes the resistances to be large resulting in lower current and lower power output. For the same load voltage at higher temperature, the resistances are lower resulting in increased current and power. The temperature of the fuel cell also affects the pressure in the channels, which affects the Nernst potential. The temperature dynamics for the SOFC are important since it affects the performance of the SOFC. Regulating the SOFC temperature is an important control parameter to ensure efficient operation.

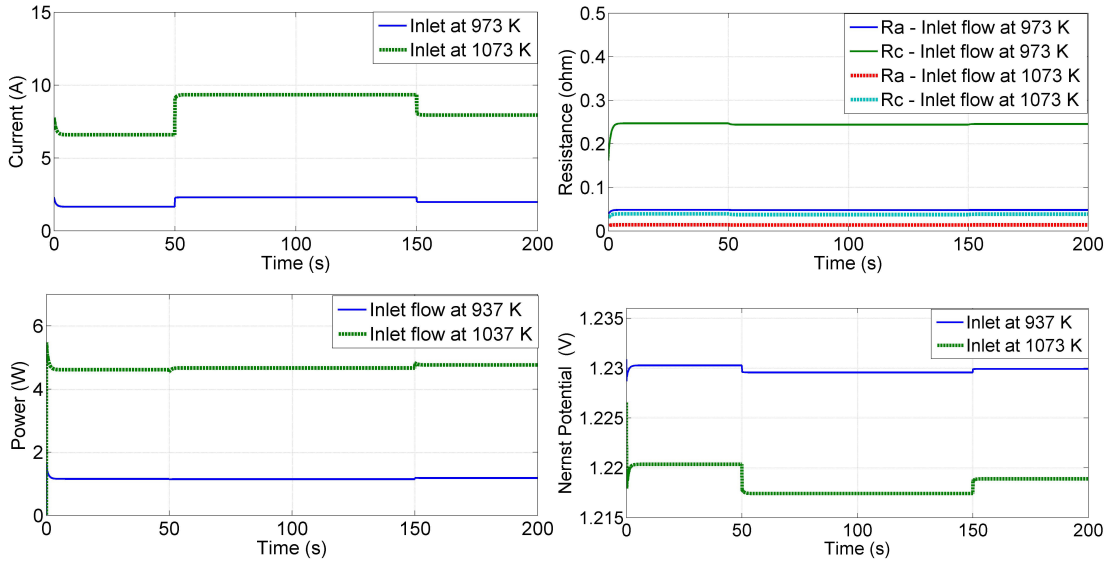

Figure 4.17 – Effect of inlet feed temperatures on SOFC performance

Effect of operating pressure on fuel cell performance

The results in Figure 4.18 show the comparison between the fuel cell operating at pressures 2.6 bar and 3 bar. All the other feed conditions were maintained the same as discussed for the results in Figure 4.12- Figure 4.16. The current, power produced, equivalent resistances and Nernst potential at operating pressure of 2.6 bar show a reduction when compared to those at 3 bar. This indicates the fuel cell gives an improved performance at high pressures and is a feature, which must be considered for control.

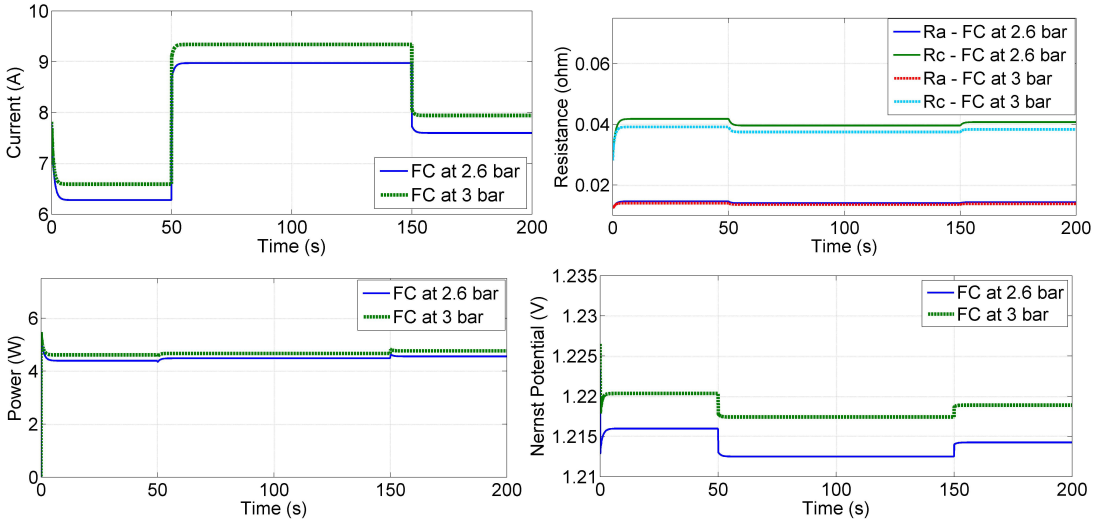

Figure 4.18 – Effect of operating pressure on SOFC performance

4.1.6. Summary

This section describes the fundamentals of the solid oxide fuel cell and demonstrates the mass flow and temperature dynamics for a single cell with the help of a lumped model. The model was verified against the results obtained experimentally and by modelling by Xue et al [35] and showed a close match. The comparison of the lumped model with the distributed model developed by Xue et al [35], indicates differences in temperature changes for load variation. This effect is due to the differences between the electrochemical models of the lumped and distributed model. The lumped model overestimates the temperatures as compared to the distributed model. The lumped model can be further developed to evaluate the SOFC performance with other fuels with appropriate reaction rate data.

In order to develop a control system for the fuel cell, it is essential to control the air and fuel flows to prevent starvation and ensure the load demand is met. An optimum amount of

fuel must be supplied to ensure a high fuel usage without causing starvation at any point within the fuel cell. Similarly the air flow supplied must be above stoichiometric to prevent air starvation, but also ensure that the compressor power required to supply this air is optimum. The temperature dynamics in the SOFC affects all parameters of the fuel cell and have a direct influence on the performance of the fuel cell. The air and fuel must be supplied at the optimum temperature and pressure to ensure an efficient response from the fuel cell while maintaining the temperatures and pressures within the SOFC material tolerance limits. The results from this section are further used to support control development for the hybrid system.

4.2. *Reformer Modelling*

4.2.1. Introduction

Fuel cell technology has emerged as a possible solution for the growing green house gases. The PEM fuel cell is dependent on the availability of a source of hydrogen, whereas SOFCs can not only reform various fuels but also give highest productivity with the use of hydrogen as a fuel. While novel technologies for hydrogen manufacturing, compact storage advances, fuel processing technology is well established and provides viable options for on-board hydrogen generation. In automotive applications involving fuel cells, on-board fuel processing provides an alternative to hydrogen cylinder storage.

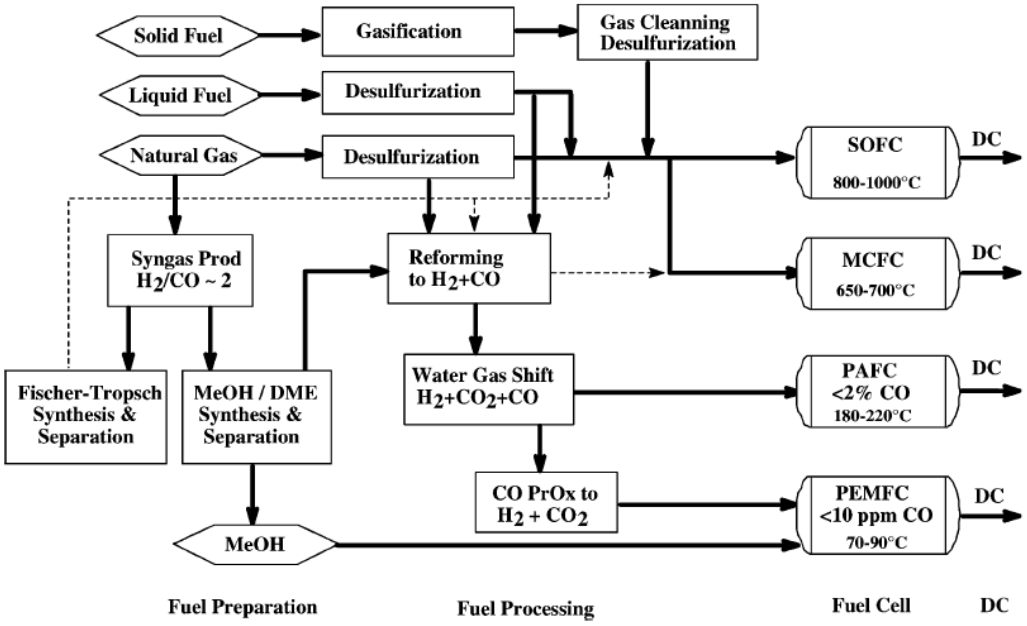

Figure 4.19– Steps involved in fuel processing for HT and LT fuel cells [45]

Fuel processing is the generic term for the processes that convert higher hydrocarbons to lighter hydrocarbons and hydrogen. Depending on the requirement for fuel quality, fuel processing involves a number of steps. The key steps include de-sulphurisation, reforming, and control of CO content. Sulphur can damage reforming catalysts such as Pt/CeO_2 and Ni catalysts [44] rendering the reformer inactive, hence the need for desulphurisation. Fuel cells such as the SOFC, PEM, PAFC, MCFC [6] have a low tolerance for sulphur as it poisons the electrodes. Figure 4.19 shows the steps involved in the fuel processing as required by different types of fuel cells.

The reformer is central to the fuel processing unit, which may consist of various other components to ensure that the fuel is delivered at the right composition. These components conventionally include HDS (hydro-desulphuriser), WGS (Water Gas Shift reactor), CO selectivity. The WGS and CO selectivity reactors are mainly utilised to reduce the concentration of carbon monoxide in the reformate and may not be used for fuel cells such as the SOFC.

The SOFC can process carbon monoxide as a fuel and eliminates the need for its removal. The SOFC–IC engine system described in Chapter 12 (The System and its Attributes), proposes a novel method of operating the system such that the exhaust flows of the reformer and the fuel cell are utilised to condition the fuel quality of the IC engine. Solid oxide fuel cells, operate at high temperatures and can reform various fuels. SOFCs give improved performance with pure hydrogen. The cell voltage produced with hydrogen is much higher than that produced by carbon monoxide [100]. This effect is due to the dependence of Gibbs free energy on temperature [100]. The proposed system utilises an external reformer to deliver fuel to the fuel cell at the right conditions to ensure a timely start-up and optimum fuel cell performance. The reformer must provide hydrogen to the fuel cell during load changes with a high utilisation factor and prevent fuel starvation at all times to ensure its optimum performance.

There are three types of reformers commonly used, steam reformer, catalytic partial oxidation reformer and the autothermal reformer. Steam reforming is an endothermic process, requiring a supply of heat. The steam reforming reaction for a hydrocarbon described by the general form $C_xH_yO_z$ as described by Kolb [44] is given in Eqn. 4.34.

$$C_xH_yO_z + (x-z)H_2O \rightarrow \left(x - z + \frac{y}{2}\right)H_2 + xCO$$

Eqn. 4.34

The catalytic partial oxidation is an exothermic process, which involves fuel conversion in an oxygen deficient atmosphere [44]. The reaction is described in Eqn. 4.35.

$$C_xH_yO_z + \left(\frac{x-z}{2}\right)(O_2 + 3.76N_2) \rightarrow xCO + \frac{y}{2}H_2 + 3.76\left(\frac{x-z}{2}\right)N_2$$

Eqn. 4.35

The autothermal reforming also known as oxidative steam reforming combines the advantages of the steam reformer and the partial oxidation process. In this reformer, air is added to the steam reforming process. The reaction occurring is described by Eqn. 4.36.

$$C_xH_yO_z + n\left(O_2 + 3.76N_2\right) + \left(x - 2n - z\right)H_2O \rightarrow xCO + \left(x - 2n - z + \frac{y}{2}\right)H_2 + 3.76nN_2$$

Eqn. 4.36

Energy is generated by partial oxidation reaction and the steam reforming reaction consumes this energy, causing the reaction to be autothermal [44]. The steam reforming process, for all fuels, has a number of advantages over autothermal reforming and partial oxidation reforming as described by Qi et al [101] and is listed below:

1. Hydrogen content in reformate stream is higher.
2. Reformate pressures can be increased by pumping liquid fuel and water without the need for compressing air.
3. Waste anode gas can be utilised as fuel to provide heat.

Methanol as a fuel for reforming is popular since it has the potential to produce highest efficiencies and requires mild reforming conditions, with a possibility to obtain it from renewable sources [101]. A methanol steam reformer is modelled for the system described in Chapter 2 (The System and its Attributes), due to the availability of data in literature for methanol and its reforming. The modelling task allows answering some basic questions about the overall system performance. Ideally, the system as described in Chapter 2, would use a single fuel such as diesel for the engine and the fuel cell system.

The purpose of using a reformer in this system is two-fold: to supply hydrogen to the fuel cell and to supply the remaining effluents as a form of external EGR for the IC engine. A steam reformer is selected for this system application mainly due to its advantage over other methods for resulting in higher hydrogen content in the exhaust stream.

The aim of this chapter is to characterize the steam reformer by

- Describing the fundamental principles of operation and modelling of a steam reformer,
- Determining the dynamic response of the reformer and hence its suitability for fast start-up and load changes.

- Determining the outlet conditions and compositions to develop an understanding of the auxiliary component requirement in the system and control systems required for the reformer.

4.2.2. Reformer physical characteristics

The chemical reactions taking place in the steam reformer are endothermic and require a source of thermal energy. This energy is provided by a catalytic burner with a plate-to-plate geometry with the reformer as shown in Figure 4.20.

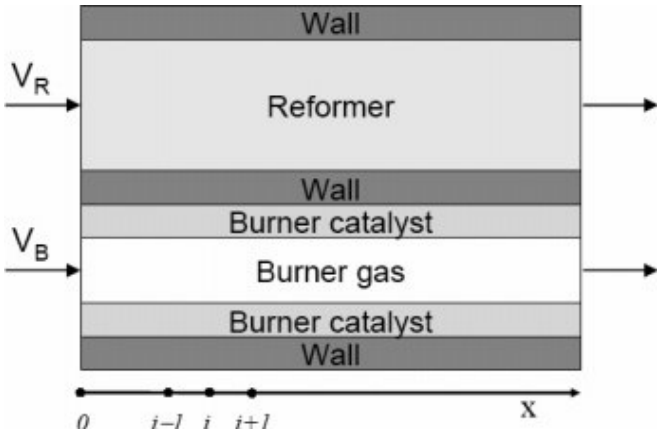

Figure 4.20 – Plate to plate geometry of reformer-burner [16]

The metallic plate between the burner and the reformer transfers heat generated by combustion in the burner to the reformer via the burner catalyst layer. The reactions in the steam reformer are strongly dependent on temperature. Consequently, the dynamic response of the reformer is temperature dependent.

The catalyst used for reforming methanol is generally copper based. Copper based catalysts such as copper/zinc oxide, copper/ceria/alumina, copper/zirconia, copper/chrome oxide and palladium based catalysts such as palladium/zinc oxide, palladium/ceria/zinc oxide, palladium/zirconia have been studied extensively for methanol steam reforming [44]. The reaction kinetics for the $CuO/ZnO/Al_2O_3$ catalyst describing the reaction rates for reforming is used in the model. The reformer-burner unit can function efficiently as long as the catalyst de-activation/ degradation does not take place. At excessive temperatures, catalyst sintering occurs and results in lower methanol conversion in the reformer [16]. The catalyst degradation is greatest along the reactor length where methanol conversion is

maximum [16].The catalyst degradation is dependent on the methanol conversion and the reformer temperature. Catalyst deactivation can also occur if sulphur is present in the fuel. The steam to carbon ratio is normally maintained at 1.5 to avoid carbon formation, which degrades the reformer performance. The effects of steam to carbon ratio are further discussed in the simulation results.

4.2.3. Steam Reformer Modelling

A reformer-burner model is described in this section. The model developed by Varesano et al [16] is solved to understand and explain the principles of modelling flow and temperature distribution in the burner, reformer and the reaction chemistry.

The paper by Varesano et al [16] discusses the reformer-burner model to design an optimum reactor to ensure the reformer temperature does not exceed 573 K and methanol conversion is above 90%. The model by Varesano et al [16] is described here and solved using the upwind Crank-Nicolson method of finite differences. The results are examined to determine the outlet flow and temperature conditions and main control variables for the reformer-burner unit.

The reformer model described in this chapter assumes the reactor as a plug flow reactor. The other basic assumptions of a plug flow reactor analysis are [102]:

- All gases are treated as ideal gases
- Plug flow- an idealized flow of fluids, all particles of fluid in a given cross section have identical velocity and direction of motion with negligible axial dispersion
- Particles of different age do not mingle and no back-mixing occurs
- All particles enter and leave the reactor simultaneously
- No longitudinal (axial) mixing of fluid elements as they move from reactor inlet to outlet.

The burner is a pseudo-homogenous reactor with two phases, the gas phase and the solid catalyst phase.

4.2.3.1. Chemical Kinetics

The chemical reactions for steam reforming over $CuO/ZnO/Al_2O_3$ catalyst are:

$$CH_3OH + H_2O \xleftrightarrow{k_1} CO_2 + 3H_2$$

Eqn. 4.37

$$CH_3OH \xleftrightarrow{k_2} CO + 2H_2$$

Eqn. 4.38

The constant k_1 is the reaction rate constant for the forward reaction while that for the reverse reaction is $-k_1$. Hydrogen production from Eqn. 4.37 and Eqn. 4.38 is considered irreversible for this model. The reaction rates for the above chemical reactions are described by Amphlett et al [103] are given in Eqn. 4.39 and Eqn. 4.40. The rate constants are of the Arrhenius type and demonstrate temperature dependence. The values for the pre-exponential coefficients and activation energies are taken from Amphlett et al [103].

$$r_1 = k_1 C_{R,1}$$

Eqn. 4.39

where the $C_{R,1}$ represents the concentration of methanol in the reformer.

$$r_2 = k_2$$

Eqn. 4.40

$$k_1 = \frac{\left[A_1 + B_1 \ln\left(\frac{C_{R,2,0}}{C_{R,1,0}}\right)\right] e^{-\left(\frac{E_1}{RT_R}\right)}}{\left(\frac{P_R}{P_{atm}}\right)^{D_1}} \rho_{cat}\left(1-\in_R\right)$$

Eqn. 4.41

where the $C_{R,1,0}$ and $C_{R,2,0}$ represent the concentration of methanol and water vapour in the reformer at the inlet.

$$k_2 = \frac{A_2 e^{-\left(\frac{E_2}{RT_R}\right)}}{\left(\frac{P_R}{P_{atm}}\right)^{D_2}} \rho_{cat}\left(1-\in_R\right)$$

Eqn. 4.42

Eqn. 4.43 gives the reaction occurring in the burner gas and solid phase. The rate equations developed by Ito et al [104] are described in Eqn. 4.44 - Eqn. 4.45.

$$CH_3OH + \frac{3}{2}O_2 \xrightarrow{k_{4,s} \quad k_{4,g}} CO_2 + 2H_2O$$

Eqn. 4.43

$$r_{4,s} = k_{4,s} C_{B,s,1}$$

Eqn. 4.44

where the $C_{B,s,1}$ represents the concentration of methanol in the burner solid.

$$r_{4,g} = k_{4,g} C_{B,g,1}$$

Eqn. 4.45

where the $C_{B,s,1}$ represents the concentration of methanol in the burner gas

$$k_{4,s} = \exp\left(\frac{-5.9\times10^{4}}{RT_{B,s}} + 22.45\right) \text{ for } T_{B,s} < 380K$$

Eqn. 4.46

$$k_{4,s} = \exp\left(\frac{-6.4\times10^{3}}{RT_{B,s}} + 5.8\right) \text{ for } 3T_{B,s} < 380 \quad K$$

Eqn. 4.47

$$k_{4,s} = \exp\left(\frac{-6.1\times10^{3}}{RT_{B,g}} + 3.2\right)$$

Eqn. 4.48

A set of 19 partial differential equations were developed by Varesano et al [16] to represent the mass and energy balances for the reformer and burner. These equation are described below.

The mass balances for the burner gas phase, burner solid phase and the reformer are described in Eqn. 4.49-Eqn. 4.52. The first term in equations Eqn. 4.49 - Eqn. 4.50 and Eqn. 4.52 are due to the convection. The second term in Eqn. 4.49 is due to mass transfer between the burner, solid and gas phases, while the last term in Eqn. 4.49, Eqn. 4.51 and Eqn. 4.52 is due to reaction chemistry.

$$\frac{\partial C_{B,g,j}}{\partial t} = -\psi_B \frac{\partial\left(T_{B,g,j} C_{B,g,j}\right)}{\partial x} - \tau_B (C_{B,g,j} - C_{B,s,j}) + G_{4j} r_{4,g} \qquad j = 1-3,6$$

Eqn. 4.49

Where $\psi_B = \frac{v_{B,0}}{T_{B,0}}\left(\frac{\overline{MM}_{B,0}}{\overline{MM}_B}\right)$

$$\frac{\partial C_{B,g,j}}{\partial t} = -\psi_B \frac{\partial T_{B,g,j} C_{B,g,7}}{\partial x} \qquad j = 7$$

Eqn. 4.50

$$\frac{\partial C_{B,s,j}}{\partial t} = \xi h (C_{B,g,j} - C_{B,s,j}) + G_{4j} r_{4,s} \qquad j = 1-3,6,7$$

Eqn. 4.51

The rate of change of concentration for the reformer species is given by Eqn. 4.52.

$$\frac{\partial C_{R,j}}{\partial t} = -\psi_R \frac{\partial \left(T_R C_{Rj}\right)}{\partial x} + \frac{G_{1j} r_1 + G_{2j} r_2}{\in_R} \qquad j = 1-5$$

Eqn. 4.52

Where $\psi_R = \frac{v_{R,0}}{T_{R,0}} \left(\frac{\overline{MM}_{R,0}}{\overline{MM}_R} \right)$

The energy balances of the burner gas phase, burner solid phase, wall and reformer are given in Eqn. 4.53 - Eqn. 4.56, respectively. The first term on the right hand side of Eqn. 4.53 - Eqn. 4.56 is based on Fourier's first law of conduction. The last term in each of the Eqn. 4.53, Eqn. 4.54 and Eqn. 4.56 is due to the heat transfer and chemical reaction terms. All the other terms in Eqn. 4.55 are due to convection of heat between the burner gas phase, solid phase, wall, reformer, and ambient.

$$\frac{\partial T_{B,g}}{\partial t} = -T_{B,g} \psi_B \frac{\partial T_{B,g}}{\partial x} + \frac{-\tau_B (T_{B,g} - T_{B,s}) \left(\frac{U_1}{h} + C_{gas} \right) - \frac{\pi_e}{\in_B} (T_{B,g} - T_e) + r_{4,g} \Delta H_4}{\overline{c}_{p,B,0} \overline{\rho}_B}$$

Eqn. 4.53

$$\frac{\partial T_{B,s}}{\partial t} = \frac{K_{cat,B} \frac{\partial^2 T_{B,s}}{\partial x^2} + \xi h \left(T_{B,g} - T_{B,s} \right) \left(\frac{U_1}{h} + C_{gas} \right) + \frac{2 f U_2}{s_B \left(1 - \in_B \right)} \left(T_W - T_{B,s} \right) + r_{4,s} \Delta H_4}{C_{cat,B}}$$

Eqn. 4.54

$$\frac{\partial T_W}{\partial t} = \frac{K_W \frac{\partial^2 T_W}{\partial x^2} + \frac{f}{s_W} \left[U_2 \left(T_{B,s} - T_W \right) + U_3 \left(T_R - T_W \right) \right] - \pi_e \left(T_W - T_e \right)}{C_W}$$

Eqn. 4.55

$$\frac{\partial T_R}{\partial t} = \frac{-\psi_R \frac{P_R}{R} \overline{c}_{P,R,0} \in_R \frac{\partial T_R}{\partial x} - \frac{2 f U_3}{s_R} \left(T_R - T_W \right) - \pi_e \left(T_R - T_e \right) + r_1 \Delta H_1 + r_2 \Delta H_2}{C_{cat,R} \left(1 - \in_R \right)}$$

Eqn. 4.56

The initial and boundary conditions for the partial difference equations are given in Eqn. 4.57 - Eqn. 4.63. The index '*j*' in the following equations, represents the species methanol (*j*=1), water vapour (*j*=2), carbon dioxide (*j*=3), carbon monoxide (*j*=4), hydrogen (*j*=5), oxygen (*j*=6), nitrogen (*j*=7).

$C_{R,j}(0,t) = C_{R,j,in}(t)$ for $j = 1-5$.

Eqn. 4.57

$$T_R(0,t) = T_{R,in}(t)$$

Eqn. 4.58

$C_{B,g,j}(0,t) = C_{B,g,j,in}(t)$ for $j = 1-3,6,7$

Eqn. 4.59

$$\left.\frac{\partial T_{B,s}(x,t)}{\partial x}\right|_{x=0} = 0$$

Eqn. 4.60

$$\left.\frac{\partial T_{B,s}(x,t)}{\partial x}\right|_{x=L} = 0$$

Eqn. 4.61

$$\left.\frac{\partial T_W(x,t)}{\partial x}\right|_{x=0} = 0$$

Eqn. 4.62

$$\left.\frac{\partial T_W(x,t)}{\partial x}\right|_{x=L} = 0$$

Eqn. 4.63

The Crank Nicolson scheme is a second order (in time and space) scheme and provides stability of solution over the implicit and explicit schemes. Crank Nicolson method is also unconditionally stable [105, 106]. The upwind discretisation for first order derivatives is used to provide better stability [105] of the numerical solution. The nonlinear partial differential equations were solved using Matlab® Version 7.5 (R2007b).

The discretisation done using upwind and Crank-Nicolson methods is described below for a partial differential equation given below:

$$\frac{\partial A}{\partial t} = \alpha \frac{\partial^2 A}{\partial x^2} + \beta \frac{\partial A}{\partial x} + A(x,t)$$

Eqn. 4.64

Using the Crank Nicolson method of finite differences, we have:

$$\frac{\partial A}{\partial t} = \frac{A_i^{n+1} - A_i^n}{\Delta t}$$

Eqn. 4.65

$$\frac{\partial^2 A}{\partial x^2} = \frac{\left(A_{i+1}^{n+1} - 2A_i^{n+1} + A_{i-1}^{n+1}\right) + \left(A_{i+1}^{n} - 2A_i^{n} + A_{i-1}^{n}\right)}{2(\Delta x)^2}$$

Eqn. 4.66

$$A(x,t) = \frac{A_i^{n+1}(x,t) + A_i^{n}(x,t)}{2}$$

Eqn. 4.67

The upwind discretisation for the first order derivative is described below:

$$\beta \frac{\partial A}{\partial x} = \beta \frac{\left(A_i^{n+1} - A_{i-1}^{n+1}\right) + \left(A_i^{n} - A_{i-1}^{n}\right)}{2\Delta x} \quad for\ \beta > 0$$

Eqn. 4.68

$$\beta \frac{\partial A}{\partial x} = \beta \frac{\left(A_{i+1}^{n+1} - A_i^{n+1}\right) + \left(A_{i+1}^{n} - A_i^{n}\right)}{2\Delta x} \quad for\ \beta < 0$$

The spatial discretisation of 50 points steps for a simulation time of 1000 seconds was applied to the model. This method allowed solving the complex partial differential equations with simplicity and the solution obtained is stable, however it was noted that the time step Δt had a significant impact on the temperatures of the reformer and burner. This is further discussed in the results section. The steps followed for the reformer-burner modelling is shown in Figure 4.21.

4.2.4. Results

Initially, the model was compared against the results obtained by Varesano et al [16]. The reformer model was then tested at various feed conditions to examine the effect of feed temperatures, steam-to-carbon ratio, load on the reformer and determine control parameters.

4.2.4.1. Validation of the model

The reaction mechanism described in this chapter is taken from validated sources of the literature [16, 103]. The results obtained from the simulation were validated against the results obtained by Varesano et al [16]. The feed conditions for validating the model are given below in Table 4-1.

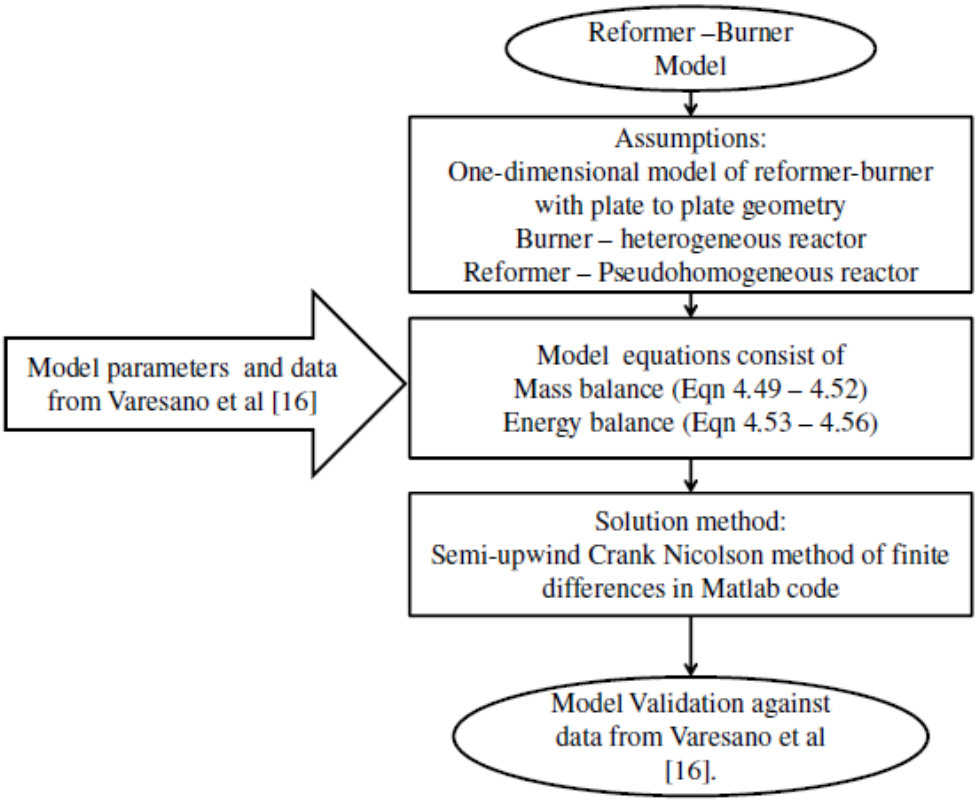

Figure 4.21- Reformer-Burner model flowchart

Table 4-1 – Feed Conditions

Feed Condition	Value	Unit
Methanol concentration in reformer	0.0325	$kmol/m^3$
Steam concentration in reformer	0.0487	$kmol/m^3$
Methanol concentration in burner	0.0054	$kmol/m^3$
Oxygen concentration in burner	0.0102	$kmol/m^3$
Nitrogen concentration in burner	0.0385	$kmol/m^3$
Feed temperature for reformer and burner	450	K

Figure 4.22 and Figure 4.23 show the steady state concentration distribution (expressed as percentage) in the reformer and temperature distribution in the reformer and burner, respectively. The temperatures and concentrations in the reformer and burner had reached steady state values within 1000 seconds of simulation. The time step used for the simulation was $\Delta t=1$. The methanol concentration drops from 40 % at the inlet to 1.3 % at the exit. Water vapour, carbon dioxide, carbon monoxide and hydrogen are 10.5 %, 21 %,

1.3 % and 65.7 % respectively. Varesano et al [16] obtained 13.7 % water vapour, 20 % carbon dioxide, 2 % carbon monoxide, 63.7 % hydrogen and 0.6 % methanol. Figure 4.22 shows the concentration profiles and the concentration values at the exit of the reformer.

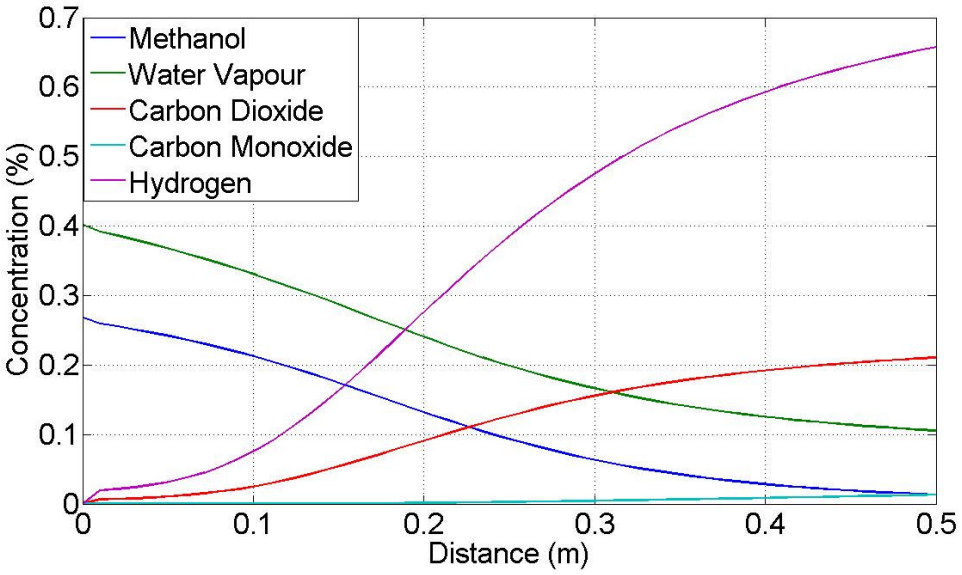

Figure 4.22 – Concentration percentages in the reformer

The temperature distribution along the length of the reactor obtained by the solution of the model is shown in Figure 4.23 while those reported by Varesano et al are in Figure 4.24. Results in Figure 4.23 show that the reformer achieves a maximum temperature of 574.5 K. The burner catalyst and wall temperature are almost equal while the burner gas phase shows a maximum temperature of 670 K. However, the temperature profiles evaluated from the model do not match with those reported by Varesano et al. The trends are similar but the burner gas temperature is only 670 K as compared to the 1100 K achieved by the model by Varesano et al. The reformer temperature rises above 550 K and occurs only after 0.15 m of the reactor length, while results in Figure 4.24 show temperature rise well within 0.1 m of the reactor length. This difference in the reformer temperature is because of the low burner gas temperature achieved by solution of the model.

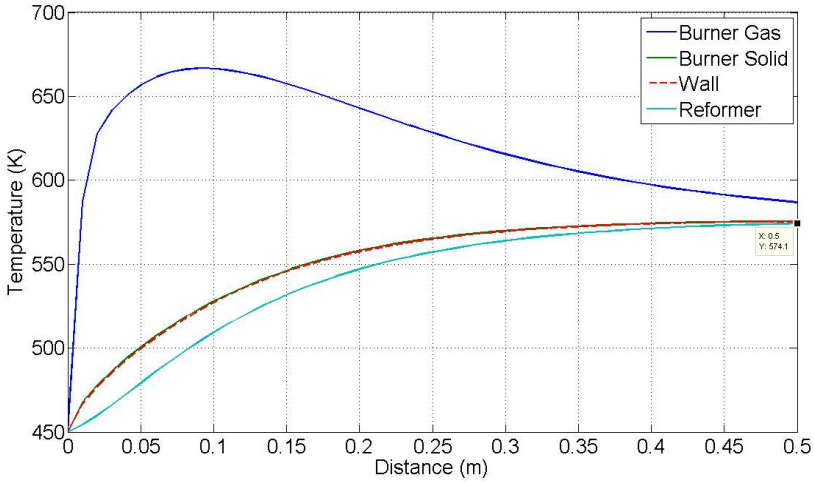

Figure 4.23 – Temperature profiles of burner and reformer for simulation time step $\Delta t=1$.

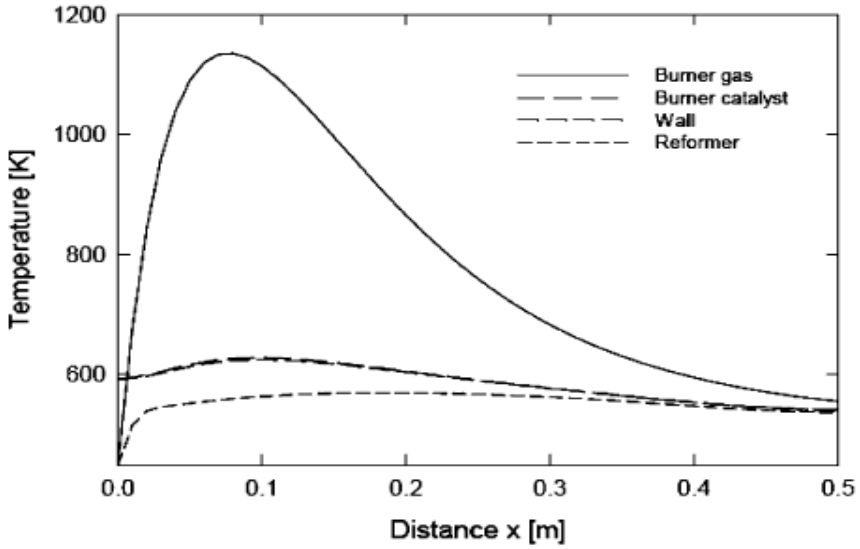

Figure 4.24 - Temperature profiles of burner and reformer obtained by Varesano et al [16].

It was noted that all temperatures in the reformer and burner increased when the step size of time in integration was reduced. Finally, when the time step for the simulation was reduced to $\Delta t=0.067$, the resulting temperature profiles for the reformer and burner were much higher and are shown in Figure 4.25. Any further reduction in the time step did not increase the temperatures indicating a stable solution. As seen, the peak burner temperature is in close agreement with that in Figure 4.24, but the burner catalyst, wall and reformer temperature are much higher. Temperatures above 573 K are not acceptable for this reformer, as it can cause catalyst de-activation [16].

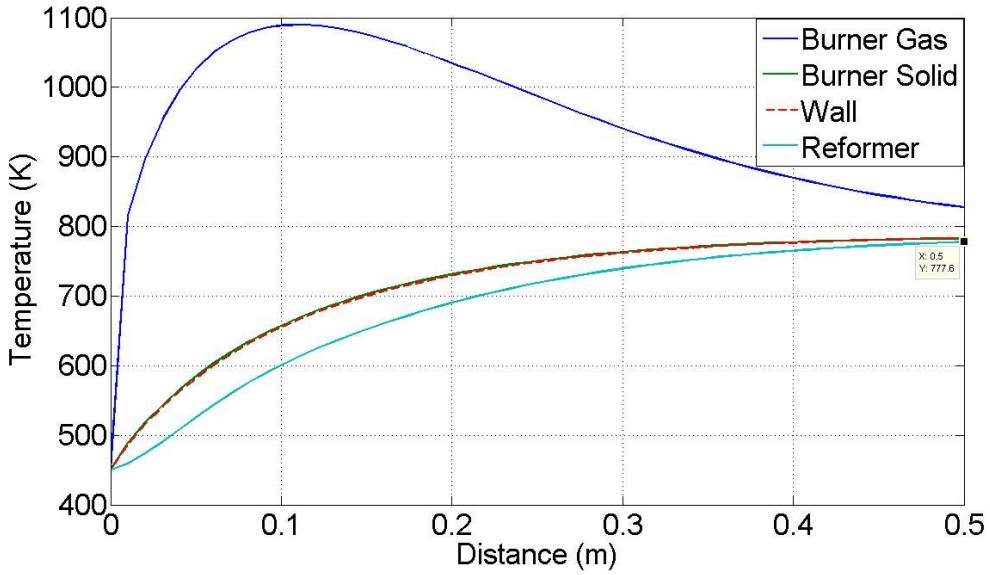

Figure 4.25 – Temperature profiles of burner and reformer for simulation time step Δt=0.067.

The results shown in Figure 4.22 and Figure 4.23 indicate that the reformer outputs are in close agreement with those reported in Varesano et al but the burner outputs do not agree. Some errors were noted in the paper by Varesano et al, which may have caused the disagreement in the results obtained. The errors in the paper and the assumptions made for the simulation are listed below:

- The catalyst pellet density given wrongly in the paper by Varesano et al [16] is 2 kg/m^3. This value affects the reaction rates of the steam reforming reaction significantly. The value was assumed to be 2000 kg/m^3 in this chapter.
- The term τ_B is incorrectly given as $\tau_B = \xi h\left(\frac{\varepsilon_B}{\varepsilon_B}\right)$ by Varesano et al which gave infinite values in the results. This term affects the heat transfer to the burner solid phase significantly. This term was assumed as $\tau_B = \xi h\left(\frac{1-\varepsilon_B}{\varepsilon_B}\right)$ for the simulation in this work.

Although the model does not predict accurate burner temperatures, for time step Δt=1 the model can still indicate factors that will influence control of the reformer but will be unable to quantify the effects of burner temperature on the reformer. Hence, further discussion includes the effects of varying feed conditions on the reformer performance. All simulation results presented in the following section are obtained by solving the model at time step Δt=1.

Figure 4.26 shows percentage conversion of methanol along the length of the reformer. The methanol conversion is given by Eqn. 4.69.

$$Methanol\ conversion = \frac{C_{CH3OH,x=0} - C_{CH3OH,x=L}}{C_{CH3OH,x=0}}$$

Eqn. 4.69

By 100 seconds of simulation time, the methanol conversion reached 40% and at 200 seconds it was 78%. After 400 seconds the methanol conversion achieved was 97.5%. Beyond 400 seconds, the conversion profiles were found to be constant.

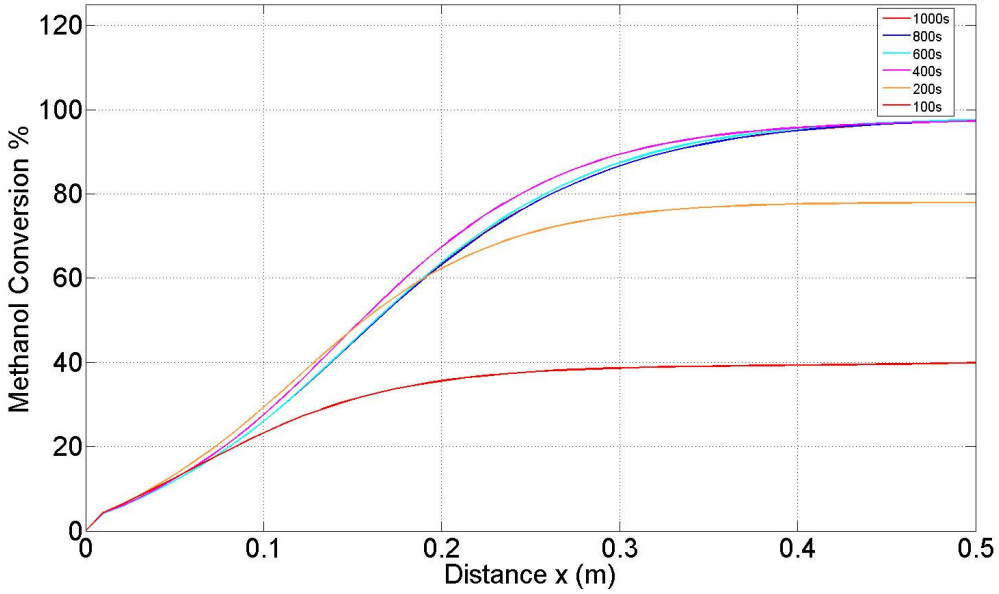

Figure 4.26 – Methanol Conversion along the length of the reactor at feed temperature of 450 K

The increase in reformer temperature at various simulation times is shown in Figure 4.27. The temperature exceeds the maximum allowable temperature of 573 K after 600 seconds. The catalyst in the last 0.1 m, where methanol conversion is highest and the temperature exceeds the recommended temperature is likely to be more degraded over a period of time. This tendency can be controlled by regulating the feed temperature of the flows to the reformer or by increasing the steam-to-carbon ratio.

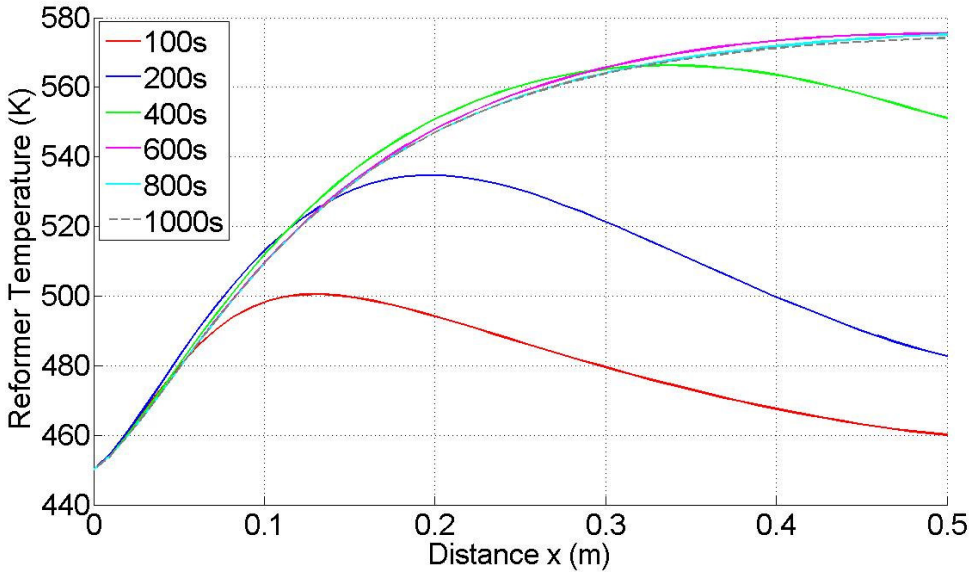

Figure 4.27 – Reformer temperature variation at various simulation times

From Figure 4.26 and Figure 4.27 it can be observed that almost 78 % of methanol conversion is achieved within 200 seconds with a maximum temperature of 540 K. These two figures show the temperature dependence of methanol conversion. The reformer, with a feed temperatures of 450 K can be expected to deliver reasonable amount of hydrogen to the fuel cell in around 200 seconds after starting up. Any unconverted methanol at this stage can either be re-circulated or fed into the SOFC to be reformed internally [15]. Figure 4.28 shows the concentration of gases in the reformer with time. For an initial temperature of 450 K for reformer and burner feed, the gases achieve steady state values after 400 seconds. For automotive applications 400 seconds is considerable amount of time for start-up. A conventional diesel fuelled vehicle would normally start-up within a couple of seconds. Before steady state is achieved for the reformer, the concentration of methanol will have a decreasing trend while that of hydrogen will be increasing. If the unused methanol as well as carbon monoxide is fed to the fuel cell along with hydrogen generated in the reformer, the fuel cell output is likely to be affected. Avoiding carbon deposits during this transient phase will be an important control parameter.

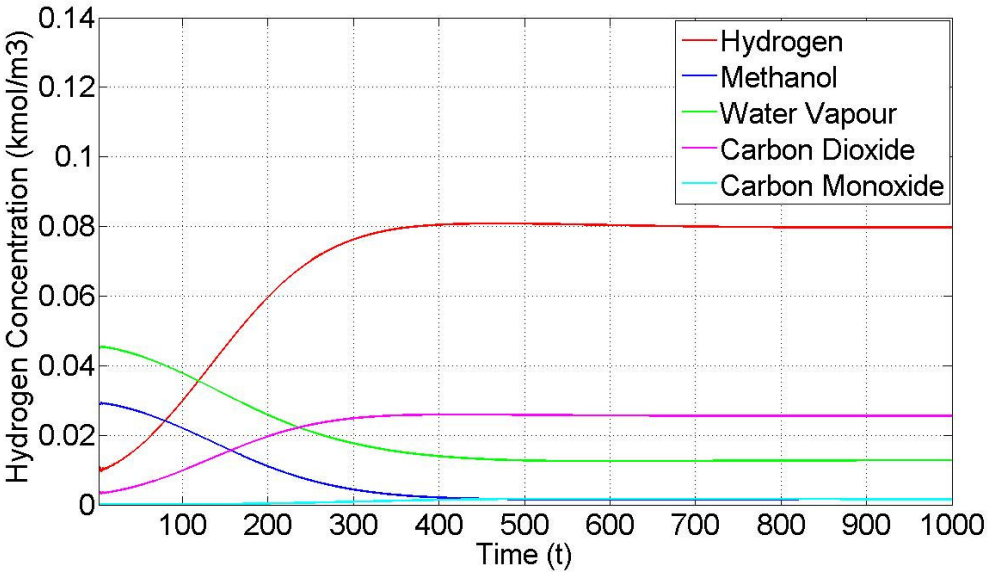

Figure 4.28 – Concentration variation in the reformer with time

For higher feed temperatures of 550 K, the methanol conversion is shown in Figure 4.29. It shows that 96.5 % of methanol conversion is achieved in 5 seconds, which reaches to 98.5 % in 50 seconds. A reformer operated at a higher feed temperature is more suitable for applications requiring fast start-up, however the temperature of the reformer must be regulated at all times to limit it below 573 K.

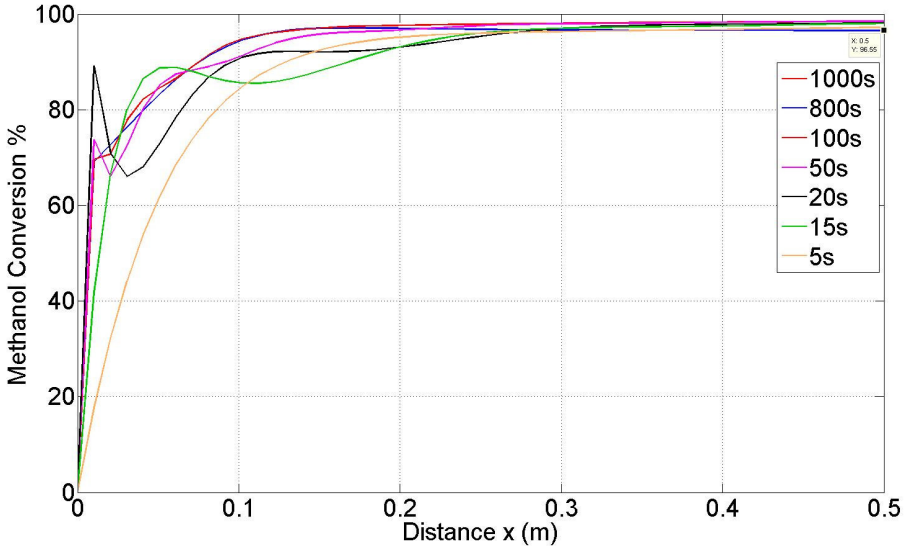

Figure 4.29 – Methanol conversion with initial feed temperature 550 K

4.2.4.2. Effect of changing feed temperature on reformer output

The model was tested for reformer feed temperatures of 450 K, 500 K and 550 K and its effects on the outputs were studied. In each case the steam-to-carbon ratio was 3 and the input concentrations of methanol and water vapour were maintained the same for all cases.

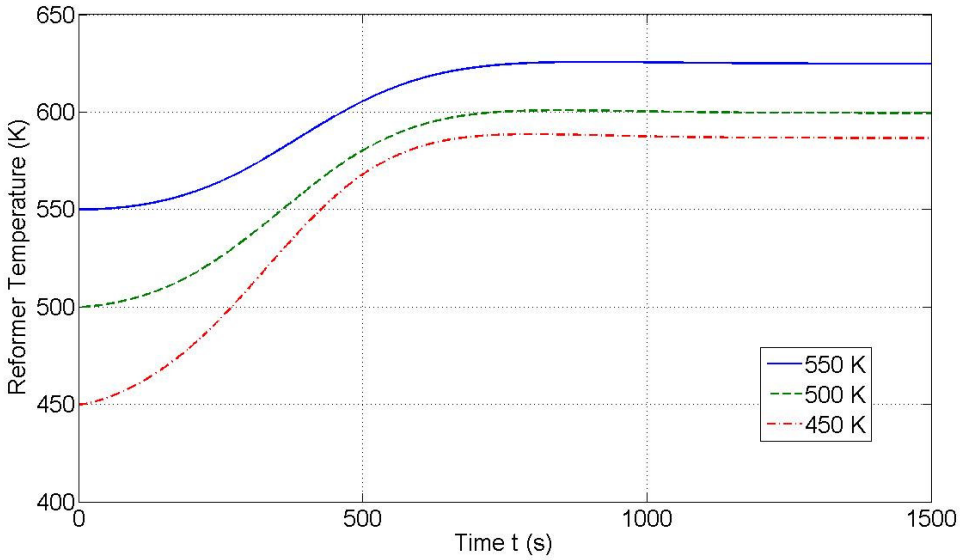

Figure 4.30 – Effect of changing feed temperatures on reformer temperature at the reformer exit.

Figure 4.30 shows the comparison of reformer temperatures at the exit of the reactor when the feed temperatures are 450 K, 500K and 550K. When the feed temperature is 450 K, the reformer achieves a maximum temperature of 575 K. When the feed temperature are 500 K or 550K the reformer temperature increases beyond 573 K which is the catalyst sintering limit. The reformer temperature depends on the heat supplied by the burner for the endothermic reactions to occur. Hence, to limit the temperature to a maximum of 573 K, the burner feed should be accordingly regulated when the reformer feed temperatures are 500 K and 550 K.

The production of hydrogen is dependent on the reformer temperature as can be seen from Figure 4.31. For the same input concentrations of methanol and steam, the higher the reformer feed temperature, higher is the hydrogen production. Since the concentration of hydrogen within the first 100 seconds is highest, when the reformer feed temperature is

550 K, a high feed temperature is desirable for automotive applications which typically require fast start up.

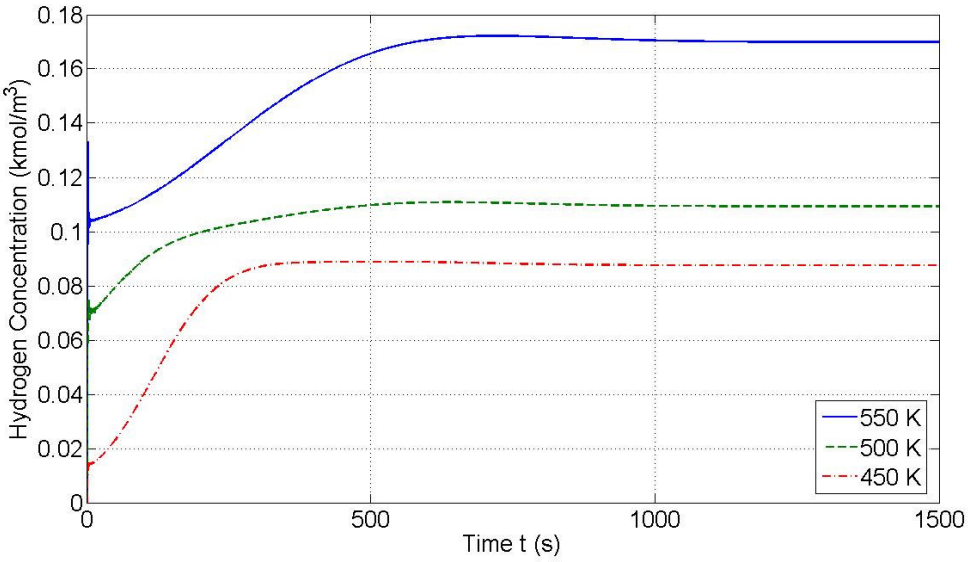

Figure 4.31 - Effect of changing feed temperatures on hydrogen concentration at the reformer exit.

The water vapour concentration at the reformer exit is shown in Figure 4.32. For a higher reformer feed temperature, the figure shows an increased water vapour consumption. The water vapour concentration in the reformer affects the methanol conversion. The effect of steam-to-carbon ratio is further discussed in the following section.

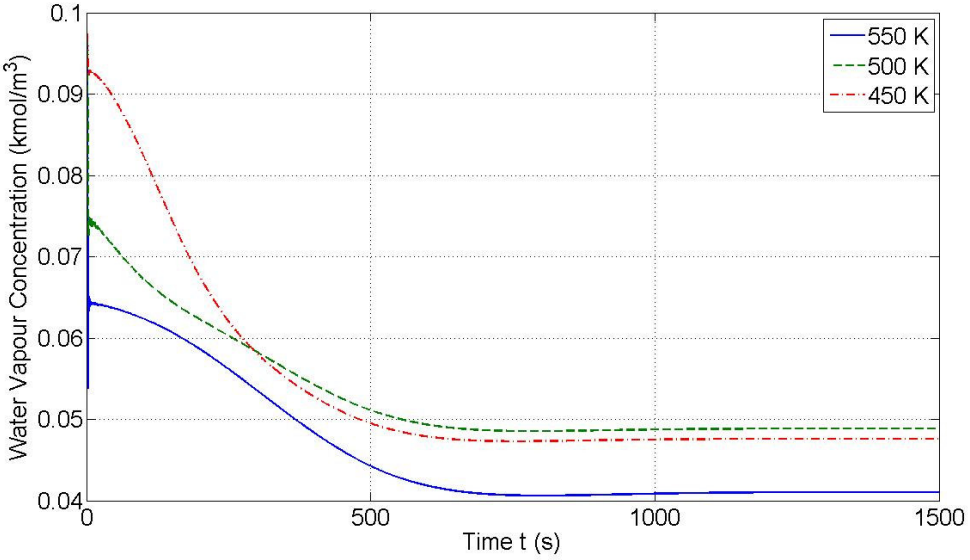

Figure 4.32 - Effect of changing feed temperatures on steam-to-carbon ratio at the reformer exit.

Figure 4.33 shows that the methanol conversion when the reformer feed temperatures are changed. At 550 K, the methanol conversion reaches a maximum within 0.15 m of the reactor length. For 500 K and 450 K the methanol conversion reaches a maximum only after 0.25 m of the reactor length, indicating a faster dynamic response of the reformer at 550 K. The methanol conversion is highly temperature dependent and can achieve higher values if the reformer temperature is well controlled.

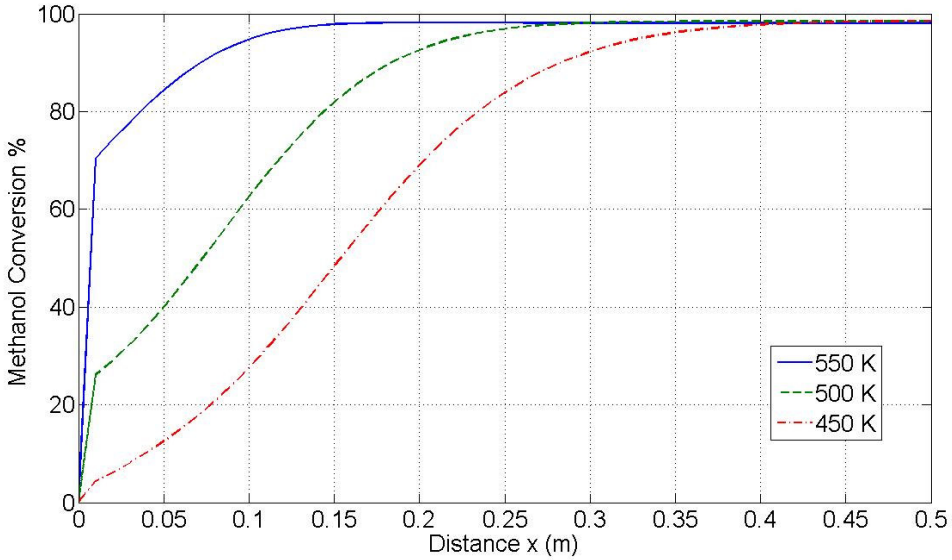

Figure 4.33 - Effect of changing feed temperatures on methanol conversion at reformer exit.

The temperature of the reformer must achieve a value high enough to allow maximum methanol conversion in a short period of time and at the same time must not exceed the catalyst sintering temperature limit. Hence, the reformer temperature is an important control parameter.

4.2.4.3. Effect of changing steam-to-carbon ratio on reformer output

The steam-to-carbon ratio in inlet is varied every 1000 seconds for feed temperatures of 450 K and 550 K. The dotted lines in Figure 4.34 - Figure 4.37 show the steam-to-carbon ratio at the reformer exit for feed temperatures of 550 K. Figure 4.34 shows negative values for steam-to-carbon ratio at the reformer exit from 0-1000 seconds for feed temperature of 450 K and 0-5000 seconds when feed temperature is 550 K. The negative

values indicate that all the steam supplied is consumed. The figure also shows that the steam consumption is higher at higher feed temperatures.

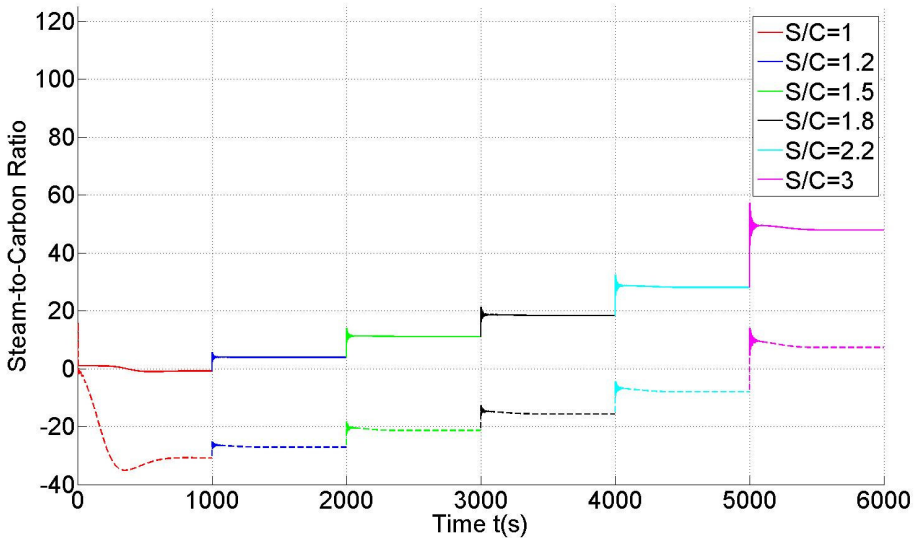

Figure 4.34 – Steam-to-carbon ratio variation at reformer exit

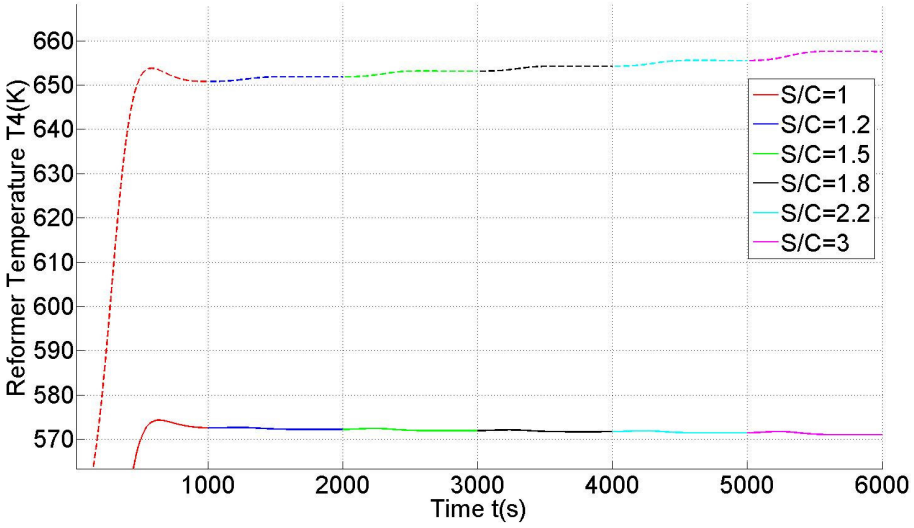

Figure 4.35 – Effect of varying steam-to-carbon ratio on reformer temperature

Figure 4.35 shows the effect of increasing steam-to-carbon ratio on reformer temperature. At 550 K feed temperature (shown with the dotted line), the reformer temperature increases with increasing steam-to-carbon ratio, while for feed temperature of 450 K (shown with the solid line), the reformer temperature decreases with increasing steam-to-carbon ratio. This could be attributed to the fact that Eqn. 4.37 and Eqn. 4.38 are both endothermic reactions. At a feed temperature 550 K, the steam-to-carbon ratio is negative

for 0-5000 seconds indicating insufficient steam for reaction described in Eqn. 4.37 to proceed. Hence, only the reaction for methanol decomposition (Eqn. 4.38) will occur. The total thermal energy provided from the burner supports only one reaction causing the reformer temperature to rise with increasing steam-to-carbon ratio. On the other hand, at feed temperature of 450 K, the reformer temperature drops only slightly with each increment of the steam-to-carbon ratio. In this case, the thermal energy provided to the reformer from the burner supports both, methanol steam reforming and methanol decomposition reactions causing the reformer temperature to remain between 572-575 K.

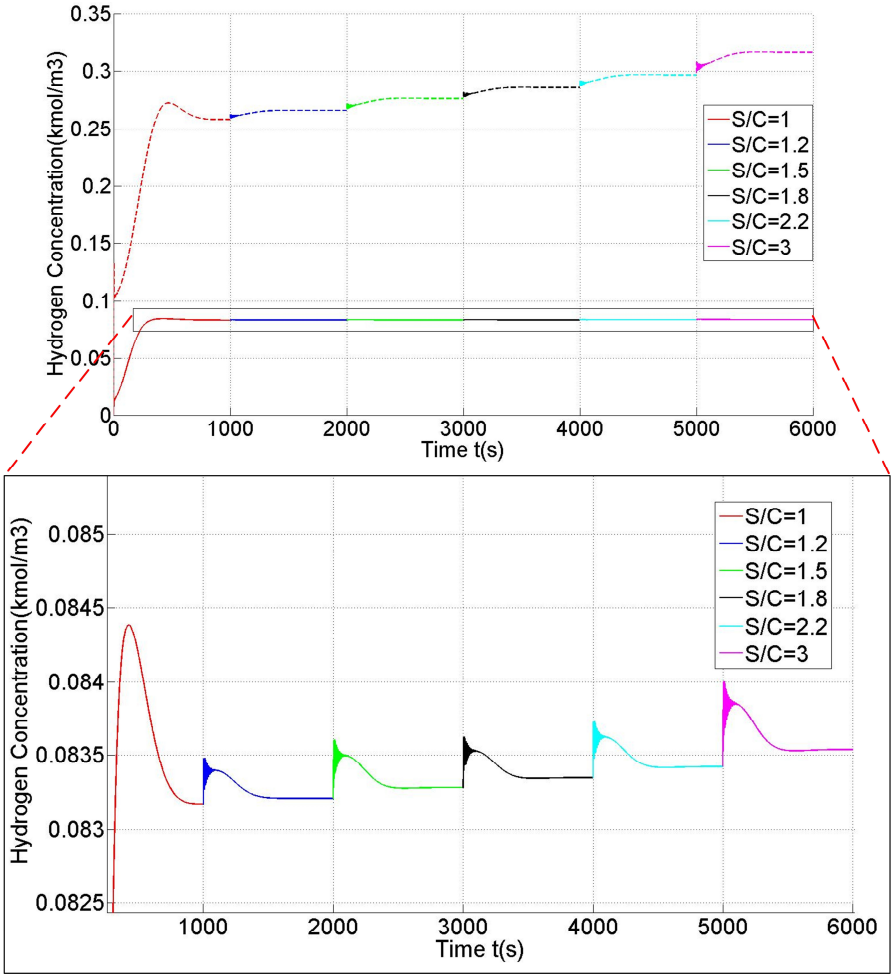

Figure 4.36 – Effect of varying steam-to-carbon ratio on hydrogen concentration

Figure 4.36 shows that increase in steam-to-carbon ratio causes the hydrogen concentration to increase. A high steam-to-carbon ratio is hence favourable for production of hydrogen. The methanol conversion profile at a feed temperature of 550 K (shown with the dotted line) with increasing steam-to-carbon ratio is shown in Figure 4.37. The methanol

conversion at the reformer exit decreases rapidly with increasing steam-to-carbon ratio at feed conditions. As previously described, at 550 K, insufficient steam causes only the methanol decomposition reaction (Eqn. 4.40) to occur, hence a decrease in methanol conversion. At 450 K feed temperature (shown with the solid line), the methanol conversion is higher than that at 550 K feed temperature, because of methanol conversion occurring due to both the reactions in Eqn. 4.37 and Eqn. 4.38.

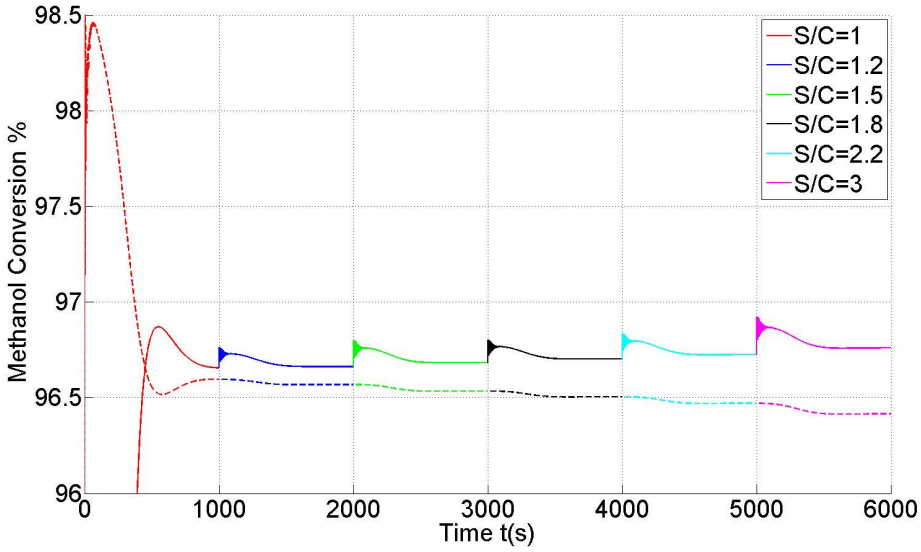

Figure 4.37 – Effect of varying steam-to-carbon ratio on methanol conversion

Hence, it can be observed that steam-to-carbon ratio regulation is important to ensure high methanol conversion. When sufficient steam is provided for the reforming reaction to occur, the reformer temperature may be regulated by increasing the steam-to-carbon ratio.

4.2.4.4. Effect of changing loads on reformer output

In order to examine the effect of changing loads, i.e. demand for hydrogen (by the fuel cell), on the reformer, the methanol concentration in the feed to the reformer is varied. The methanol feed is 0.0325 kmol/m^3 at 0 seconds, 0.0585 kmol/m^3 at 1000 seconds and 0.0487 kmol/m^3 at 2000 seconds. The water vapour is proportionately increased to ensure the same steam-to-carbon ratio at feed conditions. The feed temperatures are maintained at 550 K. The burner feed conditions will also significantly alter the reformer outputs. The temperature rise in the burner gas directly affects the reformer temperature and

consequently the methanol conversion. The burner feed conditions must regulated in proportion to the load on the reformer to ensure that the reformer temperature does not exceed its catalyst sintering limit.

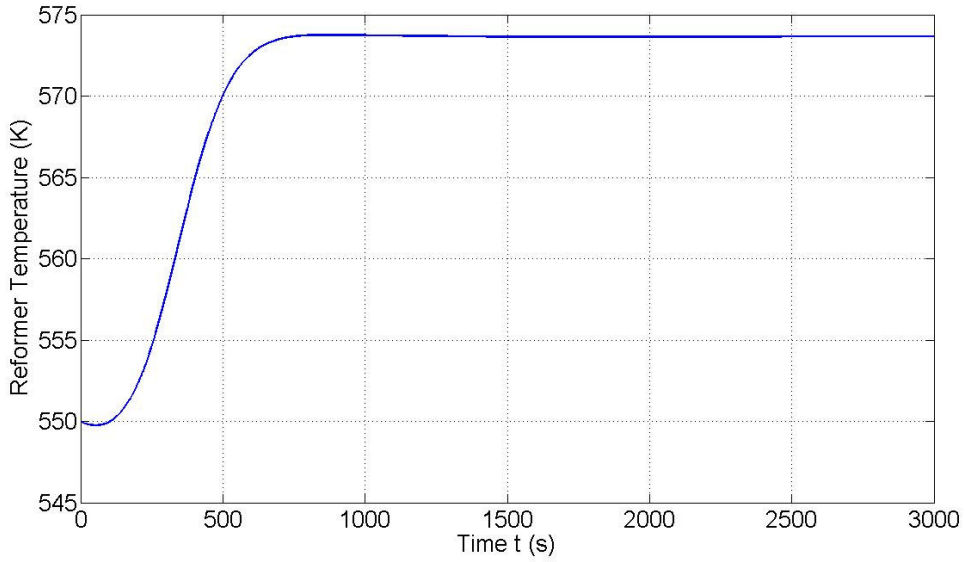

Figure 4.38 - Effect of varying reformer load on reformer temperature

Figure 4.38 shows the effect on the reformer temperature is negligible when the reformer load changes. Once the reformer reaches its maximum temperature, the reformer temperature remains almost constant for changing loads.

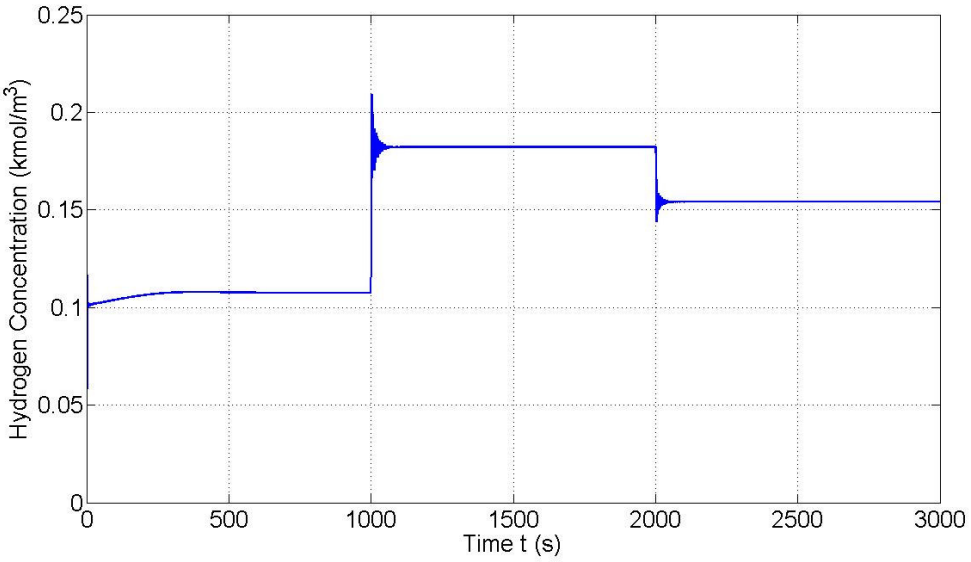

Figure 4.39 – Effect of varying reformer load on hydrogen concentration

The hydrogen production shown in Figure 4.39, being dependent on the reformer temperature (Figure 4.38), shows a slow dynamic response until the reformer temperature reaches its peak value. With any increase or decrease in load, the hydrogen production response is rapid and achieves its final value in about 60 seconds.

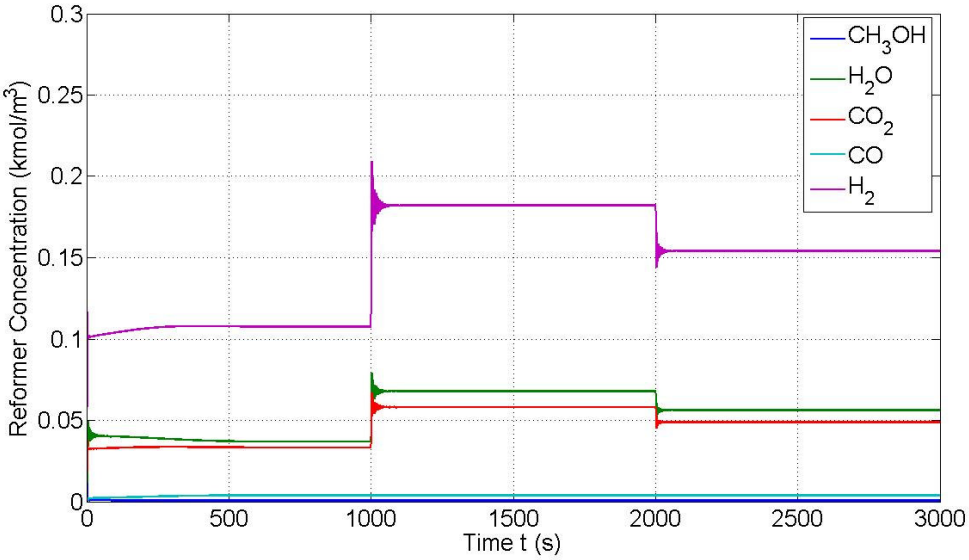

Figure 4.40 - Effect of varying reformer load on reformer species concentration

Similarly, the production of the other species in the reformer show a similar response to that of hydrogen production in Figure 4.40.

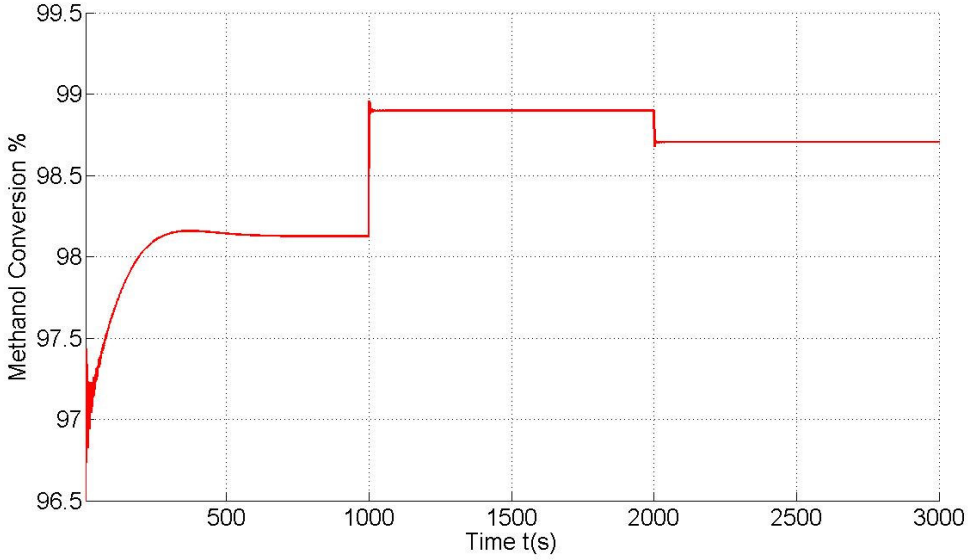

Figure 4.41 - Effect of varying reformer load on methanol conversion

Figure 4.41 shows the response of methanol conversion with changing reformer loads. Between 0-1000 seconds, the methanol conversion, which is dependent on the reformer temperature, shows slow dynamics until reformer temperature achieves a steady state value. Thereafter, the methanol conversion follows the load changes very effectively. It can be noted that the response of the reformer to changing loads depends on the reformer temperature.

4.2.5. Summary

The reformer model developed was tested to examine the output response of concentrations and temperatures in the reformer-burner unit with varying feed conditions and load changes. Although validation was not achieved for the burner temperatures, the concentration of species at the exit of reformer were in close agreement with the paper by Varesano et al [16]. The model is able to predict the effects of changes to feed conditions to the reformer. The results allow understanding of the distribution of species in the reformer, temperature dependence of reactions in the reformer and burner, and the main control parameters. A higher feed temperature is desirable for fast start-up of the reformer.

The model shows 96.5 % of methanol conversion in 5 seconds at feed temperatures of 550 K as compared to 98 % methanol conversion in 600 seconds for feed temperatures of 450 K. Increasing the reformer feed temperature results in increased in better methanol conversion and increased hydrogen production. The steam-carbon ratio affects the methanol conversion and a high value is desired. Hydrogen produced at the outlet of the reactor is dependent on the temperature dynamics. Once the reformer reaches its operating temperature, any change in load demand on the reformer thereafter, results in a faster response for hydrogen production.

The main control loops for the reformer-burner will involve the following:

- Regulation of steam-to-carbon ratio to ensure maximum methanol conversion.
- Regulation of reformer temperature to ensure maximum methanol conversion and to avoid catalyst degradation.
- Regulating the burner feed conditions in proportion to the load requirement on the reformer.

4.3. *IC Engine*

4.3.1. Introduction

The IC engine has been widely applied for propulsion and power generation. The most visible application is in the automotive sector. The automotive industry has thrived on this invention since the first mass produced cars emerged . Depending on the technology choice and engine size, the IC engine has efficiencies in the range of 25-40%. Since the late 1960s, there has been substantial investment by the automotive engine industry in emissions control technologies to meet a wave of legislation. There is progressive shift in technology from conventional engine systems to novel propulsion systems such as electric hybrids which can have lower emissions and improved system efficiencies.

This chapter describes the combustion modelling for the IC engine to operate with effluents from the fuel cell and reformer as described in the system configuration in Chapter 2 (The System and its Attributes). The system proposed involves a hybrid system with the load shared by the engine and the fuel cell. The engine and the fuel cell system are coupled via exhaust flows along with load distribution. The conventional operation of the diesel fuelled engine is significantly changed when fed with effluents from the fuel cell and the reformer. The role of the engine and the effects on its operation due to the specific system configuration are also discussed in this chapter. The purpose of the fuel cell system, besides sharing the load on the system is to condition the engine fuel such that the pollutants and fuel consumption are minimised.

The focus of this combustion modelling is to evaluate the effect of introducing effluents from the fuel cell and reformer in the engine, on the pollutants. The fuel cell stack, while supplying effluents to the engine for conditioning its fuel and inlet charge, also produces electric power. The fuel cell is operated at a steady base load while the engine is operated only when the load requirement is higher than that supplied by the fuel cell. Such a configuration of load distribution avoids the operation of the engine at very low and idle load conditions when emissions are high and fuel economy poor.

4.3.2. The effects of EGR and dual fuel operation

Stricter emission constraints have resulted in various techniques for emission reduction. Nitrogen oxide (NOx) emission regulations are severe and diesel passenger cars are

restricted to 0.18g/km of NOx emissions as per the EURO 5 emission standards [107]. NOx emissions can be controlled by a combination of EGR, after-treatment and in-cylinder emission reduction techniques. One promising in-cylinder method uses homogeneous charge compression ignition (HCCI) operation. Other techniques include water injection and hydrogen substitution. The effects of EGR and hydrogen substitution are discussed below.

4.3.2.1. Exhaust Gas Recirculation

Exhaust gas recirculation is a technique used in the diesel engine to reduce NOx emissions. The hot burned gases from the engine exhaust are cooled and fed back into the engine cylinder to dilute the charge. The effects of EGR on the engine as described by Maiboom et al [108] as also listed below:

- Thermal effect due to higher specific heat capacities of carbon dioxide and water vapour.
- Chemical effect caused by dissociation of carbon dioxide and water vapour resulting in different combustion behaviour.
- Dilution effect which is reduction in oxygen concentration in the engine, slowing the mixing of fuel and oxygen.
- Increase in soot formation
- Increase in ignition delay

As discussed in other sources of literature [54-57], the effect of various EGR concentration has different effects on combustion, emissions and engine outputs. The determination of the exact effects of such mixtures on the engine combustion, emissions and power output is complex and requires an experimental evaluation.

The exhaust from the fuel cell cathode consists of depleted oxygen and nitrogen. Introducing this oxygen depleted air in the engine inlet charge, results in a reduction of oxygen fraction in the total engine charge. The effects of oxygen displacement in the engine have been discussed by Ladommatos et al [55]. The replacement of the oxygen fraction by gases of similar heat capacities to oxygen is done by Ladommatos et al [55]. Oxygen displacement in the engine charge results in an ignition delay, increased PM and CO emissions. Dilution does not significantly affect the engine output power and efficiency but affects combustion and emissions [55]. The authors also observed a reduction of NOx and increase in PM concentrations.

Carbon dioxide addition (at oxygen fractions of 17.3 as discussed in [55]) results in lower NOx emissions and causes thermal, chemical and dilution effects in the engine. These effects are described further by Ladommatos et al [56]. The chemical effects of CO_2 addition causes its dissociation which results in the reduction of NOx and particulates. The thermal effect due to its higher specific heat capacity has the least effect on emissions. The dilution effect is achieved by replacing oxygen in the charge by carbon dioxide which results in ignition delay with increased particulate matter emissions. The dilution and chemical effects of CO_2 are more prominent than the thermal effect on the engine emissions. The chemical effect, which is caused by dissociation of carbon dioxide, results in the reduction of NOx up to 10 percent. This effect also reduces the particulate matter emissions caused by the dilution effect [56].

As described by Ladommatos et al [54] conventional EGR consists of a higher amount of carbon dioxide as compared to water vapour resulting in a more prominent effect on combustion and consequently emissions. When water vapour and carbon dioxide are introduced in the engine in equal amounts, the water vapour is more effective in reducing NOx emissions but causes an increase in particulate and smoke emissions [54]. As indicated by Ladommatos et al [54], EGR use in diesel engines is achieved by displacing the inlet charge with recirculated gases, resulting in lowering of NOx emissions but increase in PM and smoke due to reduced oxygen concentration in the inlet charge. The authors in [54] suggest that, using EGR in a way such that the oxygen concentration in the engine remains the same and introducing EGR as additional charge to the inlet air can reduce NOx as well as maintain low PM and smoke emissions. This technique of introducing EGR as additional charge is analogous to the that adopted in the engine simulations discussed in the following sections.

EGR is normally cooled before being fed back into the engine. The use of hot EGR results in an increased combustion temperature leading to formation of NOx [58]. Cooled EGR also improves the volumetric efficiency of the engine and allows more inlet charge to be inducted into the engine.

Based on the results and conclusions of the work discussed by Ladommatos et al [54-58], the use of fuel cell exhausts along with the reformer exhausts can clearly function as a

source of external EGR supplied as an additional charge to the fresh air supply to the engine.

The introduction of effluents from the fuel cell system in the engine has two effects. First, the combustion in the cylinder is modified. The second effect is the elimination of the conventional EGR valve from the engine exhaust system. The exhaust gases from the fuel cell and the exhaust gas from the reformer (except hydrogen which is fed to the fuel cell) form a source of gases which is similar in composition with normal recirculated exhaust gas. The conventional EGR system for an engine is difficult to control as compared to an externally supplied mixture which can be regulated directly. The air-path control of the engine with the VGT vane position and EGR valve position is complicated because of the interaction of the flow paths for the EGR and VGT in the exhaust manifold, nonlinear behaviour of turbochargers and common shaft between the compressor and turbine [109]. In contrast, the externally supplied inert gases or external EGR greatly simplifies the control requirement.

4.3.2.2. Dual fuel effects in the engine

A number of studies on dual fuelled IC engines have been conducted. The purpose of using dual fuels in the engine can be to reduce emissions, develop a fuel flexible engine or reduce operating costs. Hydrogen introduction with diesel has been studied mainly for emission and performance improvements of the engine [12-14, 110, 111] . In the recent years, biofuels have been introduced into IC engines in small quantities in order to lower the dependence on conventional fossil fuels and reduce carbon dioxide emissions.

The work reported by Mathur et al [14] describes the effect of hydrogen substitution in the diesel engine. The hydrogen substitution was based on the equivalent fuel energy. The results show that the increase in hydrogen substitution up to 20 % results in increasing thermal efficiency and decrease thereafter. The efficiency loss and the power loss is nominal up to 38 % of hydrogen substitution after which there is rapid loss along with knocking behaviour [14]. Effect of diluents such as helium, nitrogen and water vapour to counter the efficiency loss, power loss and knocking behaviour was examined by the authors. The results described previously [14] indicate that nitrogen dilution showed improvement in efficiency, power and prevented knocking when it was maintained at 30 %

by volume of hydrogen used. Water dilution allowed hydrogen substitution of up to 66 % without adverse effects on the engine.

The effects of hydrogen induction in a diesel engine include the reduction of smoke emissions but increased NOx emissions [13]. Effects of diluents such as helium, nitrogen and water on the emissions were examined by Mathur et al [12]. Water as a diluent resulted in negligible smoke emissions and lowest NOx levels as compared to the other two diluents [13]. Nitrogen as a diluent was better for engine performance while water as diluent is better for emission reduction [12].

Hydrogen and diesel duel fuel tests were conducted by injecting hydrogen and inducting hydrogen by Masood et al [110]. The results show that the induction of hydrogen through the inlet manifold created a homogenous mixture causing faster and complete combustion even at low loads. The pressure and heat release rate were higher when hydrogen was inducted as compared to that with injection of hydrogen. With an increase in hydrogen percentage, the trends showed decrease in NOx formation. This was attributed to the increase in water vapour concentration which reduced the peak temperatures. The NOx formation tendency is greater with inducted hydrogen than injected due to higher heat release [110].

The effect of hydrogen as a secondary fuel for a diesel engine with EGR was examined by Saravanan et al [111]. The addition of hydrogen without EGR resulted in decrease in carbon monoxide, HC and smoke emissions whereas the NOx concentrations were lowest when the EGR was 25 % [111].

Based on the experimental results discussed by [12-14, 108, 110, 111], the effect of hydrogen addition causes increased NOx emissions and requires diluents to counter performance losses and emissions. The work on EGR composition by Ladommatos et al [54] describes the use of EGR as additional charge rather than charge substitution. Based on these results from literature, it is propose that the hydrogen from the fuel cell anode can be inducted into the engine up to a marginal value of 20 %, which prevents knocking behaviour and performance degradation. The increase in NOx due to the hydrogen inducted in the cylinder can be countered by nitrogen, water vapour, and carbon dioxide exhausts from the fuel cell cathode as well as the reformer. The unused oxygen from the

fuel cell cathode is also fed to the engine. This oxygen from the fuel cell and that from the air inducted from the engine compressor ensure the concentration of oxygen is above stoichiometric requirements.

The fuel cell is operated at an utilisation factor below one to avoid fuel starvation in the fuel cell. The hydrogen from fuel cells is often recirculated within the fuel cell or used in a combustor to produce hot exhaust gas to drive a turbine. However, the addition of hydrogen even in small quantities can improve the engine performance and reduce pollutants [12-14, 110, 111].

4.3.2.3. NOx emission formation

Exhaust gas recirculation is a technique used to dilute the charge in the engine cylinder with inert gases. The inclusion of these inert gases in the cylinder helps in reduction of combustion peak temperature. The formation of oxides of nitrogen (NOx) emissions is dependent on the peak combustion temperature.

The term 'NOx' emissions includes nitric oxide (NO) and nitrogen dioxide (NO_2). The source of nitrogen in the engine is from the air inducted and/or from the nitrogen present in fuel. The formation of NOx emission can be described by the following principle equations called the Zeldovich mechanism [112].

$$O + N_2 = NO + N$$
$$N + O_2 = NO + O$$
$$N + OH = NO + H$$

Eqn. 4.70

These reactions occur at around 2000 K [112]. The peak combustion temperature directly affects the formation of NOx emissions. The use of diluents or cooled EGR can lower peak combustion temperature and results in lower NOx emissions. The following section discusses the use of fuel cell and reformer effluents as externally supplied EGR.

The aim of this section is to determine the effects of the following, on engine operation and pollutants

- Substitution of part of the engine fuel by the hydrogen available from the fuel cell exhausts

- Hydrogen substitution along with charge dilution by water vapour and oxygen depleted air available from the fuel cell exhausts
- Hydrogen substitution along with charge dilution by water vapour and oxygen depleted air available from the fuel cell exhausts and carbon dioxide, carbon monoxide and water vapour from the reformer exhausts.

In addition, the effect of the effluents at various engine speeds on the pollutants is examined and means of controlling emissions are proposed. The main control variables for developing a control system will also be identified.

4.3.3. Chemkin Model and Reaction Mechanism

The combustion within the engine is modelled using the software Chemkin-PRO developed by Reaction Design. The engine model is a zero-dimension homogenous reactor model. The governing equations for this model are given below [113]. The mass balance for the engine is given below.

$$\frac{d(\rho V)}{dt} = \dot{m}_{in} - \dot{m}_{out} + A_m \dot{s}_k M_k$$

Eqn. 4.71

The volume available for combustion is a function of time and given below.

$$\frac{V(t)}{V_c} = 1 + \frac{C-1}{2}\left[R + 1 - \cos\theta - \sqrt{R^2 - \sin^2\theta}\right]$$

Eqn. 4.72

The time derivative of the volume is given by Eqn. 4.73.

$$\frac{d(V/V_c)}{dt} = \Omega\left(\frac{C-1}{2}\right)\sin\theta\left[1 + \frac{\cos\theta}{\sqrt{R^2 - \sin^2\theta}}\right] \text{ where } \Omega = \frac{d\theta}{dt}$$

Eqn. 4.73

Eqn. 4.74 gives the energy balance for the engine.

$$\frac{dU_t}{dt} = \dot{m}_{in}\sum_{k=1}^{n} Y_{k,in} h_{k,in} - \dot{m}_{out}\sum_{k=1}^{n} Y_{k,out} h_{k,out} - Q_{loss} + Q_{source} - P\frac{dV}{dt}$$

Eqn. 4.74

The term Q_{source} represent the energy deposited into the gas in the reactor. The heat loss (Q_{loss}) from the cylinder walls by convection is computed by the software package with input of wall temperature and coefficients a, b, c for the equation given below

$$Nu = a.\mathrm{Re}^{b}\ \mathrm{Pr}^{c}$$

Eqn. 4.75

Where *Nu* is the Nusselt number for heat transfer, Re is the Reynolds number and Pr is the Prandtl number. The values for coefficients *a*, *b* and *c* are obtained from Heywood [112]. Woschini's correlation relates the gas mean velocity to the piston mean velocity and to the pressure rise during combustion [113], given in Eqn. 4.76. It gives a more accurate estimation of the average gas speed

$$w = \left[\left(C_{11} + C_{12}\frac{v_{swirl}}{\overline{S}_p}\right)\right]\overline{S}_p + C_2\frac{V_d T_i}{P_i V_i}\left(P - P_{motored}\right)$$

Eqn. 4.76

$$\frac{P_{motored}}{P} = \left(\frac{V}{V_{ref}}\right)^{\gamma}$$

Eqn. 4.77

Where C_{11}, C_{12},C_2 are modelling parameters, v_{swirl} is the swirl velocity, $\overline{S}_p$ is the mean piston speed, $P_{motored}$ is the motored cylinder pressure, V_d is the displacement volume.
The data input for the engine model in Chemkin consists of thermodynamic data of species and reaction mechanism data for the combustion. The molar fractions of the species with the cylinder are specified by the user. The input parameters for the engine model are given in the below in Table 4-2.

The characteristics of n-heptane combustion are similar to those of diesel. Hence, n-heptane reaction mechanism is used in the combustion model. This reaction mechanism was developed by Lawrence National Livermore Laboratory [114]. The n-heptane reaction mechanism does not include a mechanism for NOx formation. Hence, the mechanism for combustion of natural gas, developed by the Gas Research Institute (GRI) [115] has been combined with the n-heptane combustion mechanism. The GRI mechanism includes formation of NOx emissions and the combined reaction mechanism has 181 species and 1747 reactions.

Table 4-2 – Model input parameters

Parameter	Value	Units
Engine compression ratio	16	-
Engine cylinder clearance volume	87.5	cm^3
Engine connecting rod to crank radius ratio	3.5	-
Starting crank angle	-147	deg
Heat transfer correlation		
coefficient a	0.35	-
coefficient b	0.7	-
coefficient c	1	-
Chamber bore diameter	115	mm
Wall temperature	500	K
Woschini's Correlation of average cylinder gas velocity		
C_{11}	2.28	-
C_{12}	0.308	-
C_2	0.00324	-
Ratio of swirl velocity to mean piston speed	1	-
Air/Fuel Ratio	25	-
Engine Speed	1500	RPM
Inlet temperature	315	K

4.3.4. Methodology

In order to evaluate the effect of effluent addition on the engine, three cases with 5%, 15% and 20% of hydrogen substitution (based on equivalent energy) in the engine cylinder were examined. The engine simulation for each of these cases was tested for combustion with the following fuel and charge compositions:

- N-heptane and air
- N-heptane and air + hydrogen
- N-heptane and air+ hydrogen + fuel cell effluents (water vapour, oxygen depleted air)
- N-heptane and air+ hydrogen+fuel cell effluents (water vapour, oxygen depleted air)+reformer effluents (water vapour, carbon dioxide, trace values of carbon monoxide)

All three cases were examined at the same air-fuel ratio, and engine speed as given in Table 4-2. The fuel cell was operated at full load while the engine load is varied in each case from 100% in Case 1, to 34% in Case 2 and 25% in Case 3. The test conditions are shown in the Table 4-3.

Table 4-3 – Test conditions

	Case 1	**Case 2**	**Case 3**
Engine load %	100	34	25
Fuel cell load %	100	100	100
Hydrogen % in engine	5	15	20
EGR % (effluents from reformer and fuel cell)	10.2	27.2	35.1

Further, the effect of addition of these effluents in the engine at various speeds was investigated and possible means to lower emissions have been discussed. The steps involved the developing the engine model are given in Figure 4.42.

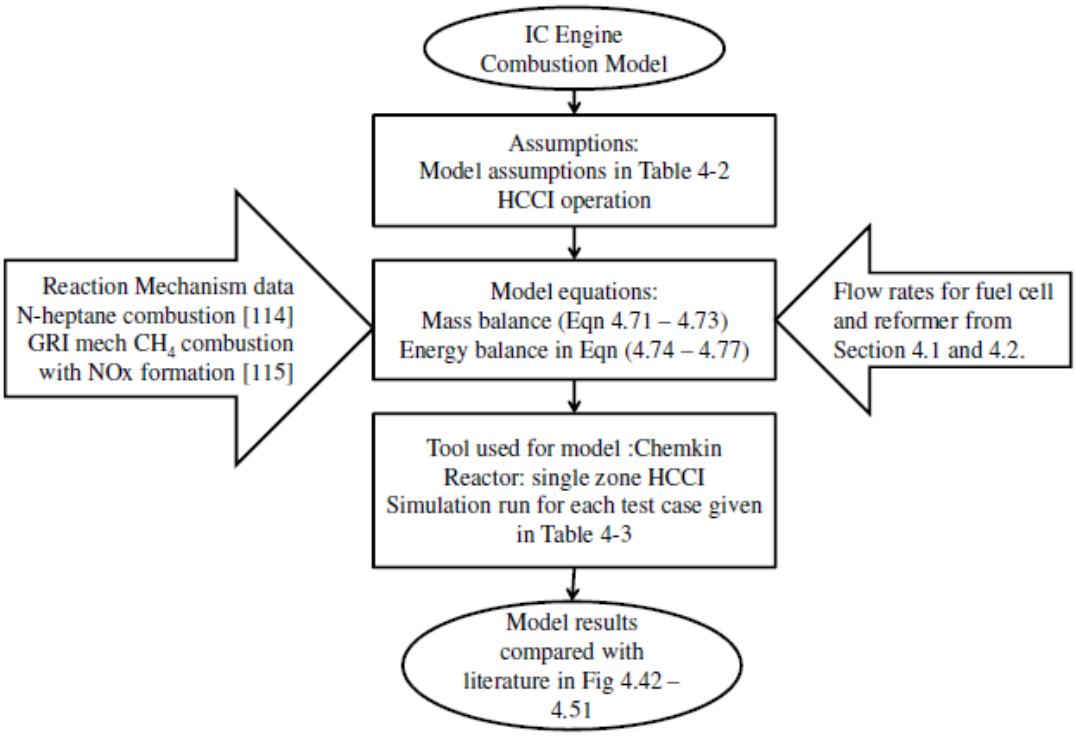

Figure 4.42 – Engine combustion model flowchart

4.3.5. Results

The results obtained by simulating various external EGR and hydrogen levels in the engine model are described in this section.

4.3.5.1. Effect of hydrogen and effluents from fuel cell and reformer on engine operation and emissions

Figure 4.43 to Figure 4.45 show the pressure, temperature and NOx emissions for each cases given in Section 4.3.4. It was observed in all three cases, that the addition of hydrogen to the cylinder with n-heptane resulted in increased peak pressure, temperature and NOx emissions. The increase in NOx emissions on addition of hydrogen is consistent with the results obtained by Mathur et al [13]. The dependence of NOx emissions on the peak temperature in the cylinder is also observed in these figures.

When the engine is supplied with hydrogen along with other effluents from the fuel cell (which acts as a source of external EGR), water vapour, oxygen depleted air, the peak pressure and temperature reduce. As a result, the NOx emission levels are lower than those produced by n-heptane combustion.

Further addition of effluents from the reformer along with effluents from the fuel cell results in an ignition delay, much lower peak pressure, temperature and NOx emissions. These NOx emissions range from 0.5-3.6% of those produced by combustion of n-heptane. The reformer effluents include carbon dioxide and water vapour which begin to dissociate at high temperatures [56]. Carbon dioxide has a higher specific heat capacity than atmospheric air and results in a reduced flame temperature and an ignition delay [56]. The introduction of water vapour in the engine inlet charge results in decreased peak gas pressure and temperature, significant reduction in NOx and an increase in unburned hydrocarbons [57]. The results obtained in Figure 4.43 to Figure 4.45 reflect the effects of NOx reduction and ignition delay as described in references [54, 56, 57]. N-heptane shows a dual stage ignition and the effect was observed in all the three cases. The induction period between the two stages increases with the addition of external EGR in all three cases.

The NOx emissions for the three cases when supplied with external EGR, were 29.8 ppm, 45.6 ppm, and 6.3 ppm for Case 1,2 and 3 respectively. The highest NOx emissions were for Case 2 when the hydrogen percentage in the cylinder was 15% and the engine was operating at 34% of its full load capacity. This indicates that the percentage of hydrogen supplied for the engine load condition is high and/or the EGR percentage is low. Increasing the EGR percentage or reducing the hydrogen percentage may result in lower NOx emissions.

In order to supply 15% of hydrogen to the engine, the fuel cell was simulated at an utilisation factor of 66%. The external EGR supplied was 27%. The effluents from the fuel cell and reformer depend on the fuel cell load as well as the hydrogen supplied to the engine. As a result, there is a limit on the fraction of external EGR that can be supplied to the engine cylinder in each case. The maximum possible external EGR that could be supplied to the engine, for full load operation of the fuel cell at 66% utilisation factor, for Case 2 was limited to 27%. Additionally, the composition of the external EGR may be manipulated by choosing to introduce effluents from either the fuel cell or the reformer or both. However, the manipulation of composition of the EGR will add to the complexity of the control system.

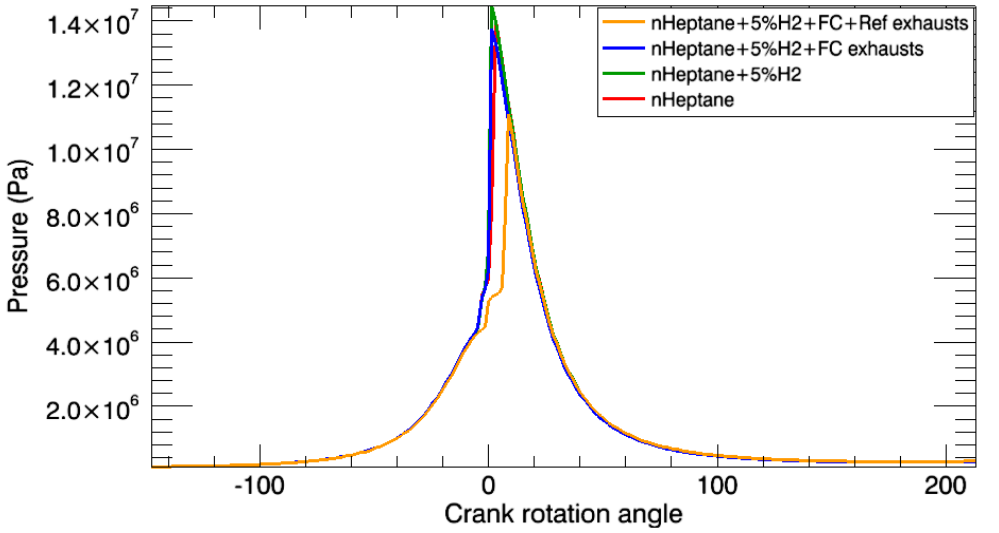

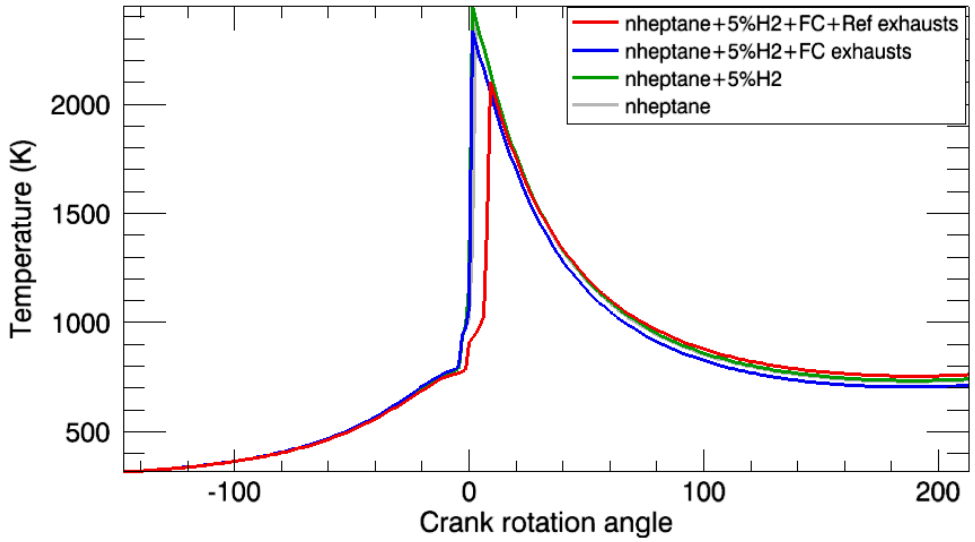

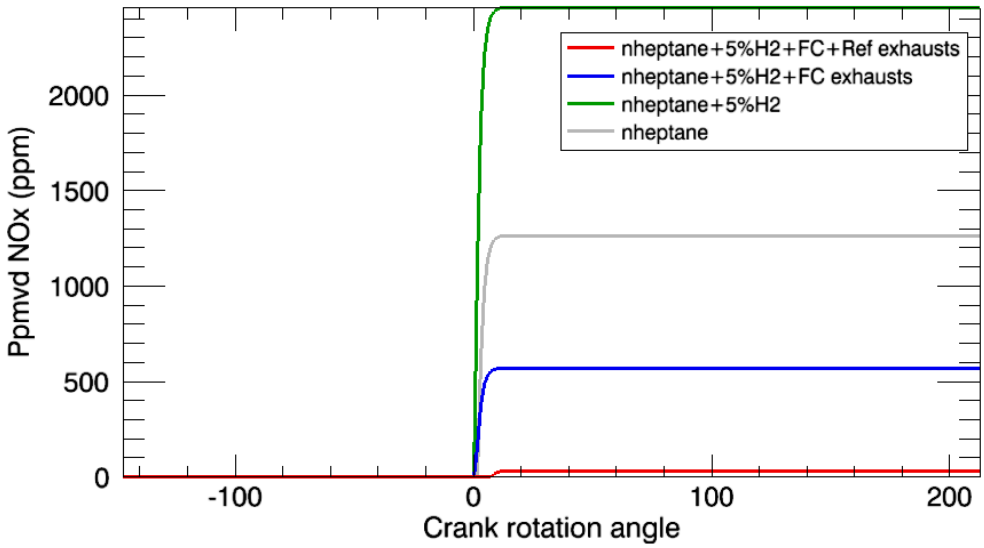

Figure 4.43 – Case 1 – Pressure, Temperature, NOx emissions

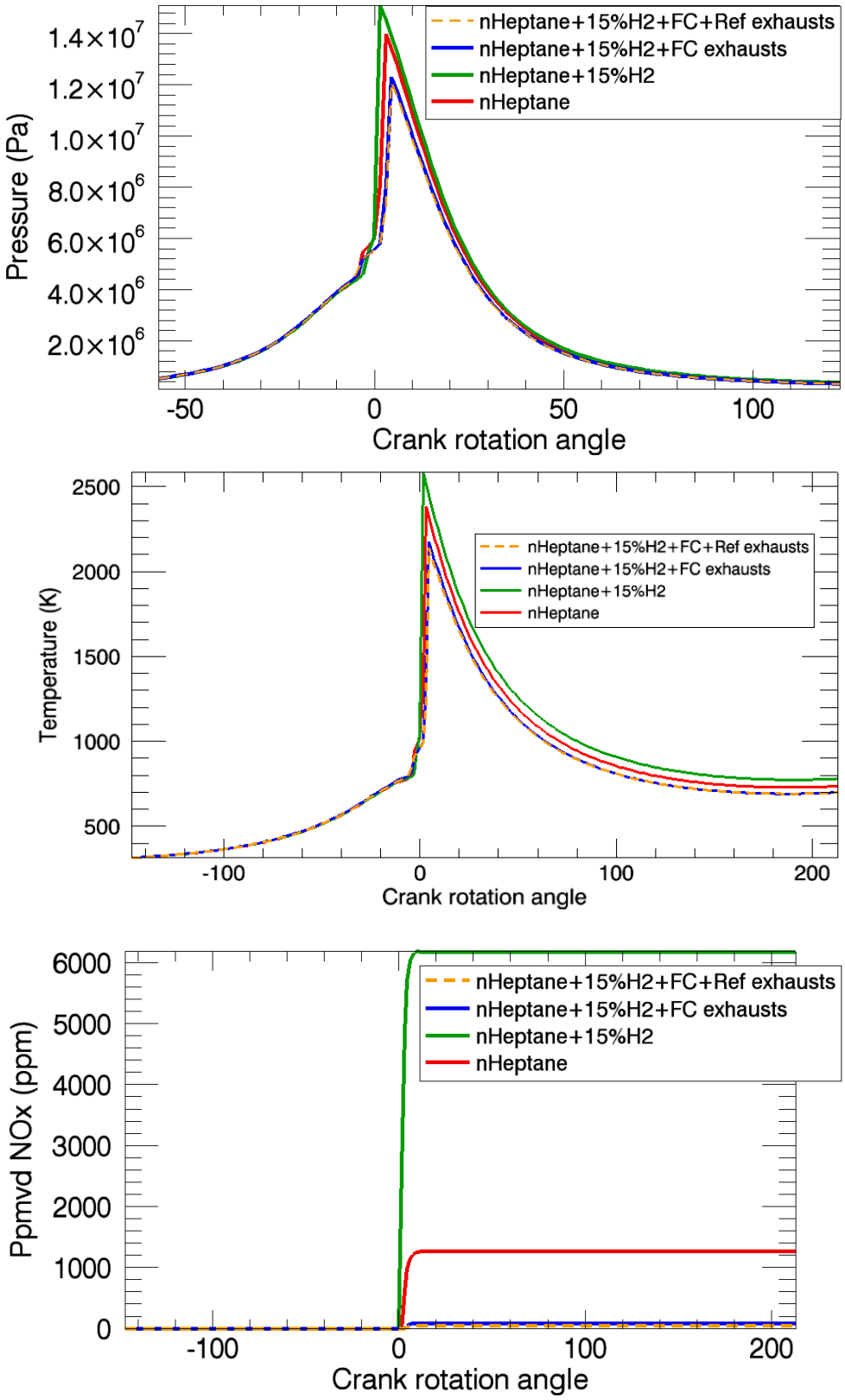

Figure 4.44 – Case 2 – Pressure, Temperature, NOx emissions

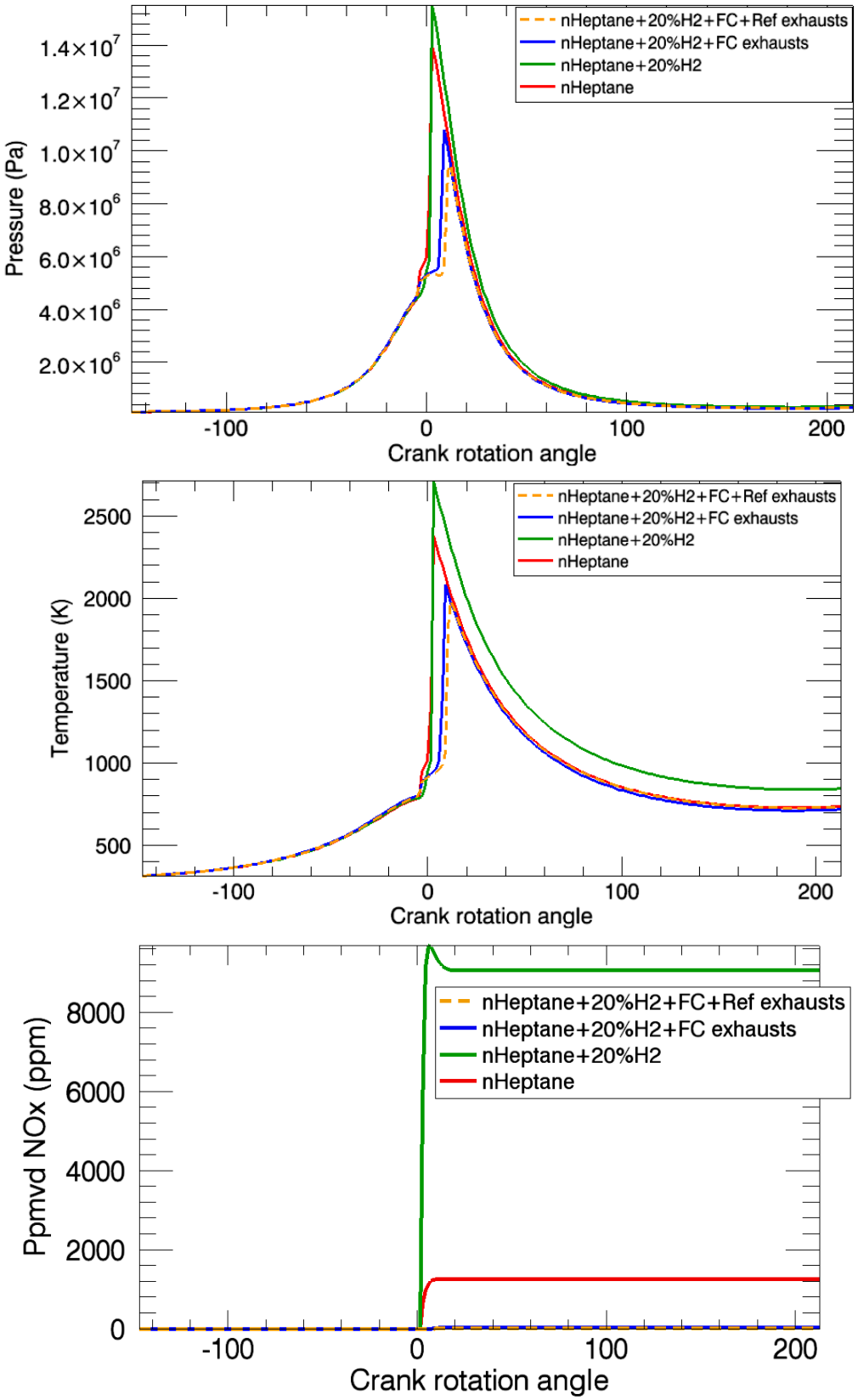

Figure 4.45– Case 3 – Pressure, Temperature, NOx emissions

4.3.5.2. Effect of engine speed on emissions

The effect of engine speeds from 1500 RPM – 3000 RPM was examined for Case 1, when the hydrogen was 5%, and effluents from fuel cell and reformer were supplied to the engine. The engine simulation is that of a single zone combustion model. The time taken for the ignition of the species within the cylinder is dependent on the reaction rates and independent of the engine speed. However, as the engine speed increases, the piston travels faster from the top dead centre to the bottom dead centre, reducing the engine cycle duration and the ignition timing is delayed. A dual stage ignition is observed at 1500 RPM and the second stage of ignition for speeds above 1500 RPM does not occur. Since the cylinder temperature at speeds above 1500 RPM does not exceed 1000 K, there are no NOx emissions, but the carbon monoxide and unburned hydrocarbon emissions are very high. Comparing the results in Figure 4.43, it is observed that the ignition delay is introduced when effluents from the reformer are also fed to the engine. At high speeds, it may be advisable to introduce the effluents only from the fuel cell to prevent an ignition delay.

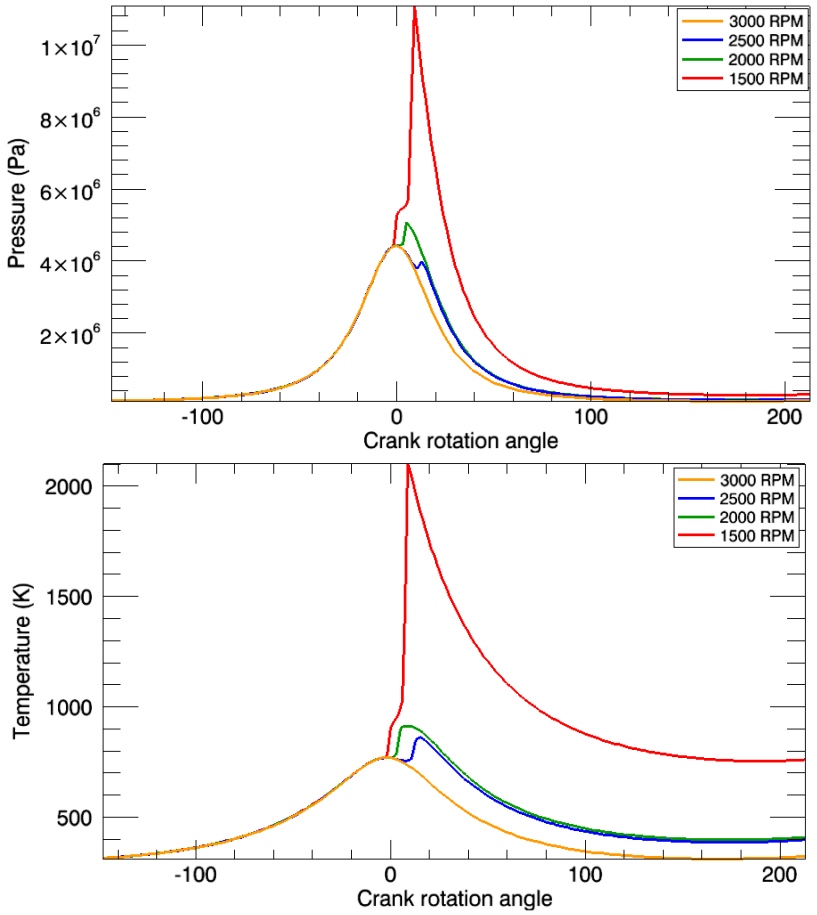

Figure 4.46– Effect of speed variation on cylinder pressure and temperature

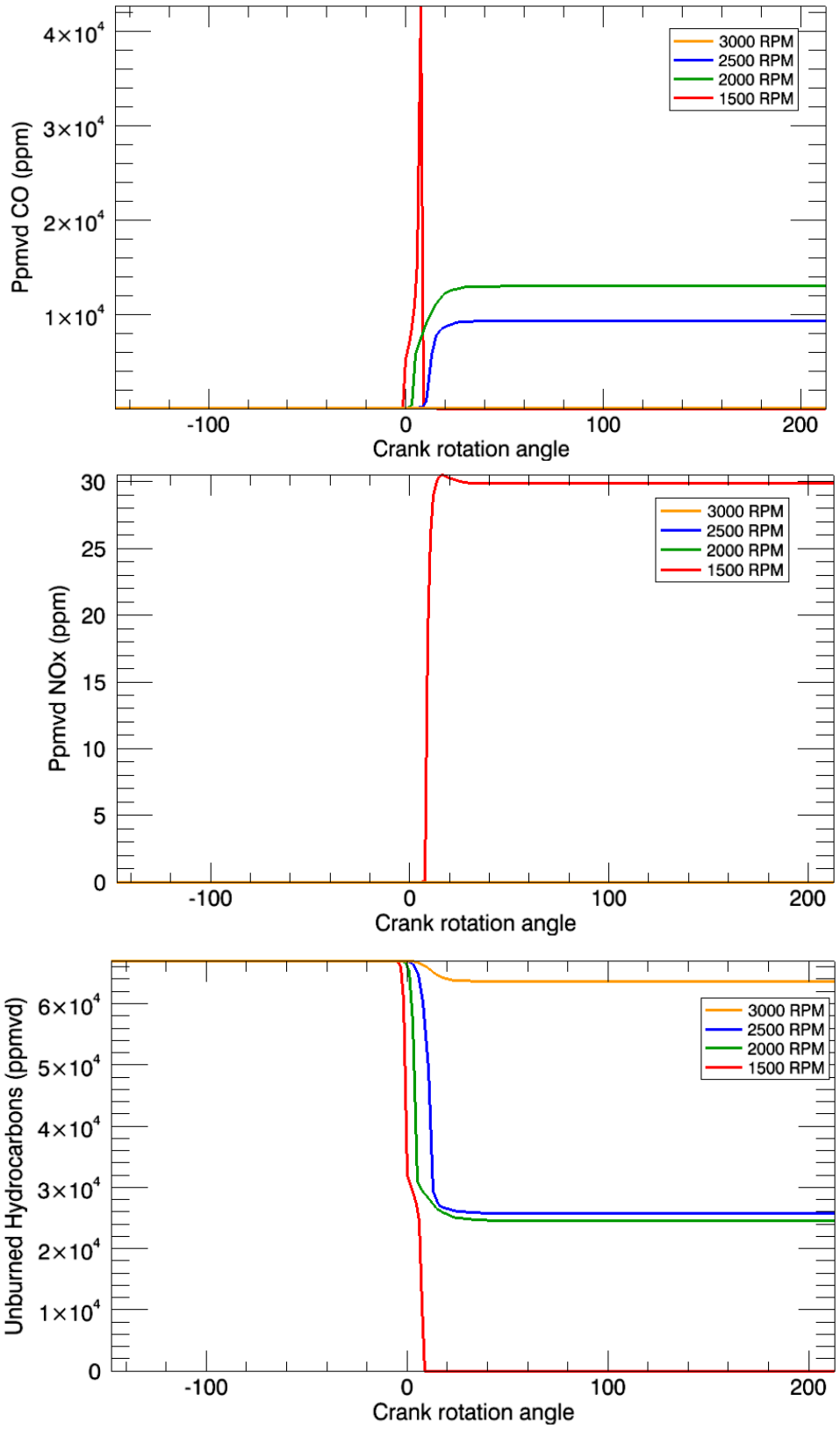

Figure 4.47- Effect of engine speed variation on emissions

4.3.5.3. Effect of external EGR composition at various engine speeds on emissions

As seen in Figure 4.46 and Figure 4.47, increasing engine speed results in an ignition delay and incomplete combustion. In order to reduce the ignition delay, the effluents from only the fuel cell are added in the engine. The pressure and temperature levels indicate a sharp rise during the ignition. The emission levels indicate that a complete combustion has occurred at all speeds except 3000 RPM.

It is particularly noted that for 2500 RPM engine speed, the second stage of ignition occurs after a significant delay as compared to lower speeds. At 3000 RPM, the temperature is lower than that at other speeds with high unburned hydrocarbons and carbon monoxide emissions.

As discussed earlier, water vapour and carbon dioxide together can cause ignition delays, by inhibiting the peak pressure and temperature in the cylinder. This effect is undesirable at high speeds and hence effluents from only the fuel cell should be used. These effluents from the fuel cell will still function to counter the NOx emissions produced by adding hydrogen to the engine cylinder.

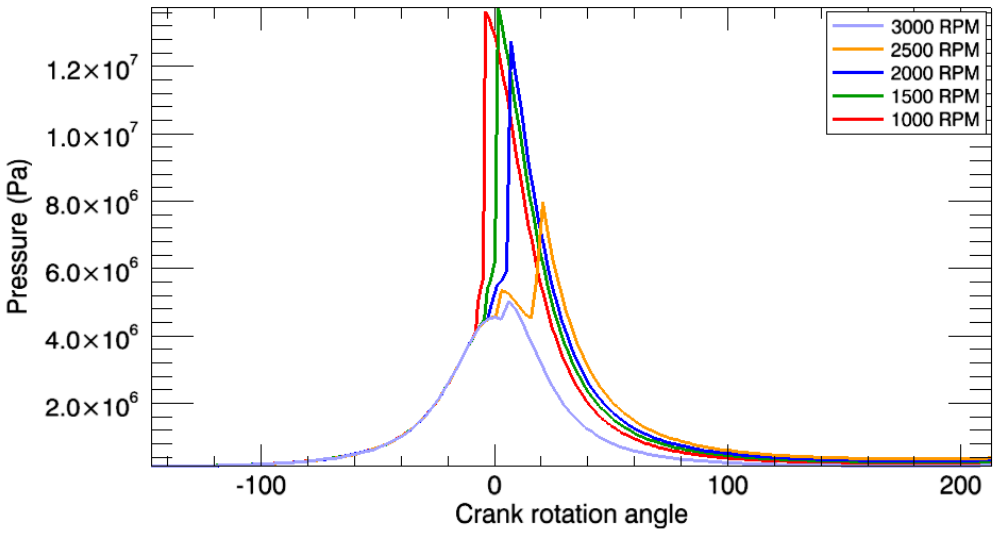

Figure 4.48 – Effect of external EGR composition at varying engine speeds on cylinder pressure

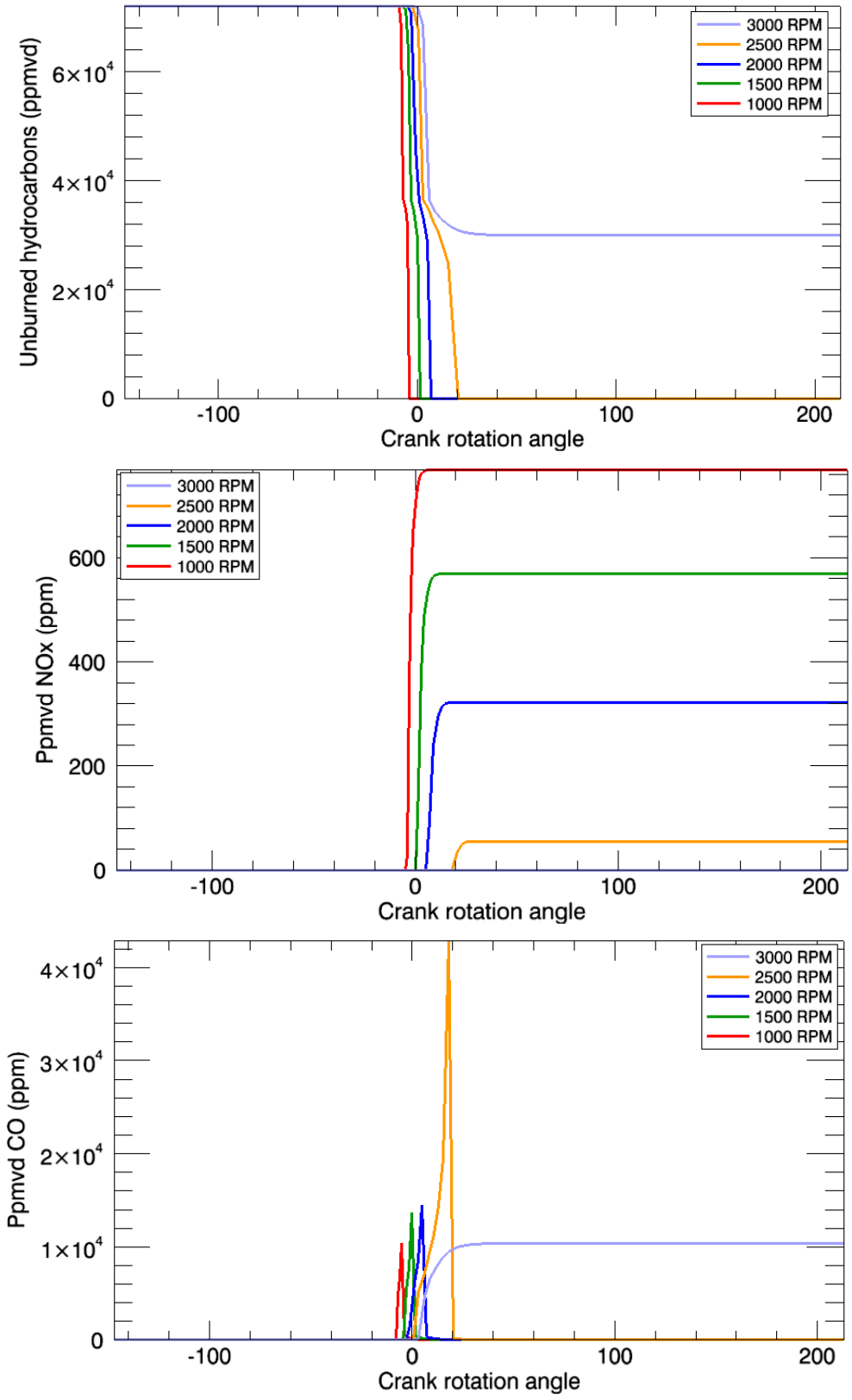

Figure 4.49 – Effect of external EGR composition at varying engine speeds on emissions

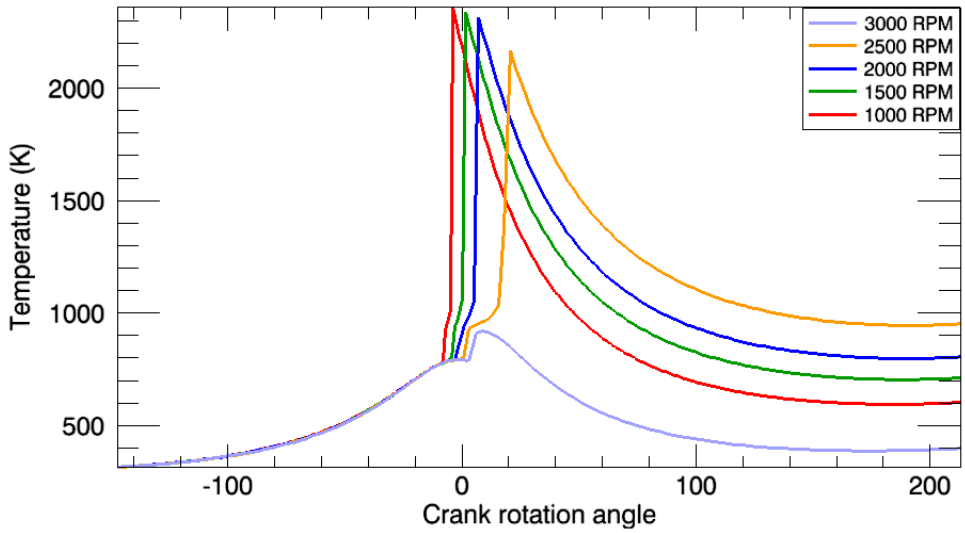

Figure 4.50 – Effect of external EGR composition at varying engine speeds on cylinder temperature

4.3.5.4. Effect of varying inlet charge temperature at high speeds on emissions

In the last two sections, it was observed that incomplete combustion occurs at high speeds and results in significant pollutants. The simulation was tested for inlet charge temperatures of 315 K, 360 and 405 K for engine speed of 3000 RPM with 5% hydrogen and external EGR from the reformer and fuel cell. The results are shown in Figure 4.51. The pressure and temperature in the cylinder show a sharp rise at 360 K and 405 K. The ignition delay is reduced as the inlet charge temperature increases.

As expected the NOx emissions would be higher at 406 K than those at 360 K. The simulation results indicated that other pollutants such as carbon monoxide and unburned hydrocarbons were negligible at 360 K and 405 K.

4.3.6. Summary

This section evaluated the emissions produced by the engine when varying amounts of hydrogen was introduced into the engine, with effluents from the fuel cell and reformer supplied as external EGR.

The key findings in this section are as follows:

- Part substitution of n-heptane by hydrogen results in increased engine peak temperatures and high NOx emissions.

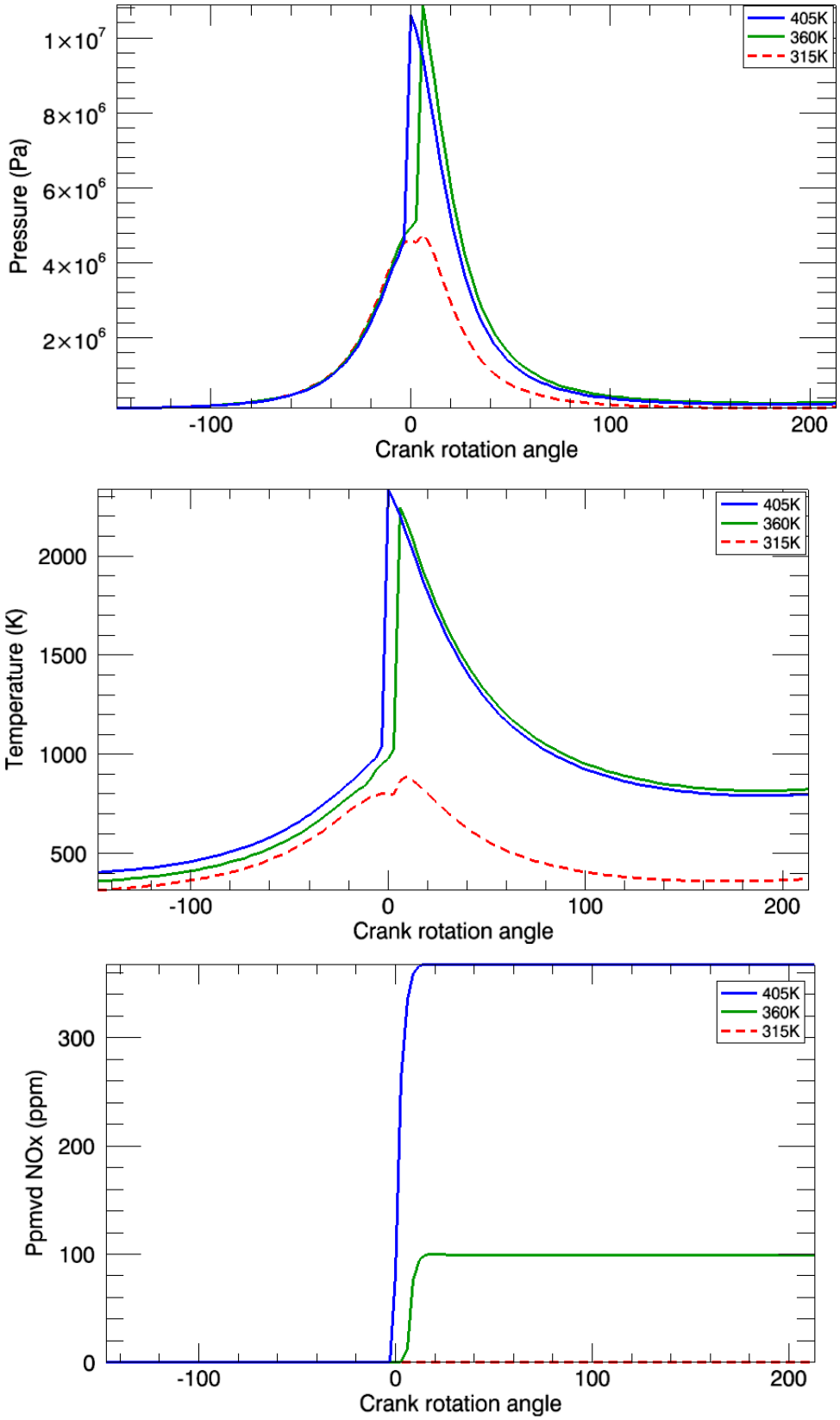

Figure 4.51 - Effect of varying inlet charge temperature at high speeds on emissions

- The induction of effluents from the fuel cell including oxygen depleted air and water vapour along with hydrogen lowered the NOx levels.
- The induction of effluents from the fuel cell and the reformer including oxygen depleted air, water vapour, carbon dioxide and trace quantities of carbon monoxide resulted in an ignition delay, lower peak pressures and up to 99.5% reduction in NOx levels (as compared to those produced by n-heptane combustion)
- When the engine was operated with effluents from both fuel cell and reformer, increase in engine speeds resulted in incomplete combustion with high levels of carbon monoxide and unburned hydrocarbon emissions.
- At higher speeds, it is desirable to introduce effluents only from the fuel cell and increase the inlet charge temperature to ensure complete combustion and minimal production of NOx emissions.
- The flow rate of hydrogen fed to the engine is mainly dependent on the utilisation factor and the load on the fuel cell. The fuel cell must be able to supply hydrogen to the engine without significantly compromising its efficiency.
- The amount of hydrogen and other effluents from the fuel cell and reformer supplied to the engine depends on the loads on the fuel cell and the engine. As a result, the percentage of the externally supplied EGR depends on these load conditions. However, the composition of the EGR may be varied by regulating the exhaust flows from the reformer and fuel cell.

The effects observed in the results of the combustion simulation regarding ignition delays, peak pressures and emissions due to addition of hydrogen, and external EGR including water vapour, carbon dioxide and nitrogen dilution are consistent with those obtained in literature sources such as [13, 54-57, 108].

It was observed that when the fuel cell was operated on a full load, and the engine load was varied to 100%, 34% and 25%, the maximum amount of effluents available from both, the fuel cell and reformer were successful in reducing the NOx emissions to 29.9, 45.7 and 6.3 ppm respectively. The carbon monoxide and unburned hydrocarbon emissions for all these cases were negligible. This proves that the effluents from fuel cell and reformer available at a certain load condition are normally sufficient to maintain emissions at a low level. At

high speeds, hydrogen percentage, EGR fraction and inlet charge temperature can be manipulated to ensure complete combustion and low level of pollutants.
The main factors that influence emissions for the engine are:

- Air-fuel ratio
- Providing appropriate composition of externally supplied EGR for the amount of hydrogen supplied to the engine depending on its load and speed
- Inlet charge temperature

The results from this section are used for defining control limits for the fraction of external EGR, which are used in Chapter 8 (Feedback Control Design Using PID Controllers) and Chapter 9 (Model Predictive Control Design).

The exact effect on emissions and ignition delay require experimental validation. The model is further used to develop a control-oriented integrated system modelling in Chapter 7 (System Integration). Control systems will be devised to regulate values of oxygen-to fuel ratio, fraction and composition of external EGR and hydrogen substitution in the engine.

4.4. *Turbocharger*

4.4.1. Introduction

Turbocharging has emerged as a common technique to improve engine performance. The purpose of turbocharging is to provide boost, i.e. compressed charge, which allows more fuel inclusion and gives more power. The turbocharger consists of two main components – the turbine and the compressor which are mechanically coupled through a shaft. The exhaust gases from the engine drive turbine and produce useful work.

Due to the mechanical connection between the turbine and compressor, the turbine powers the compressor and hence determines the air flow into the engine from the compressor. In order to deliver the right amount of air required by the engine, the turbine exhaust is equipped with a wastegate valve or a variable geometry. This enables adjusting the flow through the turbine and deliver the required air to the engine through the compressor. The wastegate valve releases some of the exhaust gases to regulate the flow to the turbine while a variable geometry turbine has adjustable vanes to manipulate the flow through the turbine.

This section describes the modelling principles of a turbocharger for control purposes. The model is used for a turbocharged engine which is further used in an integrated system model.

4.4.2. Modelling Principles

Compressor and turbine maps provided by the manufacturers are usually in the form of tables. The data for modelling used in this section is for a variable geometry turbocharger Garrett *AVNT37*.

For control purposes, look up table models are not suitable [116], hence a method based on least square regression fits to the compressor and turbine maps was used to develop the turbocharger model.

4.4.3. Compressor

The method used for modelling the turbine and compressor was the Jensen and Kristensen method described by Moraal et al [116]. This method is suitable for control oriented modelling of the turbocharger.

The compressor power is given by Eqn. 4.78.

$$P_c = Wc_p(T_{02} - T_{01})$$

Eqn. 4.78

The pressure ratio for an isentropic process is given below.

$$\frac{T_{02,is}}{T_{01}} = \left(\frac{P_{02}}{P_{01}}\right)^{\frac{\gamma-1}{\gamma}}$$

Eqn. 4.79

The isentropic efficiency of the compressor is given by Eqn. 4.80

$$\eta_{c,is} = \frac{T_{02,is} - T_{01}}{T_{02} - T_{01}}$$

Eqn. 4.80

Combining equations Eqn. 4.79 and Eqn. 4.80 results in the following:

$$\left(\frac{T_{02}}{T_{01}}\right) = 1 + \frac{1}{\eta_{c,is}}\left[\left(\frac{P_{02}}{P_{01}}\right)^{\frac{\gamma-1}{\gamma}} - 1\right]$$

Eqn. 4.81

$$P_c = Wc_p T_{01}\frac{1}{\eta_{c,is}}\left[\left(\frac{P_{02}}{P_{01}}\right)^{\frac{\gamma-1}{\gamma}} - 1\right]$$

Eqn. 4.82

The Jensen and Kristensen method for compressor modelling as described by Moraal et al [116] is given in Eqn. 4.83 to Eqn. 4.88. A dimensionless head parameter equivalent to the slip factor is represented by ψ,

$$\psi = \frac{C_p T_a\left[\left(\frac{P_{out}}{P_{1in}}\right)^{\frac{\gamma-1}{\gamma}} - 1\right]}{\left(\frac{U_c^2}{2}\right)}$$

Eqn. 4.83

where U_c is the compressor blade tip speed.

$$U_c = \frac{\pi}{60} d_c N_{tc}$$

Eqn. 4.84

The normalised compressor flow rate φ, is given by Eqn. 4.85.

$$\phi = \frac{W_c}{\rho_a \frac{\pi}{4} d_c^2 N_{tc}}$$

Eqn. 4.85

The head parameter and the compressor efficiency are represented by the following equations in terms of φ and M. The coefficients *k* and *a* were determined by using least square regression fits.

$$\psi = \frac{k_1 + k_2\phi}{k_3 - \phi} \quad k_i = k_{i1} + k_{i2}M,\ i = 1,2,3$$

Eqn. 4.86

where *M* is the inlet Mach number

$$M = \frac{U_c}{\sqrt{\gamma R T_a}}$$

Eqn. 4.87

The compressor efficiency is modelled as a function of φ and the inlet Mach number.

$$\eta = a_1\phi^2 + a_2\phi + a_3 \quad a_i = \frac{a_{i1} + a_{i2}M}{a_{i3} - M}, i = 1,2,3$$

Eqn. 4.88

4.4.4. Turbine model

The power generated by the turbine using the first law of thermodynamics is given as

$$P_t = W c_p (T_{01} - T_{02})$$

Eqn. 4.89

Assuming isentropic expansion the turbine outlet temperature is given by the following equation.

$$\left(\frac{P_{02}}{P_{01}}\right)^{\frac{\gamma-1}{\gamma}} = \frac{T_{01}}{T_{02,is}}$$

Eqn. 4.90

The isentropic efficiency of the turbine is in Eqn. 4.91.

$$\eta_{t,is} = \frac{T_{01} - T_{02}}{T_{01} - T_{2,is}}$$

Eqn. 4.91

From Eqn. 4.90and Eqn. 4.91 the turbine power is given below.

$$P_t = Wc_p T_{01} \eta_{t,is} \left[1 - \left(\frac{P_2}{P_{01}} \right)^{\frac{\gamma-1}{\gamma}} \right]$$

Eqn. 4.92

The outlet temperature of the turbine is given by Eqn. 4.93.

$$T_{02} = T_{01} \left(1 - \eta_{t,is} \left(1 - \left(\frac{P_2}{P_{01}} \right)^{\frac{\gamma-1}{\gamma}} \right) \right)$$

Eqn. 4.93

The blade-speed ratio is defined as in Eqn. 4.94.

$$\frac{U}{C} = \frac{\pi D N_{tc}}{60 \sqrt{2c_p T_{01} \left(1 - \left(\frac{p_{out}}{p_{in}} \right)^{\frac{\gamma-1}{\gamma}} \right)}}$$

Eqn. 4.94

The variable geometry turbine is modelled as described by Kolmanovsky et al [117]. The mass flow rate through the variable geometry turbocharger is given by the equation below [117].

$$W_{2t} = \frac{A_{vgt}(\chi_{vgt}) p_{out}}{\sqrt{T_2}} \psi(p_{out}, \chi_{vgt})$$

Eqn. 4.95

Where

$$\psi(p_{out}, \chi_{vgt}) = \begin{cases} \sqrt{\left(\frac{p_{in}}{p_{out}} - g(\chi_{vgt}) + 1 \right)^{2/\gamma} - \left(\frac{p_{in}}{p_{out}} - g(\chi_{vgt}) + 1 \right)^{\frac{\gamma+1}{\gamma}}} & for \quad \left(\frac{p_{in}}{p_{out}} \right) > p_{crit}(\chi_{vgt}) \\ A_t \sqrt{(p_{crit}(\chi_{vgt}) - g(\chi_{vgt}) + 1)^{2/\gamma} - (p_{crit}(\chi_{vgt}) - g(\chi_{vgt}) + 1)^{\frac{\gamma+1}{\gamma}}} & for \quad \left(\frac{p_{in}}{p_{out}} \right) > p_{crit}(\chi_{vgt}) \end{cases}$$

Eqn. 4.96

where A_{vgt} is the effective flow area for the turbine, which is modelled as a polynomial function of the VGT vane position χ_{vgt}. The pressure ratio where the flow becomes zero is given by the quantity $g(\chi_{vgt})$ [117].

The turbine efficiency is modelled as a function of the VGT vane position and the blade-speed ratio [117].

$$\eta_{t,isentropic} = f_1\left(U/C\right) f_2\left(\chi_{vgt}\right)$$

Eqn. 4.97

where f_1 and f_2 are obtained by regression fits to the experimental data.

The dynamics of the turbocharger speed are derived from Newton's second law to give turbocharger angular acceleration as a function of turbocharger net power.

$$\dot{\omega}_{tc} = \frac{1}{J_{tc}\omega_{tc}}\left(\eta_m P_t - P_c\right)$$

Eqn. 4.98

The steps followed in the turbocharger model are given in Figure 4.52.

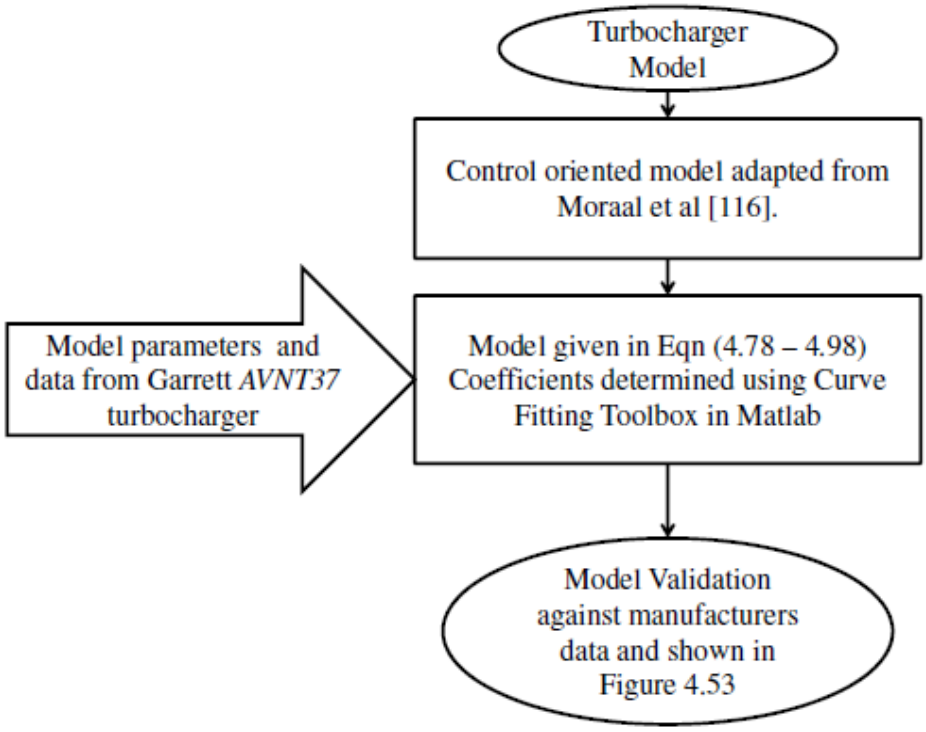

Figure 4.52 – Turbocharger model flowchart

4.4.5. Modelling Results

The model results are superimposed on the data provided by the manufacturer and shown in Figure 4.53. The data supplied by the manufacturer is shown by the cross shaped markers and the results of the curve fit model are shown by the solid lines. In Figure 4.53(a) the compressor map shows curves at various compressor speeds. Figure 4.53(b) represents the turbine map with mass flow rates and pressure ratios at various VGT settings. The model is in agreement with the data supplied by the manufacturer.

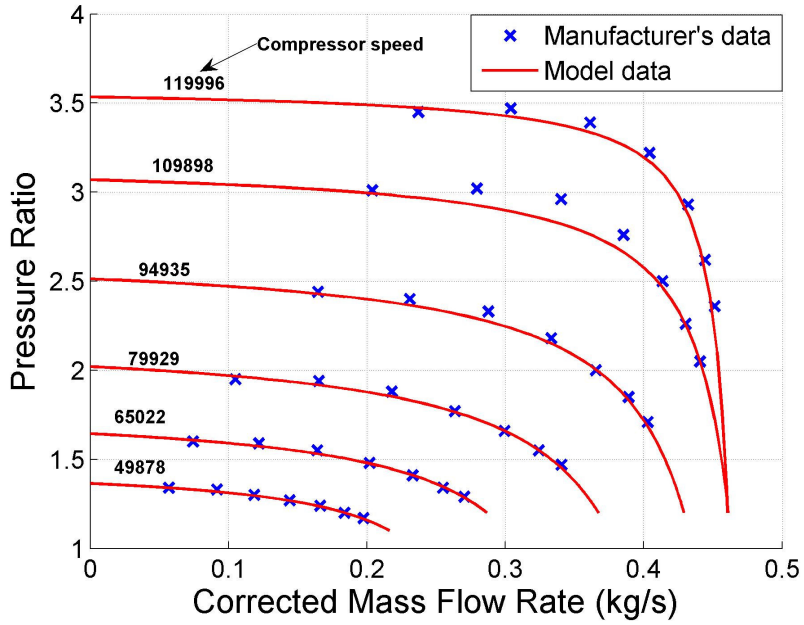

(a) Compressor map at various compressor speeds

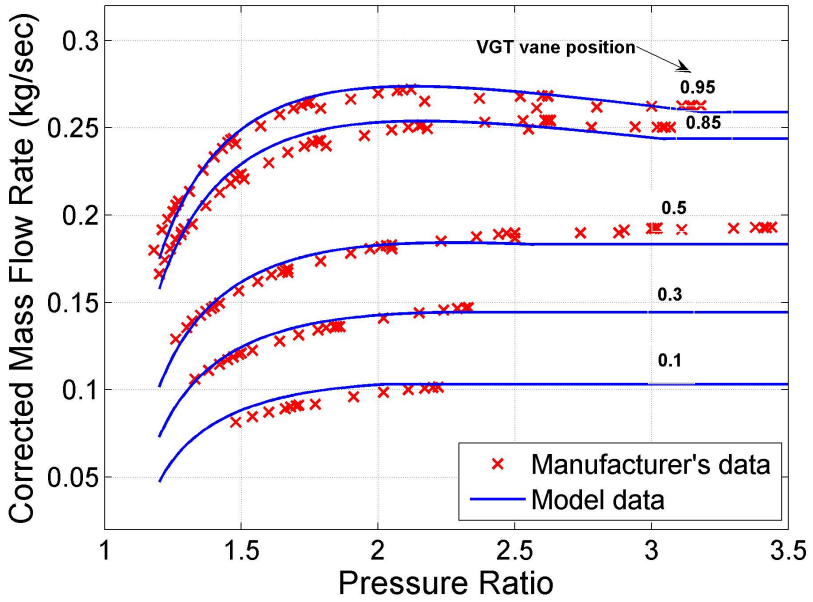

(b) Turbine maps for various VGT settings

Figure 4.53 – Curve fits for compressor (a) and turbine (b)

4.4.6. Summary

This section described the control oriented modelling of a turbocharger. The model results are a close match with the maps provided by the manufacturer (Garrett). This compressor model is integrated with the fuel cell model in the integrated system model. The turbocharger model is integrated with the engine control oriented model in Chapter 7 (System Integration).

Chapter 5. Investigation of Optimum Operating Range

5.1. *Introduction*

Various fuel cell hybrid systems for power production have emerged in the last two decades in efforts to explore possibilities of emission reduction and use of alternative fuels. Fuel cell hybrids with reciprocating internal combustion engines are, however, limited. Typically, fuel cells are used to supplement power of the engine by providing for an auxiliary load on the system. These fuel cells are independent of the main power producing components. The use of SOFC, as an auxiliary power unit (APU), is common in automotive applications. The control for such APU systems can be completely de-centralized from the main power producing component.

The concept of using SOFC effluents to condition the engine fuel in order to improve engine performance with reduced pollutants and using the fuel cell to supply a part of main load is novel. The efficient power production by the system components can be hampered by altering the flow in the fuel cell and that between the fuel cell and the engine. The fuel cell operation is not independent of the engine operation; hence the system will involve additional control parameters.

As discussed in Chapter 2 (The System and its Attributes), the system consists of an SOFC and IC engine working simultaneously to supply the power requirement. The exhaust gas streams from the fuel cell anode and cathode are fed into the IC Engine. The excess fuel from the anode assists in improving the combustion, while the oxygen depleted air from the cathode is used for lean combustion in the IC Engine as a form of exhaust gas re-circulation (EGR) or dilution. The key to the efficient operation of this system is management of flows to and between the fuel cell and the IC Engine. The flows of air and fuel in each component will determine the power distribution, efficiency, quality of

combustion and emissions for the whole system. The objective of this study is to determine the performance of the system at various load conditions of the fuel cell and the IC engine. This analysis will also determine the key components affecting the control development for the system.

In order to supply the engine with residual fuel from the fuel cell, the utilisation factor of the fuel cell has to be manipulated. The utilisation factor is the ratio of the mass flow rate of fuel to the amount of fuel used during the fuel cell operation. Conventionally utilisation factor is maintained for efficient operation of the fuel cell system between 80% to 95%. Utilisation of the fuel above 95% in a fuel cell poses a risk of running out of fuel and a resulting sharp drop in the voltage [6]. Lower values of the utilisation factor result in lower efficiency for the fuel cell. Further, when the engine is fed with hydrogen as a residual fuel from the fuel cell, knocking behaviour in the cylinder may arise due to properties of hydrogen [12].

A hybrid system, as the one described in Chapter 2 (The System and its Attributes), combines power producing components in order to produce a more efficient system. Such systems require an optimal operation to ensure a stable system operation and minimal fuel consumption. An optimum operating range for the combined SOFC-IC Engine system is therefore sought.

As a first step towards investigating the control strategy required for the system, a steady state model of the fuel cell and IC engine is developed. The feasibility of achieving a better performance of the combined system as compared to a conventional diesel engine is investigated.

Diesel engine emissions at idle conditions are considerably higher and hence inefficient. The use of fuel cell power instead of the engine power during idling can prove to be efficient and low polluting. This aspect is further examined in this chapter.

The aim of this work was:

- To determine the feasibility of improving the engine performance without largely compromising the fuel cell performance, based on the assumptions of sizes of the components,

- To determine if the amounts of exhaust stream flows from the fuel cell are appropriate to achieve the improved system efficiency and charge dilution.
- To determine and improve the performance of conventional diesel engine at various load conditions and idle condition.

5.2. *Modelling and analysis*

5.2.1. Fuel Cell

A steady state fuel cell model developed based on mass balances and some simplifying assumptions is described in this section. The fuel cell stack has a maximum power rating of 20 kW. The hydrogen flow rate to the fuel cell stack is usually varied depending on the desired power output from the Solid Oxide Fuel Cell (SOFC). At any constant fuel flow rate into the SOFC, the fuel utilisation decreases as the load is increased [118]. The fuel utilisation factor μ_f determines the power output and efficiency of the fuel cell. It also influences the amount of hydrogen flowing into the IC Engine. A controller can be designed to ensure that the fuel cell efficiency does not drop below 40%.

The electrical work done of moving a charge around the circuit in a fuel cell is given by -2*FE* Joules, where *E* is the voltage of the fuel cell and *F* is Faraday constant. If the system is reversible the electrical work done is equal to the gibbs free energy released as shown in Eqn. 5.1.

$$\Delta\bar{g}_f = -2F.E \text{ and } E = \frac{\Delta\bar{g}_f}{-2F}$$

Eqn. 5.1

Eqn. 5.1 gives the reversible open circuit voltage for a fuel cell. The efficiency of the fuel cell is defines as the ratio of the electrical energy produced to the gibbs free energy change. However, the approach suggested by Larminie et al [6] describes that since fuel cells use materials that are burnt to release energy, it is more appropriate to compare electrical energy to heat produced by burning fuel. Hence, Larminie et al [6] define efficiency as the ratio of electrical energy produced per mole to the enthalpy of formation (Δh_f). The enthalpy of formation for water has two values, i.e. the higher heating value (HHV) for the liquid state and the lower heating value (LHV) for steam. If all the energy from hydrogen is transformed into electrical energy the electromotive force is given by Eqn. 5.2.

$$E = \frac{\Delta \bar{h}_f}{-2F} = 1.48\ (HHV)$$
$$= 1.25\ (LHV)$$

Eqn. 5.2

Hence then actual cell effienciency based on the lower heating value is given by Eqn. 5.3.

$$Cell\ efficiency = \frac{V_c}{1.25}$$

Eqn. 5.3

The fuel cell efficiency is defined as [6]:

$$\eta_{FC} = \mu_f \frac{V_c}{1.25}$$

Eqn. 5.4

The fuel utilisation factor of the fuel cell defines the amount of fuel consumed to produce the power. The amount of fuel required depends on the active area of the fuel cell and the load current drawn from the stack. The active area of the fuel cell is a physical parameter assumed to be 38.955 cm^2 [35]. The amount of hydrogen required by the fuel cell can be calculated as follows [6]:

$$Hydrogen\ usage\ rate = \frac{P_{fc}}{2V_{fc}F} moles / s$$

Eqn. 5.5

The fuel utilisation factor is defined as [6]:

$$\mu_f = \frac{Mass\ \ flow\ rate\ of\ \ hydrogen}{Hydrogen\ usage\ rate}$$

Eqn. 5.6

The polarization curve assumed for a single cell of the SOFC stack is given in Figure 5.1. The single cell voltage is 0.7 V at full load, 0.75 V at half load and 0.8 V at a quarter load. The maximum current density is 0.5A/cm^2. If the fuel cell draws higher current, the voltage drops on account of increasing the overpotentials [6].

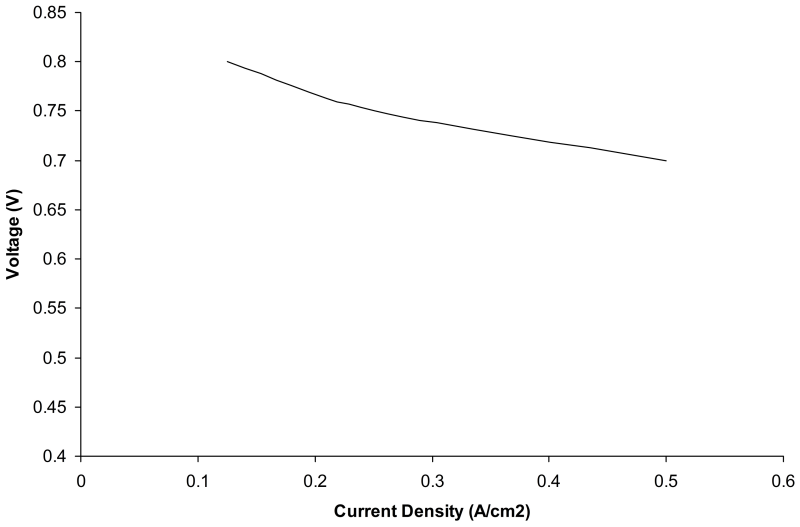

Figure 5.1 – Polarization Curve of SOFC

Based on the polarization curve shown in Figure 5.1, for a design point of 0.75V at 0.25A/cm^2, the number of cells in the stack are 2739.

The excess oxygen ratio for the fuel cell is the amount of oxygen supplied in excess of the oxygen required for the reaction. If the air supplied to the fuel cell is not sufficient, it results in a drop in the voltage due to the falling partial pressure of oxygen [6]. In order to avoid oxygen starvation, the excess oxygen ratio is maintained at $\lambda_{O_2} = 2$.

$$\lambda_{O_2} = \frac{Mass\ \ flow\ rate\ of\ \ oxygen}{Oxygen\ usage\ rate}$$

Eqn. 5.7

$$Oxygen\ usage\ rate = \frac{P_{fc}}{4V_{fc}F} moles/s$$

Eqn. 5.8

$$Water\ \ production\ rate = \frac{P_{fc}}{2V_{fc}F} moles/s$$

Eqn. 5.9

The exhausts from the fuel cell cathode and anode can be calculated by the steady state equations given below:

Cathode exhaust air flow rate = Cathode inlet air flow rate – Oxygen usage rate

Anode exhaust flow rate = Hydrogen inflow rate –Hydrogen usage rate+ Water production rate

With the excess oxygen ratio $\lambda_{O_2} = 2$, the flow rate of air required in the cathode is calculated. Corresponding values for the compressor power, efficiency and air flow rate are computed from the manufacturer's compressor map provided by Garrett.

5.2.2. IC Engine

The amount of diesel flowing into the IC Engine will depend on the power requirement. Any excess fuel from the fuel cell anode is fed to the IC Engine. The hydrogen flowing into the engine affects the specific fuel consumption. Addition of hydrogen as a supplementary fuel in a diesel fuelled engine, results in higher combustion temperatures. Hydrogen has a very low cetane number and causes knocking in the engine. In order to avoid knocking, nitrogen is added as a diluent [13]. The oxygen depleted air from the fuel cell serves as a source of nitrogen.

The oxygen depleted air varies the air-fuel ratio (AFR) of the IC Engine. At idle and full load conditions, no oxygen depleted air is fed to the IC Engine. A lean mixture during full load conditions can affect fuel conversion efficiency and emissions [112]. Hence, dilution is avoided during the full load conditions. During idle conditions, when the IC Engine is very sensitive to changes in the Air-Fuel ratio [112], the oxygen depleted air is released into the atmosphere. It is assumed that at an air-fuel ratio of 28:1, the NOx emissions are minimal and knocking is prevented.

The modelling work for the engine is based on the efficiency characteristics of a medium duty diesel engine. The amount of fuel required for a conventional diesel engine at various load conditions is calculated from the specific fuel consumption. The values for the diesel specific fuel consumption are taken from literature reports [112]. The engine rated power is 100 kW at a maximum speed of 2400rpm. The percentage of hydrogen in the engine is computed based on the fuel equivalent energy as:

$$\%\ of\ \ Hydrogen = \frac{m_{H_2}.Q_{HV_{H_2}}}{m_{diesel}.Q_{HV_{diesel}} + m_{H_2}.Q_{HV_{H_2}}}$$

Eqn. 5.10

Fuel conversion efficiency of the engine is given by:

$$\eta_f = \frac{P_{ice}}{m_{diesel}.Q_{HV_{diesel}} + m_{H_2}.Q_{HV_{H_2}}}$$

Eqn. 5.11

The brake specific fuel consumption of the diesel engine is given by the following relation [112]

$$bsfc = \frac{m_{diesel}}{P_{ice}}$$

Eqn. 5.12

Figure 5.2 shows the steps followed for the steady state model.

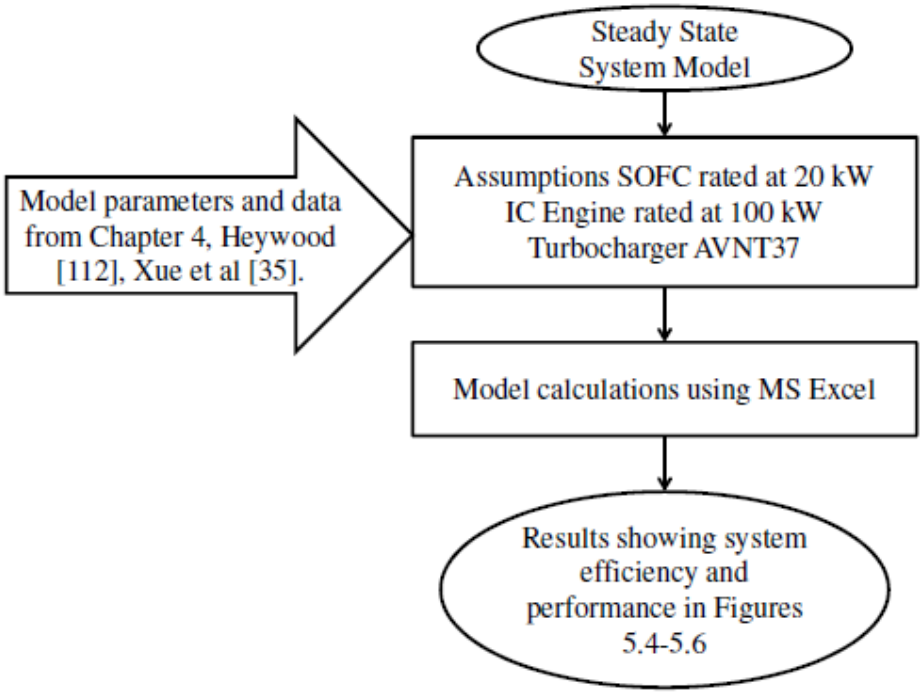

Figure 5.2 – Steady state model flowchart

5.2.3. Combined SOFC-IC Engine Efficiency:

The combined efficiency of the SOFC and IC Engine is investigated at the following conditions:

i). Full load operation of the Fuel cell, IC Engine load.

ii). Half load operation of fuel cell, IC Engine load.

iii). Idle load operation of the system.

The combined efficiency of the SOFC and the engine is defined as below:

$$\eta_{SOFC-ICE} = \frac{Net\ system\ power\ output}{Overall\ fuel\ consumption}$$

Eqn. 5.13

The system components are assumed to be operating at steady state conditions. The controls for the system can be designed such that the fuel cell handles the base load while majority of the load will be handled by the IC engine using the effluent gases from the SOFC.

The analysis of the system is based on the following considerations:

i). Effect of fuel utilisation factor, μ_f on SOFC efficiency and IC Engine fuel consumption at various load conditions.

ii). Amount of oxygen depleted air required to achieve a desired condition to prevent knocking and reduce the NOx emissions.

iii). Overall efficiency of the system at various load conditions of the SOFC and IC engine.

An optimum operating range of conditions for the combined operation is suggested.

5.3. *Results*

The fuel utilisation factor of the SOFC reduces almost linearly as the load on the fuel cell increases. This results in a fall in the efficiency of the fuel cell with increasing load. Figure 5.3 and Figure 5.4, show the performance maps of the system when the SOFC operates on full load and half load respectively. Each of these maps depicts the percentage of hydrogen fed to the IC Engine as its load is varied. The values are plotted for different fuel utilisation factors of the fuel cell and specific fuel consumption of the engine. Both the performance maps are plotted with the assumption that the SOFC efficiency is no less than 40%.

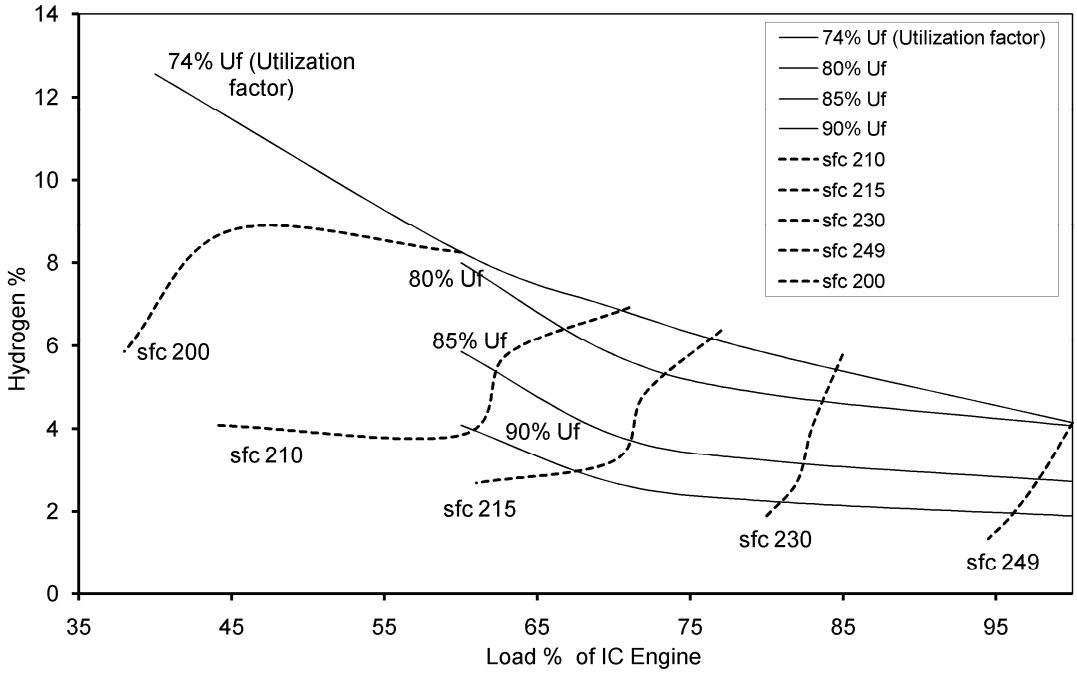

Figure 5.3 – Load variation of IC Engine with SOFC at full-load

The results presented in the Figure 5.3 and Figure 5.4 are for the engine load at a constant torque of 397 Nm. The stoichiometric air-fuel ratio of 15.25 was calculated based on the following stoichiometric equation [112] (n-dodecane representing the diesel):

$$C_{12}H_{26} + H_2 + 19O_2 + 19(3.76)N_2 \rightarrow 12CO_2 + 7.5H_2O + 19(3.76)N_2$$

Eqn. 5.14

When hydrogen is induced in the diesel engine, 30% of nitrogen by volume of the hydrogen flow gives better performance as compared to other values between 0-40% of nitrogen [12, 14]. If 4.15% of hydrogen (0.0001 kg/s) introduced in the engine at full load operation of the fuel cell and engine, the amount of nitrogen required for a knock-free operation is 30% by volume of hydrogen, which is then only 2.77% (4.479×10^{-4}), kg/s) of the nitrogen flowing out from the fuel cell. Hence, the amount of nitrogen required for smooth operation of the engine is much less compared to the actual amount of nitrogen exiting from the fuel cell cathode. The amount of nitrogen flowing out from the fuel cell at this condition is 13% by fraction of the amount in the engine.

The SOFC is fuel flexible and can reform various fuels [15]. If the fuel cell is fed with a mixture of carbon monoxide and hydrogen, then the exhausts will contain carbon dioxide, water vapour and oxygen depleted air. The carbon dioxide and oxygen depleted air can be fed to the engine as an external supply of EGR.

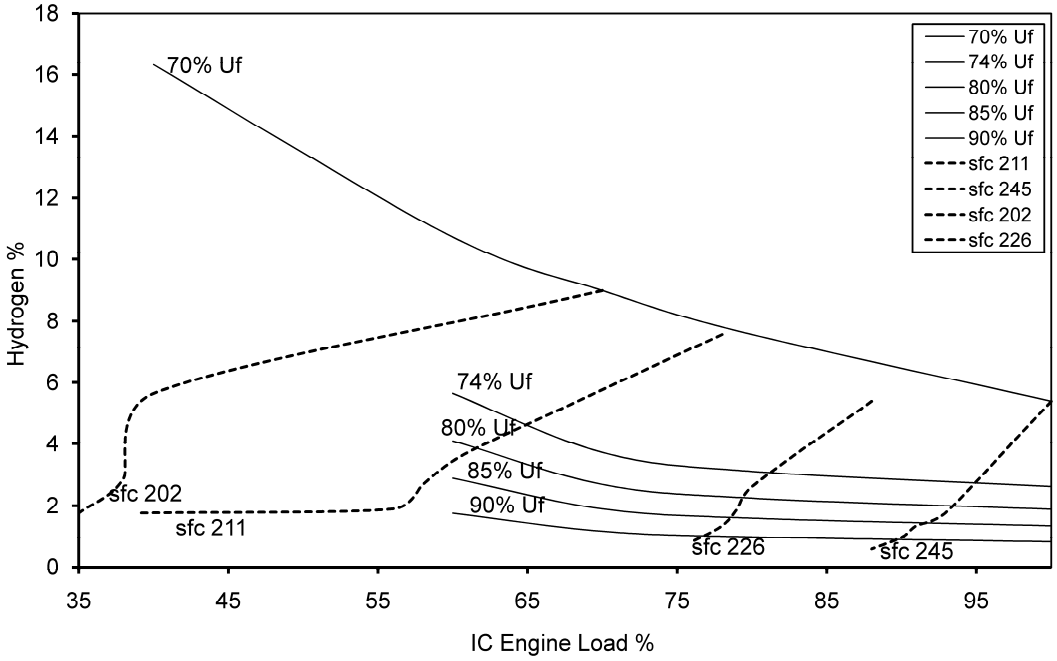

Figure 5.4 – Load variation of IC Engine with SOFC on half-load

From Figure 5.3, the SOFC is operating at full load providing 20 kW at a utilisation factor of 74%. The 26% unused fuel is fed into the IC Engine. The percentage of hydrogen entering the engine changes as the load demand on the engine changes. At low engine loads, the excess hydrogen from the fuel cell constitutes almost 16% of the equivalent energy value of the fuel required in the engine at the specific load condition. At full load condition, the same amount of excess hydrogen from the fuel cell will now constitute 4.15% of the equivalent fuel energy.

In Figure 5.3, the minimum utilisation factor is 74%, while in Figure 5.4, the minimum utilisation factor is 70% which corresponds to the efficiencies of the fuel cell at 41% and 42% respectively. As the utilisation factor of the SOFC improves, the efficiency of the SOFC improves, the amount of hydrogen injected into the IC Engine reduces and the specific fuel consumption increases.

The optimum operating ranges of the SOFC and the IC Engine are determined from the performance map. From Figure 5.3, for full load operation of the SOFC, it is observed that it is best to have a minimum of 4% hydrogen flowing into the IC Engine from the fuel cell. This helps achieve optimum efficiencies for the fuel cell, IC Engine, as well as the

combined SOFC-IC Engine efficiency. The area in the performance maps between 4% of hydrogen and the lowest utilisation factor curve in Figure 5.3, is the optimum operating range for the system when the fuel cell is at full load.

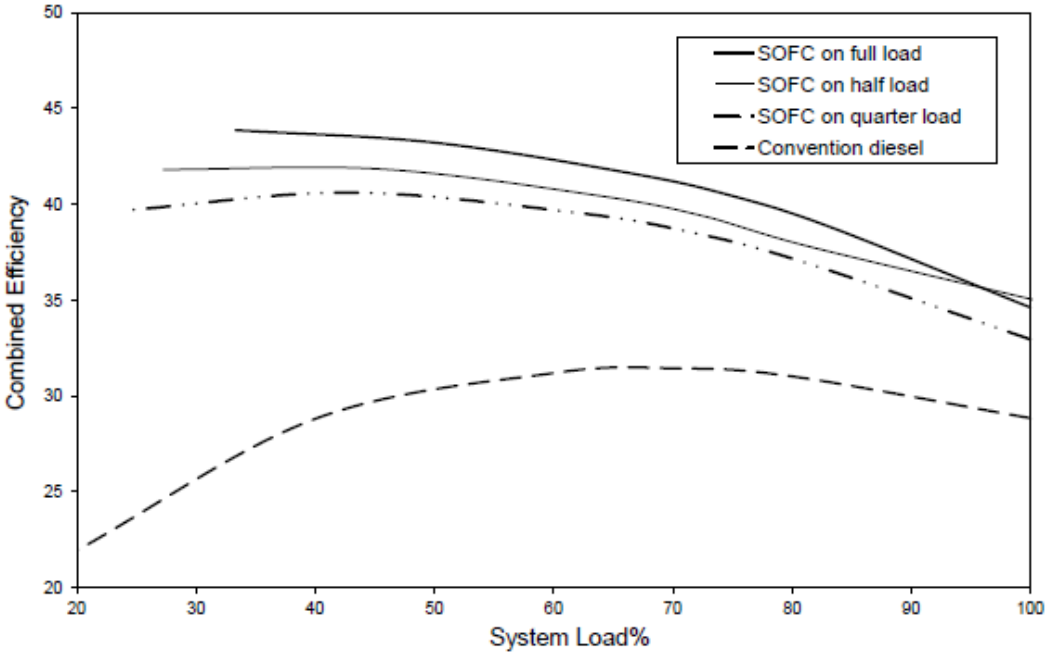

Figure 5.5 – Comparison of combined system efficiency with conventional diesel engine

Similarly, from Figure 5.4, for optimum efficiencies of the fuel cell and IC Engine, the minimum hydrogen percentage must be 2%. The operating range for the system is the area between 2% of hydrogen and the lowest utilisation factor curve when the fuel cell is on half load.

During the idle load condition, the fuel cell handles a greater percentage of the total load than the IC Engine. The specific fuel consumption of the IC Engine improves by 10% as compared to a conventional diesel engine. At the idle load condition, the efficiency of the conventional diesel engine is 27% while the hybrid system has 39 % showing significant improvement.

The change in combined efficiency of the fuel cell and the IC Engine as per the system load variation is shown in Figure 5.5. The system, when compared to a conventional diesel engine proves to be more efficient.

5.4. *Chapter Summary*

The hybrid combination of an SOFC and IC Engine in a configuration discussed here has proved to be more efficient than the conventional diesel engine. At full load and half load operation of the SOFC, optimum efficiency is obtained when the hydrogen injected into the IC Engine is at least 4% and 2 % respectively.

The fuel cell can provide a means of supplying excess fuel and oxygen depleted air to the engine, hence conditioning the engine fuel to produce power with low emissions and higher efficiency. The utilisation factor of the fuel cell plays an important role in determining the efficiency of the fuel cell and the improvement in combustion in the engine. At the same time, the oxygen depleted air flowing into the engine requires appropriate control to ensure that the knocking behaviour is avoided and emissions are minimal. The development of dynamic models for the system should help understand the response of the system components in the suggested hybrid configuration. The results from this analysis will form the basis for control strategy development of the system.

The following chapters will include an enhanced dynamic model and control design of the system. The transient response of the system and its components will be investigated.

Chapter 6. Exergy Analysis

6.1. *Introduction*

Stationary power generation systems with fuel cells have a great potential for efficient operation because of the potential to manage component efficiencies across the load range. High temperature fuel cells hybrids used for stationary power production can be applied to Combined Heat and Power (CHP) systems as developed by Sulzer Hexis Ltd and Ceres Power Ltd [119]. Conventional methods of power generation include the combustion of fossil fuels in internal combustion engines– a process which is highly irreversible because of substantial energy flow across large temperature differences. The potential to extract work from the fuel with minimum irreversibilities is explored with the help of an exergy or availability analysis. Exergy analysis can help determine the possible use of rejected heat or mass flows from a system and help identify those aspects of systems where energy recovery can be best deployed. The performance of the system developed in this thesis can be established by calculating the maximum reversible work that could be obtained from heat transfers through exhaust energy flows and to the environment.

In contrast to combustion based power sources, fuel cells have a greater potential to extract useful work from the fuel supplied. As described by Barclay [75] the reaction in fuel cells can be an isothermal charge exchange at the electrode-electrode interface whereas combustion is a chain reaction caused by rapid collisions of the reactants. The heat released during the fuel cell electrochemical reaction is considerably less as compared to that during combustion of the fuel; hence, there are fewer irreversibilities.

The electrochemical reaction at the fuel cell electrodes is not combustion. Hence, the efficiency calculations of the fuel cell cannot be based on the lower calorific value of fuel. IC Engines are limited by the Carnot temperature limit. Fuel cells do not follow a thermal cycle and hence are not limited by the Carnot efficiency with the implied heat exchange with two thermal reservoirs.

A first law analysis for a system explores the energy balance whereas the second law or exergy analysis investigates the destruction of work potential. The irreversibilities determined by an exergy analysis indicate imperfection in the system due to process imperfections and reactor imperfections. The process can be affected by reactor imperfections and vice-versa.

This chapter presents the exergy analysis of the system described in Chapter 2 (The System and its Attributes), at a steady state operating condition. The aim of this chapter is to determine the following:

- Maximum work potential
- Causes for excessive exergy losses
- Rational efficiency of each component and the system
- Where and how control methods should be used to minimise work destruction.

6.2. *Exergy concept*

Exergy is defined as the amount of work obtainable when some matter is brought to a state of thermodynamic equilibrium with the common components of the natural surroundings by means of reversible processes. Interactions take place only with the environment.

The environment is normally considered as the natural surrounding or the *dead-state*. The dead state corresponds to a large reservoir in a restricted equilibrium, that is a state of perfect thermal and mechanical equilibrium. When the system is also in chemical equilibrium along with thermal and mechanical equilibrium, the condition is said to be unrestricted equilibrium.

Unlike energy, exergy is not conserved. Exergy destruction or exergy losses are caused by entropy generation in an irreversible process. Exergy analysis highlights the imperfections in a thermal process. A process is completely reversible only if it is both, internally and externally reversible. For any system, internal exergy losses are those due to process irreversibilities within the system, while external exergy losses are wasted outputs that occur across the system boundary.

The exergy balance for a control volume with a flow process is given by Eqn. 6.1:

$$\sum\left(1-\frac{T_o}{T_j}\right)\dot{Q}_{cv}-\dot{W}_{cv}+\sum_{in}\dot{n}\times ex_{f_{in}}-\sum_{out}\dot{n}\times ex_{f_{out}}=\dot{I}_{cv}$$

Eqn. 6.1

Where $\dot{I}_{cv}$ is the irreversibility, ex_f is the exergy flow through the system and is a sum of physical, chemical kinetic and potential exergy as shown below in Eqn. 6.2

$$ex_f = ex_{ph} + ex_{ch} + ex_k + ex_p$$

Eqn. 6.2

Rational efficiency as defined by Kotas [70], given by Eqn. 6.3 is the ratio of the desired output exergy ($\dot{E}x_{desired\ output}$) of the control volume to the sum of exergies flowing into ($\sum \dot{E}x_{IN}$) the system required for the process to occur.

$$\eta_R = \frac{\dot{E}x_{desired\ output}}{\sum \dot{E}x_{IN}}$$

Eqn. 6.3

For a system with a reversible process, the irreversibility $\dot{I}_{cv}$ is identically zero.

One important aim of exergy analysis of systems is to determine the principal sources of irreversibility and to identify what work producing potential is being lost. The exergy analysis leads to the suggestion of a number of energy recovery processes each of which in turn converts the irreversible change of state into a reversible one. This aspect of exergy analysis leads to the problem statement.

6.3. *Problem statement and methodology*

The aim of this analysis is to determine the maximum possible work output of the proposed system and hence to assess the impact of the major irreversibilities in the system. The analysis follows a progressive method, first by determining the maximum work potential of a fully reversible system, including internal and external exergy losses, step by step, to determine the deviation of the system from the ideal conditions. The approach is partly similar to that described by Horlock et al [120] in which the authors have described three ideal processes for combustion of hydrocarbon fuel with inlet and outlet conditions at different states. The rational efficiency of each case is evaluated and discussed by Horlock

et al [120]. The approach followed in this chapter is described further with the help of Figure 6.1.

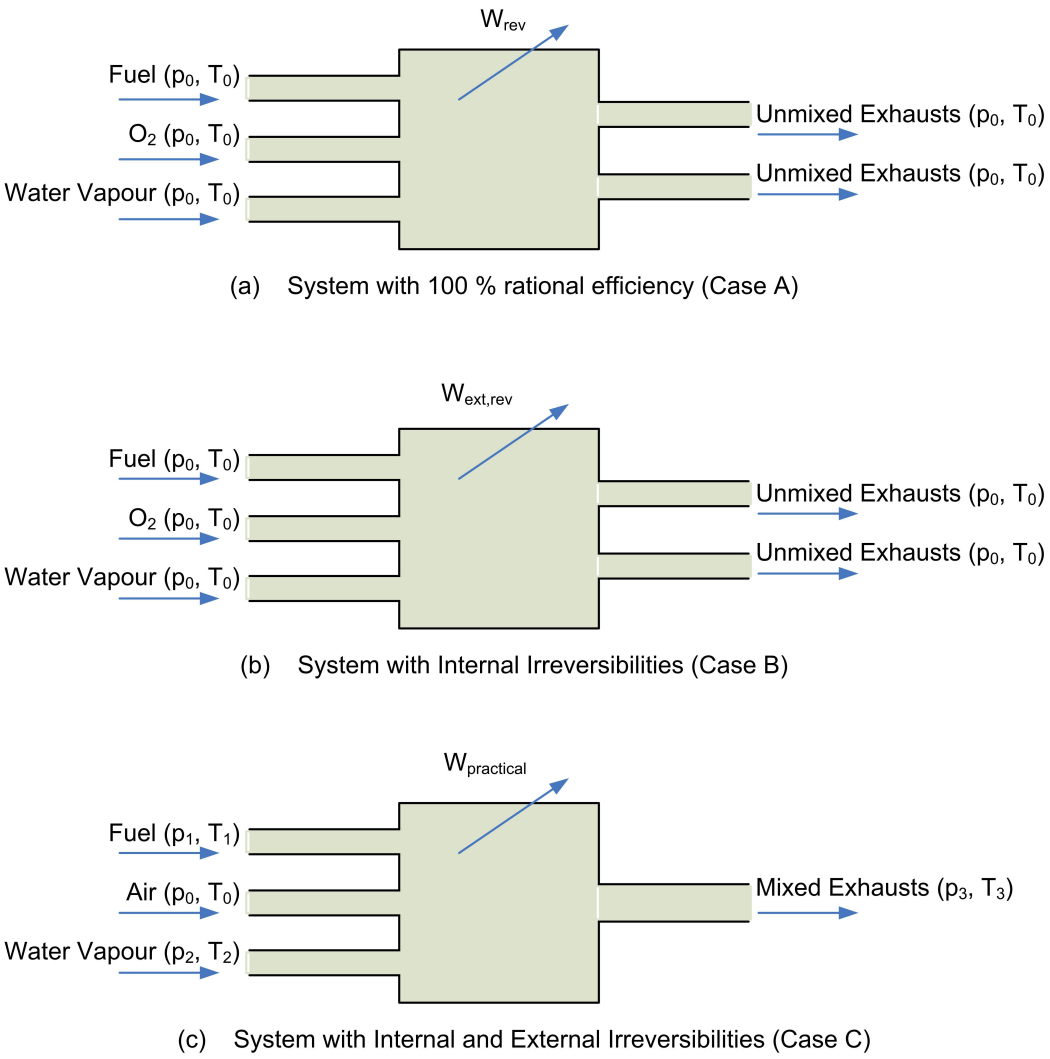

Figure 6.1 – Progressive steps followed for exergy analysis

The key steps followed for this analysis:

- The amount of work produced by the system is calculated with the initial assumption that all components work at 100% rational efficiency, i.e. the system is completely reversible producing a work output W_{rev} as shown in Figure 6.1(a). The matter streams are delivered, unmixed, to and from the system at environmental conditions. (Case A)

- Considering that all the internal exergy losses are present and external exergy losses are absent, the analysis is applied again to determine maximum work potential. The system in this case is said to be externally reversible producing a work output $W_{ext,rev}$. As shown in Figure 6.1(b), the process in the system is irreversible, while the input and exhaust flows through the system are delivered reversibly to the environment. (Case B)
- Finally, useful work produced by the system when internal and external exergy losses occur is computed. This case presents a practical system, producing work $W_{practical}$, with various irreversible processes occurring within the system. As shown in Figure 6.1(c), the system process is irreversible and the matter streams are delivered to and from the stream irreversibly(Case C).

This progressive analysis allows determining main locations of exergy losses in the system. The effect of utilising heat (which is normally rejected to the environment) internally within the system is also investigated.

6.4. *Exergy Analysis – System Components at 100% rational efficiency (Case A)*

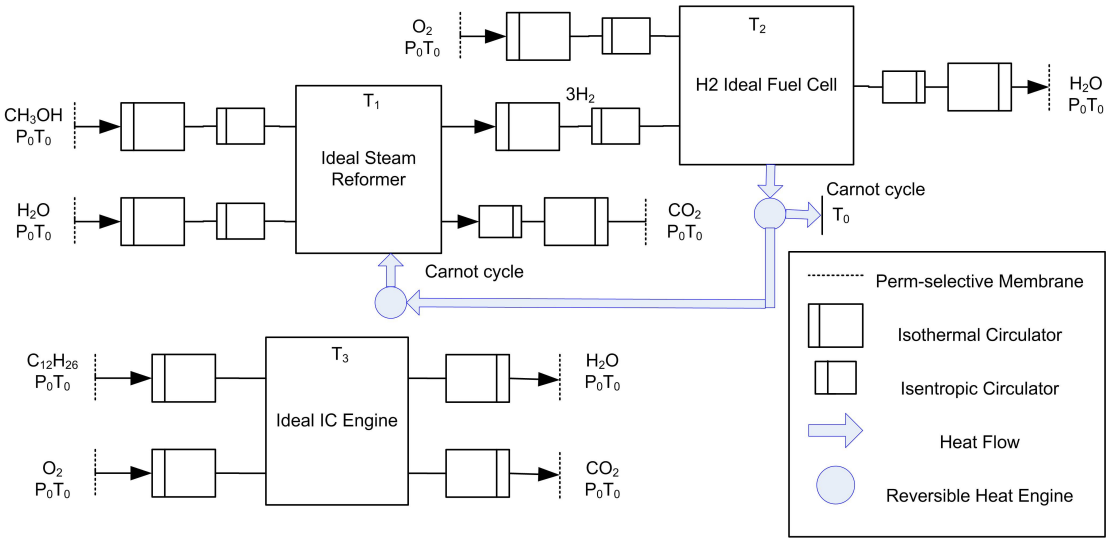

Figure 6.2 - System with all reversible processes (Case A)

As described by Haywood [86], a quasi-static or reversible process is one in which the system passes uninterruptedly through a continuous succession of quasi-static stable states. The process occurs infinitely slowly and settles to a stable state at the end of each infinitesimal step of the process. All processes are irreversible in nature and irreversibility represents a lost opportunity for producing work [86]. The study of ideal systems is essential to understand the energy conversion and potential for maximising work output in practical systems.

Ideal or reversible fuel cells have been studied and discussed in literature by authors such as Moran et al [121], Kotas [70], Haywood [86] and Barclay [75]. Kotas [70] has described the evaluation of maximum work of a reversible fuel cell without the consideration of equilibrium concentrations of species in the fuel cell. An ideal isothermal reversible reaction can occur only at equilibrium concentration of species and hence the approach followed by Haywood [86] and Barclay [75] is correct and followed in this chapter.

Work is produced by a system in a control volume when it is at conditions different from the environment. Most processes used for power production involve irreversibilities due to the process and reactor imperfections. In order to assess the maximum work potential or useful work of a completely reversible component, it is necessary to include apparatus which allows exchange of heat and mass flows with the environment reversibly. The extra apparatus to demonstrate a reversible behaviour are circulators, perm-selective membranes, reversible fuel cells and reversible heat engines as shown in Figure 6.2 and defined below.

Perm selective membrane is an idealised membrane which allows only a single species to pass through them, hence delivering the species to the fuel cell without interacting with the environment. *Circulators* are idealised compressors or expanders which enable delivery of the species to the fuel cell at the necessary equilibrium pressures.

A *reversible fuel cell* is an idealised fuel cell in which the materials (electrodes and electrolytes) are assumed to be ideal allowing an isothermal reversible reaction to occur.

A *reversible heat engine* is hypothetical engine that operates on the reversible Carnot cycle and produces work.

To achieve internal reversibility of the system components, the components are assumed to be manufactured with ideal materials. As described by Haywood and Barclay [75, 86], the reversible chemical reaction in the system can occur at only one specific set of concentrations of the reactants and products, i.e. equilibrium concentrations. A completely reversible reaction requires the reaction to progress very slowly, stepping through stable states to achieve equilibrium at each state. The reaction taking place in the system component is assumed to be ideal, where the reactants and products are delivered to and from the system at equilibrium concentrations.

The system configuration as described in Chapter 2 (The System and its Attributes) involves an interconnected system of reformer-fuel cell and IC Engine. It is however interesting to note that the advantage of such a combined system is that it compensates for the irreversible operation of the components. As shown in Figure 6.2, it can be seen that the maximum work potential can be derived from the system when the reformer and fuel cell are interconnected but the engine is independent of any flow feeds from the fuel cell or the reformer. The terms required to compute the maximum reversible potential for the system are listed below and the methods for their calculation is described in Appendix E.

- Equilibrium concentrations
- Power of Isothermal circulators
- Power of Isentropic circulators
- Carnot cycle/reversible heat engine
- Chemical exergy of the fuel

The operating parameters for the reversible system are listed in Table 6-1. Sections 6.4.1-6.4.2 describes the reversible operation of each component to enable 100 % rational efficiency with the help of Figure 6.2.

6.4.1. Reversible Reformer-SOFC system

On the basis of equilibrium thermodynamics for fuel cells demonstrated with the help of Van Hoff's equilibrium box [75, 86], for complete internal reversibility, an ideal fuel cell with perfect electrodes and equilibrium concentrations of reactants and products is considered.

Table 6-1 – Reversible System Operating Parameters

	Reversible system operating parameters	
SOFC temperature	1200	K
Reformer temperature	500	K
IC Engine temperature	298	K

For external reversibility, the circulators and perm-selective membranes function to ensure the reactants and products are delivered reversibly to and from the fuel cell. The reactants are delivered from standard atmospheric conditions to equilibrium concentrations while the products are delivered from equilibrium concentrations to standard atmospheric conditions by the circulators. The perm-selective membranes ensure no change in the concentration of the substances across the membrane [75]. This ideal fuel cell setup, as shown in Figure 6.2, generates power by isothermal oxidation of hydrogen at the electrodes. The SOFC is a high temperature fuel cell and the reactants are required to be supplied at equilibrium concentration at the necessary operating temperature. The isothermal circulators deliver the reactants from atmospheric conditions to the equilibrium concentrations while another set of isentropic circulators delivers the reactants to the fuel cell at the operating temperature. Similarly the products leaving the fuel cell are cooled through isentropic circulators and delivered at atmospheric conditions by the isothermal circulator. The operation of the fuel cell chemical reaction occurs at a high temperature and vacuum pressures, which feeds a Carnot cycle. The T-S (temperature-entropy) diagram given in Figure 6.3 shows that the Carnot cycle operates between the fuel cell temperature (T2=1273 K) and the atmospheric temperature (T0=298 K) or the dead state temperature. The area under T0-T2-S3-S2 shows the heat rejected by the fuel cell reversibly to the environment by the Carnot engine.

However, for the combined reversible operation of the reformer and fuel cell, the reformer is supplied with reactants at equilibrium concentrations and the operating temperature of 500 K via isothermal and isentropic circulators respectively. The hydrogen exhaust from the reformer is fed at 500 K to the fuel cell which is delivered to the fuel cell through an isentropic circulator at 1200 K. As a result, the shaded region in Figure 6.3, represents the heat required by the methanol steam reforming reaction.

The idealised circulators, fuel cell and reformer are a series of interconnected reversible processes. The total work potential of these processes is the sum of the electrochemical

work (Gibbs free energy at operating temperature of fuel cell), the circulator work and work produced by the Carnot cycle [75].

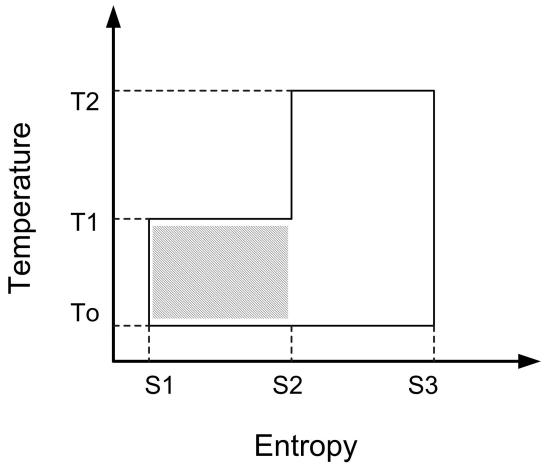

Figure 6.3 – Temperature-Entropy Diagram for reversible reformer-fuel cell process

A steam reformer is normally supplied with heat from a burner to support the endothermic chemical reaction. In order to consider a fully reversible reformer, the heat required to support the endothermic reaction is provided by the heat generated by the fuel cell Carnot cycle. The approach described by Barclay [75], for calculating the chemical exergy of methane via the reformer route is applied here. The overall methanol steam reforming electrochemical reaction for the reformer is

$$CH_3OH + H_2O \rightarrow CO_2 + 3H_2$$

Eqn. 6.4

The reformer is supplied with reactants at a temperature higher than atmospheric and hence isentropic circulators are required along with the isothermal circulators to deliver reactants and products at equilibrium concentrations to and from the reformer. The hydrogen produced by the reformer is further fed through an isentropic circulator to increase its temperature to the fuel cell operating temperature. The chemical exergy of methanol is calculated by the reformer route as described by Barclay [75]. The total work potential of the reformer is the sum of Gibbs free energy of methanol at the reformer operating temperature, work done by circulators and the work produced by the Carnot cycle.

6.4.2. Reversible IC Engine

An ideal IC engine (Figure 6.2) is supplied with reactants at equilibrium concentrations at atmospheric temperature. The chemical reaction occurring within the engine is assumed to be that of isothermal oxidation rather than the highly irreversible process of combustion. Based on the assumptions stated in Table 6-1, the products are delivered to the environment at atmospheric conditions with the help of isothermal circulators only. Since the engine operates at atmospheric temperature, the total work potential of the engine is the sum of Gibbs free energy of the fuel and the work produced by the circulators.

The steps followed to calculate work potential for the system shown in Figure 6.2 include:

- Determining the equilibrium concentrations required for the process
- Determining circulator power required for reactants and products to deliver them to and from the system at equilibrium pressures and temperatures
- ΔG for the equilibrium chemical reaction
- Determining heat dissipated through the system to the environment reversibly by the Carnot engine.
- Summing up the ΔG values from circulators, chemical reaction and Carnot engine

6.5. *System with Internal irreversibilities, externally reversible (Case B)*

Internal irreversibilities are those which are caused by factors internal to the components which may include uncontrolled chemical reactions, friction, mismatched heat capacities (in case of heat exchangers) or design faults [70]. The effect of these internal irreversibilities in the system results in reduction of work potential. The transition from a completely reversible system in Figure 6.2 to a system with internal irreversibilities is shown in Figure 6.4. Because of internal irreversibilities occurring in each component, non-ideal reactions take place and result in production of effluents.

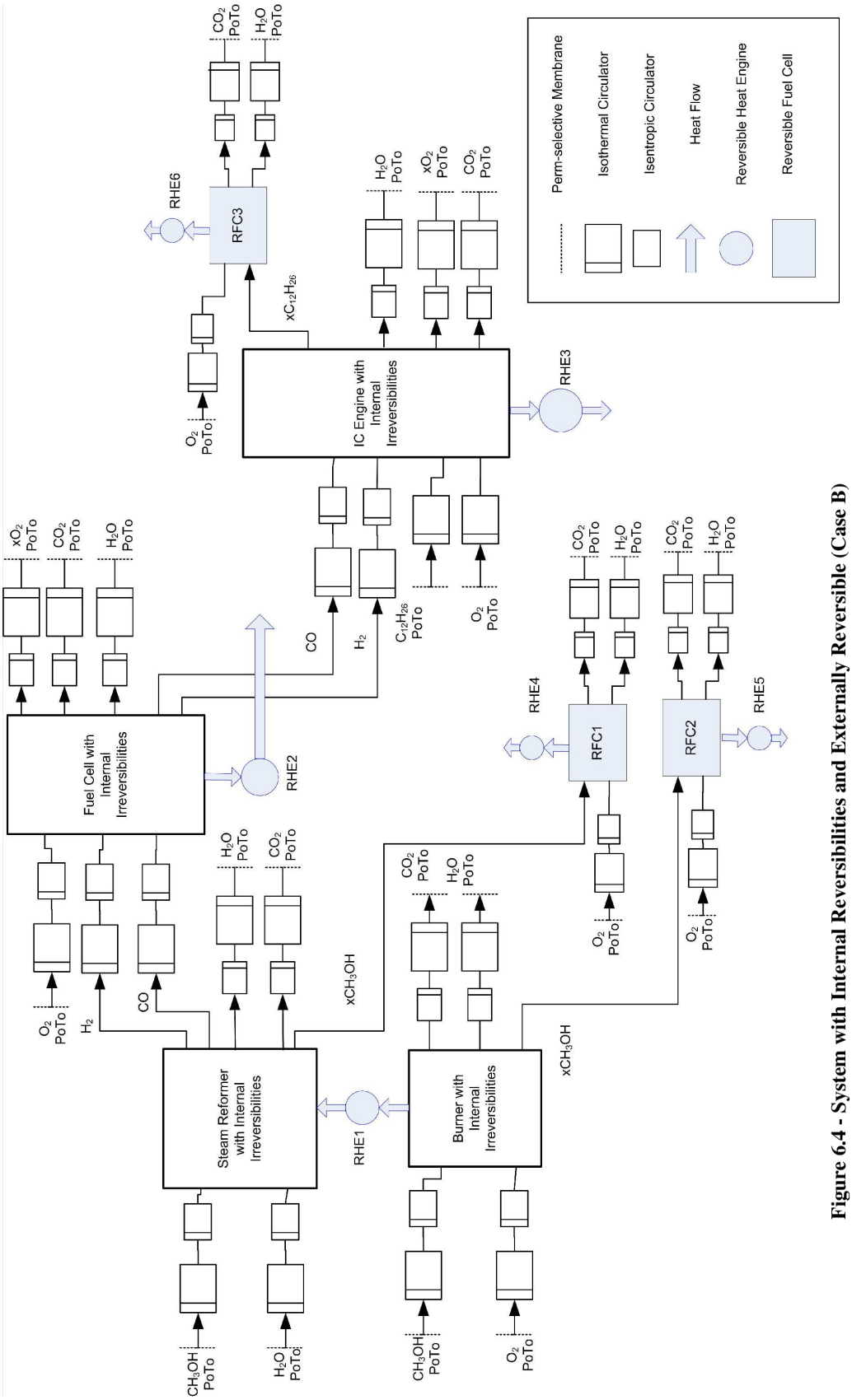

Figure 6.4 - System with Internal Reversibilities and Externally Reversible (Case B)

Table 6-2 – System with external reversibility

System with external reversibility	Case B (i)	Case B (ii)	Units
SOFC			
Temperature in	1200	1200	K
Pressure	3	3	Bar
Flow rate of H_2 in	0.2322	0.2322	mol/s
fuel utilisation factor	60	52	%
Reformer			
Temperature in	500	500	K
Pressure	3	3	Bar
Flow rate of CH_3OH	0.167	0.167	mol/s
Flow rate of H_2O	0.2504	0.2504	mol/s
Mole fraction of products			
Hydrogen	0.637	0.637	-
carbon monoxide	0.02	0.02	-
carbon dioxide	0.2	0.2	-
H_2O	0.137	0.137	-
CH_3OH	0.006	0.006	-
Burner			
Temperature in	352	352	K
Temperature out	600	600	K
Pressure in	3	3	Bar
Flow rate of CH_3OH	0.0842	0.0842	mol/s
Flow rate of O_2	0.159	0.159	mol/s
% of unburned fuel	3	14	%
IC Engine			
Temperature in	415	415	K
Temperature out	700	700	K
Pressure in	1.8	1.8	Bar
Pressure out	2	2	Bar
Flow rate of $C_{12}H_{26}$	0.0404	0.0404	mol/s
Flow rate of O_2	1.819	1.819	mol/s
% of unburned fuel	2	15	%

The system shown in Figure 6.2 is completely reversible. With the introduction of internal exergy losses or internal irreversibilities in the system, it takes the form of the system as shown in Figure 6.4. In this case the reactants and products for each component are not at equilibrium conditions resulting in incomplete usage of fuel and spontaneous reactions that result in heat transfer. The external exergy losses associated with the matter streams are idealized using circulators, perm selective membranes, reversible heat engines (RHE) and reversible fuel cells (RFC). Table 6-2 presents a list of assumptions and parameters for this case. Two sub-cases have been discussed to see the effect of internal irreversibilities on the work potential of the system. In Case B (ii) the fuel cell, burner and engine have higher process imperfections as compared to Case B (i). The following sections 6.5.1 - 6.5.3 describe how each component operation is affected by the introduction of internal irreversibilities.

6.5.1. Reformer

A practical reformer with internal irreversibilities deviates from the equilibrium reaction and produces carbon monoxide and unused methanol, unused water vapour along with hydrogen and carbon dioxide. The hydrogen and carbon monoxide exhausts from the reformer, are fed to the fuel cell as fuel. The unused methanol is fed to a completely reversible fuel cell RFC1 at equilibrium concentrations to avoid external irreversibilities. The water vapour and carbon dioxide is brought to environmental condition with the help of the circulators.

The heat required for the reforming reaction in this case is supplied by a burner. The combustion of methanol in the burner causes the formation of carbon dioxide, water vapour, some unused methanol and thermal energy. There is a reversible heat transfer from the products of this irreversible reaction to the reformer via RHE1, while the unused methanol is fed to an ideal fuel cell RFC2. The heat transfer from RFC2 to the environment is done using a reversible heat engine RHE4. The remaining effluents are released to the environment through circulators.

6.5.2. SOFC

The practical fuel cell which has electrical resistance is supplied with fuel from the reformer exhausts. It is only able to utilise part of the fuel causing the exhaust flow to consist of unused hydrogen, unused carbon monoxide, water vapour, carbon dioxide and

unused oxygen. The unused fuel is supplied to the IC engine in order to improve the performance of the engine and ensure maximum work extraction from any unused fuel. The remaining exhausts are brought to environment conditions by the ideal circulators.

6.5.3. IC Engine

The IC engine is supplied with primary fuel along with unused fuel from the fuel cell. For the sake of simplicity, it is assumed that no pollutants are formed, but the exhaust stream consists of unused oxygen, unused primary fuel, carbon dioxide and water vapour. The thermal energy that would normally be rejected to the environment directly, is instead directed to a reversible heat engine RHE3 producing further useful work while the unused primary fuel is fed to an ideal fuel cell RFC3 at equilibrium conditions. The remaining matter streams are exhausted to the environment through isentropic and isothermal circulators.

6.6. *System with Internal and External Irreversibilities (Case C)*

Irreversibilities are inherent in all processes. The main categories of irreversible processes as mentioned by Haywood [86] include the following:

- Frictional processes
- Unresisted expansion
- Heat transfer across a finite temperature difference
- Combustion of a fuel
- Diffusive mixing of fuel streams

A system with internal and external irreversibilities represents a practical scenario for the system and is shown in Figure 6.5. Inclusion of external reversibilities to the system represented in Figure 6.4 involves replacement of the ideal circulators and heat engines by practical expanders, compressors and heat exchangers. Removal of perm-selective membranes results in losses due to mixing or diffusion of species in the system. The unused fuel can either be re-circulated to the input of a component or exhausted to the environment. The system now accounts for exergy losses produced by all of the above listed categories for irreversible processes.

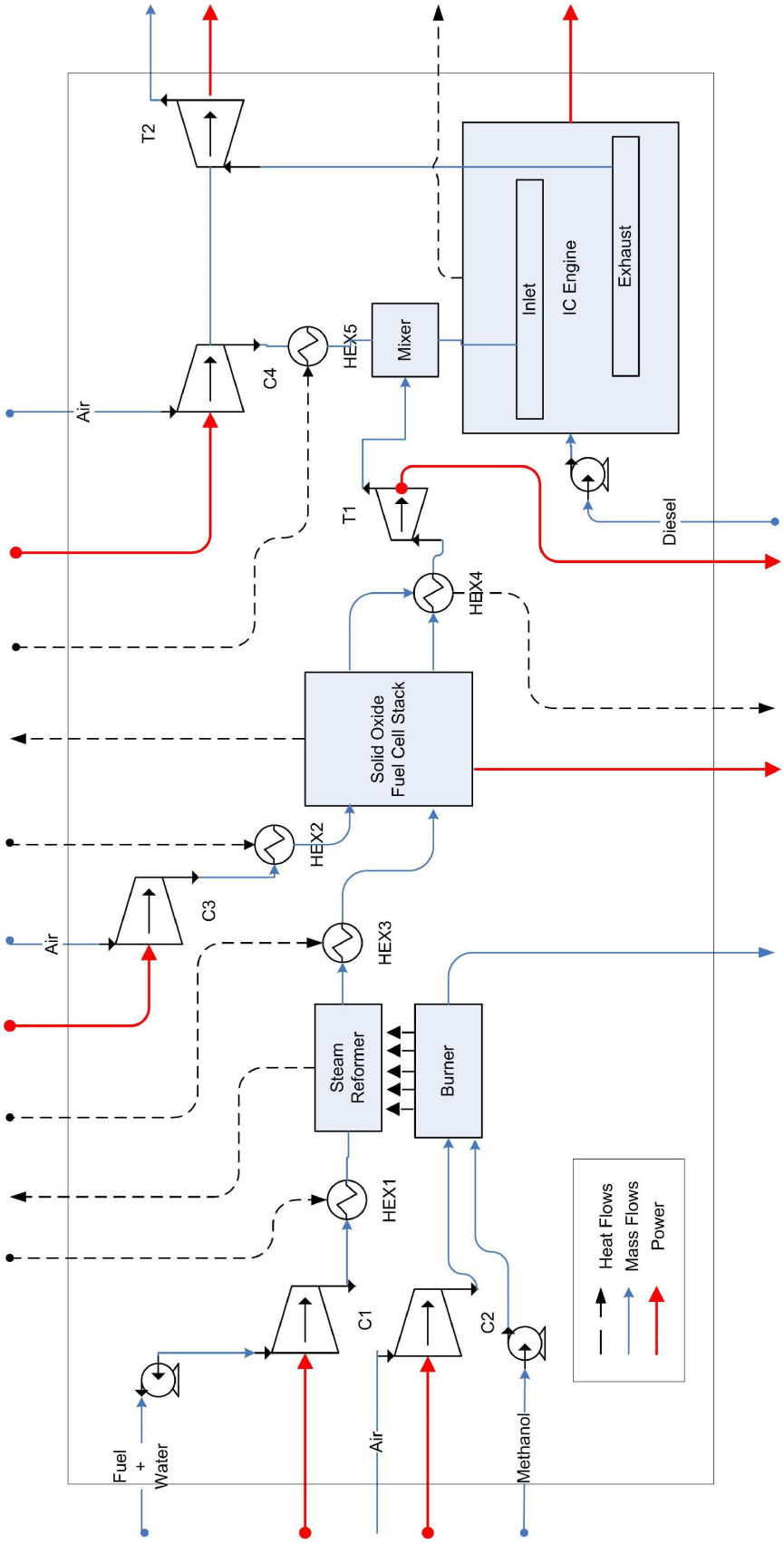

Figure 6.5 – Control Volume of the Practical System Internal and External Irreversibilities (Case C)

A steady state condition is considered for the analysis for Case C. The exergy balances for each component of the system are described below. If each individual component is considered to be in a control volume, the exergy balance for the control volume surrounding each component is described in sections 6.6.1-6.6.6. Further, the exergy balance of the whole system is computed (control volume shown in Figure 6.5), with one component feeding effluents or heat as proposed by the system configuration in Chapter 2 (The System and its Attributes) to take advantage of exergy losses. The exergy balance and rational efficiency equations given in Eqn. 6.1-Eqn. 6.3 are applied for each component. All thermochemical data for hydrogen, carbon monoxide, carbon dioxide, water vapour, oxygen, nitrogen are from taken from JANAF thermochemical table by Stull [122] and Perry's Chemical Handbook by Perry et al [123]. The fuel flow rates and operating temperatures for Case C are maintained the same as in Case B(i).

6.6.1. Reformer-Burner:

In practical conditions, the reformer deviates from the reversible reaction. The methanol reforming considered here is a two-stage reaction and is given in Eqn. 6.5 and Eqn. 6.6.

$$CH_3OH + H_2O \xleftrightarrow{k1} CO_2 + 2H_2$$

Eqn. 6.5

$$CH_3OH \xleftrightarrow{k2} CO + H_2$$

Eqn. 6.6

The methanol combustion reaction in the burner is given in Eqn. 6.7. It is assumed that 4 % of the methanol fed to the burner is unused while the rest is completely burned to produce carbon dioxide and water vapour.

$$CH_3OH + O_2 \xleftrightarrow{k1} CO_2 + 2H_2O$$

Eqn. 6.7

The reaction rates and flows for the reformer and burner reactions are determined from modelling work in Chapter 4 (Component Modelling-Reformer Modelling) and Varesano et al [16]. The thermodynamic properties of methanol are obtained from Chao et al [124].

For a control volume around the reformer and burner, the energy balances are given by Eqn. 6.8.

$$\sum_{out} \dot{n}_{out} \times h_{out} - \sum_{in} \dot{n}_{in} \times h_{in} = \dot{Q}_{REF} \text{ and } \sum_{in} \dot{n}_{in} \times h_{in} - \sum_{out} \dot{n}_{out} \times h_{out} = \dot{Q}_{BUR}$$

Eqn. 6.8

The irreversibilities in the reformer-burner unit are given by Eqn. 6.9.

$$\dot{I}_{REF-BUR} = \sum \dot{E}x_{mass,in} - \sum \dot{E}x_{mass,out} + \sum \dot{E}x_{heat}$$

Eqn. 6.9

The exergy transfer by mass for the reformer is given by Eqn. 6.10 and Eqn. 6.11.

$$\sum \dot{E}x_{mass,in} = (\dot{n}_R \times ex)_{CH_3OH,in} + (\dot{n}_R \times ex)_{H_2O,in} + (\dot{n}_B \times ex)_{CH_3OH,in} + (\dot{n}_B \times ex)_{O_2,in}$$

Eqn. 6.10

$$\sum \dot{E}x_{mass,out} = (\dot{n}_R \times ex)_{H_2,out} + (\dot{n}_R \times ex)_{CO,out} + (\dot{n}_R \times ex)_{CO_2,out} + (\dot{n}_R \times ex)_{H_2O,out}$$
$$+ (\dot{n}_R \times ex)_{CH_3OH,out} + (\dot{n}_B \times ex)_{CO_2,out} + (\dot{n}_B \times ex)_{H_2O,out} + (\dot{n}_B \times ex)_{CH_3OH,out}$$

Eqn. 6.11

The exergy transfer due to heat for the reformer-burner unit is given by Eqn. 6.12.

$$\sum \dot{E}x_{heat} = \left(1 - \frac{T_o}{T_{BUR}}\right)\dot{Q}_{BUR} - \left(1 - \frac{T_o}{T_{REF}}\right)\dot{Q}_{REF}$$

Eqn. 6.12

6.6.2. Fuel Cell:

The fuel cell exergy balance is given in Eqn. 6.13.

$$\sum \dot{E}x_{mass,in} = \sum \dot{E}x_{mass,out} - \sum \dot{E}x_{heat} + \sum \dot{E}x_{work} + \dot{I}_{FC}$$

Eqn. 6.13

It is assumed that the fuel cell operates at a full load of 20 kW and at a utilisation factor of 60 %. The mass flow rates and electrochemical data have been obtained by scaling up the single cell model discussed in Chapter 4 (Component Modelling-Solid Oxide Fuel Cell – Fundamentals and modelling principles). The exergy transfer due to mass flowing into the fuel cell is given in Eqn. 6.14 while that due to the mass flowing out from the fuel cell is given in Eqn. 6.15.

$$\sum \dot{E}x_{mass,in} = \dot{E}x_{H_2,in} + \dot{E}x_{O_2,in} = (\dot{n} \times ex)_{H_2,in} + (\dot{n} \times ex)_{O_2,in}$$

Eqn. 6.14

$$\sum \dot{E}x_{mass,out} = \dot{E}x_{H_2,out} + \dot{E}x_{O_2,out} + \dot{E}x_{H_2O,out}$$
$$= (\dot{n} \times ex)_{H_2,out} + (\dot{n} \times ex)_{O_2,out} + (\dot{n} \times ex)_{H_2O,out}$$

Eqn. 6.15

The electrical work done by the fuel cell is the product of the stack voltage and current as shown in Eqn. 6.16.

$$\sum \dot{E}x_{work} = V_{FC} \times I$$

Eqn. 6.16

The energy balance for the fuel cell, given in Eqn. 6.17, is used to determine heat generated by the fuel cell reaction.

$$\sum_{in} \dot{n}_{in} \times h_{in} - \sum_{out} \dot{n}_{out} \times h_{out} = \dot{Q}_{FC} + W_{FC}$$

Eqn. 6.17

The exergy transfer due to the heat generated in the fuel cell is given below.

$$\sum \dot{E}x_{heat} = \left(1 - \frac{To}{T_{FC}}\right).\dot{Q}_{FC}$$

Eqn. 6.18

6.6.3. IC Engine

For the IC engine, it is assumed that the engine operates at 100 kW with 2% of the input fuel unused and the rest is completely burned to form carbon dioxide and water vapour. The fuel dodecane $C_{12}H_{26}$ is used for calculation instead of diesel. The flow rates and feed and exhaust temperatures are determined from the model discussed in Chapter 4 (Component Modelling-IC Engine). The energy balance equation of the engine is used to determine the heat generated.

$$\sum_{in} \dot{n}_{in} \times h_{in} - \sum_{out} \dot{n}_{out} \times h_{out} = \dot{Q}_{ICE} + W_{ICE}$$

Eqn. 6.19

The exergy change due to heat transfer to the environment is given by Eqn. 6.20.

$$\sum \dot{E}x_{heat} = \left(1 - \frac{To}{T_{ICE}}\right)\dot{Q}_{ICE}$$

Eqn. 6.20

The exergy balance for the engine is given in Eqn. 6.21, while the exergy transfer due to the streams of matter flowing in and out of the engine is given in Eqn. 6.22 and Eqn. 6.23 respectively.

$$\dot{I}_{ICE} = \sum \dot{E}x_{mass,in} - \sum \dot{E}x_{mass,out} + \sum \dot{E}x_{heat} - \sum \dot{E}x_{work}$$

Eqn. 6.21

$$\sum \dot{E}x_{mass,in} = (\dot{n} \times ex)_{H_2,in} + (\dot{n} \times ex)_{CO,in} + (\dot{n} \times ex)_{Diesel,in} + (\dot{n} \times ex)_{O_2,AIR,in} + (\dot{n} \times ex)_{N_2,AIR,in} + (\dot{n} \times ex)_{O_2,FC,in} + (\dot{n} \times ex)_{N_2,FC,in}$$

Eqn. 6.22

$$\sum \dot{E}x_{mass,out} = (\dot{n} \times ex)_{H_2O,out} + (\dot{n} \times ex)_{CO_2,out} + (\dot{n} \times ex)_{Diesel,out} + (\dot{n} \times ex)_{O_2,out} + (\dot{n} \times ex)_{N_2,out}$$

Eqn. 6.23

6.6.4. Compressor and Turbines:

The isentropic efficiency of all compressors and turbines is assumed to be 70% and data for flow rates is obtained from the model for the Garrett turbocharger maps described in Chapter 4 (Component Modelling-Turbocharger).

$$\dot{I}_{CMP} = \sum \dot{E}x_{mass,in} - \sum \dot{E}x_{mass,out} + \sum \dot{E}x_{heat} - \sum \dot{E}x_{work}$$

Eqn. 6.24

The exergy change due to heat transfer from the compressor is determined using the energy balance equation given in Eqn. 6.25.

$$\sum_{in} \dot{n}_{in} \times h_{in} - \sum_{out} \dot{n}_{out} \times h_{out} = \dot{Q}_C - W_C$$

Eqn. 6.25

The exergy change due to heat transferred to the environment is given in Eqn. 6.26.

$$\sum \dot{E}x_{heat} = \left(1 - \frac{To}{T_C}\right).\dot{Q}_C$$

Eqn. 6.26

The exergy change due to work consumed by the compressor is given by Eqn. 6.27.

$$\sum \dot{E}x_{work} = W_C = \frac{c_p T_{out}}{\eta_c}\left(\left(\frac{Pout}{Pin}\right)^{\frac{(\gamma-1)}{\gamma}} - 1\right)$$

Eqn. 6.27

For the turbines:

$$\dot{I}_{TUR} = \sum \dot{E}x_{mass,in} - \sum \dot{E}x_{mass,out} - \sum \dot{E}x_{heat} - \sum \dot{E}x_{work}$$

Eqn. 6.28

The exergy change due to heat transfer is determined by the energy balance for the turbine given below:

$$\sum_{in} \dot{n}_{in} \times h_{in} - \sum_{out} \dot{n}_{out} \times h_{out} = \dot{Q}_T + W_T$$

Eqn. 6.29

The exergy gain due to the work produced by the turbine by expansion of gases is given by Eqn. 6.30.

$$\sum \dot{E}x_{work} = W_T = \eta_t c_p T_{out}\left(1 - \left(\frac{Pout}{Pin}\right)^{\frac{(\gamma-1)}{\gamma}}\right)$$

Eqn. 6.30

The exergy loss due to heat transfer to the environment is given in Eqn. 6.31.

$$\sum \dot{E}x_{heat} = \left(1 - \frac{To}{T_T}\right).\dot{Q}_T$$

Eqn. 6.31

6.6.5. Heat Exchangers

The energy balance for the heat exchanger determines the heat lost to the cooling or heating medium.

$$\sum_{in} \dot{n}_{in} \times h_{in} - \sum_{out} \dot{n}_{out} \times h_{out} = \dot{Q}_{med} - \dot{Q}_{surr}$$

Eqn. 6.32

$$\dot{Q}_{HEX} = \dot{Q}_{med} - \dot{Q}_{surr}$$

Eqn. 6.33

The operating temperature of the heat exchanger is given below.

$$T_{hex} = \frac{T_{in} - T_{out}}{2}$$

Eqn. 6.34

The heat lost to the surrounding in the heat exchanger is given below in Eqn. 6.35.

$$\dot{Q}_{surr} = \alpha T_{hex} S_{hex}$$

Eqn. 6.35

The exergy transfer due to heat from the heat exchanger is given by Eqn. 6.36

$$\sum \dot{E}x_{heat} = \left(1 - \frac{To}{T_{hex}}\right).\dot{Q}_{HEX}$$

Eqn. 6.36

$$\dot{I}_{HEX} = \sum \dot{E}x_{mass,in} - \sum \dot{E}x_{mass,out} + \sum \dot{E}x_{heat}$$

Eqn. 6.37

6.6.6. Mixer

The exergy losses for the mixer are given in Eqn. 6.38. It is assumed that the heat transfer to the environment in the mixer is negligible.

$$\dot{I}_{MIX} = \sum \dot{E}x_{mass1,in} + \sum \dot{E}x_{mass2,in} - \sum \dot{E}x_{mass,out}$$

Eqn. 6.38

6.6.7. System Exergy Balance

The exergy balance of the system enclosed in the control volume as shown in Figure 6.5 is given as follows:

$$\dot{I}_{SYS} = \sum \dot{E}x_{mass,in} - \sum \dot{E}x_{mass,out} + \sum \dot{E}x_{heat} - \sum \dot{E}x_{work}$$

Eqn. 6.39

The first term on the right hand side of the above equation consists of the sum of $\dot{E}x_{mass,in}$ of compressors C1, C2, C3, C4, reformer, burner and the IC engine. The second term consists of sum of $\dot{E}x_{mass,out}$ of burner, turbine T2 and CO2 and H2O exhausts from the reformer. The third term consist of the sum of $\dot{E}x_{heat}$ of compressors C1, C2, C3, C4, turbines T1, T2, heat exchangers HEX1, HEX2, HEX3, HEX4, HEX5, reformer-burner, fuel cell and IC engine. The last term is the sum of $\dot{E}x_{work}$ of all compressors, turbine, fuel cell and IC engine.

The results for Case C in the following section will indicate the contribution of the matter and energy flows for each component in the overall assessment of exergy change.

6.7. *Results and Discussion*

The maximum useful work for Case A, from the system in Figure 6.2 with 100% rational efficiency is the sum of the maximum work produced by reformer, fuel cell and the IC Engine. Table 6-3, Table 6-4 and Table 6-5 shows the exergy calculations for Case A, B and C respectively.

Table 6-3 – Case A

	Reformer	**Fuel Cell**	**IC Engine**
ΔG_1 Isentropic circulator power (kJ/mol)	89.33	21.6	0
ΔG_2 Isothermal circulator power (kJ/mol)	-147.2	-155.5	-522.9
ΔC_t Carnot cycle power (kJ/mol)	40.2	-152.4	0
ΔG of fuel at operating temperature (kJ/mol)	-41.6	-181.5	-7752.7
Chemical exergy of fuel $\Delta G_1 + \Delta G_2 + \Delta C_{t+}$ ΔG (kJ/mol)	-59.3	-467.7	-8275.6
Total in kW	**-9.9**	**-108.6**	**-334.2**

As seen in Figure 6.2 for Case A, the components are a network of reversible processes including isothermal and isentropic energy exchanges and idealised chemical reactions.

The reactions in each component, i.e., the reformer, fuel cell and engine are fully reversible occurring at equilibrium concentrations. As described by Barclay [75], these equilibrium reactions are a source of electrochemical, circulator and Carnot work potentials. Hence, the total work potential or exergy of these networks of reversible processes is the sum of ΔGs across each component. Table 6-3 shows the power produced by the circulators, Carnot cycle and Gibbs function for each fuel for the reformer, fuel cell and engine. The high value of isothermal circulator power for the reformer is due to the hydrogen produced, which is supplied to the fuel cell. The negative sign in table indicates power produced.

The maximum useful work that produced by the system at 100% rational efficiency is 452.7 kW. In order to have minimum exergy losses, the system must be operated as closely as possible to the reversible system described in Figure 6.2. The ideal circulators in the reversible system, which deliver reactants and products to and from vacuum pressures for equilibrium concentrations, have extremely high pressure ratios. As a result, the actual implementation of such a system may not be feasible or may be extremely expensive.

For Case B(i), when the system is externally reversible with internal irreversibilities, the maximum useful work output of the system reduces to 349.15 kW with the system rational efficiency dropping to 77.13 %. The rational efficiency is calculated with reference to the maximum work potential of the reversible system obtained in Table 6-3. The rational efficiency is the ratio of work potential in Case A to that in Case B. Due to internal irreversibilities, unused methanol from the burner, the unreformed methanol from the reformer and the unburnt fuel from the engine is produced. In order to ensure external reversibilities, this unused fuel, which has work potential, is exploited by feeding these fuel streams through a fully reversible fuel cell. The heat generated due to the internal irreversibilities runs a Carnot engine. The Carnot engines and the reversible fuel cells ensure external reversibility of the system.

Case B(ii) allows to evaluate the sensitivity of internal irreversibilities. In Case B(ii) it is assumed that the utilisation factor of the fuel cell is lower than Case B(i), and higher percentages of unburnt fuel is produced by the burner and the IC engine. Table 6-4, shows the results obtained in both cases, and it is evident that the work potential reduces as internal irreversibilities increase.

Table 6-4 – Case B

Case B(i)	Reformer	Burner	Fuel Cell	IC Engine
Isentropic circulator power (kW)	2.53	0.28	2.29	-28.02
Isothermal circulator power (kW)	-2.06	-1.57	2.12	-15.85
heat	4.76	-8.19	-6.81	-14.78
Reversible Fuel Cell + reversible heat engine power for unused fuel (kW)	-0.12	-0.21	0	-1.51
Chemical exergy (kW)	-6.86	-12.82	-25.28	-237.04
Total in kW	**-1.76**	**-22.51**	**-27.67**	**-297.21**
Total system power (kW)	-349.15			
Rational efficiency of the system	77.13 %			
Case B(ii)	**Reformer**	**Burner**	**Fuel Cell**	**IC Engine**
Isentropic circulator power (kW)	2.53	0.54	2.84	-14.93
Isothermal circulator power (kW)	-2.06	-1.36	2.14	-17.29
heat	4.76	-8.19	-5.20	-5.73
Reversible Fuel Cell + reversible heat engine power for unused fuel (kW)	-0.12	-0.66	0	-45.31
Chemical exergy (kW)	-6.86	-12.02	-20.20	-202.50
Total in kW	-1.76	-21.68	-20.43	-285.77
Total system power (kW)	-329.64			
Rational efficiency of the system	73.64%			

In Case B, any external exergy losses that would have been produced are eliminated by feeding them through reversible components and producing additional work. As the internal irreversibilities increase, the power produced by these reversible components increases. Since the power production contribution of the IC engine is the highest in the system, a change in its internal irreversibilities will have a greater effect on the external

irreversibilities as compared to any other component. In order to evaluate the external exergy losses for the system, we examine Case C.

The practical system in Case C, as shown in Table 6-5 produces maximum useful work of 128.90 kW with a rational efficiency of only 25.43 %. Case C has the same assumption for fuel flows and operating temperatures as in Case B (i). The rational efficiency for each component and the system is calculated using Eqn. 6.3. Table 6-5 shows the exergy analysis for each individual component and the system as a whole as well. The results in Table 6-5 are represented in a Sankey diagram in Figure 6.6 as percentages of the total system input exergy to the control volume. Figure 6.6 shows that the maximum percentages of irreversibilities are in the reformer, engine and then the burner in descending order. The fuel cell has extremely low irreversibilities (0.33 %) because the exhausts are utilised within the turbine T1 and the IC engine. However, if the fuel cell exhausts were let out to the environment, the irreversibilities would increase to 8.75 %. This clearly shows the advantages of the hybrid configuration.

The heat rejected to the environment is significant and can be used internally in the system to reduce exergy losses. The IC engine rejects a significant amount of heat (17.03 %) to the environment. If this heat was utilised by the reformer, the burner and compressor C2 would be redundant and the system rational efficiency would improve. Similarly, the heat from the IC engine can be provided to the heat exchangers. The result would be an increase in work potential to 132.96 kW and an increase in rational efficiency from 25.43 % to 36.01 %.

The system components which produce work using combustion, i.e. the IC engine and the burner have rational efficiencies of 28. 28 % and 40.78 % respectively. The high degree of irreversibility is due to dissipation of large amounts of heat due to the combustion process and the hot pressurized and unburned fuel in the exhausts. The use of combustion based devices in a system must be accompanied with other components which can utilise the thermal, chemical and pressure exergy flowing out from the device. The fuel cell has a low rational efficiency of 27.50 % since it is operated at a low utilisation factor. Amongst the auxiliary components required in the system, the rational efficiency of the mixer is lower as compared to heat exchangers, compressor and turbines.

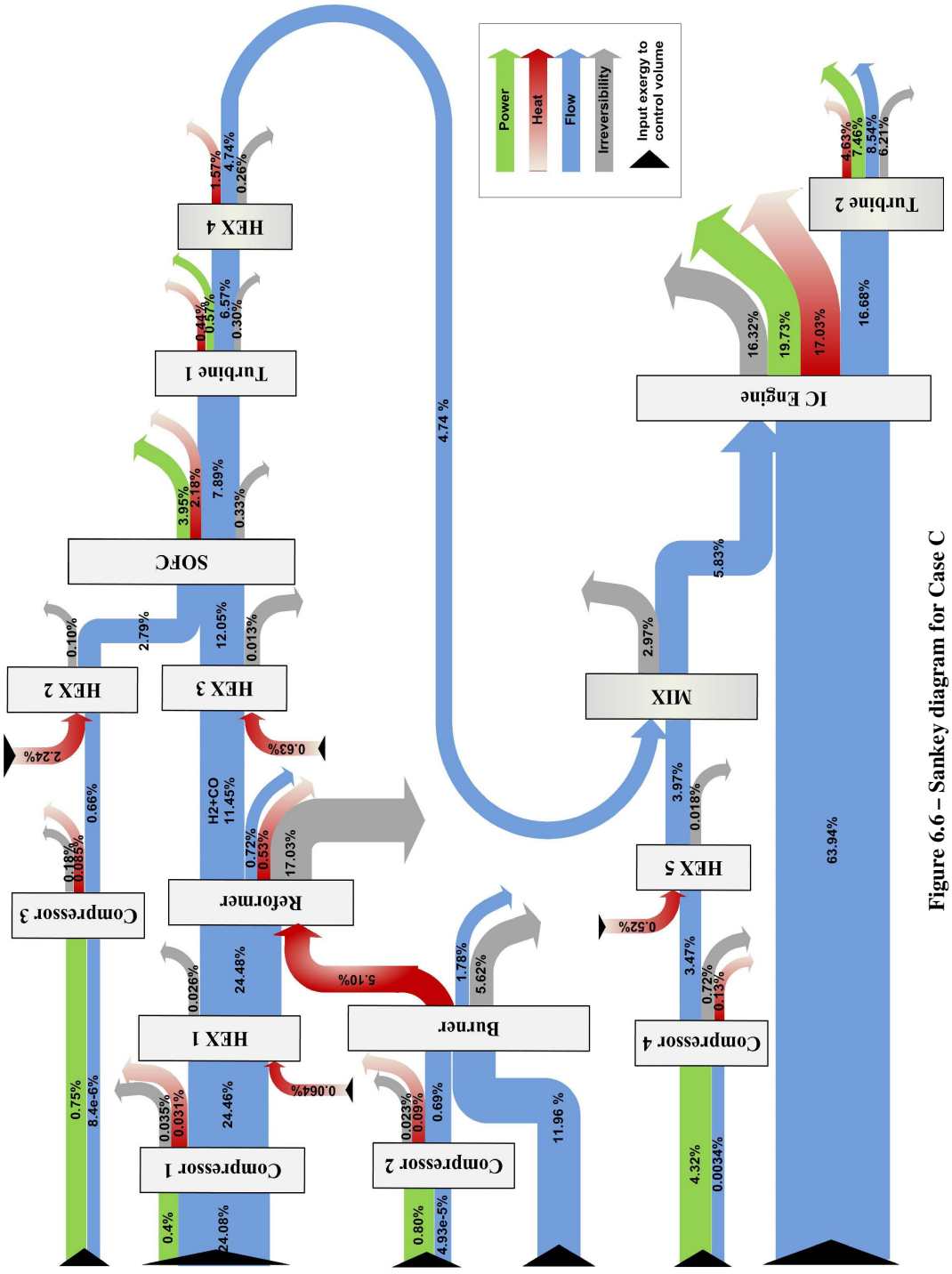

Figure 6.6 – Sankey diagram for Case C

Table 6-5 – Case C

	Exergy IN (kW)	Exergy OUT (kW)	Heat Exergy (kW)	Work (kW)	Irreversibilities (kW)	Rational efficiency
C1	122.10	123.81	-0.16	2.04	0.18	99.73%
HEX1	124.01	124.20	0.32	-	0.14	99.89%
Reformer	124.12	60.91	23.12	-	86.33	25.84%
HEX3	58.06	61.21	3.21	-	0.07	99.89%
C2	2.50E-04	3.49	-4.57E-01	4.06	0.12	85.89%
Burner	63.34	9.02	-25.83	0.00	28.49	40.78%
C3	4.28E-05	3.32	-4.28E-01	3.80	0.90	87.57%
HEX2	3.32	14.17	11.36	-	0.52	96.45%
Fuel Cell	72.73	40.01	-11.04	20.00	1.68	27.50%
T1	39.93	33.30	-2.26	2.87	1.51	90.57%
HEX4	33.30	24.03	-7.95	-	1.32	72.14%
C4	1.70E-02	17.59	-0.67	21.90	3.67	80.22%
HEX5	17.59	20.11	2.61	-	0.09	99.55%
MIX	44.62	29.58	-	-	15.04	66.30%
IC Engine	353.55	84.54	-86.32	100.00	82.70	28.28%
T2	89.13	43.27	-23.46	37.83	31.49	90.98%
System Control Volume	**506.86**	**53.51**	**-117.93**	**128.90**	**254.23**	**25.43 %**

Case A represents the ideal case with 453.7 kW of power; Case B(i), shows a drop in power produced to 349.1 kW due to the introduction of internal exergy losses; and finally Case C, shows a further drop to 128.90 kW due to the introduction of internal and external exergy losses. The exergy balance for the system in the control volume is shown in Figure 6.5 and the combined results of the exergy analysis are shown in the Sankey diagram, Figure 6.7. The figure shows that the system has 103.6 kW (22.9 %) of internal exergy losses and 220.2 kW (48.64 %) of external exergy losses. The exergy analysis for Case C, with the assumption for fuel flow rates and temperatures as in Case B(ii), results in a work potential of 118.90 kW with a rational efficiency of 23.46 %. Hence the internal exergy

losses increase to 120.1 kW (27.2 %) and the external exergy losses decrease to 210.7 kW (46.5 %).

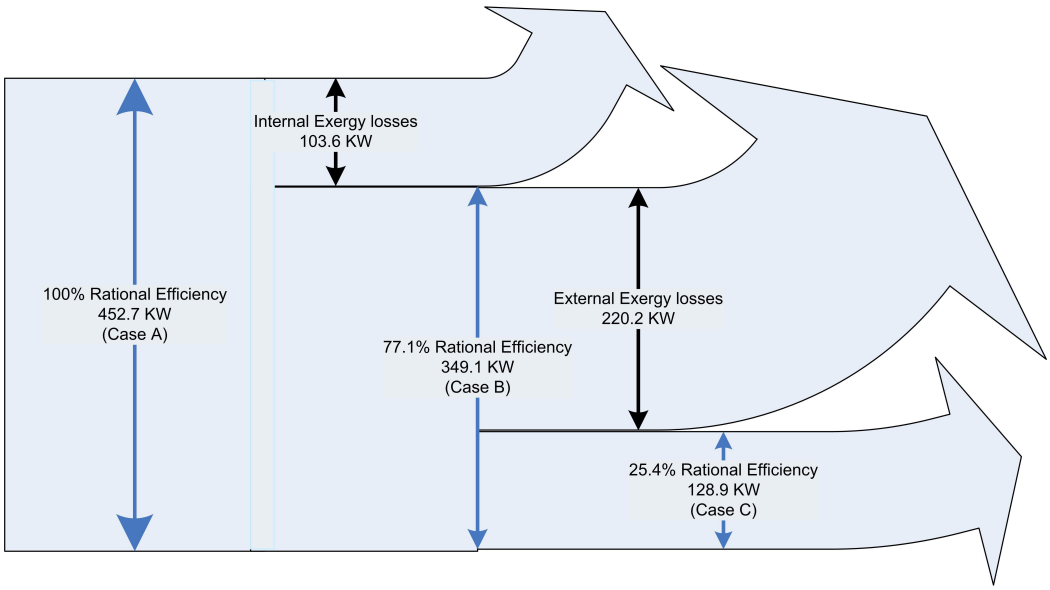

Figure 6.7 – Sankey Diagram for fuel cell-engine hybrid system

6.8. *Chapter summary*

The exergy analysis results show the progressive decrease in maximum work potential of the system from the reversible condition to the practical condition. The rational efficiencies for are 100 %, 77.1 % and 25.4 % for Case A, Case B(i) and Case C respectively. The heat dissipated to the environment from the system can be utilised within the system to reduce exergy losses. As discussed in the earlier section, the heat dissipated by the IC engine and the fuel cell can be utilised to supply heat required by the reformer and heat exchangers resulting in rational efficiency for Case C to increase from 25.43 % to 36.01 %.

When the internal irreversibilities were increased by 4.3% as in Case B(ii), the external irreversibilities decreased by 2.14 % and the work potential of the system dropped from 128.9 kW to 118.9 kW. This shows that the work potential of the system is a function of the internal irreversibilities. Internal exergy losses are mainly due to process irreversibilities which affect the external exergy losses. The external exergy losses depend on the process as well as the reactor material properties which affect the exergy transfer due to heat. Hence, the external exergy losses are dependent on the internal exergy losses.

The methodology followed here for the exergy analysis of a complex hybrid system can be applied to any system with complex matter and energy interactions. The method allowed to evaluate the extent of deviation of the practical system from the ideal system. The analysis showed that the internal irreversibilities have a direct impact on the work potential of the system, hence the focus of system optimisation should be to improve the processes within each component. The heat rejected to the environment by the IC engine, which is a form of external exergy losses, when utilised within the system results in elimination of the burner and the compressor C2. Hence, external exergy losses can indicate a potential for improved system design which has a higher rational efficiency.

The exergy analysis results presented in this chapter are for a specific set of conditions. Investigating the exergy losses for a dynamic system model can provide useful insight into the requirement for reducing exergy losses at different load conditions and during transients. Operating the system at optimum conditions can reduce irreversibilities in the system. The above exergy analysis considers the ideal case (Case A) where all components are fully reversible. This reversibility is possible when the system undergoes a number of quasi-static processes over infinite time. What is of significant interest for control development is the work potential of a practical system operating in finite time, and the extent to which entropy can be minimised or work potential maximised. This is discussed further as a control strategy based on exergy analysis in Chapter 11 (Future Work).

The exergy losses are also associated with material and design issues. The possibilities to reduce irreversibilities by improving component design for the hybrid system, according to priority for components with highest irreversibilities, is given below.

- improved catalysts in the reformer
- improved cylinder design for the IC Engine to allow complete combustion of fuel with minimum frictional losses.
- improved reactor design for efficient heat transfer and complete combustion in the burner
- improved materials or structure for the SOFC
- better designs for heat dissipation/absorption in heat exchangers.

Chapter 7. System Integration

7.1. *Introduction*

In fuel cell systems, the amount of fuel and air necessary to be supplied to the fuel cell must always be in excess to avoid degradation of its performance and structure. Hence there is the need to utilize the excess fuel and air.

Solid oxide fuel cell – gas turbine (SOFC-GT) systems exploit this potential of the hot pressurized exhausts by utilizing them to operate a turbine and produce extra power. The excess fuel is fed to the turbine through an afterburner [27]. Similarly the fuel cell exhausts, if utilized in an IC engine are highly advantageous. The solid oxide fuel cell is fuel flexible. The exhausts from the SOFC will consist of residual fuel, carbon dioxide and oxygen depleted air. Such a fuel cell provides means to improve combustion in the engine and eliminates the need for the conventional exhaust gas recirculation (EGR) system required by the engine.

Effects of hydrogen induction in a diesel fuelled engine have been studied by Mathur et al [12, 14]. The studies show improvement in thermal efficiency of the engine with increasing amount of hydrogen in the engine. However, when the amount of hydrogen in the cylinder is increased above 20 %, the thermal efficiency rapidly decreases. With the use of nitrogen as a diluent, the amount of hydrogen added can be increased, without deteriorating the thermal efficiency. It also assists in reducing knocking in the engine caused by introduction of hydrogen.

This chapter investigates the design of a control system for a hybrid system utilizing a fuel cell to condition the air and fuel input of the engine. The fuel cell provides efficient power production along with effluents which when introduced in the engine assist in improving combustion. The control design strategy, to manage flows required in the fuel cell and IC engine to ensure optimum operation of each component, is discussed in this chapter.

7.2. *Modelling Assumptions*

The system, as shown in Figure 7.2, consists of a solid oxide fuel cell supplied by fuel from hydrogen cylinders. The exhausts from the fuel cell are fed into the IC engine. The engine is supplied by a primary liquid fuel such as diesel.

The steady state analysis discussed in Chapter 5 (Investigation of Optimum Operating Range) on the fuel cell – IC Engine system suggested that effective management of the flows into and out of the system can result in optimum operation of the system. Introducing trace amount of hydrogen into a diesel engine can improve the combustion and thermal efficiency [12]. The high cetane number of hydrogen can cause knocking and hence requires a diluent such as nitrogen [12]. The oxygen depleted air from the fuel cell cathode serves this purpose. The amount of oxygen depleted air fed to the engine from the fuel cell cathode can be controlled by adjusting the excess air ratio of the fuel cell. The excess air ratio of the fuel cell is defined as the ratio of air consumed to the amount of air supplied to the fuel cell.

$$\lambda_{O_2} = \frac{W_{cathode}}{W_{O_2,used}}$$

Eqn. 7.1

The amount of hydrogen entering the engine depends on the amount of excess fuel supplied to the fuel cell. This can be controlled by controlling the utilisation factor defined as the ratio of hydrogen consumed to the hydrogen supplied to the fuel cell.

$$\mu_f = \frac{W_{H_2,used}}{W_{H_2,in}}$$

Eqn. 7.2

The efficiency of the fuel cell is proportional to the utilisation factor [6]; hence a very low utilisation factor results in greater amount of hydrogen in the engine but lower fuel cell efficiency. Since the fuel cell operation can be potentially more efficient than the engine, it is suggested to maintain an optimum utilisation factor. This ensures optimum overall system efficiency. The steps following in this chapter for an integrated system model is given in Figure 7.1.

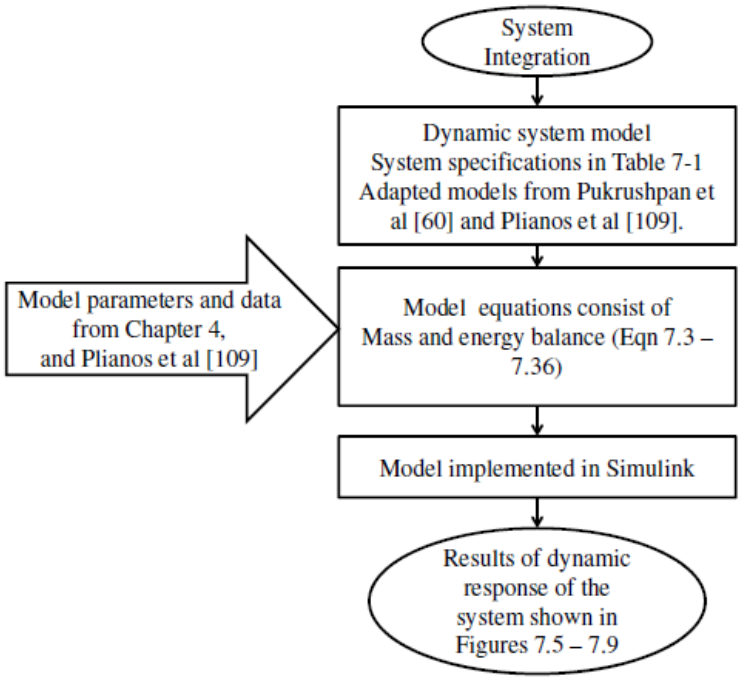

Figure 7.1 – Integrated system model flowchart

7.3. *System Modelling*

A dynamic control oriented model of the solid oxide fuel cell-IC Engine system is developed. The fuel cell model includes electrochemical and mass transfer effects. The temperature of the stack is assumed to be constant. The compressors and turbine model in the system is for a Garrett turbocharger as discussed in section 4.4 (Component Modelling-Turbocharger). The transient response of the integrated fuel cell and IC engine models is discussed. The models are implemented using Matlab®/Simulink®. The physical parameters of the system components are given in Table 7-1.

Table 7-1 – System Parameters

System Parameters	
Fuel Cell	
Maximum power output	25 kW
Number of cells	2627
IC Engine	
No of cylinders	4
Maximum power output	100kW at 2200 RPM
Bore Diameter	0.11 m
Stroke	0.127 m

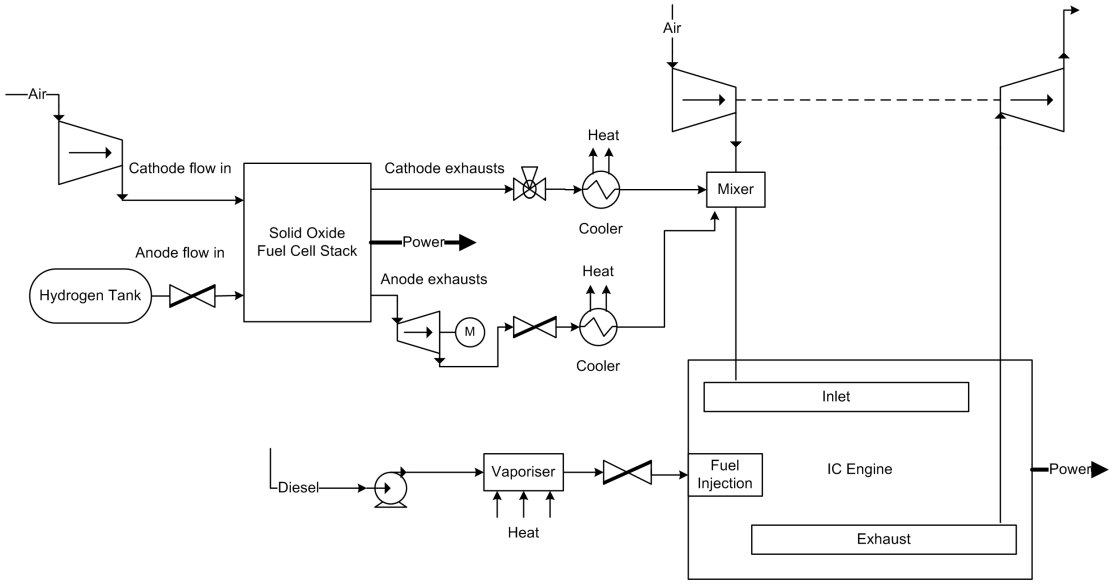

Figure 7.2 – System schematic of a solid oxide fuel cell – Internal combustion engine hybrid system

7.3.1. Fuel Cell Model

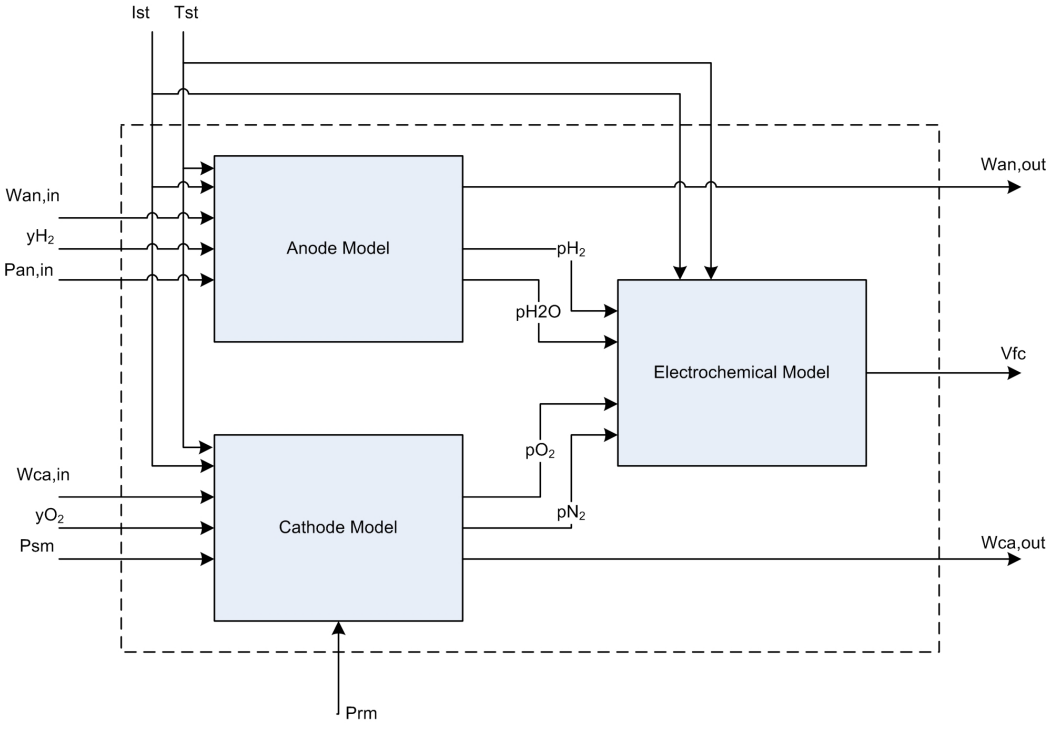

Figure 7.3 – Structure of Fuel Cell Model

The structure of the fuel cell model developed is shown in Figure 7.3.

- Electrochemical Model

The electrochemical model for the solid oxide fuel cell is described in the following equations. The parameters used for simulation of the fuel cell stack are taken from [35].

$$E_{Nernst} = -\frac{\Delta G^o}{2F} + \frac{RT}{2F}\ln\left(\frac{p_{H_2} p_{O_2}^{1/2}}{p_{H_2O}}\right)$$

Eqn. 7.3

The equivalent resistances of the cathode R_C and anode R_A are based on experimental characterization [99] for a single cell are given in Eqn. 7.4 and Eqn. 7.5. The single cell is scaled up to a 25 kW stack with 2627 cells.

$$R_A = \left[\frac{2F}{RT} k_A A_a^c \left(\frac{p_{H_2}}{P_{anode}}\right)^{0.25} \exp\left(-\frac{E_A}{RT}\right)\right]^{-1}$$

Eqn. 7.4

$$R_C = \left[\frac{4F}{RT} k_C A_c^c \left(\frac{p_{O_2}}{P_{cathode}}\right)^{0.25} \exp\left(-\frac{E_C}{RT}\right)\right]^{-1}$$

Eqn. 7.5

$$V_{fc} = E_{Nernst} - (R_A + R_C + R_\Omega) I$$

Eqn. 7.6

- Supply Manifold

The fuel cell supply manifold dynamics are given below:

$$\frac{dm_{sm}}{dt} = W_{cp1} - W_{sm,out}$$

Eqn. 7.7

$$\frac{dp_{sm}}{dt} = \frac{\gamma R_a}{V_{sm}}\left(W_{cp1} T_{cp1,out} - W_{sm,out} T_{sm}\right)$$

Eqn. 7.8

The supply manifold outlet mass flow is given by the following equation.

$$W_{sm,out} = k_{sm,out}\left(p_{sm} - P_{cathode}\right)$$

Eqn. 7.9

- Return Manifold

The return manifold model below assumes that the changes in temperature of the air from the stack into the return manifold are negligible.

$$\frac{dp_{sm}}{dt} = \frac{\gamma R_a}{V_{sm}}\left(W_{cp}T_{cp,out} - W_{sm,out}T_{sm}\right)$$

Eqn. 7.10

The return manifold outlet mass flow, $W_{rm,out}$ is governed by the orifice equation. The pressure ratio in the orifice equation will depend on the pressure at the inlet manifold of the IC Engine.

- Cathode Flow Model

The cathode is fed with pressurized air from a compressor. The mass flow balance equation and ideal gas law relations are used to develop the flow models. The flow models are developed on lines of a control oriented model for a PEM fuel cell system proposed by Pukrushpan et al [61].

$$\frac{dm_{O_2}}{dt} = W_{O_2\,in} - W_{O_2\,out} - W_{O_2\,used}$$

Eqn. 7.11

$$\frac{dm_{N_2}}{dt} = W_{N_2\,in} - W_{N_2\,out}$$

Eqn. 7.12

The mass flow rate of oxygen used in the fuel cell is a function of the load demand or the stack current.

$$W_{O_2\,used} = M_{O_2} \times \frac{nI_{st}}{4F}$$

Eqn. 7.13

The total pressure in the cathode is given by:

$$P_{cathode} = p_{O_2} + p_{N_2}$$

Eqn. 7.14

The partial pressure of oxygen is used to determine the mass fraction and the mass flows out from the cathode as shown in Eqn. 7.15-Eqn. 7.18.

$$y_{O_2,out} = \frac{p_{O_2}}{P_{cathode}}$$

Eqn. 7.15

$$x_{O_2,out} = \frac{y_{O_2,out} \times M_{O_2}}{y_{O_2,out} \times M_{O_2} + (1 - y_{O_2,out}) \times M_{N_2}}$$

Eqn. 7.16

The mass flow rate exiting the cathode ($W_{cathode,out}$) is calculated using the simplified orifice equation, which allows to calculate the following two equations.

$$W_{O_2\,out} = x_{O_2,out} \times W_{cathode,out}$$

Eqn. 7.17

$$W_{N_2\,out} = \left(1 - x_{O_2,out}\right) \times W_{cathode,out}$$

Eqn. 7.18

- Anode Flow Model

The fuel cell anode receives fuel from a hydrogen tank. This flow can be changed by adjusting the valve of the hydrogen tank. The mass balances for the anode species are given in Eqn. 7.19 and Eqn. 7.20

$$\frac{dm_{H_2}}{dt} = W_{H_2\,in} - W_{H_2\,out} - W_{H_2\,used}$$

Eqn. 7.19

$$\frac{dm_{H_2O}}{dt} = W_{H_2O_{in}} - W_{H_2O_{out}} + W_{H_2O_{gen}}$$

Eqn. 7.20

The hydrogen used during the reaction and the water vapour generated is given below.

$$W_{H_2\,used} = M_{H_2} \times \frac{nI_{st}}{2F}$$

Eqn. 7.21

$$W_{H_2O_{used}} = M_{H_2O} \times \frac{nI_{st}}{2F}$$

Eqn. 7.22

The total anode pressure is the sum of partial pressures of the gases in the anode.

$$P_{anode} = p_{H_2} + p_{H_2O}$$

Eqn. 7.23

The partial pressures, mole and mass fraction, and flow rates exiting the anode are given in Eqn. 7.24-Eqn. 7.27.

$$y_{H_2,out} = \frac{p_{H_2}}{P_{anode,out}}$$

Eqn. 7.24

$$x_{H_2,out} = \frac{y_{H_2,out} \times M_{H_2}}{y_{H_2,out} \times M_{H_2} + (1 - y_{H_2,out}) \times M_{H_2O}}$$

Eqn. 7.25

$$W_{H_2\,out} = x_{H_2,out} \times W_{anode,out}$$

Eqn. 7.26

$$W_{H_2O\,out} = \left(1 - x_{H_2,out}\right) \times W_{anode,out}$$

Eqn. 7.27

The integration of the mass balance equations determines the mass, which is used to calculate the partial pressure in both the channels using the ideal gas law.

7.4. *Mean Value Model – Engine*

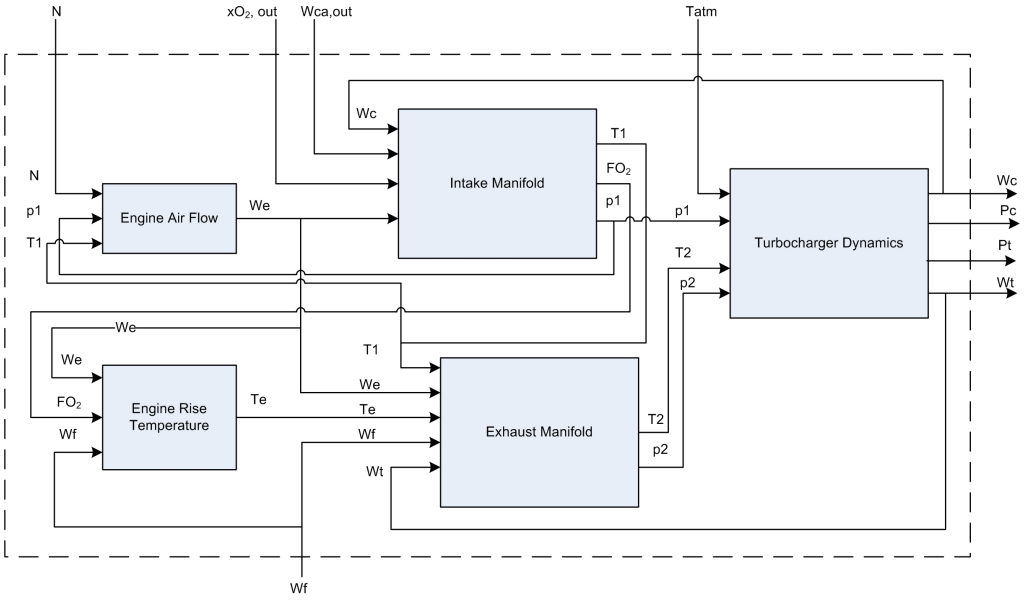

Figure 7.4 – Structure of Engine Model

The structure of the engine model is shown in Figure 7.4. Following the development path of a turbocharged engine with EGR [125], a mean value model to suit this application was developed. The EGR flow is replaced by exhaust from the fuel cell cathode.

Since, the exhaust from the fuel cell cathode contains a depleted percentage of oxygen, the calculation of oxygen-to-fuel ratio would be more appropriate for the engine. The oxygen-to-fuel ratio of the engine is given by

$$OFR = \frac{F_{O_2} \times W_e}{W_f + W_{H_2}}$$

Eqn. 7.28

Where, F_{O_2} is the fraction of oxygen in the engine intake manifold. The dynamics of F_{O_2} are given below. The mass and energy balance equations for the inlet and exhaust manifold of the engine as discussed by Jankovic et al [125] are given below.

$$\dot{F}_{O_2} = \frac{(0.21 - F_{O_2})W_{cp2} + (y_{O_2} - F_{O_2})W_{ce}}{m_1}$$

Eqn. 7.29

$$\dot{m}_1 = W_{cp2} + W_{ce} - W_e + W_{ae}$$

Eqn. 7.30

$$\dot{m}_2 = W_e + W_f - W_t$$

Eqn. 7.31

$$\dot{p}_1 = \frac{\gamma R}{V_1}\left(W_{cp2}T_{cp2} + W_{ce}T_{fce} + W_{ae}T_{fce} - W_e T_1\right)$$

Eqn. 7.32

$$\dot{p}_2 = \frac{\gamma R}{V_2}\left((W_e + W_f)T_e - W_t T_2\right)$$

Eqn. 7.33

The dynamics of the turbocharger speed is derived from Newton's second law with both parts of the equation multiplied by the turbocharger speed to give turbocharger angular acceleration as a function of turbocharger net power.

$$\dot{\omega}_{tc} = \frac{1}{J_{tc}\omega_{tc}}\left(\eta_m P_t - P_c\right)$$

Eqn. 7.34

The mass flow into the engine, compressor flow, engine outlet temperature and turbocharger net powers have been parameterized using experimental data and data supplied from the turbocharger manufacturer and adopted from the work done by Plianos et al [109] .

The fraction of oxygen depleted air entering the engine is given by Eqn. 7.35.

$$F_{O_2,dep} = \frac{W_{ce}}{W_e}$$

Eqn. 7.35

The fraction of hydrogen entering the engine is given by the equivalent energy in the fuel.

$$F_{H_2} = \frac{W_{H_2} \times Q_{H_2}}{W_f \times Q_f + W_{H_2} \times Q_{H_2}}$$

Eqn. 7.36

Where Q_{H2} and Q_f are the heating values of hydrogen and the engine fuel diesel.

7.5. *Simulation Results*

The control oriented models described in the previous section are integrated to form the complete system model. The behaviour of the engine and fuel cell is investigated for various flows into the system. On the basis of the simulation results, a control strategy to develop localized controllers for the SOFC and the IC Engine is suggested.

A series of steps for stack current, compressor motor voltage and flow of hydrogen into the anode is shown. The transient behaviour of the simulated fuel cell model can be seen in Figure 7.6 and Figure 7.7.

From Figure 7.6, the variation in utilisation factor can be noted. The utilisation factor is affected by the load demand. Since, the hydrogen flow in the fuel cell is increased in steps as the current increases; the utilisation factor is between 0.48 and 0.60.

For a given flow of fuel in the fuel cell, increase in current or the load demand causes the utilisation factor to increase. At low load conditions the utilisation is very low, lowering the efficiency of the fuel cell. For efficient operation of the fuel cell, the flow rate of hydrogen should be changed according to the load demand and maintain a utilisation factor at least of 70% (as described in Chapter 5). In order to achieve a utilisation factor between 70-95%, the fuel flow must be manipulated as the load demand changes.

As the utilisation factor increases, the amount of hydrogen and oxygen content leaving the fuel cell decrease. The fuel supply can be controlled by regulating the valve position of the hydrogen tank.

In Figure 7.6, the amount of excess oxygen supplied and the air-to-fuel ratio are increasing at each step. The excess oxygen ratio will reduce with increasing current or load demand. As more fuel is supplied, more oxygen is consumed to produce power. This increasing excess oxygen ratio causes the compressor to draw excess power from the motor to supply the air flow into the fuel cell and affects the net system power. In order to avoid air starvation in the fuel cell, the excess air ratio is maintained at λ_{O2}= 2. The compressor

motor voltage can be adjusted according to the load demand on the fuel cell to provide the necessary supply of air.

The pressures in the cathode and anode exhausts are fairly equal for lower loads. As the load increases, the pressure difference between the cathode and the anode rapidly rises. To ensure structural integrity of the electrolyte and for the electrochemical reaction to take place, this difference should be kept below 8 kPa [38]. The simulation results stay well within this value.

Figure 7.7, shows that increasing load demand results in higher power from the fuel cell. At the same time, the power required by the compressor increases much more than the fuel cell can provide. Hence, it is necessary to maintain the excess oxygen ratio at a pre-defined value. The stack voltage rapidly decreases with increase in load. The fuel cell stack voltage settles to a steady value after at least 5 seconds of simulation time. This delay is a result of the compressor operation.

The control of the air supply in the cathode depends on the amount of fuel supplied in the anode of the fuel cell. A localized controller for the fuel cell can be developed to adjust the flows into the cathode and anode with the following control objectives:

- Maintain excess air ratio in the fuel cell $\lambda_{O2}=2$,
- Regulate the flow of hydrogen such that the utilisation factor is at least 70%,
- Within the limits of the above two objectives, ensure the fuel cell supplies a steady base load.

In order to achieve the objectives for the fuel cell controller the following can be assumed:

- Inputs – Compressor Voltage
- Disturbance – Fuel cell stack current
- Performance variables – Difference between the desired power and actual power output, excess air ratio, utilisation factor
- Measurements – Stack voltage, Flow rate of fuel cell compressor, pressure input to the fuel cell

The addition of excess hydrogen from the fuel cell to the engine is preferred rather than recirculating into the fuel cell. Since the fuel cell power capacity is comparatively smaller than the engine power capacity, the amount of hydrogen entering the engine is small. The

fuel cell assists in conditioning the fuel properties of the engine in order to improve its performance.

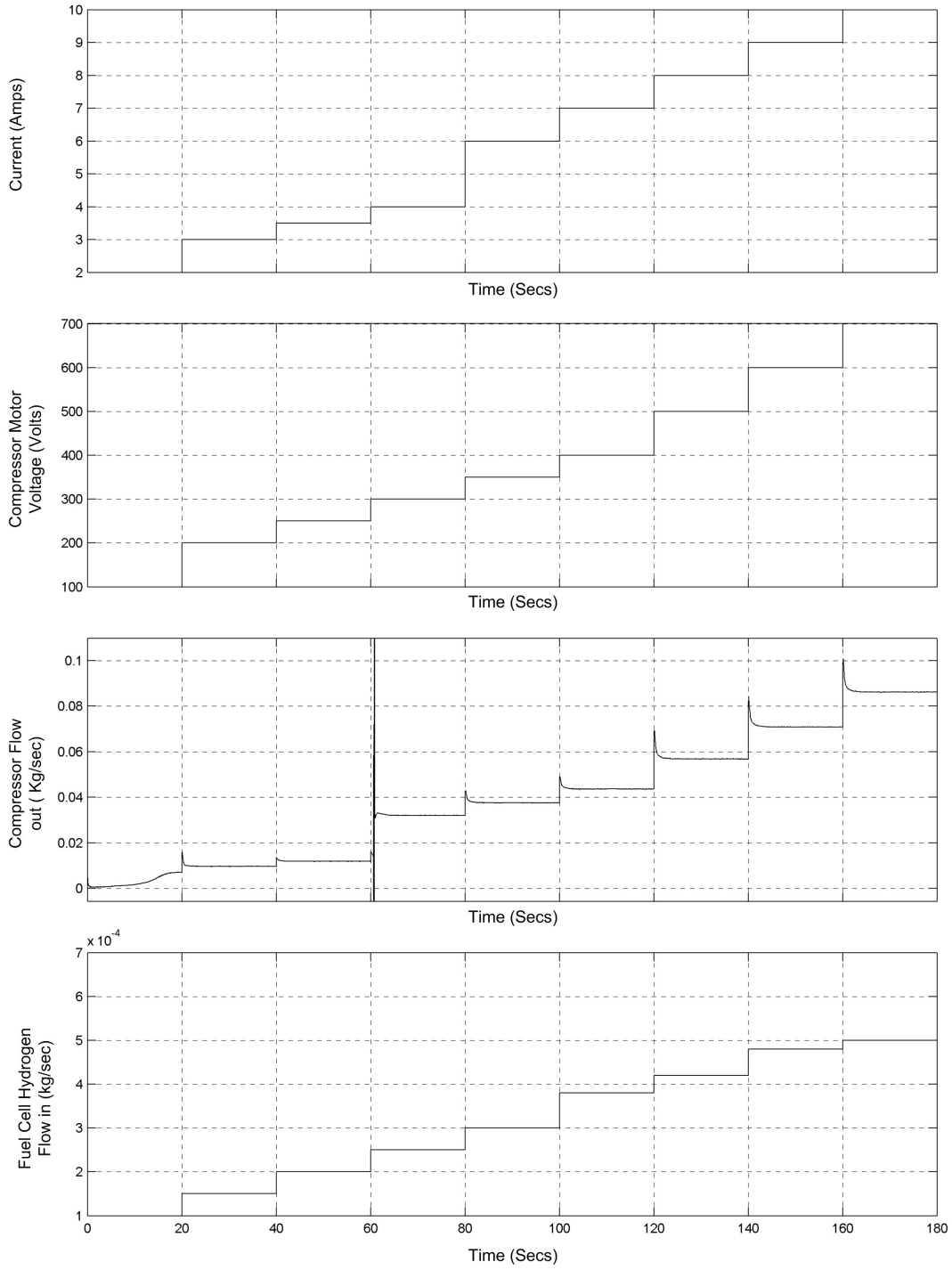

Figure 7.5 – Inputs To The Fuel Cell System Model

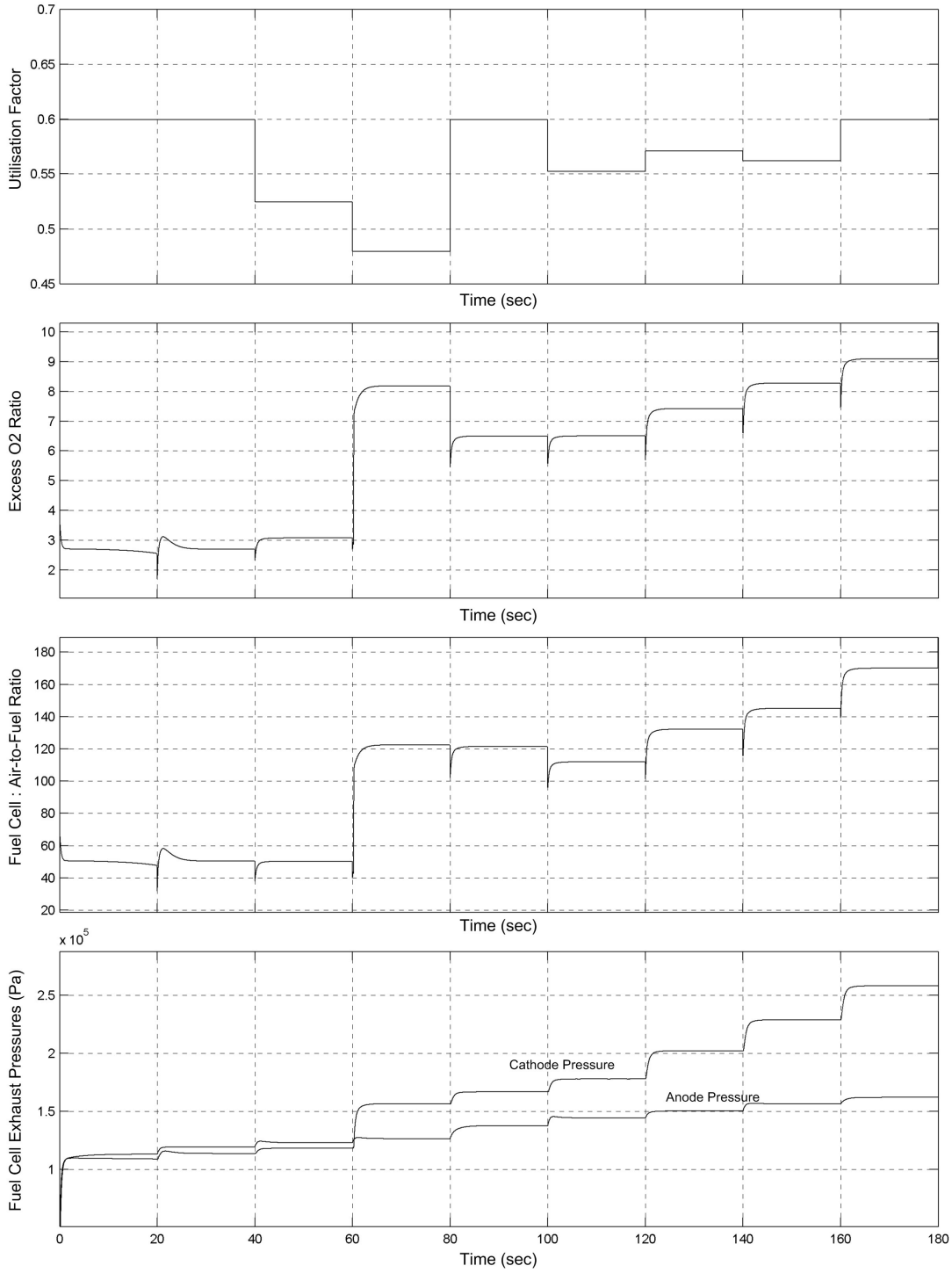

Figure 7.6 – Fuel cell performance

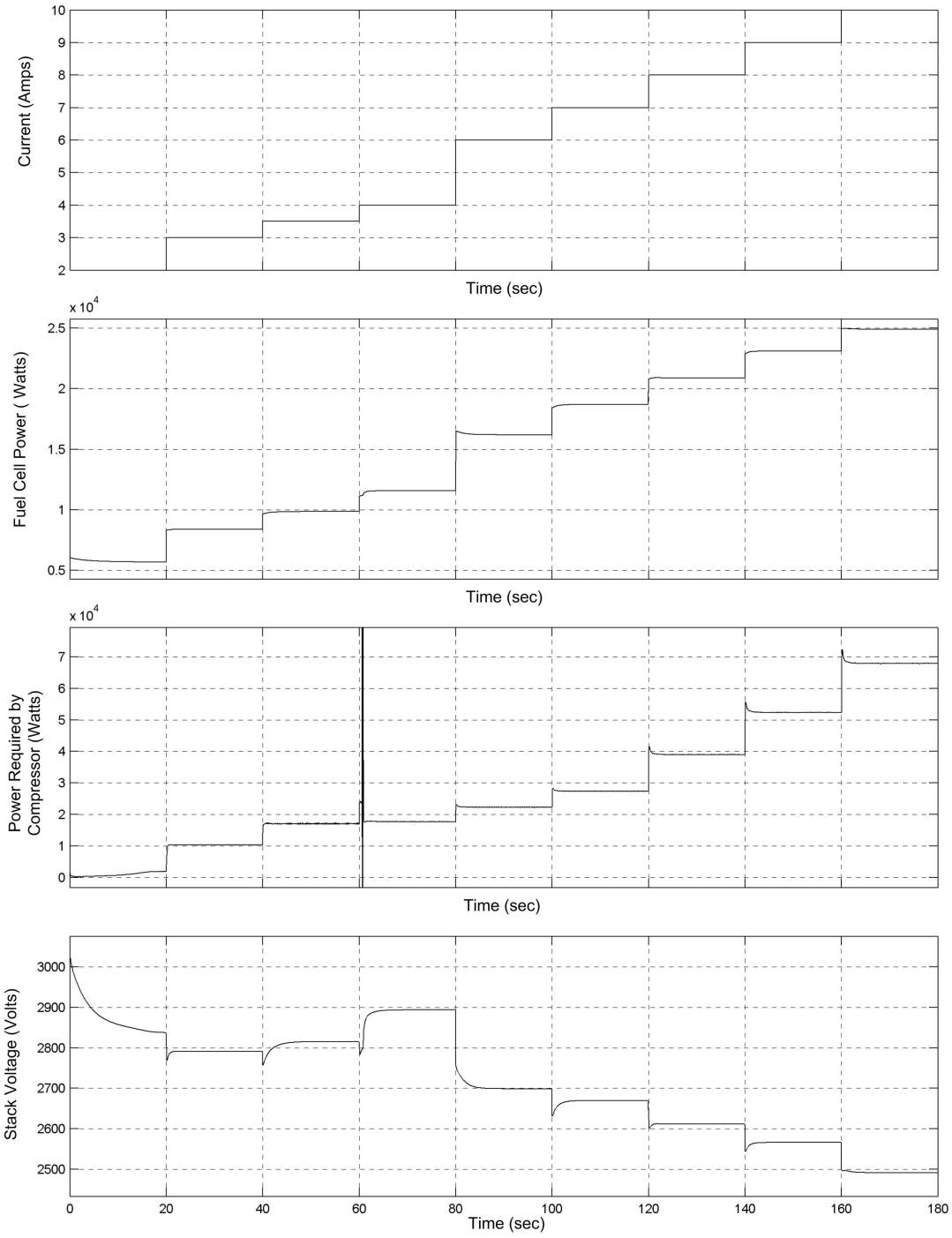

Figure 7.7 – Fuel cell output characteristics

The simulation results of the engine when fed with exhausts from the fuel cell are shown in Figure 7.8 and Figure 7.9. These effluents leave the fuel cell at a temperature of 1273 K. The engine temperature rises almost by 200 K if the effluents are fed at the same temperature. Such a temperature rise can cause pre-ignition of the fuel causing detonation in the engine cylinders. In order to avoid detonation, the effluents are cooled before entering the engine. The detailed thermal effects of combustion chemistry are not included in the model.

The cooling of the fuel cell exhausts from 1273 K to approximately 373 K results in higher heat rejection (8-95kW) as compared to conventional EGR coolers. This rejected heat can be utilized to pre-heat the incoming air into the supply manifold of the fuel cell.

In a conventional EGR fed engine system, the fraction of burned gases fed back into the cylinder consists of inert gases. For this system, the fuel cell cathode exhausts may contain significant percentage of oxygen. It is convenient to compute the oxygen-to-fuel ratio required in the engine rather than the air-to-fuel ratio. The air from the compressor to the engine provides fixed percentage of oxygen in the incoming air, whereas the percentage of oxygen in the fuel cell cathode can be computed. For control purposes, it is easier to determine the OFR as compared to the AFR for this particular system.

Figure 7.8 shows the transient characteristics of the total mass flow rate of air in the engine, percentage of hydrogen present in the fuel, mass flow rate of fuel and the oxygen-fuel ratio. An initial transient is observed for the mass flows of air and the OFR due to the compressor dynamics. The excess oxygen ratio in the fuel cell will directly affect the OFR in the engine. This is evident from Figure 7.8, where the OFR increases with increase in excess oxygen ratio of the fuel cell.

If the stoichiometric OFR for combustion of diesel and hydrogen is approximately 3.54, then the amount of oxygen available in the engine is approximately 200% in excess. Depending on the set-point for OFR, the amount of oxygen-depleted air entering the engine can be controlled in two ways; controlling the excess air ratio of the fuel cell or using a three way valve between the fuel cell and the engine. The excess air ratio of the fuel cell can be changed by adjusting the voltage input to the compressor motor. A

feedback controller can be developed to handle this exhaust from the cathode. This controller design

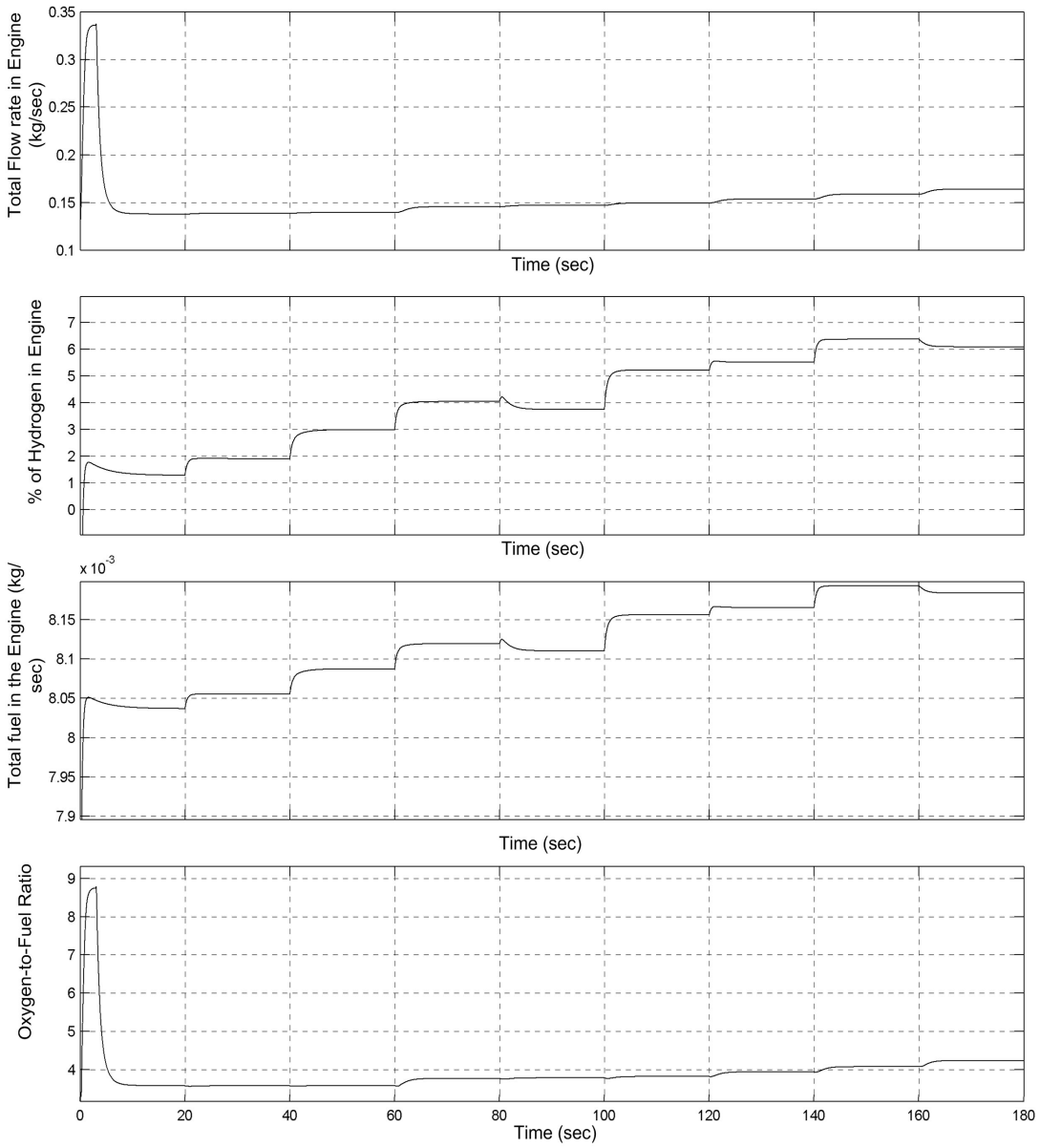

Figure 7.8- Simulation results of engine fed with exhausts from fuel cell

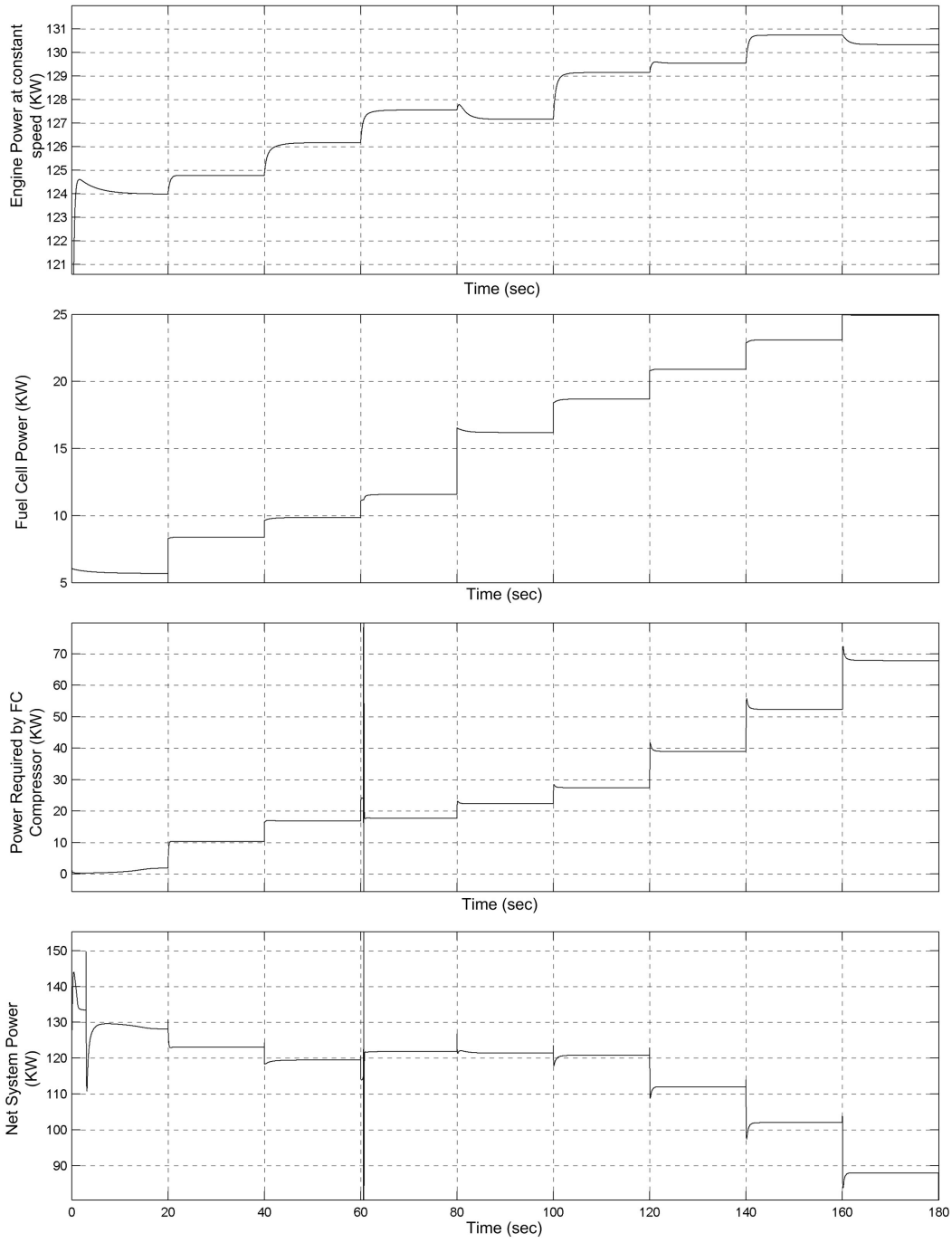

Figure 7.9– Engine output characteristics and net system power

must be such that it does not cause the fuel cell compressor to draw excessive power and eventually causes a drastic reduction in the net system power. At any time, the controller must ensure that the excess air ratio for the fuel cell is at least 2.

The use of a three way valve to control the cathode exhausts between the fuel cell and the engine can facilitate the development of localized controllers for the fuel cell and the engine. The OFR setting determines the position of the three way valve. The minimum amount of oxygen depleted air that must be present in the engine at any time must be predetermined. The excess air ratio in the fuel cell is adjusted such that it always supplies this minimum value required. In case the amount of depleted air is in excess of the requirement, the valve can direct the gases to the atmosphere or a thermal cycle. A thermal cycle facilitates the use of hot and cold exhaust streams within the system. This can be done by utilizing heat rejected from coolers to provide heat to other components in the hybrid system such as vaporizers and heat exchangers.

The mass flow rate of fuel in the engine is constant while the amount of hydrogen entering depends on the load demand on the fuel cell. When a series of increasing loads demand is applied to the fuel cell, it is observed that at any point the percentage of hydrogen in the engine is never above 10%. At the same time, the utilisation factor of the fuel cell is considerably low. Hence, a controller to optimize the amount of hydrogen entering the engine, while supplying the demand on the fuel cell and a utilisation factor above 70% is required. Based on the study by Mathur et al [12], the thermal efficiency of the engine increases only up to around 20% hydrogen in the engine. The percentage of hydrogen and the exhausts from the cathode must be controlled together such that knocking behaviour is avoided. A controller using feedback from the engine to the fuel cell to manipulate the utilisation factor and the oxygen depleted air can be developed for this purpose.

Figure 7.9 shows the power output of the engine at a speed of 1600 RPM and power output of the fuel cell. It also shows the net power output from the system including the power produced by the fuel cell, engine and turbine and the power consumed by the compressors. From Figure 7.9, the power output from the components can be compared. It is observed that with increasing load demand on the fuel cell, while operating the engine at constant speed, the net system power goes on decreasing. This is a result of excessive power consumed by the fuel cell compressor.

The increase in the engine power output is proportional to the percentage of hydrogen entering the engine. When the utilisation factor of the fuel cell is lower, the engine produces more power.

The control of the net power output of the system will depend largely on how efficiently the flows to the fuel cell and engine are controlled. An optimal controller can be developed which ensures the control of the flows within the constraints imposed by the set-points results in delivering the required power by the system.

The engine responds better to fast changing loads than the fuel cell. The engine power output increases with increase in percentage of hydrogen in the system. The fuel cell stack voltage takes a significant amount of time to settle to a steady value. A constant change in the load of fuel cell will not provide steady voltage. Hence, the fuel cell can be operated at a base load, supplying the highest possible amount of hydrogen to the engine within the utilisation factor limits.

The amount of oxygen depleted air supplied by the fuel cell can be varied by manipulating the valve position.

A controller for the engine operation can be developed with the following objectives:

- Regulate the OFR to a determined set point.
- Regulate the amount of hydrogen to a minimum of 5% and a maximum of 16%.
- Regulate the fraction of oxygen depleted air to a determined set point.
- Supply power to the load demand within the above constraints.

In order to develop a controller with the above objectives, the control problem formulation for the engine is suggested as follows:

- Inputs to the engine controller –Mass flow rate of oxygen depleted air in engine, Mass flow rate of hydrogen in the engine, Mass flow rate of air from engine compressor.
- Disturbance – Fuel required, Speed
- Performance variables – Difference between desired and actual engine power, OFR and fraction of oxygen depleted air in the engine.
- Measurements – Air flow rate from engine compressor, pressure in the inlet manifold of engine.

The control strategy suggested above can result in localized controllers for the fuel cell and IC engine ensuring that component operates at an optimum condition. A schematic of the control strategy is shown in Figure 7.10.

.

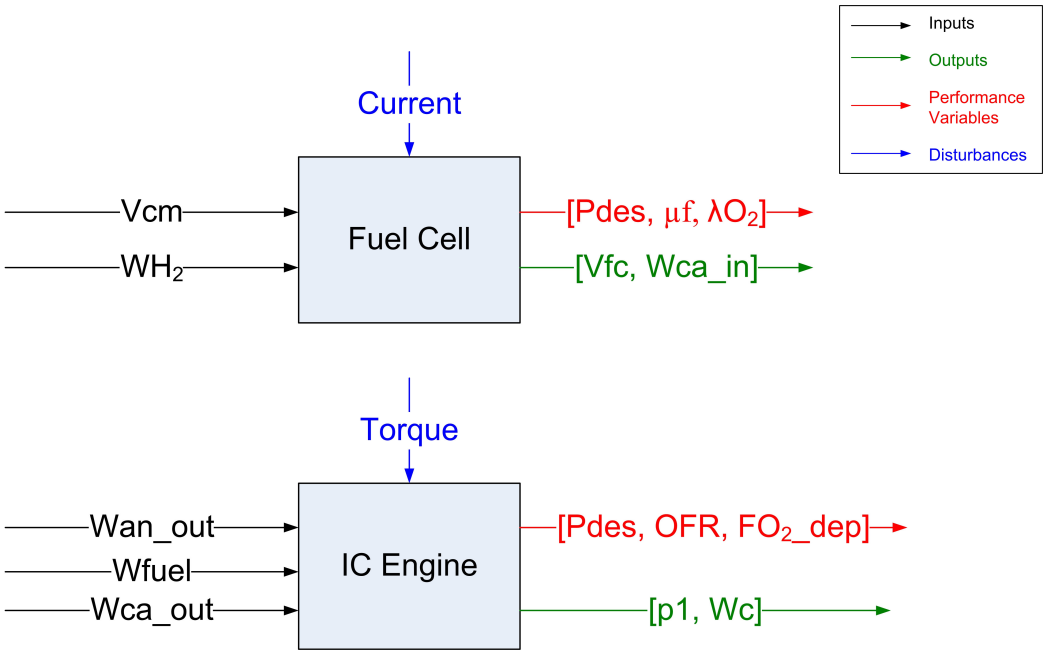

Figure 7.10 – Control Parameters for Fuel Cell and Engine

7.6. *Linearisation*

The integrated system model described in this chapter is highly nonlinear. The development of control around equilibrium points of the system requires a linearized system model. The method followed for linearisation of the model in the thesis is system identification rather than direct linearization. The control parameters established in this chapter determine the inputs, output and disturbances for the system, which allows extracting data for developing a linearized model using the system identification. The main steps followed for linearization of a system include:

- Identifying inputs and output for control purposes
- Creating data sets by running nonlinear simulation model. The model is excited with pseudorandom binary sequence (PRBS) at the operating points to obtain the data sets.

- Developing a linear state space model using the system identification toolbox in Matlab/Simulink®. The prediction error method (PEM) is used to identify state space linearized model for the specified operating points.
- Investigating step and impulse response of the model.
- Validating the linearized model

The need and methodology for linearisation of the system model with control system design are discussed and developed in the following chapters.

7.7. *Chapter Summary*

This chapter provides the pre-requisites to control development for the system. The system simulation results show that there are various controllable parameters. The efficient operation of the fuel cell system at any load condition depends on utilisation factor control and the excess oxygen ratio control. The engine operation in this system is directly affected by the utilisation factor and the excess oxygen ratio of the fuel cell. Further, the net system power is also dependent on these. Hence, utilisation factor and excess oxygen ratio control will mainly influence the performance of the system. The feasible operation of the system will be dependent on the response of the flow controllers.

The simulation results of the system are open-loop and require the following basic controllers:

- Compressor motor voltage variation according to load demand
- Hydrogen valve control for pressure regulation in electrodes
- Feedback controllers based on engine set-point for controlling fuel cell exhausts.

The hybrid system model described in this chapter uses a hydrogen tank as a source of fuel rather than a reformer, which results in fast dynamics for the system. This model has allowed focusing on the complex interactions between the fuel cell and diesel engine, which are the main power producing components. In the following chapters, the reformer is used to supply fuel to the fuel cell, which significantly affects the system dynamics.

The results obtained in this chapter indicate the need for air and fuel path control and power management in the system. The types of controllers that can be developed for the system are described in Chapter 8 (Feedback Control Design Using PID Controllers), Chapter 9 (Model Predictive Control Design) and Chapter 11 (Future Work).

Chapter 8. Feedback Control Design Using PID Controllers

8.1. *Introduction*

Hybrid systems are made up of a number of power producing components. The fundamental requirement of a control system is the minimisation of fuel consumption consistent with the overall system performance. The optimisation task is required at the local component level as well the global system level. The low level optimisation of the system components can be implemented using simple control structures. In processes involving complex interactions between the system components, there is also a need for global optimisation. Global optimisation will ensure the minimum usage of fuel in the complete system, while the local optimisation will ensure that the components operate within their constraints. This results in a hierarchical control structure, which allows lower costs and complexity for the hardware.

Conventional control objectives and strategies for fuel cells include temperature control by maintaining mass flow temperatures, air and fuel path control by regulating air and fuel utilisation and power control by limiting the current in the fuel cell [59]. Similarly, for the internal combustion engine, the air-to-fuel ratio (AFR) and engine load control are achieved by adjusting the fuel flow, air flow, fraction of exhaust gas recirculation in the charge and peak engine temperature. The control objectives for AFR control can assist in local component optimisation, while the control of power output forms a part of the global optimisation.

This chapter is structured as follows. Section 8.2 discusses the need for control of each control variable and constraints for designing the controller. Section 8.3 describes the methodology followed for designing the decentralized PID control. Section 8.4 elaborates on the results of the PID controllers designed to achieve the control objectives. Section 8.4 summarises the findings of the control design.

System Control Structure: The aim of the control design for this system is to regulate air and fuel flows through the system such that they satisfy efficiency and operating constraints. A successful control strategy will also demonstrate the feasibility of operating the system with load distributed to the fuel cell and the engine, with each component operating within its local constraints. Since, the target application of the system is in the automotive sector, fast dynamic response of each component forms another aspect of the investigation. The operating temperature of the system components affects the chemical reaction rates while heat dissipation by the components affects the rational efficiency.

The system has various control variables due to the multi-component interactions and the need for optimal system behaviour. The modelling, analyses and simulation results presented in Chapter 4 (Component Modelling), Chapter 5 (Investigation of Optimum Operating Range), Chapter 6 (Exergy Analysis) and Chapter 7 (System Integration) evidently identify the major control loops required for the system as follows:

- Fuel and air flow control
- Temperature management and thermal dissipation control
- Power distribution management

A cause and effect diagram for the system interactions, which highlight the control loops for the system, is shown in Figure 8.1. The cause and effect diagram for the diesel engine from Guzzella et al [66] has been adapted for the hybrid system described in this thesis.

The dynamic response of processes in the system is diverse, since the rate of production of matter streams from one component is different from that of another component. The main components involving chemical reactions are the reformer, fuel cell and the engine. The rate of reaction in each of these components is dependent on operating conditions. The synergistic operation of the system components, feeding effluents from one component to another, affects the dynamic response and performance of the overall system. The fuel cell response is delayed due to the slow transient response of the steam reformer resulting in a delayed voltage production from the fuel cell. Similarly, the exhaust flow dynamics of the fuel cell can affect the engine combustion and performance.

For example, a sudden change in the hydrogen flow in the engine will require appropriate changes to the air and diluent flows into the engine cylinder, which in turn can affect the power output of the engine. The hydrogen fraction in the engine charge has to be limited to a certain value, since it can affect the thermal efficiency and power output of the engine. The transients in the fuel cell exhausts, which exceed the limiting fraction of hydrogen in the charge, can mar the performance of the engine cycle and potentially cause detonation.

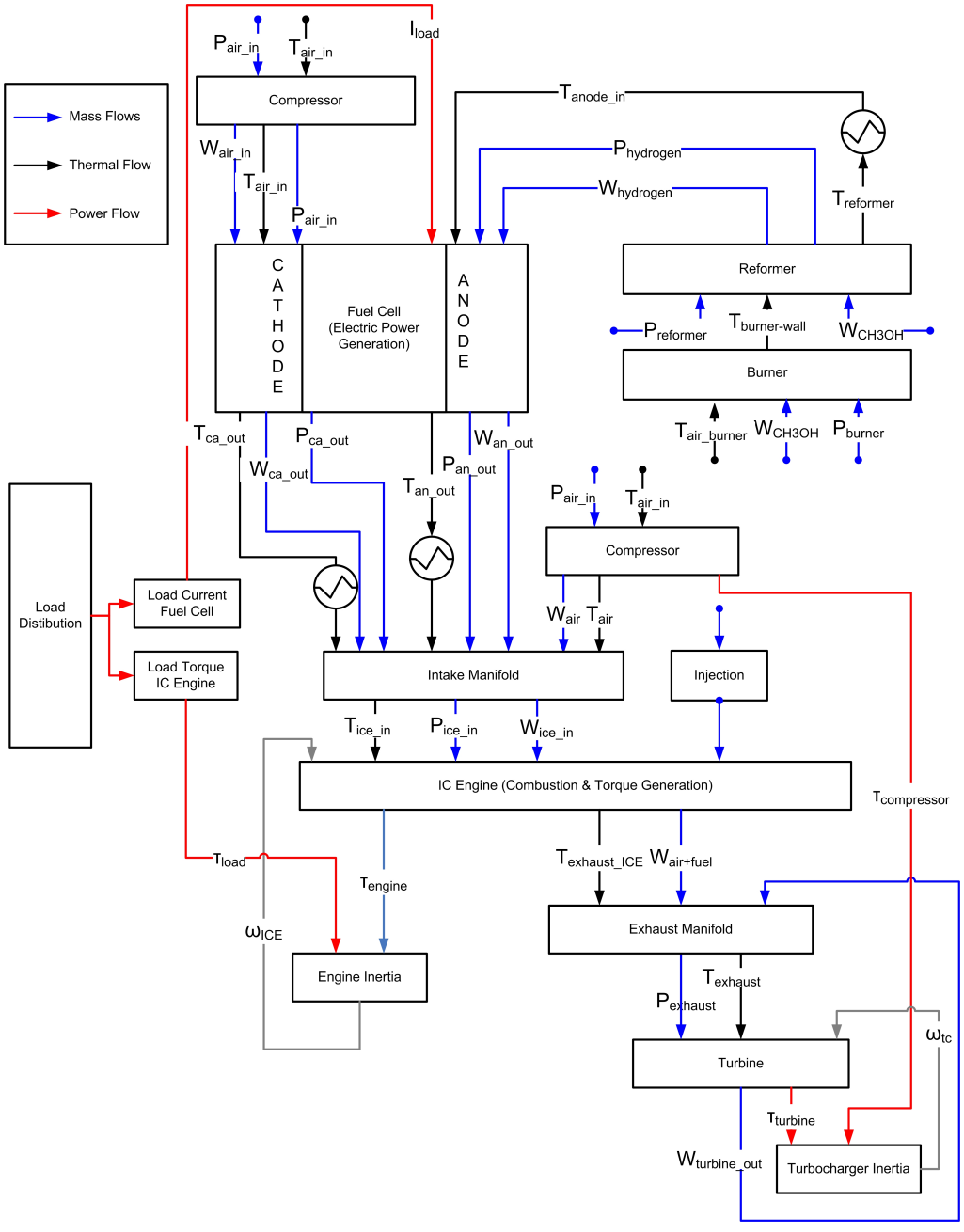

Figure 8.1 – Cause and Effect Diagram for SOFC-IC Engine Hybrid System

Whilst the components are operating at the design temperatures, the air and fuel management is crucial to the performance of the system and the subsystem components. The management of power can be visualised as a higher level control function, which can be realised in the form of a supervisory controller.

The results from Chapter 4-Chapter 7 have created a development path for control design. These analyses suggest the subsystem component interaction offers many operating constraints, hence necessitate the development of a controller. Initially, the constraints on the fuel cell range of operation and the engine were defined in Chapter 5 (Investigation of Optimum Operating Range) with a steady state analysis. A dynamic analysis of the system in Chapter 7 (System Integration) further highlighted the effect of fuel cell operation on the engine operation. The key control parameters were identified in this chapter, which are further explained in section 8.2. Decentralised PID controllers are developed to satisfy the control requirements and the behaviour of the system was investigated as discussed in the following sections.

Introduction to PID controllers

PID (proportional integral derivative) or three term control is effective for most process systems and has found a large number of industrial applications [126]. PID controllers are simple and yet provide good control performance. A block diagram of the structure of a feedback controller is depicted in Figure 8.2.

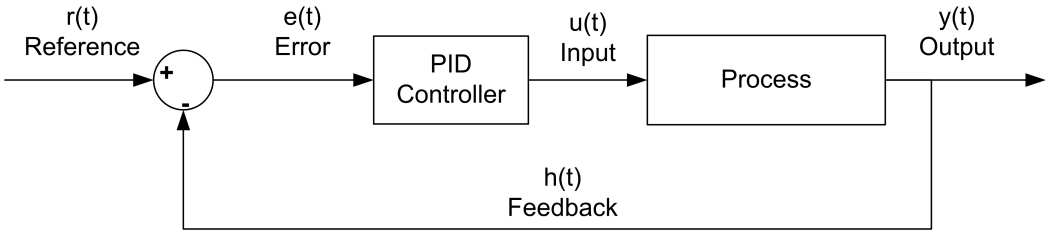

Figure 8.2 – Structure of a Feedback Control System

The difference between the reference signal r(t) and the feedback signal h(t) gives rise to the error e(t) between the desired output and the actual output signal y(t). The controller manipulates the input signal u(t) according to the error signal fed as input to the controller. The PID controller shown in Figure 8.2 is a Single-Input-Single-Output controller, such that the control variable u(t) is formed of proportional, integral and derivative parts given

by:

$$u(t) = K\left(e(t) + \frac{1}{T_i}\int_0^t e(\tau)d\tau + T_d \frac{de(t)}{dt} \right)$$

Eqn. 8.1

Where, e is the control error, K the proportional gain, T_i the integral gain (strictly the reset time) and T_d the derivative gain. PID control is very effective and applicable for SISO systems. It can also be adapted to multivariable systems by explicitly identifying cross-coupling and tuning accordingly. The integral term ensures that the steady state error becomes zero while the derivative term ensures closed-loop stability and allows prediction of future error [126].

The main aim of this work was to analyze and identify issues with controller design and successfully implement decentralized control for air and fuel paths for the system. The development of PID controllers is discussed and by analysing their performance, the need for advanced controllers such as the model predictive controller is established.

8.2. *The Control Requirement*

The cause and effect diagram shown in Figure 8.1, depicts reservoirs of energy or mass or information with rectangular boxes and circles, while the flows between the reservoirs are shown by arrows.

The main components of the cause and effect diagram are the fuel cell and the diesel engine. The objective for each, the fuel cell and the engine is the production of power as per the load requirement. The fuel cell produces electric power, through an electrochemical reaction, while the engine produces torque, as mechanical energy through combustion.

As shown in Figure 8.1, the power production in the fuel cell is an effect of consumption of air, hydrogen and load demand on the fuel cell. The air supply system of the fuel cell consists of the compressor. The production of compressed air is due to consumption of power and air supply into the compressor. The fuel supply system of the fuel cell consists of the reformer-burner unit. The consumption of methanol and air causes heat production in the burner. The reformer produces hydrogen, which is due to the heat supply from the burner and methanol supply to the reformer. The supply of fuel and air to the reformer,

burner, compressor and finally to the fuel cell, at appropriate operating temperatures and pressures results in the production of electric power from the fuel cell. The fuel cell will clearly have two control loops, i.e. the fuel path and the air path. Hence, the regulation of air and fuel can be done by controlling the excess oxygen ratio and the fuel utilisation factor of the fuel cell.

Similarly, from Figure 8.1 the production of torque from the engine is due to the consumption of air and fuel through combustion. The fuel is injected into the engine cylinder while the air supply along with charge dilution and hydrogen is provided from the compressor and the fuel cell exhaust. The inlet and exhaust manifolds are reservoirs of mass and thermal energy. The outputs of these blocks are the pressures and temperatures of the gases within them. The turbine inertia and the engine inertia blocks are reservoirs of kinetic energy. The engine has three main control loops, i.e. the air path, fuel path and externally supplied charge diluents path. The regulation of air and fuel can be done by controlling the oxygen-to-fuel ratio, while the regulation of the externally supplied diluents can be done by controlling the fraction of these gases in the intake manifold.

The control variables for fuel path control of the system are: the fuel cell utilisation factor, engine oxygen-to-fuel ratio and engine power. The control variables for air path control are the fuel cell excess oxygen ratio and the engine oxygen-to-fuel ratio.

Excess Oxygen Ratio

The system integration simulation described in Chapter 7 (System Integration) demonstrates the need for regulating the air in the fuel cell to be above stoichiometric. Oxygen starvation in fuel cells causes a sharp drop in voltage. In order to account for any sudden transients, the excess oxygen ratio is regulated at the value of λ_{O2}=2. A higher value of excess oxygen ratio results in excessive power drawn from the compressor supplying air to the fuel cell. The chosen value of the excess oxygen ratio prevents oxygen starvation and ensures that the compressor power required is optimal.

Utilisation Factor

The fuel supplied to the reformer-fuel cell must be sufficient to provide some unused fuel to the IC engine without compromising the fuel cell utilisation factor and fuel cell

efficiency. The optimum operating region for the fuel cell and the IC engine is described in Chapter 5 (Investigation of Optimum Operating Range).

While the fuel utilisation factor of the fuel cell is above unity, indicating complete usage of fuel supplied, the stack voltage drops to zero. To avoid fuel starvation, the utilisation factor must be maintained at a value below 95%. This value is chosen to avoid voltage drop during transients.

The fuel cell efficiency, defined according to the lower heating value of hydrogen is given by Eqn. 8.2. The utilisation factor is directly proportional to the fuel cell efficiency and affects the hydrogen percentage in the engine cylinder. A low utilisation factor indicates the amount of hydrogen entering the engine is higher.

$$\eta_{fc} = \mu_f \frac{V_{fc}}{1.25}$$

Eqn. 8.2

As per steady state simulation results in Chapter 5 (Investigation of Optimum Operating Range) identifying the optimum operating region for the fuel cell and engine, a minimum of 70% utilisation factor is assumed. The control objective for the utilisation factor control is to regulate its value between 70% and 95%.

During the fuel cell operation, air and fuel starvation must be prevented to avoid damaging the stack. The fuel cell failure occurs in the condition when the fuel cell is starved by air, fuel, or both. The air and fuel required in the system depend on the required load. In the decentralised structure, the value of excess oxygen ratio must remain above unity and the utilisation factor is below unity. In such a case, when the failure conditions are avoided, the fuel cell automatically receives the appropriate proportion of air and fuel. As a result, the effect of the air input on the utilisation factor and that of fuel input on the excess oxygen ratio will be negligible.

Hydrogen Supply to the Engine

The utilisation factor in the fuel cell determines the hydrogen percentage in the engine cylinder. Any changes in hydrogen content in the engine requires an appropriate change in diesel content and the air content to maintain power output and air-to-fuel ratio. Hence, the

fuel flow through the fuel cell affects the air and fuel path of the engine. If the hydrogen percentage in the engine is maintained to a minimum of 5 % (Chapter 5) it will lead to an improved engine performance. The maximum limit is set to 20 % above which the thermal efficiency of the engine begins to drop and possibility of knocking increases [12-14]. The controller set point is however maintained at 18 % (the maximum percentage of hydrogen) to account for transient conditions.

The control of the utilisation factor within its upper and lower limits does not necessarily ensure the control of percentage of hydrogen within 5 % and 18 % respectively. This largely depends on the load distribution between the fuel cell and the engine as illustrated in the Figure 8.3. There can be only one exact load condition for the fuel cell and the engine at which the fuel cell utilisation factor is 95 % and the hydrogen fraction in the engine is 5 %. Hence, the utilisation factor cannot be easily maintained at say 95 % and ensure the hydrogen percentage in the engine is 5 %. The regulation of flow to maintain utilisation factor results in set-point changes for the hydrogen value in the engine and vice-versa. Such effects are further explained with the help of Figure 8.3.

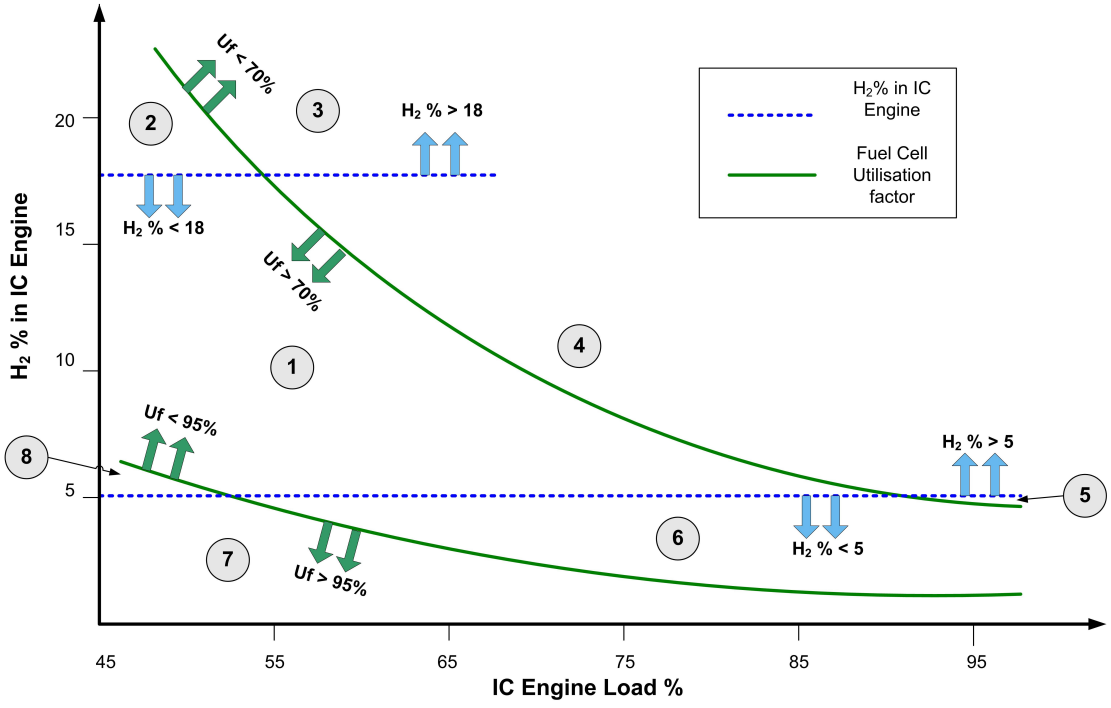

Figure 8.3 – Effect of Load Condition on Fuel Cell Utilisation Factor and Hydrogen Content in Engine

The manipulated variable for both utilisation factor control and hydrogen percentage control is the fuel input to the reformer. With a set of four possible conditions, namely

utilisation factor μ_f>=70%, μ_f <=95%, hydrogen percentage in the engine H_2%>=5% and H_2 %<=18%, the selection of set-points will be dependent on the loads on the fuel cell and the engine. Based on the assumption that the maximum power output of the fuel cell is a fifth of that of the engine, the operating conditions occurring for each region shown in Figure 8.3, are listed below.

1. Region 1: The utilisation factor and the hydrogen percentage in the engine are within prescribed limits. This region occurs over most engine load conditions.
2. Region 2: The utilisation factor is above 70%, but the hydrogen percentage is above 18%. This condition occurs mainly at low engine load conditions.
3. Region 3: The utilisation factor is below 70% and the hydrogen percentage is above 18%. This condition indicates very high load operation of the fuel cell and low load operation of the engine.
4. Region 4: The utilisation factor is below 70% and the hydrogen percentage is within 5-18% limits. This condition can occur for most load conditions for the fuel cell and engine.
5. Region 5: This region has utilisation factor below 70% and hydrogen percentage in the engine is below 5%. This occurs at very high engine load conditions.
6. Region 6: The utilisation factor is within limits of 70-95% and hydrogen percentage below 5%. This can occur over most engine load conditions and for very low load conditions of the fuel cell.
7. Region 7: The utilisation factor is above 95% and the hydrogen percentage is below 5%. This occurs for very low fuel cell load conditions.
8. Region 8: The utilisation factor is above 95% and the hydrogen percentage is above 5%. This condition occurs at low engine loads.

Oxygen-to-Fuel Ratio (OFR)

To avoid smoke formation, the air to fuel ratio in the engine must be maintained above stoichiometric. In this system, besides the oxygen from the compressor, the unused oxygen from the fuel cell stack is mixed with the incoming air and supplied to the engine cylinders. As a result, the oxygen-to-fuel ratio is a more appropriate value for regulation. The fraction of oxygen depleted air from the fuel cell cathode, affects the overall OFR and the fraction of nitrogen in the engine. The fraction of nitrogen must provide sufficient dilution to the engine to counter the effects of adding excessive (above 18%) hydrogen in

the cylinder along with the primary fuel. The OFR of the engine is regulated by adjusting air flow into the engine by means of the manifold pressure and the exhaust air from the fuel cell stack.

Engine Diesel Fuel Regulation

The torque demand sets the fuel required by the engine. This diesel fuel flow required to produce the torque is supplied to the engine. As soon as the fuel cell exhausts produce hydrogen, which is then supplied to the engine, the total fuel in the engine is in excess of that required to produce the necessary torque. Hence, for a given load condition of the engine, when hydrogen content of the charge air varies, the diesel fuel fraction will vary to meet the load demand.

External Exhaust Gas Recirculation (EGR)

The EGR fraction entering the engine is water vapour, and cathode exhausts from the fuel cell and the remainder of the exhaust flow other than hydrogen from the reformer. The water vapour and nitrogen flow from the fuel cell is treated as an external form of exhaust gas recirculation (EGR). The control of EGR fraction is done by varying a valve position, which regulates the flow of recirculated gases in the engine. As discussed in Chapter 4 (Component Modelling-IC Engine), the introduction of up to 35 % of available external EGR along with hydrogen from the fuel cell was successful in reducing NOx emissions above 99% of those by produced by combustion of pure n-heptane without any EGR. However, to account for transients the set-point for regulating external EGR is maintained at 30 %.

The feasibility of each control objective is demonstrated by developing a PID controller for a set point. Since the model is nonlinear, an adaptive or parameter estimation technique can be developed to adjust the PID gains to account for the different underlying behaviour of the system at each operating point.

8.3. *Control design and methodology*

The methodology for control design and implementation for each of the above described control variables is discussed below. Figure 8.4 shows the controllers proposed for each control variable.

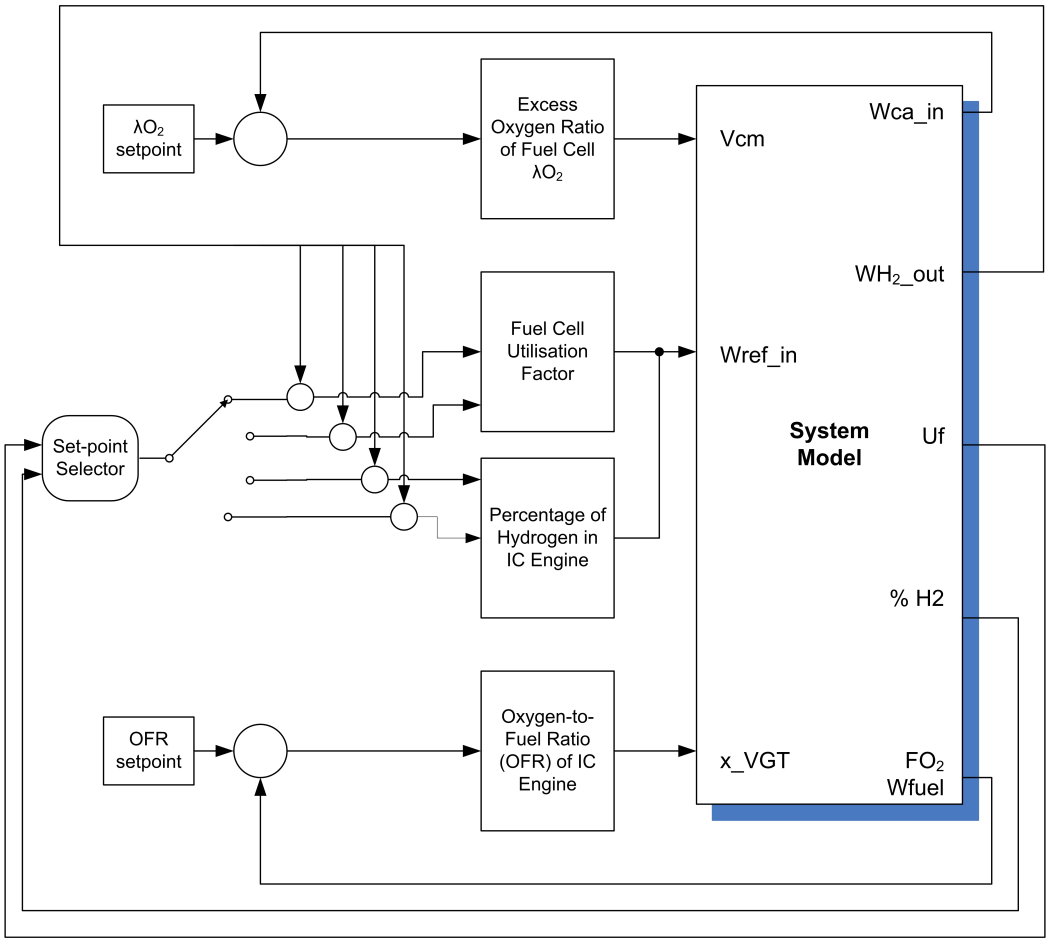

Figure 8.4 – Proposed Control Structure

1. Excess Oxygen Ratio λ_{O2} Control

The air-path of the fuel cell is regulated by excess oxygen ratio control. The difference in the air flow out from the compressor and the desired air flow is used to determine controller error. The error serves as input to a PI controller. A static linear relationship between the current and the voltage to the compressor motor is developed as a static feed forward controller. The feed forward controller along with PI controller together regulate the air flow into the fuel cell to ensure an excess ratio of λ_{O2}=2.

2. Utilisation factor control

The fuel flow into the reformer determines the hydrogen flowing into the fuel cell. The reformer dynamics is modelled as a transfer function with a time constant of 5 seconds

[38] and proportional gain K=0.86. Reformer model in Chapter 4.2 provides 86% by mass of hydrogen of the total methanol flow in the reformer.

The fuel cell utilisation factor is determined by the amount of fuel used and supplied. The utilisation factor requires regulation between 70% and 95%. From the simulation results in Chapter 7 (System Integration), it can be observed that a desired stack voltage is achieved 4-6 seconds after the utilisation factor falls below 1. The voltage settles to a steady value when the utilisation factor achieves a steady value. Hence, it is necessary for the control action to regulate the hydrogen flow into the fuel cell to achieve a fast response with minimal overshoot.

Two PID controllers for controlling the reformer input fuel flow to maintain utilisation factor at 70% and 95% are required. The error signal as input to the PID controllers is the difference between the desired hydrogen flowing out from the anode to the actual hydrogen from the anode.

3. Hydrogen percentage in engine cylinder

The regulation of the fuel flowing in the reformer is required to control the utilisation factor of the fuel cell and the hydrogen to the IC engine. Controlling the utilisation factor and the hydrogen flow to the engine together can cause conflicting targets since both require manipulation of the same input variable. In order to resolve this, a state transition approach can be implemented to select the set point for the reformer input fuel control. As shown in Figure 8.3, there are 8 possible regions of operation for the utilisation factor and the hydrogen percentage in the engine.

The state transition diagram chart shows four states each activates one PID controller at a time. The PID controllers 1,4,2,3 are designed to manipulate the fuel flow in the reformer to give hydrogen percentage at 5 %, 18 %, utilisation factor at 95 %, at 70 % respectively. The four states shown in the state flow chart are mutually exclusive, implying that only one controller can be active at a given time.

The state transition diagram has four test inputs, two each for utilisation factor and hydrogen percentage in the engine. This results in 16 possible combinations of operating regions. As shown in Figure 8.3, only 8 regions are feasible. The rest of the 8 regions cannot exist.

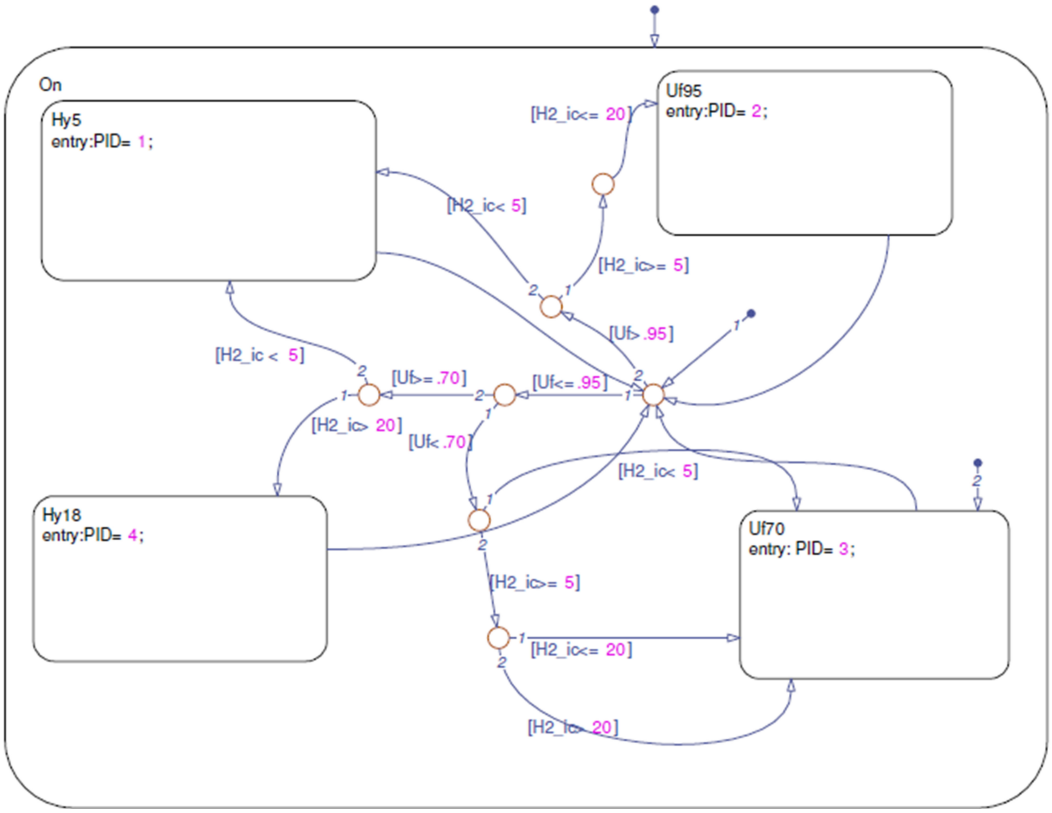

Figure 8.5 – State transition diagram for set-point selection implemented in Stateflow (version 7.0.1)

The state flow chart evaluates the utilisation factor and hydrogen percentage 4 times until the simulation time reaches 10 seconds. An activation signal in the form of pulses within the 10 seconds is applied to the state flow chart. During these 10 seconds, the state flow chart may activate a single controller throughout all pulses or different PID controllers and then finally settle to a single one after 10 seconds. The activation signal is such that it allows selection of a controller without continuous oscillations between controllers during the initial few seconds.

4. OFR control

Oxygen is fed to the engine from the fuel cell cathode exhaust and the variable geometry turbocharger (VGT). The flow from the fuel cell is kept steady while the variable geometry turbocharger vane position is manipulated to provide the balance of oxygen required, hence gives the desired OFR. The error signal for the OFR PID controller is computed with the help of the total oxygen in the engine cylinder.

5. EGR control

The exhaust water vapour, nitrogen from the fuel cell and the reformer exhausts of water vapour, carbon dioxide, carbon monoxide and trace amount of methanol, together form a source of gas composition similar to that found in the conventional EGR system. When the fuel cell utilisation factor is at 70 %, the fraction of these external EGR gases is 42 %. At various load conditions, the available external EGR and the requirement of EGR is different. A simple proportional controller can be implemented to manipulate this external-EGR fraction to the desired value.

In brief, the following controllers are implemented:

1. Feedforward+PI controller to regulate λ_{O2}, with manipulated variable compressor motor voltage (Vcm)
2. PID controller to regulate μ_f at 70 % and 95 %, with manipulated variable being the flow into the reformer (Wref_in)
3. State transition logic – set-point selector to select from four PID controllers to regulate utilisation factor or hydrogen percentage in the engine, with manipulated variable being the flow into the reformer (Wref_in).
4. PID controller to regulate OFR with manipulated variable being VGT vane position (x_vgt).
5. Proportional controller to regulate the power output of the engine with manipulated variable being the diesel flow in the engine.
6. Proportional controller to regulate external-EGR to the value required by the engine.

8.4. *Simulation Results*

1. Excess Oxygen Ratio Control

A step for the fuel cell current from 45 A to 50 A is shown in Figure 8.6(a). The PI controller is designed at a set-point for current I=50 A. The manipulated variable, i.e. compressor motor voltage and the controlled variable, i.e. excess oxygen ratio with and without the controller is compared in Figure 8.6(c) and Figure 8.6(b) respectively. When the controller is not functioning, the compressor motor voltage is kept constant. The excess

oxygen ratio achieves a steady value at the desired set-point within 10 seconds. A steady excess oxygen ratio also ensures steady compressor power.

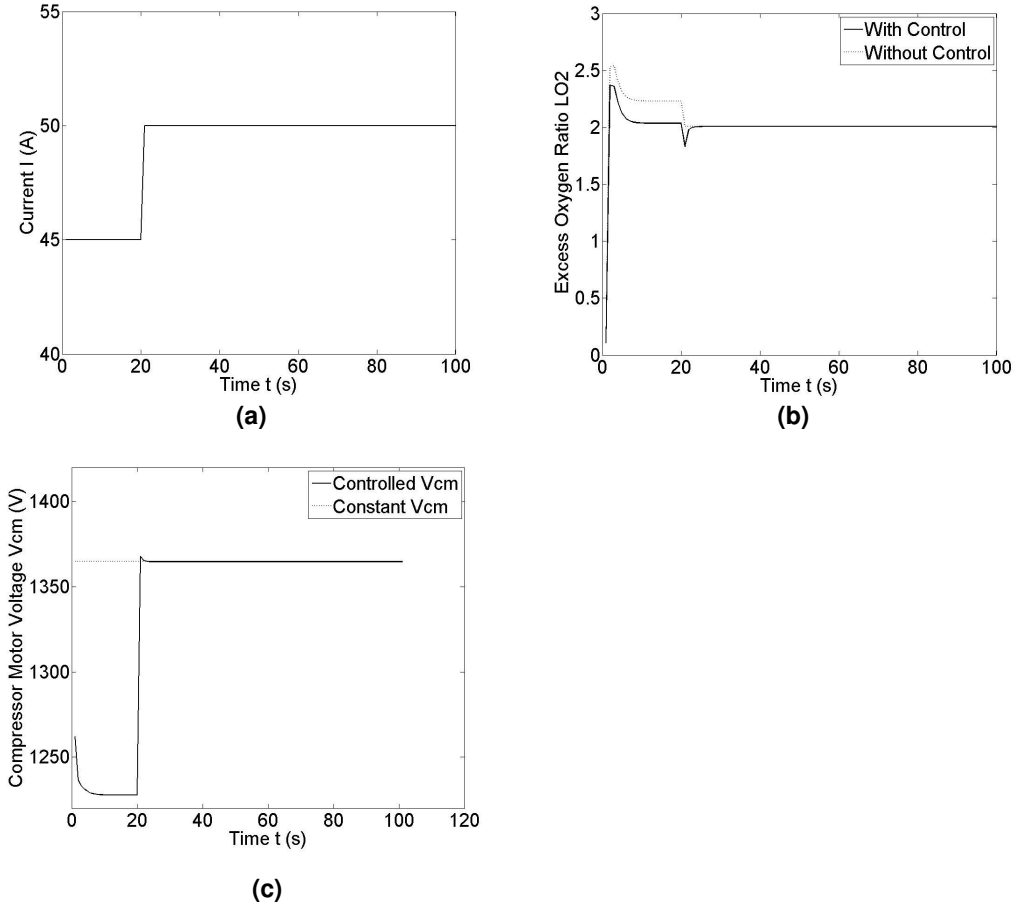

Figure 8.6 - Excess Oxygen Ratio Control

2. Utilisation Factor and Hydrogen Percentage Control

The hydrogen percentage in the charge air is controlled to 5% and is shown in Figure 8.7. The utilisation factor is controlled to 70 % and is shown in Figure 8.8. For both of these operating points the reformer fuel input is shown in Figure 8.7(a) and Figure 8.8(a) respectively. In both cases, the slow reformer dynamics results in delayed production of voltage. While the excess oxygen ratio of the fuel cell is maintained above stoichiometric, the voltage depends on the utilisation factor. The voltage rise does not occur unless the utilisation factor value is below unity, which indicates delay in hydrogen production from the reformer. The controller ensures that the utilisation factor drops to the desired value and achieves much faster response than the system without a fuel controller. This results in the voltage to rise to the set-point value within 10 seconds and ensures fast start up for the fuel cell, which is important for automotive applications. The effect of control on the

voltage output is very prominent as shown in Figure 8.7(d) and Figure 8.8(d). With a constant fuel flow to the reformer, the hydrogen set-point at 5 %, the voltage rises to a steady value only after 38 seconds. As observed from the simulations, for an open loop system without control, the higher the utilisation factor, the longer it takes the voltage to rise to a steady value. Hence the flow control is more effective at higher utilisation factors.

The values of utilisation factor and the hydrogen percentage also follow a trend similar to that of the voltage profile. Both achieve a steady value within 10 seconds as compared to those without control. This comparison for hydrogen fraction is shown in Figure 8.7(c) and Figure 8.8(c), while that for utilisation factor is shown in Figure 8.7(b) and Figure 8.8(b). Figure 8.8(c) also shows that the peak value of hydrogen fraction in the engine is lowered with application of the PID controller. The control of peak values is important since excess hydrogen can affect the performance of the IC engine.

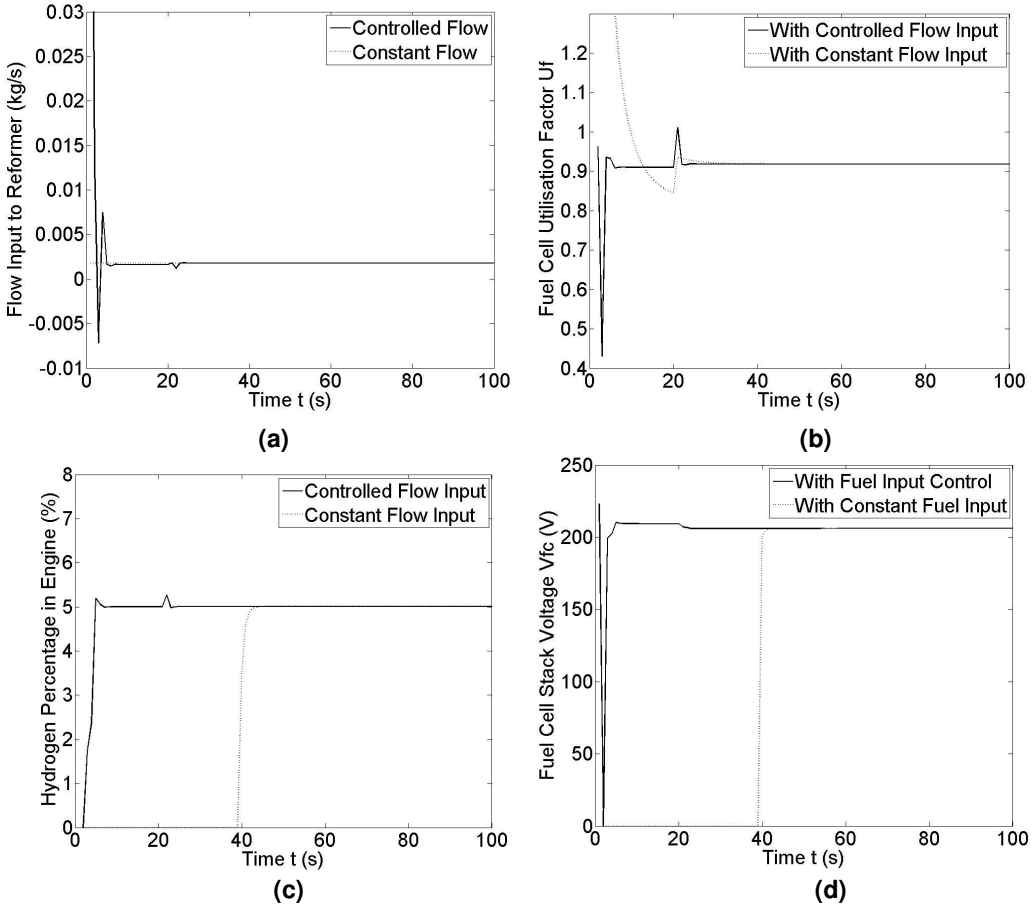

Figure 8.7 – Hydrogen Percentage Control at 5 %

Figure 8.7(a) and Figure 8.8(a) show the input response of fuel into the reformer. The response shows non-minimum phase behaviour with the signal having a negative undershoot. This behaviour is further explained in the following section.

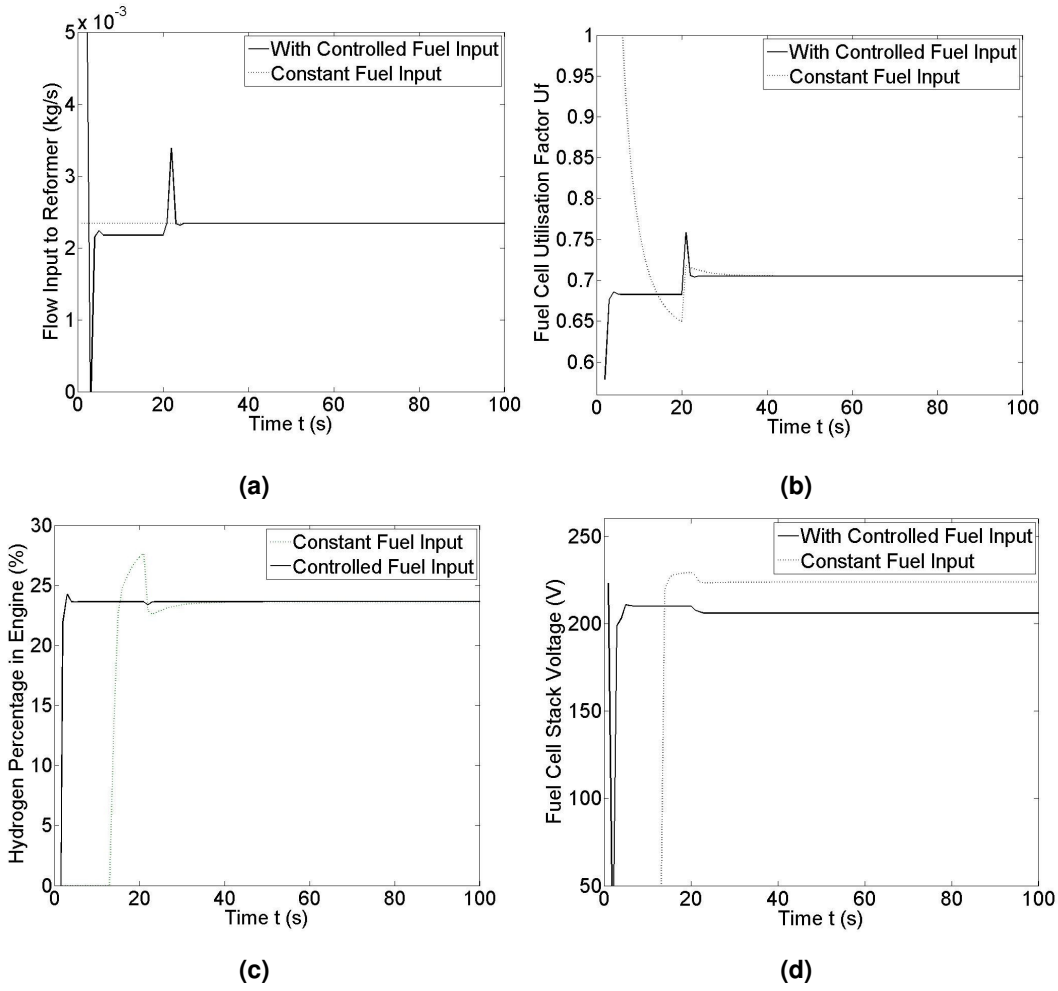

Figure 8.8 – Utilisation Factor Control at 70 %

The fast start-up of the reformer-fuel cell subsystem is also dependent on their operating temperatures. For this analysis, it is assumed that the fuel cell and reformer flows are fed at the required operating temperature, causing the electrochemical and chemical reactions to occur instantaneously. Temperature management within the system is not considered in this analysis and forms a part of future work.

3. Non-Minimum Phase Behaviour

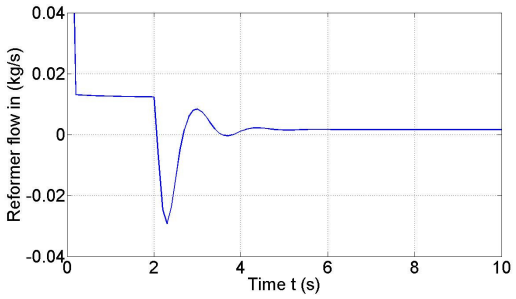

Figure 8.9 – Reformer inlet flow

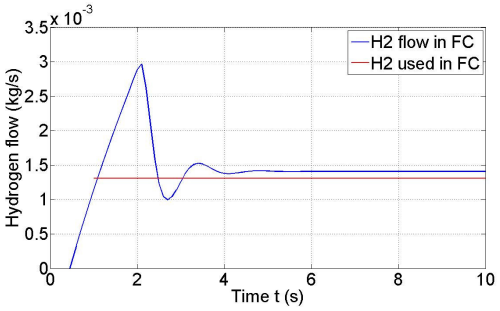

Figure 8.10 – Hydrogen flow in fuel cell

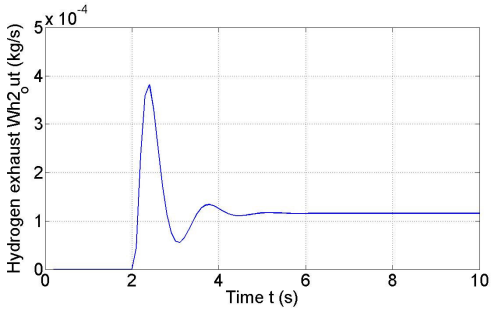

Figure 8.11 – Hydrogen exhaust from fuel cell

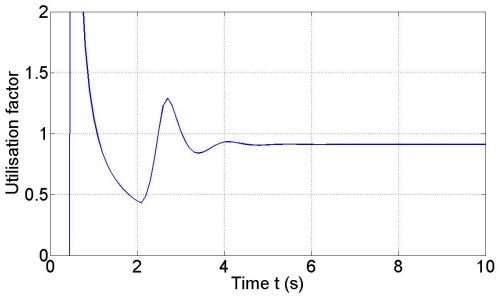

Figure 8.12 – Fuel cell utilisation factor

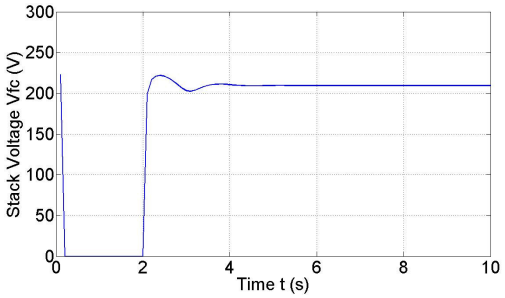

Figure 8.13 – Fuel cell stack voltage

The non-minimum phase behaviour as seen in Figure 8.7 is explained with the help of Figure 8.9 to Figure 8.13. At time 0.4 seconds, the hydrogen flowing out from the fuel cell has a negative value. This happens since the value of hydrogen flowing in the fuel cell as shown in Figure 8.10 is zero. As a result, the reformer inlet flow, which is determined by the controller and the hydrogen flowing out from the fuel cell, results in a sharp drop. Since the stack voltage is dependent on the hydrogen flow in the fuel cell, it shows a sharp

drop to zero volts. This non-minimum phase behaviour of the stack voltage is due to the dynamics between the reformer and the fuel cell.

In order to compensate for this effect, the reformer inlet flow achieves a steady value up to 2 seconds. Due to the slow dynamics of the reformer, the hydrogen flowing into the fuel cell, as shown in Figure 8.10, gradually rises to a peak at 2 seconds. The hydrogen flow required in the fuel cell must be more than the hydrogen that is used in the fuel cell. This threshold is achieved at 1 second, which results in the utilisation factor to drop below unity after 1 second. The hydrogen flowing out from the fuel cell, as shown in Figure 8.11, is zero until 2 seconds. The delay in increase of the value of hydrogen flowing out from the fuel cell is due to the fuel cell dynamics. After 2 seconds, this value increases rapidly, crosses the set-point value within a few milliseconds, and achieves a peak value, which also causes the stack voltage to rise to a peak value of 235V. In order to compensate for this, the reformer inlet flow shows a sharp drop after 2 seconds, achieves a negative peak and begins to increase, when the hydrogen flowing out from the fuel cell decreases. The reformer inlet flow is manipulated by the controller until the hydrogen flowing out from the fuel cell achieves the set-point value. During this manipulation, between 2.5-3 seconds, the utilisation factor is above unity, which reflects as a dip in the stack voltage before it achieves a steady value.

4. Set-point Selection Using a State Transition Framework

The system model is initially fed with a constant fuel input to the reformer. As soon as the state transitions activate, the control system checks the values of the utilisation factor and hydrogen percentage in engine at every sample time. According to the logic shown in the state transition diagram, a new state may be selected at each pulse with a set-point and activation of the corresponding PID controller. Figure 8.14 and Figure 8.15 show selection of two set-points – hydrogen percentage in engine at 5 % and utilisation factor at 70 % respectively. In Figure 8.14(a), the output from the state transition is shown. The output is a steady value of unity, which activates the PID controller to regulate hydrogen fraction in the charge air at 5 %. When the results in Figure 8.14 are compared to the results shown in Figure 8.7, the latter shows a faster response. This is due to the implementation of the set point selection selector. Nevertheless, the results in Figure 8.14 show improvement over a system without any control for the fuel input to the reformer.

The fuel input of the reformer affects not only the utilisation factor and the hydrogen fraction in the charge air and fuel cell voltage but also the OFR of the engine. The effect of the controller propagates through the system as observed in Figure 8.14(b-f).

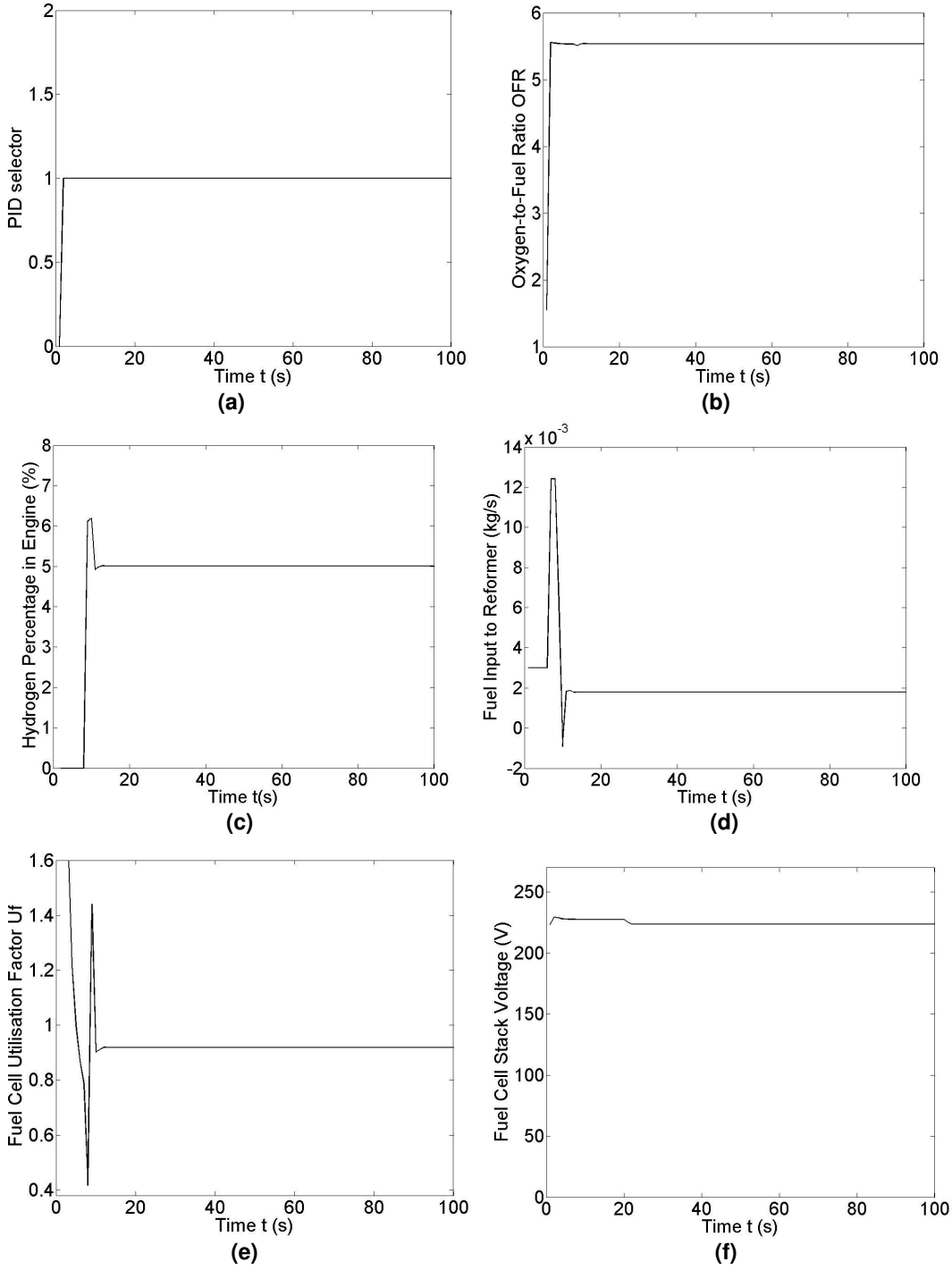

Figure 8.14 – Set-point Selector Using Stateflow - PID Controller 1 active (Hydrogen Percentage Regulation at 5%)

The reformer fuel input was set to another value to demonstrate the selection of another PID controller. In this case, the PID controller 3, which regulates the utilisation factor at 70% was selected. Figure 8.15 shows that initially when the state transition activates at

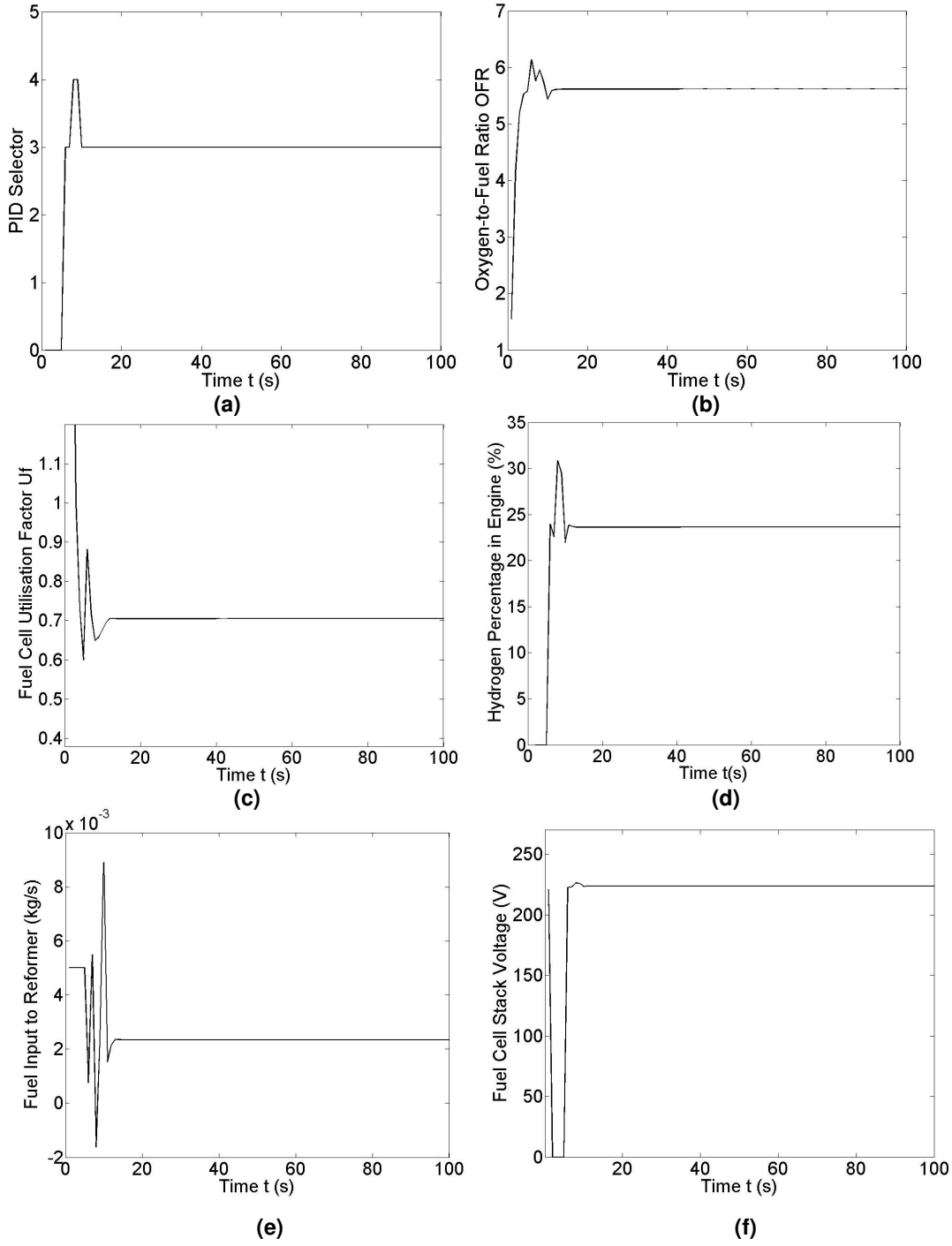

Figure 8.15 – Set-point Selector Using Stateflow - PID Controller 3 active (Utilisation factor Control at 70 %)

each sample time in the first 10 seconds, the controllers 3 and 4 are selected. As a result, some oscillations can be observed in the fuel input as well as the outputs. The oscillations in the hydrogen percentage in engine value cause the maximum peak value to reach 30%. The effect of excess hydrogen in the engine requires compensation by adding diluents to avoid detonation in the engine. The oscillations also delay the voltage response and utilisation factor response.

At various operating load conditions of the fuel cell and the engine, the load on each defines the current and torque demand from each respectively. The current and the torque are respectively measured disturbances applied to the system. The state transition framework demonstrated above can be implemented for appropriate set-point selection for such disturbances.

5. Oxygen-to-Fuel Ratio and Engine Power Control

As discussed in the previous section, as the hydrogen is supplied from the fuel cell to the engine, the complementary diesel fuel supply will correspondingly vary until the hydrogen reaches a steady value. The diesel fuel flow is adjusted as hydrogen is added to maintain a steady power output from the engine. To ensure proper combustion and avoid pollutant formation the OFR is regulated by manipulating the VGT vane position to vary engine inlet manifold pressure. Figure 8.16(b) shows the effect of controlled and uncontrolled fuel mass flow on the power output on the engine. Figure 8.16(a, c, d) compares the effect of constant VGT vane position input with the controlled position. Figure 8.16(a) and Figure 8.16(c) show the variation in diesel fuel and the total fuel in the engine. Figure 8.16(d) compares the OFR with and without controlling the VGT vane position. The controlled OFR rapidly achieves the desired value and maintains it through the fuel fluctuations.

A lean combustion, for which the OFR is higher than stoichiometric, ensures complete combustion and as a result fuel economy. A precise control of OFR is also necessary to ensure that the compressor power is maintained to a necessary minimum.

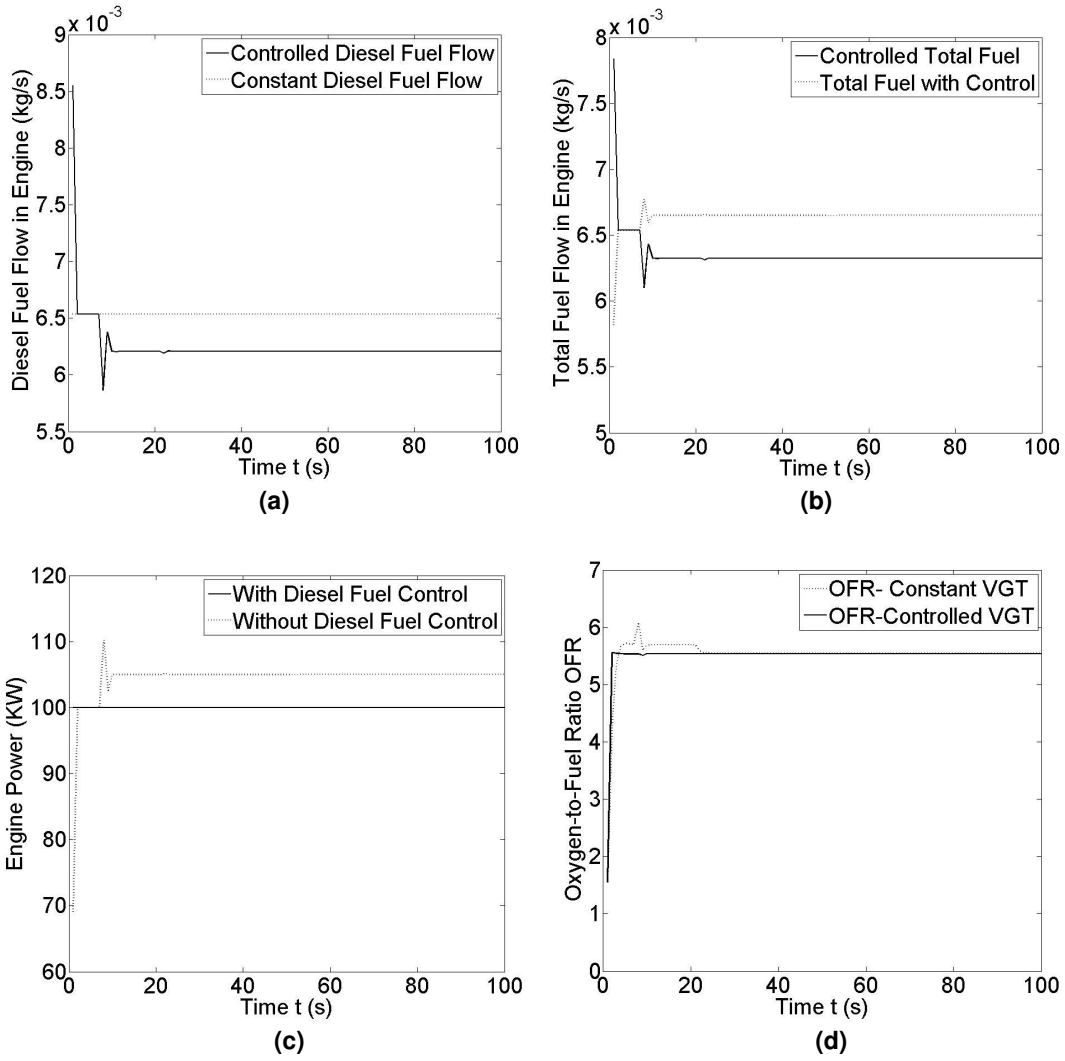

Figure 8.16 – Oxygen-to-Fuel Ratio and Engine Power Control

8.5. *Chapter Summary*

The chapter describes the implementation of PID controller for air and fuel regulation for the SOFC-IC engine system. The controllers demonstrate the improved responses of the system outputs as compared to the open loop operation of the system.

The localised PID controllers have set-points, which optimise local, as well as system performance. These set-points were selected from analyses in Chapter 5 and Chapter 7. Since the system is nonlinear, the controller gains are valid for a specified set-point only. In order to implement these controllers over a wider range of set-points, an adaptive

parameter estimation technique may be applied which gives controller gains for the respective set-points.

The conventional EGR system is replaced by utilising the exhaust flows of the fuel cell and the reformer. In the conventional EGR system, the inert gases from the exhaust manifold are cooled and recirculated to the engine. In conventional EGR systems, the control is complicated due to the nonlinear nature of the turbocharger and the interaction between the flow paths through the exhaust manifold and the common compressor-turbine shaft [127]. Since the effluents from the reformer and fuel cell can be more easily manipulated than the conventional EGR, the external-EGR proves to be advantageous from the control perspective.

Limitations:

The dynamic response of fuel cell affects the timing of introduction of hydrogen and the effluents in the engine. During start up, the fuel cell effluents may have a significant impact on the engine combustion. The steady state effects of introducing fuel cell effluents have been studied in Chapter 4 (Component Modelling-IC Engine) which allow deriving a set-point for control design. However, since the dynamic control oriented model does not include a combustion model, it cannot predict the effects of introducing fuel cell and reformer effluents in the engine.

The major disadvantage of PID controller is that these controllers are single-input-single-output (SISO) type. For complex systems, the control variables are often dependent on more than one input variable. PID controller cannot easily capture the effects of such interdependent variables. Due to this shortcoming, the state transition structure for set-point selection was developed. In its most basic form, the process causes oscillation in the controlled outputs because of the frequent changes in the control structure. The oscillatory behaviour can be managed through a slow transition between structures, but is still a complex solution.

A PID control structure with a mode switching supervisory layer has performance deficiencies due in part to the need to switch modes to deal with the non-linear nature of the hybrid power system. An advanced multiple-input-multiple-output (MIMO) control technique such as model predictive control, which can handle constraints, is more suitable

for complex process systems and will be examined in the next Chapter 9 (Model Predictive Control Design).

Chapter 9. Model Predictive Control Design

9.1. *Introduction*

Practical systems made up of multiple processes can be complex with nonlinear behaviour, with noise and various types of disturbances. Both regulation and control for load following are required and lead to a requirement for a structured control system design. The outputs of such a system are often dependent on more than a single input; hence there is a need to develop a comprehensive multivariable controller, which can accommodate a range of external factors. As described in Chapter 8 (Feedback Control Design Using PID Controllers), control methods such as PID control are effective for single-input-single-output systems, but are unable to account for effects of multiple inputs without resort to complex interlinking structures. A multivariable control method such as Model Predictive Control (MPC) can take into account the effects of input, measured and unmeasured disturbances on the output along with optimisation of the process within specified constraints. Model Predictive Control, is used extensively in the process industry [128] where it has emerged to handle multivariable constrained control requirements.

The solid oxide fuel cell – IC engine hybrid system, with its performance dependent on the flows in and through the system components, has nonlinear processes with outputs dependent on multiple inputs. The need to operate the fuel cell stack and the engine in an optimum operating region has been established in Chapter 5 (Investigation of Optimum Operating Range). Further, the dynamic system modelling in Chapter 7 (System Integration) discusses the open loop system behaviour and has allows selection of control inputs. The constraints imposed on the system components are mainly due to the limits of operating temperature to avoid degradation of materials, limitations by reaction kinetics and avoid pollutant formation. The main objective of the multivariable control design is to manage fuel, air and exhaust flows in a way to deliver the required load on the system while maximising the fuel efficiency within emissions and component temperature

constraints. The dynamic response of the system components varies, with the reformer being slower than the fuel cell and engine. The ability of the MPC to predict future control action by penalising any undesired behaviour within prescribed constraints makes it suitable for solution of the control problem proposed.

The development of a baseline controller using PID controller to demonstrate the improved system response is discussed in the previous chapter. This current chapter aims to demonstrate that the MIMO controller is a further development of a control approach in that it can perform explicit optimisation with constraints on output variables. The control of fuel flow to the reformer has demonstrated a non-minimum phase (NMP) behaviour, where the signal direction is initially opposite to that required for appropriate set-point tracking. Model predictive control can handle NMP behaviour through cancellation of the zero in the plant model, which causes the NMP behaviour. This capability of MPC will be examined in this chapter.

The following section in this chapter describes the fundamental principles of model predictive control theory and system identification, the control problem and formulation, approach followed for control design, results and discussion.

9.2. *Control Problem Formulation*

9.2.1. Introduction to Model Predictive Control

Model predictive control is a control strategy that involves online optimisation of the process and prediction of future control signals over a prediction horizon. The basic structure of a model predictive controller is given in Figure 9.1.

The MPC strategy

The MPC strategy as describe by Camacho et al [128] is described here. The future outputs are predicted for the next time instant, t+1 using prediction model. These future errors are calculated based on past input and output and future control actions. The future control actions are determined by minimizing a criterion, which consist of a quadratic cost function and constraints. This criterion is such that it maintains deviations from the reference trajectory to a minimum. N_2 is the prediction horizon, over which the input and

output signals are predicted. N_u is the control horizon after which the predicted controls are static; i.e. it defines the allowed number of changes in the control action.

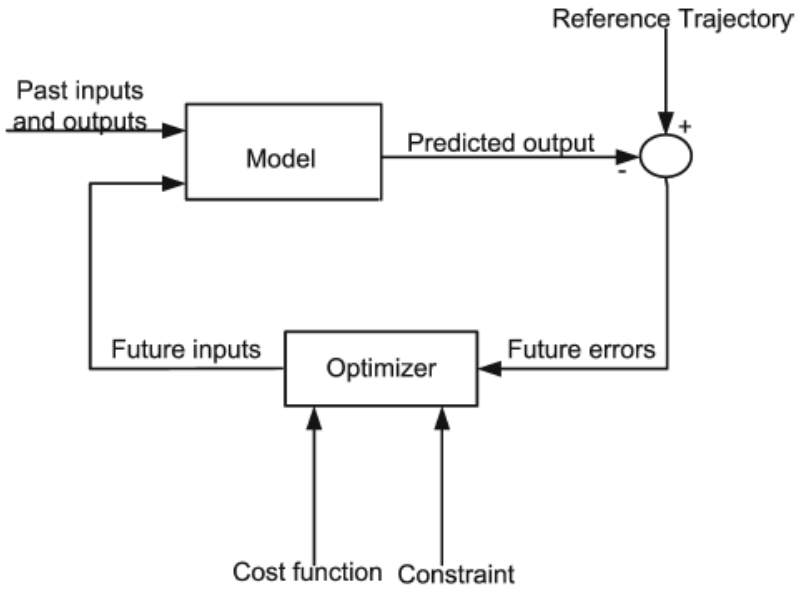

Figure 9.1 – Structure of Model Predictive Controller [128]

The model predictive controller follows a receding horizon concept. A quadratic optimisation is performed for a future time interval [i, i+N-1]. At time t=i, the optimisation results in the future control action u(t) over this horizon. The control action at the time t, u(t|t) is sent to the process model while the other signals computed are rejected. The process model then generates the future output for time (t+1) giving y(t+1). This output is further used to compute the future control action u(t+1|t+1) over the time interval [i+1, i+N]. The prediction horizon is derived from the settling time of the system to be controlled [129]. The length of this horizon can affect the speed of the control algorithm and should not be unnecessarily long [129]. The main components of the Model Predictive Controller are:

- Prediction Model

The prediction model is used to predict future outputs based on the past input and outputs as well as future control actions . The prediction model is an important part of the Model Predictive Controller and is required to be able capture the system dynamics and accurately produce outputs [128]. The prediction model can include a disturbance model along with

the process model. The inclusion of the disturbance model allows taking into effect of the disturbances on future outputs. The prediction model used in this chapter is a linear state-space model, which is typically used for multi-variable processes.

- Objective function

The weights define the penalty if the input and output values deviate from the desired values. The optimizer produces future control actions by minimising a cost function, which enshrines the control objective. The cost function is the basis for the control law [128]. The general expression for an objective function is [128]:

$$J(N_1,N_2,N_u)=E\left\{\sum_{j=N_1}^{N_2}\delta(t)\left[y(t+j|t)-r(t+j)\right]^2+\sum_{j=1}^{Nu}\lambda(j)\left[\Delta u(t+j-1)\right]^2\right\}$$

Eqn. 9.1

Where N_1, N_2 are the minimum and maximum cost horizons and N_u is the control horizon. $y(t)$ is the output, $r(t)$ is the reference trajectory, $u(t)$ is the input, $\delta(t)$ defines the weighting function on the outputs, while $\lambda(j)$ defines the weighting on the inputs. These parameters are used as controller tuning parameters. The higher the weight, the lesser is the deviation allowed for the signal. The selection of weights has an effect on stability and performance of the system [130]. The output weights ensure minimum deviation of outputs from reference trajectories while the input weights penalise the control action within the specified constraints.

The objective function is subject to constraints:

$$\begin{aligned} u_{\min} &\le u(t) \le u_{\max} && \forall t \\ du_{\min} &\le u(t)-u(t-1) \le du_{\max} && \forall t \\ y_{\min} &\le y(t) \le y_{\max} && \forall t \end{aligned}$$

Eqn. 9.2

- Control law

The control horizon defines the number of changes the control action can take. The selection of the prediction and control horizon has an effect on the system. A long prediction horizon is desirable for better performance control while a short control horizon results in a more robust system [130]. The selection of prediction horizon such that it covers the period of any NMP behaviour, ensures elimination of this behaviour from the objective function [131].

The control law is defined by the control horizon $N_{u.}$and the optimisation process. The control horizon defines the allowed number of changes in the control action during optimisation [132]. Hence for an interval $N_u<N_2$ there are no changes in the control signal.

$$\Delta u(t+j-1)=0 \qquad j>N_u$$

Eqn. 9.3

The Model Predictive Control Toolbox in Matlab®, adopts the normal convention of compensating for measured disturbances through feed forward control action and unmeasured disturbances through feedback control action.

The requirement is to develop a model predictive controller to regulate the air and fuel flows in the system. The cost function to be minimized to obtain future control actions consists of expressions for deviation of outputs from set-point values and regulation of inputs within prescribed constraints. A linear system model is used as a prediction model. The controller calculates the air and fuel flow inputs to the fuel cell and the VGT and external-EGR actuators position for the engine. The development of linear controllers for a nonlinear system is done by linearising the system model around a specific operating point. The linearization of the system can be done by direct linearization or by identifying a linear model directly with system identification.

9.2.2. Controller Objectives

The controller must adjust the flow into the fuel cell cathode and anode with the following control objectives and set-points, which have been previously identified in Chapter 7 (System Integration) and Chapter 8 (Feedback Control Design Using PID Controllers):

- Maintain excess oxygen ratio in the fuel cell to a value of 2.
- Regulate the fuel flow in the reformer such that the utilisation factor is minimum 70% and maximum 95%.
- Within the limits of the above two objectives, ensure that the fuel cell supplies a steady base load.

A controller for the engine operation must meet the following objectives, which have also been previously identified in Chapter 7 (System Integration) and Chapter 8 (Feedback Control Design Using PID Controllers):

- Regulate the oxygen to fuel ratio (OFR) of the charge to a determined set point and above the stoichiometric value of 4.3 at all times.

- Regulate the amount of hydrogen in the engine charge to a minimum of 5% and a maximum of 20%.
- Regulate the fraction of external-EGR to a determined set point, up to 30% of the engine charge.
- Within the above constraints supply power according to the load demand on the system

The control requirement for the system requires the regulation of air and fuel flow into the system to ensure that the appropriate performance variables values are achieved. The inputs to the system include:

- Fuel flow in the reformer (W_{ref_in})
- Compressor-Motor voltage for air flow in the fuel cell (V_{cm})
- Desired current of the fuel cell (I_{fc})
- Diesel fuel flow into the engine (W_{di})
- VGT vane position for air flow in the engine (χ_{vgt})
- External EGR valve position for inert gas flow in the engine (χ_{xegr})

The corresponding performance variables of the system include:

- Fuel Cell Power (P_{fc})
- Stack voltage (V_{fc})
- Excess Oxygen Ratio of fuel cell (λ_{O2})
- Utilisation factor of fuel cell (μ_f)
- IC engine power (P_{ic})
- Oxygen to Fuel Ratio in engine (OFR)
- Fraction of external EGR gases in the intake manifold (xEGR)

The outputs of the system are such that they relate to the performance variables at steady state. The output vector includes exhaust flow from cathode W_{ca_out}, hydrogen exhaust from anode W_{h2_out}, total mass flow into the engine W_e, and the fraction of oxygen in the inlet manifold F_{O2}.

Controller Design

The control oriented model for the system described in Chapter 7 (System Integration) is the basis for development of a model predictive controller for the system. The fuel input to

the fuel cell is provided by a reformer instead of a hydrogen tank. The reformer is modelled as a transfer function with time constant τ_R = 5 seconds [36]. The system model is nonlinear; hence it requires linearization around a selected operating point. The controlled outputs for the fuel cell controller are the exhaust flows from the cathode and hydrogen from the anode.

The reformer produces hydrogen, carbon monoxide, methane and trace amounts of other high molecular weight hydrocarbons. The hydrogen is supplied to the fuel cell, while the rest of the exhaust streams are supplied to the engine as inert gases for dilution of the charge air. This mixture functions like an externally supplied EGR (exhaust gas recirculation) flow.

The exhausts from the fuel cell system have the following effects on the engine:

- The hydrogen from the anode exhaust modifies the proportion of hydrogen in the engine charge gas.
- The depleted oxygen and nitrogen mixture from the cathode exhaust modifies the OFR and EGR fractions in the intake manifold and consequently the specific heat capacity.
- The exhaust gases from the reformer other than hydrogen affect the EGR value in the engine.

The system simulation results indicate the potential to deliver more than 40% of external exhaust gas fraction to the engine under full load conditions of the fuel cell and the engine. A valve to regulate this externally supplied exhaust gas recirculation (xEGR) is included in the model.

9.2.3. Linearization of System Model using System Identification

In order to develop a linear model predictive controller, the first step is to identify a linear model at an operating point. Identification is the process of constructing mathematical models of dynamical system from observations and prior knowledge [133]. There are various purposes as to why system identification is used to evaluate the models for system behaviour. The most common reasons for identifying models as stated by Norton [133] are – to satisfy scientific curiosity for prediction and control, to create models for state estimation, diagnosis of faults and inadequacies and for simulation and operator training. In this chapter, system identification is used to develop linear models for prediction and control design.

The steps involved in system identification are [132]:

1. Experiment planning to obtain data

The sampling period for the data must be small enough to incorporate all process information and the input signals must also be persistently exciting such as of PRBS form [132]. The data can be pre-processed to remove any offsets/trends. De-trending data removes any mean values and linear trends from data [134]. Detrending data is not necessary in certain cases such as [134]:

- Physical levels of data are built into the model
- Inputs to integrators require absolute signal levels
- When working with transient data (step inputs, impulse inputs)

Since the modelling data of the hybrid system used for system identification included transient responses, data detrending was avoided.

2. Selection of model structure

The selection of model inputs and outputs is required in order to achieve models, which capture the necessary system dynamics. The input-output signals, which define the structure of model, are selected from prior knowledge of the system's dynamic behaviour (Chapter 7). From the PID controllers developed in Chapter 8, the performance variables are functions of the measured outputs. The open loop simulation of the system in Chapter 7 (System Integration) provides some insight into the system behaviour, allowing selection of appropriate inputs and outputs. A state-space model structure is suitable for MIMO system and has been chosen for the control design in this chapter

3. Parameter estimation

The selection of a parameter estimation method depends on structure of the model and properties of the data [132]. The parameter estimation technique used for the model predictive control development is the prediction error method (PEM) which gives the model in a state-space format.

4. Model Validation

Model validation is done by comparing the identified model outputs with a part of output data not used for estimation. The validity of the model is generally based on the difference between simulated and measured output.

The identification of data from the system model results in a linear model, which is valid only for a small range of values around the specified operating point. The development of linear model predictive controllers for a nonlinear system can be done by using a number of linear controllers at various operating points. The appropriate controller is selected when the set-point changes. Such a method is further demonstrated in this section by developing two model predictive controllers for two operating points.

The system inputs are fed with pseudo – random binary sequence (PRBS) of appropriate frequency for the purpose of system identification. The persistently excited inputs in the form of PRBS signals and the corresponding outputs are used to create datasets. The System Identification Toolbox version 7.1 in Matlab® version R2007b is used to identify a state-space model using the datasets obtained from simulations.

Prediction Error Method – this method minimises the error between the predicted and observed values of output based on minimisation of a cost function, J [132]. The algorithm for this method is included in the System identification Toolbox of Matlab®. The prediction error method (PEM) is used to identify linear models of the following form:

$$x(t+k) = Ax(t) + B_u u(t) + B_w w_m(t) + Ke(t)$$

Eqn. 9.4

$$y(t) = Cx(t) + D_u u(t) + D_w w_m(t) + e(t)$$

Eqn. 9.5

The identified model includes a process model along with a disturbance model. The model has six inputs, the four manipulated variables are - V_{cm}, W_{ref_in}, χ_{egr}, χ_{vgt}, with two measured disturbances – desired current for fuel cell and diesel fuel flow input for the engine. The model structure is defined as follows:

Model Inputs $u = \left[Vcm \;\; W_{ref\_in} \;\; \chi_{egr} \;\; \chi_{vgt}\right]^T$

Measured Disturbances $w_m = \left[I \;\; W_{di}\right]^T$

Measured Output $y = [W_{ca\_out} \;\; W_{h2\_out} \;\; W_e \;\; F_{O2}]^T$

Performance Variables $z = \left[P_{fc} \;\; V_{fc} \;\; \lambda_{O_2} \;\; \mu_f \;\; P_{ic} \;\; OFR \;\; xEGR\right]$

Models are identified around two operating points selected for two different load conditions for the fuel cell and the engine. The model order was determined by trial-and-error method. The identified model for each operating point is a fourteenth order model. The accuracy of the model is shown by fit percentage (i.e. comparison of identified model with data used for identification) of each output signal in the System Identification Toolbox. The fit percentage for models of each operating point are given in Table 9-1.

Table 9-1 – Quality of identified models

Identified Model Outputs	Set-point 1 (fit %)	Set-point 2 (fit %)
Cathode exhaust W_{ca_out}	99.3%	99.12%
Hydrogen exhaust from anode W_{h2_out}	82.53%	67.21%
Engine flow rate W_e	93.82%	86.88%
Fraction of oxygen F_{O2}	96.04%	87.76%

The accuracy of the models was further verified by comparing it with the control oriented system model for the given operating points. The linear models are used to develop a model predictive controller using Model Predictive Control Toolbox in Matlab®. The structure of the controller is shown in Figure 9.2.

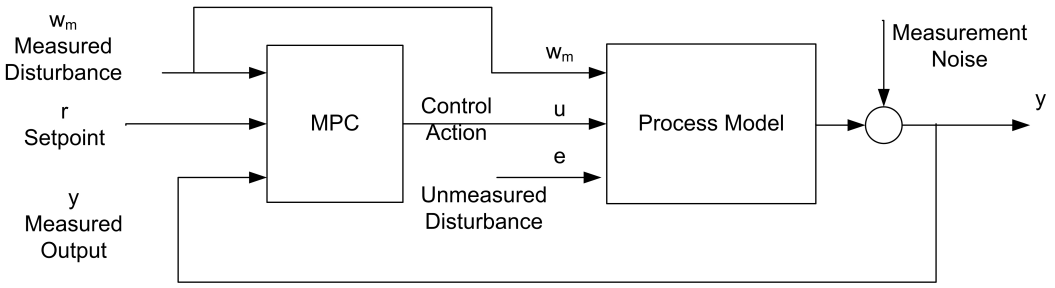

Figure 9.2 – Model Predictive Controller and Process Model

The weights for the inputs and outputs are selected such that the set-point tracking is with minimum deviation. The rate weight for the reformer fuel input is the highest, so that the deviation of its value is minimum. This ensures a steady utilisation factor and a steady value of hydrogen percentage in the engine cylinder. The control horizon selected is N_u =2, the prediction horizon is N_2=10 with the control interval as 0.1.

9.3. *Simulation results*

The validation of the control design is achieved by applying the controllers to the fuel cell-IC engine hybrid system model. Once the controllers were individually validated, the nonlinear system is fed with measured input disturbances in the form of a sequence of step changes from set-point 1 to set-point 2 and vice versa. As the set-point changes one to another, the appropriate controller is selected for the duration of the pulse. The set-point values are tabulated in Table 9-2.

Table 9-2 – Set-points for Control Design and Estimation.

	Set-point 1	**Set-point 2**	**Units**
Inputs			
Compressor Motor Voltage (Vcm)	1400	1700	V
Reformer Fuel Input (Wref_in)	0.0022	0.0024	kg/s
VGT Vane position (χvgt)	0.81	0.7	
xEGR Valve position (χxegr)	0.65	0.4	
Measured Disturbances			
Fuel Cell Current Demand (I)	50	60	A
Engine Diesel Input	6.54E-03	5.23E-03	kg/s
Outputs			
Cathode Exhaust (Wca_out)	0.08	0.095	kg/s
Hydrogen Exhaust from anode (Wh2_out)	0.0005	0.00036	kg/s
Engine (We)	0.18	0.143	kg/s
Fraction of Oxygen in Engine (FO2)	0.18	0.181	
Performance variables			
Fuel Cell Power (Pfc)	10	12.7	kW
Excess Oxygen Ratio	2	2.05	
Utilisation Factor	0.75	0.85	
Engine Power (Pic)	100	80	kW
Oxygen-to-fuel Ratio (OFR)	5.5	5.7	
Fraction of external dilution gases (xEGR)	0.3	0.26	

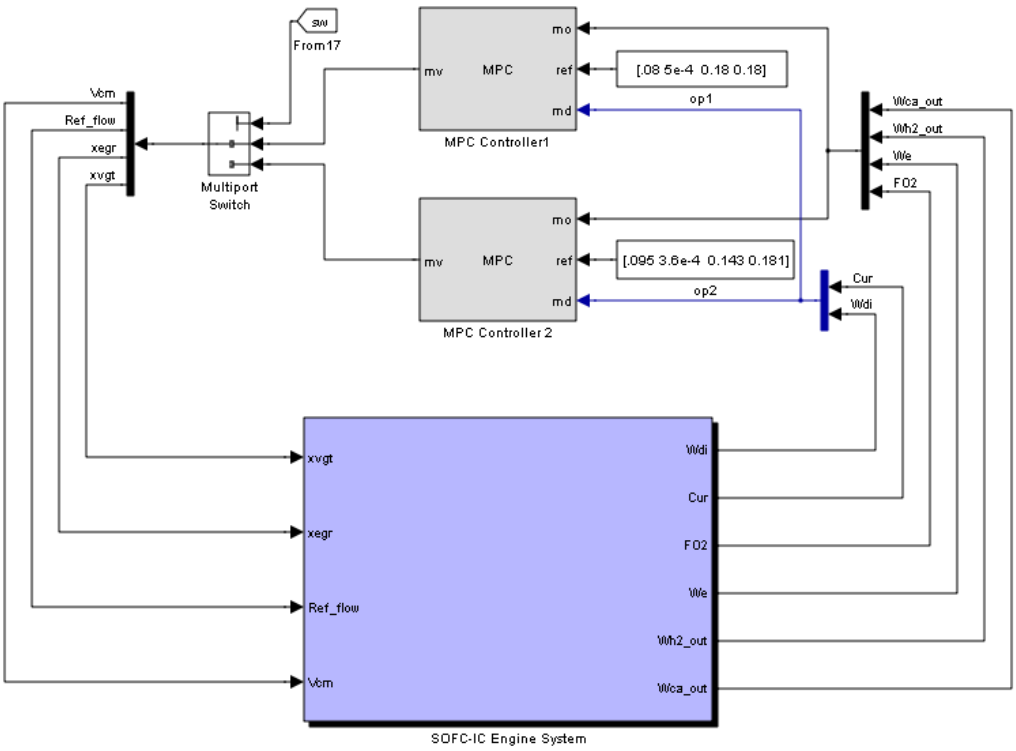

Figure 9.3 – Architecture of the controller for two set-points

The controller simulations applied to the nonlinear model are shown in Figure 9.4 - Figure 9.8. The results of the model predictive controller are strongly influenced by the identified model. As shown in Table 9-1, the fit quality is poorest for the hydrogen exhaust from the anode and will affect the controller performance as shown in the following discussion.

Output response

The exhaust flow rate from the fuel cell cathode, as shown in Figure 9.4(a), tracks the set-points accurately with an average error of 0.09%. The response is dependent on the compressor dynamics.

The hydrogen exhaust flow rate, as shown in Figure 9.4(b) from the fuel cell anode has a delayed response due to the reformer dynamics. The reformer fuel input is manipulated by the controller to compensate for the reformer response. Although, the average error in tracking the reference trajectory is 20%, the results are acceptable since the hydrogen percentage in the engine is within the necessary limits as shown in Figure 9.5(b).

The total mass flow in the engine and the fraction of oxygen in the engine, shown in Figure 9.4(c) and (d), are both dependent on the air flow input from the compressor and the externally provided dilution gases, that is the external EGR. The control action results in

set-point tracking of the mass flow in the engine with an average error of 1.26 % and the fraction of oxygen with an average error of 0.068 %. A higher initial value is observed in the total engine mass flow and the fraction of oxygen are during the first 20 seconds of simulation time. During this time, the hydrogen input to the engine is zero and only diesel fuel is supplied to the engine. The deviation in these engine outputs during this time, is due to the higher quantity of fuel. When hydrogen is supplied to the engine, the quantity of diesel fuel is reduced to maintain the equivalent fuel energy of the mixture, and the set-point tracking is with minimum error.

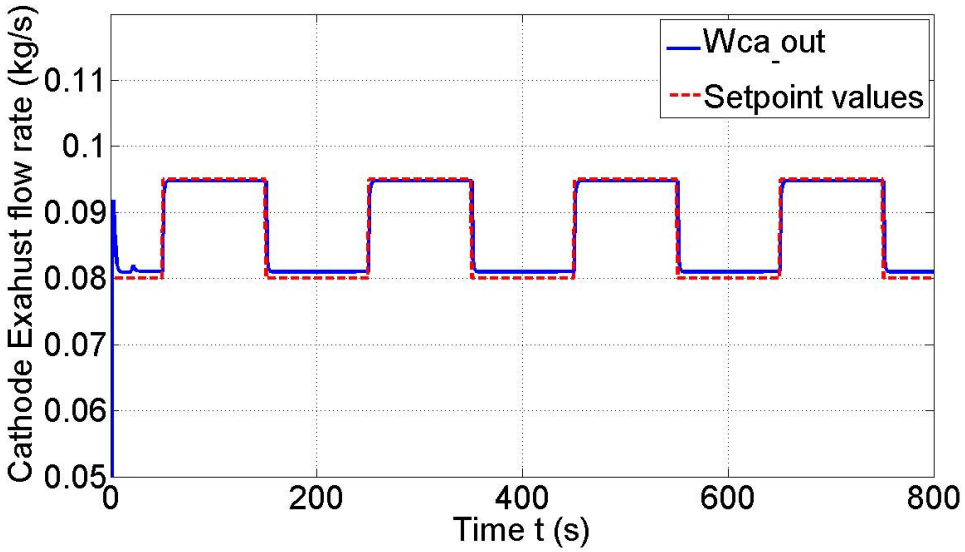

(a)

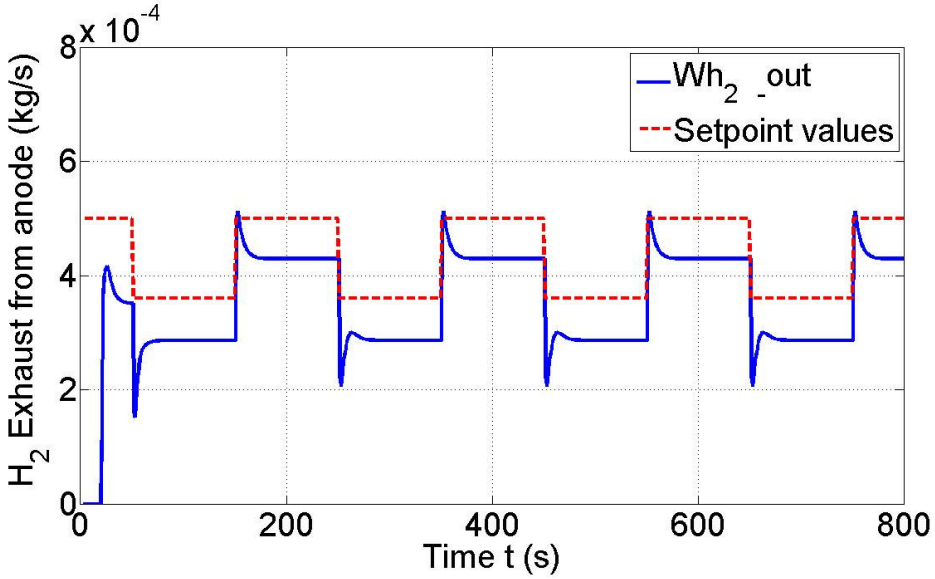

(b)

Figure 9.4 – Controlled Outputs

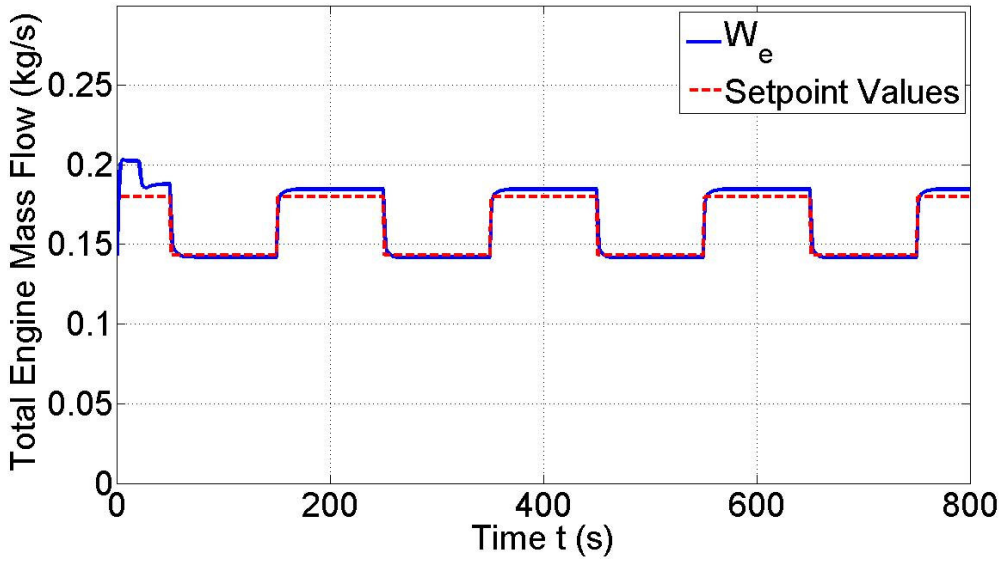

(c)

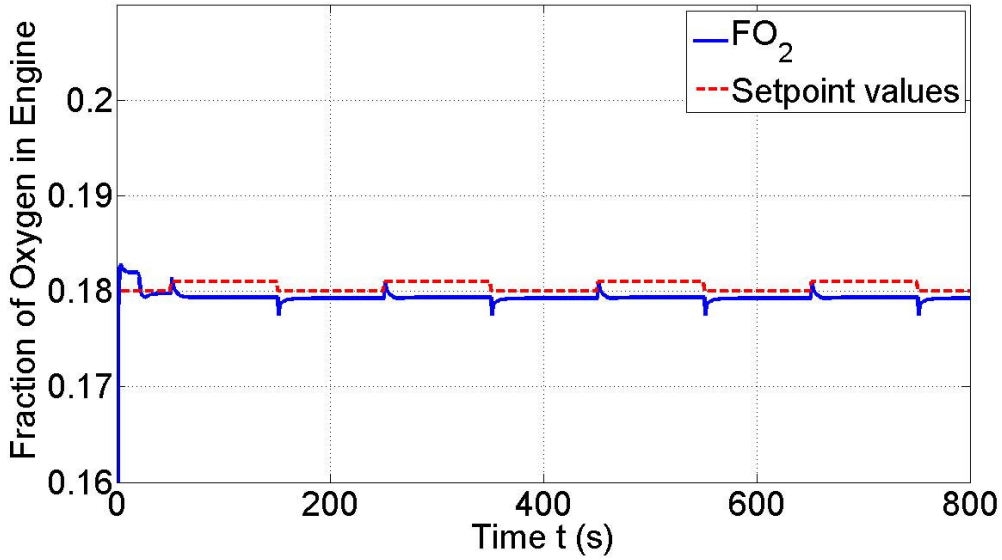

(d)

Figure 9.4 – Controlled Outputs

Performance Variables

Excess Oxygen Ratio

The performance variables of the fuel cell are shown in Figure 9.5. The excess oxygen ratio is maintained at the set-points with values 2 and 2.05. The response of the flow is dependent on the compressor dynamics. From Figure 9.5(a), during the step changes,

transients are observed and the lowest peak value of excess oxygen ratio is 1.7. Hence the controller action is satisfactory to prevent oxygen starvation in the fuel cell at any point.

Utilisation Factor

The response of the hydrogen exhaust from the fuel cell anode is directly reflected in the utilisation factor response shown in Figure 9.5(b). The utilisation factor values are 0.85 and 0.75 for set-point 1 and set-point 2 respectively. The reformer fuel input control action is such that it ensures that the utilisation factor is within 70-95% range during transient behaviour.

Fuel Cell Power and Stack Voltage

The fuel cell stack voltage and the fuel cell power output are similarly maintained at desired values as shown in Figure 9.5(c) and (d). The delay in voltage and power rise is due to the reformer response causing delayed production of hydrogen. The reformer dynamics are the slowest – the penalty on the weight is higher for the reformer to improve the response.

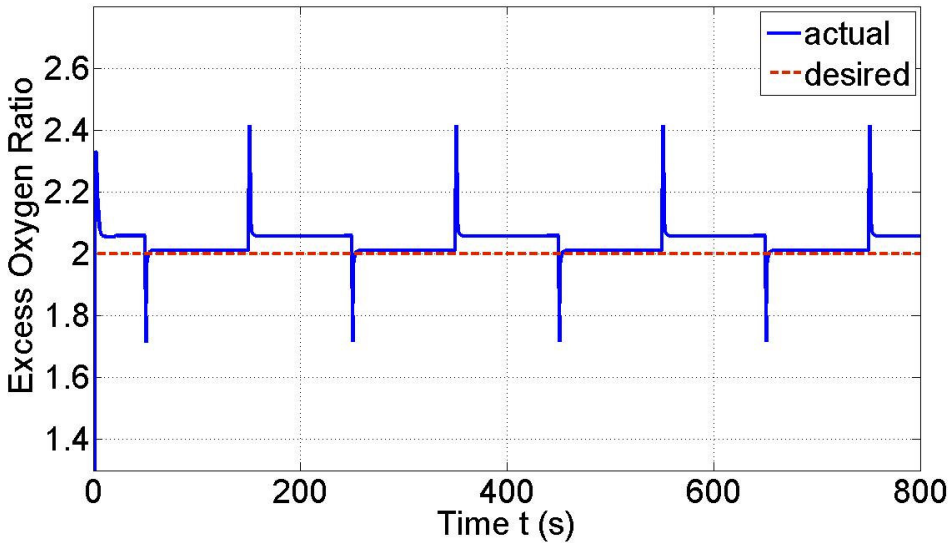

(a)

Figure 9.5 – Performance Variables of Fuel Cell

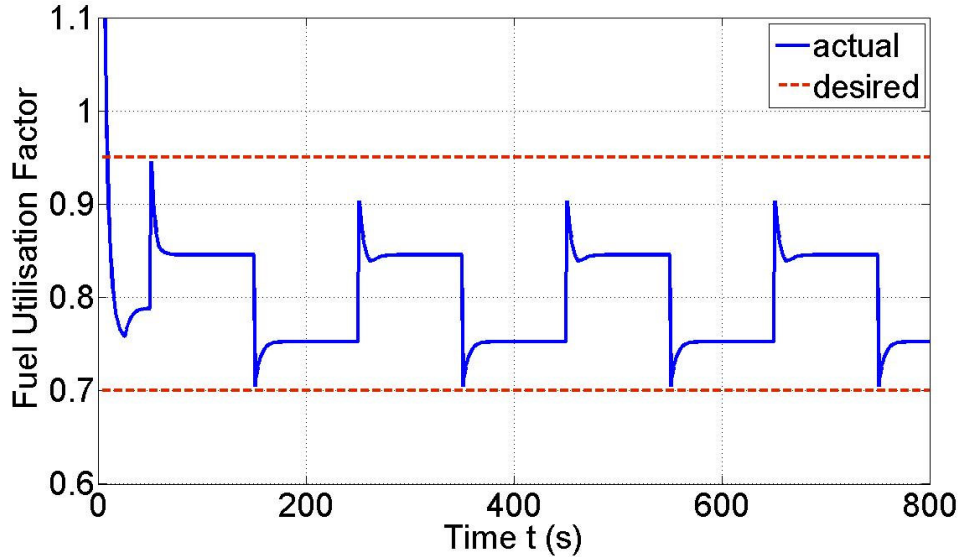

(b)

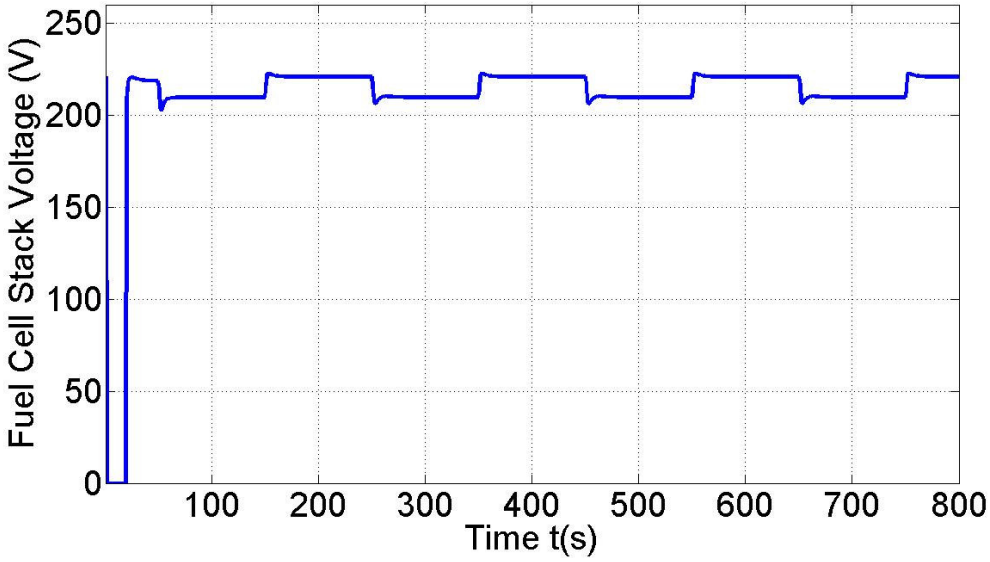

(c)

Figure 9.5 – Performance Variables of Fuel Cell

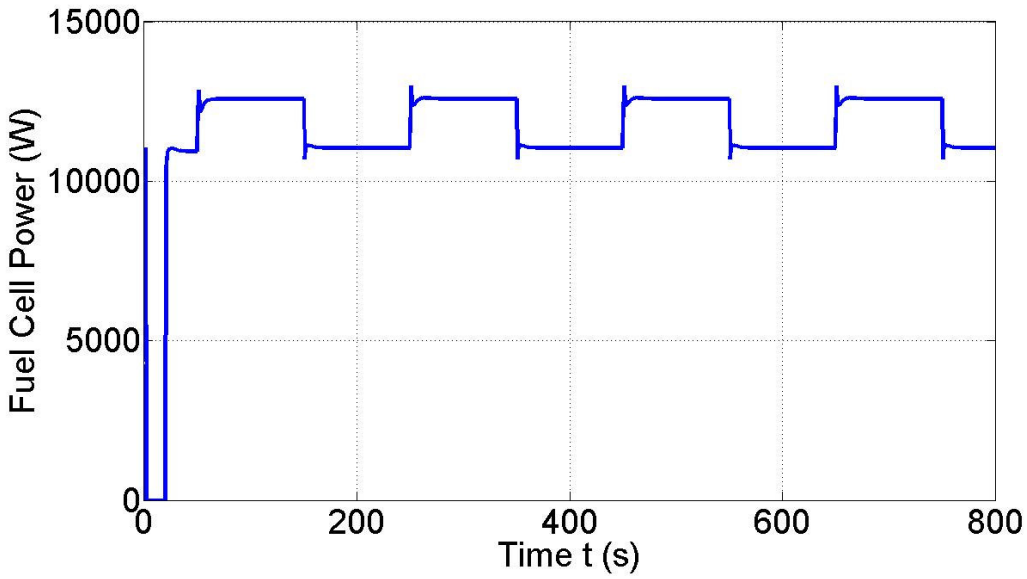

(d)

Figure 9.5 – Performance Variables of Fuel Cell

The engine performance variables are shown in Figure 9.6. The effects on each performance variable are described below.

Engine Power

As the hydrogen flow increases, the diesel flow in the engine reduces such that the total fuel equivalent energy stays the same, ensuring a constant power output. The engine power is derived from static relationships and does not include engine dynamics. The engine power produced is shown in Figure 9.6(a).

Oxygen-to-Fuel Ratio and Fraction of external EGR

The OFR has to be maintained at all times above 4.3 to avoid formation of smoke. The regulation of the engine outputs by the controller appropriately ensures the OFR is maintained at desired values with minimum peak response value of 4.85. In Figure 9.6(b), the first overshoot at approximately 20 seconds of simulation time reflects the addition of hydrogen in the engine cylinder along with diesel. This effect is also seen in the hydrogen percentage in the engine and the fraction of external EGR.

Hydrogen percentage in Engine

The hydrogen percentage in the engine as shown in Figure 9.6(c) varies from a minimum peak value of 8 % to a maximum peak value of 23 %. Ideally the maximum value should be maintained around 20 % [12-14] to ensure high thermal efficiency and avoid knocking

in engine. Any higher value of hydrogen in the engine requires dilution to avoid knocking behaviour.

The peak values observed in the OFR and external EGR fraction during step changes should be able to provide excess oxygen and dilution to track the hydrogen supplied.

Fraction of external EGR

The fraction of external EGR can be easily manipulated to provide dilution in the engine. The response of this fraction is shown in Figure 9.6(d). The response of the VGT actuator has a greater influence on the OFR as compared to that of the external EGR actuator

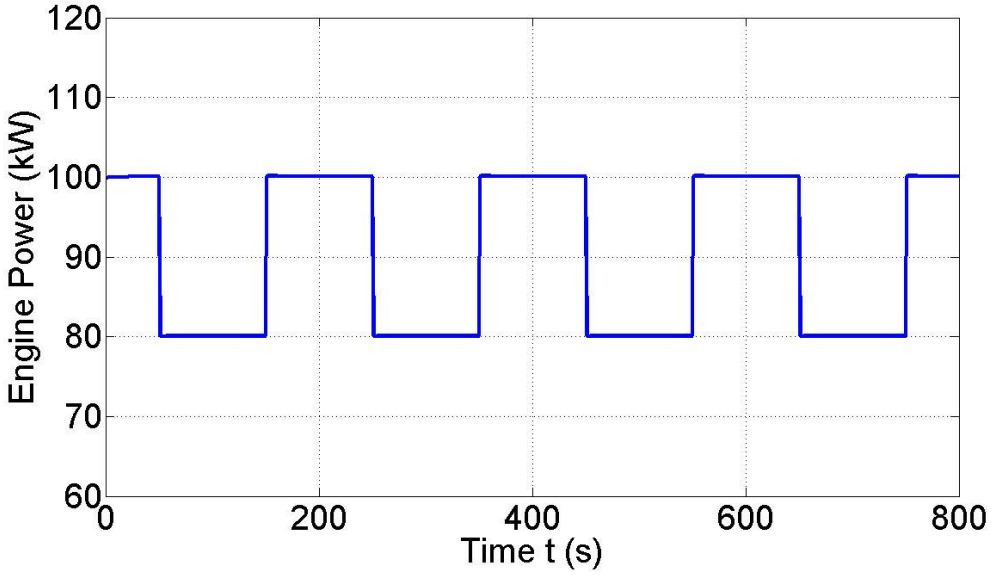

(a)

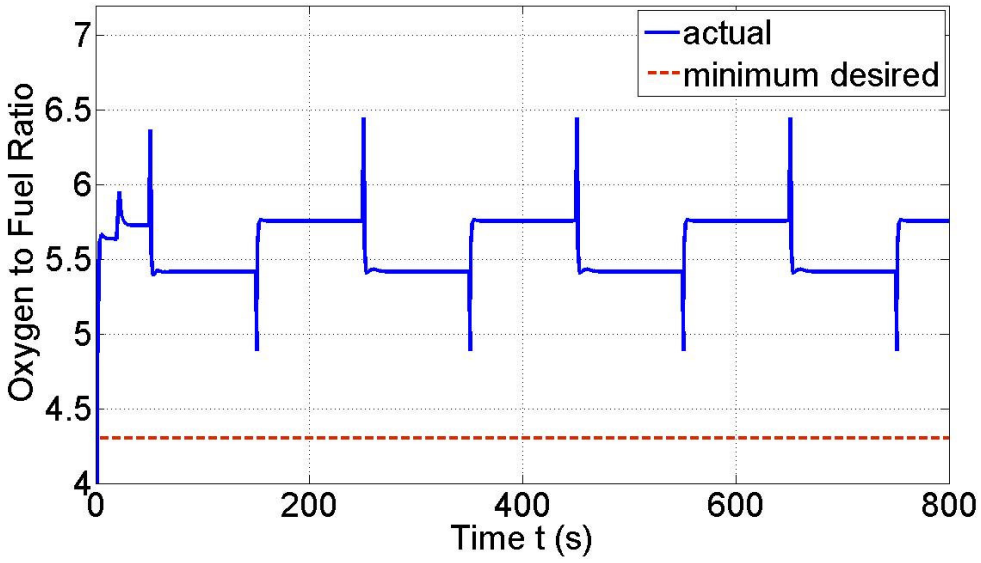

(b)

Figure 9.6 - Performance Variables of IC Engine

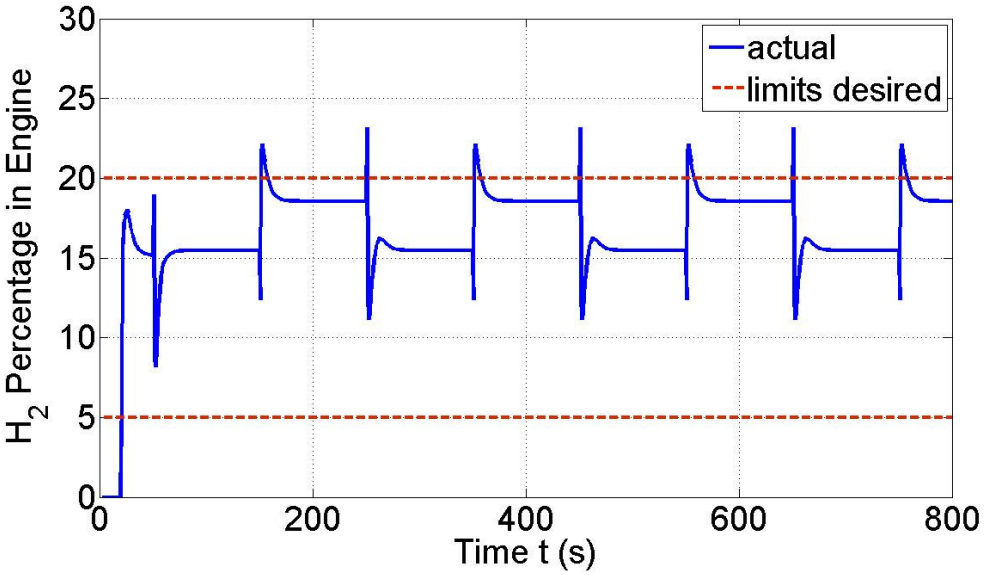

(c)

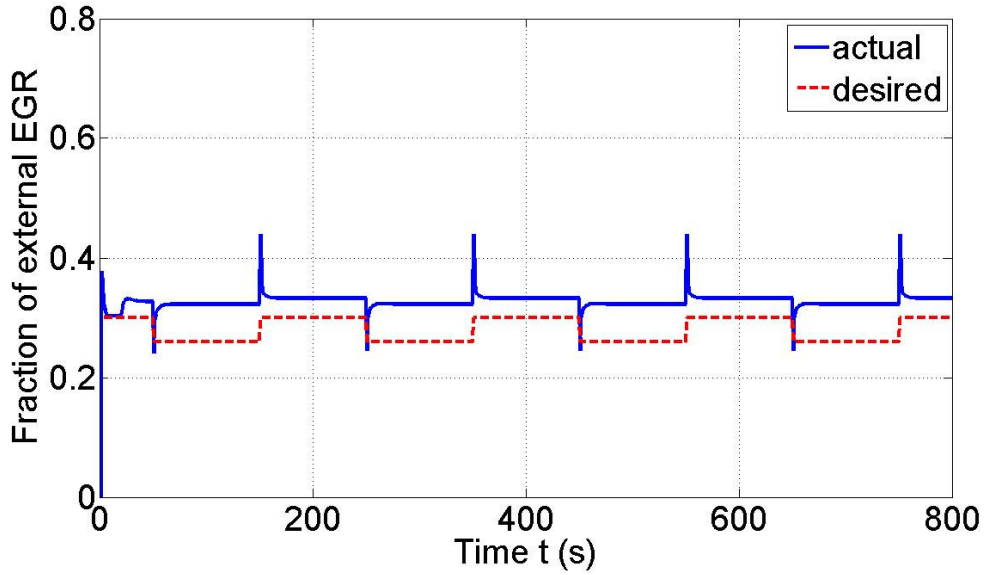

(d)

Figure 9.6 – Performance Variables of IC Engine

Manipulated Variables

The control actions of the two model predictive controllers are seen in Figure 9.7. The input values are within constraints designed for the controllers. The reformer fuel input, as shown in Figure 9.7(d), with overshoots shows the controller action to compensate for the slow reformer dynamics.

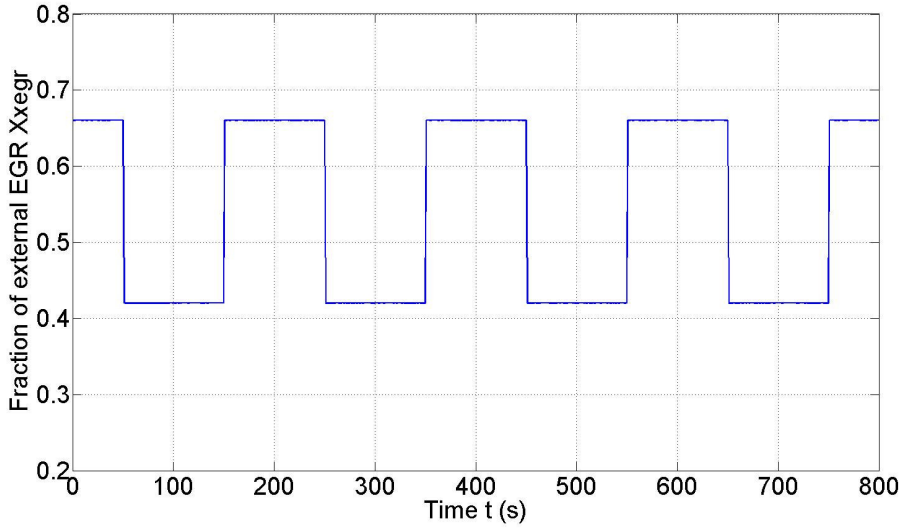

(a)

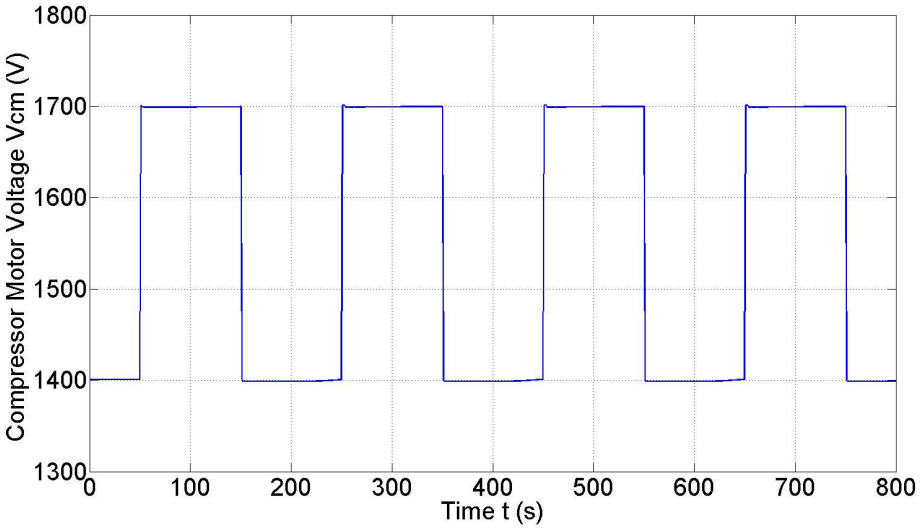

(b)

Figure 9.7 – Manipulated Inputs

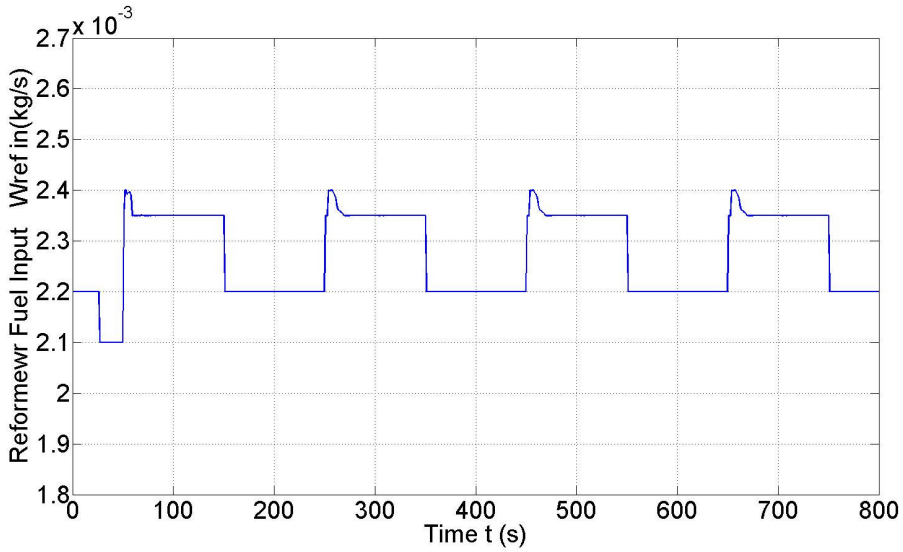

(c)

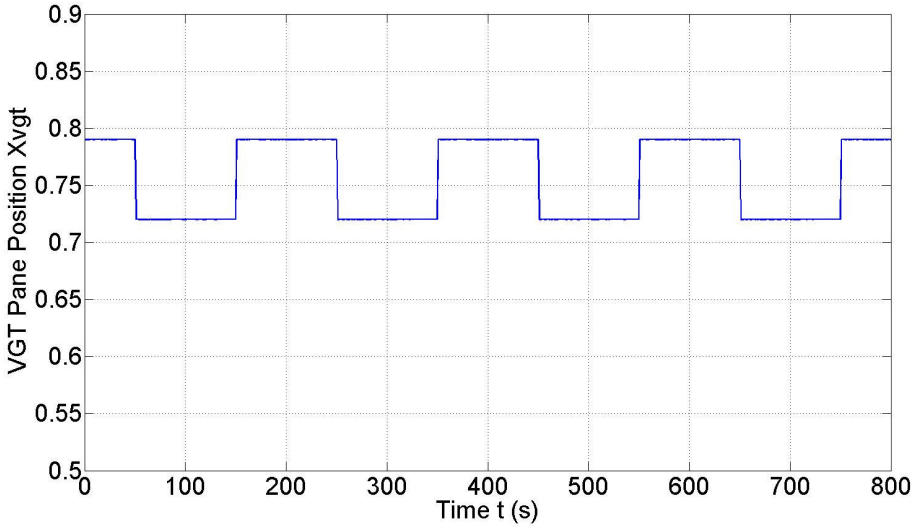

(d)

Figure 9.7 – Manipulated Inputs

Measured Disturbances

The current of the fuel cell and the diesel fuel input for the engine form the measured disturbances for the process which are compensated with feedforward control. The diesel fuel shows peaks during the step values to accommodate any change in the equivalent fuel energy due to addition of hydrogen in the engine. These signals are shown in Figure 9.8.

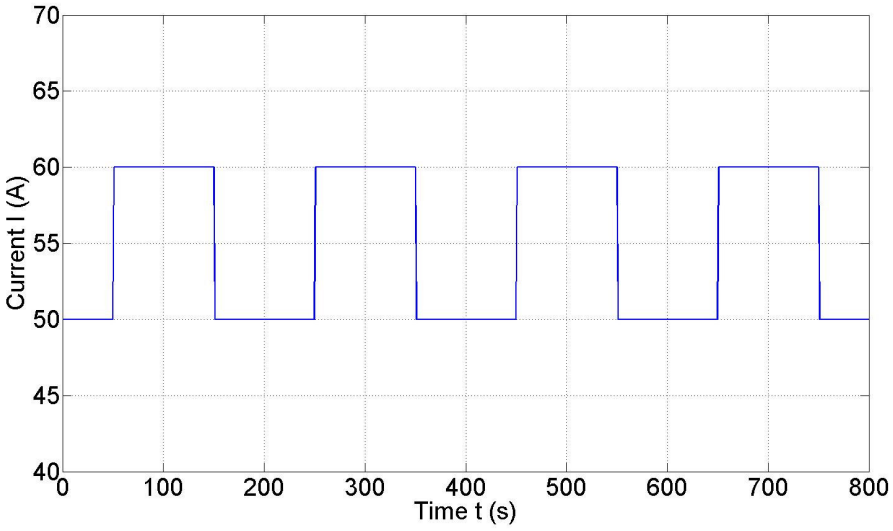

(a)

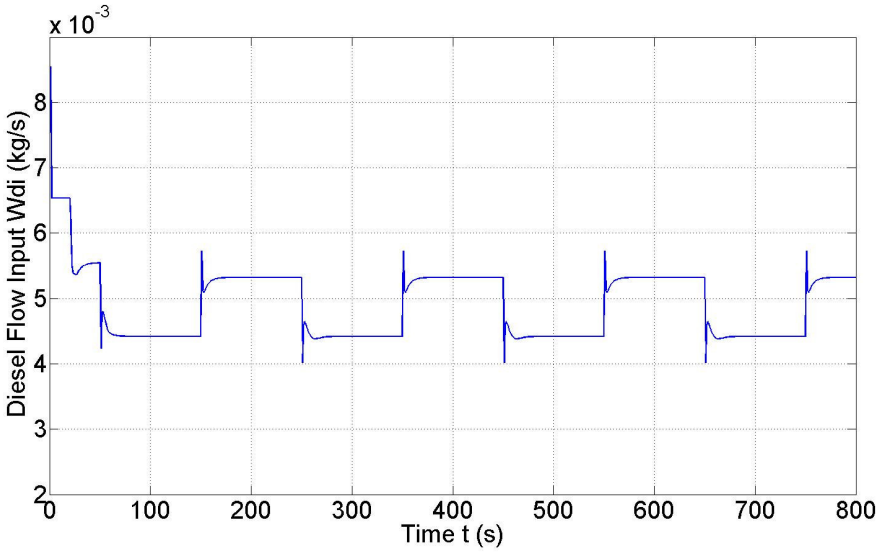

(b)

Figure 9.8 – Measured Disturbances

The effect of drop in diesel fuel when hydrogen leaves the fuel cell anode is reflected as a small overshoot at time 20 seconds in the OFR. The charge dilution provided by the external EGR gases affects the fraction of oxygen in the engine and the total mass flow to the engine. Since a fraction of the oxygen is supplied from the fuel cell exhausts, while most oxygen in the engine is from the air intake, both actuators, VGT vane position and the external EGR gases affect both outputs of the engine.

9.4. *Chapter summary*

This paper describes the design of a multivariable controller using model predictive control theory. A linearised system model was identified using data from the control-oriented system model for the chosen operating points. The identified model was a fourteenth order model and the fit percentages of the outputs were ranging from 67 % to 99 %. The MPC results show the effectiveness of the model predictive controller in handling all constraints and tracking set-points with minimum error, hence achieving optimum system performance. The controller is able to reject noise and any unmeasured disturbance within the limits of the operating point of the linearised model. The controller achieves the following:

- Prevention of air and fuel starvation in fuel cell
- Regulation of fuel cell utilisation factor and hence efficiency.
- Prevention of smoke formation by regulating OFR above stoichiometric.
- Regulating external EGR to provide dilution in the engine.

The model predictive controller is highly suitable over conventional control strategies for this system because

- There is a need to optimize flows to maintain overall system efficiency.
- All controlled variables need to be regulated simultaneously due to their effect on one or more performance variable.

Thus, the model predictive controller achieves a good transient response within the constraints on the system and demonstrates its superiority over SISO control. Such a single controller handling all local constraints of the system is ideal for the development a supervisory controller.

The superiority of the model predictive controller over the baseline control design with PID control is seen:

1. The PID controller developed for regulating the reformer fuel input displayed a non-minimum phase behaviour. This behaviour is eliminated by using a model predictive controller.
2. The need for stateflow logic to select set-points for the utilisation factor and hydrogen percentage in the engine (described in section 8.2) is eliminated using MPC. The controllers are designed such that at any point the utilisation factor and

the hydrogen percentage are within the prescribed limits.

The identified models used for MPC development were valid for a very small range of values around the operating points. Thus, in order to develop a control system operating over a wide range of operating points, an adaptive prediction model can be used which updates according to operating point changes.

The measured input disturbances of the MPC controller, which define the load on the fuel cell and the engine, form the output signals of a top level controller, i.e. a supervisory controller. A strategy for development of such a controller is described in Chapter 11 (Future Work).

Chapter 10. Conclusion

The potential of hybrid systems in aiding reduced fuel consumption and emissions has caused development of a wide number of such applications. This thesis provides a methodology for assessment of a hybrid system at the system level. The solid oxide fuel cell – diesel engine hybrid system proposed is examined in terms of efficiency improvement, fuel consumption, emissions and qualitative use of fuel and the methods of control design to improve the overall system performance. The main contributions of this thesis are the exergy approach followed for evaluating system efficiency and the design of controls for such a complex hybrid system. The conclusions from this work are given in the sections below.

10.1. *System Efficiency*

The proposed system is novel and raises a number of research questions. The first and foremost issue is regarding the efficiency improvement of the hybrid system over the conventional diesel engine systems. Chapter 5 (Investigation of Optimum Operating Range) confirms the fuel consumption improvements by indicating system efficiency of the hybrid system to be higher than that of a diesel engine. An idle load efficiency of 39 % for the hybrid system was obtained as compared to 27% for the conventional diesel engine. In order to improve engine efficiency by introducing hydrogen in the charge, the fuel cell is required to be at a low efficiency. A trade-off between the two conflicting requirements has allowed defining an optimum operating region for the system, which forms the main basis of the control design. The engine requires at least 4% hydrogen with the fuel cell at 74% utilisation factor to ensure visible efficiency improvements when the system components are at full load.

An exergy analysis of the system shows the rational efficiencies drop from 100 % for the reversible system to 77.1 % for the system with internal irreversibilities and finally 25.4 % for the practical system. When waste heat from the engine was utilised within the system,

the rational efficiency increased from 25.43 % to 36.01 %. The exergy analysis results indicate the potential for improving the system design to ensure a high rational efficiency. The results also show that work potential of the system is more dependent on the internal exergy losses than the external ones.

10.2. *Engine Emissions*

The results from the Chemkin engine model for n-heptane combustion, describes the effects of introducing hydrogen and effluents from the fuel cell and reformer (which constitute the external EGR) in the engine charge on pollutant formation. The results show that introducing the fuel cell exhausts and reformer exhausts (except hydrogen) along with hydrogen to the engine charge results in lowering of NOx emissions by 99 % of those produced for combustion of pure n-heptane. This combustion model confirms the hypothesis of reduced NOx emissions by introducing effluents from the fuel cell and reformer into the engine.

10.3. *Control Design*

The main control loops for the system are control for air and fuel flow, heat and temperature management and power distribution management between system components. Two approaches towards control design, i.e., PID and MPC controllers are developed with the focus on air-path and fuel-path control, which showed an improved dynamic system response. The feedback control design approach resulted in a set of PID controllers for each control variable with complex interactions, while the MPC design approach handles the constraints on the MIMO system more effectively. MPC also eliminates the NMP behaviour, an undesirable effect, which was observed with PID controllers. The MPC control action results in set-point tracking for the outputs of cathode exhaust with 0.09 % error, hydrogen exhaust from the anode with 20 % error, engine mass flow rate with 1.26 % error and the fraction of oxygen with 0.68 % error. This showed that the performance of the MPC controller is limited by the accuracy of the linearised plant model. The improved results of the MPC strategy over the feedback control design indicate the suitability of the MPC control technique for such complex systems. Such an effective control system is essential for an efficient operation of such a complex hybrid system.

10.4. *Modelling*

Chapter 4 describes the fundamental operating principles and dynamic behaviour of each component. The models and its parameters are adopted from literature, but require experimental validation. The dynamic behaviour of these models for changing system parameters was examined. Models for the SOFC and a steam reformer were adopted from literature. The SOFC model achieved validated with a distributed model from literature. Although complete validation was not achieved for the reformer-burner model, the model allowed identifying the control parameters. Similarly, the engine combustion model predicted the effects of the effluents on the combustion and emissions as described in literature, however it requires experimental validation. A turbocharger model, suited for control applications was developed to match data for a Garrett *AVNT37* turbocharger. These individual component models are further used in the integrated control-oriented system model developed for control design in Chapter 7. The component models and the system model identify the operating limits and set-points which form the framework for control design.

The thesis focuses on steady state analyses and dynamic system modelling to assess transient response and investigate control development methodologies. This work provides a methodology of assessing the potential of hybrid power plants. The first law and second law analyses can together support the development of a comprehensive controller for this system. This study integrates research areas of powertrain design, thermodynamics analysis of process systems and control system design.

Chapter 11. Future Work

11.1. *Future Work and Research Limitations*

The future work for this system modelling, analysis and control can be extended in a number of directions and is as discussed in the following sections. The following figure shows an overview of the work done in this thesis. The boxes with dotted lines indicate the areas of future work.

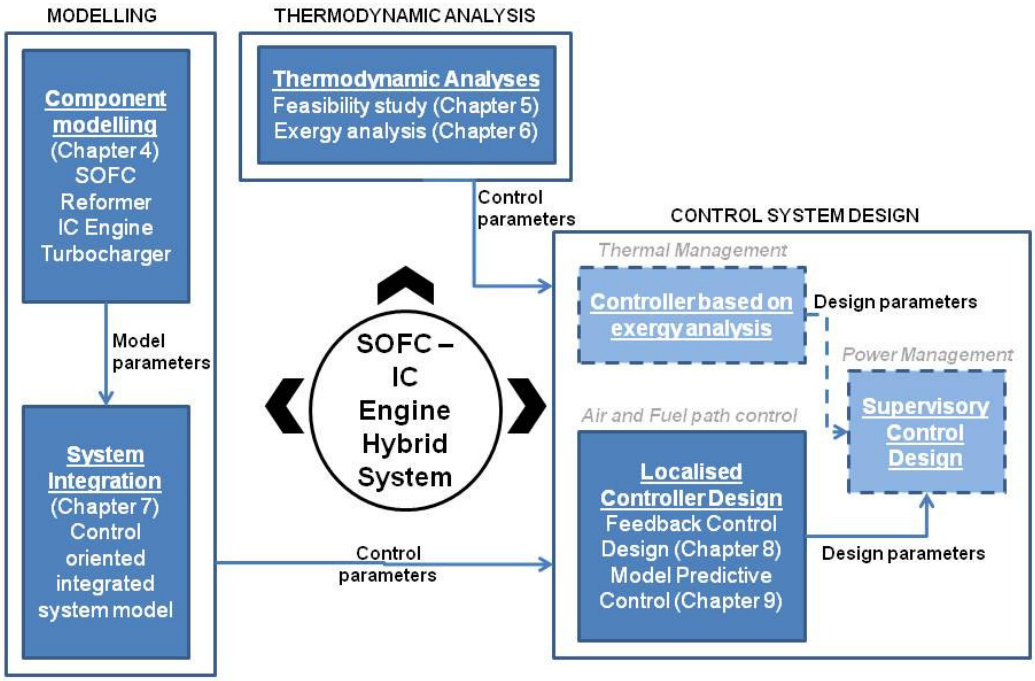

Figure 11.1 – Overview of thesis

The system can be further studied by a multidisciplinary group working on modelling, experimental work, analysis and control design. Three main work packages are given below for future development of this system. The immediate next steps to the work in this thesis is given in detail within each work package.

Work Package 1 – This work will involve experimental study of each components, data acquisition and development of validated high fidelity models to understand issues around each component. These experimentally validated models with sensors and measurements will predict more realistic dynamics.

- Fuel processing unit model with diesel reforming to consumes a single fuel in the whole system. Modelling and experimental work can include the development of a diesel reformer with its exhausts fed to the SOFC. Diesel reformate fed into the SOFC will pose a new set of challenges for control design and require experimental investigation to determine carbon formation and prevention strategies. Similarly, the use of a different type of reformer, partial oxidation or autothermal reformer may be investigated for a faster dynamics response of the reformer.
- For purposes of fuel flexibility, the ability to internally reform fuels such as methane, methanol and carbon monoxide can be studied experimentally and included in the SOFC model.
- The engine model developed using Chemkin requires experimental validation to know the precise effect of hydrogen addition and the external EGR on transient operation of the engine. The effect on emissions of HCCI operation or diesel injection with inducted effluents can be examined.

Work Package 2 – This work package will involve implementing improvements to existing models in this thesis. Low fidelity models of the components and the system suited for control purposes will be developed with experimental results and data obtained in work package 1.

- The control oriented model for the fuel cell is assumed to be operating at constant temperature. The control oriented model assumes a simply transfer function for the steam reformer to represent its dynamics. Future work can include the development of a control oriented model capable of completely capturing dynamics of flows as well as temperature of the reformer. Simplified lumped models to include temperature dynamics can be developed to further the control development. To determine the effectiveness of the control action on pollutants, future work can include a simplified combustion model within the engine model.

Work Package 3 – This work package involves control strategy and design for the system. The control strategies implemented in this thesis will be studied for the experimentally

validated models developed in work package 2. In addition, control loops for thermal management and a top level supervisory controller design will be developed.

- The work done by Stobart et al [135] describes the system behaviour with and without hybridisation. The model developed discusses the performance of the system over the New York bus cycle and the Braunsweig cycles. This model can be further developed to include the suggested supervisory controller based on the ECMS strategy and is discussed in section 11.2. The system efficiency will be examined for various drive cycles. A vehicle model can also be developed to evaluate performance of system and control strategy over drive cycles.
- A thermal management strategy based on exergy analysis can be developed. A dynamic exergy model along with an optimal control system to minimise exergy losses can be developed as discussed in Section 11.3.

11.2. *Supervisory Control*

The growth of novel propulsion systems has created a completely new set of issues where single system solutions alone cannot be implemented and also demand unconventional control techniques. The controller design for the SOFC-IC engine system is described in Chapter 8 (Feedback Control Design Using PID Controllers) and Chapter 9 (Model Predictive Control Design). These are localised controllers for the system air and fuel path, which ensure that each component operates within specified parameters and constraints. The current desired from the fuel cell and the torque required from the engine defines the power for the fuel cell and the engine respectively. The system requires a supervisory controller or a top-level controller managing the power distribution between power producing components. The advantage of such a hierarchical control system results in reduction of costs and complexity of the controller. The objective of the supervisory controller can be to manages the power distribution between components, which would result in optimised fuel consumption and overall system efficiency.

Supervisory controller can be classified into three categories heuristic methods, instantaneous optimisation and global optimisation [136]. The instantaneous optimization – Equivalent Consumption Minimisation Strategy is most suitable and advantageous since it requires knowledge of efficiency maps of the system components, torque and power limits [69]. It can be implemented in real-time optimisation by fast minimisation of the cost

function for equivalent fuel [69]. The equivalent consumption minimization strategy (ECMS) is an instantaneous optimization algorithm [136] based on the idea that for charge-sustaining hybrid vehicles, the instantaneous (charging/discharging) usage of a reversible energy storage device will decrease or increase the future fuel use of the irreversible energy storage device [136]. Figure 11.2 shows the powertrain schematic. The IC Engine and the fuel cell powered electric motor together drive the belt. The function of the battery and ultra-capacitor is to provide start-up power while the fuel cell warms up and produces desired power. The battery and ultra-capacitor also store energy captured by regenerative braking and can supply this energy to eliminate any power fluctuations. Figure 11.3 shows the structure of the supervisory control. The model required for development of the supervisory controller for the system must constitute APS and BPS models, electric motor model, engine and fuel cell operating region and fuel consumption maps and transmission and vehicle load model.

11.3. *Finite-time thermodynamics, exergy analysis and optimal control*

Reversible thermodynamics as discussed in Chapter 6 (Exergy Analysis), considers the maximum work potential by a process over an infinite amount of time when it undergoes a number of quasi-static changes. Real processes are compared to the ideal reversible process in section 6.6 for the hybrid system. As discussed by Andresen et al [137], limits on reversible processes are far from those of real processes, however more realistic limits for performance of irreversible processes can be defined based on finite time and finite size components. Finite time thermodynamics as discussed by Salamon et al [93] or entropy generation minimisation as discussed by Bejan [138] or control thermodynamics describes actual irreversible thermodynamic processes. This approach is based on optimisation of these processes occurring in finite time or rate constraints for finite size components. Finite time availability or exergy is maximum work produced within this finite time interval. The work on finite time thermodynamics in literature is discussed mainly by authors like Bejan [138], Salamon [93, 139, 140], Berry, Andresen, Tsirlin [141-143]. For developing an optimal control strategy, models of the system can be developed on principles of finite-time thermodynamics to identify limits of operation, define constraints and controls. The performance criteria can be based on entropy production or exergy losses obtained by an exergy analysis for the finite-time processes. While the goal of the optimisation would be to maximise work potential, it may also be possible to optimise the time in which the

process occurs [137]. The approach of finite-time thermodynamics along with control theory can be developed for the hybrid system described in this thesis. This novel approach can result in an optimised efficiency for the system as well as an optimised time path for the processes within the system.

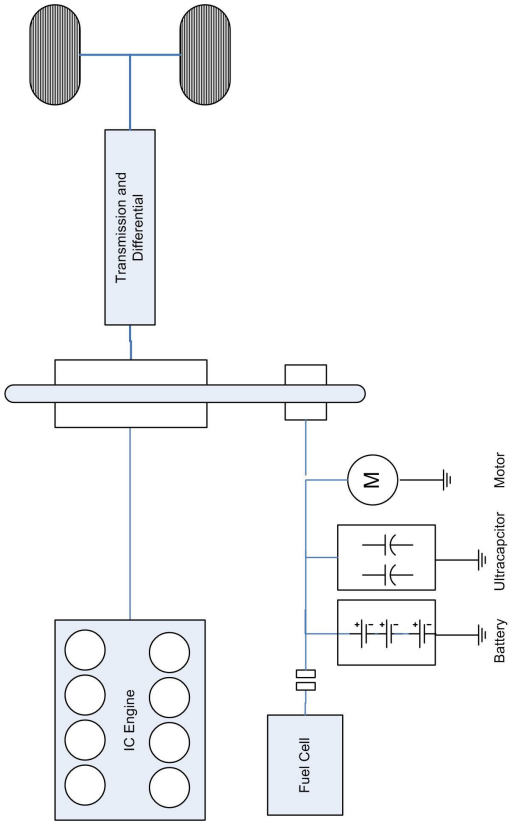

Figure 11.2 - Powertrain Schematic

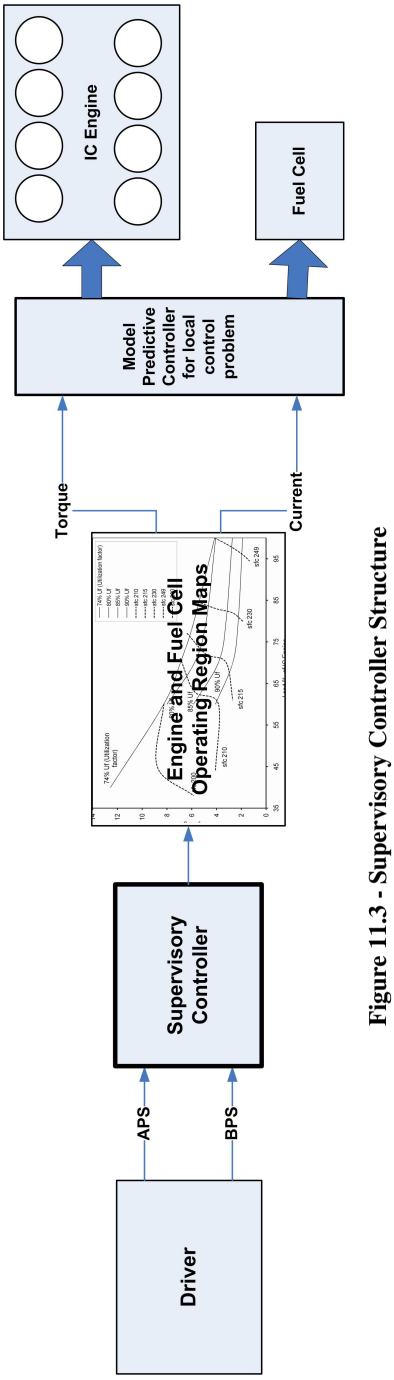

Figure 11.3 - Supervisory Controller Structure

References

[1] D. B. Hibbert, *Introduction to electrochemistry*: Macmillan Physical Science, 1993.

[2] "http://www.sae.org/fuelcells/fuelcells-history.htm."

[3] H. S. Lee, K. S. Jeong, and B. S. Oh, "An experimental study of controlling strategies and drive forces for hydrogen fuel cell hybrid vehicles," *International Journal of Hydrogen Energy*, vol. 28, pp. 215-222, 2003.

[4] "http://www.fch-ju.eu/page/who-we-are."

[5] "http://www.utcfuelcells.com/fs/com/bin/fs_com_Page/0,11491,0106,00.html."

[6] J. Larminie and A. Dicks, *Fuel cell systems explained*, 2nd ed. Chichester: Wiley, 2003.

[7] E. Eckermann, *World History of the Automobile*: SAE, 2001.

[8] M. G. Lay, *Ways of the World: A History of the World's Roads and of the Vehicles That Used Them*: Rutgers University Press, 1992.

[9] P. Capros, N. Kouvaritakis , and L. Mantzos, "Top-down Analysis of Greenhouse Gas Emission Reduction Possibilities in the EU," National Technical University of Athens 2001.

[10] J. Bates, C. Brand, P. Davison, and N. Hill, "Economic Evaluation of Emissions Reductions in the Transport Sector of the EU - Bottom-up Analysis," AEA Technology Environment 2001.

[11] C. Hendriks, D. de Jager, J. de Beer, M. van Brummelen, K. Blok, and M. Kerssemeeckers, "Economic Evaluation of Emission Reduction of Greenhouse Gases in the Energy Supply Sector in the EU - Bottom-up Analysis," ECOFYS 2001.

[12] H. B. Mathur, L. M. Das, and T. N. Patro, "Hydrogen fuel utilization in CI engine powered end utility systems," *International Journal of Hydrogen Energy*, vol. 17, pp. 369-374, 1992.

[13] H. B. Mathur, L. M. Das, and T. N. Patro, "Effects of charge diluents on the emission characteristics of a hydrogen fueled diesel engine," *International Journal of Hydrogen Energy*, vol. 17, pp. 635-642, 1992.

[14] H. B. Mathur, L. M. Das, and T. N. Patro, "Hydrogen-fuelled diesel engine: Performance improvement through charge dilution techniques," *International Journal of Hydrogen Energy*, vol. 18, pp. 421-431, 1993.

[15] G. J. Saunders and K. Kendall, "Reactions of hydrocarbons in small tubular SOFCs," *Journal of Power Sources*, vol. 106, pp. 258-263, 2002.

[16] A. Varesano, I. Guaglio, G. Saracco, and P. L. Maffettone, "Dynamics of a Methanol Reformer for Automotive Applications," *Ind. Eng. Chem. Res.*, vol. 44, pp. 759-768, 2005.

[17] A. Chaudhari and R. Stobart, "Investigation of Optimum Operating Range for a Solid Oxide Fuel Cell-IC Engine Hybrid System," *IEEE Conference on Electric and Hybrid Vehicles, 2006. ICEHV '06.* , pp. 1-6, 2006.

[18] P. Mock and S. A. Schmid, "Fuel cells for automotive powertrains--A techno-economic assessment," *Journal of Power Sources*, vol. 190, pp. 133-140, 2009.

[19] K. Rajashekara, J. A. Macbain, and M. J. Grieve, "Evaluation of SOFC Hybrid Systems for Automotive Propulsion Applications," presented at Industry Applications Conference, 41st IAS Annual Meeting. Conference Record of the 2006 IEEE 2006.

[20] J. Zizelman, S. Shaffer, and S. Mukerjee, " Solid Oxide Fuel Cell Auxiliary Power Unit A Development Update," *Society of Automotive Engineers, 2002-01-0411*, 2002.

[21] "Diesel Engine Idle Reduction in Class 8 Trucks Using On-Vehicle Equipment with Optional Shore Power: A National Demonstration Project. ," EPRI, Palo Alto, CA, and U.S. Environmental Protection Agency, Washington, DC: 1012920., 2006.

[22] N. Lutsey, J. Wallace, C. J. Brodrick, H. A. Dwyer, and D. Sperling, "Modelling Stationary Power for Heavy-Duty Trucks: Engine Idling vs. Fuel Cell APU," *Society of Automotive Engineers, 2004-01-1479*, 2004.

[23] T. Yokoyama, Y. Naganuma, K. Kuriyama, and M. Arimoto, "Development of Fuel-Cell Hybrid Bus," *Society of Automotive Engineers, 2003-01-0417*, 2003.

[24] J. H. J. Thijssen, J. P. Mello, and J.-R. B. Linna, "Cost Competitiveness of Fuel Cell Vehicles Through Novel Hybridization Approaches," *Society of Automotive Engineers, 2003-01-0809*, 2003.

[25] A. Lamm Vehicle having a driving internal-combustion engine and having a fuel cell system for the power supply to electric consuming devices of the vehicle and method for operating such a vehicle. 2001-11-06, 2001.

[26] R. H. E. Van Doorn, J. A. Almkermann, and M. Kah Vehicle Driving System Comprising an Internal Combustion Engine. Patent Number. WO03006814, 2003-01-23.

[27] P. Costamagna, L. Magistri, and A. F. Massardo, "Design and part-load performance of a hybrid system based on a solid oxide fuel cell reactor and micro gas turbine," *Jounal of Power Sources*, vol. 96, pp. 352-368, 2001.

[28] A. Bauen and D. Hart, "Assessment of the environmental benefits of transport and stationary fuel cells," *Journal of Power Sources*, vol. 86, pp. 482-494, 2000.

[29] G. J. Saunders, J. Preece, and K. Kendall, "Formulating liquid hydrocarbon fuels for SOFCs," *Journal of Power Sources*, vol. 131, pp. 23-26, 2004.

[30] Y. Yi, A. D. Rao, J. Brouwer, and G. S. Samuelsen, "Fuel flexibility study of an integrated 25 kW SOFC reformer system," *Journal of Power Sources*, vol. 144, pp. 67-76, 2005.

[31] H. Fukunaga, M. Ihara, K. Sakaki, and K. Yamada, "The relationship between overpotential and the three phase boundary length," *Solid State Ionics*, vol. 86-88, pp. 1179-1185, 1996.

[32] X. Deng and A. Petric, "Geometrical modeling of the triple-phase-boundary in solid oxide fuel cells," *Journal of Power Sources*, vol. 140, pp. 297-303, 2005.

[33] L. Petruzzi, S. Cocchi, and F. Fineschi, "A global thermo-electrochemical model for SOFC systems design and engineering," *Journal of Power Sources*, vol. 118, pp. 96-107, 2003.

[34] T. Ota, M. Koyama, C.-j. Wen, K. Yamada, and H. Takahashi, "Object-based modeling of SOFC system: dynamic behavior of micro-tube SOFC," *Journal of Power Sources*, vol. 118, pp. 430-439, 2003.

[35] X. Xue, J. Tang, N. Sammes, and Y. Du, "Dynamic modeling of single tubular SOFC combining heat/mass transfer and electrochemical reaction effects," *Journal of Power Sources*, vol. 142, pp. 211-222, 2005.

[36] J. Padullés, G. W. Ault, and J. R. McDonald, "An integrated SOFC plant dynamic model for power systems simulation," *Journal of Power Sources*, vol. 86, pp. 495-500, 2000.

[37] F. Jurado, "Modeling SOFC plants on the distribution system using identification algorithms," *Journal of Power Sources*, vol. 129, pp. 205–215, 2004.

[38] X. Wang, B. Huang, and T. Chen, "Data-driven predictive control for solid oxide fuel cells," *Journal of Process Control*, vol. 17, pp. 103-114, 2007.

[39] S. H. Chan, K. A. Khor, and Z. T. Xia, "A complete polarization model of a solid oxide fuel cell and its sensitivity to the change of cell component thickness," *Journal of Power Sources*, vol. 93, pp. 130-140, 2001.

[40] R. Peters, R. Dahl, U. Klüttgen, C. Palm, and D. Stolten, "Internal reforming of methane in solid oxide fuel cell systems," *Journal of Power Sources*, vol. 106, pp. 238-244, 2002.

[41] P. Aguiar, D. Chadwick, and L. Kershenbaum, "Modelling of an indirect internal reforming solid oxide fuel cell," *Chemical Engineering Science*, vol. 57, pp. 1665-1677, 2002.

[42] S. Nagata, A. Momma, T. Kato, and Y. Kasuga, "Numerical analysis of output characteristics of tubular SOFC with internal reformer," *Journal of Power Sources*, vol. 101, pp. 60-71, 2001.

[43] C. O. Colpan, I. Dincer, and F. Hamdullahpur, "Thermodynamic modeling of direct internal reforming solid oxide fuel cells operating with syngas," *International Journal of Hydrogen Energy*, vol. 32, pp. 787-795, 2007.

[44] G. Kolb, *Fuel Processing: For Fuel Cells*: Wiley-VCH, 2008.

[45] C. Song, "Fuel processing for low-temperature and high-temperature fuel cells: Challenges, and opportunities for sustainable development in the 21st century," *Catalysis Today*, vol. 77, pp. 17-49, 2002.

[46] S. G. Goebel, D. P. Miller, W. H. Pettit, and M. D. Cartwright, "Fast starting fuel processor for automotive fuel cell systems," *International Journal of Hydrogen Energy*, vol. 30, pp. 953-962, 2005.

[47] R. Peters, H. G. Düsterwald, and B. Höhlein, "Investigation of a methanol reformer concept considering the particular impact of dynamics and long-term stability for use in a fuel-cell-powered passenger car," *Journal of Power Sources*, vol. 86, pp. 507-514, 2000.

[48] S. Biset, L. Nieto Deglioumini, M. Basualdo, V. M. Garcia, and M. Serra, "Analysis of the control structures for an integrated ethanol processor for proton exchange membrane fuel cell systems," *Journal of Power Sources*, vol. 192, pp. 107-113, 2009.

[49] H. Görgün, M. Arcak, S. Varigonda, and S. A. Bortoff, "Observer designs for fuel processing reactors in fuel cell power systems," *International Journal of Hydrogen Energy*, vol. 30, pp. 447-457, 2005.

[50] J. Pukrushpan, A. Stefanopoulou, S. Varigonda, J. Eborn, and C. Haugstetter, "Control-oriented model of fuel processor for hydrogen generation in fuel cell applications," *Control Engineering Practice*, vol. 14, pp. 277-293, 2006.

[51] S.-T. Lin, Y.-H. Chen, C.-C. Yu, Y.-C. Liu, and C.-H. Lee, "Dynamic modeling and control structure design of an experimental fuel processor," *International Journal of Hydrogen Energy*, vol. 31, pp. 413-426, 2006.

[52] Y. Hu, D. J. Chmielewski, and D. Papadias, "Autothermal reforming of gasoline for fuel cell applications: Controller design and analysis," *Journal of Power Sources*, vol. 182, pp. 298-306, 2008.

[53] V. Hosseini and M. D. Checkel, "Reformer Gas Composition Effect on HCCI Combustion of n-Heptane, iso-Octane, and Natural Gas," *Society of Automotive Engineers*, vol. 2008-01-0049, 2008.

[54] N. Ladommatos, S. M. Abdelhalim, H. Zhao, and Z. Hu, "The Dilution, Chemical, and Thermal Effects of Exhaust Gas Recirculation on Diesel Engine Emissions--Part 4: Effects of Carbon Dioxide and Water Vapor," *Society of Automotive Engineers*, vol. 971660, 1997.

[55] N. Ladommatos, S. M. Abdelhalim, H. Zhao, and Z. Hu, "The Dilution, Chemical, and Thermal Effects on Exhaust Gas Recirculation on Diesel Engine Emissions--Part 1: Effects of Reducing Inlet Charge Oxygen," *Society of Automotive Engineers*, vol. 961165, 1996.

[56] N. Ladommatos, S. M. Abdelhalim, H. Zhao, and Z. Hu, "The Dilution, Chemical, and Thermal Effects on Exhaust Gas Recirculation on Diesel Engine Emissions--Part 2: Effects of Carbon Dioxide," *Society of Automotive Engineers*, vol. 961167, 1996.

[57] N. Ladommatos, S. M. Abdelhalim, H. Zhao, and Z. Hu, "The Dilution, Chemical, and Thermal Effects on Exhaust Gas Recirculation on Diesel Engine Emissions--Part 3: Effects of Water Vapor," *Society of Automotive Engineers*, vol. 971659, 1997.

[58] N. Ladommatos, S. M. Abdelhalim, H. Zhao, and Z. Hu, "Effects of Egr on Heat Release in Diesel Combustion," *Society of Automotive Engineers*, vol. 980184 1998.

[59] F. Mueller, F. Jabbari, R. Gaynor, and J. Brouwer, "Novel solid oxide fuel cell system controller for rapid load following," *Journal of Power Sources*, vol. 172, pp. 308-323, 2007.

[60] J. T. Pukrushpan, H. Peng, and A. G. Stefanopoulou, "Control-Oriented Modeling and Analysis for Automotive Fuel Cell Systems," *Journal of Dynamic Systems, Measurement, and Control*, vol. 126, pp. 14-25, 2004.

[61] J. T. Pukrushpan, A. G. Stefanopoulou, and H. Peng, *Control of fuel cell power systems : principles, modeling, analysis, and feedback design*. London ; New York: Springer, 2004.

[62] A. Vahidi, A. Stefanopoulou, and H. Peng, "Model predictive control for starvation prevention in a hybrid fuel cell system," *Proceedings of the 2004 American Control Conference*, vol. 1, pp. 834-839, 2004.

[63] A. Vahidi, A. Stefanopoulou, and H. Peng, "Current Management in a Hybrid Fuel Cell Power System: A Model-Predictive Control Approach," *IEEE Transactions on Control Systems Technology*, vol. 14, pp. 1047-1057, 2006.

[64] C. Bao, M. Ouyang, and B. Yi, "Modeling and control of air stream and hydrogen flow with recirculation in a PEM fuel cell system--II. Linear and adaptive nonlinear control," *International Journal of Hydrogen Energy*, vol. 31, pp. 1897-1913, 2006.

[65] C. Bao, M. Ouyang, and B. Yi, "Modeling and control of air stream and hydrogen flow with recirculation in a PEM fuel cell system--I. Control-oriented modeling," *International Journal of Hydrogen Energy*, vol. 31, pp. 1879-1896, 2006.

[66] P. Rodatz, G. Paganelli, A. Sciarretta, and L. Guzzella, "Optimal power management of an experimental fuel cell/supercapacitor-powered hybrid vehicle," *Control Engineering Practice*, vol. 13, pp. 41-53, 2005.

[67] Y. Guezennec, T.-y. Choi, G. Paganelli, and G. Rizzoni, "Supervisory Control of Fuel Cell Vehicles and its Link to Overall System Efficiency and Low-Level Control Requirements," presented at Proceedings of the American Control Conference, Denver, Colorado, 2003.

[68] P. Pisu and G. Rizzoni, "A Comparative Study Of Supervisory Control Strategies for Hybrid Electric Vehicles," *IEEE Transactions on Control Systems Technology*, vol. 15, pp. 506-518, 2007.

[69] P. Pisu and G. Rizzoni, "A Supervisory Control Strategy for Series Hybrid Electric Vehicles with Two Energy Storage Systems," presented at 2005 IEEE Conference Vehicle Power and Propulsion, 2005.

[70] T. J. Kotas, *The Exergy Method of Thermal Plant Analysis*: Butterworths, 1985.

[71] S. H. Chan and O. L. Ding, "Simulation of a solid oxide fuel cell power system fed by methane," *International Journal of Hydrogen Energy*, vol. 30, pp. 167-179, 2005.

[72] E. R. Delsman, C. U. Uju, M. H. J. M. d. Croon, J. C. Schouten, and K. J. Ptasinski, "Exergy analysis of an integrated fuel processor and fuel cell (FP-FC) system," *Energy*, vol. 31, pp. 3300-3309, 2006.

[73] M. M. Hussain, I. Dincer, and X. Li, "Energy and Exergy Analysis of an Integrated SOFC Power System," *CSME Forum 1*, 2004.

[74] K. Ayoub, "Exergoeconomic analysis of a PEM fuel cell at various operating conditions," *Energy Conversion and Management*, vol. 46, pp. 1073-1081, 2005.

[75] F. J. Barclay, *Fuel cells, engines, and hydrogen : an exergy approach*. Chichester: John Wiley, 2006.

[76] S. Douvartzides, F. Coutelieris, and P. Tsiakaras, "Exergy analysis of a solid oxide fuel cell power plant fed by either ethanol or methane," *Journal of Power Sources*, vol. 131, pp. 224-230, 2004.

[77] S. L. Douvartzides, F. A. Coutelieris, and P. E. Tsiakaras, "On the systematic optimization of ethanol fed SOFC-based electricity generating systems in terms of energy and exergy," *Journal of Power Sources*, vol. 114, pp. 203-212, 2003.

[78] N. Hotz, S. M. Senn, and D. Poulikakos, "Exergy analysis of a solid oxide fuel cell micropowerplant," *Journal of Power Sources*, vol. 158, pp. 333-347, 2006.

[79] F. Calise, M. D. d'Accadia, A. Palombo, and L. Vanoli, "Simulation and exergy analysis of a hybrid Solid Oxide Fuel Cell (SOFC)-Gas Turbine System," *Energy*, vol. 31, pp. 3278-3299, 2006.

[80] K. W. Bedringås, I. S. Ertesvåg, S. Byggstøyl, and B. F. Magnussen, "Exergy analysis of solid-oxide fuel-cell (SOFC) systems," *Energy*, vol. 22, pp. 403-412, 1997.

[81] R. Cownden, M. Nahon, and M. A. Rosen, "Exergy analysis of a fuel cell power system for transportation applications," *Exergy: An International Journal*, vol. 1, pp. 112-121, 2001.

[82] N. Hotz, S. M. Senn, and D. Poulikakos, "Exergetic analysis of fuel cell micropowerplants fed by methanol" presented at Proceedings of 3rd Fuel Cell Research Symposium - Modelling and Experimental Validation EMPA, Dübendorf, Switzerland, 2005.

[83] C. D. Rakopoulos and E. G. Giakoumis, "Availability analysis of a turbocharged diesel engine operating under transient load conditions," *Energy*, vol. 29, pp. 1085-1104, 2004.

[84] R. K. Stobart, "An availability approach to thermal energy recovery in vehicles," *Proceedings of the I MECH E Part D Journal of Automobile Engineering*, vol. 221, pp. 1107-1124, 2007.

[85] F. J. Barclay, "Fundamental thermodynamics of fuel cell, engine, and combined heat and power system efficiencies," *Proc Instn Mech Engrs Part A: J Power and Energy*, vol. 216, 2002.

[86] R. W. Haywood, *Equilibrium Thermodynamics for Engineers and Scientists*: Wiley, 1980.

[87] L. G. Alves and S. A. Nebra, "Basic chemically recuperated gas turbines--power plant optimization and thermodynamics second law analysis," *Energy*, vol. 29, pp. 2385-2395, 2004.

[88] R. D. Robinett and D. G. Wilson, "Exergy and irreversible entropy production thermodynamic concepts for control system design: robotic servo applications," presented at Proceedings 2006 IEEE International Conference on Robotics and Automation, 2006. ICRA 2006. , 2006.

[89] R. D. Robinett and D. G. Wilson, "Exergy and Irreversible Entropy Production Thermodynamic Concepts for Control System Design: Regulators," presented at IEEE International Conference on Control Applications, 2006. CCA '06. , Munich, Germany, 2006.

[90] R. D. Robinett and D. G. Wilson, "Exergy and Irreversible Entropy Production Thermodynamic Concepts for Control Design: Nonlinear Systems," presented at 14th Mediterranean Conference on Control and Automation, 2006, 2006.

[91] A. A. Alonso, B. E. Ydstie, and J. R. Banga, "From irreversible thermodynamics to a robust control theory for distributed process systems," *Journal of Process Control*, vol. 12, pp. 507-517, 2002.

[92] B. E. Ydstie, "Passivity based control via the second law," *Computers & Chemical Engineering*, vol. 26, pp. 1037-1048, 2002.

[93] P. Salamon, J. D. Nulton, G. Siragusa, T. R. Andersen, and A. Limon, "Principles of control thermodynamics," *Energy*, vol. 26, pp. 307-319, 2001.

[94] S. C. Singhal and K. Kendall, *High-temperature Solid Oxide Fuel Cells: Fundamentals, Design and Applications*: Elsevier, 2003.

[95] Y. Lu, L. Schaefer, and P. Li, "Numerical study of a flat-tube high power density solid oxide fuel cell: Part I. Heat/mass transfer and fluid flow," *Journal of Power Sources*, vol. 140, pp. 331-339, 2005.

[96] S. Campanari and P. Iora, "Definition and sensitivity analysis of a finite volume SOFC model for a tubular cell geometry," *Journal of Power Sources*, vol. 132, pp. 113-126, 2004.

[97] P. Iora, P. Aguiar, C. S. Adjiman, and N. P. Brandon, "Comparison of two IT DIR-SOFC models: Impact of variable thermodynamic, physical, and flow properties. Steady-state and dynamic analysis," *Chemical Engineering Science*, vol. 60, pp. 2963-2975, 2005.

[98] Y. Qi, B. Huang, and J. Luo, "Dynamic modeling of a finite volume of solid oxide fuel cell: The effect of transport dynamics," *Chemical Engineering Science*, vol. 61, pp. 6057-6076, 2006.

[99] E. Achenbach, "Three-dimensional and time-dependent simulation of a planar solid oxide fuel cell stack," *Journal of Power Sources*, vol. 49, pp. 333-333, 1994.

[100] Y. Inui, A. Urata, N. Ito, T. Nakajima, and T. Tanaka, "Performance simulation of planar SOFC using mixed hydrogen and carbon monoxide gases as fuel," *Energy Conversion and Management*, vol. 47, pp. 1738-1747, 2006.

[101] A. Qi, B. Peppley, and K. Karan, "Integrated fuel processors for fuel cell application: A review," *Fuel Processing Technology*, vol. 88, pp. 3-22, 2007.

[102] A. K. Coker, "Modeling of chemical kinetics and reactor design." Boston, Mass. ; Oxford: Gulf Professional Pub, 2001.

[103] J. C. Amphlett, K. A. M. Creber, J. M. Davis, R. F. Mann, B. A. Peppley, and D. M. Stokes, "Hydrogen production by steam reforming of methanol for polymer electrolyte fuel cells," *International Journal of Hydrogen Energy*, vol. 19, pp. 131-137, 1994.

[104] K. Ito, B. Choi, and O. Fujita, "The start-up characteristics of a catalytic combustor using a methanol mixture," *JSME Int. J.*, vol. 33, pp. 778, 1990.

[105] M. N. Ozisik, *Finite difference methods in heat transfer*. Boca Raton: CRC P., 1994.

[106] S. V. Patankar, *Numerical Heat Transfer and Fluid Flow*: Hemisphere, 1980.

[107] "http://www.dieselnet.com/standards/eu/ld.php."

[108] A. Maiboom, X. Tauzia, and J.-F. Hétet, "Experimental study of various effects of exhaust gas recirculation (EGR) on combustion and emissions of an automotive direct injection diesel engine," *Energy*, vol. 33, pp. 22-34, 2008.

[109] A. Plianos and R. Stobart, "Modeling and Control of Diesel Engines Equipped with a Two-Stage Turbo-System," *Society of Automotive Engineers*, vol. 2008-01-1018, 2008.

[110] M. Masood, M. M. Ishrat, and A. S. Reddy, "Computational combustion and emission analysis of hydrogen-diesel blends with experimental verification," *International Journal of Hydrogen Energy*, vol. 32, pp. 2539-2547, 2007.

[111] N. Saravanan, G. Nagarajan, K. M. Kalaiselvan, and C. Dhanasekaran, "An experimental investigation on hydrogen as a dual fuel for diesel engine system with exhaust gas recirculation technique," *Renewable Energy*, vol. 33, pp. 422-427, 2008.

[112] J. B. Heywood, *Internal combustion engine fundamentals*. New York, N.Y. ; London: McGraw-Hill, 1988.

[113] "Theory Manual, CHEMKIN-PRO Software," *Reaction Design*, 2008.

[114] H. Seiser, H. Pitsch, K. Seshadri, W. J. Pitz, and H. J. Curran, "Extinction and Autoignition of n-Heptane in Counterflow Configuration," in *Proceedings of the Combustion Institute* vol. 28. Lawrence Livermore National Laboratory, Livermore, CA, UCRL-JC-137080., 2000, pp. 2029-2037.

[115] Gregory P. Smith, David M. Golden, Michael Frenklach, Nigel W. Moriarty, Boris Eiteneer, Mikhail Goldenberg, C. Thomas Bowman, Ronald K. Hanson, Soonho Song, William C. Gardiner, V. V. L. Jr., and Z. Qin, "GRI-Mech 3.0," *http://www.me.berkeley.edu/gri_mech/*.

[116] P. K. Moraal, I., "Turbocharger Modeling for Automotive Control Applications," *SAE paper 1999-01-0908*, 1999.

[117] I. Kolmanovsky, P. Moraal, M. vanNieuwstadt, and A. Stefanopoulou, " Issues in modeling and control of intake flow in variable geometry turbocharged engines.," presented at Proc. 18th IFIP Conf. Syst. Modeling and Optimization, Detroit, Michigan, 1997.

[118] B. Ozpineci, L. M. Tolbert, and D. Zhong, "Optimum fuel cell utilization with multilevel inverters," presented at 35th Annual Power Electronics Specialists Conference 2004.

[119] "http://www.cerespower.com/technology/markets.htm."

[120] J. H. Horlock, J. B. Young, and G. Manfrida, "Exergy Analysis of Modern Fossil-Fuel Power Plants," *Journal of Engineering for Gas Turbines and Power*, vol. 122, 2000.

[121] M. J. Moran and H. N. Shapiro, *Fundamentals of engineering thermodynamics*, 3rd ed. New York: Wiley, 1997.

[122] D. R. Stull and H. Prophet, *JANAF thermochemical tables*, 2nd ed: Washington D.C. : U.S. Government Printing Office, 1971.

[123] R. H. Perry and D. W. Green, "Perry's Chemical Engineers' Handbook (7th Edition)," McGraw-Hill, 1997.

[124] J. Chao and K. Hall, "Ideal gas thermodynamic properties of simple alkanols," *International Journal of Thermophysics*, vol. 7, pp. 431-442, 1986.

[125] M. Jankovic and I. Kolmanovsky, "Constructive Lyapunov control design for turbocharged diesel engines," *IEEE Transactions on Control Systems Technology*, vol. 8, pp. 288 - 299, 2000.

[126] K. J. Astrom and T. Hagglund, *PID Controllers: Theory, Design, and Tuning*, 2nd ed: International Society for Measurement and Control, 1995.

[127] A. Plianos, A. Achir, R. Stobart, N. Langlois, and H. Chafouk, "Dynamic feedback linearization based control synthesis of the turbocharged Diesel engine," presented at American Control Conference, 2007. ACC '07, 2007.

[128] E. F. Camacho and C. Bordons, *Model Predictive Control in the Process Industry*: Springer, 1995.

[129] M. Huzmezan and J. Maciejowski, "RCAM Design Challenge Presentation Document: The Model Based Predictive Control Approach," Group for Aeronautical Research and Technology in Europe 1997.

[130] E. C. Kerrigan and J. M. Maciejowskiy, "Fault-Tolerant Control Of A Ship Propulsion System Using Model Predictive Control," presented at Proceedings of European Control Conference, 1999.

[131] D. W. Clarke, C. Mohtadi, and P. S. Tuffs, "Generalized predictive control--Part I. The basic algorithm," *Automatica*, vol. 23, pp. 137-148, 1987.

[132] E. Ikonen and K. Najim, *Advanced Process Identification and Control*: Marcel Dekker, 2002.

[133] J. P. Norton, *An Introduction to Identification*: Academic Press, 1985.

[134] L. Ljung, *System Identification Toolbox™ 7 User's Guide*, 2007.

[135] R. K. Stobart and A. Chaudhari, "A Novel Hybrid Powerplant for Passenger Bus Applications," presented at SAE Powertrain & Fluid Systems Conference and Exhibition, October 2007, Chicago, IL, USA, 2007-01-4120.

[136] J. Liu, "Modeling, Configuration And Control Optimization Of Power-Split Hybrid Vehicles," in *Mechanical Engineering*, vol. Doctor of Philosophy: The University of Michigan, 2007.

[137] B. Andresen, P. Salamon, and R. S. Berry, "Thermodynamics in finite time " in *Physic Today : American Institute of Physics*, vol. 37, 1984.

[138] A. Bejan, "Thermodynamic optimization of geometry in engineering flow systems," *Exergy,An International Journal*, vol. 1, pp. 269-277, 2001.

[139] P. Salamon, B. Andresen, and R. S. Berry, "Thermodynamics in finite time. II. Potentials for finite-time processes," *Physical Review A*, vol. 15, pp. 2094, 1977.

[140] P. Salamon, A. Nitzan, B. Andresen, and R. S. Berry, "Minimum entropy production and the optimization of heat engines," *Physical Review A*, vol. 21, pp. 2115, 1980.

[141] B. Andresen, M. H. Rubin, and R. S. Berry, "Availability for finite-time processes. General theory and a model," *The Journal of Physical Chemistry*, vol. 87, pp. 2704-2713, 1983.

[142] B. Andresen, "Finite-time thermodynamics and thermodynamic length," *Revue Générale de Thermique*, vol. 35, pp. 647-650, 1996.

[143] A. M. Tsirlin, V. A. Mironova, S. A. Amelkin, and V. Kazakov, "Finite-time thermodynamics: Conditions of minimal dissipation for thermodynamic process with given rate," *Physical Review E*, vol. 58, pp. 215, 1998.

Bibliography

1. R. K. Stobart, Peng, Z., Chaudhari, A.R., Heikal, M.R., Monaghan, M.L., Methods And Apparatus For Use With Power Supply System. Patent Number. WO/2007/113507, 2007.
2. R. K. Stobart, Peng, Z., Chaudhari, A.R., Heikal, M.R., Monaghan, M.L., Ladommatos, N., Hardalupas, I., Taylor, A.M.K.P., Zhao, H., Jiang, X., Ma, T.T.-H., Power Supply System. Patent Number. WO/2007/113509, 2007.
3. S. C. Singhal and K. Kendall, High-temperature Solid Oxide Fuel Cells: Fundamentals, Design and Applications: Elsevier, 2003.
4. J. Larminie and A. Dicks, Fuel cell systems explained, 2nd ed. Chichester: Wiley, 2003.
5. Y. Lu and L. Schaefer, "Numerical study of a flat-tube high power density solid oxide fuel cell: Part II: Cell performance and stack optimization," Journal of Power Sources, vol. 153, pp. 68-75, 2006.
6. D. Larrain, J. Van herle, F. Maréchal, and D. Favrat, "Generalized model of planar SOFC repeat element for design optimization," Journal of Power Sources, vol. 131, pp. 304-312, 2004.
7. P. Kuchonthara, S. Bhattacharya, and A. Tsutsumi, "Energy recuperation in solid oxide fuel cell (SOFC) and gas turbine (GT) combined system," Journal of Power Sources, vol. 117, pp. 7-13, 2003.
8. F. J. Gardner, M. J. Day, N. P. Brandon, M. N. Pashley, and M. Cassidy, "SOFC technology development at Rolls-Royce," Journal of Power Sources, vol. 86, pp. 122-129, 2000.
9. H.-S. Chu, F. Tsau, Y.-Y. Yan, K.-L. Hsueh, and F.-L. Chen, "The development of a small PEMFC combined heat and power system," Journal of Power Sources, vol. 176, pp. 499-514, 2008.

10. D. Bhattacharyya and R. Rengaswamy, "A Review of Solid Oxide Fuel Cell (SOFC) Dynamic Models," Industrial & Engineering Chemistry Research, vol. 48, pp. 6068-6086, 2009.
11. H. Xi, J. Sun, and V. Tsourapas, "A control oriented low order dynamic model for planar SOFC using minimum Gibbs free energy method," Journal of Power Sources, vol. 165, pp. 253–266, 2007.
12. F. Mueller, J. Brouwer, F. Jabbari, and S. Samuelsen, "Dynamic Simulation of an Integrated Solid Oxide Fuel Cell System Including Current-Based Fuel Flow Control," Journal of Fuel Cell Science and Technology, vol. 3, pp. 144-154, 2006.
13. F. Mueller, F. Jabbari, R. Gaynor, and J. Brouwer, "Novel solid oxide fuel cell system controller for rapid load following," Journal of Power Sources, vol. 172, pp. 308-323, 2007.
14. T. W. Song, J. L. Sohn, J. H. Kim, T. S. Kim, S. T. Ro, and K. Suzuki, "Performance analysis of a tubular solid oxide fuel cell/micro gas turbine hybrid power system based on a quasi-two dimensional model," Journal of Power Sources, vol. 142, pp. 30-42, 2005.
15. F. A. Coutelieris, S. Douvartzides, and P. Tsiakaras, "The importance of the fuel choice on the efficiency of a solid oxide fuel cell system," Journal of Power Sources, vol. 123 pp. 200–205, 2003.
16. P. Bance, N. P. Brandon, B. Girvan, P. Holbeche, S. O'Dea, and B. C. H. Steele, "Spinning-out a fuel cell company from a UK University--2 years of progress at Ceres Power," Journal of Power Sources, vol. 131, pp. 86-90, 2004.
17. A. Chaisantikulwat, C. Diaz-Goano, and E. S. Meadows, "Dynamic modelling and control of planar anode-supported solid oxide fuel cell," Computers & Chemical Engineering, vol. 32, pp. 2365-2381, 2008.
18. J. B. Heywood, Internal combustion engine fundamentals. New York, N.Y. ; London: McGraw-Hill, 1988.
19. W. W. Pulkrabek, Engineering fundamentals of the internal combustion engine. Upper Saddle River, N.J.: Prentice Hall, 1997.
20. M. Jung, "Mean-Value Modelling and Robust Control of the Airpath of a Turbocharged Diesel Engine," in Department of Engineering, vol. Doctor of Philosophy. Cambridge: University of Cambridge, 2003.
21. E. Hendricks, "Engine Modelling for Control Applications: A Critical Survey," Meccanica, vol. 32, pp. 387-396, 1997.

22. R. P. Lindstedt and L. Q. Maurice, "Detailed Kinetic Modelling of n-Heptane Combustion," Combustion Science and Technology, vol. 107, pp. 317 - 353, 1995.
23. L. Guzzella and A. Sciarretta, Vehicle Propulsion Systems - Introduction to Modeling and Optimization: Springer, 2005.
24. L. Guzzella and C. H. Onder, Introduction to Modeling and Control of Internal Combustion Engine Systems: Springer, 2004.
25. N. Saravanan, G. Nagarajan, K. M. Kalaiselvan, and C. Dhanasekaran, "An experimental investigation on hydrogen as a dual fuel for diesel engine system with exhaust gas recirculation technique," Renewable Energy, vol. 33, pp. 422-427, 2008.
26. A. G. Stefanopoulou, I. Kolmanovsky, and J. S. Freudenberg, "Control of Variable Geometry Turbocharged Diesel Engines for Reduced Emissions," IEEE Transactions on Control Systems Technology, vol. 8, 2000.
27. P. Amnéus, F. Mauss, M. Kraft, A. Vressner, and B. Johansson, "NOx and N2O formation in HCCI engines," Society of Automotive Engineers, vol. 2005-01-0126, 2005.
28. "Theory Manual, CHEMKIN-PRO Software," Reaction Design, 2008.
29. L. McWilliam, T. Megaritis, and H. Zhao, "Experimental Investigation of the Effects of Combined Hydrogen and Diesel Combustion on the Emissions of a HSDI Diesel Engine," Society of Automotive Engineers, vol. 2008-01-1787, 2008.
30. V. Hosseini and M. D. Checkel, "Reformer Gas Composition Effect on HCCI Combustion of n-Heptane, iso-Octane, and Natural Gas," Society of Automotive Engineers, vol. 2008-01-0049, 2008.
31. M. N. Ozisik, Finite difference methods in heat transfer. Boca Raton: CRC P., 1994.
32. S. V. Patankar, Numerical Heat Transfer and Fluid Flow: Hemisphere, 1980.
33. J. C. Amphlett, K. A. M. Creber, J. M. Davis, R. F. Mann, B. A. Peppley, and D. M. Stokes, "Hydrogen production by steam reforming of methanol for polymer electrolyte fuel cells," International Journal of Hydrogen Energy, vol. 19, pp. 131-137, 1994.
34. A. K. Coker, "Modeling of chemical kinetics and reactor design." Boston, Mass. ; Oxford: Gulf Professional Pub, 2001.
35. P. J. de Wild and M. J. F. M. Verhaak, "Catalytic production of hydrogen from methanol," Catalysis Today, vol. 60, pp. 3-10, 2000.
36. C. J. Jiang, D. L. Trimm, M. S. Wainwright, and N. W. Cant, "Kinetic mechanism for the reaction between methanol and water over a Cu-ZnO-Al2O3 catalyst," Applied Catalysis A: General, vol. 97, pp. 145-158, 1993.

37. C. J. Jiang, D. L. Trimm, M. S. Wainwright, and N. W. Cant, "Kinetic study of steam reforming of methanol over copper-based catalysts," Applied Catalysis A: General, vol. 93, pp. 245-255, 1993.
38. S. G. Goebel, D. P. Miller, W. H. Pettit, and M. D. Cartwright, "Fast starting fuel processor for automotive fuel cell systems," International Journal of Hydrogen Energy, vol. 30, pp. 953-962, 2005.
39. A. Qi, B. Peppley, and K. Karan, "Integrated fuel processors for fuel cell application: A review," Fuel Processing Technology, vol. 88, pp. 3-22, 2007.
40. B. A. Peppley, J. C. Amphlett, L. M. Kearns, and R. F. Mann, "Methanol-steam reforming on Cu/ZnO/Al2O3. Part 1: the reaction network," Applied Catalysis A: General, vol. 179, pp. 21-29, 1999.
41. R. B. Bird, W. E. Stewart, and E. N. Lightfoot, Transport Phenomena, 2nd ed: John Wiley & Sons, Inc., 2002.
42. K. Ito, B. Choi, and O. Fujita, "The start-up characteristics of a catalytic combustor using a methanol mixture," JSME Int. J., vol. 33, pp. 778, 1990.
43. G. Kolb, Fuel Processing: For Fuel Cells: Wiley-VCH, 2008.
44. Y. Guezennec, T.-y. Choi, G. Paganelli, and G. Rizzoni, "Supervisory Control of Fuel Cell Vehicles and its Link to Overall System Efficiency and Low-Level Control Requirements," presented at Proceedings of the American Control Conference, Denver, Colorado, 2003.
45. J. B. Heywood, M. A. Weiss, A. Schafer, S. A. Bassene, and N. V.K, "The Performance of Future ICE and Fuel Cell Powered Vehicles and Their Potential Fleet Impact," Society of Automotive Engineers, 2004-01-1011, 2004.
46. B. Ozpineci, L. M. Tolbert, and D. Zhong, "Optimum fuel cell utilization with multilevel inverters," presented at 35th Annual Power Electronics Specialists Conference 2004.
47. A. Plianos and R. Stobart, "Modeling and Control of Diesel Engines Equipped with a Two-Stage Turbo-System," Society of Automotive Engineers, vol. 2008-01-1018, 2008.
48. K. G. Denbigh, "The second-law efficiency of chemical processes," Chemical Engineering Science, vol. 6, pp. 1-9, 1956.
49. S.-T. Lin, Y.-H. Chen, C.-C. Yu, Y.-C. Liu, and C.-H. Lee, "Dynamic modeling and control structure design of an experimental fuel processor," International Journal of Hydrogen Energy, vol. 31, pp. 413-426, 2006.

50. T. J. Kotas, The Exergy Method of Thermal Plant Analysis: Butterworths, 1985.
51. R. W. Haywood, Equilibrium Thermodynamics for Engineers and Scientists: Wiley, 1980.
52. F. J. Barclay, "Fundamental thermodynamics of fuel cell, engine, and combined heat and power system efficiencies," Proc Instn Mech Engrs Part A: J Power and Energy, vol. 216, 2002.
53. F. J. Barclay, Fuel cells, engines, and hydrogen : an exergy approach. Chichester: John Wiley, 2006.
54. M. J. Moran and H. N. Shapiro, Fundamentals of engineering thermodynamics, 3rd ed. New York: Wiley, 1997.
55. G. J. Kabo, O. V. Govin, and A. A. Kozyro, "Additivity of chemical exergies of alkanes," Energy, vol. 23, pp. 383-391, 1998.
56. D. R. Stull and H. Prophet, JANAF thermochemical tables, 2nd ed: Washington D.C. : U.S. Government Printing Office, 1971.
57. R. H. Perry and D. W. Green, "Perry's Chemical Engineers' Handbook (7th Edition)," McGraw-Hill, 1997.
58. C. D. Rakopoulos and E. G. Giakoumis, "Availability analysis of a turbocharged diesel engine operating under transient load conditions," Energy, vol. 29, pp. 1085-1104, 2004.
59. R. K. Stobart, "An availability approach to thermal energy recovery in vehicles," Proceedings of the I MECH E Part D Journal of Automobile Engineering, vol. 221, pp. 1107-1124, 2007.
60. M. M. Hussain, I. Dincer, and X. Li, "Energy and Exergy Analysis of an Integrated SOFC Power System," CSME Forum 1, 2004.
61. S. O. Mert, I. Dincer, and Z. Ozcelik, "Exergoeconomic analysis of a vehicular PEM fuel cell system," Journal of Power Sources, vol. 165, pp. 244-252, 2007.
62. R. Cownden, M. Nahon, and M. A. Rosen, "Exergy analysis of a fuel cell power system for transportation applications," Exergy: An International Journal, vol. 1, pp. 112-121, 2001.
63. N. Hotz, S. M. Senn, and D. Poulikakos, "Exergy analysis of a solid oxide fuel cell micropowerplant," Journal of Power Sources, vol. 158, pp. 333-347, 2006.
64. H. Nico, M. S. Stephan, and P. Dimos, "Exergy analysis of a solid oxide fuel cell micropowerplant," Journal of Power Sources, vol. 158, pp. 333-347, 2006.

65. J. H. Horlock, J. B. Young, and G. Manfrida, "Exergy Analysis of Modern Fossil-Fuel Power Plants," Journal of Engineering for Gas Turbines and Power, vol. 122, 2000.
66. I. Akimitsu, M. Shigenori, K. Nobuyuki, and O. Ken-ichiro, "Exergy analysis of polymer electrolyte fuel cell systems using methanol," Journal of Power Sources, vol. 126, pp. 34-40, 2004.
67. K. W. Bedringås, I. S. Ertesvåg, S. Byggstøyl, and B. F. Magnussen, "Exergy analysis of solid-oxide fuel-cell (SOFC) systems," Energy, vol. 22, pp. 403-412, 1997.
68. D. R. Morris and J. Szargut, "Standard chemical exergy of some elements and compounds on the planet earth," Energy, vol. 11, pp. 733-755, 1986.
69. J. Szargut, D. R. Morris, and F. R. Steward, Exergy analysis of thermal, chemical and metallurgical processes: Hemispere Publishing Corporation, 1988.
70. J. A. Caton, "A Review of Investigations Using the Second Law of Thermodynamics to Study Internal-Combustion Engines," Society of Automotive Engineers, vol. 2000–01–1081, 2000.
71. W. S. Levine, The Control Handbook: CRC Press Inc, 1999.
72. V. Tsourapas, A. G. Stefanopoulou, and J. Sun, "Model-Based Control of an Integrated Fuel Cell and Fuel Processor With Exhaust Heat Recirculation," IEEE Transactions on control systems technology, vol. 15, 2007
73. J. Golbert and D. R. Lewin, "Model-based control of fuel cells (2): Optimal efficiency," Journal of Power Sources, vol. 173, pp. 298-309, 2007.
74. J. Golbert and D. R. Lewin, "Model-based control of fuel cells:(1) Regulatory control," Journal of Power Sources, vol. 135, pp. 135–151, 2004.
75. R. Kandepu, L. Imsland, B. A. Foss, C. Stiller, B. Thorud, and O. Bolland, "Modeling and control of a SOFC-GT-based autonomous power system," Energy, vol. 32, pp. 406–417, 2007.
76. A. M. Phillips, M. Jankovic, and K. E. Bailey, "Vehicle System Controller Design for a Hybrid Electric Vehicle," presented at Proceedings of the 2000 IEEE International Conference on Control Applications, Anchorage, Alaska, USA 2000.
77. J. P. Norton, An Introduction to Identification: Academic Press, 1985.
78. C. A. Smith and A. B. Corripio, Principles and Practice of Automatic Process Control, 2nd ed: John Wiley & Sons, Inc., 1997.
79. K. J. Astrom and T. Hagglund, PID Controllers: Theory, Design, and Tuning, 2nd ed: International Society for Measurement and Control, 1995.

80. E. F. Camacho and C. Bordons, Model predictive control, 2nd ed. London: Springer, 2004.
81. M. Morari and J. H. Lee, "Model Predictive Control: Past, Present & Future," presented at 30th European Symposium on Computer Aided Process Engineering (ESCAPE-7), Trondheim, Norway, 1997.
82. D. W. Clarke, C. Mohtadi, and P. S. Tuffs, "Generalized predictive control--Part I. The basic algorithm," Automatica, vol. 23, pp. 137-148, 1987.
83. R. Beck, S. Saenger, F. Richert, A. Bollig, K. Neiß, T. Scholt, K.-E. Noreik, and D. Abel, "Model Predictive Control of a Parallel Hybrid Vehicle Drivetrain," presented at 44th IEEE Conference on Decision and Control, and the European Control Conference 2005, Seville, Spain, 2005.
84. M. J. Moran, "On second-law analysis and the failed promise of finite-time thermodynamics," Energy, vol. 23, pp. 517-519, 1998.
85. C. Wu and R. L. Kiang, "Finite-time thermodynamic analysis of a Carnot engine with internal irreversibility," Energy, vol. 17, pp. 1173-1178, 1992.

Appendix A. – SOFC Model

The solution of the equations for the SOFC model is solved using the Crank-Nicolson method. The code is written in Matlab® version R2007b.

```
%%
clc % clear command window
clear % clear workspace

%%
L=200e-3;        %m length of FC
F=96485.34;    % Coulombs/mol
R=8.314       ;    %J/mol K

T=1073;
dG(1,1)=1.2723-2.7645e-4*T;

N=42000;
t_f=200;
t_0=0;
dt =(t_f-t_0)/N;
t=(0:dt:t_f-dt)';

aa=27.5;% cm2 active area

% Load Voltage
Eo(1:N/4,1)=0.7;
Eo((N/4)+1:N*0.75,1)=0.5;
Eo((N*0.75)+1:N,1)=0.6;

x=60;% scaling for mass flow rate
y=2.05;%scaling for outlet coefficients
```

```
%--------------------
% ANODE %%%%
%--------------------
% Flow IN

kaa=y*4.3827e-011*6.5;% %kg/Pa.s   %anode outlet coefficient
P=1.01e5;   %Pa
P1=1.01e5;  %Pa;
Pa_in=3e5;  %Pa

MM_h2=2.016e-3;         %kg/mol
MM_h2o=18.02e-3;        %kg/mol
Aa=pi*((3.1e-3)^2);     %m2      cross section area of anode
Rh2=4124.3;             %H2 gas constant  J/kg K
Rh2o=188.5;             %H2O gas constant J/kg K

Ya1(1,1)=0.97;  % mass fraction of H2
Ya2(1,1)=0.03;  % mass fraction of H2O

fa_in=x*1.0399e-6*1.9;

h2_in=Ya1(1,1)*fa_in;%  kg/s
h2o_in=Ya2(1,1)*fa_in;% kg/s

fa1(1,1)=h2_in;
fa2(1,1)=h2o_in;

fa(1,1)=fa_in;  %kg/s

dya=2*(3.1e-3);          %m   anode diameter
Aca=2*pi*(3.1e-3)*L;     % m2  Circumferential area of anode

Via=Aa*L;               %m3 Anode Volume

Cp_h2o(1,1)=4.184*(8.22+0.00015*T+0.00000134*T^2)/MM_h2o;%J/kg K
Cp_h2(1,1)=4.184*(6.62+0.00081*T)/MM_h2;%J/kg K

Cv_h2o(1,1)=(2.075e4+12.15*T)/(1e3*MM_h2o);%   %J/kg K
Cv_h2(1,1)=(1.829e4+3.719*T)/(1e3*MM_h2);%     %J/kg K
```

```
ha= 2987;   %W/m2K   Convective Coefficient of anode channel

%--------------------
% CATHODE %%%%
%--------------------
% Flow IN

Pc_in=3e5;   %Pa
kcc=y*1.5813e-11*250;%kg/Pa.s   %cathode outlet coeffiecient

MM_o2=32.016e-3;    %kg/mol
MM_n2=28e-3;    %kg/mol
Ac=pi*((7-3.9)*1e-3)^2;     %cross section area of cathode
Ro2=259.8;  % J/kg.K  O2 gas constant
Rn2=296.8;  % J/kg.K  N2 gas constant

Yc1(1,1)=0.23; % mass fraction of O2
Yc2(1,1)=0.77; % mass fraction of N2

o2_in=x*8.0099e-6*0.8;%kg/s  Mass flow rate of O2
n2_in=x*2.6816e-5*0.8;%kg/s  Mass flow rate of N2

fc1(1,1)=o2_in;
fc2(1,1)=n2_in;

fc_in=fc1(1,1)+fc2(1,1);   %kg/s
fc(1,1)=fc_in;

dyc=2*((7-3.9)*1e-3);    %m Diameter of cathode
Accp=2*pi*(3.9e-3)*L;   % Circumferential area (pen)
Acci=2*pi*(7e-3)*L;   % Circumferential area (insulator)

Vic=Ac*L;   %m3  Cathode Volume

Cp_o2(1,1)=4.184*(6.5+0.001*T)/MM_o2;%J/kg K
Cp_n2(1,1)=4.184*(8.27+0.000258*T-(187700/T^2))/MM_n2;%J/kg K

Cv_o2(1,1)=(2.201e4+4.936*T)/(1e3*MM_o2);%J/kg K
```

```
Cv_n2(1,1)=(1.91e4+5.126*T)/(1e3*MM_n2);%J/kg K

hc=1322.8;  %W/m2K   Convective Coefficient of cathode channel

T0=303; % Ambient temperature

%--------------------
%PEN
%--------------------
rho_pen=6337.3;                  %kg/m3 density of PEN
Vpen=pi*L*(((3.9-3.1)*1e-3)^2);   %m3 Volume of PEN
Apen=pi*(((3.9-3.1)*1e-3)^2);     %m2 Cross section area of PEN
Acpen=2*pi*((3.9-3.1)*1e-3)*L;     %m2 Circumferential area of PEN
Cp_pen=594.3;                    %J/kg K Specific heat of PEN

kpen=2.53;                   %W/m K  Thermal conductivity of PEN

sigma=5.669e-8;                  %W/m2 K4 Stefen Boltzmann constant
epsi_pen=0.33;          %Average emissivity of PEN
r_pen=3.9e-3;    %m Radius of PEN

rho_ins=480;  %kg/m3 Density of insulator
Vins=pi*L*(((9-7)*1e-3)^2);  %m3 Volume of insulator
Ains=pi*((9-7)*1e-3)^2; %Cross sectional area of insulator
Cp_ins=1047;  %J/kg K Specific heat of insulator
Acins=2*pi*(9e-3)*L; % Circumferential area of insulator
kins=0.059;   %W/m K thermal conductivity of insulator

hins=10; %W/m2 K  Convective heat transfer coefficient of insulator
epsi_ins=0.09; % emissivity of insulator
r_ins=9e-3;  %m radius of insulator

Ea=110e3;  %J/mol Activation energy of anode
Ec=160e3;  %J/mol Activation energy of cathode
ka=2.13e8;   %A/m2 anode pre-exponential factor
kc=1.49e10;  %A/m2 cathode pre-exponential factor

dHh2=1.196e8;   % J  LHV of H2
Rohm=0.0257;    % Ohmic resistance of fuel cell
```

```
Hh2f=((-0.9959e4+30.73*T)/MM_h2);     %  J/kg Enthalpy of formation
Hh2of=((-25.790e4+42.47*T)/MM_h2o);   %  J/kg Enthalpy of formation

Ho2f=(-1.2290e4+35.12*T)/MM_o2;       %  J/kg Enthalpy of formation
Hn2f=(-1.059e4+31.40*T)/MM_n2;        %  J/kg Enthalpy of formation

%% Constants
md_h2=MM_h2*Cp_h2/(2*F);

md_h2o=MM_h2o*Cp_h2o/(2*F);

md_o2=MM_o2*Cp_o2/(4*F);

rad=sigma*Acins/((1/epsi_pen)+((r_pen/r_ins)*((1/epsi_ins)-1)));

gen=MM_h2*dHh2/(2*F);

%% Input data
Pa(1,1)=3e5;
Pc(1,1)=3e5;

xh2(1,1)=(Ya1(1,1)/MM_h2)/((Ya1(1,1)/MM_h2)+(Ya2(1,1)/MM_h2o)); %mol
fraction
xh2o(1,1)=(Ya2(1,1)/MM_h2o)/((Ya1(1,1)/MM_h2)+(Ya2(1,1)/MM_h2o)); %mol
fraction

xo2(1,1)=(Yc1(1,1)/MM_o2)/((Yc1(1,1)/MM_o2)+(Yc2(1,1)/MM_n2)); %mol
fraction
xn2(1,1)=(Yc2(1,1)/MM_n2)/((Yc1(1,1)/MM_o2)+(Yc2(1,1)/MM_n2)); %mol
fraction

Cva(1,1)=Ya1(1,1)*Cv_h2(1,1)+Ya2(1,1)*Cv_h2o(1,1);
Cvc(1,1)=Yc1(1,1)*Cv_o2(1,1)+Yc2(1,1)*Cv_n2(1,1);

MMa(1,1)=xh2(1,1)*MM_h2+xh2o(1,1)*MM_h2o; % kg/mol
MMc(1,1)=xo2(1,1)*MM_o2+xn2(1,1)*MM_n2; % kg/mol
```

```
pph2(1,1)=xh2(1,1)*Pa(1,1); % Pa partial pressure
pph2o(1,1)=xh2o(1,1)*Pa(1,1);% Pa partial pressure
ma1(1,1)=xh2(1,1)*Pa(1,1)*Via/(Rh2*T);% kg mass
ma2(1,1)=xh2o(1,1)*Pa(1,1)*Via/(Rh2o*T);%kg mass
ma(1,1)=ma1(1,1)+ma2(1,1);

ppo2(1,1)=xo2(1,1)*Pc(1,1); % Pa partial pressure
ppn2(1,1)=xn2(1,1)*Pc(1,1); % Pa partial pressure
mc1(1,1)=xo2(1,1)*Pc(1,1)*Vic/(Ro2*T);%kg
mc2(1,1)=xn2(1,1)*Pc(1,1)*Vic/(Rn2*T);%kg
mc(1,1)=mc1(1,1)+mc2(1,1); % kg

da(1,1)=ma(1,1)/Via; %kg/m3
dc(1,1)=mc(1,1)/Vic;
da_in=da(1,1);
dc_in=dc(1,1);

Ta(1,1)=T;
Tc(1,1)=T;
Tp(1,1)=T;
Ts(1,1)=T;

Hh2(1,1)=(-0.9959e4+30.73*Ta(1,1))/MM_h2;
Hh2o(1,1)=(-25.790e4+42.47*Ta(1,1))/MM_h2o;

Ho2(1,1)=(-1.2290e4+35.12*Tc(1,1))/MM_o2;
Hn2(1,1)=(-1.059e4+31.40*Tc(1,1))/MM_n2;

Ra(1,1)=1/(2*F*ka*Aca*(1/(R*Ta(1,1)))*((pph2(1,1)/Pa(1,1))^0.25)*exp(-
Ea/(R*Ta(1,1))));
Rc(1,1)=1/(4*F*kc*Accp*(1/(R*Tc(1,1)))*((ppo2(1,1)/Pc(1,1))^0.25)*exp(-
Ec/(R*Tc(1,1))));
Ener(1,1)=(dG(1,1))+(R*Tp(1,1)*(1/(2*F))*log((pph2(1,1)*(1e-
5)*(((ppo2(1,1)*1e-5)^0.5))/(pph2o(1,1)*1e-5)))); % V Nernst potential
I(1,1)=(-Eo(1,1)+Ener(1,1))/(Ra(1,1)+Rc(1,1)+Rohm); % Current

%%
for i=2:N
    j=i+1
```

```
%%Density Anode %%

%da1

A11(1,1)=1;
A11(i,1)=1;

%da2

A22(1,1)=1;
A22(i,1)=1;

%% Density Cathode %%

%dc1

C44(1,1)=1;
C44(i,1)=1;

%dc2

C55(1,1)=1;
C55(i,1)=1;

%% Temperature Anode %%

%Ta

A33(i,1)=ma1(i-1,1)*Cv_h2(i-1,1)+ma2(i-1,1)*Cv_h2o(i-1,1)+...
        (0.5*dt)*(ha*Aca+md_h2*I(i-1,1)+md_h2o*I(i-1,1));

%ma

A31(i,1)=Cv_h2(i-1,1)*Ta(i-1,1);
A32(i,1)=Cv_h2o(i-1,1)*Ta(i-1,1);

%Tp
```

```
A37(i,1)=-(0.5*dt)*(ha*Aca+ md_h2*I(i-1,1)+ md_h2o*I(i-1,1));

%% Temperature Cathode %%

%Tc

C66(i,1)=mc1(i-1,1)*Cv_o2(i-1,1)+mc2(i-1,1)*Cv_n2(i-1,1)+...
        (0.5*dt)*(hc*Accp +hc*Acci +md_o2*I(i-1,1));

%mc

C64(i,1)=Cv_o2(i-1,1)*Tc(i-1,1);
C65(i,1)=Cv_n2(i-1,1)*Tc(i-1,1);

% Tp
C67(i,1)=-(0.5*dt)*(hc*Accp +md_o2*I(i-1,1));

%Ts
C68(i,1)=-(0.5*dt)*(hc*Acci);

%% Temperature Cell %%

%Tp

P77(i,1)=1+(dt/(rho_pen*Vpen*Cp_pen))*0.5*(ha*Aca +hc*Accp +md_h2*I(i-
1,1) +md_h2o*I(i-1,1) +md_o2*I(i-1,1));%-rad*Tp(i-1,1)^3);

%Ta
P73(i,1)=-(dt/(rho_pen*Vpen*Cp_pen))*0.5*(ha*Aca +md_h2*I(i-1,1)
+md_h2o*I(i-1,1));

%Tc

P76(i,1)=-(dt/(rho_pen*Vpen*Cp_pen))*0.5*(hc*Accp +md_o2*I(i-1,1));


%% Temperature Insulator %%
```

```
%Ts
S88(i,1)=1+(dt/(rho_ins*Vins*Cp_ins))*0.5*(hc*Acci+hins*Acins);%+rad*(Ts(
i-1,1)^3));

%Tc

S86(i,1)=-(dt/(rho_ins*Vins*Cp_ins))*0.5*hc*Acci;



%% LHS Matrix

FC=blkdiag(A11(i,1),A22(i,1),A33(i,1),C44(i,1),C55(i,1),C66(i,1),P77(i,1)
,S88(i,1));

FC(3,1)=A31(i,1);
FC(3,2)=A32(i,1);
FC(3,7)=A37(i,1);

FC(6,4)=C64(i,1);
FC(6,5)=C65(i,1);
FC(6,7)=C67(i,1);
FC(6,8)=C68(i,1);

FC(7,3)=P73(i,1);
FC(7,6)=P76(i,1);

FC(8,6)=S86(i,1);

%% Density Anode %%

%da1

B1(i,1)=ma1(i-1,1)+dt*(h2_in-(Ya1(i-1,1)*fa(i-1,1))-(MM_h2*I(i-
1,1)/(2*F)));
B2(i,1)=ma2(i-1,1)+dt*(h2o_in-(Ya2(i-1,1)*fa(i-1,1))+(MM_h2o*I(i-
1,1)/(2*F)));

%% Density Cathode %%
```

```
%dc1

B4(i,1)=mc1(i-1,1)+ dt*(o2_in-(Yc1(i-1,1)*fc(i-1,1))-(MM_o2*I(i-
1,1)/(4*F)));
B5(i,1)=mc2(i-1,1)+ dt*(n2_in-(Yc2(i-1,1)*fc(i-1,1)));

%% Temperature Anode %%

%Ta

B3(i,1)=2*(ma1(i-1,1)*Cv_h2(i-1,1)+ma2(i-1,1)*Cv_h2o(i-1,1))*Ta(i-
1,1)+...
        dt*((h2_in*Hh2(1,1)+h2o_in*Hh2o(1,1))+...
        -((Ya1(i-1,1)*Hh2(i-1,1)+Ya2(i-1,1)*Hh2o(i-1,1))*fa(i-1,1))+...
        -0.5*ha*Aca*(Ta(i-1,1)-Tp(i-1,1))+...
        -0.5*md_h2*I(i-1,1)*(Ta(i-1,1)-Tp(i-1,1))+...
        -0.5*md_h2o*I(i-1,1)*(Ta(i-1,1)-Tp(i-1,1)));

 %% Temperature Cathode %%

%Tc

B6(i,1)=2*(mc1(i-1,1)*Cv_o2(i-1,1)+mc2(i-1,1)*Cv_n2(i-1,1))*Tc(i-1,1)+...
        dt*((o2_in*Ho2(1,1)+n2_in*Hn2(1,1))+...
        -((Yc1(i-1,1)*Ho2(i-1,1)+Yc2(i-1,1)*Hn2(i-1,1))*fc(i-1,1))+...
        -0.5*hc*Accp*(Tc(i-1,1)-Tp(i-1,1))+...
        -0.5*hc*Acci*(Tc(i-1,1)-Ts(i-1,1))+...
       -0.5*md_o2*I(i-1,1)*(Tc(i-1,1)-Tp(i-1,1)));

%% Temperature Cell %%

%Tp

B7(i,1)=Tp(i-1,1)+(dt/(rho_pen*Vpen*Cp_pen))*((kpen*Apen/L)*(T-Tp(i-
1,1))+...
    0.5*hc*Accp*(Tc(i-1,1)-Tp(i-1,1))+...
    0.5*ha*Aca*(Ta(i-1,1)-Tp(i-1,1))+...
    0.5*md_h2*I(i-1,1)*(Ta(i-1,1)-Tp(i-1,1))+...
```

```
    0.5*md_h2o*I(i-1,1)*(Ta(i-1,1)-Tp(i-1,1))+...
    0.5*md_o2*I(i-1,1)*(Tc(i-1,1)-Tp(i-1,1))+...
    rad*(Tp(i-1,1)^4-Ts(i-1,1)^4)+...
    gen*I(i-1,1)+I(i-1,1)^2*(Ra(i-1,1)+Rc(i-1,1)+Rohm));

%% Temperature Insulator %%

%Ts

B8(i,1)=Ts(i-1,1)+(dt/(rho_ins*Vins*Cp_ins))*((kins*Ains/L)*(T-Ts(i-
1,1))+...
    0.5*hc*Acci*(Tc(i-1,1)-Ts(i-1,1))+...
    0.5*hins*Acins*(2*T0-Ts(i-1,1))+...
    -rad*(Ts(i-1,1)^4-Tp(i-1,1)^4));

%% RHS Matrix

B=vertcat(B1(i,1),B2(i,1),B3(i,1),B4(i,1),B5(i,1),B6(i,1),B7(i,1),B8(i,1)
);

%% Solve Matrix

X=FC\B;

%% Assign values to solution

ma1(i,1)=X(1);  %kg
ma2(i,1)=X(2);  %kg
Ta(i,1)=X(3);   %K

mc1(i,1)=X(4);  %kg
mc2(i,1)=X(5);  %kg
Tc(i,1)=X(6);   %K

Tp(i,1)=X(7);  %K
Ts(i,1)=X(8);  %K

ma(i,1)=ma1(i,1)+ma2(i,1);
pph2(i,1)=ma1(i,1)*Rh2*Ta(i,1)/Via;
```

```
pph2o(i,1)=ma2(i,1)*Rh2o*Ta(i,1)/Via;
Pa(i,1)=pph2(i,1)+pph2o(i,1);
xh2(i,1)=pph2(i,1)/Pa(i,1);
xh2o(i,1)=pph2o(i,1)/Pa(i,1);
fa(i,1)=kaa*(Pa(i,1)-P);% flow out from anode

Ya1(i,1)=xh2(i,1)*MM_h2/(xh2(i,1)*MM_h2+xh2o(i,1)*MM_h2o);
Ya2(i,1)=xh2o(i,1)*MM_h2o/(xh2(i,1)*MM_h2+xh2o(i,1)*MM_h2o);
MMa(i,1)=xh2(i,1)*MM_h2+xh2o(i,1)*MM_h2o;
da(i,1)=ma(i,1)/Via;

mc(i,1)=mc1(i,1)+mc2(i,1);
ppo2(i,1)=mc1(i,1)*Ro2*Tc(i,1)/Vic;
ppn2(i,1)=mc2(i,1)*Rn2*Tc(i,1)/Vic;
Pc(i,1)=ppo2(i,1)+ppn2(i,1);
xo2(i,1)=ppo2(i,1)/Pc(i,1);
xn2(i,1)=ppn2(i,1)/Pc(i,1);
fc(i,1)=kcc*(Pc(i,1)-P1);% flow out from cathode

Yc1(i,1)=xo2(i,1)*MM_o2/(xo2(i,1)*MM_o2+xn2(i,1)*MM_n2);
Yc2(i,1)=xn2(i,1)*MM_n2/(xo2(i,1)*MM_o2+xn2(i,1)*MM_n2);
MMc(i,1)=xo2(i,1)*MM_o2+xn2(i,1)*MM_n2;
dc(i,1)=mc(i,1)/Vic;

fa1(i,1)=Ya1(i,1)*fa(i,1);
fa2(i,1)=Ya2(i,1)*fa(i,1);

fc1(i,1)=Yc1(i,1)*fc(i,1);
fc2(i,1)=Yc2(i,1)*fc(i,1);

Cv_h2o(i,1)=(2.075e4+12.15*Ta(i,1))/(1e3*MM_h2o);%J/kg K
Cv_h2(i,1)=(1.829e4+3.719*Ta(i,1))/(1e3*MM_h2);%J/kg K

Cv_o2(i,1)=(2.201e4+4.936*Tc(i,1))/(1e3*MM_o2);%J/kg K
Cv_n2(i,1)=(1.91e4+5.126*Tc(i,1))/(1e3*MM_n2);%J/kg K

Cva(i,1)=Ya1(i,1)*Cv_h2(i,1)+Ya2(i,1)*Cv_h2o(i,1);
Cvc(i,1)=Yc1(i,1)*Cv_o2(i,1)+Yc2(i,1)*Cv_n2(i,1);
```

```
Cp_h2o(i,1)=4.184*(8.22+0.00015*Ta(i,1)+0.00000134*(Ta(i,1)^2))/MM_h2o;
%J/kg K
Cp_h2(i,1)=4.184*(6.62+0.00081*Ta(i,1))/MM_h2;                    %J/kg K

Cp_o2(i,1)=4.184*(6.5+0.001*Tc(i,1))/MM_o2;%     %J/kg K
Cp_n2(i,1)=4.184*(8.27+0.000258*Tc(i,1)-(187700/(Tc(i,1)^2)))/MM_n2;%

Hh2(i,1)=(-0.9959e4+30.73*Ta(i,1))/MM_h2;
Hh2o(i,1)=(-25.790e4+42.47*Ta(i,1))/MM_h2o;

Ho2(i,1)=(-1.2290e4+35.12*Tc(i,1))/MM_o2;
Hn2(i,1)=(-1.059e4+31.40*Tc(i,1))/MM_n2;

dG(i,1)=1.2723-2.7645e-4*Tp(i,1);% Xi, Sun, Tsourapas

Ra(i,1)=1/(2*F*ka*Aca*(1/(R*Ta(i,1)))*((pph2(i,1)/Pa(i,1))^0.25)*exp(-
Ea/(R*Ta(i,1))));
Rc(i,1)=1/(4*F*kc*Accp*(1/(R*Tc(i,1)))*((ppo2(i,1)/Pc(i,1))^0.25)*exp(-
Ec/(R*Tc(i,1))));
Ener(i,1)=(dG(i,1))+(R*Tp(i,1)/(2*F))*log(pph2(i,1)*(1e-
5)*((ppo2(i,1)*1e-5)^0.5)/(pph2o(i,1)*1e-5));% Eo(i,1)=Ener(i,1)-
I(i,1)*(Ra(i,1)+Rc(i,1)+Rohm);
I(i,1)=(-Eo(i,1)+Ener(i,1))/(Ra(i,1)+Rc(i,1)+Rohm);
Pwr(i,1)=Eo(i,1)*I(i,1);
end

%% Data from Xue et al
%Polarisation curve
x1=[.025;.08;.16;.24;.32;.36];
y1=[1.05;.94;.82;.72;.64;.6];

Ixs=[0.025;.04;.07;.11;.16;.21;.27;.32;.34];
Vys=[.9;.86;.82;.8;.77;.75;.73;.72;.71];

Ixe=[0.025;.08;.16;.24;.32;.36];
Vye=[1.05;.94;.82;.72;.64;.6];

%power curve - experimental
Ix=[0;0.025;0.04;0.05;0.11;0.14;0.19;0.24;0.31;0.38];
```

```
Py=[0;0.025;0.045;0.055;0.09;0.11;0.14;0.18;0.22;0.27];
% simulation
Pyy=[0;0.05;0.09;0.14;0.17;0.22];
Ixx=[0;0.05;0.1;0.17;0.25;0.36];
```

Appendix B. – Reformer Model

Reformer Model Parameters

The values of the parameters and constants used for modelling of the reformer are listed below in Table 1.

Table 1 – Reformer Model parameters

	Value	Unit	
ϵ_B	0.909	-	Burner void fraction
ϵ_R	0.7	-	Reformer void fraction
ΔH_1	5.24E+04	J/mol	Reaction enthalpy
ΔH_2	9.32E+04	J/mol	Reaction enthalpy
ΔH_4	-6.38E+06	J/mol	Reaction enthalpy
ξ	2700	m^2/m^3	Catalyst specific surface
π_e		$J/m^3.s.K$	
ρ	$P\overline{MM}/RT$	kg/ m^3	Density
ρ_{cat}	2700	kg/ m^3	Catalyst pellet density
T		s^{-1}	
ψ_R	$(v_{R,0}/T_{R,0})/(\overline{MM}_{R,0}\ /\overline{MM}_R)$	m/s.K	
ψ_B	$(v_{B,0}/T_{B,0})/(\overline{MM}_{B,0}/\overline{MM}_B)$	m/s.K	
a	0.2	m	reactor width
A_1	1.15E+06	$m^3/s.kg$	Kinetic parameters
A_2	7.09E+07	mol/s.kg	Kinetic parameters
B_1	9.45E+05	$m^3/s.kg$	Kinetic parameters
D_1	1.46	-	Kinetic parameters

D_2	0.3	-	Kinetic parameters
C_{Bg}	-	$kmol/m^3$	Concentration in burner gas phase
C_{Bs}	-	$kmol/m^3$	Concentration in burner solid phase
C_W	2.77E+06	J/m^3K	Wall thermal capacity
C_R	-	$kmol/m^3$	Concentration in reformer
C_{gas}	$\sum_j \left(C_{B,g,j} - C_{B,s,j}\right) MM_j cp_j$	J/m^3K	
C_{catR}	3.68E+06	J/m^3K	Catalyst thermal capacity
C_{catB}	3.68E+06	J/m^3K	Catalyst thermal capacity
c_p	-	J/kgK	specific heat
E_1	84100	J/mol	Kinetic parameters
E_2	111200	J/mol	Kinetic parameters
F	1		Wall shape factor
G	-	-	Stoichiometric coefficient
h	0.00264	m/s	burner mass-transfer coefficient
k	-	s^{-1}	reaction rate coefficient
K_{cat}	26	J/m.s.K	Catalyst conductivity
K_W	240	J/m.s.K	Wall conductivity
MM	-	kg/kmol	Molar Mass
P	-	kPa	Pressure
P_{atm}	1.00E+05	kPa	Ambient Pressure
P_R	3.00E+05	kPa	Reformer Pressure
P_B	2.00E+05	kPa	Burner Pressure
R	8.31E+00	J/mol.K	Ideal gas constant
r	-	$kmol/m^3.s$	reaction rate
s_B	1.10E-02	m	burner thickness
s_{Bs}	1.00E-03	m	burner catalyst thickness

s_R	3.00E-02	m	reformer thickness
s_W	1.00E-03	m	wall thickness
t	-	s	time
T_{Bg}	-	K	Temperature burner gas phase
T_{Bs}	-	K	Temperature burner solid phase
T_e	298	K	Temperature ambient
T_W	-	K	Temperature wall
T_R	-	K	Temperature Reformer
U_1	45	$J/m^2.s.K$	heat exchange coefficient
U_2	10000	$J/m^2.s.K$	heat exchange coefficient
U_3	470	$J/m^2.s.K$	heat exchange coefficient
U_e	5	$J/m^2.s.K$	heat exchange coefficient
v	0.25 and 0.4	m/s	reformer and burner gas speed
x	-	m	axial coordinate

Reformer Code

The solution for the 19 partial differential equations of the reformer model are solved using the upwind Crank-Nicolson method. The code is written in Matlab® version R2007b.

```
%-------------------------------------------------------------------------%
Reformer Model - solution of 19 PDE by upwind Crank-Nicolson method
%-------------------------------------------------------------------------
%% Clear workspace
clear
%%
%Define mesh in space                                          |
%N mesh points                                                 |
% delta x is dx                                              %  |
N= 50;
dx= 0.5/(N-1);
x= 0:dx:0.5;

%Define mesh in time                                           |
```

```
%t0 initial time                                          |
%tf final time                                            |
%M time step                                              |
%delta t is dt

M=1000;
t_f=1000;
t_0=0;
dt =(t_f-t_0)/M;
t=0:dt:999.9;
t1=0:20:980;
                                                      %   |
%Define constants                      |
MM_ch3oh = 32.0416; % kg/kmol
MM_h2o = 18.0148;   % kg/kmol
MM_co2 = 44.009;    % kg/kmol
MM_co = 28.01;      % kg/kmol
MM_h2 = 2.0158;     % kg/kmol
MM_o2 = 31.998;     % kg/kmol
MM_n2 = 28.014;     % kg/kmol

Cp_ch3oh = 3.2635;    %  kJ/ kg K
Cp_h2o = 2.1966;      %  kJ/ kg K
Cp_co2 = 1.5481;      %  kJ/ kg K
Cp_co = 1.2134;       %  kJ/ kg K
Cp_h2 = 1.4435e1;     %  kJ/ kg K
Cp_o2 = 1.2343;       %  kJ/ kg K
Cp_n2 = 1.2134;       %  kJ/ kg K

dH1=5.24e4*1000;     % J/kmol
dH2=9.316e4*1000;    % J/kmol
dH4=6.38e5*1000;     % J/kmol



yBch3oh=0.0054/(0.0054+0.0102+0.0385);
yBo2=0.0102/(0.0054+0.0102+0.0385);
yBn2=0.0385/(0.0054+0.0102+0.0385);



yRch3oh(1,1)=0.0325/(0.0325+0.0487);
```

```
yRh2o(1,1)=0.0487/(0.0325+0.0487)'

xRh2o=(yRh2o(1,1)*MM_h2o)/(yRh2o(1,1)*MM_h2o+yRch3oh(1,1)*MM_ch3oh);
xRch3oh=(yRch3oh(1,1)*MM_ch3oh)/(yRh2o(1,1)*MM_h2o+yRch3oh(1,1)*MM_ch3oh)
;

MMR0=((yRh2o(1,1)*MM_h2o)+(yRch3oh(1,1)*MM_ch3oh))*1e-3
%% kg/mol
MMR=((.137*MM_h2o)+(.006*MM_ch3oh)+(.2*MM_co2)+(.02*MM_co)+(.637*MM_h2))*
1e-3   %% kg/mol
CpR= (Cp_ch3oh*xRch3oh + Cp_h2o*xRh2o )*1e3;
% J/kgK mean & at entrance

xBo2=(yBo2*MM_o2)/(yBo2*MM_o2+yBch3oh*MM_ch3oh+yBn2*MM_n2)
xBch3oh=(yBch3oh*MM_ch3oh)/(yBo2*MM_o2+yBch3oh*MM_ch3oh+yBn2*MM_n2)
xBn2=(yBn2*MM_n2)/(yBo2*MM_o2+yBch3oh*MM_ch3oh+yBn2*MM_n2)

MMB0=((yBo2*MM_o2)+(yBch3oh*MM_ch3oh)+(yBn2*MM_n2))*1e-3
%% kg/mol
MMB=((.0996*MM_o2)+(0*MM_ch3oh)+(.732486*MM_n2)+(.102876*MM_co2)+(.065046
*MM_h2o))*1e-3 %% kg/mol
CpB= (Cp_ch3oh*xBch3oh + Cp_o2*xBo2 + Cp_n2*xBn2)*1e3;              % mass
basis - mean & at entrance J/kg K



Vb0=0.4;
TBg0= 450;

xita=2700       % m2/m3
h=0.00264       %m/s
tauB=xita*h*.1;

p1 = tauB*(dt/2);
q1 = dt/2;  % Burner solid % gas source term coefficient
r2= xita*h*(dt/2);

Vr0=0.25;
TRg0= 450;
```

```
p2= dt/(2*0.7);     %% reformer equation (10)
rhocat=2700  %kg/m3 catalyst density

rhoR= 3e5*MMR0/(8.314*450);              %kg/m3
rhoB= 2e5*MMB0/(8.314*450);              %kg/m3 density
pie=50;

u1=45      % J/m2.s.K
u2=10000   % J/m2.s.K
u3=470     % J/m2.s.K

a1= (tauB/(CpB*rhoB))*q1;       % 2nd term eqn 11 coefficient

S= u1/h;
b1= (pie/(.9090*CpB*rhoB))*q1;

d1= q1*(1/(CpB*rhoB));     %%Burner gas equation (11) source term
coefficient

Kcat=26     %J/m s K
Ccat=3.68e6 %J/m3 K
sb=0.011    %m
r4= Kcat*dt/(2*Ccat*(dx^2));
a2= xita*h*q1/Ccat; % 2nd term eqn 12 coefficient
b2= 2*1*u2*q1/((1-.9090)*sb*Ccat);
d2= q1/Ccat;           %% Catalayst Layer equation (12) source tem coeff

Kw=240  % J/m.s.K
Cw=2.772e6   %J/m3.K
sw=0.001    % m
r5=Kw*dt/(Cw*2*(dx^2));

a3=q1*1*u2/(Cw*sw); % 2nd term eqn (13) coefficient
b3=q1*1*u3/(Cw*sw);
d3=q1*pie/Cw;

Te = 298;
sr=0.03 %m
a4= 2*1*u3*q1/(sr*Ccat*0.3); % 2nd term eqn (14) coefficient
```

```
b4= pie*q1/(Ccat*0.3);
d4= q1/(Ccat*0.3);      %

MMR1(1,1)=MMR0
psiR(1,1)= (Vr0/TRg0)*(MMR0/MMR1(1,1));
r3(1,1)= psiR(1,1)*(dt/(2*dx));
r6(1,1)=((psiR(1,1)*(3e5)*0.7*MMR0*CpR*dt)/(8.314*2*dx*Ccat*0.3));

MMB1(1,1)=MMB0
psiB(1,1)= (Vb0/TBg0)*(MMB0/MMB1(1,1));
r1(1,1) = psiB(1,1)*(dt/(2*dx));

A_1= 1.15e6;    % m3/s.kg
A_2= 7.09e7/1000;    % kmol/s.kg
B_1= 9.41e5;    % m3/s.kg
D_1= 1.46;
D_2= 0.3;
E_1= 84100;     % J/mol
E_2= 111200;    % J/mol

% Nomenclature
% Indexes 1,2,3,4,5,6,7 replaced by a,b,c,d,e,f,g for CH3OH,
%  H2O,CO2,CO,H2,O2,N2 respectively

%% Feed Conditions % Feed/Initial Conditions
    C1a(N,M)= 0;
    C1b(N,M)= 0;
    C1c(N,M)= 0;
    C1f(N,M)=0;
    C1g(N,M)=0;
    C2a(N,M)= 0;
    C2b(N,M)= 0;
    C2c(N,M)= 0;
    C2f(N,M)=0;
    C2g(N,M)=0;
    C3a(N,M)= 0;
    C3b(N,M)= 0;
    C3c(N,M)= 0;
    C3d(N,M)=0;
    C3e(N,M)=0;
```

```
    T1(N,M)=0;
    T2(N,M)=0;
    T3(N,M)=0;
    T4(N,M)=0;

    Cgas(N,M)=0;

    %% burner gas
    C1a(1,1)= 0.0054;       % Methanol
    C1b(1,1)= 0;            % Water vapour
    C1c(1,1)= 0;            % Carbon dioxide
    C1f(1,1)=0.0102;        % Oxygen
    C1g(1,1)=0.0385;        % Nitrogen


    %% Burner solid
    C2a(1,1)= 0;            % Methanol
    C2b(1,1)= 0;            % Water vapour
    C2c(1,1)= 0;            % Carbon dioxide
    C2f(1,1)=0;             % Oxygen
    C2g(1,1)=0;             % Nitrogen

    %% Reformer
    C3a(1,1)= 0.0325;       % Methanol
    C3b(1,1)= 0.0487;       % Water vapour
    C3c(1,1)= 0;            % CO2
    C3d(1,1)=0;             % CO
    C3e(1,1)=0;             % Hydrogen


    T1(1,1)=450;            % Burner gas
    T2(1,1)=450;            % Burner Solid
    T3(1,1)=450;            % Wall
    T4(1,1)=450;            % Reformer


%%
for i=1:N
```

```
  C1f(i,1)=0.0102;
  C1g(i,1)=0.0385;
  C3a(i,1)= 0.0325;
  C3b(i,1)= 0.0487;
  T1(i,1)=450;
  T2(i,1)=450;
  T3(i,1)=450;
  T4(i,1)=450;

end

for j=1:M

    C1a(1,j)= 0.0054;
    C1f(1,j)=0.0102;
    C1g(1,j)=0.0385;
    C3a(1,j)= 0.0325;
    C3b(1,j)= 0.0487;
    T1(1,j)=450;
    T2(1,j)=450;
    T3(1,j)=450;
    T4(1,j)=450;

    Cgas(1,j)=1e3*((C1a(1,j)-C2a(1,j))*MM_ch3oh*Cp_ch3oh + ...
    (C1b(1,j)-C2b(1,j))*MM_h2o*Cp_h2o + ...
    (C1c(1,j)-C2c(1,j))*MM_co2*Cp_co2 + ...
    (C1f(1,j)-C2f(1,j))*MM_o2*Cp_o2 +  ...
    (C1g(1,j)-C2g(1,j))*MM_n2*Cp_n2);

end



% Nomenclature
% Indexes 1,2,3,4,5,6,7 replaced by a,b,c,d,e,f,g for CH3OH,
%  H2O,CO2,CO,H2,O2,N2 respectively

%%                                                    %for j=1:M
for j=2:M
    k=j+1     %(no of iterations)
```

```
for i=2:N
yRh2o1(i,1)=C3b(i,j-1)/(C3a(i,j-1)+C3b(i,j-1)+C3c(i,j-1)+C3d(i,j-
1)+C3e(i,j-1));
yRch3oh1(i,1)=C3a(i,j-1)/(C3a(i,j-1)+C3b(i,j-1)+C3c(i,j-1)+C3d(i,j-
1)+C3e(i,j-1));
yRco21(i,1)=C3c(i,j-1)/(C3a(i,j-1)+C3b(i,j-1)+C3c(i,j-1)+C3d(i,j-
1)+C3e(i,j-1));
yRco1(i,1)=C3d(i,j-1)/(C3a(i,j-1)+C3b(i,j-1)+C3c(i,j-1)+C3d(i,j-
1)+C3e(i,j-1));
yRh21(i,1)=C3e(i,j-1)/(C3a(i,j-1)+C3b(i,j-1)+C3c(i,j-1)+C3d(i,j-
1)+C3e(i,j-1));

MMR1(i,1)=((yRh2o1(i,1)*MM_h2o)+(yRch3oh1(i,1)*MM_ch3oh)+(yRco21(i,1)*MM_
co2)+(yRco1(i,1)*MM_co)+(yRh21(i,1)*MM_h2))*1e-3;

psiR(i,1)= (Vr0/TRg0)*(MMR0/MMR1(i,1));
r3(i,1)= psiR(i,1)*(dt/(2*dx));
r6(i,1)=((psiR(i,1)*(3e5)*0.7*MMR0*CpR*dt)/(8.314*2*dx*Ccat*0.3));

yBch3oh1(i,1)=C1a(i,j-1)/(C1a(i,j-1)+C1b(i,j-1)+C1c(i,j-1)+C1f(i,j-
1)+C1g(i,j-1));
yBh2o1(i,1)=C1b(i,j-1)/(C1a(i,j-1)+C1b(i,j-1)+C1c(i,j-1)+C1f(i,j-
1)+C1g(i,j-1));
yBco21(i,1)=C1c(i,j-1)/(C1a(i,j-1)+C1b(i,j-1)+C1c(i,j-1)+C1f(i,j-
1)+C1g(i,j-1));
yBo21(i,1)=C1f(i,j-1)/(C1a(i,j-1)+C1b(i,j-1)+C1c(i,j-1)+C1f(i,j-
1)+C1g(i,j-1));
yBn21(i,1)=C1g(i,j-1)/(C1a(i,j-1)+C1b(i,j-1)+C1c(i,j-1)+C1f(i,j-
1)+C1g(i,j-1));

MMB1(i,1)=((yBo21(i,1)*MM_o2)+(yBch3oh1(i,1)*MM_ch3oh)+(yBn21(i,1)*MM_n2)
+(yBco21(i,1)*MM_co2)+(yBh2o1(i,1)*MM_h2o))*1e-3;

psiB(i,1)= (Vb0/TBg0)*(MMB0/MMB1(i,1));
r1(i,1) = psiB(i,1)*(dt/(2*dx));
end

%CH3OH MATRIX
%%%%%%%%%%%%%%%%%%%%%%%%%%%%%%%%%%%%%%%%%%%%%%%%%%%%%%%%%%%%%%%%%%%%%%%
```

```
% Equation(7) - Burner Gas
% CH3OH
%%%%%%%%%%%%%%%%%%
% T1

R1_16(1,1)= 0;
for i= 2:N
    R1_16(i,i)= r1(i,1)*C1a(i,j-1);
    R1_16(i,i-1)= -r1(i,1)*C1a(i,j-1);
end



% C2a
R16 = -p1*eye(N);

% C1a
R11 = zeros(N);
for i= 2:N
    R11(i,i)= 1+r1(i,1)*T1(i,j-1)+p1+(-q1*(-1*exp(((-6.1e3/(8.314*T1(i,j-
1)))+3.2))));
    R11(i,i-1)= -r1(i,1)*T1(i,j-1);
end
R11(1,1)= 1+p1+(-q1*(-1*exp(((-6.1e3/(8.314*T1(1,j-1)))+3.2))));



%--------------------------------
% H2O
%--------------------------------
% T1
R2_16 = zeros(N,N);
for i= 2:N
    R2_16(i,i)= r1(i,1)*C1b(i,j-1);
    R2_16(i,i-1)= -r1(i,1)*C1b(i,j-1);
end
R2_16(1,1)= 0;

% C1b
R22 = zeros(N);
for i= 2:N
    R22(i,i)= 1+r1(i,1)*T1(i,j-1)+p1;
```

```
    R22(i,i-1)= -r1(i,1)*T1(i,j-1);
end
R22(1,1)= 1+p1;

% C2b
R27 = -p1*(eye(N));

% C1a
for i=1:N
R21= -q1*eye(N)*(2*exp(((-6.1e3/(8.314*T1(i,j-1)))+3.2)));
end
%--------------------------------
% CO2
%--------------------------------
% T1
R3_16 = zeros(N);
for i= 2:N
    R3_16(i,i)= r1(i,1)*C1c(i,j-1);
    R3_16(i,i-1)= -r1(i,1)*C1c(i,j-1);
end
R3_16(1,1)= 0;

% C1c
R33 = zeros(N);
for i= 2:N
    R33(i,i)= 1+r1(i,1)*T1(i,j-1)+p1;
    R33(i,i-1)= -r1(i,1)*T1(i,j-1);
end
R33(1,1)= 1+p1;

% C2c
R38 = -p1*(eye(N));

% C1a

for i=1:N
R31=-q1*eye(N)*(1*exp(((-6.1e3/(8.314*T1(i,j-1)))+3.2)));
end
%--------------------------------
% O2
```

```
%--------------------------------
% T1
R4_16 = zeros(N);
for i= 2:N
    R4_16(i,i)= r1(i,1)*C1f(i,j-1);
    R4_16(i,i-1)= -r1(i,1)*C1f(i,j-1);
end
R4_16(1,1)= 0;

% C1f
R44 = zeros(N);
for i= 2:N
    R44(i,i)= 1+r1(i,1)*T1(i,j-1)+p1;
    R44(i,i-1)= -r1(i,1)*T1(i,j-1);
end
R44(1,1)= 1+p1;

% C2f
R49 = -p1*(eye(N));

% C1a

for i=1:N
R41=-q1*eye(N)*(-1.5*exp(((-6.1e3/(8.314*T1(i,j-1)))+3.2)));
end
%%%%%%%%%%%%%%%%%%%%%%%%%%%%%%%%%%%%%%%%%%%%%%%%%%%%%%%%%%%%%%%%%%%%%%%

% Equation(8) - Burner Gas - N2
% T1
R5_16 = zeros(N);
for i=2:N
    R5_16(i,i)= r1(i,1)*C1g(i,j-1);
    R5_16(i,i-1)= -r1(i,1)*C1g(i,j-1);
end
R5_16(1,1)=0;

% C1g
R55 = zeros(N);
for i=2:N
    R55(i,i)= 1+r1(i,1)*T1(i,j-1);
```

```
    R55(i,i-1)= -r1(i,1)*T1(i,j-1);
end
R55(1,1)=1;

%%%%%%%%%%%%%%%%%%%%%%%%%%%%%%%%%%%%%%%%%%%%%%%%%%%%%%%%%%%%%%%%%%%%%%%
% Equation(9) - Burner Solid
%------------------------------
% CH3OH
%------------------------------
% C1a
for i=1:N
R61(i,i) = -r2;
end

% C2a
for i=1:N
    if T2(i,j-1)<380
        R66(i,i)= (1+r2+(-q1*(-1*exp((-5.9e4/(8.314*T2(i,j-
1))+22.45)))));
    end
    if 380<T2(i,j-1)<830
        R66(i,i)= (1+r2+(-q1*(-1*exp((-6.4e3/(8.314*T2(i,j-1))+5.8)))));
    end
end

%------------------------------
% H2O
%------------------------------
% C1b
R72 = -r2*(eye(N));

% C2b
R77= (1+r2)*(eye(N));

% C2a
for i=1:N
if T2(i,j-1)<380
    R76(i,i)=-q1*(2*exp((-5.9e4/(8.314*T2(i,j-1))+22.45)));
end
if 380<T2(i,j-1)<830
```

```
    R76(i,i)=-q1*(2*exp((-6.4e3/(8.314*T2(i,j-1))+5.8)));
end
end

%-----------------------------
% CO2
%-----------------------------
% C1c
R83 = -r2*(eye(N));

% C2c
R88= (1+r2)*(eye(N));

% C2a
for i=1:N
    if T2(i,j-1)<380
    R86(i,i)=-q1*(1*exp((-5.9e4/(8.314*T2(i,j-1))+22.45)));
    end
    if 380<T2(i,j-1)<830
    R86(i,i)=-q1*(1*exp((-6.4e3/(8.314*T2(i,j-1))+5.8)));
    end
end

%-----------------------------
% O2
%-----------------------------
% C1f
R94 = -r2*(eye(N));

% C2f
R99= (1+r2)*(eye(N));

% C2a
for i=1:N
    if T2(i,j-1)<380
    R96(i,i)=-q1*(-1.5*exp((-5.9e4/(8.314*T2(i,j-1))+22.45)));
    end
    if 380<T2(i,j-1)<830
    R96(i,i)=-q1*(-1.5*exp((-6.4e3/(8.314*T2(i,j-1))+5.8)));
    end
```

```
end



%-----------------------------
% N2
%-----------------------------
% C1g
R10_5 = -r2*(eye(N));

% C2g
R10_10= (1+r2)*(eye(N));

%%%%%%%%%%%%%%%%%%%%%%%%%%%%%%%%%%%%%%%%%%%%%%%%%%%%%%%%%%%%%%%%%%%%%%%
% Equation(10) - Reformer Equation

%-----------------------------
% CH3OH
%-----------------------------

% C3a
R11_11 = zeros(N);
for i= 2:N
    R11_11(i,i)= 1+r3(i,1)*T4(i,j-1)+(p2*((-1*(-
1)*(((A_1+B_1*log(.0487/.0325))*exp(-E_1/(8.314*T4(i,j-
1))))*((rhocat*0.3)/(3^D_1))))));
    R11_11(i,i-1)= -r3(i,1)*T4(i,j-1);
end
R11_11(1,1)= 1+(p2*((-1*(-1)*(((A_1+B_1*log(.0487/.0325))*exp(-
E_1/(8.314*T4(1,j-1))))*((rhocat*0.3)/(3^D_1))))));;

% T4
R11_19 = zeros(N);
for i= 2:N
    R11_19(i,i)= r3(i,1)*C3a(i,j-1);
    R11_19(i,i-1)= -r3(i,1)*C3a(i,j-1);
end
R11_19(1,1)= 0;

%-----------------------------
```

```
% H2O
%------------------------------

% C3b
R12_12 = zeros(N);
for i= 2:N
    R12_12(i,i)= 1+r3(i,1)*T4(i,j-1);
    R12_12(i,i-1)= -r3(i,1)*T4(i,j-1);
end
R12_12(1,1)= 1;

% T4
R12_19 = zeros(N);
for i= 2:N
    R12_19(i,i)= r3(i,1)*C3b(i,j-1);
    R12_19(i,i-1)= -r3(i,1)*C3b(i,j-1);
end
R12_19(1,1)= 0;

% C3a
for i=1:N
R12_11(i,i)=p2*((-1*(-1)*(((A_1+B_1*log(.0487/.0325))*exp(-
E_1/(8.314*T4(i,j-1))))*((rhocat*0.3)/(3^D_1)))));
end
%------------------------------
% CO2
%------------------------------

% C3c
R13_13 = zeros(N);
for i= 2:N
    R13_13(i,i)= 1+r3(i,1)*T4(i,j-1);
    R13_13(i,i-1)= -r3(i,1)*T4(i,j-1);
end
R13_13(1,1)= 1;

% T4
R13_19 = zeros(N);
for i= 2:N
    R13_19(i,i)= r3(i,1)*C3c(i,j-1);
```

```
    R13_19(i,i-1)= -r3(i,1)*C3c(i,j-1);
end
R13_19(1,1)= 0;

% C3a
for i=1:N
R13_11(i,i)= p2*((1*(-1)*(((A_1+B_1*log(.0487/.0325))*exp(-
E_1/(8.314*T4(i,j-1))))*((rhocat*0.3)/(3^D_1)))));
end
%-----------------------------
% CO
%-----------------------------

% C3d
R14_14 = zeros(N);
for i= 2:N
    R14_14(i,i)= 1+r3(i,1)*T4(i,j-1);
    R14_14(i,i-1)= -r3(i,1)*T4(i,j-1);
end
R14_14(1,1)= 1;

% T4
R14_19 = zeros(N);
for i= 2:N
    R14_19(i,i)= r3(i,1)*C3d(i,j-1);
    R14_19(i,i-1)= -r3(i,1)*C3d(i,j-1);
end
R14_19(1,1)= 0;

%-----------------------------
% H2
%-----------------------------

% C3e
R15_15 = zeros(N);
for i= 2:N
    R15_15(i,i)= 1+r3(i,1)*T4(i,j-1);
    R15_15(i,i-1)= -r3(i,1)*T4(i,j-1);
end
R15_15(1,1)= 1;
```

```
% T4
R15_19 = zeros(N);
for i= 2:N
    R15_19(i,i)= r3(i,1)*C3e(i,j-1);
    R15_19(i,i-1)= -r3(i,1)*C3e(i,j-1);
end
R15_19(1,1)= 0;

% C3a
for i=1:N
R15_11(i,i)= p2*((3*(-1)*(((A_1+B_1*log(.0487/.0325))*exp(-
E_1/(8.314*T4(i,j-1))))*((rhocat*0.3)/(3^D_1)))));
end

%%%%%%%%%%%%%%%%%%%%%%%%%%%%%%%%%%%%%%%%%%%%%%%%%%%%%%%%%%%%%%%%
% Equation(11) - Heat Balances - Burner Gas

for i=2:N

    Cgas(i,j-1)=1e3*((C1a(i,j-1)-C2a(i,j-1))*MM_ch3oh*Cp_ch3oh + ...
    (C1b(i,j-1)-C2b(i,j-1))*MM_h2o*Cp_h2o + ...
    (C1c(i,j-1)-C2c(i,j-1))*MM_co2*Cp_co2 + ...
    (C1f(i,j-1)-C2f(i,j-1))*MM_o2*Cp_o2 +  ...
    (C1g(i,j-1)-C2g(i,j-1))*MM_n2*Cp_n2);
end

% T1
R16_16 = zeros(N);
for i= 2:N

    R16_16(i,i)= 1+(a1*S)+(a1*Cgas(i,j-1))+(r1(i,1)*T1(i,j-1))+b1;

    R16_16(i,i-1)= -r1(i,1)*T1(i,j-1);
end
R16_16(1,1)= 1+(a1*S)+(a1*Cgas(i,j-1))+b1;

% T2
for i=1:N
```

```
R16_17= -a1*(Cgas(i,j-1)+S)*(eye(N));
end

% C1a
for i=1:N
R16_1=-d1*eye(N)*(dH4*exp((-6.1e3/(8.314*T1(i,j-1))+3.2)));
end
%%%%%%%%%%%%%%%%%%%%%%%%%%%%%%%%%%%%%%%%%%%%%%%%%%%%%%%%%%%%%%%%%%%%%%%
% Equation(12) - Heat Balances - Burner Solid
% T1
for i=1:N

R17_16 =(-a2*(S+Cgas(i,j-1)))*eye(N);
end

% T2
R17_17 = zeros(N);
for i= 2:N-1



    R17_17(i,i)= 1+2*r4+a2*S+a2*Cgas(i,j-1)+b2;
    R17_17(i,i-1)= -r4;
    R17_17(i,i+1)= -r4;
end
R17_17(1,1)= 1+r4+a2*S+a2*Cgas(1,j-1)+b2;
R17_17(1,2)= -r4;
R17_17(N,N)= 1+r4+a2*S+a2*Cgas(N,j-1)+b2;
R17_17(N,N-1)= -r4;

% T3
R17_18= -b2*eye(N);

% C2a
for i=1:N
    if T2(i,j-1)<380
        R17_6(i,i)= -d2*(dH4*exp((-5.9e4/(8.314*T2(i,j-1))+22.45)));
    end
    if 380<T2(i,j-1)<830
```

```
        R17_6(i,i)=-d2*(dH4*exp((-6.4e3/(8.314*T2(i,j-1))+5.8)));
    end
end
%%%%%%%%%%%%%%%%%%%%%%%%%%%%%%%%%%%%%%%%%%%%%%%%%%%%%%%%%%%%%%%%%%%%%%%
% Equation(13) - Heat Balances - Wall

% T2
R18_17= -a3*eye(N);

% T3
R18_18 = zeros(N);
for i= 2:N-1
    R18_18(i,i)= (1+2*r5+a3+b3+d3);
    R18_18(i,i-1)= -r5;
    R18_18(i,i+1)= -r5;
end
R18_18(1,1)= 1+r5+a3+b3+d3;
R18_18(1,2)= -r5;
R18_18(N,N)= 1+r5+a3+b3+d3;
R18_18(N,N-1)= -r5;

% T4
R18_19= -b3*eye(N);

%%%%%%%%%%%%%%%%%%%%%%%%%%%%%%%%%%%%%%%%%%%%%%%%%%%%%%%%%%%%%%%%%%%%%%%
% Equation(14) - Heat Balances - Reformer

% T3
R19_18= -a4*(eye(N));

% T4
R19_19 = zeros(N);
for i= 2:N
    R19_19(i,i)= (1+r6(i,1)+a4+b4);
    R19_19(i,i-1)= -r6(i,1);
end
R19_19(1,1)= 1+a4+b4;

% C3a
for i=1:N
```

```
R19_11(i,i)= -d4*((dH1*(-1)*(((A_1+B_1*log(.0487/.0325))*exp(-
E_1/(8.314*T4(i,j-1))))*((2*0.3)/(3^D_1)))));
end
%
%%%%%%%%%%%%%%%%%%%%%%%%%%%%%%%%%%%%%%%%%%%%%%%%%%%%%%%%%%%%%%%%
% The complete Matrix R :
R = blkdiag(R11, R22, R33, R44,R55, R66, R77, R88, R99, R10_10, R11_11,
R12_12, R13_13, R14_14, R15_15, R16_16, R17_17, R18_18, R19_19);
R(1:50,251:300)= R16;
R(1:50,751:800)= R1_16;

R(51:100,301:350)= R27;
R(51:100,751:800)= R2_16;

R(101:150,351:400)= R38;
R(101:150,751:800)= R3_16;

R(151:200,401:450)= R49;
R(151:200,751:800)= R4_16;

R(201:250,751:800)= R5_16;

R(251:300, 1:50)= R61;

R(301:350,51:100)= R72;

R(351:400,101:150)= R83;

R(401:450,151:200)= R94;

R(451:500,201:250)= R10_5;

R(501:550,901:950)= R11_19;

R(551:600,901:950)= R12_19;

R(601:650,901:950)= R13_19;
```

```
R(651:700,901:950)= R14_19;

R(701:750,901:950)= R15_19;

R(751:800,801:850)= R16_17;

R(801:850,751:800)= R17_16;
R(801:850,851:900)= R17_18;

R(851:900,801:850)= R18_17;
R(851:900,901:950)= R18_19;

R(901:950,851:900)= R19_18;

R(51:100,1:50) = R21;
R(101:150,1:50) = R31;
R(151:200,1:50) = R41;

R(301:350,251:300) = R76;
R(351:400,251:300) = R86;
R(401:450,251:300) = R96;

R(551:600,501:550)= R12_11;
R(601:650,501:550)= R13_11;
R(701:750,501:550)= R15_11;

R(751:800,1:50)= R16_1;

R(801:850,251:300)= R17_6;

R(901:950,501:550)= R19_11;

%%%%%%%%%%%%%%%%%%%%%%%%%%%%%%%%%%%%%%%%%%%%%%%%%%%%%%%%%%%%%%%%%%%%%%%%

% RHS Column Matrix

% Equation(7) - Burner Gas
%=====================================
```

```
% CH3OH
%=======================================
%for j=1:M

   B1(1,1)=((1-p1)*C1a(1,j-1))+ (p1*C2a(1,j-1))+(q1*(-1*C1a(1,j-1)*exp((-
6.1e3/(8.314*T1(1,j-1))+3.2))));
    for i=2:N
        B1(i,1)= (1-2*r1(i,1)*T1(i,j-1)-p1+r1(i,1)*T1(i-1,j-1))*C1a(i,j-
1) + ...
        (r1(i,1)*T1(i,j-1))*C1a(i-1,j-1) + ...
        p1*C2a(i,j-1)+ ...
        q1*C1a(i,j-1)*(-1*exp(((-6.1e3/(8.314*T1(i,j-1)))+3.2)));
    end



%=======================================
% H2O
%=======================================
    B2(1,1)=(1-p1)*C1b(1,j-1)+p1*C2b(1,j-1)+q1*(2*C1a(1,j-1)*exp((-
6.1e3/(8.314*T1(1,j-1))+3.2)));
        for i=2:N
            B2(i,1)= (1-2*r1(i,1)*T1(i,j-1)-p1+r1(i,1)*T1(i-1,j-
1))*C1b(i,j-1) + ...
            (r1(i,1)*T1(i,j-1))*C1b(i-1,j-1) + ...
            p1*C2b(i,j-1)+ ...
            q1*C1a(i,j-1)*(2*exp(((-6.1e3/(8.314*T1(i,j-1)))+3.2)));
        end

%=======================================
% CO2
%=======================================

    B3(1,1)=(1-p1)*C1c(1,j-1)+p1*C2c(1,j-1)+q1*(1*C1a(1,j-1)*exp(((-
6.1e3/(8.314*T1(1,j-1)))+3.2)));
    for i=2:N
        B3(i,1)= (1-2*r1(i,1)*T1(i,j-1)-p1+r1(i,1)*T1(i-1,j-1))*C1c(i,j-
1) + ...
        (r1(i,1)*T1(i,j-1))*C1c(i-1,j-1) + ...
        p1*C2c(i,j-1)+ ...
        q1*C1a(i,j-1)*(1*exp(((-6.1e3/(8.314*T1(i,j-1)))+3.2)));
```

```
    end


%=====================================
% O2
%=====================================

    B4(1,1)=(1-p1)*C1f(1,j-1)+p1*C2f(1,j-1)+q1*C1a(1,j-1)*(-1.5*exp(((-
6.1e3/(8.314*T1(1,j-1)))+3.2)));
    for i=2:N
        B4(i,1)= (1-2*r1(i,1)*T1(i,j-1)-p1+r1(i,1)*T1(i-1,j-1))*C1f(i,j-
1) + ...
        (r1(i,1)*T1(i,j-1))*C1f(i-1,j-1) + ...
        p1*C2f(i,j-1)+ ...
        q1*C1a(i,j-1)*(-1.5*exp(((-6.1e3/(8.314*T1(i,j-1)))+3.2)));
    end

%%%%%%%%%%%%%%%%%%%%%%%%%%%%%%%%%%%%%%%%%%%%%%%%%%%%%%%%%%%%%%%%%%%

% Equation(8) Burner Gas - N2
    B5(1,1)=C1g(1,j-1);
    for i= 2:N
        B5(i,1)= C1g(i,j-1)*(1-2*r1(i,1)*T1(i,j-1)+r1(i,1)*T1(i-1,j-
1))+(C1g(i-1,j-1)*r1(i,1)*T1(i,j-1)) ;
    end
%%%%%%%%%%%%%%%%%%%%%%%%%%%%%%%%%%%%%%%%%%%%%%%%%%%%%%%%%%%%%%%%%%%

% Equation(9) - Burner Solid
%=====================================
% CH3OH
%=====================================
for i=1:N
    if T2(1,j-1) < 380
            B6(i,1)= (1-r2)*C2a(i,j-1) + ...
                r2* C1a(i,j-1) + ...
                q1*C2a(i,j-1)*(-1*exp((-5.9e4/(8.314*T2(1,j-1))+22.45)));
        end
   if 380<T2(1,j-1)<830
            B6(i,1)= (1-r2)*C2a(i,j-1) + ...
               r2* C1a(i,j-1) + ...
```

```
                q1*C2a(i,j-1)*(-1*exp((-6.4e3/(8.314*T2(1,j-1))+5.8)));
        end
end

%=====================================
% H2O
%=====================================

for i=1:N
    if T2(1,j-1) < 380

        B7(i,1)= (1-r2)*C2b(i,j-1) + ...
        r2* C1b(i,j-1) + ...
        q1*C2a(i,j-1)*(2*exp((-5.9e4/(8.314*T2(1,j-1))+22.45)));
    end



   if 380<T2(1,j-1)<830
            B7(i,1)= (1-r2)*C2b(i,j-1) + ...
            r2* C1b(i,j-1) + ...
            q1*C2a(i,j-1)*(2*exp((-6.4e3/(8.314*T2(1,j-1))+5.8)));
        end
end

%=====================================
% CO2
%=====================================
for i=1:N
    if T2(1,j-1) < 380
        B8(i,1)= (1-r2)*C2c(i,j-1) + ...
        r2* C1c(i,j-1) + ...
        q1*C2a(i,j-1)*(1*exp((-5.9e4/(8.314*T2(1,j-1))+22.45)));
    end

  if 380<T2(1,j-1)<830
        B8(i,1)= (1-r2)*C2c(i,j-1) + ...
        r2* C1c(i,j-1) + ...
        q1*C2a(i,j-1)*(1*exp((-6.4e3/(8.314*T2(1,j-1))+5.8)));
    end
end
```

```
%=====================================
% O2
%=====================================
for i=1:N
  if T2(1,j-1) < 380
        B9(i,1)= (1-r2)*C2f(i,j-1) + ...
        r2* C1f(i,j-1) + ...
        q1*C2a(i,j-1)*(-1.5*exp((-5.9e4/(8.314*T2(1,j-1))+22.45)));
    end

 if 380<T2(1,j-1)<830
        B9(i,1)= (1-r2)*C2f(i,j-1) + ...
        r2* C1f(i,j-1) + ...
        q1*C2a(i,j-1)*(-1.5*exp((-6.4e3/(8.314*T2(1,j-1))+5.8)));
   end

 end
%=====================================
% N2
%=====================================



    for i=1:N
        B10(i,1)= (1-r2)*C2g(i,j-1) + r2* C1g(i,j-1);
    end



%%%%%%%%%%%%%%%%%%%%%%%%%%%%%%%%%%%%%%%%%%%%%%%%%%%%%%%%%%%%%%%%%%%%%%%
% Equation(10) - Reformer

%=====================================
% CH3OH
%=====================================



    B11(1,1)= C3a(1,j-1) + p2*((-1*(C3a(1,j-
1))*(((A_1+(B_1*log(.0487/.0325)))*exp(-E_1/(8.314*T4(1,j-
1))))*((rhocat*0.3)/(3^D_1))))+ ...
        (2*-1*A_2*((rhocat*0.3)/(3^D_2))*exp(-E_2/(8.314*T4(1)))));
```

```
    for i=2:N
        B11(i,1)= (1-2*r3(i,1)*T4(i,j-1)+r3(i,1)*T4(i-1,j-1))*C3a(i,j-1)
+ ...
        (r3(i,1)*T4(i,j-1))*C3a(i-1,j-1)+ ...
        p2*((-1*(C3a(i,j-1))*(((A_1+B_1*log(.0487/.0325))*exp(-
E_1/(8.314*T4(i,j-1))))*((rhocat*0.3)/(3^D_1))))+ ...
        (2*-1*(-1*A_2*((rhocat*0.3)/(3^D_2))*exp(-E_2/(8.314*T4(i,j-
1))))));
    end



%=====================================
% H2O
%=====================================



    B12(1,1)= C3b(1,j-1) + p2*((-1*(C3a(1,j-
1))*(((A_1+B_1*log(.0487/.0325))*exp(-E_1/(8.314*T4(1,j-
1))))*((rhocat*0.3)/(3^D_1))))+0);
        for i=2:N
            B12(i,1)=(1-2*r3(i,1)*T4(i,j-1)+r3(i,1)*T4(i-1,j-1))*C3b(i,j-
1) + ...
            (r3(i,1)*T4(i,j-1))*C3b(i-1,j-1)+ ...
            p2*((-1*(C3a(i,j-1))*(((A_1+B_1*log(.0487/.0325))*exp(-
E_1/(8.314*T4(i,j-1))))*((rhocat*0.3)/(3^D_1)))));
        end;



%=====================================
% CO2
%=====================================



    B13(1,1)= C3c(1,j-1) + p2*((1*(C3a(1,j-
1))*(((A_1+B_1*log(.0487/.0325))*exp(-E_1/(8.314*T4(1,j-
1))))*((rhocat*0.3)/(3^D_1))))+0);
    for i=2:N
        B13(i,1)= (1-2*r3(i,1)*T4(i,j-1)+r3(i,1)*T4(i-1,j-1))*C3c(i,j-1)
+ ...
```

```
        (r3(i,1)*T4(i,j-1))*C3c(i-1,j-1)+ ...
        p2*((1*(C3a(i,j-1))*(((A_1+B_1*log(.0487/.0325))*exp(-
E_1/(8.314*T4(i,j-1))))*((rhocat*0.3)/(3^D_1))))+0);
    end


%=====================================
% CO
%=====================================


    B14(1,1)= C3d(1,j-1) + 2*p2*(1*A_2*((rhocat*0.3)/(3^D_2))*exp(-
E_2/(8.314*T4(1,j-1))));
    for i=2:N
        B14(i,1)= (1-2*r3(i,1)*T4(i,j-1)+r3(i,1)*T4(i-1,j-1))*C3d(i,j-1)
+ ...
        (r3(i,1)*T4(i,j-1))*C3d(i-1,j-1)+ ...
        p2*2*(1*A_2*((rhocat*0.3)/(3^D_2))*exp(-E_2/(8.314*T4(i,j-1))));
    end


%=====================================
% H2
%=====================================


    B15(1,1)= C3e(1,j-1) + p2*(( 3*(C3a(1,j-
1))*(((A_1+B_1*log(.0487/.0325))*exp(-E_1/(8.314*T4(1,j-
1))))*((rhocat*0.3)/(3^D_1))))+ ...
    (2*2*A_2*((rhocat*0.3)/(3^D_2))*exp(-E_2/(8.314*T4(1,j-1)))));
    for i=2:N
        B15(i,1)= (1-2*r3(i,1)*T4(i,j-1)+r3(i,1)*T4(i-1,j-1))*C3e(i,j-1)
+ ...
        (r3(i,1)*T4(i,j-1))*C3e(i-1,j-1)+ ...
        p2*(( 3*(C3a(i,j-1))*(((A_1+B_1*log(.0487/.0325))*exp(-
E_1/(8.314*T4(i,j-1))))*((rhocat*0.3)/(3^D_1))))+ ...
        (2*2*A_2*((rhocat*0.3)/(3^D_2))*exp(-E_2/(8.314*T4(i,j-1)))));
    end


%%%%%%%%%%%%%%%%%%%%%%%%%%%%%%%%%%%%%%%%%%%%%%%%%%%%%%%%%%%%%%%%%%%
```

```
% Equation(11) - Burner Gas - Heat Balance


    B16(1,1)=(1-a1*S-a1*Cgas(1,j-1)-b1)*T1(1,j-1)  ...
    + (a1*S+a1*Cgas(1,j-1))*T2(1,j-1)  ...
    + 2*b1*Te + d1*(dH4*C1a(1,j-1)*exp((-6.1e3/(8.314*T1(1,j-1))+3.2)));


    for i=2:N
        B16(i,1)= (1-(T1(i,j-1)*r1(i,1))- a1*S-a1*Cgas(i,j-1)+
r1(i,1)*T1(i-1,j-1)- b1)*T1(i,j-1)  ...
        + (a1*S+a1*Cgas(i,j-1))*T2(i,j-1)  ...
        + 2*b1*Te + d1*(dH4*C1a(i,j-1)*exp((-6.1e3/(8.314*T1(i,j-
1))+3.2)));
    end


%%%%%%%%%%%%%%%%%%%%%%%%%%%%%%%%%%%%%%%%%%%%%%%%%%%%%%%%%%%%%%%%%%%%%%%
% Equation(12) - Burner Solid - Heat Balance
   if T2(1,j-1) < 380
        B17(1,1)=(1-r4-a2*S-a2*Cgas(1,j-1)-b2)*T2(1,j-1) ...
        + r4* T2(2,j-1) ...
        +(a2*S+a2*Cgas(1,j-1))*T1(1,j-1)  ...
        + b2*T3(1,j-1)  ...
        + d2*(dH4*C2a(1,j-1)*exp((-5.9e4/(8.314*T2(1,j-1))+22.45)));
   end


    if 380<T2(1,j-1)<830


        B17(1,1)=(1-r4-a2*S-a2*Cgas(1,j-1)-b2)*T2(1,j-1) ...
        +r4* T2(2,j-1) ...
        +(a2*S+a2*Cgas(1,j-1))*T1(1,j-1)  ...
        + b2*T3(1,j-1)  ...
        + d2*(dH4*C2a(1,j-1)*exp((-6.4e3/(8.314*T2(1,j-1))+5.8)));


    end



    for i=2:N-1
```

```
    if T2(i,j-1) < 380

    B17(i,1)= (1-2*r4-a2*S-a2*Cgas(i,j-1)-b2)*T2(i,j-1) ...
    + r4*T2(i+1,j-1)  ...
    +r4* T2(i-1,j-1) ...
    +(a2*S+a2*Cgas(i,j-1))*T1(i,j-1)  ...
    +b2*T3(i,j-1)  ...
    + d2*(dH4*C2a(i,j-1)*exp((-5.9e4/(8.314*T2(i,j-1))+22.45)));
    end

    if 380<T2(1,j-1)<830

    B17(i,1)= (1-2*r4-a2*S-a2*Cgas(i,j-1)-b2)*T2(i,j-1) ...
    + r4*T2(i+1,j-1)  ...
    +r4* T2(i-1,j-1) ...
    +(a2*S+a2*Cgas(i,j-1))*T1(i,j-1)  ...
    + b2*T3(i,j-1)  ...
    + d2*(dH4*C2a(i,j-1)*exp((-6.4e3/(8.314*T2(i,j-1))+5.8)));

    end
end

    if T2(N,j-1) < 380
    B17(N,1)=(1-r4-a2*S-a2*Cgas(N,j-1)...
    -b2)*T2(N,j-1)...
    +r4* T2(N-1,j-1)+ ...
    (a2*S+a2*Cgas(N,j-1))*T1(N,j-1) ...
    +b2*T3(N,j-1) ...
    + d2*(dH4*C2a(N,j-1)*exp((-5.9e4/(8.314*T2(N,j-1))+22.45)));
    end

    if 380<T2<830
    B17(N,1)=(1-r4-a2*S-a2*Cgas(N,j-1)...
    -b2)*T2(N,j-1)...
    +r4* T2(N-1,j-1)+ ...
    (a2*S+a2*Cgas(N,j-1))*T1(N,j-1) ...
    +b2*T3(N,j-1) ...
    + d2*(dH4*C2a(N,j-1)*exp((-6.4e3/(8.314*T2(N,j-1))+5.8)));
    end
```

```
%%%%%%%%%%%%%%%%%%%%%%%%%%%%%%%%%%%%%%%%%%%%%%%%%%%%%%%%%%%%%%%%%%%%%%%%
% Equation(13) - Wall - Heat Balance



    B18(1,1)=(1-r5-a3-b3-d3)*T3(1,j-1) + (r5)*T3(2,j-1) +a3*T2(1,j-1)
+b3*T4(1,j-1)+2*d3*Te;
    for i=2:N-1
        B18(i,1)= (1-2*r5-a3-b3-d3)*T3(i,j-1) + r5*T3(i-1,j-1) + r5
*T3(i+1,j-1) +a3*T2(i,j-1) + b3*T4(i,j-1)+2*d3*Te;
    end
    B18(N,1)= (1-r5-a3-b3+d3)*T3(N,j-1) + r5*T3(N-1,j-1)+ a3*T2(N,j-1) +
b3*T4(N,j-1)+2*d3*Te;

%%%%%%%%%%%%%%%%%%%%%%%%%%%%%%%%%%%%%%%%%%%%%%%%%%%%%%%%%%%%%%%%%%%%%%%%
% Equation(14) - Reformer - Heat Balance

    B19(1,1)=(1-a4-b4)*T4(1,j-1)  ...
    + a4*T3(1,j-1)  ...
    + d4*((dH1*(-C3a(1,j-1))*(((A_1+B_1*log(.0487/.0325))*exp(-
E_1/(8.314*T4(1,j-1))))*((2*0.3)/(3^D_1)))) ...
    +2*(dH2*A_2*((2*0.3)/(3^D_2))*exp(-E_2/(8.314*T4(1,j-1))))  ...
    + 2*b4*Te;
    for i=2:N
        B19(i,1)= (1-r6(i,1)-a4-b4)*T4(i,j-1)  ...
        + r6(i,1)*T4(i-1,j-1)  ...
        + a4*T3(i,j-1)  ...
        + d4*((dH1*(-C3a(i,j-1))*(((A_1+B_1*log(.0487/.0325))*exp(-
E_1/(8.314*T4(i,j-1))))*((2*0.3)/(3^D_1)))) ...
        + 2*(dH2*A_2*((2*0.3)/(3^D_2))*exp(-E_2/(8.314*T4(i,j-1)))))  ...
        + 2*b4*Te;
    end

%%%%%%%%%%%%%%%%%%%%%%%%%%%%%%%%%%%%%%%%%%%%%%%%%%%%%%%%%%%%%%%%%%%%%%%%
% The complete RHS matrix is
B=
cat(1,B1,B2,B3,B4,B5,B6,B7,B8,B9,B10,B11,B12,B13,B14,B15,B16,B17,B18,B19)
;
%%%%%%%%%%%%%%%%%%%%%%%%%%%%%%%%%%%%%%%%%%%%%%%%%%%%%%%%%%%%%%%%%%%%%%%%
```

```
        P1 = R\B;
        q(950,1)=0;

        Q=[q P1];



        C1a(2:50,j) = Q(2:50,2);
        C1b(2:50,j)=Q(52:100,2);
        C1c(2:50,j)=Q(102:150,2);
        C1f(2:50,j)=Q(152:200,2);
        C1g(2:50,j)=Q(202:250,2);

        C2a(2:50,j)=Q(252:300,2);
        C2b(2:50,j)=Q(302:350,2);
        C2c(2:50,j)=Q(352:400,2);
        C2f(2:50,j)=Q(402:450,2);
        C2g(2:50,j)=Q(452:500,2);

        C3a(2:50,j)=Q(502:550,2);
        C3b(2:50,j)=Q(552:600,2);
        C3c(2:50,j)=Q(602:650,2);
        C3d(2:50,j)=Q(652:700,2);
        C3e(2:50,j)=Q(702:750,2);

        T1(2:50,j)=Q(752:800,2);
        T2(2:50,j)=Q(802:850,2);
        T3(2:50,j)=Q(852:900,2);
        T4(2:50,j)=Q(902:950,2);



P0=cat(1,C1a,C1b,C1c,C1f,C1g,C2a,C2b,C2c,C2f,C2g,C3a,C3b,C3c,C3d,C3e,T1,T
2,T3,T4);

  errC(1:50,1)=0.00001;
  errT(1:50,1)=0.01;
  if P0(:,j)-P0(:,j-
1)<=cat(1,errC,errC,errC,errC,errC,errC,errC,errC,errC,errC,errC,errC,err
C,errC,errC,errT,errT,errT,errT);
```

```
  end
end


%%
    grid on
    plot(x,T1(1:50,M), '-r', 'LineWidth',2)
    xlabel('Distance x (m)')
    ylabel('Temperature (K)')
    hold on
    plot(x,T2(1:50,M), '-g', 'LineWidth',2)
    hold on
    plot(x,T3(1:50,M), '-b', 'LineWidth',2)
    hold on
    plot(x,T4(1:50,M), '-m', 'LineWidth',2)
    grid on
    legend('Burner Gas','Burner Solid','Wall','Reformer')
%
```

Appendix C. – Engine Model

```
     ************************************************************
     *                  CHEMKIN-PRO Release 15082                 *
     *                      CHEM Application                      *
     *               GAS-PHASE MECHANISM INTERPRETER              *
     * Copyright(c) 1997-2008 Reaction Design.  All Rights Reserved. *
     ************************************************************


Initializing CHEMKIN Gas-phase Interpreter a component of CHEMKIN-PRO Release
15082, Build date: Sep 26, 2008
This and All Other CHEMKIN(R) Libraries are Copyright (c) 1997-2008 Reaction
Design.  All rights reserved.


LICENSE INFORMATION:


LicNum: 5069
 Licensed to Loughborough University
 Contact: Richard Stobart
 Expiring: 14-mar-2011
 Platform: win32


                WORKING SPACE REQUIREMENTS
                 PROVIDED        REQUIRED
 LOGICAL              181             181
 INTEGER           126618          126618
 REAL              196225          196225
 CHARACTER          17842           17842

This problem requires      1.497MB of memory for the REAL array.
                          --------------------
                          ELEMENTS     ATOMIC
                          CONSIDERED   WEIGHT
                          --------------------
                           1. n       14.0067
                           2. c       12.0112
                           3. h       1.00797
                           4. o       15.9994
                           5. ar      39.9480
                          --------------------
 ------------------------------------------------------------------------------
                          C
                       P  H
                       H  A
                       A  R
 SPECIES               S  G  MOLECULAR  TEMPERATURE  ELEMENT COUNT
 CONSIDERED            E  E  WEIGHT     LOW    HIGH          n         c
h         o         ar
 ------------------------------------------------------------------------------
   1. n2               G  0 2.8013E+01   300   5000          2         0
0         0         0
```

```
   2. ch3               G  0 1.5035E+01   300   5000          0          1
3          0          0
   3. h                 G  0 1.0080E+00   300   5000          0          0
1          0          0
   4. ch4               G  0 1.6043E+01   300   5000          0          1
4          0          0
   5. h2                G  0 2.0159E+00   300   5000          0          0
2          0          0
   6. oh                G  0 1.7007E+01   300   5000          0          0
1          1          0
   7. h2o               G  0 1.8015E+01   300   5000          0          0
2          1          0
   8. o                 G  0 1.5999E+01   300   5000          0          0
0          1          0
   9. c2h6              G  0 3.0070E+01   300   5000          0          2
6          0          0
  10. c2h5              G  0 2.9062E+01   300   5000          0          2
5          0          0
  11. hco               G  0 2.9019E+01   300   5000          0          1
1          1          0
  12. co                G  0 2.8011E+01   300   5000          0          1
0          1          0
  13. co2               G  0 4.4010E+01   300   5000          0          1
0          2          0
  14. o2                G  0 3.1999E+01   300   5000          0          0
0          2          0
  15. h2o2              G  0 3.4015E+01   300   5000          0          0
2          2          0
  16. ho2               G  0 3.3007E+01   300   5000          0          0
1          2          0
  17. c2h4              G  0 2.8054E+01   300   5000          0          2
4          0          0
  18. ch3oh             G  0 3.2042E+01   300   5000          0          1
4          1          0
  19. ch2oh             G  0 3.1034E+01   250   4000          0          1
3          1          0
  20. ch3o              G  0 3.1034E+01   300   3000          0          1
3          1          0
  21. ch2o              G  0 3.0026E+01   300   5000          0          1
2          1          0
  22. c2h2              G  0 2.6038E+01   300   5000          0          2
2          0          0
  23. c2h3              G  0 2.7046E+01   300   5000          0          2
3          0          0
  24. c2h               G  0 2.5030E+01   300   4000          0          2
1          0          0
  25. hcco              G  0 4.1030E+01   300   4000          0          2
1          1          0
  26. ch2               G  0 1.4027E+01   250   4000          0          1
2          0          0
  27. ch                G  0 1.3019E+01   300   5000          0          1
1          0          0
  28. ch2co             G  0 4.2038E+01   300   5000          0          2
2          1          0
  29. ch2(s)            G  0 1.4027E+01   300   4000          0          1
2          0          0
  30. pc2h4oh           G  0 4.5062E+01   300   5000          0          2
5          1          0
  31. ch3co             G  0 4.3046E+01   300   5000          0          2
3          1          0
  32. ch3cho            G  0 4.4054E+01   300   5000          0          2
4          1          0
  33. c3h5-s            G  0 4.1073E+01   300   5000          0          3
5          0          0
  34. c3h4-p            G  0 4.0065E+01   300   4000          0          3
4          0          0
  35. c3h5-a            G  0 4.1073E+01   300   5000          0          3
5          0          0
```

```
  36. c3h6              G  0 4.2081E+01   300   5000          0          3
6         0         0
  37. c3h4-a            G  0 4.0065E+01   300   4000          0          3
4         0         0
  38. ch3chco           G  0 5.6065E+01   300   5000          0          3
4         1         0
  39. c3h5-t            G  0 4.1073E+01   300   5000          0          3
5         0         0
  40. c4h6              G  0 5.4092E+01   300   5000          0          4
6         0         0
  41. nc3h7             G  0 4.3089E+01   300   5000          0          3
7         0         0
  42. ic3h7             G  0 4.3089E+01   300   5000          0          3
7         0         0
  43. c3h8              G  0 4.4097E+01   300   5000          0          3
8         0         0
  44. c5h9              G  0 6.9127E+01   300   5000          0          5
9         0         0
  45. c4h7              G  0 5.5100E+01   300   5000          0          4
7         0         0
  46. c4h8-1            G  0 5.6108E+01   300   5000          0          4
8         0         0
  47. sc4h9             G  0 5.7116E+01   300   5000          0          4
9         0         0
  48. pc4h9             G  0 5.7116E+01   300   5000          0          4
9         0         0
  49. ch3coch3          G  0 5.8081E+01   300   5000          0          3
6         1         0
  50. ch3coch2          G  0 5.7073E+01   300   5000          0          3
5         1         0
  51. c2h5co            G  0 5.7073E+01   300   5000          0          3
5         1         0
  52. c2h5cho           G  0 5.8081E+01   300   5000          0          3
6         1         0
  53. c5h10-1           G  0 7.0135E+01   300   5000          0          5
10         0         0
  54. ch2cho            G  0 4.3046E+01   300   5000          0          2
3         1         0
  55. c5h11-1           G  0 7.1143E+01   300   5000          0          5
11         0         0
  56. c5h11-2           G  0 7.1143E+01   300   5000          0          5
11         0         0
  57. c2h5o             G  0 4.5062E+01   300   5000          0          2
5         1         0
  58. c2h5o2            G  0 6.1061E+01   300   5000          0          2
5         2         0
  59. ch3o2             G  0 4.7034E+01   300   5000          0          1
3         2         0
  60. ch3o2h            G  0 4.8042E+01   300   5000          0          1
4         2         0
  61. c3h2              G  0 3.8049E+01   150   4000          0          3
2         0         0
  62. o2c2h4oh          G  0 7.7060E+01   300   5000          0          2
5         3         0
  63. c2h4o2h           G  0 6.1061E+01   300   5000          0          2
5         2         0
  64. c2h3co            G  0 5.5057E+01   300   5000          0          3
3         1         0
  65. c2h3cho           G  0 5.6065E+01   300   5000          0          3
4         1         0
  66. c3h5o             G  0 5.7073E+01   300   5000          0          3
5         1         0
  67. c3h6o1-2          G  0 5.8081E+01   300   5000          0          3
6         1         0
  68. c3h6ooh1-2        G  0 7.5088E+01   300   5000          0          3
7         2         0
  69. c3h6ooh2-1        G  0 7.5088E+01   300   5000          0          3
7         2         0
```

```
  70. nc3h7o            G  0 5.9089E+01   300   5000           0          3
7         1         0
  71. ic3h7o            G  0 5.9089E+01   300   5000           0          3
7         1         0
  72. nc3h7o2           G  0 7.5088E+01   300   5000           0          3
7         2         0
  73. ic3h7o2           G  0 7.5088E+01   300   5000           0          3
7         2         0
  74. c4h7o             G  0 7.1100E+01   300   5000           0          4
7         1         0
  75. c4h8ooh1-3o2      G  0 1.2111E+02   300   5000           0          4
9         4         0
  76. c4h8ooh1-3        G  0 8.9115E+01   300   5000           0          4
9         2         0
  77. nc4ket13          G  0 1.0411E+02   300   5000           0          4
8         3         0
  78. c4h8ooh1-2        G  0 8.9115E+01   300   5000           0          4
9         2         0
  79. c4h8o1-3          G  0 7.2108E+01   300   5000           0          4
8         1         0
  80. pc4h9o2           G  0 8.9115E+01   300   5000           0          4
9         2         0
  81. c3h3              G  0 3.9057E+01   300   4000           0          3
3         0         0
  82. hocho             G  0 4.6026E+01   300   5000           0          1
2         2         0
  83. c2h3o1,2          G  0 4.3046E+01   300   5000           0          2
3         1         0
  84. nc3h7cho          G  0 7.2108E+01   300   5000           0          4
8         1         0
  85. nc3h7co           G  0 7.1100E+01   300   5000           0          4
7         1         0
  86. c3h6cho-2         G  0 7.1100E+01   300   5000           0          4
7         1         0
  87. ch2ch2coch3       G  0 7.1100E+01   300   5000           0          4
7         1         0
  88. c2h5coch2         G  0 7.1100E+01   300   5000           0          4
7         1         0
  89. c2h5coc2h4p       G  0 8.5127E+01   300   5000           0          5
9         1         0
  90. nc3h7coch2        G  0 8.5127E+01   300   5000           0          5
9         1         0
  91. nc4h9cho          G  0 8.6135E+01   300   5000           0          5
10         1         0
  92. nc4h9co           G  0 8.5127E+01   300   5000           0          5
9         1         0
  93. hoch2o            G  0 4.7034E+01   300   5000           0          1
3         2         0
  94. c6h13-1           G  0 8.5171E+01   300   5000           0          6
13         0         0
  95. c6h12-1           G  0 8.4163E+01   300   5000           0          6
12         0         0
  96. c6h11             G  0 8.3155E+01   300   5000           0          6
11         0         0
  97. nc7h16            G  0 1.0021E+02   300   5000           0          7
16         0         0
  98. c7h15-1           G  0 9.9198E+01   300   5000           0          7
15         0         0
  99. c7h15-2           G  0 9.9198E+01   300   5000           0          7
15         0         0
 100. c7h15-3           G  0 9.9198E+01   300   5000           0          7
15         0         0
 101. c7h15-4           G  0 9.9198E+01   300   5000           0          7
15         0         0
 102. c7h15o2-1         G  0 1.3120E+02   300   5000           0          7
15         2         0
 103. c7h15o2h-1        G  0 1.3220E+02   300   5000           0          7
16         2         0
```

```
 104. c7h15o2-2         G  0 1.3120E+02   300   5000          0         7
15         2         0
 105. c7h15o2h-2        G  0 1.3220E+02   300   5000          0         7
16         2         0
 106. c7h15o2-3         G  0 1.3120E+02   300   5000          0         7
15         2         0
 107. c7h15o2h-3        G  0 1.3220E+02   300   5000          0         7
16         2         0
 108. c7h14-1           G  0 9.8190E+01   300   5000          0         7
14         0         0
 109. c7h14-2           G  0 9.8190E+01   300   5000          0         7
14         0         0
 110. c7h14-3           G  0 9.8190E+01   300   5000          0         7
14         0         0
 111. c7h13             G  0 9.7182E+01   300   5000          0         7
13         0         0
 112. c7h15o2-4         G  0 1.3120E+02   300   5000          0         7
15         2         0
 113. c7h15o-1          G  0 1.1520E+02   300   5000          0         7
15         1         0
 114. c7h15o-2          G  0 1.1520E+02   300   5000          0         7
15         1         0
 115. c7h15o-3          G  0 1.1520E+02   300   5000          0         7
15         1         0
 116. c7h14ooh1-2       G  0 1.3120E+02   300   5000          0         7
15         2         0
 117. c7h14ooh1-3       G  0 1.3120E+02   300   5000          0         7
15         2         0
 118. c7h14ooh1-4       G  0 1.3120E+02   300   5000          0         7
15         2         0
 119. c7h14ooh2-3       G  0 1.3120E+02   300   5000          0         7
15         2         0
 120. c7h14ooh2-4       G  0 1.3120E+02   300   5000          0         7
15         2         0
 121. c7h14ooh2-5       G  0 1.3120E+02   300   5000          0         7
15         2         0
 122. c7h14ooh3-1       G  0 1.3120E+02   300   5000          0         7
15         2         0
 123. c7h14ooh3-2       G  0 1.3120E+02   300   5000          0         7
15         2         0
 124. c7h14ooh3-4       G  0 1.3120E+02   300   5000          0         7
15         2         0
 125. c7h14ooh3-5       G  0 1.3120E+02   300   5000          0         7
15         2         0
 126. c7h14ooh3-6       G  0 1.3120E+02   300   5000          0         7
15         2         0
 127. c7h14ooh4-2       G  0 1.3120E+02   300   5000          0         7
15         2         0
 128. c7h14ooh4-3       G  0 1.3120E+02   300   5000          0         7
15         2         0
 129. c7h14o1-3         G  0 1.1419E+02   300   5000          0         7
14         1         0
 130. c7h14o1-4         G  0 1.1419E+02   300   5000          0         7
14         1         0
 131. c7h14o2-4         G  0 1.1419E+02   300   5000          0         7
14         1         0
 132. c7h14o2-5         G  0 1.1419E+02   300   5000          0         7
14         1         0
 133. c7h14o3-5         G  0 1.1419E+02   300   5000          0         7
14         1         0
 134. c7h14ooh1-3o2     G  0 1.6320E+02   300   5000          0         7
15         4         0
 135. c7h14ooh2-3o2     G  0 1.6320E+02   300   5000          0         7
15         4         0
 136. c7h14ooh2-4o2     G  0 1.6320E+02   300   5000          0         7
15         4         0
 137. c7h14ooh2-5o2     G  0 1.6320E+02   300   5000          0         7
15         4         0
```

```
 138. c7h14ooh3-1o2    G  0 1.6320E+02   300   5000           0          7
15          4          0
 139. c7h14ooh3-2o2    G  0 1.6320E+02   300   5000           0          7
15          4          0
 140. c7h14ooh3-4o2    G  0 1.6320E+02   300   5000           0          7
15          4          0
 141. c7h14ooh3-5o2    G  0 1.6320E+02   300   5000           0          7
15          4          0
 142. c7h14ooh3-6o2    G  0 1.6320E+02   300   5000           0          7
15          4          0
 143. c7h14ooh4-2o2    G  0 1.6320E+02   300   5000           0          7
15          4          0
 144. c7h14ooh4-3o2    G  0 1.6320E+02   300   5000           0          7
15          4          0
 145. nc7ket13         G  0 1.4619E+02   300   5000           0          7
14          3          0
 146. nc7ket23         G  0 1.4619E+02   300   5000           0          7
14          3          0
 147. nc7ket24         G  0 1.4619E+02   300   5000           0          7
14          3          0
 148. nc7ket25         G  0 1.4619E+02   300   5000           0          7
14          3          0
 149. nc7ket31         G  0 1.4619E+02   300   5000           0          7
14          3          0
 150. nc7ket32         G  0 1.4619E+02   300   5000           0          7
14          3          0
 151. nc7ket34         G  0 1.4619E+02   300   5000           0          7
14          3          0
 152. nc7ket35         G  0 1.4619E+02   300   5000           0          7
14          3          0
 153. nc7ket36         G  0 1.4619E+02   300   5000           0          7
14          3          0
 154. nc7ket42         G  0 1.4619E+02   300   5000           0          7
14          3          0
 155. nc7ket43         G  0 1.4619E+02   300   5000           0          7
14          3          0
 156. nc4h9coch2       G  0 9.9154E+01   300   5000           0          6
11          1          0
 157. c4h7ooh1-4       G  0 8.8107E+01   300   5000           0          4
8           2          0
 158. c5h9ooh1-4       G  0 1.0213E+02   300   5000           0          5
10          2          0
 159. c4h7o1-4         G  0 7.1100E+01   300   5000           0          4
7           1          0
 160. c5h9o1-4         G  0 8.5127E+01   300   5000           0          5
9           1          0
 161. c                G  0 1.2011E+01   200   3500           0          1
0           0          0
 162. hccoh            G  0 4.2038E+01   300   5000           0          2
2           1          0
 163. n                G  0 1.4007E+01   200   6000           1          0
0           0          0
 164. nh               G  0 1.5015E+01   200   6000           1          0
1           0          0
 165. nh2              G  0 1.6023E+01   200   6000           1          0
2           0          0
 166. nh3              G  0 1.7031E+01   200   6000           1          0
3           0          0
 167. nnh              G  0 2.9021E+01   200   6000           2          0
1           0          0
 168. no               G  0 3.0006E+01   200   6000           1          0
0           1          0
 169. no2              G  0 4.6005E+01   200   6000           1          0
0           2          0
 170. n2o              G  0 4.4013E+01   200   6000           2          0
0           1          0
 171. hno              G  0 3.1014E+01   200   6000           1          0
1           1          0
```

```
 172. cn                G  0 2.6018E+01   200   6000          1         1
0         0         0
 173. hcn               G  0 2.7026E+01   200   6000          1         1
1         0         0
 174. h2cn              G  0 2.8034E+01   300   4000          1         1
2         0         0
 175. hcnn              G  0 4.1033E+01   300   5000          2         1
1         0         0
 176. hcno              G  0 4.3025E+01   300   5000          1         1
1         1         0
 177. hocn              G  0 4.3025E+01   300   5000          1         1
1         1         0
 178. hnco              G  0 4.3025E+01   300   5000          1         1
1         1         0
 179. nco               G  0 4.2017E+01   200   6000          1         1
0         1         0
 180. ar                G  0 3.9948E+01   300   5000          0         0
0         0         1
 181. c3h7              G  0 4.3089E+01   300   5000          0         3
7         0         0
 ---------------------------------------------------------------------------
```

```
                                                          (k = A T**b exp(-E/RT))
     REACTIONS CONSIDERED                                   A        b        E

   1. ch3+h(+m)=>ch4(+m)                                 2.14E+15   -0.4        0.0
      h2              Enhanced by    2.000E+00
      h2o             Enhanced by    5.000E+00
      co              Enhanced by    2.000E+00
      co2             Enhanced by    3.000E+00
      Low pressure limit:  0.33100E+31 -0.40000E+01  0.21080E+04
      TROE centering:      0.00000E+00  0.10000E-14  0.10000E-14  0.40000E+02
   2. ch4(+m)=>ch3+h(+m)                                 1.05E+21   -1.4   107900.1
      h2              Enhanced by    2.000E+00
      h2o             Enhanced by    5.000E+00
      co              Enhanced by    2.000E+00
      co2             Enhanced by    3.000E+00
      Low pressure limit:  0.16300E+37 -0.50000E+01  0.11001E+06
      TROE centering:      0.00000E+00  0.10000E-14  0.10000E-14  0.40000E+02
   3. ch4+h=>ch3+h2                                      1.73E+04    3.0     8224.0
   4. ch3+h2=>ch4+h                                      6.61E+02    3.0     7744.0
   5. ch4+oh=>ch3+h2o                                    1.93E+05    2.4     2106.1
   6. ch3+h2o=>ch4+oh                                    4.82E+02    2.9    14859.9
   7. ch4+o=>ch3+oh                                      2.13E+06    2.2     6479.9
   8. ch3+oh=>ch4+o                                      3.56E+04    2.2     3919.9
   9. c2h6+ch3=>c2h5+ch4                                 1.51E-07    6.0     6047.1
  10. c2h5+ch4=>c2h6+ch3                                 9.65E-10    6.6    10219.9
  11. hco+oh=>co+h2o                                     1.02E+14    0.0        0.0
  12. co+h2o=>hco+oh                                     2.90E+15    0.0   105200.1
  13. co+oh=>co2+h                                       1.40E+05    1.9    -1347.0
  14. co2+h=>co+oh                                       1.57E+07    1.9    20990.0
  15. h+o2=>o+oh                                         1.97E+14    0.0    16539.9
  16. o+oh=>h+o2                                         1.56E+13    0.0      424.9
  17. o+h2=>h+oh                                         5.08E+04    2.7     6292.1
  18. h+oh=>o+h2                                         2.23E+04    2.7     4196.9
  19. o+h2o=>2oh                                         2.97E+06    2.0    13400.1
  20. 2oh=>o+h2o                                         3.01E+05    2.0    -3849.9
  21. oh+h2=>h+h2o                                       2.16E+08    1.5     3430.0
  22. h+h2o=>oh+h2                                       9.35E+08    1.5    18580.1
  23. hco+m=>h+co+m                                      1.86E+17   -1.0    17000.0
      h2              Enhanced by    2.500E+00
      h2o             Enhanced by    1.200E+01
      co              Enhanced by    1.900E+00
      co2             Enhanced by    3.800E+00
  24. h+co+m=>hco+m                                      6.47E+13    0.0     -441.9
      h2              Enhanced by    2.500E+00
```

```
    h2o             Enhanced by    1.200E+01
    co              Enhanced by    1.900E+00
    co2             Enhanced by    3.800E+00
 25. h2o2+oh=>h2o+ho2                                 1.00E+12    0.0        0.0
    Declared duplicate reaction...
 26. h2o+ho2=>h2o2+oh                                 1.68E+11    0.3    31460.1
    Declared duplicate reaction...
 27. c2h4+o=>ch3+hco                                  1.02E+07    1.9      179.0
 28. ch3+hco=>c2h4+o                                  2.85E+08    1.1    31770.1
 29. h+c2h4(+m)=>c2h5(+m)                             1.08E+12    0.5     1821.9
    h2              Enhanced by    2.000E+00
    h2o             Enhanced by    5.000E+00
    co              Enhanced by    2.000E+00
    co2             Enhanced by    3.000E+00
    Low pressure limit:  0.11120E+35 -0.50000E+01  0.44479E+04
    TROE centering:      0.10000E+01  0.10000E-14  0.95000E+02  0.20000E+03
 30. c2h5(+m)=>h+c2h4(+m)                             3.59E+14   -0.3    39570.0
    h2              Enhanced by    2.000E+00
    h2o             Enhanced by    5.000E+00
    co              Enhanced by    2.000E+00
    co2             Enhanced by    3.000E+00
    Low pressure limit:  0.36900E+37 -0.57900E+01  0.42196E+05
    TROE centering:      0.10000E+01  0.10000E-14  0.95000E+02  0.20000E+03
 31. ch3oh(+m)=>ch3+oh(+m)                            1.90E+16    0.0    91729.9
    h2              Enhanced by    2.000E+00
    h2o             Enhanced by    1.600E+01
    co              Enhanced by    2.000E+00
    co2             Enhanced by    3.000E+00
    Low pressure limit:  0.29500E+45 -0.73500E+01  0.95460E+05
    TROE centering:      0.41400E+00  0.27900E+03  0.54590E+04  0.10000+101
 32. ch3+oh(+m)=>ch3oh(+m)                            9.18E+10    1.0      745.0
    h2              Enhanced by    2.000E+00
    h2o             Enhanced by    1.600E+01
    co              Enhanced by    2.000E+00
    co2             Enhanced by    3.000E+00
    Low pressure limit:  0.14250E+40 -0.63500E+01  0.44751E+04
    TROE centering:      0.41400E+00  0.27900E+03  0.54590E+04  0.10000+101
 33. c2h6+h=>c2h5+h2                                  5.54E+02    3.5     5167.1
 34. c2h5+h2=>c2h6+h                                  1.36E-01    4.1     8857.1
 35. ch3oh+ho2=>ch2oh+h2o2                            3.98E+13    0.0    19400.1
 36. ch2oh+h2o2=>ch3oh+ho2                            3.13E+15   -0.9    10750.0
 37. c2h5+o2=>c2h4+ho2                                1.22E+30   -5.8    10099.9
 38. c2h4+ho2=>c2h5+o2                                1.26E+30   -5.6    22310.0
 39. c2h6+oh=>c2h5+h2o                                5.12E+06    2.1      854.9
 40. c2h5+h2o=>c2h6+oh                                1.01E+07    2.1    22979.9
 41. c2h6+o=>c2h5+oh                                  1.13E+14    0.0     7849.9
 42. c2h5+oh=>c2h6+o                                  2.08E+13    0.0    12719.9
 43. ch3+ho2=>ch3o+oh                                 1.10E+13    0.0        0.0
 44. ch3o+oh=>ch3+ho2                                 4.78E+14   -0.3    24550.0
 45. co+ho2=>co2+oh                                   3.01E+13    0.0    23000.0
 46. co2+oh=>co+ho2                                   6.44E+15   -0.3    84609.9
 47. 2ch3(+m)=>c2h6(+m)                               9.21E+16   -1.2      635.8
    h2              Enhanced by    2.000E+00
    h2o             Enhanced by    5.000E+00
    co              Enhanced by    2.000E+00
    co2             Enhanced by    3.000E+00
    Low pressure limit:  0.11350E+37 -0.52460E+01  0.17051E+04
    TROE centering:      0.40500E+00  0.11200E+04  0.69600E+02  0.10000E+16
 48. c2h6(+m)=>2ch3(+m)                               4.71E+21   -1.7    87409.9
    h2              Enhanced by    2.000E+00
    h2o             Enhanced by    5.000E+00
    co              Enhanced by    2.000E+00
    co2             Enhanced by    3.000E+00
    Low pressure limit:  0.58010E+41 -0.57760E+01  0.88479E+05
    TROE centering:      0.40500E+00  0.11200E+04  0.69600E+02  0.10000E+16
 49. h2o+m=>h+oh+m                                    1.84E+27   -3.0   122599.9
    h2              Enhanced by    2.500E+00
    h2o             Enhanced by    1.200E+01
```

```
    co              Enhanced by    1.900E+00
    co2             Enhanced by    3.800E+00
 50. h+oh+m=>h2o+m                                  2.25E+22   -2.0        0.0
    h2              Enhanced by    2.500E+00
    h2o             Enhanced by    1.200E+01
    co              Enhanced by    1.900E+00
    co2             Enhanced by    3.800E+00
 51. h+o2(+m)=>ho2(+m)                              1.48E+12    0.6        0.0
    h2              Enhanced by    2.500E+00
    h2o             Enhanced by    1.200E+01
    co              Enhanced by    1.900E+00
    co2             Enhanced by    3.800E+00
    Low pressure limit:  0.35000E+17 -0.41000E+00 -0.11159E+04
    TROE centering:      0.50000E+00  0.10000E-29  0.10000E+31  0.10000+101
 52. ho2(+m)=>h+o2(+m)                              5.05E+14   -0.1    49960.1
    h2              Enhanced by    2.500E+00
    h2o             Enhanced by    1.200E+01
    co              Enhanced by    1.900E+00
    co2             Enhanced by    3.800E+00
    Low pressure limit:  0.11990E+20 -0.10800E+01  0.48844E+05
    TROE centering:      0.50000E+00  0.10000E-29  0.10000E+31  0.10000+101
 53. co+o(+m)=>co2(+m)                              1.80E+10    0.0     2384.1
    h2              Enhanced by    2.500E+00
    h2o             Enhanced by    1.200E+01
    co              Enhanced by    1.900E+00
    co2             Enhanced by    3.800E+00
    Low pressure limit:  0.13500E+25 -0.27880E+01  0.41910E+04
 54. co2+m=>co+o+m                                  1.67E+16   -1.0   130099.9
    h2              Enhanced by    2.500E+00
    h2o             Enhanced by    1.200E+01
    co              Enhanced by    1.900E+00
    co2             Enhanced by    3.800E+00
 55. co+o2=>co2+o                                   1.07E-15    7.1    13320.0
 56. co2+o=>co+o2                                   9.44E-15    7.1    19539.9
 57. hco+h=>co+h2                                   7.34E+13    0.0        0.0
 58. co+h2=>hco+h                                   4.81E+14    0.0    90000.0
 59. hco+o=>co+oh                                   3.02E+13    0.0        0.0
 60. co+oh=>hco+o                                   8.70E+13    0.0    87900.1
 61. ch2o+m=>hco+h+m                                6.28E+29   -3.6    93200.1
 62. hco+h+m=>ch2o+m                                2.66E+24   -2.6      427.1
 63. ch2o+oh=>hco+h2o                               3.43E+09    1.2     -446.9
 64. hco+h2o=>ch2o+oh                               1.19E+09    1.2    29380.0
 65. ch2o+h=>hco+h2                                 9.33E+08    1.5     2976.1
 66. hco+h2=>ch2o+h                                 7.45E+07    1.5    17650.1
 67. ch2o+o=>hco+oh                                 4.16E+11    0.6     2761.9
 68. hco+oh=>ch2o+o                                 1.46E+10    0.6    15340.1
 69. ch3+oh=>ch2o+h2                                2.25E+13    0.0     4299.9
 70. ch2o+h2=>ch3+oh                                6.76E+14    0.0    76030.1
 71. ch3+o=>ch2o+h                                  8.00E+13    0.0        0.0
 72. ch2o+h=>ch3+o                                  1.06E+15    0.0    69630.0
 73. ch3+o2=>ch3o+o                                 2.00E+18   -1.6    29210.1
 74. ch3o+o=>ch3+o2                                 3.58E+18   -1.6    -1631.0
 75. ch2o+ch3=>hco+ch4                              3.64E-06    5.4      998.1
 76. hco+ch4=>ch2o+ch3                              7.58E-06    5.4    16150.1
 77. hco+ch3=>ch4+co                                1.21E+14    0.0        0.0
 78. ch4+co=>hco+ch3                                2.07E+16    0.0    90479.9
 79. ch3o(+m)=>ch2o+h(+m)                           5.45E+13    0.0    13500.0
    Low pressure limit:  0.23440E+26 -0.27000E+01  0.30600E+05
 80. ch2o+h+m=>ch3o+m                               3.81E+09    1.0    -7489.0
 81. c2h4(+m)=>c2h2+h2(+m)                          1.80E+13    0.0    76000.0
    Low pressure limit:  0.15000E+16  0.00000E+00  0.55443E+05
 82. c2h2+h2+m=>c2h4+m                              1.88E+11    0.2    34780.1
 83. ho2+o=>oh+o2                                   3.25E+13    0.0        0.0
 84. oh+o2=>ho2+o                                   7.86E+14   -0.3    55390.1
 85. hco+ho2=>ch2o+o2                               2.97E+10    0.3    -3860.9
 86. ch2o+o2=>hco+ho2                               2.05E+13    0.0    38950.1
 87. ch3o+o2=>ch2o+ho2                              5.50E+10    0.0     2424.0
 88. ch2o+ho2=>ch3o+o2                              1.32E+09    0.3    31390.1
```

```
 89. ch3+ho2=>ch4+o2                                   3.60E+12    0.0        0.0
 90. ch4+o2=>ch3+ho2                                   5.18E+15   -0.3    57960.1
 91. hco+o2=>co+ho2                                    7.58E+12    0.0      409.9
 92. co+ho2=>hco+o2                                    9.03E+11    0.3    32930.0
 93. ho2+h=>2oh                                        7.08E+13    0.0      299.9
 94. 2oh=>ho2+h                                        1.35E+14   -0.3    39570.0
 95. ho2+h=>h2+o2                                      1.66E+13    0.0      820.0
 96. h2+o2=>ho2+h                                      9.14E+14   -0.3    58299.9
 97. ho2+oh=>h2o+o2                                    2.89E+13    0.0     -500.0
 98. h2o+o2=>ho2+oh                                    6.89E+15   -0.3    72140.1
 99. h2o2+o2=>2ho2                                     5.94E+17   -0.7    53150.1
     Declared duplicate reaction...
100. 2ho2=>h2o2+o2                                     4.20E+14    0.0    11979.9
     Declared duplicate reaction...
101. 2oh(+m)=>h2o2(+m)                                 1.24E+14   -0.4        0.0
     h2              Enhanced by    2.500E+00
     h2o             Enhanced by    1.200E+01
     co              Enhanced by    1.900E+00
     co2             Enhanced by    3.800E+00
     Low pressure limit:  0.30410E+31 -0.46300E+01  0.20490E+04
     TROE centering:      0.47000E+00  0.10000E+03  0.20000E+04  0.10000E+16
102. h2o2(+m)=>2oh(+m)                                 3.14E+19   -1.4    51859.9
     h2              Enhanced by    2.500E+00
     h2o             Enhanced by    1.200E+01
     co              Enhanced by    1.900E+00
     co2             Enhanced by    3.800E+00
     Low pressure limit:  0.77210E+36 -0.56300E+01  0.53909E+05
     TROE centering:      0.47000E+00  0.10000E+03  0.20000E+04  0.10000E+16
103. h2o2+h=>h2o+oh                                    2.41E+13    0.0     3969.9
104. h2o+oh=>h2o2+h                                    7.75E+12    0.0    74710.1
105. ch4+ho2=>ch3+h2o2                                 3.42E+11    0.0    19289.9
106. ch3+h2o2=>ch4+ho2                                 3.36E+11   -0.3     2501.9
107. ch2o+ho2=>hco+h2o2                                5.82E-03    4.5     6556.9
108. hco+h2o2=>ch2o+ho2                                1.19E-02    4.2     4920.9
109. oh+m=>o+h+m                                       3.91E+22   -2.0   105299.9
     h2              Enhanced by    2.500E+00
     h2o             Enhanced by    1.200E+01
     co              Enhanced by    1.900E+00
     co2             Enhanced by    3.800E+00
110. o+h+m=>oh+m                                       4.72E+18   -1.0        0.0
     h2              Enhanced by    2.500E+00
     h2o             Enhanced by    1.200E+01
     co              Enhanced by    1.900E+00
     co2             Enhanced by    3.800E+00
111. o2+m=>2o+m                                        6.47E+20   -1.5   121500.0
     h2              Enhanced by    2.500E+00
     h2o             Enhanced by    1.200E+01
     co              Enhanced by    1.900E+00
     co2             Enhanced by    3.800E+00
112. 2o+m=>o2+m                                        6.17E+15   -0.5        0.0
     h2              Enhanced by    2.500E+00
     h2o             Enhanced by    1.200E+01
     co              Enhanced by    1.900E+00
     co2             Enhanced by    3.800E+00
113. h2+m=>2h+m                                        4.57E+19   -1.4   104400.1
     h2              Enhanced by    2.500E+00
     h2o             Enhanced by    1.200E+01
     co              Enhanced by    1.900E+00
     co2             Enhanced by    3.800E+00
114. 2h+m=>h2+m                                        2.42E+15   -0.4    -3039.9
     h2              Enhanced by    2.500E+00
     h2o             Enhanced by    1.200E+01
     co              Enhanced by    1.900E+00
     co2             Enhanced by    3.800E+00
115. c2h3+h(+m)=>c2h4(+m)                              6.10E+12    0.3      280.1
     Low pressure limit:  0.98000E+30 -0.38600E+01  0.33200E+04
     TROE centering:      0.78200E+00  0.20800E+03  0.26630E+04  0.60950E+04
116. c2h4(+m)=>c2h3+h(+m)                              1.69E+15    0.1   107099.9
```

```
     Low pressure limit:  0.27180E+33 -0.40300E+01  0.11014E+06
     TROE centering:      0.78200E+00  0.20800E+03  0.26630E+04  0.60950E+04
117. c2h5+c2h3=>2c2h4                                3.00E+12    0.0        0.0
118. 2c2h4=>c2h5+c2h3                                4.82E+14    0.0    71530.1
119. c2h2+h(+m)=>c2h3(+m)                            3.11E+11    0.6     2588.9
     h2              Enhanced by    2.000E+00
     h2o             Enhanced by    5.000E+00
     co              Enhanced by    2.000E+00
     co2             Enhanced by    3.000E+00
     Low pressure limit:  0.22540E+41 -0.72690E+01  0.65770E+04
     TROE centering:      0.10000E+01  0.10000E-14  0.67500E+03  0.10000E+16
120. c2h3(+m)=>c2h2+h(+m)                            2.03E+15   -0.4    44460.1
     h2              Enhanced by    2.000E+00
     h2o             Enhanced by    5.000E+00
     co              Enhanced by    2.000E+00
     co2             Enhanced by    3.000E+00
     Low pressure limit:  0.14700E+45 -0.82690E+01  0.48448E+05
     TROE centering:      0.10000E+01  0.10000E-14  0.67500E+03  0.10000E+16
121. c2h4+h=>c2h3+h2                                 8.42E-03    4.6     2582.9
122. c2h3+h2=>c2h4+h                                 5.72E-01    3.8     3233.0
123. c2h4+oh=>c2h3+h2o                               2.02E+13    0.0     5955.1
124. c2h3+h2o=>c2h4+oh                               1.02E+13    0.0    20219.9
125. c2h3+o2=>c2h2+ho2                               5.19E-15   -1.3     3310.0
     Declared duplicate reaction...
126. c2h2+ho2=>c2h3+o2                               2.73E-16   -0.9    11400.1
     Declared duplicate reaction...
127. c2h2+m=>c2h+h+m                                 4.20E+16    0.0   107000.0
128. c2h+h+m=>c2h2+m                                 7.13E+07    2.1   -28909.9
129. c2h2+o2=>hcco+oh                                2.00E+08    1.5    30099.9
130. hcco+oh=>c2h2+o2                                2.23E+05    1.5    25400.1
131. ch2+o2=>co+h2o                                  7.28E+19   -2.5     1809.0
132. co+h2o=>ch2+o2                                  8.51E+20   -2.5   179800.0
133. c2h2+oh=>c2h+h2o                                3.37E+07    2.0    14000.0
134. c2h+h2o=>c2h2+oh                                4.67E+03    3.1      685.0
135. o+c2h2=>c2h+oh                                  3.16E+15   -0.6    15000.0
136. c2h+oh=>o+c2h2                                  4.44E+10    0.5   -15570.0
137. c2h2+o=>ch2+co                                  6.12E+06    2.0     1900.1
138. ch2+co=>c2h2+o                                  1.15E+06    2.0    52570.0
139. c2h+o2=>hco+co                                  2.41E+12    0.0        0.0
140. hco+co=>c2h+o2                                  1.33E+16   -1.1   154099.9
141. c2h+o=>co+ch                                    1.81E+13    0.0        0.0
142. co+ch=>c2h+o                                    7.48E+16   -1.1    82130.0
143. ch2+o2=>hco+oh                                  1.29E+20   -3.3      283.9
144. hco+oh=>ch2+o2                                  5.31E+19   -3.3    73169.9
145. ch2+o=>co+2h                                    5.00E+13    0.0        0.0
146. co+2h=>ch2+o                                    0.00E+00    0.0        0.0
147. ch2+h=>ch+h2                                    1.00E+18   -1.6        0.0
148. ch+h2=>ch2+h                                    7.03E+17   -1.6     2990.0
149. ch2+oh=>ch+h2o                                  1.13E+07    2.0     3000.0
150. ch+h2o=>ch2+oh                                  3.44E+07    2.0    21150.1
151. ch2+o2=>co2+2h                                  3.29E+21   -3.3     2868.1
152. co2+2h=>ch2+o2                                  0.00E+00    0.0        0.0
153. ch+o2=>hco+o                                    3.30E+13    0.0        0.0
154. hco+o=>ch+o2                                    4.40E+13    0.0    71990.0
155. ch3oh+oh=>ch2oh+h2o                             7.10E+06    1.8     -596.1
156. ch2oh+h2o=>ch3oh+oh                             3.29E+01    3.5    22719.9
157. ch3oh+h=>ch3o+h2                                3.60E+12    0.0     6094.9
158. ch3o+h2=>ch3oh+h                                7.47E+12    0.0     7825.1
159. ch3oh+h=>ch2oh+h2                               1.44E+13    0.0     6094.9
160. ch2oh+h2=>ch3oh+h                               1.54E+07    1.7    14250.0
161. ch3oh+ch3=>ch2oh+ch4                            3.19E+01    3.2     7172.1
162. ch2oh+ch4=>ch3oh+ch3                            8.93E-04    4.8    15810.0
163. ch3oh+o=>ch2oh+oh                               3.88E+05    2.5     3080.1
164. ch2oh+oh=>ch3oh+o                               4.96E+03    2.5     8781.1
165. ch2oh+o2=>ch2o+ho2                              3.81E+06    2.0     1641.0
166. ch2o+ho2=>ch2oh+o2                              1.77E+11    0.7    24180.0
167. ch2oh(+m)=>ch2o+h(+m)                           2.80E+14   -0.7    32820.0
     Low pressure limit:  0.60100E+34 -0.53900E+01  0.36200E+05
```

```
     TROE centering:      0.96000E+00  0.67600E+02  0.18550E+04  0.75430E+04
168. ch2o+h(+m)=>ch2oh(+m)                          3.79E+16   -1.4     5402.0
     Low pressure limit:  0.81390E+36 -0.60500E+01  0.87820E+04
     TROE centering:      0.96000E+00  0.67600E+02  0.18550E+04  0.75430E+04
169. c2h3+o2=>c2h2+ho2                              2.12E-06    6.0     9484.0
     Declared duplicate reaction...
170. c2h2+ho2=>c2h3+o2                              1.11E-07    6.3    17570.0
     Declared duplicate reaction...
171. h2o2+o=>oh+ho2                                 9.55E+06    2.0     3969.9
172. oh+ho2=>h2o2+o                                 2.54E+07    1.7    19849.9
173. c2h2+o=>hcco+h                                 1.43E+07    2.0     1900.1
174. hcco+h=>c2h2+o                                 2.02E+05    2.0    13310.0
175. c2h2+oh=>ch2co+h                               2.19E-04    4.5    -1000.0
176. ch2co+h=>c2h2+oh                               2.16E-03    4.5    19669.9
177. ch2co+h=>ch3+co                                1.10E+13    0.0     3400.1
178. ch3+co=>ch2co+h                                2.40E+12    0.0    40200.1
179. ch2co+o=>ch2+co2                               1.75E+12    0.0     1349.9
180. ch2+co2=>ch2co+o                               3.74E+12    0.0    53690.0
181. ch2+o2=>ch2o+o                                 3.29E+21   -3.3     2868.1
182. ch2o+o=>ch2+o2                                 3.86E+22   -3.3    63180.0
183. ch2co(+m)=>ch2+co(+m)                          3.00E+14    0.0    70979.9
     Low pressure limit:  0.36000E+16  0.00000E+00  0.59270E+05
184. ch2+co+m=>ch2co+m                              6.91E+08    1.0    -4359.9
185. ch2co+o=>hcco+oh                               1.00E+13    0.0     8000.0
186. hcco+oh=>ch2co+o                               1.43E+10    0.0    -1255.0
187. ch2co+oh=>hcco+h2o                             1.00E+13    0.0     2000.0
188. hcco+h2o=>ch2co+oh                             1.41E+11    0.0     9995.0
189. ch2co+h=>hcco+h2                               2.00E+14    0.0     8000.0
190. hcco+h2=>ch2co+h                               6.52E+11    0.0      840.1
191. hcco+oh=>2hco                                  1.00E+13    0.0        0.0
192. 2hco=>hcco+oh                                  4.82E+13    0.0    40359.9
193. hcco+h=>ch2(s)+co                              1.10E+14    0.0        0.0
194. ch2(s)+co=>hcco+h                              6.66E+13    0.0    39260.0
195. hcco+o=>h+2co                                  8.00E+13    0.0        0.0
196. h+2co=>hcco+o                                  0.00E+00    0.0        0.0
197. c2h6+o2=>c2h5+ho2                              4.00E+13    0.0    50900.1
198. c2h5+ho2=>c2h6+o2                              3.00E+11    0.0        0.0
199. c2h6+ho2=>c2h5+h2o2                            1.70E+13    0.0    20460.1
200. c2h5+h2o2=>c2h6+ho2                            1.07E+11    0.2     7842.0
201. ch2+o2=>co2+h2                                 1.01E+21   -3.3     1507.9
202. co2+h2=>ch2+o2                                 3.05E+23   -3.3   186700.0
203. ch3+c2h3=>ch4+c2h2                             3.92E+11    0.0        0.0
204. ch4+c2h2=>ch3+c2h3                             2.96E+13    0.0    66049.9
205. ch3+c2h5=>ch4+c2h4                             1.95E+13   -0.5        0.0
206. ch4+c2h4=>ch3+c2h5                             2.90E+16   -0.7    70169.9
207. ch3oh+ch2o=>2ch3o                              3.84E+13    0.1    84719.9
208. 2ch3o=>ch3oh+ch2o                              6.03E+13    0.0        0.0
209. ch2o+ch3o=>ch3oh+hco                           1.15E+11    0.0     1280.1
210. ch3oh+hco=>ch2o+ch3o                           3.02E+11    0.0    18159.9
211. ch4+ch3o=>ch3+ch3oh                            1.57E+11    0.0     8842.0
212. ch3+ch3oh=>ch4+ch3o                            1.05E+09    0.0    50000.0
213. c2h6+ch3o=>c2h5+ch3oh                          3.00E+11    0.0     7000.0
214. c2h5+ch3oh=>c2h6+ch3o                          1.71E+10    0.0    50000.0
215. c2h3+h=>c2h2+h2                                2.00E+13    0.0     2500.0
216. c2h2+h2=>c2h3+h                                1.33E+13    0.0    68080.1
217. ch3o+ch3oh=>ch2oh+ch3oh                        3.00E+11    0.0     4074.1
218. ch2oh+ch3oh=>ch3o+ch3oh                        1.55E+05    1.7    10500.0
219. ch3oh+oh=>ch3o+h2o                             1.00E+06    2.1      496.6
220. ch3o+h2o=>ch3oh+oh                             8.98E+06    2.1    17380.0
221. c2h5+h=>2ch3                                   3.61E+13    0.0        0.0
222. 2ch3=>c2h5+h                                   5.45E+16   -1.0    16979.9
223. c2h3+o2=>ch2o+hco                              1.70E+29   -5.3     6500.0
224. ch2o+hco=>c2h3+o2                              1.66E+29   -5.3    93049.9
225. c2h6=>c2h5+h                                   2.78E+21   -1.6   103799.9
226. c2h5+h=>c2h6                                   3.61E+13    0.0        0.0
227. pc2h4oh=>c2h4+oh                               1.29E+12   -0.4    26849.9
228. c2h4+oh=>pc2h4oh                               9.93E+11    0.0     -960.1
229. c2h4+ch3=>c2h3+ch4                             6.62E+00    3.7     9500.0
```

```
230. c2h3+ch4=>c2h4+ch3                                1.44E+00    4.0     5472.0
231. ch3co(+m)=>ch3+co(+m)                             3.00E+12    0.0    16719.9
     Low pressure limit:  0.12000E+16  0.00000E+00  0.12518E+05
232. ch3+co+m=>ch3co+m                                 9.62E+11   -0.1     9778.0
233. ch3cho=>ch3+hco                                   2.61E+15    0.1    80549.9
234. ch3+hco=>ch3cho                                   2.00E+13    0.0        0.0
235. ch3cho+o2=>ch3co+ho2                              3.01E+13    0.0    39150.1
236. ch3co+ho2=>ch3cho+o2                              8.55E+10    0.3    -1940.0
237. ch3cho+oh=>ch3co+h2o                              2.00E+06    1.8     1300.0
238. ch3co+h2o=>ch3cho+oh                              1.35E+06    1.8    32849.9
239. ch3cho+h=>ch3co+h2                                1.34E+13    0.0     3299.9
240. ch3co+h2=>ch3cho+h                                2.10E+12    0.0    19690.0
241. ch3cho+o=>ch3co+oh                                5.94E+12    0.0     1868.1
242. ch3co+oh=>ch3cho+o                                4.08E+11    0.0    16169.9
243. ch3cho+ho2=>ch3co+h2o2                            3.01E+12    0.0    11930.0
244. ch3co+h2o2=>ch3cho+ho2                            1.21E+13   -0.3    12010.0
245. ch3cho+ch3=>ch3co+ch4                             2.61E+06    1.8     5911.1
246. ch3co+ch4=>ch3cho+ch3                             1.07E+07    1.8    22789.9
247. c3h5-s=>c2h2+ch3                                  9.60E+39   -8.2    42030.1
248. c2h2+ch3=>c3h5-s                                  1.61E+40   -8.6    20330.1
249. c2h2+ch3=>c3h4-p+h                                1.21E+17   -1.2    16680.0
250. c3h4-p+h=>c2h2+ch3                                1.00E+14    0.0     4000.0
251. c3h5-a=>c2h2+ch3                                  2.40E+48   -9.9    82080.1
252. c2h2+ch3=>c3h5-a                                  2.61E+46   -9.8    36950.1
253. c3h6=>c2h3+ch3                                    2.73E+62  -13.3   123200.1
254. c2h3+ch3=>c3h6                                    4.71E+59  -13.2    29539.9
255. c2h2+ch3=>c3h4-a+h                                6.74E+19   -2.1    31590.1
256. c3h4-a+h=>c2h2+ch3                                1.15E+16   -0.7    15789.9
257. c3h6=>c3h5-a+h                                    2.01E+61  -13.3   118500.0
258. c3h5-a+h=>c3h6                                    4.89E+56  -12.2    28080.1
259. c3h6+o=>ch2co+ch3+h                               2.50E+07    1.8       76.0
260. ch2co+ch3+h=>c3h6+o                               0.00E+00    0.0        0.0
261. c3h6+o=>c2h5+hco                                  1.58E+07    1.8    -1216.1
262. c2h5+hco=>c3h6+o                                  1.40E+05    1.9    26510.0
263. c3h6+o=>ch3chco+2h                                2.50E+07    1.8       76.0
264. ch3chco+2h=>c3h6+o                                0.00E+00    0.0        0.0
265. c3h6=>c3h5-s+h                                    7.71E+69  -16.1   140000.0
266. c3h5-s+h=>c3h6                                    1.22E+63  -14.6    26159.9
267. c3h6+ho2=>c3h5-a+h2o2                             1.50E+11    0.0    14190.0
268. c3h5-a+h2o2=>c3h6+ho2                             5.87E+05    1.3     9759.1
269. c3h6+ho2=>c3h5-s+h2o2                             7.50E+09    0.0    12570.0
270. c3h5-s+h2o2=>c3h6+ho2                             2.31E+04    1.3   -13419.9
271. c3h6+ho2=>c3h5-t+h2o2                             3.00E+09    0.0     9930.0
272. c3h5-t+h2o2=>c3h6+ho2                             9.23E+03    1.3   -14060.0
273. c3h6+oh=>c3h5-a+h2o                               3.12E+06    2.0     -298.0
274. c3h5-a+h2o=>c3h6+oh                               6.19E+06    2.0    31880.0
275. c3h6+oh=>c3h5-s+h2o                               2.11E+06    2.0     2778.0
276. c3h5-s+h2o=>c3h6+oh                               2.72E+04    2.5    11530.1
277. c4h6=>2c2h3                                       4.03E+19   -1.0    98150.1
278. 2c2h3=>c4h6                                       1.26E+13    0.0        0.0
279. c4h6+oh=>c2h5+ch2co                               1.00E+12    0.0        0.0
280. c2h5+ch2co=>c4h6+oh                               3.73E+12    0.0    30020.1
281. c4h6+oh=>ch2o+c3h5-a                              1.00E+12    0.0        0.0
282. ch2o+c3h5-a=>c4h6+oh                              3.50E+06    0.0    71060.0
283. c4h6+oh=>c2h3+ch3cho                              1.00E+12    0.0        0.0
284. c2h3+ch3cho=>c4h6+oh                              5.44E+11    0.0    18550.0
285. c4h6+o=>c2h4+ch2co                                1.00E+12    0.0        0.0
286. c2h4+ch2co=>c4h6+o                                6.38E+11    0.0    94340.1
287. c4h6+o=>ch2o+c3h4-a                               1.00E+12    0.0        0.0
288. ch2o+c3h4-a=>c4h6+o                               1.08E+12    0.0    79049.9
289. c2h4+o2=>c2h3+ho2                                 4.00E+13    0.0    58200.1
290. c2h3+ho2=>c2h4+o2                                 4.94E+13   -0.5     1368.1
291. ch2o+m=>co+h2+m                                   1.83E+32   -4.4    87120.0
292. co+h2+m=>ch2o+m                                   5.07E+27   -3.4    84349.9
293. nc3h7=>ch3+c2h4                                   2.28E+14   -0.6    28400.1
294. ch3+c2h4=>nc3h7                                   4.10E+11    0.0     7204.1
295. nc3h7=>h+c3h6                                     2.67E+15   -0.6    36820.0
296. h+c3h6=>nc3h7                                     1.00E+13    0.0     2500.0
```

297.	nc3h7+o2=>c3h6+ho2	3.00E+11	0.0	3000.0
298.	c3h6+ho2=>nc3h7+o2	2.00E+11	0.0	17500.0
299.	c2h4+ch3o=>c2h3+ch3oh	1.20E+11	0.0	6750.0
300.	c2h3+ch3oh=>c2h4+ch3o	1.00E+10	0.0	9000.0
301.	c3h6+oh=>c3h5-t+h2o	1.11E+06	2.0	1451.0
302.	c3h5-t+h2o=>c3h6+oh	3.28E+03	2.7	12310.0
303.	c3h6+o=>c3h5-a+oh	5.24E+11	0.7	5884.1
304.	c3h5-a+oh=>c3h6+o	1.06E+11	0.7	20820.0
305.	c3h6+o=>c3h5-s+oh	1.20E+11	0.7	8958.9
306.	c3h5-s+oh=>c3h6+o	1.57E+08	1.2	460.1
307.	c3h6+o=>c3h5-t+oh	6.03E+10	0.7	7631.9
308.	c3h5-t+oh=>c3h6+o	1.80E+07	1.4	1243.1
309.	c3h6+h=>c3h5-a+h2	1.73E+05	2.5	2492.1
310.	c3h5-a+h2=>c3h6+h	7.93E+04	2.5	19520.1
311.	c3h6+o2=>c3h5-s+ho2	2.00E+12	0.0	62900.1
312.	c3h5-s+ho2=>c3h6+o2	1.08E+08	0.8	-984.0
313.	c3h6+h=>c2h4+ch3	4.83E+33	-5.8	18500.0
314.	c2h4+ch3=>c3h6+h	2.31E+33	-5.9	31620.0
315.	ic3h7=>h+c3h6	8.57E+18	-1.6	40340.1
316.	h+c3h6=>ic3h7	1.30E+13	0.0	1560.0
317.	ic3h7+h=>c3h6+h2	2.00E+13	0.0	0.0
318.	c3h6+h2=>ic3h7+h	4.82E+09	0.7	12090.1
319.	ic3h7+o2=>c3h6+ho2	4.50E+11	0.0	5020.1
320.	c3h6+ho2=>ic3h7+o2	2.00E+11	0.0	17500.0
321.	c3h8=>ch3+c2h5	7.90E+22	-1.8	88630.0
322.	ch3+c2h5=>c3h8	3.66E+14	-0.4	989.0
323.	c3h8+o2=>ic3h7+ho2	4.00E+13	0.0	47500.0
324.	ic3h7+ho2=>c3h8+o2	2.08E+12	0.0	0.0
325.	c3h8+o2=>nc3h7+ho2	4.00E+13	0.0	47500.0
326.	nc3h7+ho2=>c3h8+o2	2.08E+12	0.0	0.0
327.	h+c3h8=>h2+ic3h7	1.30E+06	2.4	4471.1
328.	h2+ic3h7=>h+c3h8	4.71E+05	2.1	12180.0
329.	h+c3h8=>h2+nc3h7	1.88E+05	2.8	6280.1
330.	h2+nc3h7=>h+c3h8	2.76E+01	3.4	9530.1
331.	c3h8+o=>ic3h7+oh	2.81E+13	0.0	5200.1
332.	ic3h7+oh=>c3h8+o	1.87E+12	0.0	9607.1
333.	c3h8+o=>nc3h7+oh	1.13E+14	0.0	7849.9
334.	nc3h7+oh=>c3h8+o	7.53E+12	0.0	12260.0
335.	c3h8+oh=>nc3h7+h2o	1.05E+10	1.0	1586.0
336.	nc3h7+h2o=>c3h8+oh	6.93E+09	1.0	23250.0
337.	c3h8+oh=>ic3h7+h2o	4.67E+07	1.6	-34.9
338.	ic3h7+h2o=>c3h8+oh	3.07E+07	1.6	21630.0
339.	c3h8+ho2=>ic3h7+h2o2	5.60E+12	0.0	17700.0
340.	ic3h7+h2o2=>c3h8+ho2	4.16E+11	0.0	7425.9
341.	c3h8+ho2=>nc3h7+h2o2	1.68E+13	0.0	20430.0
342.	nc3h7+h2o2=>c3h8+ho2	2.33E+12	0.0	9826.0
343.	ch3+c3h8=>ch4+ic3h7	3.98E+11	0.0	9500.0
344.	ch4+ic3h7=>ch3+c3h8	1.58E+12	0.0	16479.9
345.	ch3+c3h8=>ch4+nc3h7	1.29E+12	0.0	11599.9
346.	ch4+nc3h7=>ch3+c3h8	5.13E+12	0.0	18580.1
347.	ic3h7+c3h8=>nc3h7+c3h8	3.00E+10	0.0	12900.1
348.	nc3h7+c3h8=>ic3h7+c3h8	3.00E+10	0.0	12900.1
349.	c2h3+c3h8=>c2h4+ic3h7	1.00E+11	0.0	10400.1
350.	c2h4+ic3h7=>c2h3+c3h8	1.31E+11	0.0	17800.0
351.	c2h3+c3h8=>c2h4+nc3h7	1.00E+11	0.0	10400.1
352.	c2h4+nc3h7=>c2h3+c3h8	1.31E+11	0.0	17800.0
353.	c2h5+c3h8=>c2h6+ic3h7	1.00E+11	0.0	10400.1
354.	c2h6+ic3h7=>c2h5+c3h8	3.63E+10	0.0	9934.0
355.	c2h5+c3h8=>c2h6+nc3h7	1.00E+11	0.0	10400.1
356.	c2h6+nc3h7=>c2h5+c3h8	3.63E+10	0.0	9934.0
357.	c3h8+c3h5-a=>ic3h7+c3h6	2.00E+11	0.0	16099.9
358.	ic3h7+c3h6=>c3h8+c3h5-a	3.98E+10	0.0	9700.0
359.	c3h8+c3h5-a=>nc3h7+c3h6	7.94E+11	0.0	20500.0
360.	nc3h7+c3h6=>c3h8+c3h5-a	1.00E+11	0.0	9800.0
361.	c3h8+ch3o=>nc3h7+ch3oh	3.00E+11	0.0	7000.0
362.	nc3h7+ch3oh=>c3h8+ch3o	1.22E+10	0.0	9181.9
363.	c3h8+ch3o=>ic3h7+ch3oh	3.00E+11	0.0	7000.0
364.	ic3h7+ch3oh=>c3h8+ch3o	1.22E+10	0.0	9181.9

365. c5h9=>c3h5-a+c2h4	2.50E+13	0.0	45000.0
366. c3h5-a+c2h4=>c5h9	0.00E+00	0.0	0.0
367. c5h9=>c2h3+c3h6	2.50E+13	0.0	30000.0
368. c2h3+c3h6=>c5h9	1.50E+10	0.0	7400.1
369. c4h7=>c4h6+h	1.20E+14	0.0	49299.9
370. c4h6+h=>c4h7	4.00E+13	0.0	1300.0
371. c4h7=>c2h4+c2h3	1.00E+11	0.0	37000.0
372. c2h4+c2h3=>c4h7	5.00E+10	0.0	7000.0
373. c4h8-1+c4h6=>2c4h7	2.35E+12	0.0	46719.9
374. 2c4h7=>c4h8-1+c4h6	1.60E+12	0.0	0.0
375. c4h7+ch3=>c4h6+ch4	8.00E+12	0.0	0.0
376. c4h6+ch4=>c4h7+ch3	7.05E+13	0.0	57280.1
377. c3h5-a+c4h7=>c3h6+c4h6	6.31E+12	0.0	0.0
378. c3h6+c4h6=>c3h5-a+c4h7	1.00E+10	0.0	50000.0
379. c4h7+o2=>c4h6+ho2	1.00E+09	0.0	0.0
380. c4h6+ho2=>c4h7+o2	1.00E+11	0.0	17000.0
381. h+c4h7=>c4h6+h2	3.16E+13	0.0	0.0
382. c4h6+h2=>h+c4h7	1.07E+13	0.0	56810.0
383. c2h5+c4h7=>c4h6+c2h6	3.98E+12	0.0	0.0
384. c4h6+c2h6=>c2h5+c4h7	3.21E+12	0.0	49840.1
385. c2h5+c4h7=>c2h4+c4h8-1	9.24E+06	1.5	-962.0
386. c2h4+c4h8-1=>c2h5+c4h7	7.81E+02	2.9	50960.1
387. c2h3+c4h7=>c2h4+c4h6	3.98E+12	0.0	0.0
388. c2h4+c4h6=>c2h3+c4h7	1.16E+13	0.0	57710.1
389. c4h8-1=>c3h5-a+ch3	5.00E+15	0.0	71000.0
390. c3h5-a+ch3=>c4h8-1	5.00E+12	0.0	0.0
391. c4h8-1=>c2h3+c2h5	1.00E+19	-1.0	96770.1
392. c2h3+c2h5=>c4h8-1	9.00E+12	0.0	0.0
393. c4h8-1=>h+c4h7	4.11E+18	-1.0	97349.9
394. h+c4h7=>c4h8-1	5.00E+13	0.0	0.0
395. c4h8-1+ch3=>c4h7+ch4	1.00E+11	0.0	7299.9
396. c4h7+ch4=>c4h8-1+ch3	6.00E+11	0.0	17859.9
397. c4h8-1+h=>c4h7+h2	5.00E+13	0.0	3900.1
398. c4h7+h2=>c4h8-1+h	4.00E+13	0.0	25200.0
399. c4h8-1+oh=>c4h7+h2o	2.25E+13	0.0	2217.0
400. c4h7+h2o=>c4h8-1+oh	4.77E+12	0.0	26469.9
401. c4h8-1+c3h5-a=>c4h7+c3h6	7.90E+10	0.0	12400.1
402. c4h7+c3h6=>c4h8-1+c3h5-a	1.00E+11	0.0	17500.0
403. c4h8-1+ho2=>c4h7+h2o2	1.40E+12	0.0	14900.1
404. c4h7+h2o2=>c4h8-1+ho2	3.16E+11	0.0	13000.0
405. c4h8-1+o2=>c4h7+ho2	2.70E+13	0.0	33200.1
406. c4h7+ho2=>c4h8-1+o2	3.00E+11	0.0	0.0
407. sc4h9=>c3h6+ch3	7.37E+17	-1.4	30229.9
408. c3h6+ch3=>sc4h9	3.30E+11	0.0	7200.1
409. sc4h9=>c4h8-1+h	3.59E+20	-2.1	40969.9
410. c4h8-1+h=>sc4h9	1.00E+13	0.0	1200.0
411. sc4h9+o2=>c4h8-1+ho2	4.50E-19	0.0	5020.1
412. c4h8-1+ho2=>sc4h9+o2	2.00E-19	0.0	17500.0
413. pc4h9=>c2h5+c2h4	7.50E+17	-1.4	29580.1
414. c2h5+c2h4=>pc4h9	3.30E+11	0.0	7200.1
415. pc4h9=>c4h8-1+h	1.16E+17	-1.2	38159.9
416. c4h8-1+h=>pc4h9	1.00E+13	0.0	2900.1
417. pc4h9+o2=>c4h8-1+ho2	3.00E-19	0.0	3000.0
418. c4h8-1+ho2=>pc4h9+o2	2.00E-19	0.0	17500.0
419. ch3coch3=>ch3co+ch3	1.22E+23	-2.0	83950.1
420. ch3co+ch3=>ch3coch3	1.00E+13	0.0	0.0
421. ch3coch3+oh=>ch3coch2+h2o	1.05E+10	1.0	1586.0
422. ch3coch2+h2o=>ch3coch3+oh	6.93E+09	1.0	23250.0
423. ch3coch3+h=>ch3coch2+h2	5.63E+07	2.0	7700.1
424. ch3coch2+h2=>ch3coch3+h	9.00E+12	0.0	145000.0
425. ch3coch3+o=>ch3coch2+oh	1.13E+14	0.0	7849.9
426. ch3coch2+oh=>ch3coch3+o	7.50E+12	0.0	12300.0
427. ch3coch3+ch3=>ch3coch2+ch4	3.96E+11	0.0	9783.9
428. ch3coch2+ch4=>ch3coch3+ch3	5.38E+08	0.9	17539.9
429. ch3coch3+ch3o=>ch3coch2+ch3oh	1.00E+11	0.0	7000.0
430. ch3coch2+ch3oh=>ch3coch3+ch3o	1.00E+10	0.0	9000.0
431. ch3coch2=>ch2co+ch3	1.00E+14	0.0	31000.0
432. ch2co+ch3=>ch3coch2	1.00E+11	0.0	6000.0

```
433. ch3coch3+o2=>ch3coch2+ho2                         1.20E+14    0.0    46000.0
434. ch3coch2+ho2=>ch3coch3+o2                         2.00E+12    0.0     2000.0
435. ch3coch3+ho2=>ch3coch2+h2o2                       1.70E+13    0.0    20460.1
436. ch3coch2+h2o2=>ch3coch3+ho2                       1.00E+11    0.0     8000.0
437. c2h5co=>c2h5+co                                   1.83E+15   -0.7    12909.9
438. c2h5+co=>c2h5co                                   1.51E+11    0.0     4810.0
439. c2h5cho+h=>c2h5co+h2                              3.98E+13    0.0     4200.1
440. c2h5co+h2=>c2h5cho+h                              1.78E+13    0.0    23669.9
441. c2h5cho+o=>c2h5co+oh                              5.01E+12    0.0     1789.9
442. c2h5co+oh=>c2h5cho+o                              1.00E+12    0.0    19159.9
443. c2h5cho+oh=>c2h5co+h2o                            2.69E+10    0.8     -340.1
444. c2h5co+h2o=>c2h5cho+oh                            1.70E+10    0.8    31200.0
445. c2h5cho+ch3=>c2h5co+ch4                           2.61E+06    1.8     5911.1
446. c2h5co+ch4=>c2h5cho+ch3                           9.97E+06    1.8    22780.1
447. c2h5cho+ho2=>c2h5co+h2o2                          1.00E+12    0.0    11000.0
448. c2h5co+h2o2=>c2h5cho+ho2                          1.00E+12    0.0    14000.0
449. c2h5cho+ch3o=>c2h5co+ch3oh                        1.00E+12    0.0     3299.9
450. c2h5co+ch3oh=>c2h5cho+ch3o                        3.16E+11    0.0    18000.0
451. c2h5cho+c2h5=>c2h5co+c2h6                         1.00E+12    0.0     8000.0
452. c2h5co+c2h6=>c2h5cho+c2h5                         1.58E+13    0.0    28000.0
453. c2h5cho=>c2h5+hco                                 9.85E+18   -0.7    81710.1
454. c2h5+hco=>c2h5cho                                 1.81E+13    0.0        0.0
455. c2h5cho+o2=>c2h5co+ho2                            2.00E+13    0.5    42200.1
456. c2h5co+ho2=>c2h5cho+o2                            1.91E+14    0.5     3090.1
457. c2h5cho+nc3h7=>c2h5co+c3h8                        1.70E+12    0.0     8440.0
458. c2h5co+c3h8=>c2h5cho+nc3h7                        1.90E+14    0.0    18789.9
459. c2h5cho+ic3h7=>c2h5co+c3h8                        1.70E+12    0.0     8440.0
460. c2h5co+c3h8=>c2h5cho+ic3h7                        1.90E+14    0.0    18789.9
461. c2h5cho+c2h3=>c2h5co+c2h4                         1.70E+12    0.0     8440.0
462. c2h5co+c2h4=>c2h5cho+c2h3                         2.49E+14    0.0    26190.0
463. c2h5cho+c3h5-a=>c2h5co+c3h6                       1.70E+12    0.0     8440.0
464. c2h5co+c3h6=>c2h5cho+c3h5-a                       1.00E+13    0.0    28000.0
465. c5h10-1=>c2h5+c3h5-a                              1.00E+16    0.0    71400.1
466. c2h5+c3h5-a=>c5h10-1                              1.00E+13    0.0        0.0
467. c5h10-1+h=>c5h9+h2                                2.80E+13    0.0     4000.0
468. c5h9+h2=>c5h10-1+h                                1.00E+12    0.0    14000.0
469. c5h10-1+o=>c5h9+oh                                2.54E+05    2.6    -1130.0
470. c5h9+oh=>c5h10-1+o                                7.00E+11    0.0    29900.1
471. c5h10-1+o=>pc4h9+hco                              1.00E+11    0.0        0.0
472. pc4h9+hco=>c5h10-1+o                              0.00E+00    0.0        0.0
473. c5h10-1+o=>nc3h7+ch3co                            1.00E+11    0.0        0.0
474. nc3h7+ch3co=>c5h10-1+o                            0.00E+00    0.0        0.0
475. c5h10-1+oh=>c5h9+h2o                              6.80E+13    0.0     3060.0
476. c5h9+h2o=>c5h10-1+oh                              5.00E+12    0.0    26500.0
477. c5h10-1+oh=>pc4h9+ch2o                            1.00E+11    0.0        0.0
478. pc4h9+ch2o=>c5h10-1+oh                            0.00E+00    0.0        0.0
479. c5h10-1+oh=>nc3h7+ch3cho                          1.00E+11    0.0        0.0
480. nc3h7+ch3cho=>c5h10-1+oh                          0.00E+00    0.0        0.0
481. c5h10-1+ch3=>c5h9+ch4                             1.00E+11    0.0     7299.9
482. c5h9+ch4=>c5h10-1+ch3                             6.00E+11    0.0    17900.1
483. h2o2+h=>h2+ho2                                    4.82E+13    0.0     7950.1
484. h2+ho2=>h2o2+h                                    1.88E+12    0.3    24260.0
485. hco+o=>co2+h                                      3.00E+13    0.0        0.0
486. co2+h=>hco+o                                      9.68E+15    0.0   110200.1
487. ch3+m=>ch2+h+m                                    1.97E+16    0.0    92520.1
488. ch2+h+m=>ch3+m                                    2.11E+11    1.0   -19620.0
489. ch3+h=>ch2+h2                                     9.00E+13    0.0    15099.9
490. ch2+h2=>ch3+h                                     1.82E+13    0.0    10400.1
491. ch3+oh=>ch2+h2o                                   3.00E+06    2.0     2500.0
492. ch2+h2o=>ch3+oh                                   2.62E+06    2.0    12960.1
493. ch+ch4=>c2h4+h                                    6.00E+13    0.0        0.0
494. c2h4+h=>ch+ch4                                    3.57E+14    0.0    55479.9
495. ch3oh(+m)=>ch2oh+h(+m)                            2.69E+16   -0.1    98940.0
     Low pressure limit:  0.23400E+41 -0.63300E+01  0.10310E+06
     TROE centering:      0.77300E+00  0.69300E+03  0.53330E+04  0.10000+101
496. ch2oh+h(+m)=>ch3oh(+m)                            1.53E+06    2.6     -342.0
     Low pressure limit:  0.13290E+31 -0.36700E+01  0.38179E+04
     TROE centering:      0.77300E+00  0.69300E+03  0.53330E+04  0.10000+101
```

```
497. ch3co+h=>ch2co+h2                          2.00E+13    0.0        0.0
498. ch2co+h2=>ch3co+h                          7.27E+09    0.0    83039.9
499. ch3co+o=>ch2co+oh                          2.00E+13    0.0        0.0
500. ch2co+oh=>ch3co+o                          7.27E+09    0.0    83039.9
501. ch3co+ch3=>ch2co+ch4                       5.00E+13    0.0        0.0
502. ch2co+ch4=>ch3co+ch3                       7.27E+09    0.0    83039.9
503. c2h4+o=>ch2cho+h                           3.39E+06    1.9      179.0
504. ch2cho+h=>c2h4+o                           9.48E+06    1.8    16050.0
505. c2h5+o=>ch3cho+h                           5.00E+13    0.0        0.0
506. ch3cho+h=>c2h5+o                           9.00E+13    0.0    72680.0
507. c2h6+ch=>c2h5+ch2                          1.10E+14    0.0     -260.0
508. c2h5+ch2=>c2h6+ch                          3.83E+10    0.6      440.0
509. ch2oh+ch2o=>ch3oh+hco                      1.29E-01    4.6     6596.1
510. ch3oh+hco=>ch2oh+ch2o                      9.63E+03    2.9    13109.9
511. c3h6+o2=>c3h5-t+ho2                        1.40E+12    0.0    60700.1
512. c3h5-t+ho2=>c3h6+o2                        1.73E+07    1.0    -1074.1
513. c2h3+c2h4=>c4h6+h                          5.00E+11    0.0     7299.9
514. c4h6+h=>c2h3+c2h4                          1.00E+13    0.0     4700.1
515. c5h11-1=>c2h4+nc3h7                        7.97E+17   -1.4    29789.9
516. c2h4+nc3h7=>c5h11-1                        3.30E+11    0.0     7200.1
517. c5h11-1=>h+c5h10-1                         3.48E+15   -0.7    37880.0
518. h+c5h10-1=>c5h11-1                         1.00E+13    0.0     2900.1
519. c5h11-1+o2=>c5h10-1+ho2                    3.00E-19    0.0     3000.0
520. c5h10-1+ho2=>c5h11-1+o2                    2.00E-19    0.0    17500.0
521. c5h11-1=>c5h11-2                           3.88E+09    0.3    19760.0
522. c5h11-2=>c5h11-1                           1.83E+13   -0.6    24359.9
523. c5h11-2=>c3h6+c2h5                         3.03E+21   -2.3    30960.1
524. c3h6+c2h5=>c5h11-2                         3.30E+11    0.0     7200.1
525. c5h11-2=>c5h10-1+h                         1.64E+19   -1.6    40780.1
526. c5h10-1+h=>c5h11-2                         1.00E+13    0.0     1200.0
527. c5h11-2+o2=>c5h10-1+ho2                    4.50E-19    0.0     5020.1
528. c5h10-1+ho2=>c5h11-2+o2                    2.00E-19    0.0    17500.0
529. c2h5o+m=>ch3+ch2o+m                        1.35E+38   -7.0    23800.0
530. ch3+ch2o+m=>c2h5o+m                        6.44E+36   -7.0    16849.9
531. c2h5o+o2=>ch3cho+ho2                       4.28E+10    0.0     1097.0
532. ch3cho+ho2=>c2h5o+o2                       3.87E+08    0.4    31880.0
533. h2o2+o2=>2ho2                              1.84E+14   -0.7    39549.9
     Declared duplicate reaction...
534. 2ho2=>h2o2+o2                              1.30E+11    0.0    -1629.1
     Declared duplicate reaction...
535. c2h3+o2=>ch2cho+o                          3.50E+14   -0.6     5260.0
536. ch2cho+o=>c2h3+o2                          2.59E+12    0.1     6458.9
537. c2h5o2=>c2h5+o2                            4.93E+50  -11.5    42250.0
538. c2h5+o2=>c2h5o2                            1.09E+48  -11.5    10219.9
539. ch3o2+m=>ch3+o2+m                          4.34E+27   -3.4    30469.9
540. ch3+o2+m=>ch3o2+m                          5.44E+25   -3.3        0.0
541. ch3o2h=>ch3o+oh                            6.31E+14    0.0    42299.9
542. ch3o+oh=>ch3o2h                            1.17E+11    0.6    -1771.0
543. c3h2+o2=>hcco+co+h                         5.00E+13    0.0        0.0
544. hcco+co+h=>c3h2+o2                         0.00E+00    0.0        0.0
545. ch3o2+ch2o=>ch3o2h+hco                     1.99E+12    0.0    11669.9
546. ch3o2h+hco=>ch3o2+ch2o                     8.50E+12   -0.5     7009.1
547. c2h4+ch3o2=>c2h3+ch3o2h                    1.13E+13    0.0    30430.0
548. c2h3+ch3o2h=>c2h4+ch3o2                    3.00E+12    0.0    11500.0
549. ch4+ch3o2=>ch3+ch3o2h                      1.81E+11    0.0    18479.9
550. ch3+ch3o2h=>ch4+ch3o2                      3.71E+11   -0.5    -1327.0
551. ch3oh+ch3o2=>ch2oh+ch3o2h                  1.81E+12    0.0    13710.1
552. ch2oh+ch3o2h=>ch3oh+ch3o2                  1.04E+08    1.2     2542.1
553. c2h5+ho2=>c2h5o+oh                         3.20E+13    0.0        0.0
554. c2h5o+oh=>c2h5+ho2                         3.08E+15   -0.3    27490.0
555. ch3o2+ch3=>2ch3o                           7.00E+12    0.0    -1000.0
556. 2ch3o=>ch3o2+ch3                           2.97E+16   -0.9    28310.0
557. ch3o2+c2h5=>ch3o+c2h5o                     7.00E+12    0.0    -1000.0
558. ch3o+c2h5o=>ch3o2+c2h5                     6.57E+16   -0.9    31260.0
559. ch3o2+ho2=>ch3o2h+o2                       1.75E+10    0.0    -3275.1
560. ch3o2h+o2=>ch3o2+ho2                       5.16E+13   -0.8    34880.0
561. h2o2+oh=>h2o+ho2                           5.80E+14    0.0     9560.0
     Declared duplicate reaction...
```

562.	h2o+ho2=>h2o2+oh	9.77E+13	0.3	41020.1
	Declared duplicate reaction...			
563.	2ch3o2=>ch2o+ch3oh+o2	3.11E+14	-1.6	-1050.9
564.	ch2o+ch3oh+o2=>2ch3o2	0.00E+00	0.0	0.0
565.	2ch3o2=>o2+2ch3o	1.40E+16	-1.6	1859.9
566.	o2+2ch3o=>2ch3o2	0.00E+00	0.0	0.0
567.	c2h6+ch3o2=>c2h5+ch3o2h	1.70E+13	0.0	20460.1
568.	c2h5+ch3o2h=>c2h6+ch3o2	7.50E+11	0.0	1280.1
569.	o2c2h4oh=>pc2h4oh+o2	3.90E+16	-1.0	30000.0
570.	pc2h4oh+o2=>o2c2h4oh	1.20E+11	0.0	-1099.9
571.	o2c2h4oh=>oh+2ch2o	1.25E+10	0.0	18900.1
572.	oh+2ch2o=>o2c2h4oh	0.00E+00	0.0	0.0
573.	c2h5o2=>c2h4o2h	5.64E+47	-11.4	37320.0
574.	c2h4o2h=>c2h5o2	6.99E+48	-12.2	25849.9
575.	c2h5o+m=>ch3cho+h+m	1.16E+35	-5.9	25270.1
576.	ch3cho+h+m=>c2h5o+m	3.06E+30	-4.8	6099.9
577.	ch3o2+ch3cho=>ch3o2h+ch3co	3.01E+12	0.0	11930.0
578.	ch3o2h+ch3co=>ch3o2+ch3cho	2.52E+13	-0.5	8990.9
579.	c2h3co=>c2h3+co	2.04E+14	-0.4	31450.0
580.	c2h3+co=>c2h3co	1.51E+11	0.0	4810.0
581.	c2h3cho+oh=>c2h3co+h2o	9.24E+06	1.5	-962.0
582.	c2h3co+h2o=>c2h3cho+oh	1.44E+07	1.5	36450.1
583.	c2h3cho+h=>c2h3co+h2	1.34E+13	0.0	3299.9
584.	c2h3co+h2=>c2h3cho+h	4.82E+12	0.0	25560.0
585.	c2h3cho+o=>c2h3co+oh	5.94E+12	0.0	1868.1
586.	c2h3co+oh=>c2h3cho+o	9.38E+11	0.0	22030.1
587.	c2h3cho+ho2=>c2h3co+h2o2	3.01E+12	0.0	11930.0
588.	c2h3co+h2o2=>c2h3cho+ho2	2.78E+13	-0.3	17880.0
589.	c2h3cho+ch3=>c2h3co+ch4	2.61E+06	1.8	5911.1
590.	c2h3co+ch4=>c2h3cho+ch3	2.45E+07	1.8	28650.1
591.	c2h3cho+ch3o2=>c2h3co+ch3o2h	3.01E+12	0.0	11930.0
592.	c2h3co+ch3o2h=>c2h3cho+ch3o2	5.79E+13	-0.5	14859.9
593.	c3h5o=>c2h3cho+h	1.00E+14	0.0	29099.9
594.	c2h3cho+h=>c3h5o	7.71E+11	0.5	17750.0
595.	c3h5o=>c2h3+ch2o	2.03E+12	0.1	23560.0
596.	c2h3+ch2o=>c3h5o	1.50E+11	0.0	10599.9
597.	c3h5o+o2=>c2h3cho+ho2	1.00E+12	0.0	6000.0
598.	c2h3cho+ho2=>c3h5o+o2	1.29E+11	0.0	32000.0
599.	c3h5-a+ho2=>c3h5o+oh	7.00E+12	0.0	-1000.0
600.	c3h5o+oh=>c3h5-a+ho2	2.04E+13	-0.2	12260.0
601.	c3h5-a+ch3o2=>c3h5o+ch3o	7.00E+12	0.0	-1000.0
602.	c3h5o+ch3o=>c3h5-a+ch3o2	1.99E+15	-0.7	17020.1
603.	c3h6+ho2=>c3h6o1-2+oh	1.29E+12	0.0	14900.1
604.	c3h6o1-2+oh=>c3h6+ho2	1.00E-10	0.0	0.0
605.	c3h6+ch3o2=>c3h5-a+ch3o2h	3.24E+11	0.0	14900.1
606.	c3h5-a+ch3o2h=>c3h6+ch3o2	2.00E+10	0.0	15000.0
607.	c3h6o1-2=>c2h4+ch2o	6.00E+14	0.0	60000.0
608.	c2h4+ch2o=>c3h6o1-2	2.97E+11	0.0	50000.0
609.	c3h6o1-2+oh=>ch2o+c2h3+h2o	5.00E+12	0.0	0.0
610.	ch2o+c2h3+h2o=>c3h6o1-2+oh	0.00E+00	0.0	0.0
611.	c3h6o1-2+h=>ch2o+c2h3+h2	2.63E+07	2.0	5000.0
612.	ch2o+c2h3+h2=>c3h6o1-2+h	0.00E+00	0.0	0.0
613.	c3h6o1-2+o=>ch2o+c2h3+oh	8.43E+13	0.0	5200.1
614.	ch2o+c2h3+oh=>c3h6o1-2+o	0.00E+00	0.0	0.0
615.	c3h6o1-2+ho2=>ch2o+c2h3+h2o2	1.00E+13	0.0	15000.0
616.	ch2o+c2h3+h2o2=>c3h6o1-2+ho2	0.00E+00	0.0	0.0
617.	c3h6o1-2+ch3o2=>ch2o+c2h3+ch3o2h	1.00E+13	0.0	19000.0
618.	ch2o+c2h3+ch3o2h=>c3h6o1-2+ch3o2	0.00E+00	0.0	0.0
619.	c3h6o1-2+ch3=>ch2o+c2h3+ch4	2.00E+11	0.0	10000.0
620.	ch2o+c2h3+ch4=>c3h6o1-2+ch3	0.00E+00	0.0	0.0
621.	c2h4o2h=>c2h4+ho2	9.29E+30	-6.1	19930.0
622.	c2h4+ho2=>c2h4o2h	1.88E+25	-4.5	11659.9
623.	c3h6ooh1-2=>c3h6o1-2+oh	1.25E+15	-1.2	17580.1
624.	c3h6o1-2+oh=>c3h6ooh1-2	4.96E+08	1.0	29090.1
625.	c3h6ooh2-1=>c3h6o1-2+oh	3.46E+16	-1.6	18870.0
626.	c3h6o1-2+oh=>c3h6ooh2-1	2.79E+17	-1.5	33090.1
627.	c3h6ooh1-2=>c3h6+ho2	5.50E+14	-0.8	15260.0
628.	c3h6+ho2=>c3h6ooh1-2	6.47E+10	0.2	8278.9

629.	c3h6ooh2-1=>c3h6+ho2	2.44E+19	-2.1	18229.9
630.	c3h6+ho2=>c3h6ooh2-1	5.82E+22	-3.2	13960.1
631.	nc3h7o=>c2h5+ch2o	1.39E+16	-0.9	19770.1
632.	c2h5+ch2o=>nc3h7o	1.00E+11	0.0	11900.1
633.	ic3h7o=>ch3+ch3cho	3.84E+17	-1.2	20490.0
634.	ch3+ch3cho=>ic3h7o	1.50E+11	0.0	12900.1
635.	ic3h7o=>ch3coch3+h	2.00E+14	0.0	21500.0
636.	ch3coch3+h=>ic3h7o	7.89E+12	0.2	6810.0
637.	nc3h7o=>c2h5cho+h	2.51E+14	0.0	23400.1
638.	c2h5cho+h=>nc3h7o	1.00E+12	0.0	0.0
639.	ic3h7o+o2=>ch3coch3+ho2	9.09E+09	0.0	390.1
640.	ch3coch3+ho2=>ic3h7o+o2	1.00E+11	0.0	32000.0
641.	ch3+oh=>ch2(s)+h2o	2.65E+13	0.0	2185.9
642.	ch2(s)+h2o=>ch3+oh	3.24E+10	0.9	1211.0
643.	ch3oh+o2=>ch2oh+ho2	2.05E+13	0.0	44900.1
644.	ch2oh+ho2=>ch3oh+o2	3.99E+05	2.0	-4424.0
645.	nc3h7o2+ch3o2=>nc3h7o+ch3o+o2	1.40E+16	-1.6	1859.9
646.	nc3h7o+ch3o+o2=>nc3h7o2+ch3o2	0.00E+00	0.0	0.0
647.	ic3h7o2+ch3o2=>ic3h7o+ch3o+o2	1.40E+16	-1.6	1859.9
648.	ic3h7o+ch3o+o2=>ic3h7o2+ch3o2	0.00E+00	0.0	0.0
649.	nc3h7o2=>c3h6ooh1-2	2.00E+11	0.0	26849.9
650.	c3h6ooh1-2=>nc3h7o2	1.90E+12	-0.2	17650.1
651.	ic3h7o2=>c3h6ooh2-1	6.00E+11	0.0	29400.1
652.	c3h6ooh2-1=>ic3h7o2	1.70E+12	-0.5	14359.9
653.	ic3h7o2+c2h5o2=>ic3h7o+c2h5o+o2	1.40E+16	-1.6	1859.9
654.	ic3h7o+c2h5o+o2=>ic3h7o2+c2h5o2	0.00E+00	0.0	0.0
655.	nc3h7o2+c2h5o2=>nc3h7o+c2h5o+o2	1.40E+16	-1.6	1859.9
656.	nc3h7o+c2h5o+o2=>nc3h7o2+c2h5o2	0.00E+00	0.0	0.0
657.	2ic3h7o2=>o2+2ic3h7o	1.40E+16	-1.6	1859.9
658.	o2+2ic3h7o=>2ic3h7o2	0.00E+00	0.0	0.0
659.	2nc3h7o2=>o2+2nc3h7o	1.40E+16	-1.6	1859.9
660.	o2+2nc3h7o=>2nc3h7o2	0.00E+00	0.0	0.0
661.	ic3h7o2+nc3h7o2=>ic3h7o+nc3h7o+o2	1.40E+16	-1.6	1859.9
662.	ic3h7o+nc3h7o+o2=>ic3h7o2+nc3h7o2	0.00E+00	0.0	0.0
663.	ic3h7o2+ch3=>ic3h7o+ch3o	7.00E+12	0.0	-1000.0
664.	ic3h7o+ch3o=>ic3h7o2+ch3	1.53E+13	-0.1	26320.0
665.	ic3h7o2+c2h5=>ic3h7o+c2h5o	7.00E+12	0.0	-1000.0
666.	ic3h7o+c2h5o=>ic3h7o2+c2h5	3.39E+13	-0.1	29260.0
667.	ic3h7o2+ic3h7=>2ic3h7o	7.00E+12	0.0	-1000.0
668.	2ic3h7o=>ic3h7o2+ic3h7	5.53E+11	0.5	29770.1
669.	ic3h7o2+nc3h7=>ic3h7o+nc3h7o	7.00E+12	0.0	-1000.0
670.	ic3h7o+nc3h7o=>ic3h7o2+nc3h7	8.90E+13	-0.2	29750.0
671.	ic3h7o2+c3h5-a=>ic3h7o+c3h5o	7.00E+12	0.0	-1000.0
672.	ic3h7o+c3h5o=>ic3h7o2+c3h5-a	1.03E+12	0.1	15030.1
673.	ic3h7o2+c4h7=>ic3h7o+c4h7o	7.00E+12	0.0	-1000.0
674.	ic3h7o+c4h7o=>ic3h7o2+c4h7	6.73E+06	1.3	44460.1
675.	nc3h7o2+ch3=>nc3h7o+ch3o	7.00E+12	0.0	-1000.0
676.	nc3h7o+ch3o=>nc3h7o2+ch3	1.61E+13	0.0	26130.0
677.	nc3h7o2+c2h5=>nc3h7o+c2h5o	7.00E+12	0.0	-1000.0
678.	nc3h7o+c2h5o=>nc3h7o2+c2h5	3.56E+13	0.1	29070.0
679.	nc3h7o2+ic3h7=>nc3h7o+ic3h7o	7.00E+12	0.0	-1000.0
680.	nc3h7o+ic3h7o=>nc3h7o2+ic3h7	5.81E+11	0.6	29580.1
681.	nc3h7o2+nc3h7=>2nc3h7o	7.00E+12	0.0	-1000.0
682.	2nc3h7o=>nc3h7o2+nc3h7	9.34E+13	-0.1	29560.0
683.	nc3h7o2+c3h5-a=>nc3h7o+c3h5o	7.00E+12	0.0	-1000.0
684.	nc3h7o+c3h5o=>nc3h7o2+c3h5-a	1.08E+12	0.2	14840.1
685.	nc3h7o2+c4h7=>nc3h7o+c4h7o	7.00E+12	0.0	-1000.0
686.	nc3h7o+c4h7o=>nc3h7o2+c4h7	7.06E+06	1.5	44270.1
687.	nc3h7o2=>nc3h7+o2	3.87E+18	-1.2	36080.1
688.	nc3h7+o2=>nc3h7o2	4.52E+12	0.0	0.0
689.	ic3h7o2=>ic3h7+o2	4.21E+16	-0.3	35909.9
690.	ic3h7+o2=>ic3h7o2	7.54E+12	0.0	0.0
691.	nc3h7+ho2=>nc3h7o+oh	7.00E+12	0.0	-1000.0
692.	nc3h7o+oh=>nc3h7+ho2	1.77E+15	-0.4	26979.9
693.	ic3h7+ho2=>ic3h7o+oh	7.00E+12	0.0	-1000.0
694.	ic3h7o+oh=>ic3h7+ho2	1.10E+13	0.2	27000.0
695.	ch3o2+nc3h7=>ch3o+nc3h7o	7.00E+12	0.0	-1000.0
696.	ch3o+nc3h7o=>ch3o2+nc3h7	1.72E+17	-1.0	31740.0

697.	ch3o2+ic3h7=>ch3o+ic3h7o	7.00E+12	0.0	-1000.0
698.	ch3o+ic3h7o=>ch3o2+ic3h7	1.07E+15	-0.3	31760.0
699.	ch3o2+c3h8=>ch3o2h+nc3h7	1.70E+13	0.0	20460.1
700.	ch3o2h+nc3h7=>ch3o2+c3h8	5.00E+11	0.0	6500.0
701.	ch3o2+c3h8=>ch3o2h+ic3h7	2.00E+12	0.0	17000.0
702.	ch3o2h+ic3h7=>ch3o2+c3h8	5.00E+11	0.0	6500.0
703.	c4h7o=>ch3cho+c2h3	7.94E+14	0.0	19000.0
704.	ch3cho+c2h3=>c4h7o	1.00E+10	0.0	20000.0
705.	c4h7o=>c2h3cho+ch3	7.94E+14	0.0	19000.0
706.	c2h3cho+ch3=>c4h7o	1.00E+10	0.0	20000.0
707.	c4h7+ho2=>c4h7o+oh	7.00E+12	0.0	-1000.0
708.	c4h7o+oh=>c4h7+ho2	1.34E+08	1.1	41690.0
709.	c4h7+ch3o2=>c4h7o+ch3o	7.00E+12	0.0	-1000.0
710.	c4h7o+ch3o=>c4h7+ch3o2	1.30E+10	0.5	46450.1
711.	c4h7+c2h5o2=>c4h7o+c2h5o	7.00E+12	0.0	-1000.0
712.	c4h7o+c2h5o=>c4h7+c2h5o2	8.54E+06	1.4	44289.9
713.	c4h8-1+oh=>nc3h7+ch2o	1.00E+12	0.0	0.0
714.	nc3h7+ch2o=>c4h8-1+oh	1.62E+12	0.0	13229.9
715.	c4h8-1+o=>c3h6+ch2o	7.23E+05	2.3	-1050.0
716.	c3h6+ch2o=>c4h8-1+o	2.00E+05	2.3	80280.1
717.	c4h8-1+o=>ch3cho+c2h4	1.30E+13	0.0	849.9
718.	ch3cho+c2h4=>c4h8-1+o	2.07E+12	0.0	85099.9
719.	c4h8-1+o=>ch3co+c2h5	1.30E+13	0.0	849.9
720.	ch3co+c2h5=>c4h8-1+o	2.35E+12	0.0	38150.1
721.	c4h8-1+oh=>ch3cho+c2h5	1.00E+12	0.0	0.0
722.	ch3cho+c2h5=>c4h8-1+oh	9.33E+12	0.0	19930.0
723.	c4h8-1+oh=>ch3co+c2h6	5.00E+11	0.0	0.0
724.	ch3co+c2h6=>c4h8-1+oh	9.83E+12	0.0	32430.0
725.	c4h8-1+o=>c2h5cho+ch2	1.30E+13	0.0	849.9
726.	c2h5cho+ch2=>c4h8-1+o	5.71E+09	0.0	11000.0
727.	c4h8-1+o=>c2h5co+ch3	1.30E+13	0.0	849.9
728.	c2h5co+ch3=>c4h8-1+o	4.80E+11	0.0	32550.0
729.	c4h8-1+oh=>c2h5cho+ch3	1.00E+12	0.0	0.0
730.	c2h5cho+ch3=>c4h8-1+oh	4.95E+10	0.0	16940.0
731.	c4h8-1+oh=>c2h5co+ch4	5.00E+11	0.0	0.0
732.	c2h5co+ch4=>c4h8-1+oh	2.20E+13	0.0	34270.1
733.	c4h8-1+ch3o2=>c4h7+ch3o2h	1.40E+12	0.0	14900.1
734.	c4h7+ch3o2h=>c4h8-1+ch3o2	3.16E+11	0.0	13000.0
735.	c4h8ooh1-3o2=>c4h8ooh1-3+o2	8.09E+21	-1.9	37830.1
736.	c4h8ooh1-3+o2=>c4h8ooh1-3o2	7.54E+12	0.0	0.0
737.	c4h8ooh1-3o2=>nc4ket13+oh	2.50E+10	0.0	21400.1
738.	nc4ket13+oh=>c4h8ooh1-3o2	6.51E+04	1.1	44390.1
739.	c4h8ooh1-2=>c4h8-1+ho2	2.21E+18	-1.9	16390.1
740.	c4h8-1+ho2=>c4h8ooh1-2	1.50E+11	0.0	7799.9
741.	c4h8ooh1-3=>c4h8o1-3+oh	5.00E+10	0.0	15250.0
742.	c4h8o1-3+oh=>c4h8ooh1-3	0.00E+00	0.0	0.0
743.	c4h8ooh1-3=>oh+ch2o+c3h6	6.64E+13	-0.2	29900.1
744.	oh+ch2o+c3h6=>c4h8ooh1-3	0.00E+00	0.0	0.0
745.	c4h8o1-3+oh=>ch2o+c3h5-a+h2o	5.00E+12	0.0	0.0
746.	ch2o+c3h5-a+h2o=>c4h8o1-3+oh	0.00E+00	0.0	0.0
747.	c4h8o1-3+h=>ch2o+c3h5-a+h2	5.00E+12	0.0	0.0
748.	ch2o+c3h5-a+h2=>c4h8o1-3+h	0.00E+00	0.0	0.0
749.	c4h8o1-3+o=>ch2o+c3h5-a+oh	5.00E+12	0.0	0.0
750.	ch2o+c3h5-a+oh=>c4h8o1-3+o	0.00E+00	0.0	0.0
751.	c4h8o1-3+ho2=>ch2o+c3h5-a+h2o2	1.00E+13	0.0	15000.0
752.	ch2o+c3h5-a+h2o2=>c4h8o1-3+ho2	0.00E+00	0.0	0.0
753.	c4h8o1-3+ch3o2=>ch2o+c3h5-a+ch3o2h	1.00E+13	0.0	19000.0
754.	ch2o+c3h5-a+ch3o2h=>c4h8o1-3+ch3o2	0.00E+00	0.0	0.0
755.	c4h8o1-3+ch3=>ch2o+c3h5-a+ch4	2.00E+11	0.0	10000.0
756.	ch2o+c3h5-a+ch4=>c4h8o1-3+ch3	0.00E+00	0.0	0.0
757.	pc4h9o2=>c4h8ooh1-2	2.00E+11	0.0	26849.9
758.	c4h8ooh1-2=>pc4h9o2	5.18E+10	-0.2	14300.0
759.	pc4h9o2=>c4h8ooh1-3	2.50E+10	0.0	20849.9
760.	c4h8ooh1-3=>pc4h9o2	1.74E+09	-0.1	8186.9
761.	c2h5cho+ch3o2=>c2h5co+ch3o2h	3.01E+12	0.0	11930.0
762.	c2h5co+ch3o2h=>c2h5cho+ch3o2	2.36E+13	-0.5	8983.0
763.	c2h5cho+c4h7=>c2h5co+c4h8-1	1.70E+12	0.0	8440.0
764.	c2h5co+c4h8-1=>c2h5cho+c4h7	1.00E+13	0.0	28000.0

765. c2h5o2=>c2h4+ho2	3.37E+55	-13.4	44669.9
766. c2h4+ho2=>c2h5o2	1.29E+50	-12.3	21300.0
767. c2h4o2h=>c2h5+o2	2.15E+37	-8.2	28020.1
768. c2h5+o2=>c2h4o2h	2.42E+35	-8.0	8311.9
769. c3h4-a+ho2=>c2h4+co+oh	1.00E+12	0.0	14000.0
770. c2h4+co+oh=>c3h4-a+ho2	1.00E+00	0.0	0.0
771. c3h4-a+ho2=>c3h3+h2o2	3.00E+13	0.0	14000.0
772. c3h3+h2o2=>c3h4-a+ho2	1.55E+16	-1.4	44000.0
773. ch3cho+oh=>ch3+hocho	3.00E+15	-1.1	0.0
774. ch3+hocho=>ch3cho+oh	5.35E+19	-1.7	119799.9
775. c3h5-t+o2=>c3h4-a+ho2	1.89E+30	-5.6	15539.9
776. c3h4-a+ho2=>c3h5-t+o2	1.57E+31	-5.8	26609.9
777. c3h6+o2=>c3h5-a+ho2	4.00E+12	0.0	39900.1
778. c3h5-a+ho2=>c3h6+o2	3.33E+10	0.3	-555.9
779. c3h6+ch3=>c3h5-a+ch4	2.21E+00	3.5	5674.9
780. c3h5-a+ch4=>c3h6+ch3	2.65E+01	3.5	23180.0
781. c3h6+ch3=>c3h5-s+ch4	1.35E+00	3.5	12849.9
782. c3h5-s+ch4=>c3h6+ch3	1.05E-01	4.0	6924.9
783. c3h6+ch3=>c3h5-t+ch4	8.40E-01	3.5	11659.9
784. c3h5-t+ch4=>c3h6+ch3	1.50E-02	4.2	7842.0
785. c3h6+c2h5=>c3h5-a+c2h6	1.00E+11	0.0	9800.0
786. c3h5-a+c2h6=>c3h6+c2h5	5.37E+05	1.3	16440.0
787. c3h5-t=>c2h2+ch3	2.16E+10	-8.3	45109.9
788. c2h2+ch3=>c3h5-t	1.61E+10	-8.6	20330.1
789. c3h5-a+ho2=>c2h3+ch2o+oh	1.00E-18	0.0	0.0
790. c2h3+ch2o+oh=>c3h5-a+ho2	1.00E-30	0.0	0.0
791. c3h5-a+h=>c3h4-a+h2	1.81E+13	0.0	0.0
792. c3h4-a+h2=>c3h5-a+h	1.23E+13	0.1	47229.9
793. c3h5-a+ch3=>c3h4-a+ch4	1.00E+11	0.0	0.0
794. c3h4-a+ch4=>c3h5-a+ch3	4.92E+12	0.1	47780.1
795. c3h5-a+c2h5=>c2h6+c3h4-a	4.00E+11	0.0	0.0
796. c2h6+c3h4-a=>c3h5-a+c2h5	1.80E+12	0.1	40330.1
797. c3h5-a+c2h5=>c2h4+c3h6	4.00E+11	0.0	0.0
798. c2h4+c3h6=>c3h5-a+c2h5	6.94E+16	-1.3	52799.9
799. c3h5-a+c2h3=>c2h4+c3h4-a	1.00E+12	0.0	0.0
800. c2h4+c3h4-a=>c3h5-a+c2h3	1.62E+13	0.1	48190.0
801. c3h4-a+c3h6=>2c3h5-a	8.39E+17	-1.3	33690.0
802. 2c3h5-a=>c3h4-a+c3h6	1.00E+12	0.0	0.0
803. c3h5-a+o2=>c2h3cho+oh	2.47E+13	-0.4	23020.1
804. c2h3cho+oh=>c3h5-a+o2	1.90E+14	-0.8	74880.0
805. c3h5-s+o2=>ch3cho+hco	4.34E+12	0.0	0.0
806. ch3cho+hco=>c3h5-s+o2	1.61E+17	-1.3	96530.1
807. c3h5-s+h=>c3h4-a+h2	3.33E+12	0.0	0.0
808. c3h4-a+h2=>c3h5-s+h	7.98E+12	0.1	68859.9
809. c3h5-s+ch3=>c3h4-a+ch4	1.00E+11	0.0	0.0
810. c3h4-a+ch4=>c3h5-s+ch3	6.25E+12	0.1	69340.1
811. c3h5-t+o2=>ch3coch2+o	3.81E+17	-1.4	5580.1
812. ch3coch2+o=>c3h5-t+o2	2.00E+11	0.0	17500.0
813. c3h5-t+h=>c3h4-p+h2	3.33E+12	0.0	0.0
814. c3h4-p+h2=>c3h5-t+h	2.14E+16	-0.9	71049.9
815. c3h5-t+ch3=>c3h4-p+ch4	1.00E+11	0.0	0.0
816. c3h4-p+ch4=>c3h5-t+ch3	1.68E+16	-0.9	71530.1
817. c3h4-a+m=>c3h3+h+m	1.14E+17	0.0	70000.0
818. c3h3+h+m=>c3h4-a+m	1.80E+15	-0.4	10609.9
819. c3h4-a=>c3h4-p	1.20E+15	0.0	92400.1
820. c3h4-p=>c3h4-a	3.22E+18	-1.0	96590.1
821. c3h4-a+o2=>c3h3+ho2	4.00E+13	0.0	39159.9
822. c3h3+ho2=>c3h4-a+o2	1.18E+11	0.3	38.0
823. c3h4-a+ho2=>ch2co+ch2+oh	4.00E+12	0.0	19000.0
824. ch2co+ch2+oh=>c3h4-a+ho2	1.00E+00	0.0	0.0
825. c3h3+h=>c3h2+h2	5.00E+13	0.0	0.0
826. c3h2+h2=>c3h3+h	3.85E+10	0.4	4599.9
827. c3h4-a+oh=>c3h3+h2o	1.00E+07	2.0	1000.0
828. c3h3+h2o=>c3h4-a+oh	7.00E+06	2.0	34520.1
829. c3h4-a+o=>c2h4+co	7.80E+12	0.0	1599.9
830. c2h4+co=>c3h4-a+o	8.28E+13	-0.2	124799.9
831. c3h2+oh=>c2h2+hco	5.00E+13	0.0	0.0
832. c2h2+hco=>c3h2+oh	2.91E+20	-1.4	78520.1

833.	c3h5-a=>c3h4-a+h	6.66E+15	-0.4	63219.9
834.	c3h4-a+h=>c3h5-a	2.40E+11	0.7	3006.9
835.	c3h5-t=>c3h4-a+h	3.51E+14	-0.4	40890.1
836.	c3h4-a+h=>c3h5-t	8.50E+12	0.0	2000.0
837.	c3h4-a+h=>c3h3+h2	2.00E+07	2.0	5000.0
838.	c3h3+h2=>c3h4-a+h	3.24E+06	2.0	23359.9
839.	c3h4-a+ch3=>c3h3+ch4	3.67E-02	4.0	6830.1
840.	c3h3+ch4=>c3h4-a+ch3	1.55E-01	4.0	25669.9
841.	c3h4-a+c3h5-a=>c3h3+c3h6	2.00E+11	0.0	7700.1
842.	c3h3+c3h6=>c3h4-a+c3h5-a	2.64E+19	-2.7	42140.1
843.	c3h4-a+c2h=>c3h3+c2h2	1.00E+13	0.0	0.0
844.	c3h3+c2h2=>c3h4-a+c2h	1.42E+16	-1.4	53820.0
845.	c3h4-p+m=>c3h3+h+m	1.14E+17	0.0	70000.0
846.	c3h3+h+m=>c3h4-p+m	6.71E+11	0.6	6419.9
847.	c3h4-p=>c2h+ch3	4.20E+16	0.0	100000.0
848.	c2h+ch3=>c3h4-p	1.02E+12	0.6	-1599.9
849.	c3h4-p+o2=>c3h3+ho2	2.00E+13	0.0	41599.9
850.	c3h3+ho2=>c3h4-p+o2	2.35E+11	0.1	77.9
851.	c3h4-p+ho2=>c2h4+co+oh	3.00E+12	0.0	19000.0
852.	c2h4+co+oh=>c3h4-p+ho2	1.00E+00	0.0	0.0
853.	c3h4-p+oh=>c3h3+h2o	1.00E+07	2.0	1000.0
854.	c3h3+h2o=>c3h4-p+oh	2.80E+07	1.8	32120.0
855.	c3h4-p+o=>c3h3+oh	7.65E+08	1.5	8599.9
856.	c3h3+oh=>c3h4-p+o	2.18E+08	1.3	22469.9
857.	c3h4-p+o=>c2h3+hco	3.20E+12	0.0	2010.0
858.	c2h3+hco=>c3h4-p+o	2.55E+12	-0.4	32349.9
859.	c3h4-p+o=>hcco+ch3	9.60E+08	1.0	0.0
860.	hcco+ch3=>c3h4-p+o	1.64E+10	-0.2	24090.1
861.	c3h5-t=>c3h4-p+h	1.08E+15	-0.6	38490.0
862.	c3h4-p+h=>c3h5-t	6.50E+12	0.0	2000.0
863.	c3h5-s=>c3h4-p+h	4.19E+15	-0.8	37479.9
864.	c3h4-p+h=>c3h5-s	5.80E+12	0.0	3099.9
865.	c3h4-p+h=>c3h3+h2	2.00E+07	2.0	5000.0
866.	c3h3+h2=>c3h4-p+h	1.30E+07	1.8	20960.1
867.	c3h4-p+ch3=>c3h3+ch4	1.50E+00	3.5	5599.9
868.	c3h3+ch4=>c3h4-p+ch3	2.54E+01	3.3	22039.9
869.	c3h4-p+c2h=>c3h3+c2h2	1.00E+12	0.0	0.0
870.	c3h3+c2h2=>c3h4-p+c2h	5.30E+11	-0.4	49630.0
871.	c3h4-p+c2h3=>c3h3+c2h4	1.00E+12	0.0	7700.1
872.	c3h3+c2h4=>c3h4-p+c2h3	9.54E+11	-0.4	52450.1
873.	c3h4-p+c3h5-a=>c3h3+c3h6	1.00E+12	0.0	7700.1
874.	c3h3+c3h6=>c3h4-p+c3h5-a	4.93E+16	-1.7	37950.1
875.	c3h3+o=>ch2o+c2h	1.00E+13	0.0	0.0
876.	ch2o+c2h=>c3h3+o	5.45E+14	0.0	31609.9
877.	c3h3+oh=>c3h2+h2o	1.00E+13	0.0	0.0
878.	c3h2+h2o=>c3h3+oh	1.34E+15	0.0	15680.0
879.	c3h3+o2=>ch2co+hco	3.01E+10	0.0	2870.0
880.	ch2co+hco=>c3h3+o2	4.88E+11	0.0	59469.9
881.	c3h3+ch3=>c2h5+c2h	4.56E+17	-1.1	48729.9
882.	c2h5+c2h=>c3h3+ch3	1.81E+13	0.0	0.0
883.	pc4h9o2=>pc4h9+o2	7.60E+18	-1.2	35840.1
884.	pc4h9+o2=>pc4h9o2	4.52E+12	0.0	0.0
885.	c2h3o1,2=>ch3co	8.50E+14	0.0	14000.0
886.	ch3co=>c2h3o1,2	1.14E+10	2.1	33520.1
887.	c2h3o1,2=>ch2cho	1.00E+14	0.0	14000.0
888.	ch2cho=>c2h3o1,2	1.23E+11	1.7	28300.0
889.	ch2cho=>ch2co+h	3.09E+15	-0.3	50820.0
890.	ch2co+h=>ch2cho	5.00E+13	0.0	12300.0
891.	ch2cho+o2=>ch2o+co+oh	2.00E+13	0.0	4200.1
892.	ch2o+co+oh=>ch2cho+o2	0.00E+00	0.0	0.0
893.	nc4ket13=>ch3cho+ch2cho+oh	1.05E+16	0.0	41599.9
894.	ch3cho+ch2cho+oh=>nc4ket13	0.00E+00	0.0	0.0
895.	c3h5-a+o2=>c3h4-a+ho2	2.18E+21	-2.9	30760.0
896.	c3h4-a+ho2=>c3h5-a+o2	2.69E+19	-2.4	20500.0
897.	c3h5-a+o2=>ch2cho+ch2o	7.14E+15	-1.2	21050.0
898.	ch2cho+ch2o=>c3h5-a+o2	4.94E+16	-1.4	88620.0
899.	c3h5-a+o2=>c2h2+ch2o+oh	9.72E+29	-5.7	21450.0
900.	c2h2+ch2o+oh=>c3h5-a+o2	0.00E+00	0.0	0.0

901.	hcco+o2=>co2+hco	2.40E+11	0.0	-854.0
902.	co2+hco=>hcco+o2	1.47E+14	0.0	133599.9
903.	c3h6+h=>c3h5-s+h2	8.04E+05	2.5	12280.1
904.	c3h5-s+h2=>c3h6+h	2.39E+03	3.0	5876.0
905.	ch2co+oh=>ch2oh+co	3.73E+12	0.0	-1012.9
906.	ch2oh+co=>ch2co+oh	9.43E+06	1.7	27490.0
907.	ch3+o2=>ch2o+oh	7.47E+11	0.0	14250.0
908.	ch2o+oh=>ch3+o2	7.78E+11	0.0	67770.1
909.	c2h4+h2=>2ch3	3.77E+12	0.8	84710.1
910.	2ch3=>c2h4+h2	1.00E+14	0.0	32000.0
911.	c3h5-t+o2=>ch2o+ch3co	3.71E+25	-4.0	7043.0
912.	ch2o+ch3co=>c3h5-t+o2	1.87E+27	-4.4	101200.1
913.	ic3h7+oh=>c3h6+h2o	2.41E+13	0.0	0.0
914.	c3h6+h2o=>ic3h7+oh	2.98E+12	0.6	83820.0
915.	ic3h7+o=>ch3coch3+h	4.82E+13	0.0	0.0
916.	ch3coch3+h=>ic3h7+o	1.29E+16	-0.2	79380.0
917.	ic3h7+o=>ch3cho+ch3	4.82E+13	0.0	0.0
918.	ch3cho+ch3=>ic3h7+o	1.28E+11	0.8	86479.9
919.	c3h6+h=>c3h5-t+h2	4.05E+05	2.5	9794.0
920.	c3h5-t+h2=>c3h6+h	2.76E+02	3.2	5500.0
921.	c3h6=>c3h5-t+h	5.62E+71	-16.6	139300.0
922.	c3h5-t+h=>c3h6	2.03E+64	-14.9	27550.0
923.	nc3h7cho+o2=>nc3h7co+ho2	2.00E+13	0.5	42200.1
924.	nc3h7co+ho2=>nc3h7cho+o2	1.00E+07	0.5	4000.0
925.	nc3h7cho+oh=>nc3h7co+h2o	1.00E+13	0.0	0.0
926.	nc3h7co+h2o=>nc3h7cho+oh	2.00E+13	0.0	37000.0
927.	nc3h7cho+h=>nc3h7co+h2	4.00E+13	0.0	4200.1
928.	nc3h7co+h2=>nc3h7cho+h	1.80E+13	0.0	24000.0
929.	nc3h7cho+o=>nc3h7co+oh	5.00E+12	0.0	1789.9
930.	nc3h7co+oh=>nc3h7cho+o	1.00E+12	0.0	19000.0
931.	nc3h7cho+ho2=>nc3h7co+h2o2	2.80E+12	0.0	13599.9
932.	nc3h7co+h2o2=>nc3h7cho+ho2	1.00E+12	0.0	10000.0
933.	nc3h7cho+ch3=>nc3h7co+ch4	1.70E+12	0.0	8440.0
934.	nc3h7co+ch4=>nc3h7cho+ch3	1.50E+13	0.0	28000.0
935.	nc3h7cho+ch3o=>nc3h7co+ch3oh	1.15E+11	0.0	1280.1
936.	nc3h7co+ch3oh=>nc3h7cho+ch3o	3.00E+11	0.0	18000.0
937.	nc3h7cho+ch3o2=>nc3h7co+ch3o2h	1.00E+12	0.0	9500.0
938.	nc3h7co+ch3o2h=>nc3h7cho+ch3o2	2.50E+10	0.0	10000.0
939.	nc3h7cho+oh=>c3h6cho-2+h2o	4.67E+07	1.6	-34.9
940.	c3h6cho-2+h2o=>nc3h7cho+oh	8.06E+05	1.9	21940.0
941.	nc3h7cho+ho2=>c3h6cho-2+h2o2	1.48E+04	2.6	13909.9
942.	c3h6cho-2+h2o2=>nc3h7cho+ho2	1.51E+03	2.6	4424.0
943.	nc3h7cho+ch3o2=>c3h6cho-2+ch3o2h	9.63E+03	2.6	13909.9
944.	c3h6cho-2+ch3o2h=>nc3h7cho+ch3o2	4.05E+03	2.4	3704.1
945.	nc3h7co=>nc3h7+co	1.00E+11	0.0	9599.9
946.	nc3h7+co=>nc3h7co	1.00E+11	0.0	0.0
947.	ch3chco+oh=>c2h5+co2	1.73E+12	0.0	-1010.0
948.	c2h5+co2=>ch3chco+oh	0.00E+00	0.0	0.0
949.	ch3chco+h=>c2h5+co	4.40E+12	0.0	1458.9
950.	c2h5+co=>ch3chco+h	0.00E+00	0.0	0.0
951.	ch3chco+o=>ch3cho+co	3.20E+12	0.0	-436.9
952.	ch3cho+co=>ch3chco+o	0.00E+00	0.0	0.0
953.	ch2ch2cooch3=>c2h4+ch3co	5.97E+12	0.0	20729.9
954.	c2h4+ch3co=>ch2ch2coch3	2.11E+11	0.0	7349.9
955.	c2h5coch2=>ch2co+c2h5	1.57E+13	0.0	30000.0
956.	ch2co+c2h5=>c2h5coch2	2.11E+11	0.0	7349.9
957.	c3h6cho-2=>c3h6+hco	8.25E+12	-0.2	21900.1
958.	c3h6+hco=>c3h6cho-2	1.00E+11	0.0	6000.0
959.	c2h5coc2h4p=>c2h5co+c2h4	1.55E+17	-1.5	27840.1
960.	c2h5co+c2h4=>c2h5coc2h4p	7.00E+10	0.0	9599.9
961.	nc3h7coch2=>nc3h7+ch2co	1.23E+18	-1.4	43450.1
962.	nc3h7+ch2co=>nc3h7coch2	1.00E+11	0.0	11599.9
963.	nc4h9cho+o2=>nc4h9co+ho2	2.00E+13	0.5	42200.1
964.	nc4h9co+ho2=>nc4h9cho+o2	1.00E+07	0.0	40000.0
965.	nc4h9cho+oh=>nc4h9co+h2o	1.00E+13	0.0	0.0
966.	nc4h9co+h2o=>nc4h9cho+oh	2.00E+13	0.0	37000.0
967.	nc4h9cho+h=>nc4h9co+h2	4.00E+13	0.0	4200.1
968.	nc4h9co+h2=>nc4h9cho+h	1.80E+13	0.0	24000.0

969.	nc4h9cho+o=>nc4h9co+oh	5.00E+12	0.0	1789.9
970.	nc4h9co+oh=>nc4h9cho+o	1.00E+12	0.0	19000.0
971.	nc4h9cho+ho2=>nc4h9co+h2o2	2.80E+12	0.0	13599.9
972.	nc4h9co+h2o2=>nc4h9cho+ho2	1.00E+12	0.0	10000.0
973.	nc4h9cho+ch3=>nc4h9co+ch4	1.70E+12	0.0	8440.0
974.	nc4h9co+ch4=>nc4h9cho+ch3	1.50E+13	0.0	28000.0
975.	nc4h9cho+ch3o=>nc4h9co+ch3oh	1.15E+11	0.0	1280.1
976.	nc4h9co+ch3oh=>nc4h9cho+ch3o	3.00E+11	0.0	18000.0
977.	nc4h9cho+ch3o2=>nc4h9co+ch3o2h	1.00E+12	0.0	9500.0
978.	nc4h9co+ch3o2h=>nc4h9cho+ch3o2	2.50E+10	0.0	10000.0
979.	nc4h9co=>pc4h9+co	1.00E+11	0.0	9599.9
980.	pc4h9+co=>nc4h9co	1.00E+11	0.0	0.0
981.	hoch2o=>ch2o+oh	8.54E+13	-0.1	17530.1
982.	ch2o+oh=>hoch2o	2.60E+12	0.0	-614.0
983.	hoch2o=>hocho+h	1.00E+14	0.0	14900.1
984.	hocho+h=>hoch2o	5.92E+11	0.6	12300.0
985.	hocho+m=>co+h2o+m	2.30E+13	0.0	50000.0
986.	co+h2o+m=>hocho+m	1.42E+10	0.5	46840.1
987.	hocho+m=>co2+h2+m	1.50E+16	0.0	57000.0
988.	co2+h2+m=>hocho+m	2.40E+14	0.5	61020.1
989.	hocho=>hco+oh	4.59E+18	-0.5	108299.9
990.	hco+oh=>hocho	1.00E+14	0.0	0.0
991.	hocho+oh=>h2o+co2+h	2.62E+06	2.1	916.1
992.	h2o+co2+h=>hocho+oh	0.00E+00	0.0	0.0
993.	hocho+oh=>h2o+co+oh	1.85E+07	1.5	-962.0
994.	h2o+co+oh=>hocho+oh	0.00E+00	0.0	0.0
995.	hocho+h=>h2+co2+h	4.24E+06	2.1	4868.1
996.	h2+co2+h=>hocho+h	0.00E+00	0.0	0.0
997.	hocho+h=>h2+co+oh	6.03E+13	-0.3	2988.1
998.	h2+co+oh=>hocho+h	0.00E+00	0.0	0.0
999.	hocho+ch3=>ch4+co+oh	3.90E-07	5.8	2200.1
1000.	ch4+co+oh=>hocho+ch3	0.00E+00	0.0	0.0
1001.	hocho+ho2=>h2o2+co+oh	1.00E+12	0.0	11919.9
1002.	h2o2+co+oh=>hocho+ho2	0.00E+00	0.0	0.0
1003.	hocho+o=>co+2oh	1.77E+18	-1.9	2974.9
1004.	co+2oh=>hocho+o	0.00E+00	0.0	0.0
1005.	ch2(s)+m=>ch2+m	1.00E+13	0.0	0.0
1006.	ch2+m=>ch2(s)+m	7.16E+15	-0.9	11430.0
1007.	ch2(s)+ch4=>2ch3	4.00E+13	0.0	0.0
1008.	2ch3=>ch2(s)+ch4	5.43E+15	-0.9	15650.1
1009.	ch2(s)+c2h6=>ch3+c2h5	1.20E+14	0.0	0.0
1010.	ch3+c2h5=>ch2(s)+c2h6	1.04E+14	-0.3	19820.0
1011.	ch2(s)+o2=>co+oh+h	7.00E+13	0.0	0.0
1012.	co+oh+h=>ch2(s)+o2	0.00E+00	0.0	0.0
1013.	ch2(s)+h2=>ch3+h	7.00E+13	0.0	0.0
1014.	ch3+h=>ch2(s)+h2	2.48E+17	-0.9	16130.0
1015.	ch2(s)+h=>ch+h2	3.00E+13	0.0	0.0
1016.	ch+h2=>ch2(s)+h	1.51E+16	-0.9	14419.9
1017.	ch2(s)+o=>co+2h	3.00E+13	0.0	0.0
1018.	co+2h=>ch2(s)+o	0.00E+00	0.0	0.0
1019.	ch2(s)+oh=>ch2o+h	3.00E+13	0.0	0.0
1020.	ch2o+h=>ch2(s)+oh	3.19E+18	-0.9	87859.9
1021.	ch2(s)+co2=>ch2o+co	3.00E+12	0.0	0.0
1022.	ch2o+co=>ch2(s)+co2	2.85E+15	-0.9	65520.1
1023.	ch2(s)+ch3=>c2h4+h	2.00E+13	0.0	0.0
1024.	c2h4+h=>ch2(s)+ch3	2.67E+15	-0.1	68840.1
1025.	ch2(s)+ch2co=>c2h4+co	1.60E+14	0.0	0.0
1026.	c2h4+co=>ch2(s)+ch2co	4.60E+15	-0.1	105599.9
1027.	c6h13-1+o2=>c6h12-1+ho2	3.00E-19	0.0	3000.0
1028.	c6h12-1+ho2=>c6h13-1+o2	2.00E-19	0.0	17500.0
1029.	c6h13-1=>c2h4+pc4h9	5.45E+17	-1.3	29580.1
1030.	c2h4+pc4h9=>c6h13-1	3.30E+11	0.0	7200.1
1031.	c6h13-1=>c6h12-1+h	2.09E+16	-0.9	37950.1
1032.	c6h12-1+h=>c6h13-1	1.00E+13	0.0	2900.1
1033.	c6h12-1+oh=>c6h11+h2o	3.00E+13	0.0	1229.9
1034.	c6h11+h2o=>c6h12-1+oh	9.76E+14	-0.1	39260.0
1035.	c6h12-1+h=>c6h11+h2	3.70E+13	0.0	3900.1
1036.	c6h11+h2=>c6h12-1+h	2.78E+14	-0.1	26770.1

1037. c6h12-1+ch3=>c6h11+ch4	1.00E+12	0.0	7299.9
1038. c6h11+ch4=>c6h12-1+ch3	1.96E+14	-0.1	30650.1
1039. c6h12-1+o=>c6h11+oh	2.12E+11	0.1	9125.0
1040. c6h11+oh=>c6h12-1+o	7.00E+11	0.0	29900.1
1041. c6h12-1+oh=>c5h11-1+ch2o	1.00E+11	0.0	-4000.0
1042. c5h11-1+ch2o=>c6h12-1+oh	0.00E+00	0.0	0.0
1043. c6h12-1+o=>c5h11-1+hco	1.00E+11	0.0	-1050.0
1044. c5h11-1+hco=>c6h12-1+o	0.00E+00	0.0	0.0
1045. c6h11=>c3h6+c3h5-a	2.50E+13	0.0	45000.0
1046. c3h6+c3h5-a=>c6h11	1.00E+10	0.0	17000.0
1047. c6h11=>c4h8-1+c2h3	2.50E-17	0.0	45000.0
1048. c4h8-1+c2h3=>c6h11	1.50E-20	0.0	7400.1
1049. c6h11=>c4h7+c2h4	2.50E-17	0.0	45000.0
1050. c4h7+c2h4=>c6h11	1.50E-20	0.0	7400.1
1051. c6h12-1=>nc3h7+c3h5-a	1.00E+16	0.0	71000.0
1052. nc3h7+c3h5-a=>c6h12-1	1.00E+13	0.0	0.0
1053. nc7h16=>h+c7h15-1	1.34E+88	-21.2	142800.0
1054. h+c7h15-1=>nc7h16	3.37E+82	-20.2	39609.9
1055. nc7h16=>h+c7h15-2	6.50E+87	-21.0	139500.0
1056. h+c7h15-2=>nc7h16	5.21E+80	-19.7	38890.1
1057. nc7h16=>h+c7h15-3	6.50E+87	-21.0	139500.0
1058. h+c7h15-3=>nc7h16	5.21E+80	-19.7	38890.1
1059. nc7h16=>h+c7h15-4	3.25E+87	-21.0	139500.0
1060. h+c7h15-4=>nc7h16	5.19E+80	-19.7	38890.1
1061. nc7h16=>c6h13-1+ch3	2.93E+73	-16.6	118900.1
1062. c6h13-1+ch3=>nc7h16	8.35E+66	-15.8	31830.1
1063. nc7h16=>c5h11-1+c2h5	8.10E+77	-17.6	120400.1
1064. c5h11-1+c2h5=>nc7h16	8.30E+67	-16.1	32349.9
1065. nc7h16=>pc4h9+nc3h7	1.42E+78	-17.7	120700.1
1066. pc4h9+nc3h7=>nc7h16	1.36E+68	-16.1	32460.1
1067. nc7h16+h=>c7h15-1+h2	1.88E+05	2.8	6280.1
1068. c7h15-1+h2=>nc7h16+h	8.93E+03	2.7	10550.0
1069. nc7h16+h=>c7h15-2+h2	2.60E+06	2.4	4471.1
1070. c7h15-2+h2=>nc7h16+h	3.93E+03	2.7	11260.0
1071. nc7h16+h=>c7h15-3+h2	2.60E+06	2.4	4471.1
1072. c7h15-3+h2=>nc7h16+h	3.93E+03	2.7	11260.0
1073. nc7h16+h=>c7h15-4+h2	1.30E+06	2.4	4471.1
1074. c7h15-4+h2=>nc7h16+h	3.91E+03	2.7	11260.0
1075. nc7h16+o=>c7h15-1+oh	1.93E+05	2.7	3716.1
1076. c7h15-1+oh=>nc7h16+o	4.02E+03	2.6	5892.9
1077. nc7h16+o=>c7h15-2+oh	9.54E+04	2.7	2106.1
1078. c7h15-2+oh=>nc7h16+o	6.33E+01	3.0	6798.0
1079. nc7h16+o=>c7h15-3+oh	9.54E+04	2.7	2106.1
1080. c7h15-3+oh=>nc7h16+o	6.33E+01	3.0	6798.0
1081. nc7h16+o=>c7h15-4+oh	4.77E+04	2.7	2106.1
1082. c7h15-4+oh=>nc7h16+o	6.31E+01	3.0	6798.0
1083. nc7h16+oh=>c7h15-1+h2o	1.05E+10	1.0	1590.1
1084. c7h15-1+h2o=>nc7h16+oh	1.50E+10	1.1	23330.1
1085. nc7h16+oh=>c7h15-2+h2o	9.40E+07	1.6	-34.9
1086. c7h15-2+h2o=>nc7h16+oh	6.15E+05	1.9	21909.9
1087. nc7h16+oh=>c7h15-3+h2o	9.40E+07	1.6	-34.9
1088. c7h15-3+h2o=>nc7h16+oh	6.15E+05	1.9	21909.9
1089. nc7h16+oh=>c7h15-4+h2o	4.70E+07	1.6	-34.9
1090. c7h15-4+h2o=>nc7h16+oh	6.12E+05	1.9	21909.9
1091. nc7h16+ho2=>c7h15-1+h2o2	1.68E+13	0.0	20440.0
1092. c7h15-1+h2o2=>nc7h16+ho2	2.05E+13	-0.4	8398.9
1093. nc7h16+ho2=>c7h15-2+h2o2	1.12E+13	0.0	17690.0
1094. c7h15-2+h2o2=>nc7h16+ho2	4.35E+11	0.0	8164.9
1095. nc7h16+ho2=>c7h15-3+h2o2	1.12E+13	0.0	17690.0
1096. c7h15-3+h2o2=>nc7h16+ho2	4.35E+11	0.0	8164.9
1097. nc7h16+ho2=>c7h15-4+h2o2	5.60E+12	0.0	17690.0
1098. c7h15-4+h2o2=>nc7h16+ho2	4.33E+11	0.0	8164.9
1099. nc7h16+ch3=>c7h15-1+ch4	9.04E-01	3.6	7153.9
1100. c7h15-1+ch4=>nc7h16+ch3	1.12E+00	3.6	11909.9
1101. nc7h16+ch3=>c7h15-2+ch4	5.41E+04	2.3	7287.1
1102. c7h15-2+ch4=>nc7h16+ch3	2.14E+03	2.6	14550.0
1103. nc7h16+ch3=>c7h15-3+ch4	5.41E+04	2.3	7287.1
1104. c7h15-3+ch4=>nc7h16+ch3	2.14E+03	2.6	14550.0

1105. nc7h16+ch3=>c7h15-4+ch4	2.70E+04	2.3	7287.1
1106. c7h15-4+ch4=>nc7h16+ch3	2.13E+03	2.6	14550.0
1107. nc7h16+o2=>c7h15-1+ho2	6.00E+13	0.0	52799.9
1108. c7h15-1+ho2=>nc7h16+o2	5.18E+10	0.3	-406.1
1109. nc7h16+o2=>c7h15-2+ho2	4.00E+13	0.0	50150.1
1110. c7h15-2+ho2=>nc7h16+o2	1.10E+09	0.7	-541.1
1111. nc7h16+o2=>c7h15-3+ho2	4.00E+13	0.0	50150.1
1112. c7h15-3+ho2=>nc7h16+o2	1.10E+09	0.7	-541.1
1113. nc7h16+o2=>c7h15-4+ho2	2.00E+13	0.0	50150.1
1114. c7h15-4+ho2=>nc7h16+o2	1.09E+09	0.7	-541.1
1115. nc7h16+c2h5=>c7h15-1+c2h6	1.00E+11	0.0	13400.1
1116. c7h15-1+c2h6=>nc7h16+c2h5	3.20E+11	0.0	12300.0
1117. nc7h16+c2h5=>c7h15-2+c2h6	1.00E+11	0.0	10400.1
1118. c7h15-2+c2h6=>nc7h16+c2h5	1.00E+11	0.0	12900.1
1119. nc7h16+c2h5=>c7h15-3+c2h6	1.00E+11	0.0	10400.1
1120. c7h15-3+c2h6=>nc7h16+c2h5	1.00E+11	0.0	12900.1
1121. nc7h16+c2h5=>c7h15-4+c2h6	5.00E+10	0.0	10400.1
1122. c7h15-4+c2h6=>nc7h16+c2h5	1.00E+11	0.0	12900.1
1123. nc7h16+ch3o=>c7h15-1+ch3oh	3.16E+11	0.0	7000.0
1124. c7h15-1+ch3oh=>nc7h16+ch3o	1.20E+10	0.0	9200.0
1125. nc7h16+ch3o=>c7h15-2+ch3oh	2.19E+11	0.0	5000.0
1126. c7h15-2+ch3oh=>nc7h16+ch3o	8.90E+09	0.0	7200.1
1127. nc7h16+ch3o=>c7h15-3+ch3oh	2.19E+11	0.0	5000.0
1128. c7h15-3+ch3oh=>nc7h16+ch3o	8.90E+09	0.0	7200.1
1129. nc7h16+ch3o=>c7h15-4+ch3oh	1.10E+11	0.0	5000.0
1130. c7h15-4+ch3oh=>nc7h16+ch3o	8.90E+09	0.0	7200.1
1131. nc7h16+c2h3=>c7h15-1+c2h4	1.00E+12	0.0	18000.0
1132. c7h15-1+c2h4=>nc7h16+c2h3	2.57E+12	0.0	25400.1
1133. nc7h16+c2h3=>c7h15-2+c2h4	8.00E+11	0.0	16800.0
1134. c7h15-2+c2h4=>nc7h16+c2h3	2.00E+12	0.0	24200.0
1135. nc7h16+c2h3=>c7h15-3+c2h4	8.00E+11	0.0	16800.0
1136. c7h15-3+c2h4=>nc7h16+c2h3	2.00E+12	0.0	24200.0
1137. nc7h16+c2h3=>c7h15-4+c2h4	4.00E+11	0.0	16800.0
1138. c7h15-4+c2h4=>nc7h16+c2h3	2.00E+12	0.0	24200.0
1139. nc7h16+ch3o2=>c7h15-1+ch3o2h	1.21E+13	0.0	20430.0
1140. c7h15-1+ch3o2h=>nc7h16+ch3o2	3.60E+12	0.0	9800.0
1141. nc7h16+ch3o2=>c7h15-2+ch3o2h	8.06E+12	0.0	17700.0
1142. c7h15-2+ch3o2h=>nc7h16+ch3o2	2.38E+11	0.0	3700.1
1143. nc7h16+ch3o2=>c7h15-3+ch3o2h	8.06E+12	0.0	17700.0
1144. c7h15-3+ch3o2h=>nc7h16+ch3o2	2.38E+11	0.0	3700.1
1145. nc7h16+ch3o2=>c7h15-4+ch3o2h	4.03E+12	0.0	17700.0
1146. c7h15-4+ch3o2h=>nc7h16+ch3o2	2.38E+11	0.0	3700.1
1147. nc7h16+c7h15o2-1=>c7h15-1+c7h15o2h-1	1.21E+13	0.0	20430.0
1148. c7h15-1+c7h15o2h-1=>nc7h16+c7h15o2-1	1.44E+10	0.0	15000.0
1149. nc7h16+c7h15o2-2=>c7h15-1+c7h15o2h-2	1.21E+13	0.0	20430.0
1150. c7h15-1+c7h15o2h-2=>nc7h16+c7h15o2-2	1.44E+10	0.0	15000.0
1151. nc7h16+c7h15o2-3=>c7h15-1+c7h15o2h-3	1.21E+13	0.0	20430.0
1152. c7h15-1+c7h15o2h-3=>nc7h16+c7h15o2-3	1.44E+10	0.0	15000.0
1153. nc7h16+c7h15o2-1=>c7h15-2+c7h15o2h-1	8.06E+12	0.0	17700.0
1154. c7h15-2+c7h15o2h-1=>nc7h16+c7h15o2-1	1.44E+10	0.0	15000.0
1155. nc7h16+c7h15o2-2=>c7h15-2+c7h15o2h-2	8.06E+12	0.0	17700.0
1156. c7h15-2+c7h15o2h-2=>nc7h16+c7h15o2-2	1.44E+10	0.0	15000.0
1157. nc7h16+c7h15o2-3=>c7h15-2+c7h15o2h-3	8.06E+12	0.0	17700.0
1158. c7h15-2+c7h15o2h-3=>nc7h16+c7h15o2-3	1.44E+10	0.0	15000.0
1159. nc7h16+c7h15o2-1=>c7h15-3+c7h15o2h-1	8.06E+12	0.0	17700.0
1160. c7h15-3+c7h15o2h-1=>nc7h16+c7h15o2-1	1.44E+10	0.0	15000.0
1161. nc7h16+c7h15o2-2=>c7h15-3+c7h15o2h-2	8.06E+12	0.0	17700.0
1162. c7h15-3+c7h15o2h-2=>nc7h16+c7h15o2-2	1.44E+10	0.0	15000.0
1163. nc7h16+c7h15o2-3=>c7h15-3+c7h15o2h-3	8.06E+12	0.0	17700.0
1164. c7h15-3+c7h15o2h-3=>nc7h16+c7h15o2-3	1.44E+10	0.0	15000.0
1165. nc7h16+c7h15o2-1=>c7h15-4+c7h15o2h-1	4.03E+12	0.0	17700.0
1166. c7h15-4+c7h15o2h-1=>nc7h16+c7h15o2-1	1.44E+10	0.0	15000.0
1167. nc7h16+c7h15o2-2=>c7h15-4+c7h15o2h-2	4.03E+12	0.0	17700.0
1168. c7h15-4+c7h15o2h-2=>nc7h16+c7h15o2-2	1.44E+10	0.0	15000.0
1169. nc7h16+c7h15o2-3=>c7h15-4+c7h15o2h-3	4.03E+12	0.0	17700.0
1170. c7h15-4+c7h15o2h-3=>nc7h16+c7h15o2-3	1.44E+10	0.0	15000.0
1171. nc7h16+c7h15-1=>c7h15-2+nc7h16	1.00E+11	0.0	10400.1
1172. c7h15-2+nc7h16=>nc7h16+c7h15-1	1.50E+11	0.0	12300.0

1173. nc7h16+c7h15-1=>c7h15-3+nc7h16	1.00E+11	0.0	10400.1
1174. c7h15-3+nc7h16=>nc7h16+c7h15-1	1.50E+11	0.0	12300.0
1175. nc7h16+c7h15-1=>c7h15-4+nc7h16	5.00E+10	0.0	10400.1
1176. c7h15-4+nc7h16=>nc7h16+c7h15-1	1.50E+11	0.0	12300.0
1177. nc7h16+c7h15-2=>c7h15-3+nc7h16	1.00E+11	0.0	10400.1
1178. c7h15-3+nc7h16=>nc7h16+c7h15-2	1.00E+11	0.0	10400.1
1179. nc7h16+c7h15-2=>c7h15-4+nc7h16	5.00E+10	0.0	10400.1
1180. c7h15-4+nc7h16=>nc7h16+c7h15-2	1.00E+11	0.0	10400.1
1181. nc7h16+c7h15-3=>c7h15-4+nc7h16	5.00E+10	0.0	10400.1
1182. c7h15-4+nc7h16=>nc7h16+c7h15-3	1.00E+11	0.0	10400.1
1183. c7h15-1=>c5h11-1+c2h4	8.16E+17	-1.4	30840.1
1184. c5h11-1+c2h4=>c7h15-1	1.00E+11	0.0	8200.0
1185. c7h15-1=>c7h14-1+h	4.20E+16	-0.9	37940.0
1186. c7h14-1+h=>c7h15-1	1.00E+13	0.0	2900.1
1187. c7h15-2=>pc4h9+c3h6	2.22E+16	-0.9	30130.0
1188. pc4h9+c3h6=>c7h15-2	1.00E+11	0.0	8200.0
1189. c7h15-2=>c7h14-1+h	1.34E+15	-0.6	38760.0
1190. c7h14-1+h=>c7h15-2	1.00E+13	0.0	1200.0
1191. c7h15-2=>c7h14-2+h	2.71E+15	-0.7	37590.1
1192. c7h14-2+h=>c7h15-2	1.00E+13	0.0	2900.1
1193. c7h15-3=>c4h8-1+nc3h7	3.29E+11	0.2	22909.9
1194. c4h8-1+nc3h7=>c7h15-3	1.00E+11	0.0	7700.1
1195. c7h15-3=>c6h12-1+ch3	1.03E+14	-0.4	28690.0
1196. c6h12-1+ch3=>c7h15-3	1.75E+11	0.0	7200.1
1197. c7h15-3=>c7h14-2+h	2.71E+15	-0.7	37590.1
1198. c7h14-2+h=>c7h15-3	1.00E+13	0.0	2900.1
1199. c7h15-3=>c7h14-3+h	2.02E+15	-0.7	37680.0
1200. c7h14-3+h=>c7h15-3	1.00E+13	0.0	2900.1
1201. c7h15-4=>c2h5+c5h10-1	5.43E+16	-0.9	30590.1
1202. c2h5+c5h10-1=>c7h15-4	1.00E+11	0.0	8200.0
1203. c7h15-4=>c7h14-3+h	4.02E+15	-0.7	37680.0
1204. c7h14-3+h=>c7h15-4	1.00E+13	0.0	2900.1
1205. c7h15-1+o2=>c7h14-1+ho2	3.00E-09	0.0	3000.0
1206. c7h14-1+ho2=>c7h15-1+o2	2.44E-10	0.3	17919.9
1207. c7h15-2+o2=>c7h14-1+ho2	4.50E-09	0.0	5020.1
1208. c7h14-1+ho2=>c7h15-2+o2	1.15E-08	-0.1	17419.9
1209. c7h15-2+o2=>c7h14-2+ho2	3.00E-09	0.0	3000.0
1210. c7h14-2+ho2=>c7h15-2+o2	3.79E-09	0.1	18270.1
1211. c7h15-3+o2=>c7h14-2+ho2	3.00E-09	0.0	3000.0
1212. c7h14-2+ho2=>c7h15-3+o2	3.79E-09	0.1	18270.1
1213. c7h15-3+o2=>c7h14-3+ho2	3.00E-09	0.0	3000.0
1214. c7h14-3+ho2=>c7h15-3+o2	5.09E-09	0.0	18180.0
1215. c7h15-4+o2=>c7h14-3+ho2	6.00E-09	0.0	3000.0
1216. c7h14-3+ho2=>c7h15-4+o2	5.11E-09	0.0	18180.0
1217. c7h15-1=>c7h15-3	1.39E+09	1.0	33760.0
1218. c7h15-3=>c7h15-1	4.41E+07	1.4	36280.1
1219. c7h15-1=>c7h15-4	2.54E+09	0.3	19760.0
1220. c7h15-4=>c7h15-1	1.61E+08	0.7	22280.1
1221. c7h15-2=>c7h15-3	9.59E+08	1.4	39700.1
1222. c7h15-3=>c7h15-2	9.59E+08	1.4	39700.1
1223. c7h15-1=>c7h15-2	5.48E+08	1.6	38760.0
1224. c7h15-2=>c7h15-1	1.74E+07	2.0	41280.1
1225. c7h14-1+oh=>c7h13+h2o	3.00E+13	0.0	1229.9
1226. c7h13+h2o=>c7h14-1+oh	7.92E+14	-0.5	36479.9
1227. c7h14-2+oh=>c7h13+h2o	3.00E+13	0.0	1229.9
1228. c7h13+h2o=>c7h14-2+oh	1.60E+15	-0.6	33609.9
1229. c7h14-3+oh=>c7h13+h2o	3.00E+13	0.0	1229.9
1230. c7h13+h2o=>c7h14-3+oh	1.19E+15	-0.6	33700.1
1231. c7h14-1+h=>c7h13+h2	3.70E+13	0.0	3900.1
1232. c7h13+h2=>c7h14-1+h	2.26E+14	-0.5	23990.0
1233. c7h14-2+h=>c7h13+h2	3.70E+13	0.0	3900.1
1234. c7h13+h2=>c7h14-2+h	4.57E+14	-0.6	21120.0
1235. c7h14-3+h=>c7h13+h2	3.70E+13	0.0	3900.1
1236. c7h13+h2=>c7h14-3+h	3.40E+14	-0.6	21210.1
1237. c7h14-1+ch3=>c7h13+ch4	1.00E+12	0.0	7299.9
1238. c7h13+ch4=>c7h14-1+ch3	1.59E+14	-0.5	27870.0
1239. c7h14-2+ch3=>c7h13+ch4	1.00E+12	0.0	7299.9
1240. c7h13+ch4=>c7h14-2+ch3	3.23E+14	-0.6	25000.0

```
1241. c7h14-3+ch3=>c7h13+ch4                          1.00E+12    0.0     7299.9
1242. c7h13+ch4=>c7h14-3+ch3                          2.40E+14   -0.6    25090.1
1243. c7h14-1+o=>c7h13+oh                             2.62E+11    0.5    11909.9
1244. c7h13+oh=>c7h14-1+o                             7.00E+11    0.0    29900.1
1245. c7h14-2+o=>c7h13+oh                             1.29E+11    0.6    14780.1
1246. c7h13+oh=>c7h14-2+o                             7.00E+11    0.0    29900.1
1247. c7h14-3+o=>c7h13+oh                             1.73E+11    0.6    14690.0
1248. c7h13+oh=>c7h14-3+o                             7.00E+11    0.0    29900.1
1249. c7h14-1+oh=>ch2o+c6h13-1                        1.00E+11    0.0    -4000.0
1250. ch2o+c6h13-1=>c7h14-1+oh                        0.00E+00    0.0        0.0
1251. c7h14-1+oh=>ch3cho+c5h11-1                      1.00E+11    0.0    -4000.0
1252. ch3cho+c5h11-1=>c7h14-1+oh                      0.00E+00    0.0        0.0
1253. c7h14-2+oh=>ch3cho+c5h11-1                      1.00E+11    0.0    -4000.0
1254. ch3cho+c5h11-1=>c7h14-2+oh                      0.00E+00    0.0        0.0
1255. c7h14-2+oh=>c2h5cho+pc4h9                       1.00E+11    0.0    -4000.0
1256. c2h5cho+pc4h9=>c7h14-2+oh                       0.00E+00    0.0        0.0
1257. c7h14-3+oh=>c2h5cho+pc4h9                       1.00E+11    0.0    -4000.0
1258. c2h5cho+pc4h9=>c7h14-3+oh                       0.00E+00    0.0        0.0
1259. c7h14-1+o=>ch2cho+c5h11-1                       1.00E+11    0.0    -1050.0
1260. ch2cho+c5h11-1=>c7h14-1+o                       0.00E+00    0.0        0.0
1261. c7h14-2+o=>ch3cho+c5h10-1                       1.00E+11    0.0    -1050.0
1262. ch3cho+c5h10-1=>c7h14-2+o                       0.00E+00    0.0        0.0
1263. c7h14-3+o=>ch3cho+c5h10-1                       1.00E+11    0.0    -1050.0
1264. ch3cho+c5h10-1=>c7h14-3+o                       0.00E+00    0.0        0.0
1265. c7h13=>c3h5-a+c4h8-1                            2.50E+13    0.0    45000.0
1266. c3h5-a+c4h8-1=>c7h13                            1.00E+13    0.0     9599.9
1267. c7h13=>c4h7+c3h6                                2.50E+13    0.0    45000.0
1268. c4h7+c3h6=>c7h13                                1.00E+13    0.0     9599.9
1269. c7h14-1=>pc4h9+c3h5-a                           1.00E+16    0.0    71000.0
1270. pc4h9+c3h5-a=>c7h14-1                           1.00E+13    0.0        0.0
1271. c7h14-2=>c4h7+nc3h7                             1.00E+16    0.0    71000.0
1272. c4h7+nc3h7=>c7h14-2                             1.00E+13    0.0        0.0
1273. c7h14-3=>c4h7+nc3h7                             1.00E+16    0.0    71000.0
1274. c4h7+nc3h7=>c7h14-3                             1.00E+13    0.0        0.0
1275. c7h15o2-1=>c7h15-1+o2                           2.22E+19   -1.4    36090.1
1276. c7h15-1+o2=>c7h15o2-1                           4.52E+12    0.0        0.0
1277. c7h15o2-2=>c7h15-2+o2                           9.88E+21   -2.0    37859.9
1278. c7h15-2+o2=>c7h15o2-2                           7.54E+12    0.0        0.0
1279. c7h15o2-3=>c7h15-3+o2                           9.88E+21   -2.0    37859.9
1280. c7h15-3+o2=>c7h15o2-3                           7.54E+12    0.0        0.0
1281. c7h15o2-4=>c7h15-4+o2                           9.88E+21   -2.0    37859.9
1282. c7h15-4+o2=>c7h15o2-4                           7.54E+12    0.0        0.0
1283. c7h15-1+c7h15o2-1=>2c7h15o-1                    7.00E+12    0.0    -1000.0
1284. 2c7h15o-1=>c7h15-1+c7h15o2-1                    6.65E+14   -0.4    29570.0
1285. c7h15-1+c7h15o2-2=>c7h15o-1+c7h15o-2            7.00E+12    0.0    -1000.0
1286. c7h15o-1+c7h15o-2=>c7h15-1+c7h15o2-2            4.35E+14   -0.5    29700.0
1287. c7h15-1+c7h15o2-3=>c7h15o-1+c7h15o-3            7.00E+12    0.0    -1000.0
1288. c7h15o-1+c7h15o-3=>c7h15-1+c7h15o2-3            4.35E+14   -0.5    29700.0
1289. c7h15-2+c7h15o2-1=>c7h15o-2+c7h15o-1            7.00E+12    0.0    -1000.0
1290. c7h15o-2+c7h15o-1=>c7h15-2+c7h15o2-1            1.16E+17   -1.0    31469.9
1291. c7h15-2+c7h15o2-2=>2c7h15o-2                    7.00E+12    0.0    -1000.0
1292. 2c7h15o-2=>c7h15-2+c7h15o2-2                    7.57E+16   -1.1    31599.9
1293. c7h15-2+c7h15o2-3=>c7h15o-2+c7h15o-3            7.00E+12    0.0    -1000.0
1294. c7h15o-2+c7h15o-3=>c7h15-2+c7h15o2-3            7.57E+16   -1.1    31599.9
1295. c7h15-3+c7h15o2-1=>c7h15o-3+c7h15o-1            7.00E+12    0.0    -1000.0
1296. c7h15o-3+c7h15o-1=>c7h15-3+c7h15o2-1            1.16E+17   -1.0    31469.9
1297. c7h15-3+c7h15o2-2=>c7h15o-3+c7h15o-2            7.00E+12    0.0    -1000.0
1298. c7h15o-3+c7h15o-2=>c7h15-3+c7h15o2-2            7.57E+16   -1.1    31599.9
1299. c7h15-3+c7h15o2-3=>2c7h15o-3                    7.00E+12    0.0    -1000.0
1300. 2c7h15o-3=>c7h15-3+c7h15o2-3                    7.57E+16   -1.1    31599.9
1301. c7h15o2-1=>c7h14ooh1-2                          2.00E+11    0.0    26849.9
1302. c7h14ooh1-2=>c7h15o2-1                          1.78E+10   -0.1    14210.1
1303. c7h15o2-1=>c7h14ooh1-3                          2.50E+10    0.0    20849.9
1304. c7h14ooh1-3=>c7h15o2-1                          2.23E+09   -0.1     8210.1
1305. c7h15o2-1=>c7h14ooh1-4                          3.12E+09    0.0    19050.0
1306. c7h14ooh1-4=>c7h15o2-1                          2.79E+08   -0.1     6409.9
1307. c7h15o2-2=>c7h14ooh2-3                          2.00E+11    0.0    26849.9
1308. c7h14ooh2-3=>c7h15o2-2                          1.72E+10   -0.1    14210.1
```

1309. c7h15o2-2=>c7h14ooh2-4	2.50E+10	0.0	20849.9
1310. c7h14ooh2-4=>c7h15o2-2	2.14E+09	-0.1	8210.1
1311. c7h15o2-2=>c7h14ooh2-5	3.12E+09	0.0	19050.0
1312. c7h14ooh2-5=>c7h15o2-2	2.68E+08	-0.1	6409.9
1313. c7h15o2-3=>c7h14ooh3-1	3.75E+10	0.0	24400.1
1314. c7h14ooh3-1=>c7h15o2-3	8.88E+10	-0.5	9340.1
1315. c7h15o2-3=>c7h14ooh3-2	2.00E+11	0.0	26849.9
1316. c7h14ooh3-2=>c7h15o2-3	1.72E+10	-0.1	14210.1
1317. c7h15o2-3=>c7h14ooh3-4	2.00E+11	0.0	26849.9
1318. c7h14ooh3-4=>c7h15o2-3	1.72E+10	-0.1	14210.1
1319. c7h15o2-3=>c7h14ooh3-5	2.50E+10	0.0	20849.9
1320. c7h14ooh3-5=>c7h15o2-3	2.14E+09	-0.1	8210.1
1321. c7h15o2-3=>c7h14ooh3-6	3.12E+09	0.0	19050.0
1322. c7h14ooh3-6=>c7h15o2-3	2.68E+08	-0.1	6409.9
1323. c7h15o2-4=>c7h14ooh4-2	5.00E+10	0.0	20849.9
1324. c7h14ooh4-2=>c7h15o2-4	4.29E+09	-0.1	8210.1
1325. c7h15o2-4=>c7h14ooh4-3	4.00E+11	0.0	26849.9
1326. c7h14ooh4-3=>c7h15o2-4	3.43E+10	-0.1	14210.1
1327. c7h15o2-1+ho2=>c7h15o2h-1+o2	1.75E+10	0.0	-3275.1
1328. c7h15o2h-1+o2=>c7h15o2-1+ho2	4.92E+13	-0.8	34870.0
1329. c7h15o2-2+ho2=>c7h15o2h-2+o2	1.75E+10	0.0	-3275.1
1330. c7h15o2h-2+o2=>c7h15o2-2+ho2	4.93E+13	-0.8	34880.0
1331. c7h15o2-3+ho2=>c7h15o2h-3+o2	1.75E+10	0.0	-3275.1
1332. c7h15o2h-3+o2=>c7h15o2-3+ho2	4.93E+13	-0.8	34880.0
1333. h2o2+c7h15o2-1=>ho2+c7h15o2h-1	2.40E+12	0.0	10000.0
1334. ho2+c7h15o2h-1=>h2o2+c7h15o2-1	2.40E+12	0.0	10000.0
1335. h2o2+c7h15o2-2=>ho2+c7h15o2h-2	2.40E+12	0.0	10000.0
1336. ho2+c7h15o2h-2=>h2o2+c7h15o2-2	2.40E+12	0.0	10000.0
1337. h2o2+c7h15o2-3=>ho2+c7h15o2h-3	2.40E+12	0.0	10000.0
1338. ho2+c7h15o2h-3=>h2o2+c7h15o2-3	2.40E+12	0.0	10000.0
1339. c7h15o2-1+ch3o2=>c7h15o-1+ch3o+o2	1.40E+16	-1.6	1859.9
1340. c7h15o-1+ch3o+o2=>c7h15o2-1+ch3o2	0.00E+00	0.0	0.0
1341. c7h15o2-2+ch3o2=>c7h15o-2+ch3o+o2	1.40E+16	-1.6	1859.9
1342. c7h15o-2+ch3o+o2=>c7h15o2-2+ch3o2	0.00E+00	0.0	0.0
1343. c7h15o2-3+ch3o2=>c7h15o-3+ch3o+o2	1.40E+16	-1.6	1859.9
1344. c7h15o-3+ch3o+o2=>c7h15o2-3+ch3o2	0.00E+00	0.0	0.0
1345. 2c7h15o2-1=>o2+2c7h15o-1	1.40E+16	-1.6	1859.9
1346. o2+2c7h15o-1=>2c7h15o2-1	0.00E+00	0.0	0.0
1347. c7h15o2-1+c7h15o2-2=>c7h15o-1+c7h15o-2+o2	1.40E+16	-1.6	1859.9
1348. c7h15o-1+c7h15o-2+o2=>c7h15o2-1+c7h15o2-2	0.00E+00	0.0	0.0
1349. c7h15o2-1+c7h15o2-3=>c7h15o-1+c7h15o-3+o2	1.40E+16	-1.6	1859.9
1350. c7h15o-1+c7h15o-3+o2=>c7h15o2-1+c7h15o2-3	0.00E+00	0.0	0.0
1351. 2c7h15o2-2=>o2+2c7h15o-2	1.40E+16	-1.6	1859.9
1352. o2+2c7h15o-2=>2c7h15o2-2	0.00E+00	0.0	0.0
1353. c7h15o2-2+c7h15o2-3=>c7h15o-2+c7h15o-3+o2	1.40E+16	-1.6	1859.9
1354. c7h15o-2+c7h15o-3+o2=>c7h15o2-2+c7h15o2-3	0.00E+00	0.0	0.0
1355. 2c7h15o2-3=>o2+2c7h15o-3	1.40E+16	-1.6	1859.9
1356. o2+2c7h15o-3=>2c7h15o2-3	0.00E+00	0.0	0.0
1357. c7h15o2h-1=>c7h15o-1+oh	1.50E+16	0.0	42500.0
1358. c7h15o-1+oh=>c7h15o2h-1	1.75E+09	1.5	-3745.0
1359. c7h15o2h-2=>c7h15o-2+oh	1.25E+16	0.0	41599.9
1360. c7h15o-2+oh=>c7h15o2h-2	9.51E+08	1.4	-4525.1
1361. c7h15o2h-3=>c7h15o-3+oh	1.25E+16	0.0	41599.9
1362. c7h15o-3+oh=>c7h15o2h-3	9.51E+08	1.4	-4525.1
1363. c7h15o-1=>ch2o+c6h13-1	4.68E+17	-1.3	20260.0
1364. ch2o+c6h13-1=>c7h15o-1	1.00E+11	0.0	11900.1
1365. c7h15o-2=>ch3cho+c5h11-1	8.66E+21	-2.4	21880.0
1366. ch3cho+c5h11-1=>c7h15o-2	1.00E+11	0.0	12900.1
1367. c7h15o-3=>c2h5cho+pc4h9	5.60E+21	-2.3	21359.9
1368. c2h5cho+pc4h9=>c7h15o-3	1.00E+11	0.0	12900.1
1369. c7h14ooh1-2=>c7h14-1+ho2	5.38E+17	-1.8	19060.0
1370. c7h14-1+ho2=>c7h14ooh1-2	1.00E+11	0.0	10530.1
1371. c7h14ooh2-3=>c7h14-2+ho2	8.88E+18	-2.1	21479.9
1372. c7h14-2+ho2=>c7h14ooh2-3	1.00E+11	0.0	11530.1
1373. c7h14ooh3-2=>c7h14-2+ho2	8.88E+18	-2.1	21479.9
1374. c7h14-2+ho2=>c7h14ooh3-2	1.00E+11	0.0	11530.1
1375. c7h14ooh3-4=>c7h14-3+ho2	6.62E+18	-2.0	20570.0
1376. c7h14-3+ho2=>c7h14ooh3-4	1.00E+11	0.0	10530.1

1377. c7h14ooh4-3=>c7h14-3+ho2	1.32E+19	-2.0	20570.0
1378. c7h14-3+ho2=>c7h14ooh4-3	1.00E+11	0.0	10530.1
1379. c7h14ooh1-3=>c7h14o1-3+oh	7.50E+10	0.0	15250.0
1380. c7h14o1-3+oh=>c7h14ooh1-3	0.00E+00	0.0	0.0
1381. c7h14ooh1-4=>c7h14o1-4+oh	9.38E+09	0.0	7000.0
1382. c7h14o1-4+oh=>c7h14ooh1-4	0.00E+00	0.0	0.0
1383. c7h14ooh2-4=>c7h14o2-4+oh	7.50E+10	0.0	15250.0
1384. c7h14o2-4+oh=>c7h14ooh2-4	0.00E+00	0.0	0.0
1385. c7h14ooh2-5=>c7h14o2-5+oh	9.38E+09	0.0	7000.0
1386. c7h14o2-5+oh=>c7h14ooh2-5	0.00E+00	0.0	0.0
1387. c7h14ooh3-1=>c7h14o1-3+oh	7.50E+10	0.0	15250.0
1388. c7h14o1-3+oh=>c7h14ooh3-1	0.00E+00	0.0	0.0
1389. c7h14ooh3-5=>c7h14o3-5+oh	7.50E+10	0.0	15250.0
1390. c7h14o3-5+oh=>c7h14ooh3-5	0.00E+00	0.0	0.0
1391. c7h14ooh3-6=>c7h14o2-5+oh	9.38E+09	0.0	7000.0
1392. c7h14o2-5+oh=>c7h14ooh3-6	0.00E+00	0.0	0.0
1393. c7h14ooh4-2=>c7h14o2-4+oh	7.50E+10	0.0	15250.0
1394. c7h14o2-4+oh=>c7h14ooh4-2	0.00E+00	0.0	0.0
1395. c7h14ooh1-3=>oh+ch2o+c6h12-1	8.12E+13	-0.1	31090.1
1396. oh+ch2o+c6h12-1=>c7h14ooh1-3	0.00E+00	0.0	0.0
1397. c7h14ooh2-4=>oh+ch3cho+c5h10-1	5.36E+17	-1.4	26750.0
1398. oh+ch3cho+c5h10-1=>c7h14ooh2-4	0.00E+00	0.0	0.0
1399. c7h14ooh3-1=>oh+nc4h9cho+c2h4	2.21E+19	-1.7	26979.9
1400. oh+nc4h9cho+c2h4=>c7h14ooh3-1	0.00E+00	0.0	0.0
1401. c7h14ooh3-5=>oh+c2h5cho+c4h8-1	2.47E+18	-1.6	27020.1
1402. oh+c2h5cho+c4h8-1=>c7h14ooh3-5	0.00E+00	0.0	0.0
1403. c7h14ooh4-2=>oh+nc3h7cho+c3h6	1.30E+18	-1.5	26800.0
1404. oh+nc3h7cho+c3h6=>c7h14ooh4-2	0.00E+00	0.0	0.0
1405. c7h14ooh1-3o2=>c7h14ooh1-3+o2	6.00E+23	-2.5	38390.1
1406. c7h14ooh1-3+o2=>c7h14ooh1-3o2	7.54E+12	0.0	0.0
1407. c7h14ooh2-3o2=>c7h14ooh2-3+o2	6.35E+23	-2.5	38400.1
1408. c7h14ooh2-3+o2=>c7h14ooh2-3o2	7.54E+12	0.0	0.0
1409. c7h14ooh2-4o2=>c7h14ooh2-4+o2	6.35E+23	-2.5	38400.1
1410. c7h14ooh2-4+o2=>c7h14ooh2-4o2	7.54E+12	0.0	0.0
1411. c7h14ooh2-5o2=>c7h14ooh2-5+o2	6.35E+23	-2.5	38400.1
1412. c7h14ooh2-5+o2=>c7h14ooh2-5o2	7.54E+12	0.0	0.0
1413. c7h14ooh3-1o2=>c7h14ooh3-1+o2	1.60E+21	-2.0	36520.1
1414. c7h14ooh3-1+o2=>c7h14ooh3-1o2	4.52E+12	0.0	0.0
1415. c7h14ooh3-2o2=>c7h14ooh3-2+o2	6.35E+23	-2.5	38400.1
1416. c7h14ooh3-2+o2=>c7h14ooh3-2o2	7.54E+12	0.0	0.0
1417. c7h14ooh3-4o2=>c7h14ooh3-4+o2	6.35E+23	-2.5	38400.1
1418. c7h14ooh3-4+o2=>c7h14ooh3-4o2	7.54E+12	0.0	0.0
1419. c7h14ooh3-5o2=>c7h14ooh3-5+o2	6.35E+23	-2.5	38400.1
1420. c7h14ooh3-5+o2=>c7h14ooh3-5o2	7.54E+12	0.0	0.0
1421. c7h14ooh3-6o2=>c7h14ooh3-6+o2	6.35E+23	-2.5	38400.1
1422. c7h14ooh3-6+o2=>c7h14ooh3-6o2	7.54E+12	0.0	0.0
1423. c7h14ooh4-2o2=>c7h14ooh4-2+o2	3.19E+23	-2.5	38400.1
1424. c7h14ooh4-2+o2=>c7h14ooh4-2o2	7.54E+12	0.0	0.0
1425. c7h14ooh4-3o2=>c7h14ooh4-3+o2	3.19E+23	-2.5	38400.1
1426. c7h14ooh4-3+o2=>c7h14ooh4-3o2	7.54E+12	0.0	0.0
1427. c7h14ooh1-3o2=>nc7ket13+oh	2.50E+10	0.0	21400.1
1428. nc7ket13+oh=>c7h14ooh1-3o2	9.11E+02	1.7	43840.1
1429. c7h14ooh2-3o2=>nc7ket23+oh	1.00E+11	0.0	23849.9
1430. nc7ket23+oh=>c7h14ooh2-3o2	1.31E+04	1.5	45870.0
1431. c7h14ooh2-4o2=>nc7ket24+oh	1.25E+10	0.0	17849.9
1432. nc7ket24+oh=>c7h14ooh2-4o2	5.56E+01	1.9	43479.9
1433. c7h14ooh2-5o2=>nc7ket25+oh	1.56E+09	0.0	16050.0
1434. nc7ket25+oh=>c7h14ooh2-5o2	6.95E+00	1.9	41680.0
1435. c7h14ooh3-1o2=>nc7ket31+oh	1.25E+10	0.0	17849.9
1436. nc7ket31+oh=>c7h14ooh3-1o2	4.29E+01	1.9	43750.0
1437. c7h14ooh3-2o2=>nc7ket32+oh	1.00E+11	0.0	23849.9
1438. nc7ket32+oh=>c7h14ooh3-2o2	1.17E+04	1.5	46150.1
1439. c7h14ooh3-4o2=>nc7ket34+oh	1.00E+11	0.0	23849.9
1440. nc7ket34+oh=>c7h14ooh3-4o2	1.17E+04	1.5	46150.1
1441. c7h14ooh3-5o2=>nc7ket35+oh	1.25E+10	0.0	17849.9
1442. nc7ket35+oh=>c7h14ooh3-5o2	5.56E+01	1.9	43479.9
1443. c7h14ooh3-6o2=>nc7ket36+oh	1.56E+09	0.0	16050.0
1444. nc7ket36+oh=>c7h14ooh3-6o2	6.95E+00	1.9	41680.0

```
1445. c7h14ooh4-2o2=>nc7ket42+oh                    1.25E+10    0.0    17849.9
1446. nc7ket42+oh=>c7h14ooh4-2o2                    4.15E+01    1.9    43750.0
1447. c7h14ooh4-3o2=>nc7ket43+oh                    1.00E+11    0.0    23849.9
1448. nc7ket43+oh=>c7h14ooh4-3o2                    1.17E+04    1.5    46150.1
1449. nc7ket13=>nc4h9cho+ch2cho+oh                  1.05E+16    0.0    41599.9
1450. nc4h9cho+ch2cho+oh=>nc7ket13                  0.00E+00    0.0        0.0
1451. nc7ket23=>nc4h9cho+ch3co+oh                   1.05E+16    0.0    41599.9
1452. nc4h9cho+ch3co+oh=>nc7ket23                   0.00E+00    0.0        0.0
1453. nc7ket24=>nc3h7cho+ch3coch2+oh                1.05E+16    0.0    41599.9
1454. nc3h7cho+ch3coch2+oh=>nc7ket24                0.00E+00    0.0        0.0
1455. nc7ket25=>c2h5cho+ch2ch2coch3+oh              1.05E+16    0.0    41599.9
1456. c2h5cho+ch2ch2coch3+oh=>nc7ket25              0.00E+00    0.0        0.0
1457. nc7ket31=>ch2o+nc4h9coch2+oh                  1.50E+16    0.0    42000.0
1458. ch2o+nc4h9coch2+oh=>nc7ket31                  0.00E+00    0.0        0.0
1459. nc7ket32=>ch3cho+nc4h9co+oh                   1.05E+16    0.0    41599.9
1460. ch3cho+nc4h9co+oh=>nc7ket32                   0.00E+00    0.0        0.0
1461. nc7ket34=>nc3h7cho+c2h5co+oh                  1.05E+16    0.0    41599.9
1462. nc3h7cho+c2h5co+oh=>nc7ket34                  0.00E+00    0.0        0.0
1463. nc7ket35=>c2h5cho+c2h5coch2+oh                1.05E+16    0.0    41599.9
1464. c2h5cho+c2h5coch2+oh=>nc7ket35                0.00E+00    0.0        0.0
1465. nc7ket36=>ch3cho+c2h5coc2h4p+oh               1.05E+16    0.0    41599.9
1466. ch3cho+c2h5coc2h4p+oh=>nc7ket36               0.00E+00    0.0        0.0
1467. nc7ket42=>ch3cho+nc3h7coch2+oh                1.05E+16    0.0    41599.9
1468. ch3cho+nc3h7coch2+oh=>nc7ket42                0.00E+00    0.0        0.0
1469. nc7ket43=>c2h5cho+nc3h7co+oh                  1.05E+16    0.0    41599.9
1470. c2h5cho+nc3h7co+oh=>nc7ket43                  0.00E+00    0.0        0.0
1471. c7h14o1-3+oh=>c6h12-1+hco+h2o                 2.50E+12    0.0        0.0
1472. c6h12-1+hco+h2o=>c7h14o1-3+oh                 0.00E+00    0.0        0.0
1473. c7h14o1-4+oh=>c5h10-1+ch2cho+h2o              2.50E+12    0.0        0.0
1474. c5h10-1+ch2cho+h2o=>c7h14o1-4+oh              0.00E+00    0.0        0.0
1475. c7h14o2-4+oh=>ch3co+c5h10-1+h2o               2.50E+12    0.0        0.0
1476. ch3co+c5h10-1+h2o=>c7h14o2-4+oh               0.00E+00    0.0        0.0
1477. c7h14o2-5+oh=>ch3coch2+c4h8-1+h2o             2.50E+12    0.0        0.0
1478. ch3coch2+c4h8-1+h2o=>c7h14o2-5+oh             0.00E+00    0.0        0.0
1479. c7h14o3-5+oh=>c2h5co+c4h8-1+h2o               2.50E+12    0.0        0.0
1480. c2h5co+c4h8-1+h2o=>c7h14o3-5+oh               0.00E+00    0.0        0.0
1481. c7h14o1-3+oh=>c2h4+nc4h9co+h2o                2.50E+12    0.0        0.0
1482. c2h4+nc4h9co+h2o=>c7h14o1-3+oh                0.00E+00    0.0        0.0
1483. c7h14o1-4+oh=>c2h4+nc3h7coch2+h2o             2.50E+12    0.0        0.0
1484. c2h4+nc3h7coch2+h2o=>c7h14o1-4+oh             0.00E+00    0.0        0.0
1485. c7h14o2-4+oh=>c3h6+nc3h7co+h2o                2.50E+12    0.0        0.0
1486. c3h6+nc3h7co+h2o=>c7h14o2-4+oh                0.00E+00    0.0        0.0
1487. c7h14o2-5+oh=>c3h6+c2h5coch2+h2o              2.50E+12    0.0        0.0
1488. c3h6+c2h5coch2+h2o=>c7h14o2-5+oh              0.00E+00    0.0        0.0
1489. c7h14o3-5+oh=>c2h5cho+c4h7+h2o                2.50E+12    0.0        0.0
1490. c2h5cho+c4h7+h2o=>c7h14o3-5+oh                0.00E+00    0.0        0.0
1491. c7h14o1-3+ho2=>c6h12-1+hco+h2o2               5.00E+12    0.0    17700.0
1492. c6h12-1+hco+h2o2=>c7h14o1-3+ho2               0.00E+00    0.0        0.0
1493. c7h14o1-4+ho2=>c5h10-1+ch2cho+h2o2            5.00E+12    0.0    17700.0
1494. c5h10-1+ch2cho+h2o2=>c7h14o1-4+ho2            0.00E+00    0.0        0.0
1495. c7h14o2-4+ho2=>ch3co+c5h10-1+h2o2             5.00E+12    0.0    17700.0
1496. ch3co+c5h10-1+h2o2=>c7h14o2-4+ho2             0.00E+00    0.0        0.0
1497. c7h14o2-5+ho2=>ch3coch2+c4h8-1+h2o2           5.00E+12    0.0    17700.0
1498. ch3coch2+c4h8-1+h2o2=>c7h14o2-5+ho2           0.00E+00    0.0        0.0
1499. c7h14o3-5+ho2=>c2h5co+c4h8-1+h2o2             5.00E+12    0.0    17700.0
1500. c2h5co+c4h8-1+h2o2=>c7h14o3-5+ho2             0.00E+00    0.0        0.0
1501. c7h14o1-3+ho2=>c2h4+nc4h9co+h2o2              5.00E+12    0.0    17700.0
1502. c2h4+nc4h9co+h2o2=>c7h14o1-3+ho2              0.00E+00    0.0        0.0
1503. c7h14o1-4+ho2=>c2h4+nc3h7coch2+h2o2           5.00E+12    0.0    17700.0
1504. c2h4+nc3h7coch2+h2o2=>c7h14o1-4+ho2           0.00E+00    0.0        0.0
1505. c7h14o2-4+ho2=>c3h6+nc3h7co+h2o2              5.00E+12    0.0    17700.0
1506. c3h6+nc3h7co+h2o2=>c7h14o2-4+ho2              0.00E+00    0.0        0.0
1507. c7h14o2-5+ho2=>c3h6+c2h5coch2+h2o2            5.00E+12    0.0    17700.0
1508. c3h6+c2h5coch2+h2o2=>c7h14o2-5+ho2            0.00E+00    0.0        0.0
1509. c7h14o3-5+ho2=>c2h5cho+c4h7+h2o2              5.00E+12    0.0    17700.0
1510. c2h5cho+c4h7+h2o2=>c7h14o3-5+ho2              0.00E+00    0.0        0.0
1511. nc4h9coch2=>pc4h9+ch2co                       1.55E+18   -1.4    43140.1
1512. pc4h9+ch2co=>nc4h9coch2                       1.00E+11    0.0    11599.9
```

```
1513. c7h14ooh1-3=>c4h7ooh1-4+nc3h7                    3.82E+14   -0.7    27469.9
1514. c4h7ooh1-4+nc3h7=>c7h14ooh1-3                    8.50E+10    0.0     7799.9
1515. c7h14ooh1-4=>c5h10-1+c2h4+ho2                    2.44E+16   -1.1    29450.0
1516. c5h10-1+c2h4+ho2=>c7h14ooh1-4                    0.00E+00    0.0        0.0
1517. c7h14ooh2-4=>c5h9ooh1-4+c2h5                     1.67E+18   -1.8    27669.9
1518. c5h9ooh1-4+c2h5=>c7h14ooh2-4                     9.25E+10    0.0     7799.9
1519. c7h14ooh2-5=>c4h8-1+c3h6ooh2-1                   2.13E+16   -1.0    28800.0
1520. c4h8-1+c3h6ooh2-1=>c7h14ooh2-5                   8.50E+10    0.0     7799.9
1521. c7h15-1+ho2=>c7h15o-1+oh                         7.00E+12    0.0    -1000.0
1522. c7h15o-1+oh=>c7h15-1+ho2                         1.13E+16   -0.8    26990.0
1523. c7h15-2+ho2=>c7h15o-2+oh                         7.00E+12    0.0    -1000.0
1524. c7h15o-2+oh=>c7h15-2+ho2                         1.97E+18   -1.4    28890.1
1525. c7h15-3+ho2=>c7h15o-3+oh                         7.00E+12    0.0    -1000.0
1526. c7h15o-3+oh=>c7h15-3+ho2                         1.97E+18   -1.4    28890.1
1527. c7h15-1+ch3o2=>c7h15o-1+ch3o                     7.00E+12    0.0    -1000.0
1528. c7h15o-1+ch3o=>c7h15-1+ch3o2                     1.10E+18   -1.3    31750.0
1529. c7h15-2+ch3o2=>c7h15o-2+ch3o                     7.00E+12    0.0    -1000.0
1530. c7h15o-2+ch3o=>c7h15-2+ch3o2                     1.92E+20   -1.9    33659.9
1531. c7h15-3+ch3o2=>c7h15o-3+ch3o                     7.00E+12    0.0    -1000.0
1532. c7h15o-3+ch3o=>c7h15-3+ch3o2                     1.92E+20   -1.9    33659.9
1533. c4h7ooh1-4=>c4h7o1-4+oh                          2.02E+20   -1.5    47039.9
1534. c4h7o1-4+oh=>c4h7ooh1-4                          2.00E+13    0.0        0.0
1535. c5h9ooh1-4=>c5h9o1-4+oh                          1.18E+20   -1.4    46049.9
1536. c5h9o1-4+oh=>c5h9ooh1-4                          2.00E+13    0.0        0.0
1537. c4h7o1-4=>ch2o+c3h5-a                            2.41E+16   -1.1     7549.9
1538. ch2o+c3h5-a=>c4h7o1-4                            1.00E+11    0.0    11900.1
1539. c5h9o1-4=>ch3cho+c3h5-a                          7.72E+20   -2.4     5890.1
1540. ch3cho+c3h5-a=>c5h9o1-4                          5.00E+10    0.0     9599.9
1541. o+ch<=>h+co                                      5.70E+13    0.0        0.0
1542. o+ch2<=>h+hco                                    8.00E+13    0.0        0.0
1543. o+ch2(s)<=>h2+co                                 1.50E+13    0.0        0.0
1544. o+ch2(s)<=>h+hco                                 1.50E+13    0.0        0.0
1545. o+ch2oh<=>oh+ch2o                                1.00E+13    0.0        0.0
1546. o+ch3o<=>oh+ch2o                                 1.00E+13    0.0        0.0
1547. o+ch3oh<=>oh+ch3o                                1.30E+05    2.5     5000.0
1548. o+c2h5<=>ch3+ch2o                                2.24E+13    0.0        0.0
1549. h+2o2<=>ho2+o2                                   2.08E+19   -1.2        0.0
1550. h+o2+h2o<=>ho2+h2o                               1.13E+19   -0.8        0.0
1551. h+o2+n2<=>ho2+n2                                 2.60E+19   -1.2        0.0
1552. h+o2+ar<=>ho2+ar                                 7.00E+17   -0.8        0.0
1553. 2h+h2<=>2h2                                      9.00E+16   -0.6        0.0
1554. 2h+h2o<=>h2+h2o                                  6.00E+19   -1.2        0.0
1555. 2h+co2<=>h2+co2                                  5.50E+20   -2.0        0.0
1556. h+ch<=>c+h2                                      1.65E+14    0.0        0.0
1557. h+ch2oh<=>h2+ch2o                                2.00E+13    0.0        0.0
1558. h+ch2oh<=>oh+ch3                                 1.65E+11    0.7     -284.0
1559. h+ch2oh<=>ch2(s)+h2o                             3.28E+13   -0.1      610.0
1560. h+ch3o(+m)<=>ch3oh(+m)                           2.43E+12    0.5       50.0
      Low pressure limit:  0.46600E+42 -0.74400E+01  0.14080E+05
      TROE centering:      0.70000E+00  0.10000E+03  0.90000E+05  0.10000E+05
      h2              Enhanced by    2.000E+00
      h2o             Enhanced by    6.000E+00
      ch4             Enhanced by    2.000E+00
      co              Enhanced by    1.500E+00
      co2             Enhanced by    2.000E+00
      c2h6            Enhanced by    3.000E+00
1561. h+ch3o<=>h+ch2oh                                 4.15E+07    1.6     1924.0
1562. h+ch3o<=>h2+ch2o                                 2.00E+13    0.0        0.0
1563. h+ch3o<=>oh+ch3                                  1.50E+12    0.5     -110.0
1564. h+ch3o<=>ch2(s)+h2o                              2.62E+14   -0.2     1070.0
1565. h+c2h5(+m)<=>c2h6(+m)                            5.21E+17   -1.0     1580.0
      Low pressure limit:  0.19900E+42 -0.70800E+01  0.66850E+04
      TROE centering:      0.84220E+00  0.12500E+03  0.22190E+04  0.68820E+04
      h2              Enhanced by    2.000E+00
      h2o             Enhanced by    6.000E+00
      ch4             Enhanced by    2.000E+00
      co              Enhanced by    1.500E+00
      co2             Enhanced by    2.000E+00
```

```
      c2h6            Enhanced by    3.000E+00
      ar              Enhanced by    7.000E-01
1566. h+c2h5<=>h2+c2h4                                2.00E+12    0.0        0.0
1567. h+hccoh<=>h+ch2co                               1.00E+13    0.0        0.0
1568. oh+h2o2<=>ho2+h2o                               2.00E+12    0.0      427.0
      Declared duplicate reaction...
1569. oh+h2o2<=>ho2+h2o                               1.70E+18    0.0    29410.0
      Declared duplicate reaction...
1570. oh+c<=>h+co                                     5.00E+13    0.0        0.0
1571. oh+ch<=>h+hco                                   3.00E+13    0.0        0.0
1572. oh+ch2<=>h+ch2o                                 2.00E+13    0.0        0.0
1573. oh+ch2oh<=>h2o+ch2o                             5.00E+12    0.0        0.0
1574. oh+ch3o<=>h2o+ch2o                              5.00E+12    0.0        0.0
1575. oh+c2h<=>h+hcco                                 2.00E+13    0.0        0.0
1576. oh+c2h2<=>h+hccoh                               5.04E+05    2.3    13500.0
1577. oh+c2h2<=>ch3+co                                4.83E-04    4.0    -2000.0
1578. oh+c2h3<=>h2o+c2h2                              5.00E+12    0.0        0.0
1579. 2ho2<=>o2+h2o2                                  1.30E+11    0.0    -1630.0
      Declared duplicate reaction...
1580. 2ho2<=>o2+h2o2                                  4.20E+14    0.0    12000.0
      Declared duplicate reaction...
1581. ho2+ch2<=>oh+ch2o                               2.00E+13    0.0        0.0
1582. c+o2<=>o+co                                     5.80E+13    0.0      576.0
1583. c+ch2<=>h+c2h                                   5.00E+13    0.0        0.0
1584. c+ch3<=>h+c2h2                                  5.00E+13    0.0        0.0
1585. ch+h2o<=>h+ch2o                                 5.71E+12    0.0     -755.0
1586. ch+ch2<=>h+c2h2                                 4.00E+13    0.0        0.0
1587. ch+ch3<=>h+c2h3                                 3.00E+13    0.0        0.0
1588. ch+co(+m)<=>hcco(+m)                            5.00E+13    0.0        0.0
      Low pressure limit:  0.26900E+29 -0.37400E+01  0.19360E+04
      TROE centering:      0.57570E+00  0.23700E+03  0.16520E+04  0.50690E+04
      h2              Enhanced by    2.000E+00
      h2o             Enhanced by    6.000E+00
      ch4             Enhanced by    2.000E+00
      co              Enhanced by    1.500E+00
      co2             Enhanced by    2.000E+00
      c2h6            Enhanced by    3.000E+00
      ar              Enhanced by    7.000E-01
1589. ch+co2<=>hco+co                                 1.90E+14    0.0    15792.0
1590. ch+ch2o<=>h+ch2co                               9.46E+13    0.0     -515.0
1591. ch+hcco<=>co+c2h2                               5.00E+13    0.0        0.0
1592. ch2+o2=>oh+h+co                                 5.00E+12    0.0     1500.0
1593. 2ch2<=>h2+c2h2                                  1.60E+15    0.0    11944.0
1594. ch2+ch3<=>h+c2h4                                4.00E+13    0.0        0.0
1595. ch2+ch4<=>2ch3                                  2.46E+06    2.0     8270.0
1596. ch2+hcco<=>c2h3+co                              3.00E+13    0.0        0.0
1597. ch2(s)+n2<=>ch2+n2                              1.50E+13    0.0      600.0
1598. ch2(s)+ar<=>ch2+ar                              9.00E+12    0.0      600.0
1599. ch2(s)+o2<=>co+h2o                              1.20E+13    0.0        0.0
1600. ch2(s)+h2o(+m)<=>ch3oh(+m)                      4.82E+17   -1.2     1145.0
      Low pressure limit:  0.18800E+39 -0.63600E+01  0.50400E+04
      TROE centering:      0.60270E+00  0.20800E+03  0.39220E+04  0.10180E+05
      h2              Enhanced by    2.000E+00
      h2o             Enhanced by    6.000E+00
      ch4             Enhanced by    2.000E+00
      co              Enhanced by    1.500E+00
      co2             Enhanced by    2.000E+00
      c2h6            Enhanced by    3.000E+00
1601. ch2(s)+h2o<=>ch2+h2o                            3.00E+13    0.0        0.0
1602. ch2(s)+co<=>ch2+co                              9.00E+12    0.0        0.0
1603. ch2(s)+co2<=>ch2+co2                            7.00E+12    0.0        0.0
1604. hco+h2o<=>h+co+h2o                              1.50E+18   -1.0    17000.0
1605. c2h+h2<=>h+c2h2                                 5.68E+10    0.9     1993.0
1606. hcco+o2<=>oh+2co                                3.20E+12    0.0      854.0
1607. 2hcco<=>2co+c2h2                                1.00E+13    0.0        0.0
1608. n+no<=>n2+o                                     2.70E+13    0.0      355.0
1609. n+o2<=>no+o                                     9.00E+09    1.0     6500.0
1610. n+oh<=>no+h                                     3.36E+13    0.0      385.0
```

```
1611. n2o+o<=>n2+o2                                   1.40E+12    0.0    10810.0
1612. n2o+o<=>2no                                     2.90E+13    0.0    23150.0
1613. n2o+h<=>n2+oh                                   3.87E+14    0.0    18880.0
1614. n2o+oh<=>n2+ho2                                 2.00E+12    0.0    21060.0
1615. n2o(+m)<=>n2+o(+m)                              7.91E+10    0.0    56020.0
      Low pressure limit:  0.63700E+15  0.00000E+00  0.56640E+05
      h2              Enhanced by    2.000E+00
      h2o             Enhanced by    6.000E+00
      ch4             Enhanced by    2.000E+00
      co              Enhanced by    1.500E+00
      co2             Enhanced by    2.000E+00
      c2h6            Enhanced by    3.000E+00
      ar              Enhanced by    6.250E-01
1616. ho2+no<=>no2+oh                                 2.11E+12    0.0     -480.0
1617. no+o+m<=>no2+m                                  1.06E+20   -1.4        0.0
      h2              Enhanced by    2.000E+00
      h2o             Enhanced by    6.000E+00
      ch4             Enhanced by    2.000E+00
      co              Enhanced by    1.500E+00
      co2             Enhanced by    2.000E+00
      c2h6            Enhanced by    3.000E+00
      ar              Enhanced by    7.000E-01
1618. no2+o<=>no+o2                                   3.90E+12    0.0     -240.0
1619. no2+h<=>no+oh                                   1.32E+14    0.0      360.0
1620. nh+o<=>no+h                                     4.00E+13    0.0        0.0
1621. nh+h<=>n+h2                                     3.20E+13    0.0      330.0
1622. nh+oh<=>hno+h                                   2.00E+13    0.0        0.0
1623. nh+oh<=>n+h2o                                   2.00E+09    1.2        0.0
1624. nh+o2<=>hno+o                                   4.61E+05    2.0     6500.0
1625. nh+o2<=>no+oh                                   1.28E+06    1.5      100.0
1626. nh+n<=>n2+h                                     1.50E+13    0.0        0.0
1627. nh+h2o<=>hno+h2                                 2.00E+13    0.0    13850.0
1628. nh+no<=>n2+oh                                   2.16E+13   -0.2        0.0
1629. nh+no<=>n2o+h                                   3.65E+14   -0.5        0.0
1630. nh2+o<=>oh+nh                                   3.00E+12    0.0        0.0
1631. nh2+o<=>h+hno                                   3.90E+13    0.0        0.0
1632. nh2+h<=>nh+h2                                   4.00E+13    0.0     3650.0
1633. nh2+oh<=>nh+h2o                                 9.00E+07    1.5     -460.0
1634. nnh<=>n2+h                                      3.30E+08    0.0        0.0
1635. nnh+m<=>n2+h+m                                  1.30E+14   -0.1     4980.0
      h2              Enhanced by    2.000E+00
      h2o             Enhanced by    6.000E+00
      ch4             Enhanced by    2.000E+00
      co              Enhanced by    1.500E+00
      co2             Enhanced by    2.000E+00
      c2h6            Enhanced by    3.000E+00
      ar              Enhanced by    7.000E-01
1636. nnh+o2<=>ho2+n2                                 5.00E+12    0.0        0.0
1637. nnh+o<=>oh+n2                                   2.50E+13    0.0        0.0
1638. nnh+o<=>nh+no                                   7.00E+13    0.0        0.0
1639. nnh+h<=>h2+n2                                   5.00E+13    0.0        0.0
1640. nnh+oh<=>h2o+n2                                 2.00E+13    0.0        0.0
1641. nnh+ch3<=>ch4+n2                                2.50E+13    0.0        0.0
1642. h+no+m<=>hno+m                                  4.48E+19   -1.3      740.0
      h2              Enhanced by    2.000E+00
      h2o             Enhanced by    6.000E+00
      ch4             Enhanced by    2.000E+00
      co              Enhanced by    1.500E+00
      co2             Enhanced by    2.000E+00
      c2h6            Enhanced by    3.000E+00
      ar              Enhanced by    7.000E-01
1643. hno+o<=>no+oh                                   2.50E+13    0.0        0.0
1644. hno+h<=>h2+no                                   9.00E+11    0.7      660.0
1645. hno+oh<=>no+h2o                                 1.30E+07    1.9     -950.0
1646. hno+o2<=>ho2+no                                 1.00E+13    0.0    13000.0
1647. cn+o<=>co+n                                     7.70E+13    0.0        0.0
1648. cn+oh<=>nco+h                                   4.00E+13    0.0        0.0
1649. cn+h2o<=>hcn+oh                                 8.00E+12    0.0     7460.0
```

```
1650. cn+o2<=>nco+o                                   6.14E+12    0.0     -440.0
1651. cn+h2<=>hcn+h                                   2.95E+05    2.5     2240.0
1652. nco+o<=>no+co                                   2.35E+13    0.0        0.0
1653. nco+h<=>nh+co                                   5.40E+13    0.0        0.0
1654. nco+oh<=>no+h+co                                2.50E+12    0.0        0.0
1655. nco+n<=>n2+co                                   2.00E+13    0.0        0.0
1656. nco+o2<=>no+co2                                 2.00E+12    0.0    20000.0
1657. nco+m<=>n+co+m                                  3.10E+14    0.0    54050.0
      h2              Enhanced by    2.000E+00
      h2o             Enhanced by    6.000E+00
      ch4             Enhanced by    2.000E+00
      co              Enhanced by    1.500E+00
      co2             Enhanced by    2.000E+00
      c2h6            Enhanced by    3.000E+00
      ar              Enhanced by    7.000E-01
1658. nco+no<=>n2o+co                                 1.90E+17   -1.5      740.0
1659. nco+no<=>n2+co2                                 3.80E+18   -2.0      800.0
1660. hcn+m<=>h+cn+m                                  1.04E+29   -3.3   126600.0
      h2              Enhanced by    2.000E+00
      h2o             Enhanced by    6.000E+00
      ch4             Enhanced by    2.000E+00
      co              Enhanced by    1.500E+00
      co2             Enhanced by    2.000E+00
      c2h6            Enhanced by    3.000E+00
      ar              Enhanced by    7.000E-01
1661. hcn+o<=>nco+h                                   2.03E+04    2.6     4980.0
1662. hcn+o<=>nh+co                                   5.07E+03    2.6     4980.0
1663. hcn+o<=>cn+oh                                   3.91E+09    1.6    26600.0
1664. hcn+oh<=>hocn+h                                 1.10E+06    2.0    13370.0
1665. hcn+oh<=>hnco+h                                 4.40E+03    2.3     6400.0
1666. hcn+oh<=>nh2+co                                 1.60E+02    2.6     9000.0
1667. h+hcn(+m)<=>h2cn(+m)                            3.30E+13    0.0        0.0
      Low pressure limit:  0.14000E+27 -0.34000E+01  0.19000E+04
      h2              Enhanced by    2.000E+00
      h2o             Enhanced by    6.000E+00
      ch4             Enhanced by    2.000E+00
      co              Enhanced by    1.500E+00
      co2             Enhanced by    2.000E+00
      c2h6            Enhanced by    3.000E+00
      ar              Enhanced by    7.000E-01
1668. h2cn+n<=>n2+ch2                                 6.00E+13    0.0      400.0
1669. c+n2<=>cn+n                                     6.30E+13    0.0    46020.0
1670. ch+n2<=>hcn+n                                   3.12E+09    0.9    20130.0
1671. ch+n2(+m)<=>hcnn(+m)                            3.10E+12    0.1        0.0
      Low pressure limit:  0.13000E+26 -0.31600E+01  0.74000E+03
      TROE centering:      0.66700E+00  0.23500E+03  0.21170E+04  0.45360E+04
      h2              Enhanced by    2.000E+00
      h2o             Enhanced by    6.000E+00
      ch4             Enhanced by    2.000E+00
      co              Enhanced by    1.500E+00
      co2             Enhanced by    2.000E+00
      c2h6            Enhanced by    3.000E+00
      ar              Enhanced by    1.000E+00
1672. ch2+n2<=>hcn+nh                                 1.00E+13    0.0    74000.0
1673. ch2(s)+n2<=>nh+hcn                              1.00E+11    0.0    65000.0
1674. c+no<=>cn+o                                     1.90E+13    0.0        0.0
1675. c+no<=>co+n                                     2.90E+13    0.0        0.0
1676. ch+no<=>hcn+o                                   4.10E+13    0.0        0.0
1677. ch+no<=>h+nco                                   1.62E+13    0.0        0.0
1678. ch+no<=>n+hco                                   2.46E+13    0.0        0.0
1679. ch2+no<=>h+hnco                                 3.10E+17   -1.4     1270.0
1680. ch2+no<=>oh+hcn                                 2.90E+14   -0.7      760.0
1681. ch2+no<=>h+hcno                                 3.80E+13   -0.4      580.0
1682. ch2(s)+no<=>h+hnco                              3.10E+17   -1.4     1270.0
1683. ch2(s)+no<=>oh+hcn                              2.90E+14   -0.7      760.0
1684. ch2(s)+no<=>h+hcno                              3.80E+13   -0.4      580.0
1685. ch3+no<=>hcn+h2o                                9.60E+13    0.0    28800.0
1686. ch3+no<=>h2cn+oh                                1.00E+12    0.0    21750.0
```

```
1687. hcnn+o<=>co+h+n2                                2.20E+13    0.0        0.0
1688. hcnn+o<=>hcn+no                                 2.00E+12    0.0        0.0
1689. hcnn+o2<=>o+hco+n2                              1.20E+13    0.0        0.0
1690. hcnn+oh<=>h+hco+n2                              1.20E+13    0.0        0.0
1691. hcnn+h<=>ch2+n2                                 1.00E+14    0.0        0.0
1692. hnco+o<=>nh+co2                                 9.80E+07    1.4     8500.0
1693. hnco+o<=>hno+co                                 1.50E+08    1.6    44000.0
1694. hnco+o<=>nco+oh                                 2.20E+06    2.1    11400.0
1695. hnco+h<=>nh2+co                                 2.25E+07    1.7     3800.0
1696. hnco+h<=>h2+nco                                 1.05E+05    2.5    13300.0
1697. hnco+oh<=>nco+h2o                               3.30E+07    1.5     3600.0
1698. hnco+oh<=>nh2+co2                               3.30E+06    1.5     3600.0
1699. hnco+m<=>nh+co+m                                1.18E+16    0.0    84720.0
      h2              Enhanced by    2.000E+00
      h2o             Enhanced by    6.000E+00
      ch4             Enhanced by    2.000E+00
      co              Enhanced by    1.500E+00
      co2             Enhanced by    2.000E+00
      c2h6            Enhanced by    3.000E+00
      ar              Enhanced by    7.000E-01
1700. hcno+h<=>h+hnco                                 2.10E+15   -0.7     2850.0
1701. hcno+h<=>oh+hcn                                 2.70E+11    0.2     2120.0
1702. hcno+h<=>nh2+co                                 1.70E+14   -0.8     2890.0
1703. hocn+h<=>h+hnco                                 2.00E+07    2.0     2000.0
1704. hcco+no<=>hcno+co                               9.00E+12    0.0        0.0
1705. ch3+n<=>h2cn+h                                  6.10E+14   -0.3      290.0
1706. ch3+n<=>hcn+h2                                  3.70E+12    0.1      -90.0
1707. nh3+h<=>nh2+h2                                  5.40E+05    2.4     9915.0
1708. nh3+oh<=>nh2+h2o                                5.00E+07    1.6      955.0
1709. nh3+o<=>nh2+oh                                  9.40E+06    1.9     6460.0
1710. nh+co2<=>hno+co                                 1.00E+13    0.0    14350.0
1711. cn+no2<=>nco+no                                 6.16E+15   -0.8      345.0
1712. nco+no2<=>n2o+co2                               3.25E+12    0.0     -705.0
1713. n+co2<=>no+co                                   3.00E+12    0.0    11300.0
1714. o+ch3=>h+h2+co                                  3.37E+13    0.0        0.0
1715. ch+h2(+m)<=>ch3(+m)                             1.97E+12    0.4     -370.0
      Low pressure limit:  0.48200E+26 -0.28000E+01  0.59000E+03
      TROE centering:      0.57800E+00  0.12200E+03  0.25350E+04  0.93650E+04
      h2              Enhanced by    2.000E+00
      h2o             Enhanced by    6.000E+00
      ch4             Enhanced by    2.000E+00
      co              Enhanced by    1.500E+00
      co2             Enhanced by    2.000E+00
      c2h6            Enhanced by    3.000E+00
      ar              Enhanced by    7.000E-01
1716. ch2+ch2=>2h+c2h2                                2.00E+14    0.0    10989.0
1717. ch2(s)+h2o=>h2+ch2o                             6.82E+10    0.2     -935.0
1718. c2h3+o2<=>ho2+c2h2                              1.34E+06    1.6     -384.0
      Declared duplicate reaction...
1719. o+ch3cho<=>oh+ch2cho                            2.92E+12    0.0     1808.0
1720. o+ch3cho=>oh+ch3+co                             2.92E+12    0.0     1808.0
1721. o2+ch3cho=>ho2+ch3+co                           3.01E+13    0.0    39150.0
1722. h+ch3cho<=>ch2cho+h2                            2.05E+09    1.2     2405.0
1723. h+ch3cho=>ch3+h2+co                             2.05E+09    1.2     2405.0
1724. oh+ch3cho=>ch3+h2o+co                           2.34E+10    0.7    -1113.0
1725. ho2+ch3cho=>ch3+h2o2+co                         3.01E+12    0.0    11923.0
1726. ch3+ch3cho=>ch3+ch4+co                          2.72E+06    1.8     5920.0
1727. h+ch2co(+m)<=>ch2cho(+m)                        4.86E+11    0.4    -1755.0
      Low pressure limit:  0.10120E+43 -0.76300E+01  0.38540E+04
      TROE centering:      0.46500E+00  0.20100E+03  0.17730E+04  0.53330E+04
      h2              Enhanced by    2.000E+00
      h2o             Enhanced by    6.000E+00
      ch4             Enhanced by    2.000E+00
      co              Enhanced by    1.500E+00
      co2             Enhanced by    2.000E+00
      c2h6            Enhanced by    3.000E+00
      ar              Enhanced by    7.000E-01
1728. o+ch2cho=>h+ch2+co                              1.50E+14    0.0        0.0
```

```
1729. o2+ch2cho=>oh+2hco                                2.35E+10    0.0        0.0
1730. h+ch2cho<=>ch3+hco                                2.20E+13    0.0        0.0
1731. h+ch2cho<=>ch2co+h2                               1.10E+13    0.0        0.0
1732. oh+ch2cho<=>h2o+ch2co                             1.20E+13    0.0        0.0
1733. oh+ch2cho<=>hco+ch2oh                             3.01E+13    0.0        0.0
1734. ch3+c2h5(+m)<=>c3h8(+m)                           9.43E+12    0.0        0.0
      Low pressure limit:  0.27100E+75 -0.16820E+02  0.13065E+05
      TROE centering:      0.15270E+00  0.29100E+03  0.27420E+04  0.77480E+04
      h2              Enhanced by    2.000E+00
      h2o             Enhanced by    6.000E+00
      ch4             Enhanced by    2.000E+00
      co              Enhanced by    1.500E+00
      co2             Enhanced by    2.000E+00
      c2h6            Enhanced by    3.000E+00
      ar              Enhanced by    7.000E-01
1735. o+c3h8<=>oh+c3h7                                  1.93E+05    2.7     3716.0
1736. h+c3h8<=>c3h7+h2                                  1.32E+06    2.5     6756.0
1737. oh+c3h8<=>c3h7+h2o                                3.16E+07    1.8      934.0
1738. c3h7+h2o2<=>ho2+c3h8                              3.78E+02    2.7     1500.0
1739. ch3+c3h8<=>c3h7+ch4                               9.03E-01    3.6     7154.0
1740. ch3+c2h4(+m)<=>c3h7(+m)                           2.55E+06    1.6     5700.0
      Low pressure limit:  0.30000E+64 -0.14600E+02  0.18170E+05
      TROE centering:      0.18940E+00  0.27700E+03  0.87480E+04  0.78910E+04
      h2              Enhanced by    2.000E+00
      h2o             Enhanced by    6.000E+00
      ch4             Enhanced by    2.000E+00
      co              Enhanced by    1.500E+00
      co2             Enhanced by    2.000E+00
      c2h6            Enhanced by    3.000E+00
      ar              Enhanced by    7.000E-01
1741. o+c3h7<=>c2h5+ch2o                                9.64E+13    0.0        0.0
1742. h+c3h7(+m)<=>c3h8(+m)                             3.61E+13    0.0        0.0
      Low pressure limit:  0.44200E+62 -0.13545E+02  0.11357E+05
      TROE centering:      0.31500E+00  0.36900E+03  0.32850E+04  0.66670E+04
      h2              Enhanced by    2.000E+00
      h2o             Enhanced by    6.000E+00
      ch4             Enhanced by    2.000E+00
      co              Enhanced by    1.500E+00
      co2             Enhanced by    2.000E+00
      c2h6            Enhanced by    3.000E+00
      ar              Enhanced by    7.000E-01
1743. h+c3h7<=>ch3+c2h5                                 4.06E+06    2.2      890.0
1744. oh+c3h7<=>c2h5+ch2oh                              2.41E+13    0.0        0.0
1745. ho2+c3h7<=>o2+c3h8                                2.55E+10    0.3     -943.0
1746. ho2+c3h7=>oh+c2h5+ch2o                            2.41E+13    0.0        0.0
1747. ch3+c3h7<=>2c2h5                                  1.93E+13   -0.3        0.0

 UNITS for the preceding reactions (unless otherwise noted):
       A units mole-cm-sec-K, E units cal/mole



 NO ERRORS FOUND ON INPUT:
 ASCII Vers. 4.5.0 CHEMKIN linkfile chem.asc written.

 GAS PHASE WORKING SPACE REQUIREMENTS ARE
    INTEGER:      90645
    REAL:         31577
    CHARACTER:      186

 Total CPUtime: 2 (seconds)
```

Appendix D. – Investigation of Optimum Range

The calculations for fuel cell efficiency and engine specific fuel consumption, fuel cell and engine power and the combined system power for various load conditions is given in Table 2 - Table 7 below.

Table 2 – Calculation for compressor and fuel cell at various load conditions

	Full Load operation SOFC		Half load operation of SOFC		Idle load operation	
Compressor		**Units**		**Units**		**Units**
Input pressure	1	bar	1	bar	1	bar
Output pressure	3	bar	2.4	bar	1.8	bar
Pressure ratio	3		2.4		1.8	
Mass flow rate	0.0204	kg/s	0.0095	kg/s	0.0045	kg/s
Mass flow factor	0.3522	kg/s K1/2 bar	0.1643	kg/s K1/2 bar	0.0770	kg/s K1/2 bar
Efficiency	0.76		0.74		0.68	
at rotor speed	109898		94935		79929	
Temperature in						
Tin	298	K	298	K	298	K
DT = Tout - Tin	144.75	K	114.58	K	80.22	K
Temperature out						
Tout	442.75	K	412.58	K	378.22	K
γ	1004		1004		1004	
Power used	2.96	KW	1.10	KW	0.36	KW
Electric motor power for compressor (motor efficiency 60%)	5	KW	3	KW	1.2	KW
Solid Oxide Fuel Cell						
Cell vtg	0.7		0.75		0.8	
Power output	**20**	**KW**	**10**	**KW**	**5**	**KW**
QLHV Hydrogen	1.20E+08	J/kg	1.20E+08	J/kg	1.20E+08	J/kg
Stoichiometry	2		2		2	
Fuel Utilisation	**0.90**		**0.90**		**0.88**	
Air mass flow rate in	0.0204	kg/s	0.0095	kg/s	0.0045	kg/s
Oxygen usage rate	0.0024	kg/s	0.0011	kg/s	0.0005	kg/s
Air mass flow rate out	0.0180	kg/s	0.0084		0.0039	
Fuel mass flow rate in	3.35E-04	kg/s	1.55E-04	kg/s	7.50E-05	kg/s
Hydrogen usage	3.00E-04	kg/s	1.40E-04	kg/s	6.56E-05	kg/s
Fuel mass flow rate out	3.50E-05	kg/s	1.50E-05	kg/s	9.38E-06	kg/s
Equivalent to energy of fuel supplied to fuel cell	40.23	kW	18.62	KW	9.01	KW
Fuel cell efficiency	**0.50**		**0.54**		**0.56**	
Current I	57476.4	Amp	24820.7	Amp	11259.4	Amp
Current density	0.5	A/cm2	0.5	A/cm2	0.5	A/cm2
Stack electrode area	114952.9	cm2				
Cell active area	720	cm2				
No. of cells	160	cells	160		160	
DC vtg output	180.54	V	84.07	V	39.41	V

Table 3 – Diesel engine operation at various load conditions

Engine →	Diesel Engine Operation at various speed condition & min BSFC										idle conditions	
	100% speed	Units	80% speed	Units	70% speed	Units	60% power o/p	Units	40% power o/p	Units		Units
Power	100.00	KW	80.00	KW	70.00	KW	60.00	KW	40.00	KW	8.00	KW
bore	0.1350	m	0.1350	m	0.1350	m	0.1350	m	0.1350	m	0.1350	m
stroke	0.1400	m	0.1400	m	0.1400	m	0.1400	m	0.1400	m	0.1400	m
Vd	0.0080	m3	0.0080	m3	0.0080	m3	0.0080	m3	0.0080	m3	0.0080	m3
Speed	2400.00	rpm	1920.00	rpm	1680.00	rpm	1440.00	rpm	960.00	rpm	720.00	rpm
	40.00	rps	32.00	rps	28.00	rps	24.00	rps	16.00	rps	12.00	rps
Max piston speed S	672.00	rev/min	537.60	rev/min	470.40	rev/min	403.20	rev/min	268.80	rev/min	201.60	rev/min
Torque	397.89	Nm	397.89	Nm	397.89	Nm	397.89	Nm	397.89	Nm	106.10	Nm
calculated BMEP	6.24	Bar	6.24	Bar	6.24	Bar	6.24	Bar	6.24	Bar	1.66	Bar
QHV H2	1.20E+08	J/kg	1.20E+08	J/kg	1.20E+08	J/kg	1.20E+08	J/kg	1.20E+08	J/kg	1.20E+08	J/kg
mf of H2	0.00	kg/s	0.0000	kg/s	0.0000	kg/s	0.0000	kg/s	0.0000	kg/s	0.0000	kg/s
mf*QHV of H2	0.00	W	0.0000	W	0.0000	W	0.0000	W	0.0000	W	0.0000	W
QHV Diesel	4.30E+07	J/kg	4.30E+07	J/kg	4.30E+07	J/kg	4.30E+07	J/kg	4.30E+07	J/kg	4.30E+07	J/kg
mf of Diesel	0.01	kg/s	0.005156	kg/s	0.004336	kg/s	0.003633	kg/s	0.002389	kg/s	0.000689	kg/s
mf*QHV of Diesel	3.11E+05	W	2.22E+05	W	1.86E+05	W	1.56E+05	W	1.03E+05	W	2.96E+04	W
bsfc	260.00	g/KW.h	232.00	g/KW.h	223.00	g/KW.h	218.00	g/KW.h	215.00	g/KW.h	310.00	g/KW.h
Fuel conversion efficiency	0.32		0.3609		0.3754		0.3840		0.3894		0.2701	

Table 4 – Diesel engine and SOFC hybrid operation, with fuel cell operating at full load

Engine →	Diesel Engine Operation with SOFC on full load										idle conditions	
	100% power o/p	Units	80% power o/p	Units	70% power o/p	Units	60% power o/p	Units	40% power o/p	Units		Units
Power	100.00	KW	80.00	KW	70.00	KW	60.00	KW	40.00	KW	3.00	KW
bore	0.1350	m	0.1350	m	0.1350	m	0.1350	m	0.1350	m	0.1350	m
stroke	0.1400	m	0.1400	m	0.1400	m	0.1400	m	0.1400	m	0.1400	m
Vd	0.0080	m3	0.0080	m3	0.0080	m3	0.0080	m3	0.0080	m3	0.0080	m3
Speed	2400.00	rpm	1920.00	rpm	1680.00	rpm	1440.00	rpm	960.00	rpm	720.00	rpm
	40.00	rps	32.00	rps	28.00	rps	24.00	rps	16.00	rps	12.00	rps
Max piston speed S	672.00	rev/min	537.60	rev/min	470.40	rev/min	403.20	rev/min	268.80	rev/min	201.60	rev/min
Torque	397.89	Nm	397.89	Nm	397.89	Nm	397.89	Nm	397.89	Nm	39.79	Nm
calculated bmep	6.24	Bar	6.24	Bar	6.24	Bar	6.24	Bar	6.24	Bar	0.62	Bar
QHV H2	1.20E+08	J/kg	1.20E+08	J/kg	1.20E+08	J/kg	1.20E+08	J/kg	1.20E+08	J/kg	1.20E+08	J/kg
mf of H2	3.50E-05	kg/s	3.50E-05	kg/s	3.50E-05	kg/s	3.50E-05	kg/s	3.50E-05	kg/s	9.38E-06	kg/s
mf*QHV of H2	4203.50	W	4203.50	W	4203.50	W	4203.50	W	4203.50	W	1125.94	W
QHV Diesel	4.30E+07	J/kg	4.30E+07	J/kg	4.30E+07	J/kg	4.30E+07	J/kg	4.30E+07	J/kg	4.30E+07	J/kg
mf of Diesel	0.01	kg/s	0.01	kg/s	0.00	kg/s	0.00	kg/s	0.00	kg/s	0.00	kg/s
mf*QHV of Diesel	3.06E+05	W	2.18E+05	W	1.82E+05	W	1.52E+05	W	9.85E+04	W	9.98E+03	W
bsfc	256.48	g/KW.h	229.20	g/KW.h	217.97	g/KW.h	212.12	g/KW.h	206.23	g/KW.h	278.64	g/KW.h
Fuel conversion efficiency	0.32		0.36		0.38		0.38		0.39		0.27	

Table 5 - Diesel engine and SOFC hybrid operation, with fuel cell at half load

Engine →	Diesel Engine Operation with SOFC on half load									
	100% power o/p	Units	80% power o/p	Units	70% power o/p	Units	60% power o/p	Units	40% power o/p	Units
Power	100.00	KW	80.00	KW	70.00	KW	60.00	KW	40.00	KW
bore	0.1350	m	0.1350	m	0.1350	m	0.1350	m	0.1350	m
stroke	0.1400	m	0.1400	m	0.1400	m	0.1400	m	0.1400	m
Vd	0.0080	m3	0.0080	m3	0.0080	m3	0.0080	m3	0.0080	m3
Speed	2400.00	rpm	1920.00	rpm	1680.00	rpm	1440.00	rpm	960.00	rpm
	40.00	rps	32.00	rps	28.00	rps	24.00	rps	16.00	rps
Max piston speed S	672.00	rev/min	537.60	rev/min	470.40	rev/min	403.20	rev/min	268.80	rev/min
Torque	397.89	Nm	397.89	Nm	397.89	Nm	397.89	Nm	397.89	Nm
bmep max	6.24	Bar	6.24	Pa	6.24	Pa	6.24	Pa	6.24	Pa
QHV H2	1.20E+08	J/kg	1.20E+08	J/kg	1.20E+08	J/kg	1.20E+08	J/kg	1.20E+08	J/kg
mf of H2	1.08E-04	kg/s	1.08E-04	kg/s	1.08E-04	kg/s	1.08E-04	kg/s	1.08E-04	kg/s
mf*QHV of H2	12970.80	W	12970.80		12970.80		12970.80		12970.80	
QHV Diesel	4.30E+07	J/kg	4.30E+07		4.30E+07		4.30E+07	J/kg	4.30E+07	J/kg
mf of Diesel	0.01	kg/s	0.01	kg/s	0.00	kg/s	0.00	kg/s	0.00	kg/s
mf*QHV of Diesel	3.09E+05	W	2.20E+05		1.85E+05		1.54E+05		1.01E+05	
bsfc(diesel consumption only)	258.48	g/KW.h	230.13	g/KW.h	220.83	g/KW.h	215.46	g/KW.h	211.23	g/KW.h
Fuel conversion efficiency	0.31		0.34		0.35		0.36		0.35	

The data in Table 6 and Table 7 is calculated at various system load conditions with the fuel cell operating at full load and half load respectively. The constant efficiency lines for the fuel cell and constant specific fuel consumption for the engine are shown in Chapter 5 in the results section.

Table 6 - Performance map data for diesel engine operation with SOFC at full load

Diesel engine operation with SOFC at half load								
Diesel mass flow rate kg/s	**Engine Load %**	**Hydrogen %**	**FC Efficiency**	**Engine bsfc g/KWh**	**hydrogen flow rate kg/s**	**Utilisation factor**	**Total power KW**	**SOFC-ICE efficiency**
0.006832	100	5.4	42%	245	0.0002	70%	110	**34.61%**
0.004766	80	7.56		214	0.0002		90	**39.31%**
0.003946	70	8.99		202	0.0002		80	**41.30%**
0.003243	60	10.73		194	0.0002		70	**42.82%**
0.001999	40	16.32		179	0.0002		50	**45.46%**
0.007087	100	1.8	45%	255	0.000188	74%	110	**33.61%**
0.005021	80	2.62		226	0.000188		90	**37.74%**
0.004201	70	3.11		216	0.000188		80	**39.37%**
0.003498	60	3.72		209	0.000188		70	**40.46%**
0.002254	40	5.65		202	0.000188		50	**41.84%**
0.0071244	100	1.35	48%	256	0.000175	80%	110	**33.60%**
0.0050584	80	1.89		227	0.000175		90	**37.73%**
0.0042384	70	2.25		217	0.000175		80	**39.36%**
0.0035354	60	2.69		212	0.000175		70	**40.45%**
0.0022914	40	4.09		206	0.000175		50	**41.82%**
0.007153	100	0.96	51%	257	0.000165	85%	110	**33.60%**
0.005087	80	1.34		228	0.000165		90	**37.73%**
0.004267	70	1.59		219	0.000165		80	**39.35%**
0.003564	60	1.9		213	0.000165		70	**40.45%**
0.00232	40	2.89		208	0.000165		50	**41.81%**
0.00718	100	0.58	54%	258	0.000155	90%	110	**33.60%**
0.005114	80	0.81		230	0.000155		90	**37.73%**
0.004294	70	0.97		220	0.000155		80	**39.36%**
0.003591	60	1.16		215	0.000155		70	**40.46%**
0.002347	40	1.76		211	0.000155		50	**41.83%**

Table 7 – Performance map data for diesel engine operation with SOFC at half load

Diesel engine operation with SOFC at half load								
Diesel mass flow rate kg/s	Engine Load %	Hydrogen %	FC Efficiency	Engine bsfc g/KWh	hydrogen flow rate kg/s	Utilisation factor	Total power KW	SOFC-ICE efficiency
0.006832	100	5.4	42%	245	0.0002	70%	110	**34.61%**
0.004766	80	7.56		214	0.0002		90	**39.31%**
0.003946	70	8.99		202	0.0002		80	**41.30%**
0.003243	60	10.73		194	0.0002		70	**42.82%**
0.001999	40	16.32		179	0.0002		50	**45.46%**
0.007087	100	1.8	45%	255	0.000188	74%	110	**33.61%**
0.005021	80	2.62		226	0.000188		90	**37.74%**
0.004201	70	3.11		216	0.000188		80	**39.37%**
0.003498	60	3.72		209	0.000188		70	**40.46%**
0.002254	40	5.65		202	0.000188		50	**41.84%**
0.0071244	100	1.35	48%	256	0.000175	80%	110	**33.60%**
0.0050584	80	1.89		227	0.000175		90	**37.73%**
0.0042384	70	2.25		217	0.000175		80	**39.36%**
0.0035354	60	2.69		212	0.000175		70	**40.45%**
0.0022914	40	4.09		206	0.000175		50	**41.82%**
0.007153	100	0.96	51%	257	0.000165	85%	110	**33.60%**
0.005087	80	1.34		228	0.000165		90	**37.73%**
0.004267	70	1.59		219	0.000165		80	**39.35%**
0.003564	60	1.9		213	0.000165		70	**40.45%**
0.00232	40	2.89		208	0.000165		50	**41.81%**
0.00718	100	0.58	54%	258	0.000155	90%	110	**33.60%**
0.005114	80	0.81		230	0.000155		90	**37.73%**
0.004294	70	0.97		220	0.000155		80	**39.36%**
0.003591	60	1.16		215	0.000155		70	**40.46%**
0.002347	40	1.76		211	0.000155		50	**41.83%**

Appendix E. – Exergy Analysis

Calculation of equilibrium concentrations

The calculation of equilibrium concentrations for hydrogen fuel cell, methanol reformer and $C_{12}H_{26}$ IC engine it is necessary to find the equilibrium constants for the reversible reaction.

The equilibrium constant for a reversible reaction can be found from JANAF thermochemical tables for hydrogen. Since the reforming reaction for methanol and $C_{12}H_{26}$ reactions are not listed in the JANAF table, the approach used by Barclay[75] is followed.

For a reaction $aA + bB \leftrightarrow cD + dD$ the equilibrium constant is given below.

$$K = \left(\frac{P_C{}^c P_D{}^d}{P_A{}^a P_B{}^b} \right)$$

Hydrogen Oxidation

Consider the reaction of hydrogen oxidation,

$$H_2 + \frac{1}{2} O_2 \Rightarrow zH_2 + \frac{z}{2} O_2 + (1-z) H_2O$$

The total number of moles in the mixture is $n = z + \frac{z}{2} + (1-z) = \frac{z+2}{2}$

The mole fractions or equilibrium concentrations are given by

$$\gamma_{H_2} = \frac{2z}{z+2}$$

$$\gamma_{O_2} = \frac{z}{z+2}$$

$$\gamma_{H_2O} = \frac{2(1-z)}{z+2}$$

For very small values values of z the mole fractions for hydrogen, oxygen and water vapour become z, z/2 and 1 respectively.

Hence $K = \left(\frac{\gamma_{H_2O}}{\gamma_{H_2} \gamma_{O_2}^{1/2}} \right) \times \left(\frac{P}{P_{ref}} \right)^{-1/2}$

Methanol Reforming

Similarly the equilibrium concentrations for methanol reforming reaction are calculated for the following reaction.

$$CH_3OH + H_2O \Rightarrow zCH_3OH + zH_2O + (1-z)CO_2 + 3(1-z)H_2$$

The total number of moles in the mixture are $n = z + z + (1-z) + 3(1-z) = 4 - 2z$

The equilibrium concentrations are

$$\gamma_{CH_3OH} = \gamma_{H_2O} = \frac{z}{4-2z}$$

$$\gamma_{CO_2} = \frac{1-z}{4-2z}$$

$$\gamma_{H_2} = \frac{3(1-z)}{4-2z}$$

$$K = \left(\frac{\gamma_{CO_2} (\gamma_{H_2})^3}{\gamma_{CH_3OH} \gamma_{H_2O}} \right) \times \left(\frac{P}{P_{ref}} \right)^2$$

$C_{12}H_{26}$ Oxidation

For the IC Engine reaction the fuel used is $C_{12}H_{26}$

$$C_{12}H_{26} + 18.5O_2 \Rightarrow zC_{12}H_{26} + 18.5zO_2 + 12(1-z)CO_2 + 13(1-z)H_2O$$

The total number of moles in the mixture are

$$n = z + 18.5z + 12(1-z) + 13(1-z) = (25 - 5.5z)$$

The equilibrium concentrations are

$$\gamma_{C_{12}H_{26}} = \frac{z}{25 - 5.5z}$$

$$\gamma_{O_2} = \frac{18.5z}{25 - 5.5z}$$

$$\gamma_{CO_2} = \frac{12(1-z)}{25 - 5.5z}$$

$$\gamma_{H_2O} = \frac{13(1-z)}{25 - 5.5z}$$

$$K = \left(\frac{(\gamma_{CO_2})^{12} (\gamma_{H_2O})^{13}}{\gamma_{C_{12}H_{26}} (\gamma_{O_2})^{18.5}} \right) \times \left(\frac{P}{P_{ref}} \right)^{5.5}$$

Work done by Isothermal Circulators

The work done by the isothermal circulators on an ideal gas is given below:

$$\Delta G_2 = \tilde{R}T \ln\left(\frac{P_{in}}{P_{out}} \right)$$

Work done by Isentropic Circulators

For an isentropic process $\left(\frac{P_{out}}{P_{in}} \right) = \left(\frac{T_{out}}{T_{in}} \right)^{\frac{\gamma}{\gamma - 1}}$

The enthalpy changes from T_{in} to T_{out} are determined from the JANAF tables, which is the work done by the isentropic circulators ΔG_1.

Work done by Carnot cycle/Reversible Heat Engine

The reversible system components described in Fig. 1, when operating above ambient temperature produce Carnot work or reversible heat engine work. The Carnot work is given by [75].

$$P_{CT} = (T_1 - T_0)(S_4 - S_3)$$

where the reversible system follows isothermal paths from 1-2 and 3-4 and isentropic paths from 4-1 and 2-3.

Appendix F. – Feedback Control

The top level simulink model for the feedback control design is given below in Figure. 1. The blue subsystem models are the PID controllers and marked with controller numbers for easy identification. The details of the controllers are shown in the following figures.

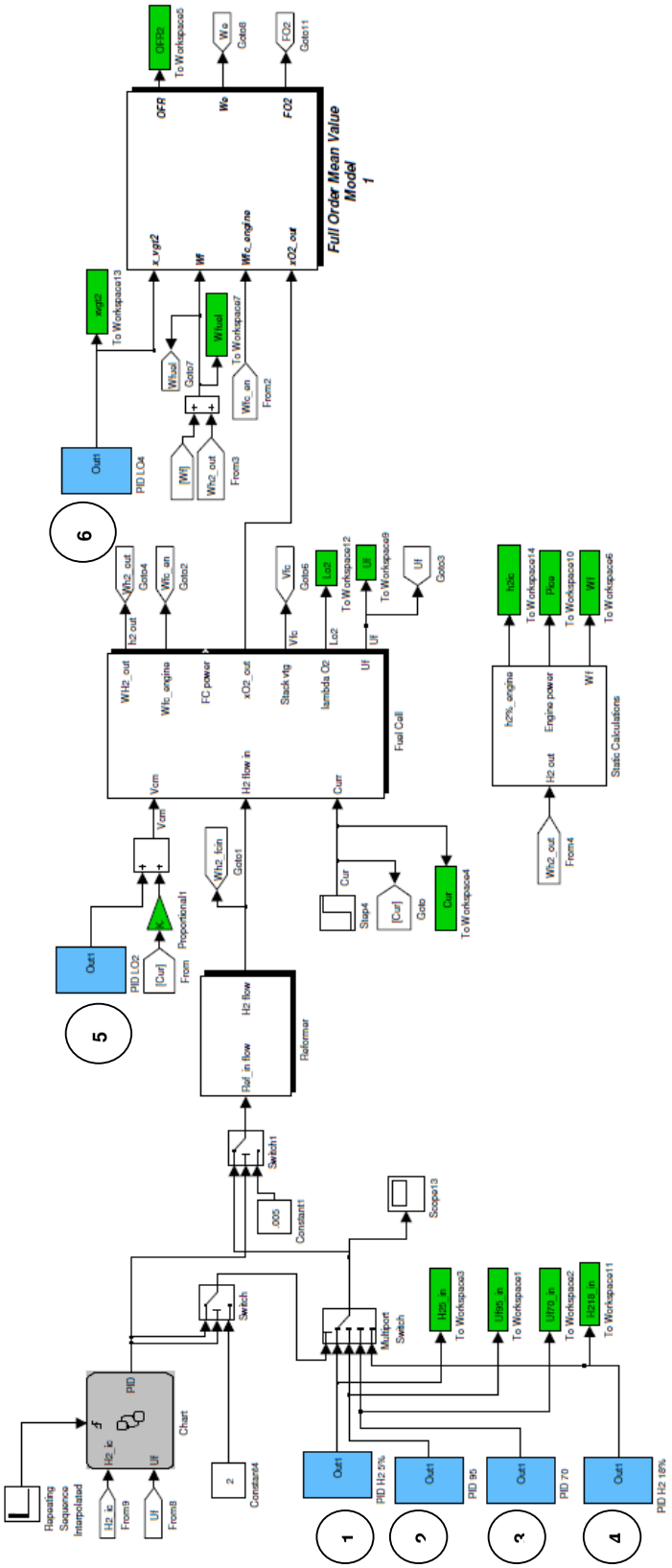

Figure. 1 – Top level Simulink model

The static calculations to estimate hydrogen percentage in the engine, the engine power and the reduction in diesel flow due to the introduction of hydrogen in the charge are given in Figure. 2.

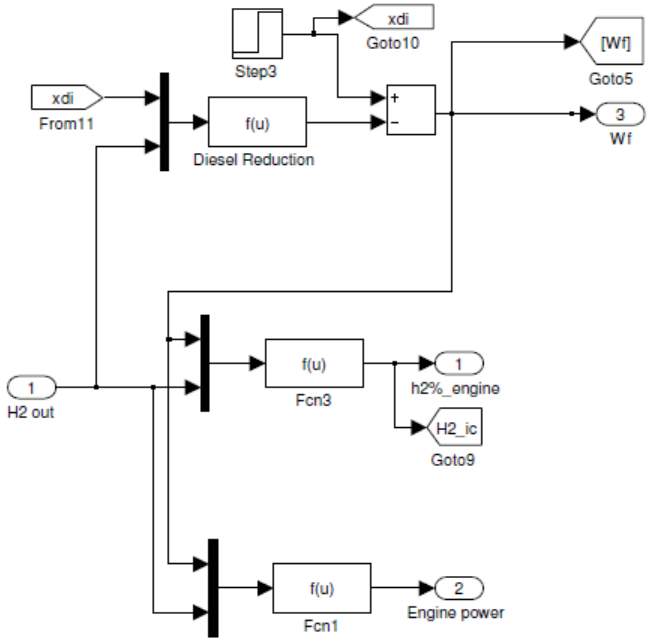

Figure. 2 – Static calculations

The details of the controller used for regulating the reformer input flow are shown at the left hand side in Figure. 1. Figure. 3-Figure. 5 show the details of the PID controller 1 to maintain the fraction of hydrogen in the engine to 5%.

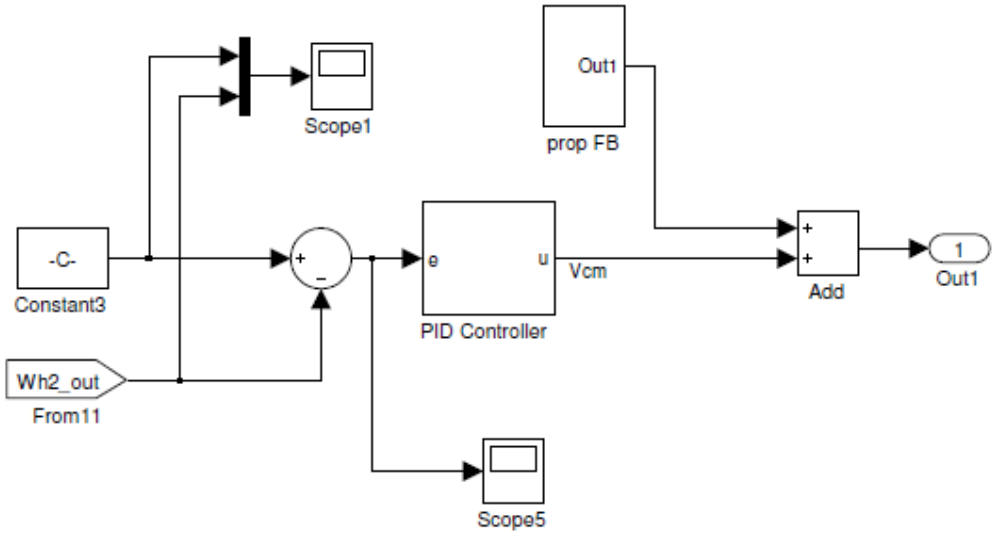

Figure. 3 – PID controller 1 to maintain fraction of hydrogen in intake charge to 5%.

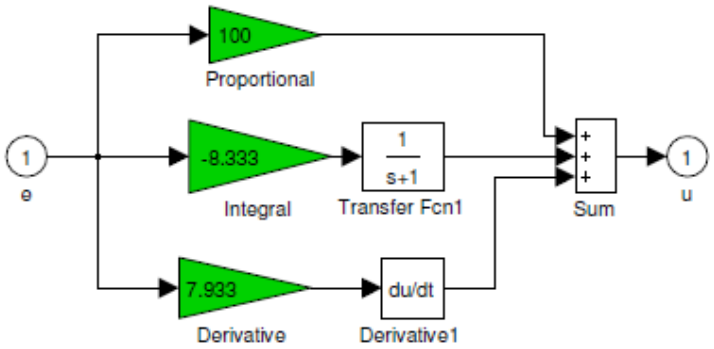

Figure. 4 – PID gains for controller 1.

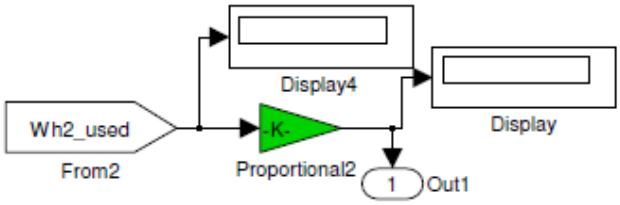

Figure. 5 – Proportional feedforward loop.

Figure. 4 shows the gains for the PID controller and Figure. 5 shows the details of a proportional feedforward loop for the fuel supply. The feedforward loop ensures that the fuel supplied is always in excess of that used in the fuel cell stack.

Similarly, the details of controllers 2-6 including PID gains for each controller are given in Figure. 6 - Figure. 18.

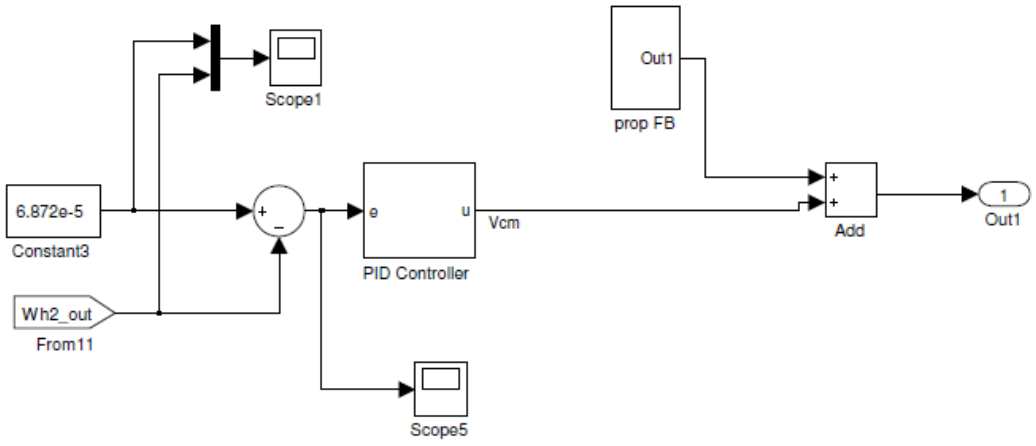

Figure. 6 - PID controller 2 to maintain fuel cell utilisation factor to 95%.

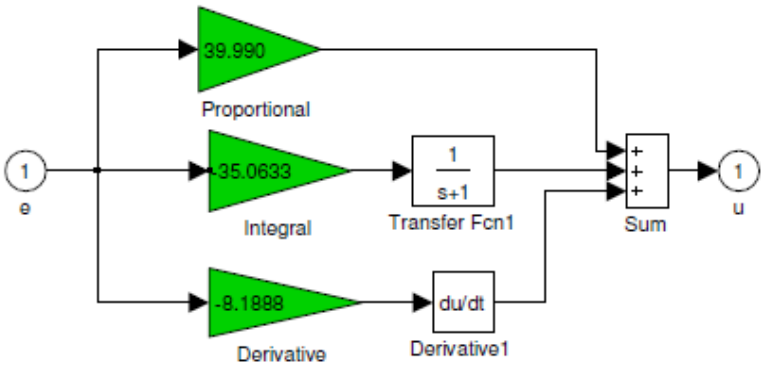

Figure. 7 – PID gains for controller 2.

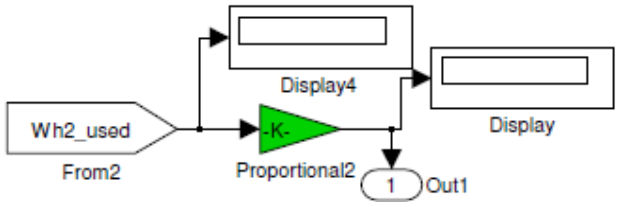

Figure. 8 – Proportional feedforward loop

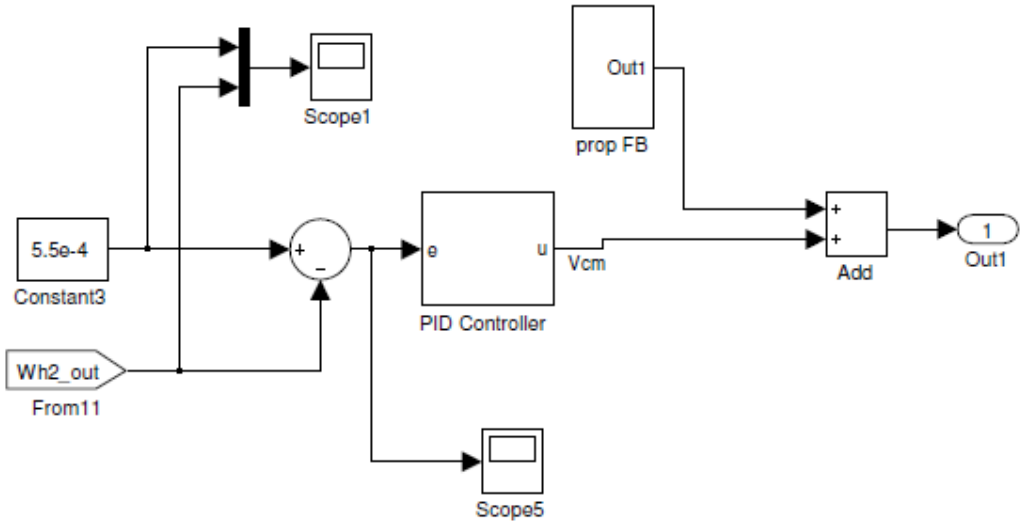

Figure. 9 - PID controller 3 to maintain fuel cell utilisation factor to 70%.

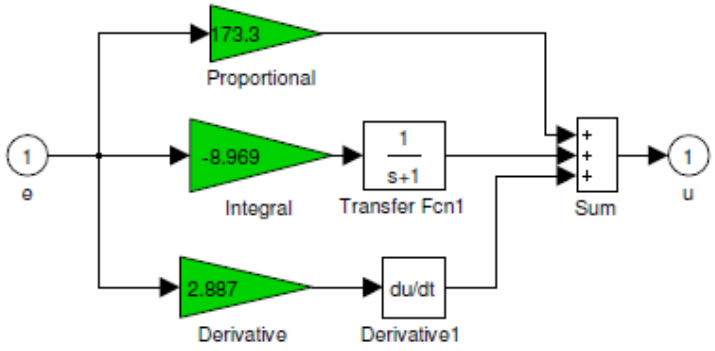

Figure. 10 – PID gains for controller 3.

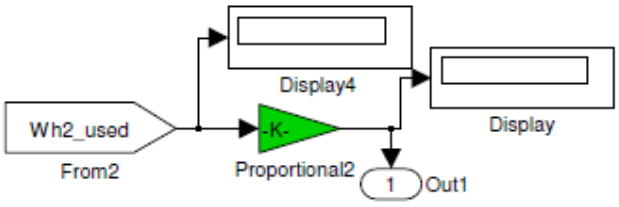

Figure. 11 – Proportional feedforward loop.

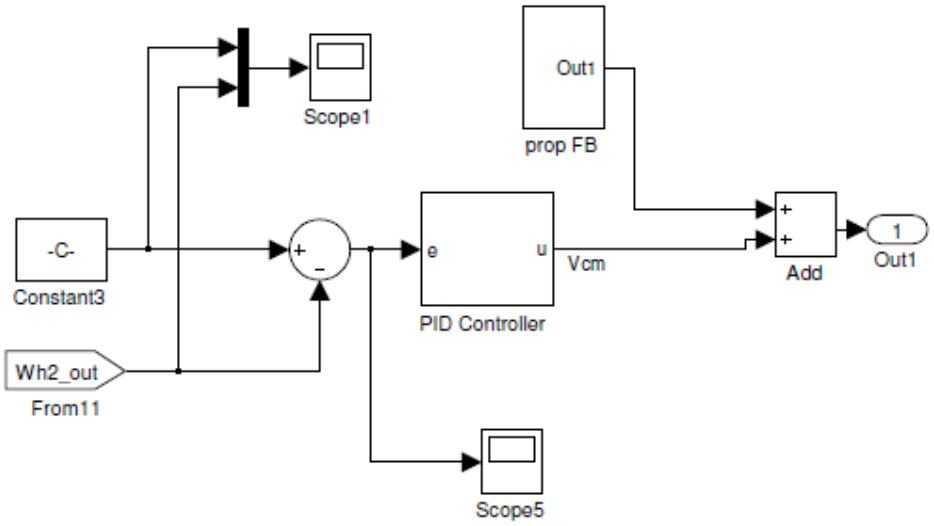

Figure. 12 - PID controller 4 to maintain fraction of hydrogen in intake charge to 20%.

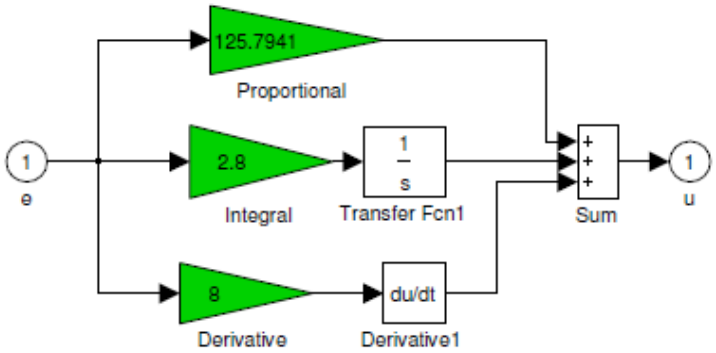

Figure. 13 – PID gains for controller 4.

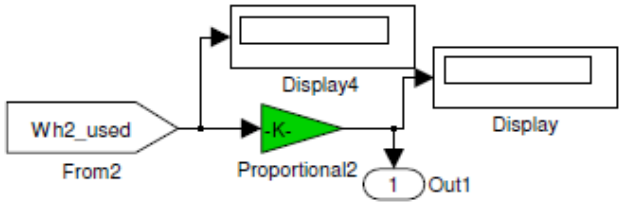

Figure. 14 – Proportional feedforward loop

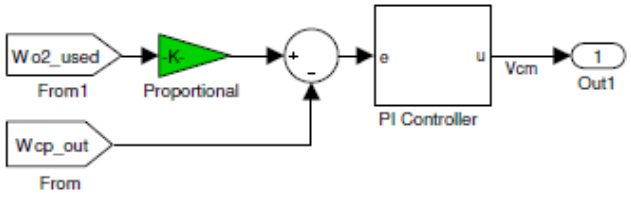

Figure. 15 - PID controller 5 to maintain excess oxygen ration to 2.

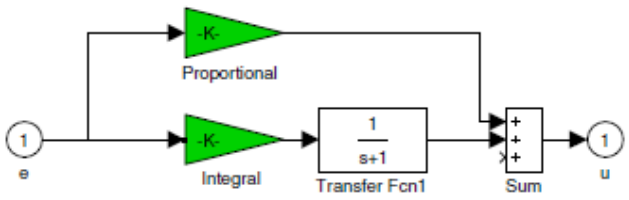

Figure. 16 – PID gains for controller 5.

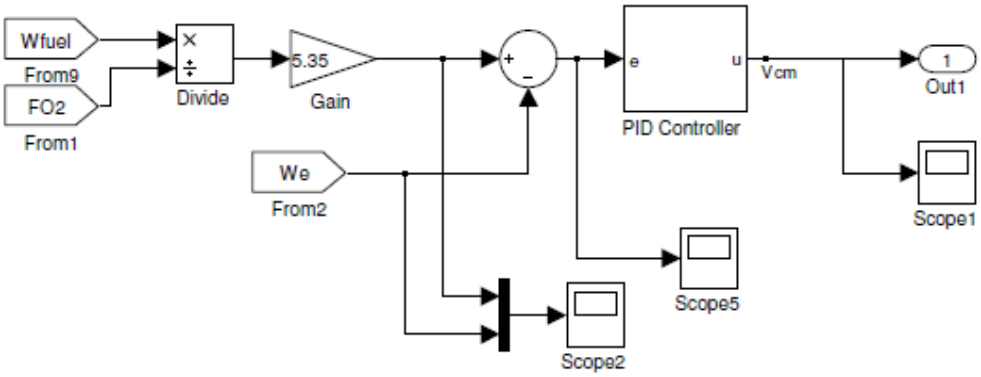

Figure. 17 - PID controller 6 to maintain fraction of oxygen-to-fuel ratio

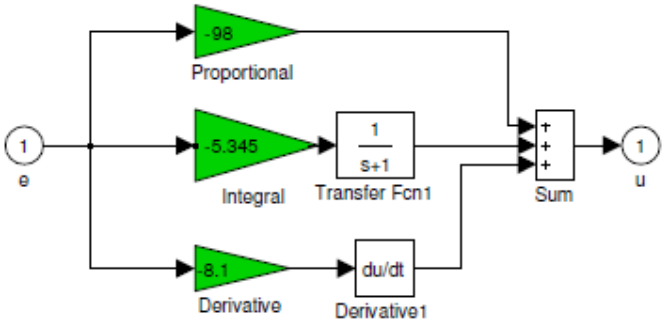

Figure. 18 – PID gains for controller 6.

Appendix G. – List of Publications

1. A. Chaudhari and R. Stobart, "Investigation of Optimum Operating Range for a Solid Oxide Fuel Cell-IC Engine Hybrid System," *IEEE Conference on Electric and Hybrid Vehicles, 2006. ICEHV '06.* , pp. 1-6, 2006.

2. R. K. Stobart, Peng, Z., Chaudhari, A.R., Heikal, M.R., Monaghan, M.L., Methods And Apparatus For Use With Power Supply System. Patent Number. WO/2007/113507, 2007.

3. R. K. Stobart, Peng, Z., Chaudhari, A.R., Heikal, M.R., Monaghan, M.L., Ladommatos, N., Hardalupas, I., Taylor, A.M.K.P., Zhao, H., Jiang, X., Ma, T.T.-H., Power Supply System. Patent Number. WO/2007/113509, 2007.

4. R. K. Stobart and A. Chaudhari, "A Novel Hybrid Powerplant for Passenger Bus Applications," presented at SAE Powertrain & Fluid Systems Conference and Exhibition, October 2007, Chicago, IL, USA, 2007-01-4120.

5. A. Chaudhari, A. Plianos, and R. Stobart, "Modelling and Control Design of SOFC-IC Engine Hybrid System," *Society of Automotive Engineers*, vol. 2008-01-0082, 2008.

6. A. Plianos, A. R. Chaudhari, and R. K. Stobart, "Modeling and Control of a novel SOFC-IC Engine Hybrid System," presented at Proceedings of UKACC Control Conference 2008, Manchester, UK, 2008.

7. A. Chaudhari, A. Plianos, and R. Stobart, "Development of Model Predictive Controller for SOFC-IC Engine Hybrid System," *SAE International Journal of Engines*, vol. 2, pp. 56-66, 2009.

8. A. R. Chaudhari and R. H. Thring, "Energy economy analysis of the G-Wiz: a two-year case study based on two vehicles," *Proceedings of the Institution of Mechanical Engineers, Part D: Journal of Automobile Engineering*, vol. 225, 2011.

Submitted for Publication

9. A. R. Chaudhari and R. K. Stobart, "Exergy Analysis of a SOFC-IC Engine Hybrid System " *Journal of Power Sources*, 2011.

10. A. R. Chaudhari and R. H. Thring, "Automotive Hydrogen Tanks: An Experimental and Modelling Study of Temperature Rise During Filling," *International Journal of Hydrogen Energy*, 2011.